

TABLE OF CONTENTS

	<u>Page</u>
INTRODUCTION	1 1/A12
I. ESTIMATES OF EXPLOSIVE YIELD	8 1/B5
1-1 Explosive Yield as a Function of Propellant Type and Accident Conditions	8 1/B5
1-2 Explosive Yield as a Function of Fluid Type and Initial Conditions for Gas Vessel Bursts	26 1/C9
List of References	29 1/C12
II. CHARACTERISTICS OF PRESSURE WAVES	31 1/C14
2-1 General	31 1/C14
2-2 Pressure Waves from Propellant Explosions	40 1/D9
2-3 Pressure Waves from Gas Vessel Bursts	56 1/E11
List of References	68 1/F9
II. A GAS VESSEL BURST	70 1/F11
2A-1 Nondimensional Parameters	70 1/F11
2A-2 Source of Data	70 1/F11
2A-3 Overpressure Calculation	71 1/F12
2A-4 Impulse Calculation	74 1/G1
2A-5 Effect of Cylindrical Geometry	74 1/G1
2A-6 Effect of Reflecting Surface (Burst at Ground Level)	74 1/G1
List of References	78 1/G5
Symbols	79 1/G6

TABLE OF CONTENTS (Cont'd)

		<u>Page</u>
III.	EFFECTS OF PRESSURE WAVES	80 1/G7
	3-1 Damage Estimates to Structures	80 1/G7
	3-2 Injury Estimates to Humans	99 2/B3
	List of References	125 2/D1
III.A	STRUCTURAL RESPONSE	128 2/D4
	3A-1 Overturning Analysis	128 2/D4
	3A-2 Development of Beam Equations	134 2/D10
	3A-3 Development of Plate Equations	142 2/E4
	3A-4 Development of Membrane Equations	153 2/F1
	List of References	158 2/F6
III.B	PRESSURE/IMPULSE COMBINATIONS PRODUCING LUNG DAMAGE	159 2/F7
	List of References	169 2/G3
III.C	PRESSURE/IMPULSE COMBINATIONS PRODUCING LOSS OF HEARING	171 2/G5
	List of References	175 2/G9
III.D	PRESSURE/IMPULSE COMBINATIONS PRODUCING WHOLE-BODY DISPLACEMENT AND SUBSEQUENT DAMAGE TO THE HEAD AND BODY	176 2/G10
	List of References	190 3/B1
IV.	CHARACTERISTICS OF FRAGMENTS	191 3/B2
	4-1 General	191 3/B2
	4-2 Methods for Estimating Fragment Initial Velocities for Spheres and Cylinders Bursting into Many Fragments	191 3/B2

TABLE OF CONTENTS (Cont'd)

		<u>Page</u>
4-3	Estimate of Initial Velocities of Fragments from Spheres and Cylinders Bursting into Two Equal Halves	218 3/D1
4-4	Determination of Appurtenance Velocity	228 3/D11
4-5	Methods for Computing Fragment Ranges and Impact Conditions	240 3/E9
4-6	Fragment Mass Distribution	279 4/All
4-7	Probability of Fragment Arrival Versus Range	286 4/B4
	List of References	292 4/B10
IV. A	METHODS FOR ESTIMATING FRAGMENT INITIAL VELOCITIES	293 4/B11
	List of References	315 4/D5
IV. B	COMPARISON OF EXPERIMENTAL RESULTS WITH CODE PREDICTIONS	316 4/D6
	List of References	318 4/D8
IV. C	ESTIMATE OF INITIAL VELOCITIES OF FRAGMENTS FROM SPHERES AND CYLINDERS BURSTING INTO TWO EQUAL HALVES	319 4/D9
	List of References	354 4/G2
IV. D	ESTIMATION OF VELOCITIES ATTAINED BY APPURTENANCES SUBJECTED TO BLAST LOADING	355 4/G3
	List of References	377 5/B2
IV. E	ANALYSES FOR FRAGMENT TRAJECTORIES	378 5/B3
	List of References	401 5/C12

TABLE OF CONTENTS (Cont'd)

	<u>Page</u>
IV.F STATISTICAL FITTING TO FRAGMENT DATA	402 5/C13
4F-1 Derivation of Figures 4-46 Through 4-49	402 5/C13
4F-2 Derivation of Figure 4-50	402 5/C13
4F-3 Rationale for Averaging Fragment Mass Distribution for Events 3, 4, and 5	403 5/C14
4F-4 Fragment Mass Distributions for Gas Vessel Bursts	406 5/D3
4F-5 Rationale for Averaging Fragment Mass Distributions for Tanks A and B and Tanks D and E	412 5/D9
4F-6 Derivation of Figure 4-57, Fragment Distance Versus Percent Yield for Propellant Explosions	413 5/D10
4F-7 Derivation of Simulated Fragment Range Distribution for Gas Vessel Bursts	415 5/D12
4F-8 Rationale for Combining Simulated Range Distribution for Tanks A and B and for Tanks D and E	423 5/E6
List of References	424 5/E7
V. EFFECTS OF FRAGMENTS	425 5/E8
5-1 Damage Estimates to Structures and Facilities	425 5/E8
5-2 Damage Estimates to People from Secondary Fragments	433 5/F2
List of References	442 5/F11
V.A EFFECTS OF FRAGMENTS ON STRUCTURES	444 5/F13
List of References	446 5/G1

TABLE OF CONTENTS (Concl'd)

		<u>Page</u>
V. B	DAMAGE ESTIMATES TO PEOPLE FROM SECONDARY FRAGMENTS	447 5/G2
	5B-1 Penetrating Fragments	447 5/G2
	5B-2 Nonpenetrating Fragments	455 5/G10
	List of References	456 5/G11
VI.	RISK ASSESSMENT AND INTEGRATED EFFECTS	458 5/G13
	6-1 Risk Assessment	458 5/G13
	6-2 Prediction of Relative Blast and Fragment Effects	461 6/A7
	List of References	507 6/D11
VII.	DISCUSSION OF RESULTS	508 6/D12
VIII.	CONCLUSIONS	511 6/E1
IX.	RECOMMENDATIONS	513 6/E3
LIST OF SYMBOLS		516 6/E6
CONVERSION FACTORS		523 6/E13
GLOSSARY OF TERMS		525 6/F1
BIBLIOGRAPHY		528 6/F4

NAS1.26:134906

OCT 26 1977

NASA CONTRACTOR REPORT 134906

COMPLETED

ORIGINAL

WORKBOOK FOR PREDICTING PRESSURE WAVE
AND FRAGMENT EFFECTS OF EXPLODING PROPELLANT
TANKS AND GAS STORAGE VESSELS

W. E. BAKER, J. J. KULESZ, R. E. RICKER,
R. L. BESSEY, P. S. WESTINE, V. B. PARR,
AND G. A. OLDHAM

CONTRACT NAS3-19231
SEPTEMBER 1977

NASA

1. Report No. NASA CR-134906	2. Government Accession No.	3. Recipient's Catalog No.	
4. Title and Subtitle WORKBOOK FOR PREDICTING PRESSURE WAVE AND FRAGMENT EFFECTS OF EXPLODING PROPELLANT TANKS AND GAS STORAGE VESSELS		5. Report Date September 1977	
		6. Performing Organization Code	
7. Author(s) W. E. Baker, J. J. Kulesz, R. E. Ricker, R. L. Bessey, P. S. Westine, V. E. Parr, and G. A. Oldham		8. Performing Organization Report No. 02-4130	
		9. Work Unit No.	
		10. Contract or Grant No. NAS3-19231	
11. Type of Report and Period Covered Contractor Report		12. Sponsoring Agency Name and Address National Aeronautics and Space Administration Washington, D.C. 20546	
		13. Sponsoring Agency Code	
15. Supplementary Notes Project Managers, Robert D. Siewert and Paul M. Ordin, Space Propulsion and Power Division, NASA Lewis Research Center, Cleveland, Ohio 44135			
16. Abstract This workbook is intended to provide the designer and the safety engineer with the best available technology for predicting damage and hazards from explosions of propellant tanks and bursts of pressure vessels, both near and far from these explosion sources. The information is presented in the form of graphs, tables, and nomographs to allow easy calculation without recourse to difficult mathematical manipulation or the use of extensive computer programs. When complex methods have been used to develop simple prediction aids, they are fully described in appendices. Topics covered in various chapters are			
<ul style="list-style-type: none"> (1) Estimation of explosive yield (2) Characteristics of pressure waves (3) Effects of pressure waves (4) Characteristics of fragments (5) Effects of fragments (6) Risk assessment and integrated effects <p>Short chapters giving a discussion of results, conclusions, and recommendations for further work are also included.</p>			
17. Key Words (Suggested by Author(s)) Fragmentation; Chemical explosions; Fragments; Compressed gases; Range safety; Debris; Blast loads; Blast effects; Ballistics; Liquid rocket propellants; Terminal ballistics		18. Distribution Statement Unclassified - unlimited STAR Category 28	
19. Security Classif. (of this report) Unclassified	20. Security Classif. (of this page) Unclassified	21. No. of Pages 557	22. Price* A24

BLANK PAGE

FOREWORD

Many staff members at Southwest Research Institute in addition to the authors contributed substantially to the work reported here. The authors gratefully acknowledge the special contributions of the following:

- . Mr. M. A. Sissung, for organization and editing of the workbook,
- . Miss C. A. Hajovsky, for extensive data reduction and curve plotting.

The technical support of our project managers at the NASA Lewis Research Center, Mr. Robert D. Siewert and Mr. Paul M. Ordin, contributed materially to the success of this work. In particular, they provided excellent technical guidance throughout the contract, and were also able to obtain for us the needed input data for all the example cases presented in Chapter VI and references to other related work.

In this printing minor errors in the test and figures have been corrected.

BLANK PAGE

SUMMARY

This workbook is intended to provide the designer and the safety engineer with the best available technology that they need to predict damage and hazards from explosions of propellant tanks and bursts of pressure vessels, both near and far from these explosion sources. The information is presented in the form of graphs, tables, and nomographs to allow easy calculation without recourse to difficult mathematical manipulation or the use of extensive computer programs. When complex methods have been used to develop simple prediction aids, they are fully described in appendices.

Topics covered in various chapters are:

- (1) Estimation of explosive yield
- (2) Characteristics of pressure waves
- (3) Effects of pressure waves
- (4) Characteristics of fragments
- (5) Effects of fragments
- (6) Risk assessment and integrated effects.

Short chapters giving discussion of results, conclusions, and recommendations for further work are also included.

INTRODUCTION

Nature of the Hazards

The likelihood of accidental explosions, in the various activities that involve liquid propellants for space vehicles, can best be decreased by improvements in design practices and operating procedures. Over the years, the frequency of occurrence of accidental explosions in the space program has decreased with advances in technology. Nevertheless, the possibility of space vehicle fuel/oxidizer explosions or pressure bursts will always exist, especially with reusable propulsion systems that must be more reliable compared with those in the "one-shot" space vehicle. Excessive cyclic stresses, wear of moving parts and the accumulation of contaminants are some of the factors that could contribute to component malfunctions or material failures during the lifetime use of such systems. These malfunctions or failures could, in turn, contribute to accidental explosions with risk of damage to facilities and hazards to people. Thus, it becomes important to predict the explosive yield and the effects of pressure wave and fragments in a quantitative manner.

It is the intent here to provide the designer and the safety engineer with the best available technology that they need to predict damage and hazards from explosions of propellant tanks and bursts of pressure vessels in the near and far fields of interest.

In a launch configuration within tankage in a rocket motor, liquid propellants and nonreacting gases are initially contained within vessels of various sizes, geometries, and strengths. Various modes of failure of these vessels are possible, from either internal or external stimuli. If the vessel is pressurized with static internal pressure, one possible mode of failure is simply fracture, instituted at a critical size flaw and propagated throughout the vessel. A similar kind of failure can occur if the vessel is accidentally immersed in a fire, and pressure increases internally because of vaporization of the internal propellant. Some launch vehicles have the liquid fuel and oxidizer separated by a common bulkhead. Accidental over-pressurization of one of these chambers can cause rupture of this bulkhead, and subsequent mixing and explosion of the propellant. External stimuli that can cause vessel failure include high-speed impact by foreign objects, accidental detonation of the warhead of a missile, dropping of a tank to the ground (as in toppling of a missile on the launch pad), as well as many other external sources. Vessel failure can result in an immediate release of energy or it can cause subsequent energy release because of mixing of propellant and oxidizer and subsequent ignition. Other modes of failure which have resulted or could result in violent explosions are fall-back immediately after launch due to loss of thrust, or low-level failure of the guidance system after launch resulting in impact

into the ground at several hundred feet per second.

Failure of a vessel containing liquid propellants or compressed gas can result in various levels of energy release, ranging from negligible to the full heat value of the combined propellant and oxidizer, or full value of stored energy in the compressed gas. Toward the lower end of the scale of energy release might be the failure of a pressurized vessel due to ductile crack propagation. Here, the stored pressure energy within the compressed propellant or gas in an ullage volume above the propellant could split the vessel or generate a weak blast wave. In the intermediate range of energy releases could lie vessel failure by external stimulus and ignition, either very rapidly or at very late times, so that only small proportions of mixed propellant and oxidizer contribute to the energy release. In this intermediate range could also lie the rapid fracture of gas storage vessels after heating or very rapid crack propagation. At the upper end of the scale could be the explosion in a vessel wherein a pre-mixed propellant and oxidizer detonate in much the same fashion as a high explosive, and explosions resulting after violent impact with the ground. In past studies of possible blast and fragmentation effects from vessel rupture, a critical problem has been to accurately assess the energy release as a result of the accident or incident. A common method of assessment of possible energy release or correlation of the results of experiments has been to assess the energy release on the basis of equivalent pounds of TNT. This method is used because a large body of experimental data and theoretical analyses exist for blast waves generated by TNT or other solid explosives (refs. 1 and 2). Although the comparison with TNT is convenient, the correlation is far from exact. Specific energies which can be released, i.e., energy per unit volume or mass of material, differ quite widely between TNT, various liquid propellants or mixtures of liquid propellants and oxidizers, and gases stored in pressure vessels. The characteristics of damaging blast waves from explosions which can occur in flight vehicle accidents can therefore be quite different from blast waves from TNT explosions. The accidental explosions usually generate waves with lower amplitudes (peak overpressures) and longer durations than equivalent energy TNT explosions, at least close to the explosion source. Reference 3 discusses in some detail the blast waves from accidental explosions of the classes covered in this handbook.

Dependent on the total energy release and the rate of this energy release, the sizes and shapes of fragments generated by bursting liquid propellant vessels and their appurtenances, and bursting gas vessels, cover a very wide spectrum. At one extreme is the case of a vessel bursting because of seam failure or crack propagation from a flaw wherein only one "fragment" is generated, the vessel itself. This fragment, from a very slow reaction, can be propelled by releasing the contents of the vessel. At the other extreme is the conversion of the vessel and parts near it into a cloud of small fragments by an explosion of the contents of a vessel at a

very rapid rate, similar to a TNT explosion (refs. 4 and 5). For most accidental vessel failures, the distribution of fragment masses and shapes undoubtedly lies between these two extremes. The modes of failure of the vessel may be dependent upon details of construction and the metallurgy of the vessel material. Some of the masses and shapes are dictated by the masses and shapes of attached or nearby appurtenances. In any event, assessment and prediction of these parameters is much more difficult than is true for the better understood phenomenon of shell casing fragmentation.

Once the masses, shapes, and initial velocities of fragments from liquid propellant vessels or bursting gas vessels have been determined in some manner, then the trajectories of these fragments and their losses in velocity due to air drag or perforation or penetration of various materials must be computed. This problem is primarily one of exterior ballistics. It differs from conventional exterior ballistic studies of trajectories of projectiles, bombs, or missiles in that the body in flight is invariably very irregular in shape and can be tumbling violently. Exact trajectories cannot be determined then in the same sense that they can be for well-designed projectiles. Only approximate trajectories can be estimated, usually by assuming relatively simple geometric shapes, such as spheres, discs or cylinders, for which exterior ballistics data and techniques exist. But, in some fashion, one can predict the ranges and impact velocities for fragments which were initially projected in specified directions from the bursting vessel with specified initial velocities.

This problem is not complete until one can assess the effects of blast waves and fragments from the accidents on various "targets." For a proper assessment of hazards, one should consider a wide variety of targets, including human beings, various classes of buildings, vehicles, and perhaps even aircraft. Problems of fragment damage are exceedingly complex, not only because of the inherent statistical nature of the characteristics of the impacting fragments but also because the terminal ballistic effects for large irregular objects impacting any of the targets described are not very well known. In most past studies of fragment damage from accidents, the investigators have been content to simply locate and approximate the size and mass of the fragments in impact areas and have ignored the important problem of the terminal ballistic effect of these fragments. Prediction of blast damage is also not simple, but much more work has been done and reasonable estimates can be made for most structures and for humans, provided the characteristics of the blast waves can be defined (refs. 6 and 7).

Means for Assessment of Risk

This handbook is directed toward estimation of blast and fragmentation effects of accidental explosions in flight vehicles. It is not intended to encompass the entire problem of risk assessment for launch and operation

of these vehicles. This more comprehensive task includes the estimation of the probability of occurrence of various types of failures or accidents, and must employ methods such as failure mode analysis or fault-tree analysis to obtain such probabilities. In this handbook, it is assumed that a specific explosive accident has occurred, and the hazardous effects of that accident are predicted. A brief discussion of methods of risk assessment is given in Chapter 6.

Scope and Significance of Material Presented

The material presented in the handbook is based on a previous study of fragmentation from bursting propellant vessels (ref. 8) and on the literature on characteristics and effects of blast waves and fragment impact. Methods are given for predicting the damage to facilities and hazards to people from exploding liquid propellant tanks or bursting gas storage bottles. Various chapters present material which allows estimation of explosive yield or energy for a variety of propellant explosions and gas vessel bursts, give predictions of characteristics of pressure waves from these explosions, and present techniques for making damage estimates for structures and facilities, and mortality or injury to people subjected to the blast waves. Other chapters include estimates of fragment initial velocities and the statistics of mass and shape, terminal velocities and impact conditions, and effects of such impact on facilities, structures and people. Throughout the workbook, presentations are made in the form of scaled graphs, equations, nomographs or tables which allow easy calculation without recourse to difficult mathematical manipulation or use of extensive computer programs. When such methods have been used to develop simple prediction aids, they are fully described in appendices.

It is believed that this workbook is the first to provide safety engineers with relatively simple yet comprehensive methods for estimating blast and fragment hazards for accidental explosions in liquid-propellant fueled flight vehicles. Some methods for estimating blast yield for classes of liquid propellant accidents are given in ref. 9, and ref. 10 discusses blast and fragmentation from such explosions. But, neither of these references allows estimation of fragment characteristics and effects for liquid propellant explosions, nor do they treat gas vessel bursts. Special features not seen elsewhere are the prediction of blast wave characteristics for gas vessel bursts, effects of fragment impact on structures and facilities, and extensive application of the pressure-impulse (P-I) damage concept to a wide variety of structures and to humans.

Intended Purpose and Limits of Use

The purpose of the workbook is to provide typical safety engineers, with training at the bachelor's degree level in some engineering specialty, with methods for rapid estimation of blast and fragment hazards from accidental explosions in flight vehicles. It should require only a desk or pocket calculator or slide rule to perform any of the needed calculations. There are, of course, a number of limits to the calculations and their applicability which the user should observe. Because almost all of the data he will use are graphical, these limits will often be self-evident from the extreme values on the graphs. In general, one should not extend or extrapolate these graphs, but should instead merely report that prediction is not possible if input parameters fall outside the range of the plot.

Factors of safety are included in the prediction methods in various ways. When curves are based on experiments, error bands are usually given. Use of average curves through the data will give most probable values for such loading parameters as blast overpressure and impulse; use of the upper limits of the error band will assure conservatism by encompassing all of the extreme values in the measured data rather than the most probable. Most of the fragment data must be presented statistically. The user is often given a choice of several regression lines through the data. Choice of such a line with a very high probability of, say, predicting that all fragments less than a certain mass will fall to earth within a given distance, will assure a high factor of safety in estimating exclusion distances for possible fragment damage. In estimating effects of blast and fragments, factors of safety are included by estimating different degrees of damage given blast envelopment or fragment impact. For structures, estimates can be made for lower limits to damage (threshold of no damage at all) through quite severe structural damage to buildings, vehicles, etc. For people, estimates can be made for threshold of ear damage through 1% chance of mortality to 99% chance of mortality. For estimation methods which are based on sparse data or analysis, we have large bands of uncertainty--the user should apply upper limits of these bands, if in doubt.

Applications to Areas Other Than Aerospace Rocket Launch and Research Facilities

This workbook was prepared primarily for use by safety engineers and site planners at aerospace rocket launch and research facilities. It emphasizes the blast and fragment hazards which could occur at such sites, and the prediction of their damaging effects. The prediction of blast and fragment hazards is specific for liquid propellant explosions and gas bottle bursts. The common use in explosive safety circles of conversion to TNT equivalency is nearly completely avoided, so the workbook cannot be easily used to predict hazards from detonations of condensed explosives such as TNT. On the other hand, the methods given in Chapters III, V and VI for

prediction of damaging effects are quite independent of the methods for estimating the hazards. Blast damage predictions could as easily be made for TNT or nuclear explosions as for propellant explosions, provided the blast wave characteristics were defined. Similarly, fragment damage predictions are independent of the sources of the fragments, and only depend on a knowledge of the impact conditions. Indeed, the treatment of damage effects is much more extensive than one would be apt to find in any other single document, and could find much wider use than for damage prediction near aerospace test and launch facilities.

Additional Areas of Research

The bases for the prediction methods given in this workbook range from a firm foundation of extensive testing and analysis, through analyses supported by limited testing or accident reporting, to some predictions which are quite speculative because of little corroborating evidence. Predictions in the latter case could often be improved by additional research.

Areas in which we feel there is a pressing need for additional study are:

- (1) Definition of fragmentation characteristics for bursting gas storage bottles. Existing data consist of only five tests for one bottle geometry and material, and one gas.
- (2) Definition of blast wave characteristics for burst of cylindrical gas storage vessels, either analytically or experimentally. Present methods are limited to essentially spherically symmetric cases.
- (3) Better definition of fragment impact effects on a variety of structures and facilities, for fragments typical of those occurring in aerospace vehicle explosions. Most fragment impact data or methods developed to date are related to high velocity, small mass penetrators which are not typical of accidentally produced fragments.
- (4) Extension of the present work to accidental explosions in thick-walled storage vessels typical of ground transport and storage vessels. The current work is directed toward explosions of flight-weight hardware. Blast and fragmentation characteristics can be drastically different for heavier vessels.

In Chapter IX, we discuss these and other areas for further work in more detail.

LIST OF REFERENCES

1. Baker, Wilfred E., Explosions in Air, Univ. of Texas Press, Austin, Texas, May 1973.
2. Kingery, C. N., and B. F. Pannill, "Peak Overpressure vs Scaled Distance for TNT Surface Burst (Hemispherical Charges)," BRL Memo Report No. 1518, Aberdeen Proving Ground, Md., April 1964. AD 443-102.
3. Strehlow, Roger A., and Wilfred E. Baker, "The Characterization and Evaluation of Accidental Explosions," NASA CR 134779, NASA Grant NSG3008, June 1975.
4. Gurney, R. W., "The Initial Velocities of Fragments from Bombs, Shells, and Grenades," BRL Report 405, 1943.
5. Henry, I. G., "The Gurney Formula and Related Approximations for the High-Explosive Deployment of Fragments," Hughes Aircraft Company, Report No. PUB-189, Culver City, California, April 1967.
6. Custard, G. H., and G. R. Thayer, "Evaluation of Explosive Storage Safety Criteria," Falcon Research and Development Co., Contract DAHC04-69-C-0095, March 1970.
7. White, Clayton S., Robert V. Jones, Edward G. Damon, E. Royce Fletcher, and Donald R. Richmond, "The Biodynamics of Airblast," Tech. Rep. to Defense Nuclear Agency, DNA 2738T, Lovelace Foundation for Medical Education and Research, July 1971. AD 734-208.
8. Baker, W.E., V. B. Parr, R. L. Bessey, and P. A. Cox, "Assembly and Analysis of Fragmentation Data for Liquid Propellant Vessels," NASA CR-134538, NASA Lewis Research Center, Jan. 1974.
9. Willoughby, A. B., C. Wilton, and J. Mansfield, "Liquid Propellant Explosion Hazards. Final Report - Dec. 1968. Vol. III - Prediction Methods," AFRPL-TR-68-92, URS 652-35, URS Research Co., Burlingame, California.
10. Jensen, Andreas V. (ed.), "Chemical Rocket/Propellant Hazards, Vol. I, General Safety Engineering Design Criteria," Chemical Propulsion Information Agency, CPIA Publication No. 194, Vol. 1, Oct. 1971.

CHAPTER I

ESTIMATES OF EXPLOSIVE YIELD

1-1 Explosive Yield as a Function of Propellant Type and Accident Conditions

1-1.1 General Discussion of Propellant Explosives

Accidents involving liquid propellant rockets, both during static firing on a test stand and during launch, have shown that liquid propellants can generate violent explosions. These explosions "drive" air blast waves, which can cause direct damage and can accelerate fragments or nearby objects. In fact, the specific energies of liquid rocket propellants, in stoichiometric mixtures, are significantly greater than for TNT (specific energy is energy per unit mass).⁽¹⁾ The estimation of explosive yield, the energy released during the explosion, is a prerequisite to the determination of expected damage resulting from the explosion. Before delving into the method of calculating explosive yield, however, a general discussion of the characteristics of propellant explosions will help the reader understand the complexities involved in the determination of explosive yield.

One extremely important fundamental fact concerning liquid propellants is that their potential explosive yield is very high, but their actual yield is much lower. This situation occurs because the propellant and oxidizer are never intimately mixed in the proper proportions before ignition. The degree of confinement of propellant and oxidizer can also seriously affect the actual explosive yield of liquid propellants. For example, a liquid propellant mixture could conceivably explode inside a storage vessel or could leak out of a containment vessel and form a shallow pool of large lateral extent before detonation. Each case produces different values for explosive yield. Presently, there are at least four methods for estimating yield from liquid propellant explosions which, unfortunately, do not necessarily give the same predictions: One method is based on Project PYRO results,⁽²⁻⁴⁾ and two of the others are the "Seven Chart Approach" and the "Mathematical Model" of Farber and Deese.⁽⁵⁾ The fourth approach, which is really based on the previous three methods, was developed by Baker, et al.,⁽¹⁾ and is easy to use and readily adaptable to the calculation of explosive yield. For further information concerning the development of this method, Reference 1 is recommended.

From the test results reported in Reference 2 and 6 through 8, a number of observations can be made regarding blast yields from liquid

propellant explosions. (1)

- (1) Yield is quite dependent on the particular fuel and oxidizer being mixed.
- (2) The yield is very dependent on the mode of mixing of fuel and oxidizer, i. e., on the type of accident which is simulated. Maximum yields are experienced when intimate mixing is accomplished before ignition.
- (3) On many of the liquid hydrogen/liquid oxygen (LH_2/LO_2) tests (regardless of investigators), spontaneous ignition occurred very early in the mixing process, resulting in very low percentage yields.
- (4) Yield is very dependent on time of ignition, even ignoring the possibility of spontaneous ignition.
- (5) Blast yield per unit mass of propellant decreases as total propellant mass increases.
- (6) Variability in yields for supposedly identical tests was great, compared to variability in blast measurements of conventional explosives.

1-1.2 Scaled Curves for Explosive Yield for Various Propellants and Types of Accidents

If a blast source is placed on or near a reflecting surface, such as the ground, then the initial shock is very quickly reflected and the reflected wave merges with the incident wave so rapidly that a single, strengthened blast wave is formed. The characteristics of this single wave are often almost identical with the characteristics of blast waves in free-air experiments, except that the blast source appears to have greater energy than for free-air tests. The proportion of energy reflected from the ground is a function of how perfect a reflector it is, that is, how little energy is imparted to the ground in cratering, ground shock, and so forth. If the ground were a perfectly rigid surface, then the equivalent free-air energy driving the air blast wave would be $E' = 2E$. The other extreme case is that of a perfect absorber, for which $E' = E$. All actual tests will have equivalent free-air energies lying between these limits.

All of the PYRO experiments, on which the prediction curves in this section are based, were conducted on the ground surface, with no cratering. When the curves are used to predict blast yields for explosions occurring in flight or far enough above the ground that the imme-

diate reflection discussed does not occur, one must account for the absence of the "perfect" reflecting surface. This is done by dividing the blast yields calculated from curves in this chapter by a factor of two.

1-1.2.1 Terminology

In this document, three types of fuel and oxidizer combinations and three different modes of mixing will be considered. The three types of propellants are:

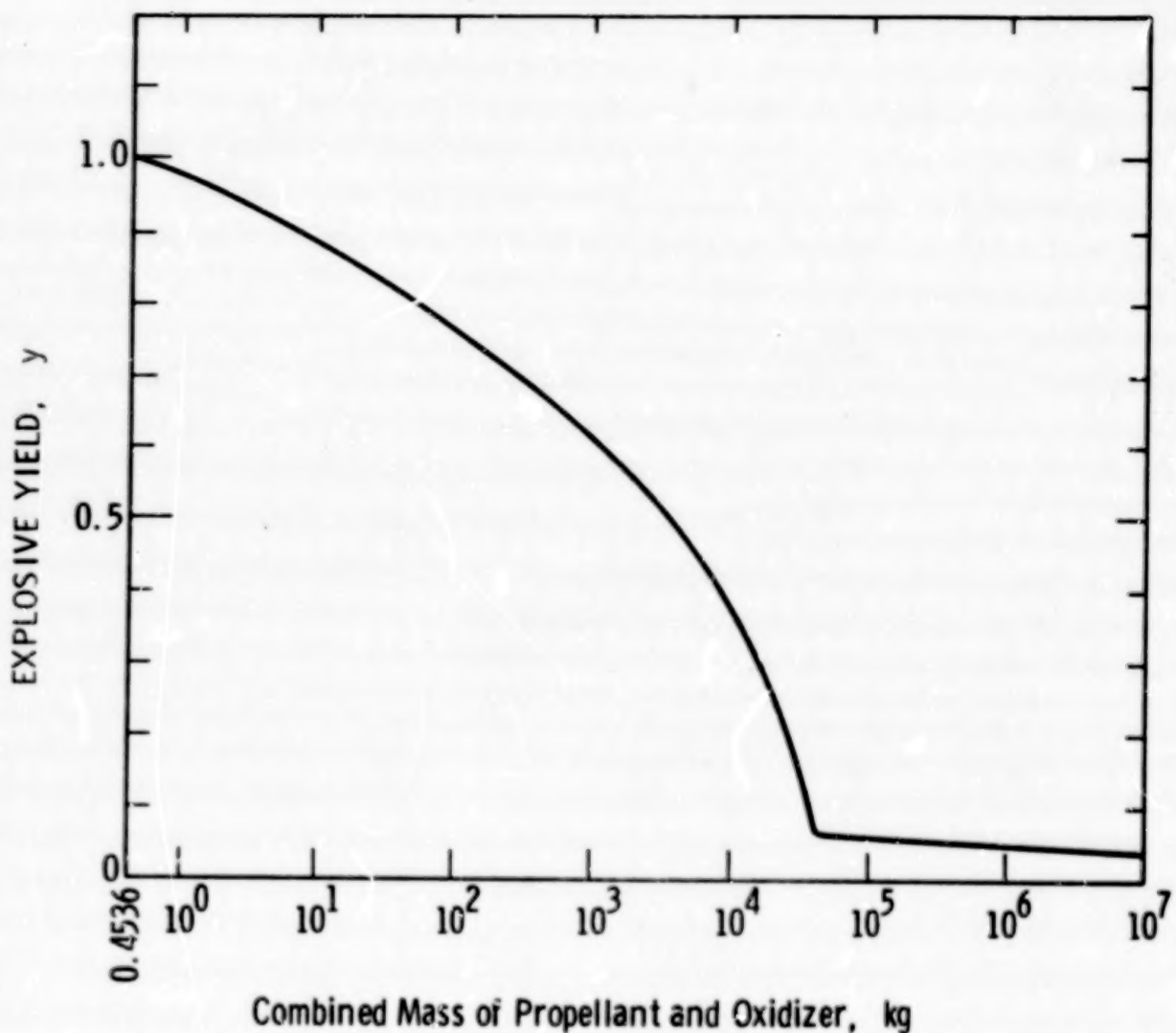
- (1) The hypergolic propellant which is in widest use. A fuel of 50% N_2H_4 - 50% UDMH and an oxidizer of N_2O_4 in a mass ratio of 1/2.
- (2) Liquid Oxygen-Hydrocarbon - This propellant uses kerosene (RP-1) as a fuel and liquid oxygen (LO_2) as the oxidizer in stoichiometric mass ratio of 1/2. 25.
- (3) Liquid Oxygen-Liquid Hydrogen - This propellant is an entirely cryogenic combination of liquid hydrogen (LH_2) fuel and liquid oxygen (LO_2) oxidizer in stoichiometric mass ratio of 1/5.

The three modes of mixing (failure modes) discussed are:

- (1) Confinement by Missile (CBM) - This type of accident consists of failure of an interior bulkhead separating fuel and oxidizer in a missile stage.
- (2) Confinement by Ground Surface (CBGS) - This type of accident includes impacts at various velocities (e.g., fall back on the launch pad) of the missile on the ground, with all tankage ruptured, and subsequent ignition.
- (3) High Velocity Impact (HVI) - This type of accident involves high velocity impact of a missile after launch.

1-1.2.2 Methods for Calculating Explosive Yield

Some parameters which become important in determining explosive yield are the type of propellant, the failure mode and in some cases, ignition time, impact velocity, and type of surface impacted. It is important to keep in mind, however, that blast yield as a percent or fraction of energy available decreases as total combined mass of propellant and oxidizer increases. Figure 1-1, which is a normalized plot for



Multiplier Factors:

(1) Hypergolic - 240%

(2) LO₂/RP-1 - 125%

(3) LO₂/LH₂ - 370%

$$(1 \text{ lb}_m = \text{kg} \times 2.2)$$

Figure 1-1. Estimated Terminal Yield as a Function of Combined Propellant and Oxidizer Mass (Ref. 9)

all propellants, depicts this relationship and should be used as an upper limit for percent explosive yield. Since this is a normalized plot, the percent yield for a particular propellant can be determined by obtaining the normalized fractional value from the graph and multiplying by the multiplier factor for the particular propellant under investigation. These multiplier factors, shown on the figure, are:

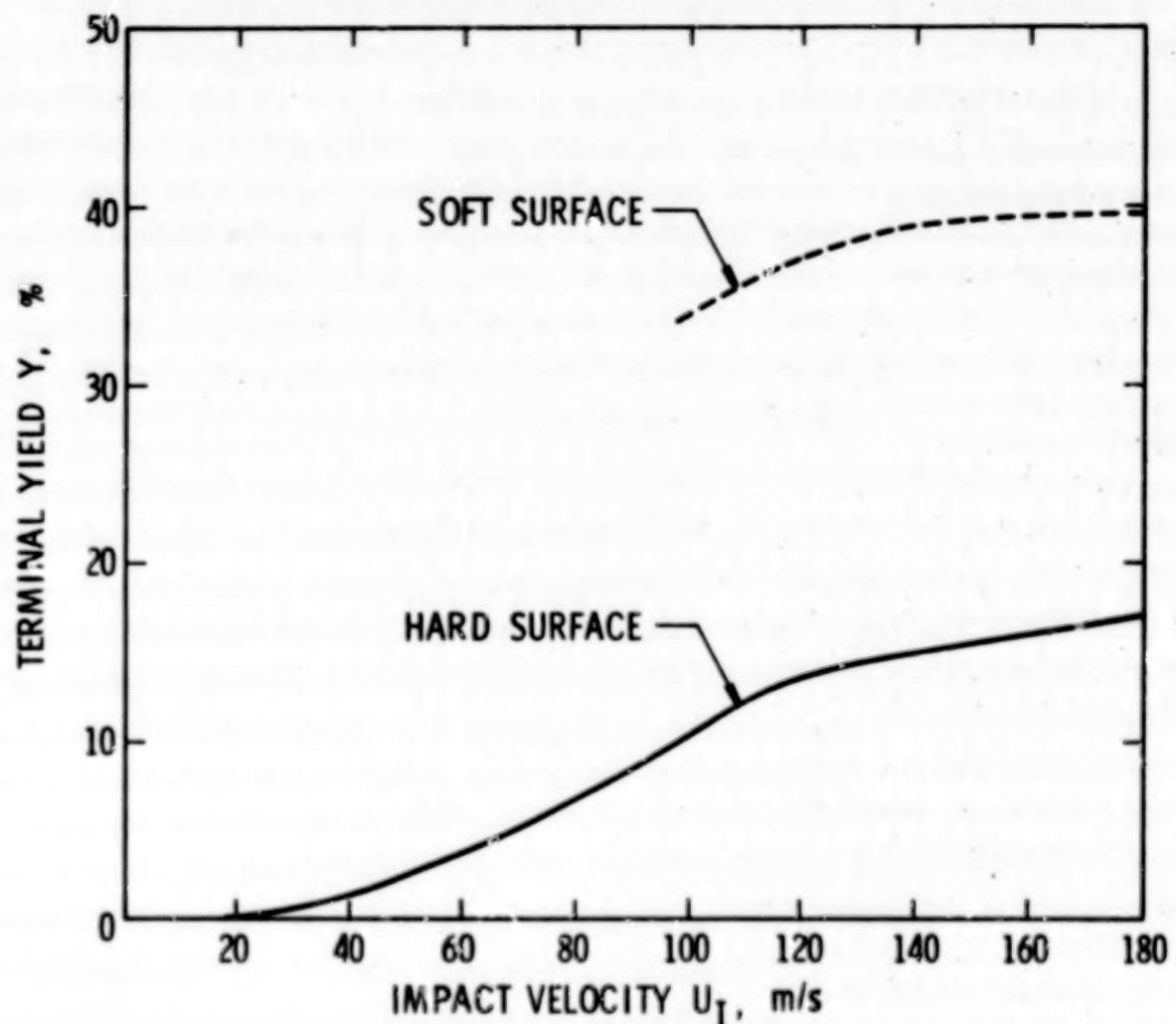
Hypergolic (50% N₂H₄ - 50% UDMH fuel and N₂O₄ oxidizer in mass ratio of 1/2) - 240%⁽¹⁰⁾

Liquid oxygen-hydrocarbon (RP-1 fuel LO₂ oxidizer in mass ratio of 1/2.25) - 125%⁽⁶⁾

Liquid oxygen-liquid hydrogen (LH₂ fuel and LO₂ oxidizer in mass ratio of 1/5) - 370%⁽⁶⁾

Careful examination of Figure 1-1 and the multiplier factors indicate that explosive yield can be greater than 100 percent. Also, in certain cases, explosive yield will be greater than 100 percent when calculated by other methods. This anomaly occurs because explosive yield, as it is used here, is really terminal yield, or yield based on "TNT equivalence". Since the specific energies of the liquid propellants involved are greater than the specific energy of TNT, terminal (TNT equivalent) yield can be greater than 100 percent. Calculations were done in this manner to correlate with other methods discussed in subsequent paragraphs. Whenever the value of percent explosive (terminal) yield determined by these other methods exceeds the value of percent explosive (terminal) yield determined by using Figure 1-1, the value from Figure 1-1 is the correct choice.

- (1) Hypergolic materials, by definition, ignite spontaneously on contact, so it is not possible to obtain appreciable mixing before ignition unless the fuel and oxidizer are thrown violently together. Ignition time is therefore not an important determinant of blast yield for hypergolics, but impact velocity and degree of confinement after impact are important factors. If a CBM or CBGS failure mode is being considered, percent explosive yield can be acquired from Table 1-1. If a HVI failure mode is assumed, then percent explosive yield can be determined from Figure 1-2. The percent yield determined by any one of these methods must then be compared to the percent yield determined from the weight of the propellant (Figure 1-1). The smaller of the two is the correct choice.



(ft/sec = m/s X 3.281)

Figure 1-2. Terminal Yield Vs Impact Velocity
for Hypergolic HVI (Ref. 3)

TABLE 1-1. ESTIMATE OF TERMINAL YIELD FOR HYPERGOLIC CBM AND CBGS (REF. 3)

Failure Mode	Terminal Yield Range (%)	Estimated Upper Limit
Diaphragm rupture (CBM)	0.01 - 0.8	1.5
Spill (CBGS)	0.02 - 0.3	0.5
Small explosive donor	0.8 - 1.2	2
Large explosive donor	3.4 - 3.7	5
Command destruct	0.3 - 0.35	0.5
310-ft drop (CBGS)	-1.5	3

(2) Because liquid oxygen/hydrocarbon propellants are not hypergolic, considerable mixing can occur in various types of accidents, and time of ignition after onset of mixing is an important determinant of blast yield. For the case of mixing and an explosion within the missile tankage (CBM), percent explosive yield can be determined by assuming an ignition time and then examining Figure 1-3.* For simulated fall-back on the launch pad (CBGS), impact velocity as well as ignition time are important parameters in estimating blast yield. A two-step approach has been developed to calculate blast yield. (1) After assuming an impact velocity, maximum percent yield Y_m can be determined from Equation (1-1):

$$Y_m = 5\% + \frac{(6.82\%)}{(m/s)} U_I, \quad 0 \leq U_I \leq 16.8 \text{ m/s} \quad (1-1)$$

*A word of explanation will help clarify the meaning of the central solid line and shaded area of this graph and similar subsequent graphs. The shaded portion represents an area in which data from actual propellant blasts was found. The central solid line is an estimate of the most likely occurrence and, for most cases, is the recommended choice. Conservative estimates of explosive yield can be made by choosing the uppermost boundary of the shaded area. The vertical depth of the shaded area at any abscissa indicates the total range of data, and therefore the total uncertainty in the estimate.

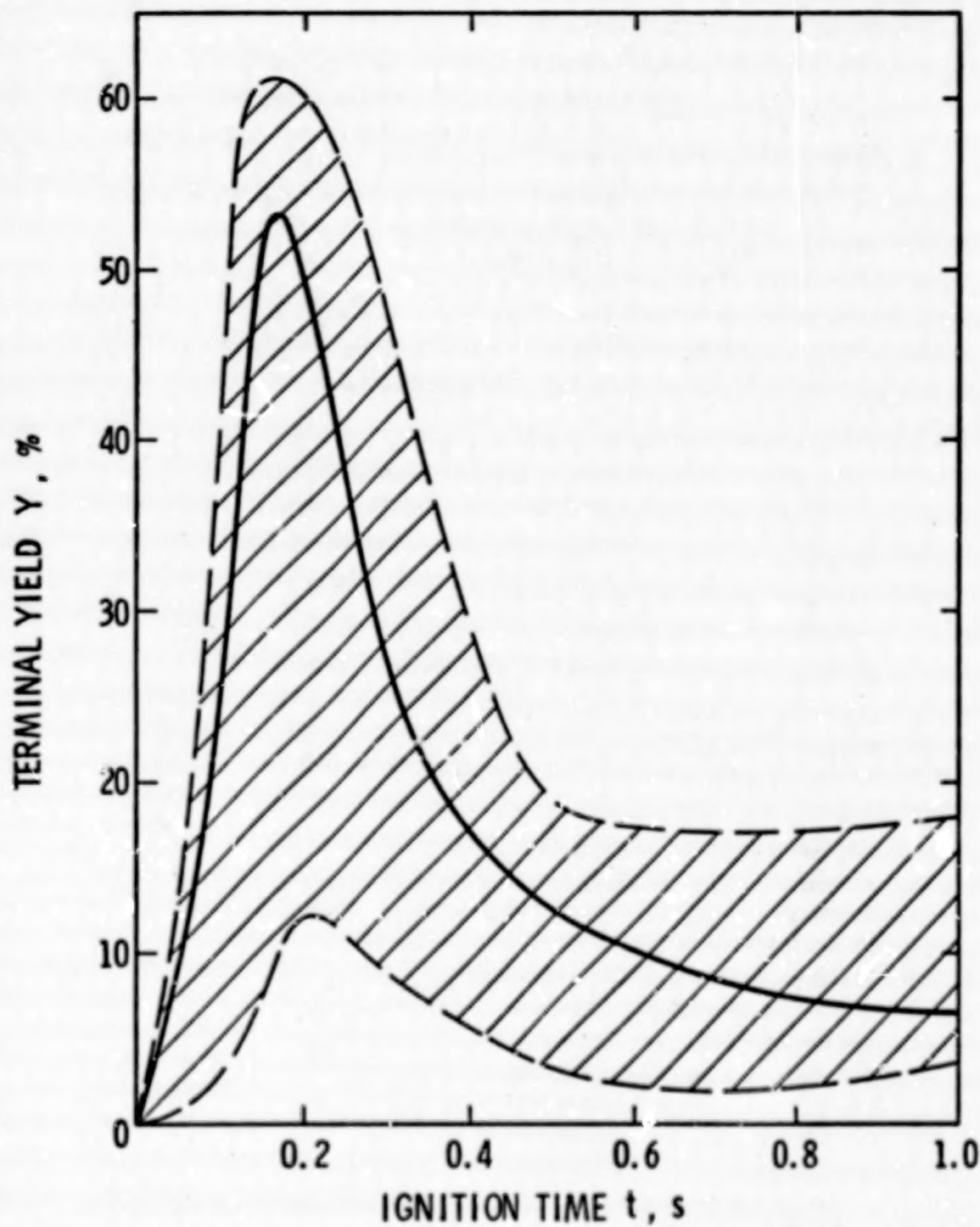


Figure 1-3. Terminal Yield Vs Ignition Time
for $\text{LO}_2/\text{RP-1 CBM}$

where Y_m is expressed in percent and U_I is in meters per second. Percent explosive yield can then be determined from Y_m , an estimate of ignition time, and Figure 1-4. The determination of explosive yield for the HVI failure mode is somewhat simpler because there is little ignition delay and therefore only impact velocity affects yield. Thus, blast yield can be acquired by using Figure 1-5 directly. The percent yield determined by any one of these methods must then be compared to the percent yield determined from the weight of the propellant (Figure 1-1). The smaller of the two is the correct choice.

- (3) The determination of explosive yield, for the entirely cryogenic combination of liquid hydrogen (LH_2) fuel and liquid oxygen (LO_2) oxidizer is similar to that of liquid oxygen-hydrocarbon propellants. For the CBM case, it is necessary for one to assume an ignition time and then use Figure 1-6 to find explosive yield. For the CBGS case, an impact velocity is assumed and maximum percent yield Y_m can be determined from Equation (1-2):

$$Y_m = 10\% + \frac{(4.43\%)}{(m/s)} U_I, \quad 0 \leq U_I \leq 24.4 \text{ m/s} \quad (1-2)$$

where Y_m is expressed in percent and U_I is in meters per second. Percent explosive yield can then be determined from Y_m , an estimate of ignition time and Figure 1-7. For high velocity impact (HVI) of this propellant, the blast yield is dependent only on the impact velocity and can be acquired from Figure 1-8 directly. The percent yield determined by any one of these methods must then be compared to the percent yield determined from the weight of the propellant (Figure 1-1). The smaller of the two is the correct choice.

Table 1-2 has been prepared to alleviate the necessity of rereading the preceding presentation each time a value of explosive yield must be determined. To use the table, all one needs to do is identify the type of propellant and type of accident. Then the proper sequence in "Part 1" should be followed after making the necessary assumptions (e.g., ignition time or impact velocity and type of surface impacted) to arrive at a value for explosive yield. Explosive yield should then be determined by using the method depicted in "Part 2" which involves the use of Figure 1-1 and multiplier factors (see page 11). The smaller value for explosive yield

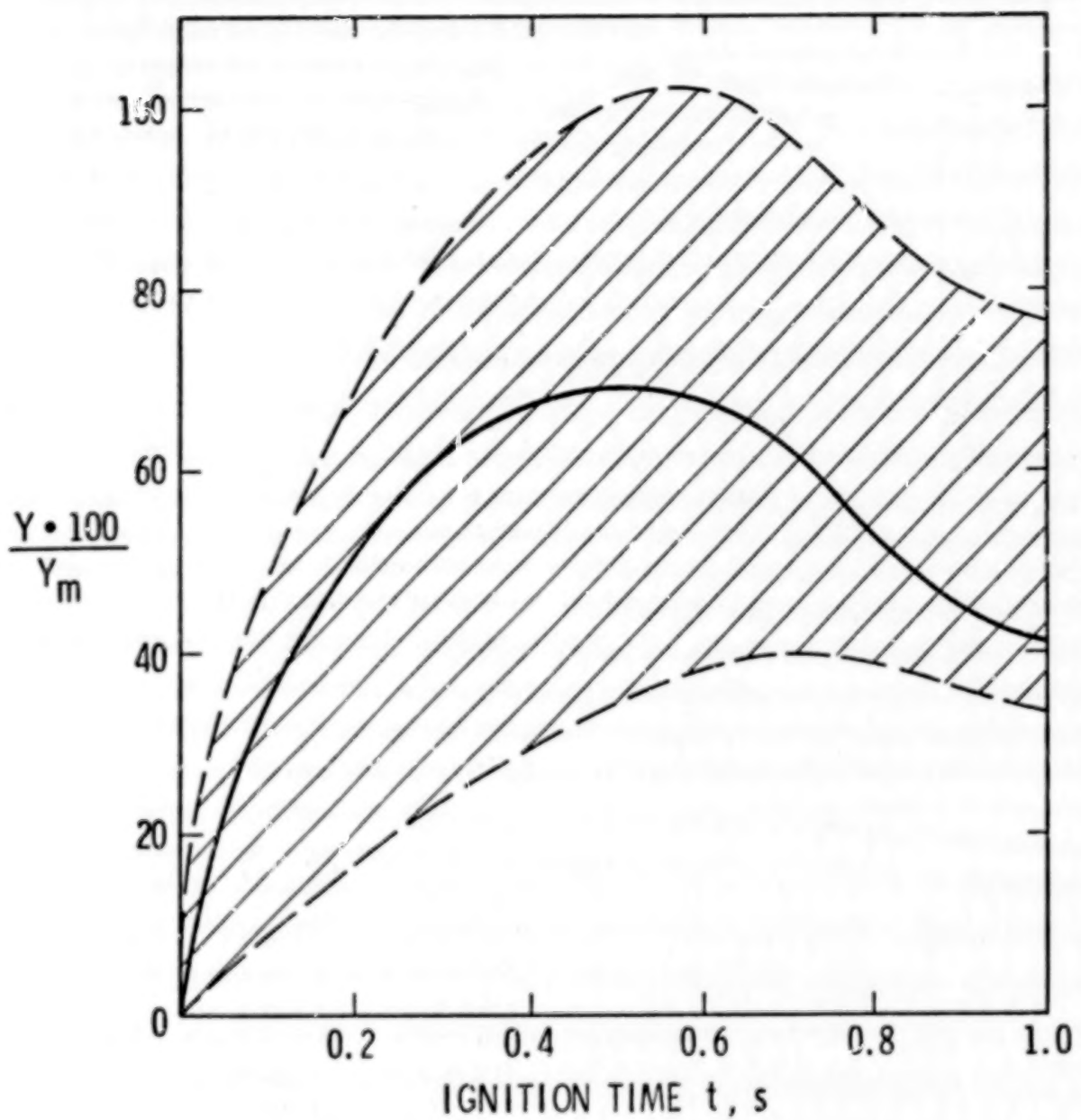
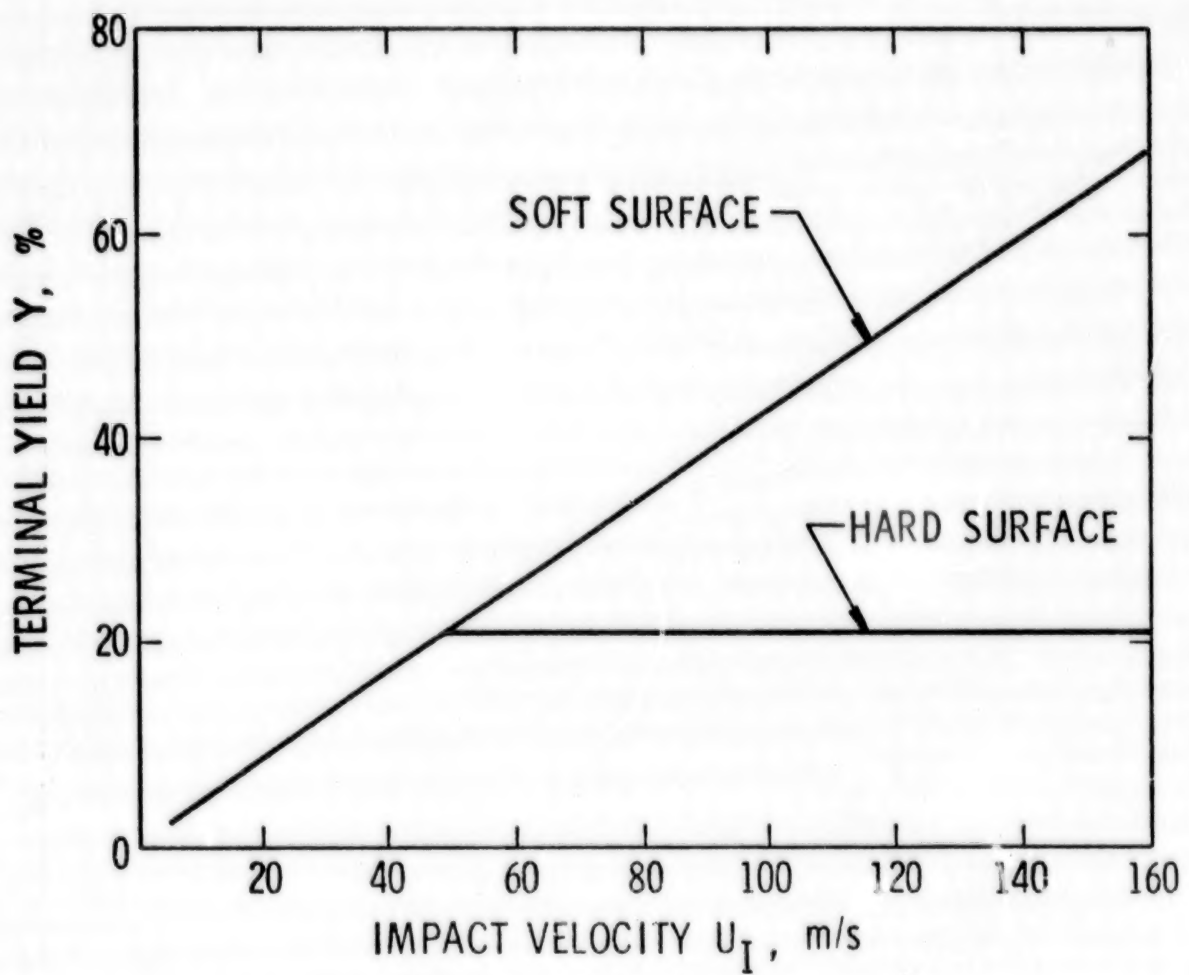


Figure 1-4. Normalized Terminal Yield Vs Ignition Time for $\text{LO}_2/\text{RP-1 CBGS}$



(ft/sec = m/s X 3.281)

Figure 1-5. Terminal Yield Vs Impact Velocity
for LO₂/RP-1 HVI (Ref. 3)

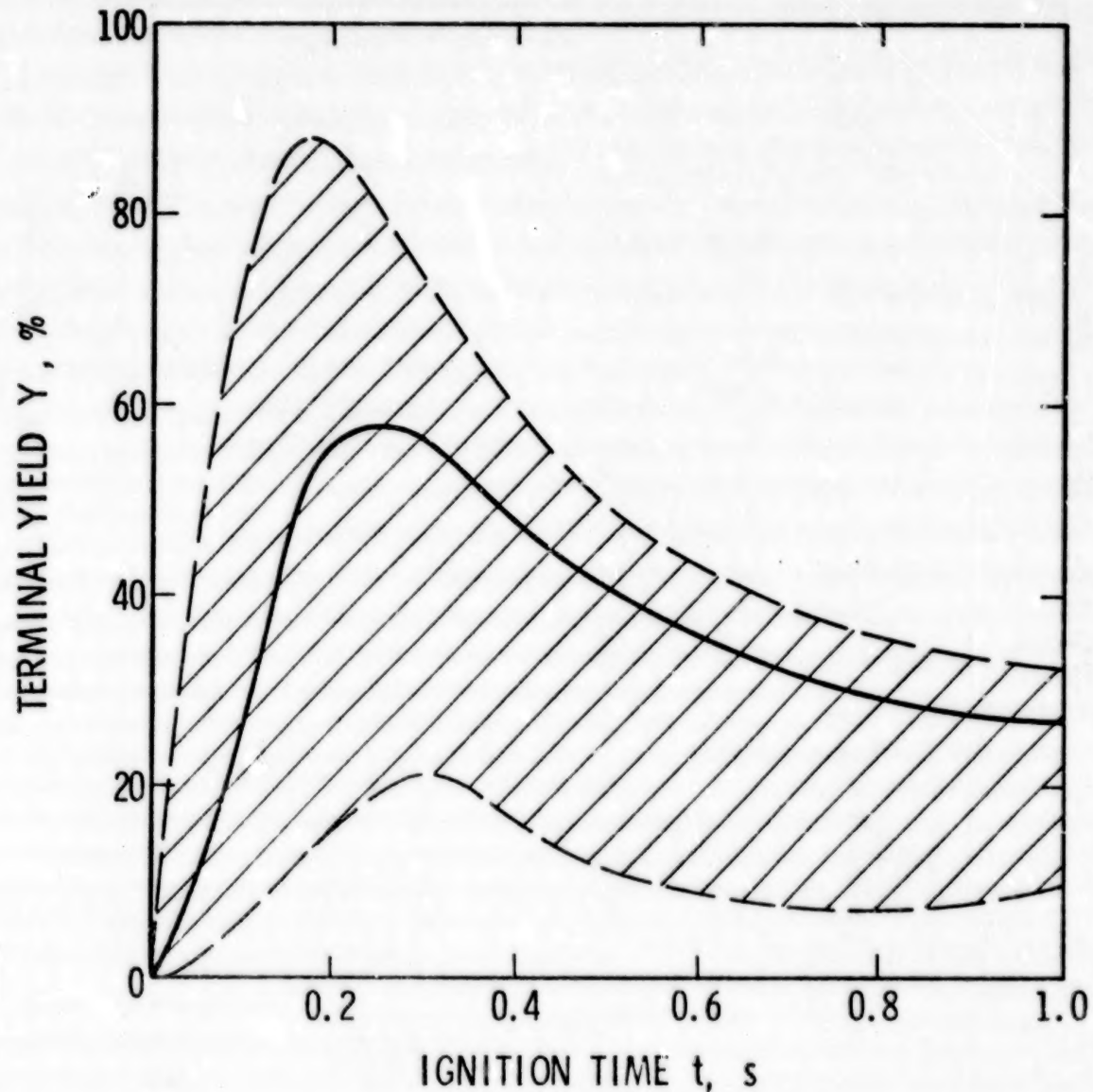


Figure 1-6. Terminal Yield Vs Ignition Time
for LO_2/LH_2 CBM

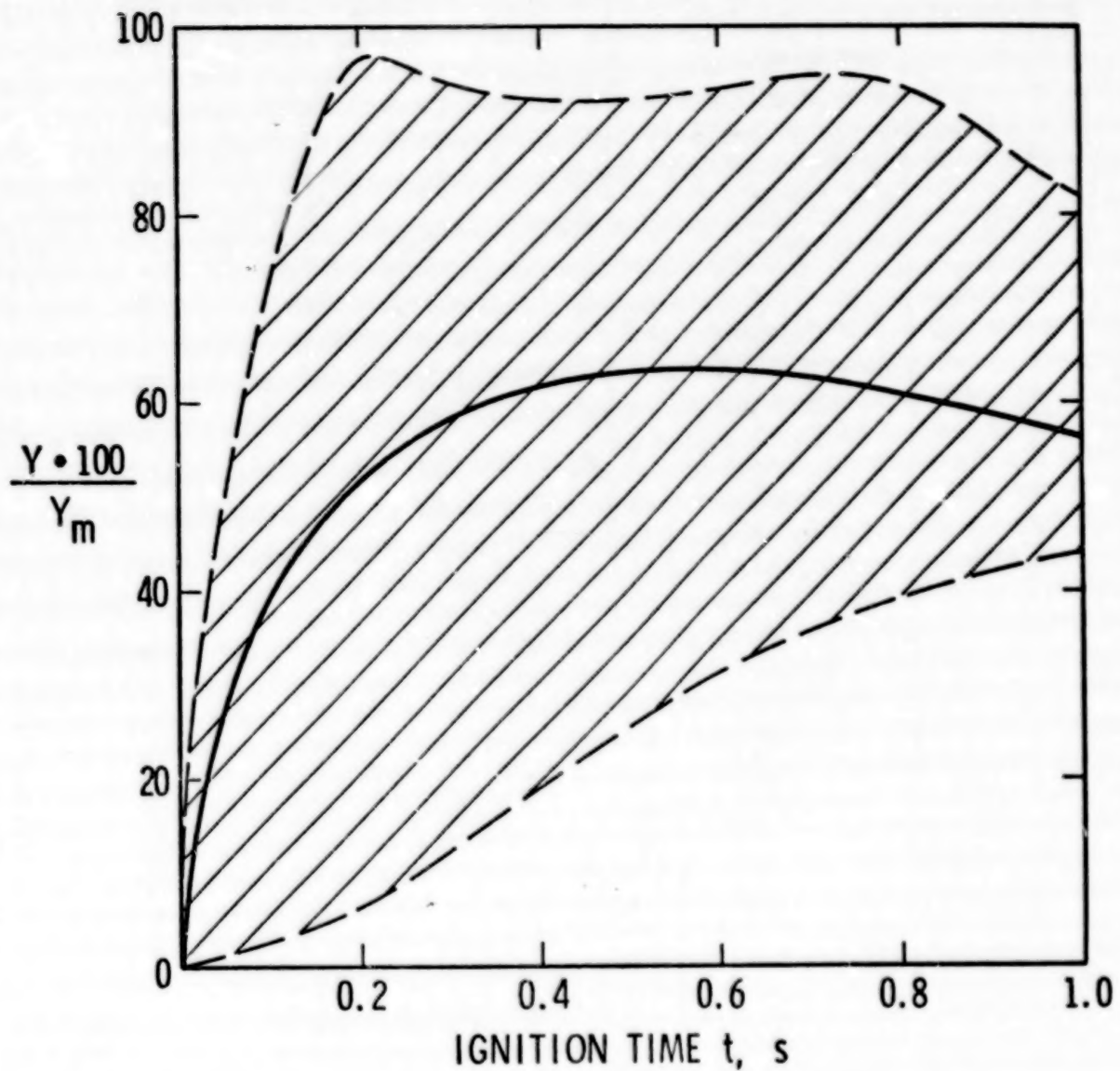
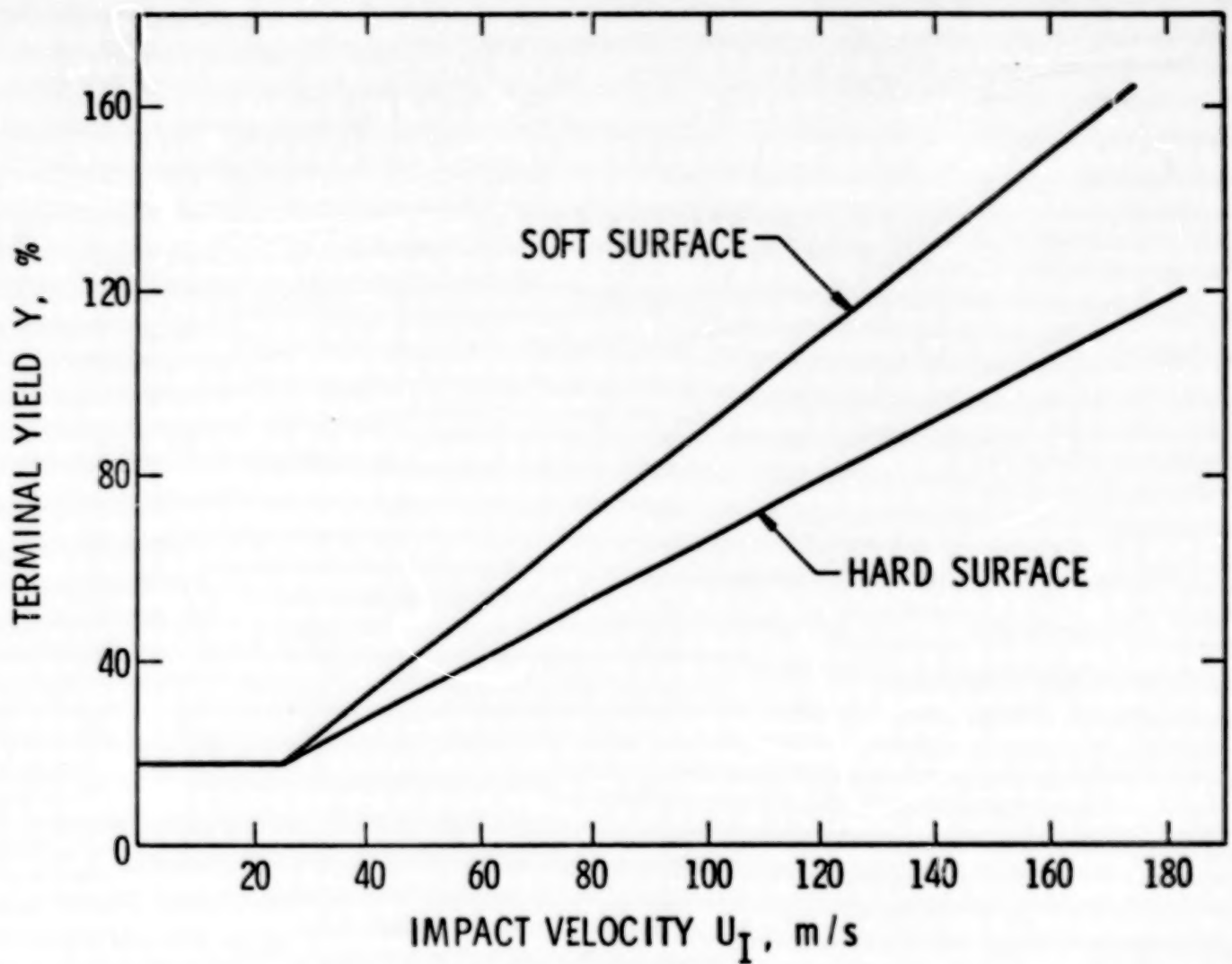


Figure 1-7. Normalized Terminal Yield Vs Ignition Time
for LO_2/LH_2 CBGS



(ft/sec = m/s X 3.281)

Figure 1-8. Terminal Yield Vs Impact Velocity
for LO_2/LH_2 HVI (Ref. 3)

determined in "Part 1" and "Part 2" is the correct value. This value can then be used to determine an effective weight of propellant, and pressure and impulse at scaled distances using the methods demonstrated in a subsequent chapter.

1-1.3 Examples for Determining Explosive Yield

Example 1:

Propellant-Hypergolic

Combined mass of propellant and oxidizer-10,000 kg (22,000 lb_m)

Failure mode - CBM

Solution: Examine Table 1-2 for "Part 1" and "Part 2" solution sequences.

Part 1: Table 1-1 implies that for the CBM failure mode,

$$Y = 0.01 - 0.8\%$$

Using the higher portion for safety reasons,

$$Y = 0.8\%$$

Part 2: Figure 1-1 implies that for a combined mass of propellant and oxidizer of 10,000 kg,

$$Y = (240\%) (0.37) = 88.8\%$$

where 240% is the hypergolic multiplier factor,

$Y = 0.8\%$, the smaller value, is the correct choice.

Example 2:

Propellant-Hypergolic

Combined mass of propellant and oxidizer-1000 kg (2200 lb_m)

Failure mode - HVI

Impact velocity (assumption) - 140 m/s (459 ft/sec)

Type of surface impacted - hard

Solution: Examine Table 1-2 for "Part 1" and "Part 2" solution sequences.

Part 1: Figure 1-2 implies that for an impact velocity of 140 m/s (459 ft/sec) onto a hard surface, $Y = 15\%$.

TABLE 1-2. SEQUENCE FOR DETERMINATION
OF EXPLOSIVE YIELD *

<u>Type of Propellant & Oxidizer</u>	<u>Type of Accident Failure Mode</u>	<u>Sequence[†]</u> <u>Part 1[‡]</u>	<u>Part 2 (check)</u>
Hypergolic (50% N ₂ H ₄ - 50% UDMH/N ₂ O ₄)	CBM	Table 1-1	Figure 1-1
	CBGS	Table 1-1	Figure 1-1
	HVI	Figure 1-2	Figure 1-1
Liquid Oxygen - Hydrocarbon (LO ₂ /RP-1)	CBM	Figure 1-3	Figure 1-1
	CBGS	Eq. (1-1) Figure 1-4	Figure 1-1
	HVI	Figure 1-5	Figure 1-1
Liquid Oxygen- Liquid Hydrogen (LO ₂ /LH ₂)	CBM	Figure 1-6	Figure 1-1
	CBGS	Eq. (1-2) Figure 1-7	Figure 1-1
	HVI	Figure 1-8	Figure 1-1

* For explosions occurring far above the ground ($H/W^{1/3} > 10 \text{ m/kg}^{1/3}$, where H is height above the ground), blast yields calculated from curves in this section should be divided by two.

† Correct choice is the smaller of Part 1 and Part 2.

‡ See footnote on page 14.

Part 2: Figure 1-1 implies that for a combined mass of propellant and oxidizer of 1000 kg (2200 lb_m)

$$Y = (240\%) (0.6) = 144\%$$

where 240% is the hypergolic multiplier factor.

Y = 15%, the smaller value, is the correct choice.

Example 3:

Propellant and oxidizer - LO₂/RP-1

Combined mass of propellant and oxidizer - 10,000 kg (22,000 lb_m)

Failure mode - CBM

Ignition time (assumption) - 0.2 seconds

Solution: Examine Table 1-2 for "Part 1" and "Part 2" solution sequences.

Part 1: Figure 1-3 implies that for an ignition time of 0.2 seconds,

$$Y = 52\%$$

Part 2: Figure 1-1 implies that for a combined mass of propellant and oxidizer of 10,000 kg (22,000 lb_m)

$$Y = (125\%) (0.37) = 46\%$$

where 125% is the LO₂/RP-1 multiplier factor.

Y = 46%, the smaller value, is the correct choice.

Example 4:

Propellant and oxidizer - LO₂/RP-1

Combined mass of propellant and oxidizer - 150,000 kg
(330,000 lb_m)

Failure mode - CBGS

Impact velocity (assumption) - 10 m/s (32.8 ft/sec)

Ignition time (assumption) - 0.5 seconds

Solution: Examine Table 1-2 for "Part 1" and "Part 2" solution sequences.

Part 1: Equation (1-1) implies that for an impact velocity of 10 m/s, (32.8 ft/sec)

$$Y_m = 5\% + \frac{(6.82\%)}{(m/s)} (10 m/s)$$

$$Y_m = 5\% + 68.2\%$$

$$Y_m = 73.2\%$$

Figure 1-4 implies that for an ignition time of 0.5 seconds

$$\frac{Y \cdot 100}{Y_m} = 70$$

or

$$Y = \frac{(70)}{(100)} Y_m$$

$$Y = \frac{(70)}{(100)} (73.2\%) = 51.2\%$$

Part 2: Figure 1-1 implies that for a combined mass of propellant and oxidizer of 150,000 kg (330,000 lb_m),

$$Y = (125\%) (0.05) = 6.25\%$$

where 125% is the LO₂/RP-1 multiplier factor.

Y = 6.25%, the smaller value, is the correct choice.

Example 5:

Propellant and Oxidizer - LO₂/LH₂

Combined mass of propellant and oxidizer - 10,000 kg (22,000 lb_m)

Failure mode - HV.

Impact velocity (assumed) - 40 m/s (131 ft/sec)

Type of surface impact - hard

Solution: Examine Table . . for "Part 1" and "Part 2" solution sequences

Part 1: Figure 1-8 implies that for impact velocity of 40 m/s (131 ft/sec),

$$Y = 30\%$$

Part 2: Figure 1-1 implies that for a combined mass of propellant and oxidizer of 10,000 kg (22,000 lb_m),

$$Y = (370\%) (.37) = 137\%$$

where 370% is the LO₂/LH₂ multiplier factor.

Y = 30%, the smaller value, is the correct choice.

1-2 Explosive Yield as a Function of Fluid Type and Initial Conditions for Gas Vessel Bursts

1-2.1 General Discussion of Gas Vessel Explosions

When a pressurized gas-filled vessel bursts, a shock wave in many ways similar to that which results from a TNT explosion propagates from the source. The overpressure behind this shock wave may be quite large and capable of causing damage. The specific impulse associated with this shock wave is also important for the prediction of damage from a gas vessel burst. These two parameters vary with distance from the source.

In the analysis that was used for the overpressure and specific impulse calculations, the effects of the containing vessel and its fragments were ignored, that is, all of the energy of the gas in the vessel was put into the flow field, rather than into the fragments as kinetic energy. For a spherical vessel, the flow field was assumed spherically symmetric. Also, the surrounding atmosphere was assumed to be air.

To determine the overpressure and impulse, one must know the initial conditions of the gas in the vessel. The pressure p_i, temperature T_i, and ratio of specific heats of the gas γ_i must be known.

The conditions of the atmosphere into which the shock wave propagates also must be known. These are the atmospheric pressure p_a, the speed of sound a_a, and the ratio of specific heats γ_a. The latter value will be a constant for all explosions in air.

1-2.2 Discussion of Energy

The energy contained in a pressurized gas vessel can be obtained by

$$E = \left(\frac{p_i - p_a}{\gamma_i - 1} \right) v_i$$

where

V_i is the volume of the vessel before it bursts⁽¹¹⁾ and

p_i indicates absolute pressures.

The overpressure and impulse are graphed versus a dimensionless scaled distance:

$$\bar{R} = \frac{r p_a}{E^{1/3}}$$

A scaled specific impulse is used:⁽¹²⁾

$$I = \frac{I_a}{p_a^{2/3} E^{1/3}}$$

Note that there is no need to calculate a TNT equivalent for gas vessel bursts.

1-2.3 Example Calculations

Example 1. Calculation of Energy

Let $p_a = 1.013 \times 10^5$ Pa (1 standard sea level atmosphere)
(14.7 psi)

$$p_1 = 41.013 \times 10^5$$
 Pa (595 psi)

$$\gamma_1 = 1.4$$
 (diatomic gas)

$$V_i = 1.0 \text{ m}^3$$
 (35.3 ft³)

$$E = \frac{(p_1 - p_a)}{\gamma_1 - 1} \leftarrow V_i = \frac{(41.013 \times 10^5 \text{ Pa} - 1.013 \times 10^5 \text{ Pa}) 1 \text{ m}^3}{1.4 - 1}$$
$$= 1.00 \times 10^7 \text{ J}$$
 (1.34 $\times 10^6$ ft-lb_f)

Example 2, Calculation of Scaled Distance

Using the same conditions as in the previous example,

$$\bar{R} = \frac{r p_a^{1/3}}{E^{1/3}} = \left[\frac{r}{\frac{(p_1/p_a - 1) V_i}{\gamma_1 - 1}} \right]^{1/3} = \left[\frac{r}{\left(\frac{\frac{41.013 \times 10^5 \text{ Pa}}{1.013 \times 10^5 \text{ Pa}} - 1}{1.4 - 1} \right) \text{ m}^3} \right]^{1/3}$$

$$= 0.216 r \text{ (r in m)} \quad [0.0658 r \text{ (r in ft)}]$$

Example 3, Calculation of Scaled Impulse

Let $a_a = 331 \text{ m/s}$ (speed of sound at standard sea level conditions) (1086 ft/sec).

For the conditions used in the previous examples,

$$\bar{I} = \frac{I a_a}{p_a^{2/3} E^{1/3}} = \frac{I (331 \text{ m/s})}{(1.013 \times 10^5 \text{ Pa})^{2/3} (1.00 \times 10^7)^{1/3}} =$$

$$7.070 \times 10^{-4} I \text{ (I in Pa} \cdot \text{s)}$$

LIST OF REFERENCES

1. Baker, W. E., V. B. Parr, R. L. Bessey and P. A. Cox, "Assembly and Analysis of Fragmentation Data for Liquid Propellant Vessels," NASA CR-134538, NASA Lewis Research Center, January 1974.
2. Willoughby, A. B., C. Wilton and J. Mansfield, "Liquid Propellant Explosive Hazards, Final Report-December 1968, Vol. I - Technical Documentary Report," AFRPL-TR-68-92, URS-652-35, URS Research Co., Burlingame, California.
3. Willoughby, A. B., C. Wilton and J. Mansfield, "Liquid Propellant Explosion Hazards, Final Report-December 1968, Vol. II - Test Data," AFRPL-TR-68-92, URS 652-35, URS Research Co., Burlingame, California.
4. Willoughby, A. B., C. Wilton and J. Mansfield, "Liquid Propellant Explosion Hazards, Final Report-December 1968, Vol. III - Prediction Methods," AFRPL-TR-68-92, URS 652-35, URS Research Co., Burlingame, California.
5. Farber, E. A., and J. H. Deese, "A Systematic Approach for the Analytical Analysis and Prediction of the Yield from Liquid Propellant Explosions," Tech. Paper No. 347, Eng. Progress at the University of Florida, XX, 3, March 1966.
6. (Anonymous), "Summary Report on a Study of the Blast Effect of a Saturn Vehicle," Report No. C63850, Arthur D. Little, Inc., Cambridge, Massachusetts, February 1962.
7. Pesante, R. E., and M. Nishibazashi, "Evaluation of the Blast Parameters and Fireball Characteristics of Liquid Oxygen/Liquid Hydrogen Propellant," Report No. 0954-01(01)FP, Aerojet-General Corp., Downey, California, April 1967.
8. Gayle, J. B., C. H. Blakewood, J. W. Bransford, W. H. Swindell, and R. W. High, "Preliminary Investigation of Blast Hazards of RP-1/LOX and LH₂/LOX Propellant Combinations," NASA TM X-53240, George C. Marshall Space Flight Center, Huntsville, Alabama, April 1965.
9. Farber, E. A., F. W. Klement, and C. F. Bonzon, "Prediction of Explosive Yield and Other Characteristics of Liquid Propellant Rocket Explosions," Final Report, October 31, 1968, Contract No. NAS 10-1255, University of Florida, Gainesville, Florida.

10. Carter, P. B., Jr., "A Method of Evaluating Blast Parameters Resulting from Detonation of Rocket Propellants," AEDC-TDR-64-200, Arnold Engineering Dev. Center, Air Force Systems Command. October 1964, AD 450-140.
11. Huang, S. L., and P. C. Chou, "Calculations of Expanding Shock Waves and Late-State Equivalence," Drexel Institute of Technology Report 125-12, April 1968.
12. Strehlow, Roger A., "Accidental Non-Ideal Explosions," Progress Report NASA NSG 3008, December 6, 1974.

CHAPTER II

CHARACTERISTICS OF PRESSURE WAVES

2-1 General

Explosions from liquid rocket propellant accidents "drive" air blast waves, which can in turn cause direct damage and can accelerate fragments or nearby objects. The launch pads at the Air Force Eastern Test Range (ETR) have for a number of years been instrumented with air blast recorders to measure the overpressures generated during launch pad explosions, so some data are available on the intensities of the blast waves generated. Such measurements, and the common practice in safety circles of comparing explosive effects on the basis of blast waves generated by TNT, have led to expression of blast yields of propellant explosions in equivalent "pounds of TNT." (Although a direct conversion of pounds of TNT to energy can easily be made -- 1 lb_m of TNT equals 1.4×10^6 ft-lb_f -- this is seldom done).

Liquid propellant explosions differ from TNT explosions in a number of ways, so that the concept of "TNT equivalence" quoted in pounds of TNT is far from exact. Some of the differences are described below.

- (1) The specific energies of liquid propellants, in stoichiometric mixtures, are significantly greater than for TNT (specific energy is energy per unit mass).
- (2) Although the potential explosive yield is very high for liquid propellants, the actual yield is much lower, because propellant and oxidizer are never intimately mixed in the proper proportions before ignition.
- (3) Confinement of propellant and oxidizer, and subsequent effect on explosive yield, are very different for liquid propellants and TNT. Degree of confinement can seriously affect explosive yield of liquid propellants, but has only a secondary effect on detonation of TNT or any other solid explosive.
- (4) The geometry of the liquid propellant mixture at time of ignition can be quite different than that of the spherical or hemispherical geometry of TNT usually used for generation of controlled blast waves. The sources of compiled data for blast waves from TNT or Pentolite invariably rely on

measurements of blasts from spheres or hemispheres of explosive. The liquid propellant mixture can, however, be a shallow pool of large lateral extent at time of detonation.

- (5) The blast waves from liquid propellant explosions show different characteristics as a function of distance from the explosion than do waves from TNT explosions. This is undoubtedly simply a manifestation of some of the differences discussed previously, but it does change the "TNT equivalence" of a liquid-propellant explosion with distance from the explosion. Fletcher (Reference 1) discusses these differences and shows them graphically (see Figures 2-1 and 2-2). These differences are very evident in the results of the many blast experiments reported in Project PYRO (References 2-4). They have caused the coinage of the phase "terminal yield", meaning the yield based on blast data taken at great enough distance from the explosion for the blast waves to be similar to those produced by TNT explosions. At closer distance, two different yields are usually reported; an overpressure yield based on equivalence of side-on peak overpressures, and an impulse yield based on equivalence of side-on positive impulses.

Accidents with bursting gas storage vessels also can generate damaging blast waves. The characteristics of the blasts from these and other accidental explosions are reviewed in Reference 5, and rather complete descriptions given of the theory of such "non-ideal" explosions. Again, these sources generate blast waves which can differ significantly from blast waves generated by condensed explosives such as TNT, with the differences being greatest close to the source. The trend is similar to that for propellant explosions, i. e., peak overpressures are less and impulses are greater than for "equivalent" TNT explosions. But, the potential maximum yield or blast energy from gas vessel bursts is much more apt to be realized than for liquid propellant explosions. The high pressure gas already contains the necessary energy and can be rapidly released without the prior mixing and ignition required for the propellants.

However, let us for the moment ignore the differences between accidental explosions and planned ones, and discuss instead the general characteristics of the blast waves generated by any explosion. References 6-8 are good general source references on air blast waves and their behavior.

As a blast wave passes through the air or interacts with and loads a structure or target, rapid variations in pressure, density, temperature and particle velocity occur. The properties of blast waves which are

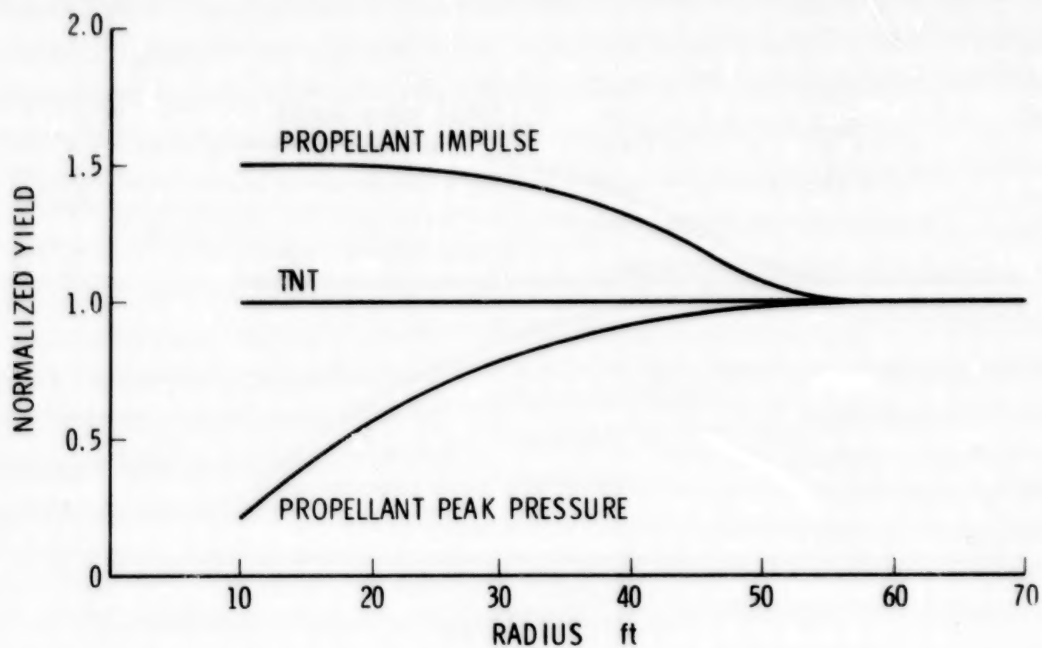


Figure 2-1. Normalized Pressure and Impulse Yields from
Explosion of N_2O_4 /Aerozine 50 (Ref. 1)

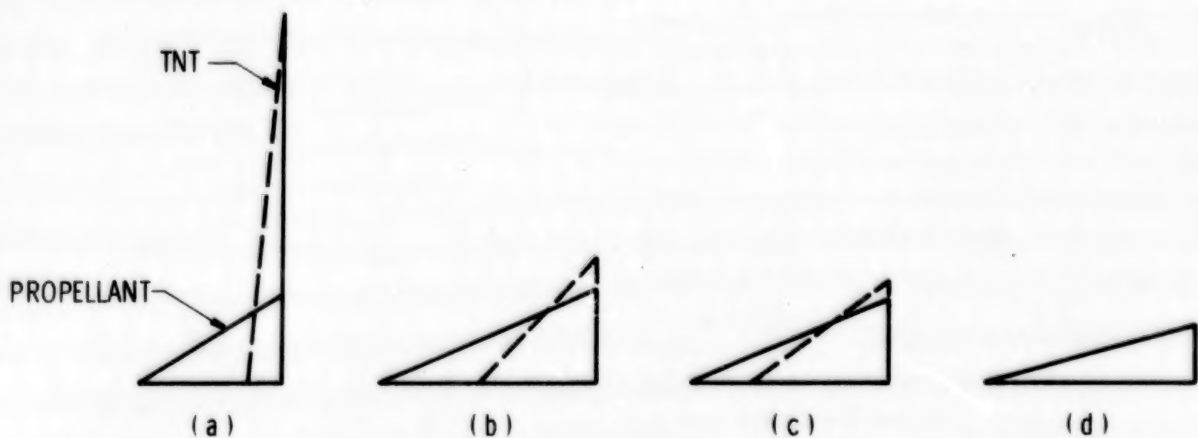


Figure 2-2. Representative Shock Impulses Showing Coalescence of Shock Waves from Dissimilar Sources [Stages (a) Through (d)] (Ref. 1)

usually defined are related both to the properties which can be easily measured or observed and to properties which can be correlated with blast damage patterns. It is relatively easy to measure shock front arrival times and velocities and entire time histories of overpressures. Measurement of density variations and time histories of particle velocity are more difficult, and no reliable measurements of temperature variations exist.

Classically, the properties which are usually defined and measured are those of the undisturbed or side-on wave as it propagates through the air. Figure 2-3 shows graphically some of these properties in an ideal wave (Reference 1).

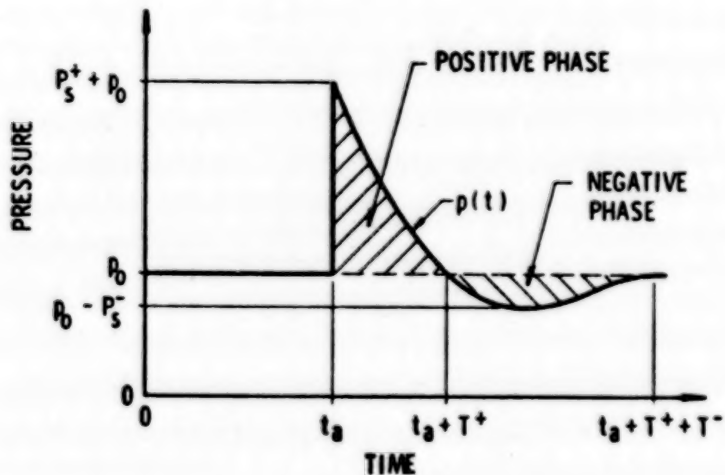


Figure 2-3. Ideal Blast Wave

Prior to shock front arrival, the pressure is ambient pressure p_o . At arrival time t_a , the pressure rises quite abruptly (discontinuously, in an ideal wave) to a peak value $P_s^+ + p_o$. The pressure then decays to ambient in total time $t_a + T^+$, drops to a partial vacuum of amplitude P_s^- , and eventually returns to p_o in total time $t_a + T^+ + T^-$. The quantity P_s^+ is usually termed the peak side-on overpressure, or merely the peak overpressure. The portion of the time history above initial ambient pressure is called the positive phase, of duration T^+ . That portion below p_o , of amplitude P_s^- and duration T^- is called the negative phase. Positive and negative impulses, defined by

$$I_S^+ = \int_{t_a}^{t_a + T^+} [p(t) - p_o] dt \quad (2-1)$$

and

$$I_S^- = \int_{t_a^- + T^+}^{t_a^- + T^-} [p_0 - p(t)] dt \quad (2-2)$$

respectively, are also significant blast wave parameters.

In most blast studies, the negative phase of the blast wave is ignored and only blast parameters associated with the positive phase are considered or reported. (The positive superscript is usually dropped). The ideal side-on parameters almost never represent the actual pressure loading applied to structures or targets following an explosion. So a number of other properties are defined to either more closely approximate real blast loads or to provide upper limits for such loads.

An upper limit to blast loads is obtained if one interposes an infinite, rigid wall in front of the wave, and reflects the wave normally. All flow behind the wave is stopped, and pressures are considerably greater than side-on. The peak overpressure in normally reflected waves is usually designated P_r . The integral of this pressure over the positive phase, defined similarly to Equation (2-1), is the reflected impulse I_r . Durations of the positive phase of normally reflected waves are designated T_r . The parameter I_r has been measured closer to high explosive blast sources than have most blast parameters.

In certain instances, damage estimates involve P_r and I_r instead of P_s and I_s . This situation can occur when one is examining the effect of an air burst on ground structures. The ground, in this case, acts as the most significant reflecting surface. Reflected pressures and impulses are also used in analyzing face-on loading of windows and structures. Fortunately, reflected pressure and impulse can be calculated directly from side-on pressure and impulse. For values of $\bar{P}_r \leq 3.5$ where \bar{P}_r is P_r/p_0 (p_0 is atmospheric pressure),

$$\bar{P}_r = 2\bar{P}_s + \frac{(\gamma + 1)\bar{P}_s^2}{(\gamma - 1)\bar{P}_s + 2\gamma} \quad (2-3)$$

where $\bar{P}_s = P_s/p_0$ and γ is the ratio of specific heats which equals 1.4 for air. For values of $\bar{P}_s > 3.5$, \bar{P}_r , and subsequently P_r , can be determined from Figure 2-4.

Over the range $0.00141 \leq \bar{P}_s \leq 1.38$, $\bar{I}_r (= I_r a_0/p_0^{1/3} E^{1/3})$ can be calculated from

$$\bar{I} = \bar{I}_s \frac{\bar{P}_r}{\bar{P}_s} \quad (2-4)$$

where $\bar{I}_s = I_s a_0 / p_0^{1/3} E^{1/3}$. For values of $\bar{P}_s < 0.00141$,

$$\bar{I}_r = 2\bar{I}_s \quad (2-5)$$

A real target feels a very complex loading during the process of diffraction of the shock front around the target. Figure 2-5 shows schematically, in three stages, the interaction of a blast wave with an irregular object. As the wave strikes the object, a portion is reflected from the front face, and the remainder diffracts around the object. In the diffraction process, the incident wave front closes in behind the object, greatly weakened locally, and a pair of trailing vortices is formed. Rarefaction waves sweep across the front face, attenuating the initial reflected blast pressure. After passage of the front, the body is immersed in a time-varying flow field. Maximum pressure on the front face during this "drag" phase of loading is the stagnation pressure.

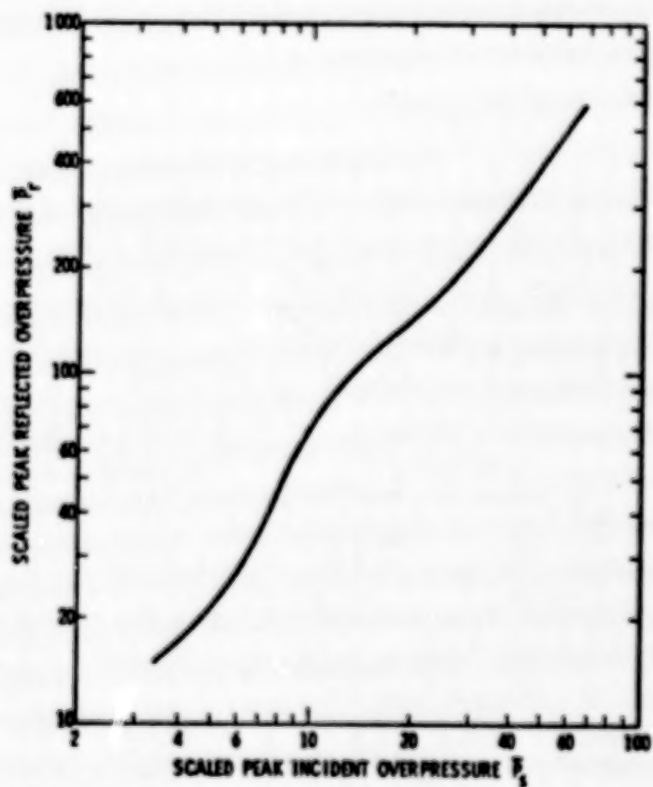


Figure 2-4. Scaled Reflected Overpressure Vs Scaled Side-on Overpressure

We are interested in the net transverse pressure on the object as a function of time. This loading, somewhat idealized, is shown in Figure 2-6 [details of the calculation are given by Glasstone (Reference 7)]. At time of arrival t_a , the net transverse pressure rises linearly from zero to maximum of P_r in time $(T_1 - t_a)$ (for a flat-faced object, this time is zero). Pressure then falls linearly to drag pressure in time $(T_2 - T_1)$, and then decays more slowly to zero in time $(T_3 - T_2)$. This time history of drag pressure q is a modified exponential, with a maximum given by

$$C_D Q = C_D \cdot (1/2) \rho_s u_s^2 \quad (2-6)$$

where C_D is the steady-state drag coefficient for the object, Q is peak dynamic pressure, and ρ_s and u_s are peak density and particle velocity respectively for the blast wave. The characteristics of the diffraction phase of the loading can be determined if the peak side-on overpressure P_s or the shock velocity U is known, together with the shape and some characteristic dimension D of the object. The peak amplitude of the drag phase of the loading can be determined if the peak side-on overpressure P_s or the shock velocity U is known, together with the shape and some characteristic dimension D of the object. The peak amplitude of the drag phase, $C_D Q$, can also be determined explicitly from P_s or u_s .

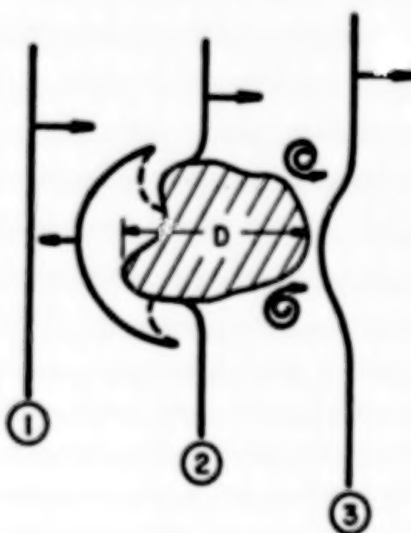


Figure 2-5. Interaction of Blast Wave with Irregular Object

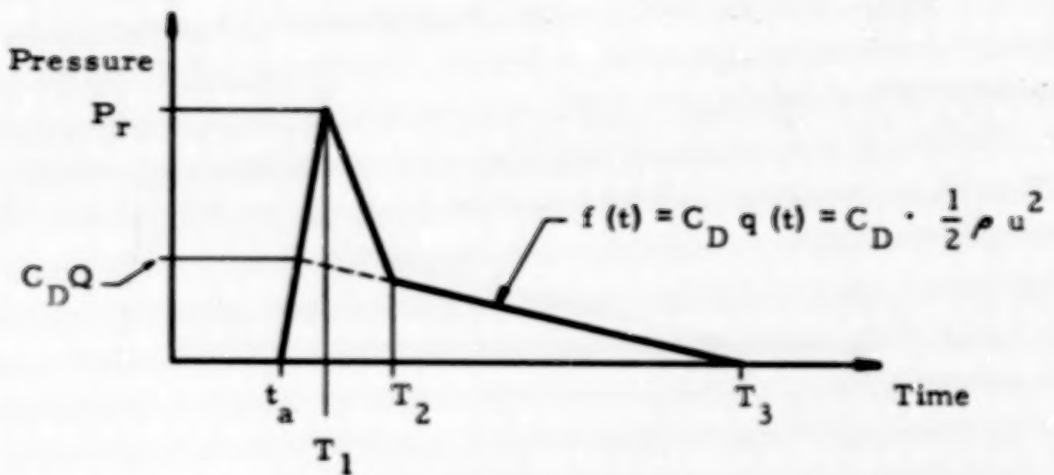


Figure 2-6. Time History of Net Transverse Pressure on Object During Passage of a Blast Wave

Because of the importance of the dynamic pressure q in drag or wind effects and target tumbling, it is often reported as a blast wave property. In some instances drag impulse I_d , defined as

$$I_d = \int_{t_a}^{t_a + T} q dt = (1/2) \int_{t_a}^{t_a + T} \rho u^2 dt \quad (2-7)$$

is also reported.

Although it is possible to define the potential or kinetic energy in blast waves, it is not customary in air blast technology to report or compute these properties. For underwater explosions, the use of "energy flux density" is more common (Reference 9). This quantity is given approximately by

$$E_f = \frac{1}{\rho_o c_o} \int_{t_a}^{t_a + T} [p(t) - p_o]^2 dt \quad (2-8)$$

Blast waves from real accidental explosions can differ in a number of ways from the essentially clean spherical waves considered in most theoretical treatments, and in many field or laboratory experiments. As an example, any explosion source which is not spherical in free air or

hemispherical in contact with a reflecting plane will generate a blast wave which is, at least in its early stages, non-spherical. The wave may well have an axis of symmetry, but requires definition in at least two space coordinates and time. Analytically, the treatment of non-spherical waves requires more mathematical complexity, and experimentally, measurement requires many more tests than for spherical waves.

The simplest type of non-spherical behavior probably results from elevation of a spherical explosion source above a reflecting plane (usually the ground). The resulting reflection process is described in Baker (Reference 6) and Glasstone (Reference 7). A structure or target on the ground feels a double shock if it is in the region of regular reflection close to the blast source, or a single strengthened shock if it is in the region of Mach reflection. Even this "simplest" case of non-spherical behavior is quite complex.

The second type of asphericity is that caused by sources which are not spherical. Most real blast sources are non-spherical, and can be of regular geometry such as cylindrical or block-shaped, or can be quite irregular in shape. Few analyses or experiments have been done for other than cylindrical geometry of solid explosive sources. For cylinders, the wave patterns are quite complex. The pressure-time histories exhibit multiple shocks, and decay in a quite different manner in the near field than do spherical waves. Fortunately, asymmetries smooth out as the blast wave progresses, and "far enough" from most real sources, the wave will become a spherical wave.

Other effects which can significantly alter blast wave properties are:

- (1) Effect of partial or total confinement.
- (2) Atmospheric propagation effects.
- (3) Absorption of energy by ground shock or cratering.
- (4) Transmission over irregular terrain.

These effects are often ignored or roughly approximated in safety studies because they are quite variable or can be adequately accounted for by use of simple safety factors or energy multipliers. They are discussed in some detail in References 5 and 6.

2-2 Pressure Waves From Propellant Explosions

2-2.1 Introduction

The characteristics of pressure waves, particularly peak side-on overpressure and specific impulse, are used extensively in developing damage estimates from propellant explosions. This portion of this chapter is therefore devoted to the calculation of pressures and specific impulses at varying distances from a propellant explosion based on methods given by Baker, et al⁽¹⁰⁾.

The same terminology used in Chapter I, Section 1-1, for propellant types and failure modes is used in this chapter. Three different types of propellant-oxidizer combinations are considered. These are hypergolic (50% N₂H₄ - 50% UDMH fuel and N₂O₄ oxidizer in a mass ratio of 1/2), liquid oxygen-hydrocarbon [Kerosene (RP-1) fuel and liquid oxygen (LO₂) oxidizer in a mass ratio of 1/2.25], and liquid oxygen-liquid hydrogen [cryogenic combination of liquid hydrogen (LH₂) fuel and liquid oxygen (LO₂) oxidizer in stoichiometric mass ratio of 1/5]. Three types of failure modes are considered; namely, confined by missile (CBM), confined by ground surface (CBGS), and high velocity impact (HVI). If needed, Chapter I should be consulted for a more complete explanation of types of propellants and failure modes.

2-2.2 Determination of Peak Side-On Overpressure and Specific Impulse

Throughout the PYRO (2-4) work, blast yield is expressed as percent yield, based on an average of pressures and impulses measured at the farthest distance from the source when compared to standard reference curves (Reference 11) for TNT surface bursts (terminal yield). Hopkinson's blast scaling is used when comparing blast data for tests with the same propellants and failure conditions, but different mass of propellant. So, the blast parameters P (peak side-on overpressure) and I/W^{1/3} (scaled impulse) are plotted as functions of R/W^{1/3} (scaled distance), after being normalized by the fractional yield. This procedure is equivalent to determining an effective mass of propellant for blast from:

$$W = W_T \times \frac{Y}{100} \quad (2-9)$$

where W_T is total mass of propellant and oxidizer, Y is terminal blast yield in percent and W is effective mass of propellant. Because the data are normalized by comparing to TNT blast data, the effective blast energy E can be obtained by multiplying W by the specific detonation energy of

TNT, 4.18×10^6 J/kg (1.4×10^6 ft lb_f/lb_m). Baker's⁽¹⁰⁾ smoothed curves through the scaled PYRO blast data, and Equation (2-9) will be used to obtain blast wave properties for particular combinations of propellants and simulated accidents.

Table 2-1 contains the different propellant failure mode combinations under consideration and the figure numbers of the graphs (following Table 2-1) needed to determine peak side-on overpressure and scaled specific impulse as a function of scaled distance for each accident situation. The procedure for finding peak side-on overpressure and specific impulse are as follows:

- (1) Calculate terminal yield Y using methods discussed in Chapter I, Section 1-1.
- (2) Determine W, effective mass of propellant and oxidizer, from Equation (2-9).
- (3) Choose a specific standoff distance R from the center of the anticipated blast and calculate scaled distance $R/W^{1/3}$.
- (4) Examine Table 1 and acquire the proper figure numbers for finding peak side-on overpressure P and scaled impulse $I/W^{1/3}$ for the particular propellant/oxidizer and failure mode under consideration.
- (5) Determine P from the appropriate Pressure versus Scaled Distance curve and the predetermined scaled distance.
- (6) Determine $I/W^{1/3}$ from the appropriate Scaled Positive Impulse versus Scaled Distance curve* and the predetermined scaled distance.
- (7) Calculate specific impulse I from scaled positive impulse $I/W^{1/3}$.

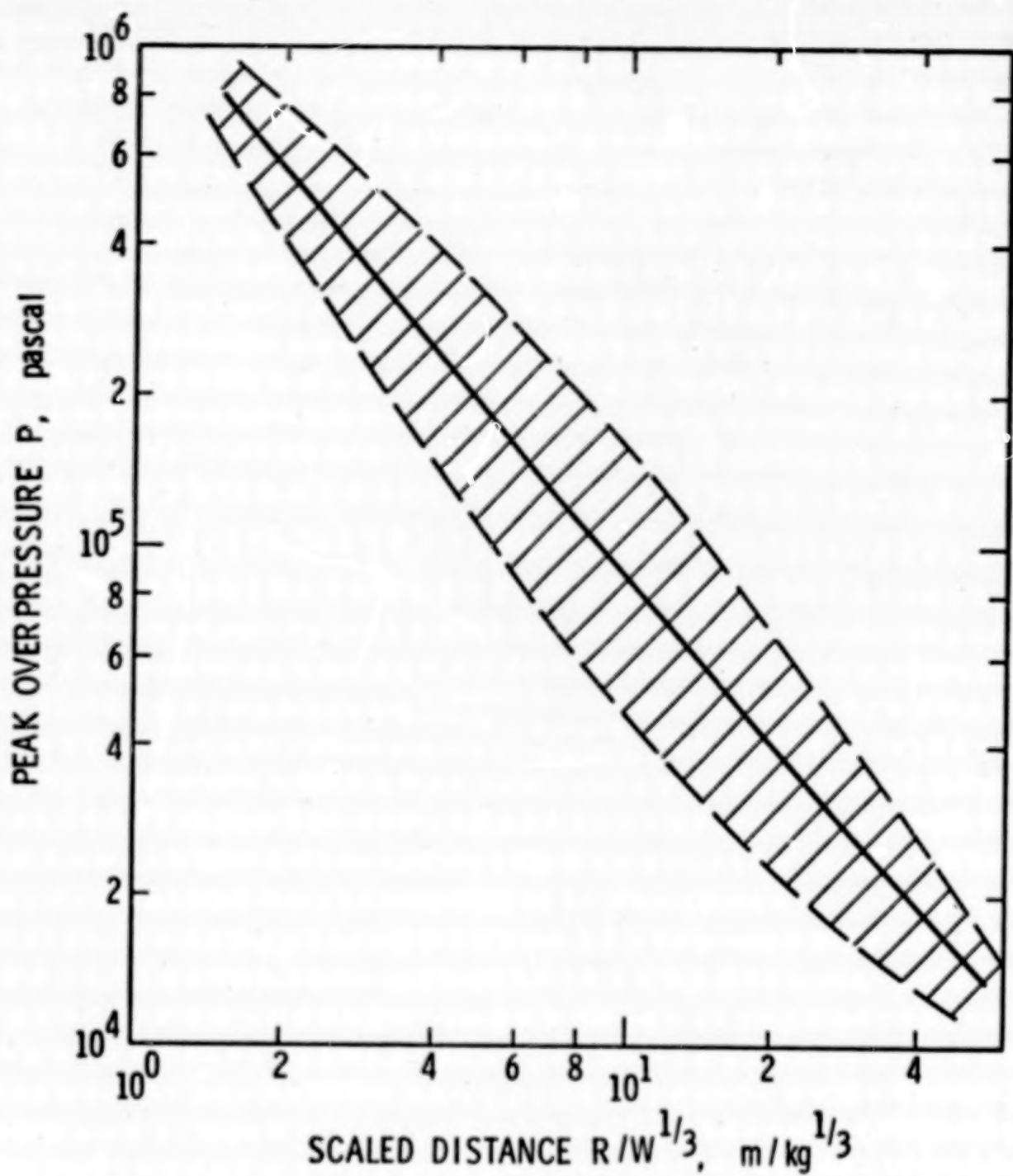
*A word of explanation will help clarify the meaning of the central solid line and shaded area of the graphs. The shaded portion represents actual data from propellant blasts. The central solid line is an estimate of the most likely occurrence and, for most cases, is the recommended choice. The vertical distance between the two dashed lines at any abscissa is a measure of the data spread, or uncertainty in a prediction from the solid line.

That is

$$I = \left(\frac{I}{W^{1/3}} \right) (W^{1/3}) \quad (2-10)$$

TABLE 2-1. GUIDE TO SELECTION OF PROPER GRAPHS FOR THE DETERMINATION OF PRESSURE AND SPECIFIC IMPULSE

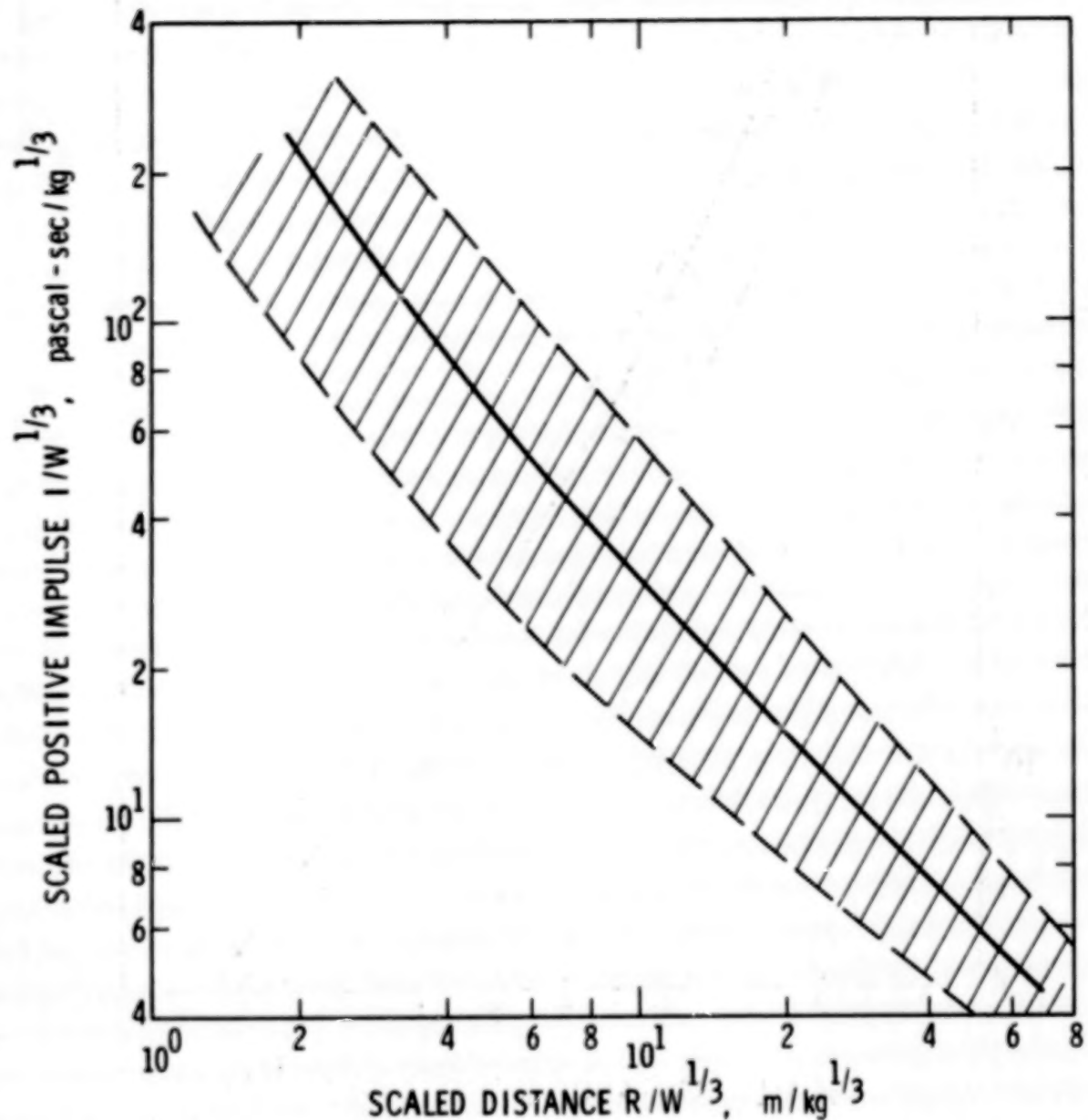
Type of Propellant & Oxidizer	Type of Accident (Failure Mode)	Peak Side-On Overpressure (P)	Scaled Impulse ($I/W^{1/3}$)
Hypergolic (50% N ₂ H ₄ 50% UDMH/N ₂ O ₄)	CBM	Figure 2-7	Figure 2-8
	CBGS	Figure 2-7	Figure 2-8
	HVI	Figure 2-9	Figure 2-8
Liquid Oxygen-Hydrocarbon (LO ₂ /RP-1)	CBM	Figure 2-10	Figure 2-11
	CBGS	Figure 2-12	Figure 2-13
	HVI	Figure 2-12	Figure 2-13
Liquid Oxygen-Liquid Hydrogen (LO ₂ /LH ₂)	CBM	Figure 2-14	Figure 2-15
	CBGS	Figure 2-16	Figure 2-17
	HVI	Figure 2-16	Figure 2-17



$$(\text{psi} = \text{Pa} \times 1.450 \times 10^{-4})$$

$$(\text{ft/lb}^{1/3}_m = \text{m/kg}^{1/3} \times 2.521)$$

Figure 2-7. Pressure vs Scaled Distance. Hypergolic Propellant; CBM and CBGS Failure Modes.



$$(\text{psi-sec/lb}_m^{-1} = \rho_a \cdot s / \text{kg}^{1/3} \times 1.114 \times 10^{-4})$$

$$(\text{ft/lb}_m^{1/3} = \text{m/kg}^{1/3} \times 2.521)$$

**Figure 2-8. Scaled Positive Impulse vs Scaled Distance.
Hypergolic Propellant; CBM, CBGS and HVI
Failure Modes.**

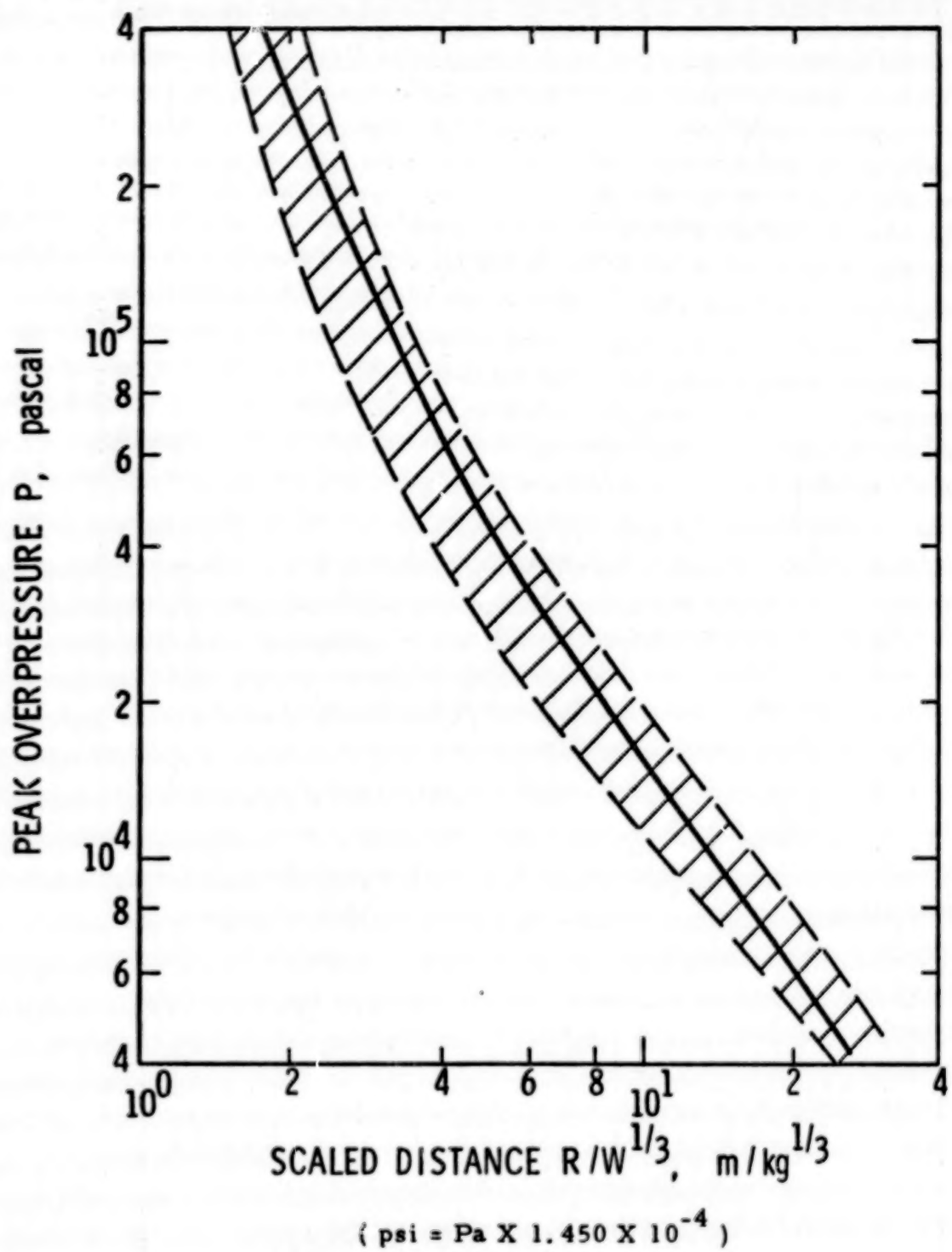


Figure 2-9. Pressure vs Scaled Distance. Hypergolic Propellant; HVI Failure Mode.

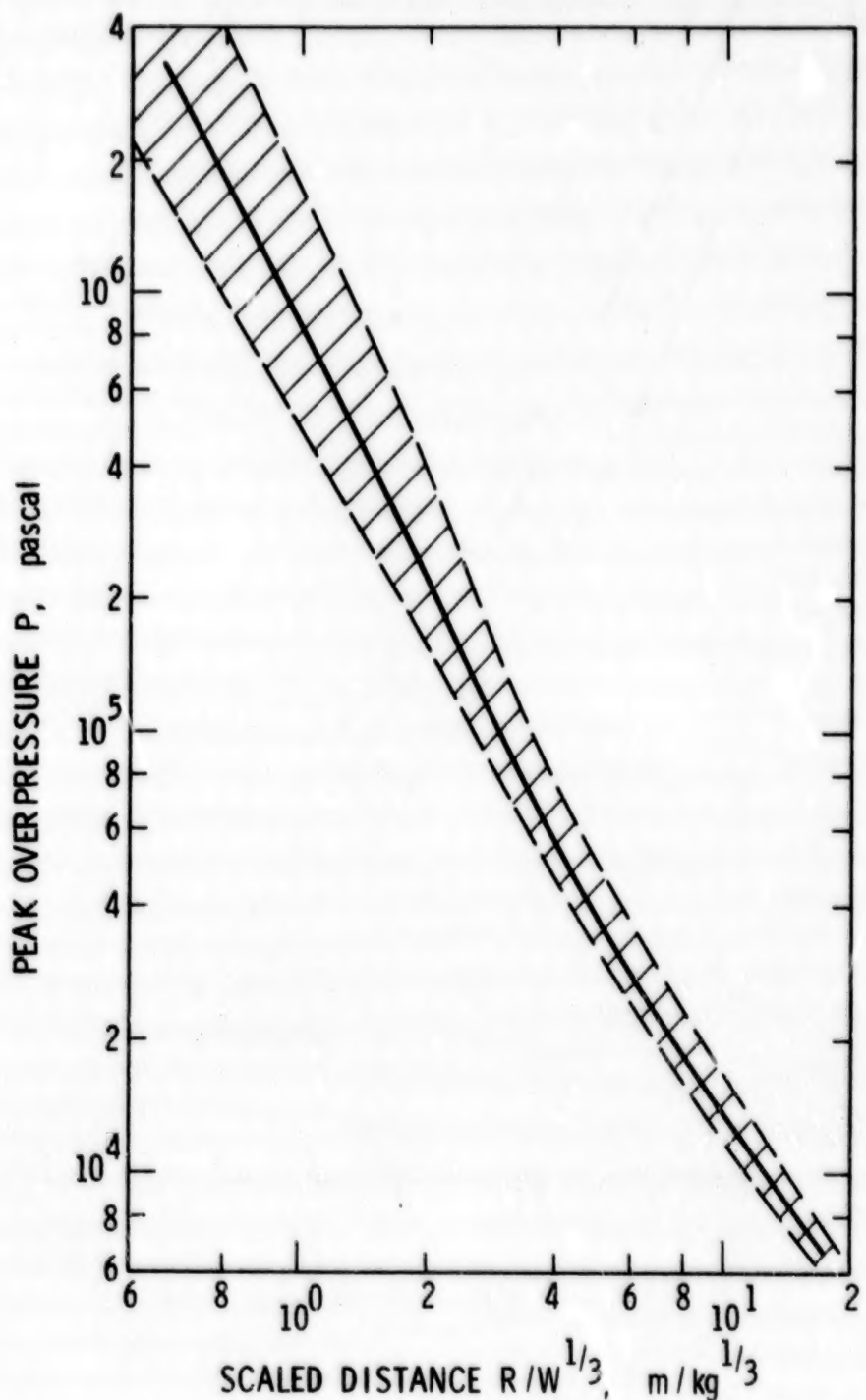
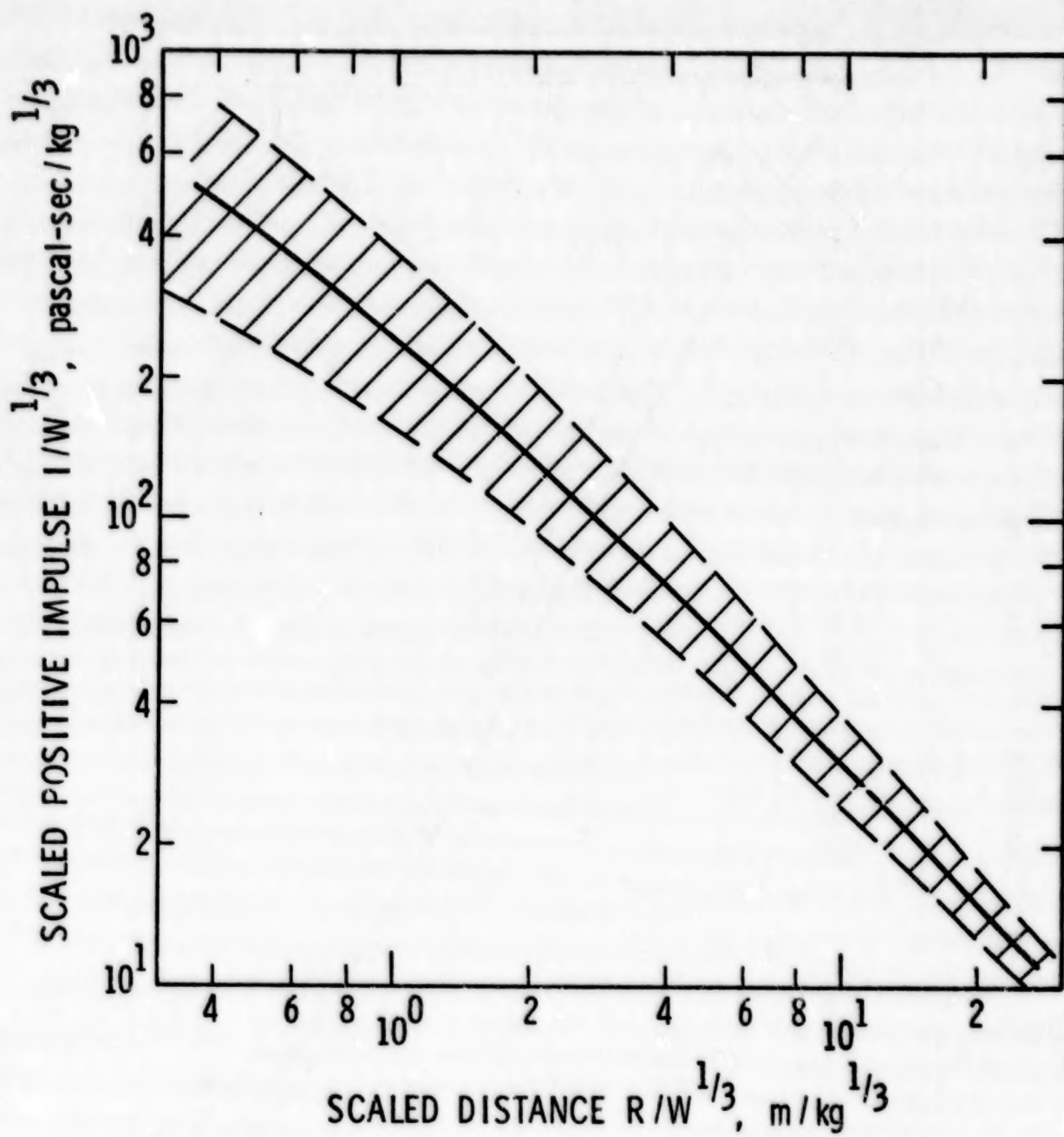


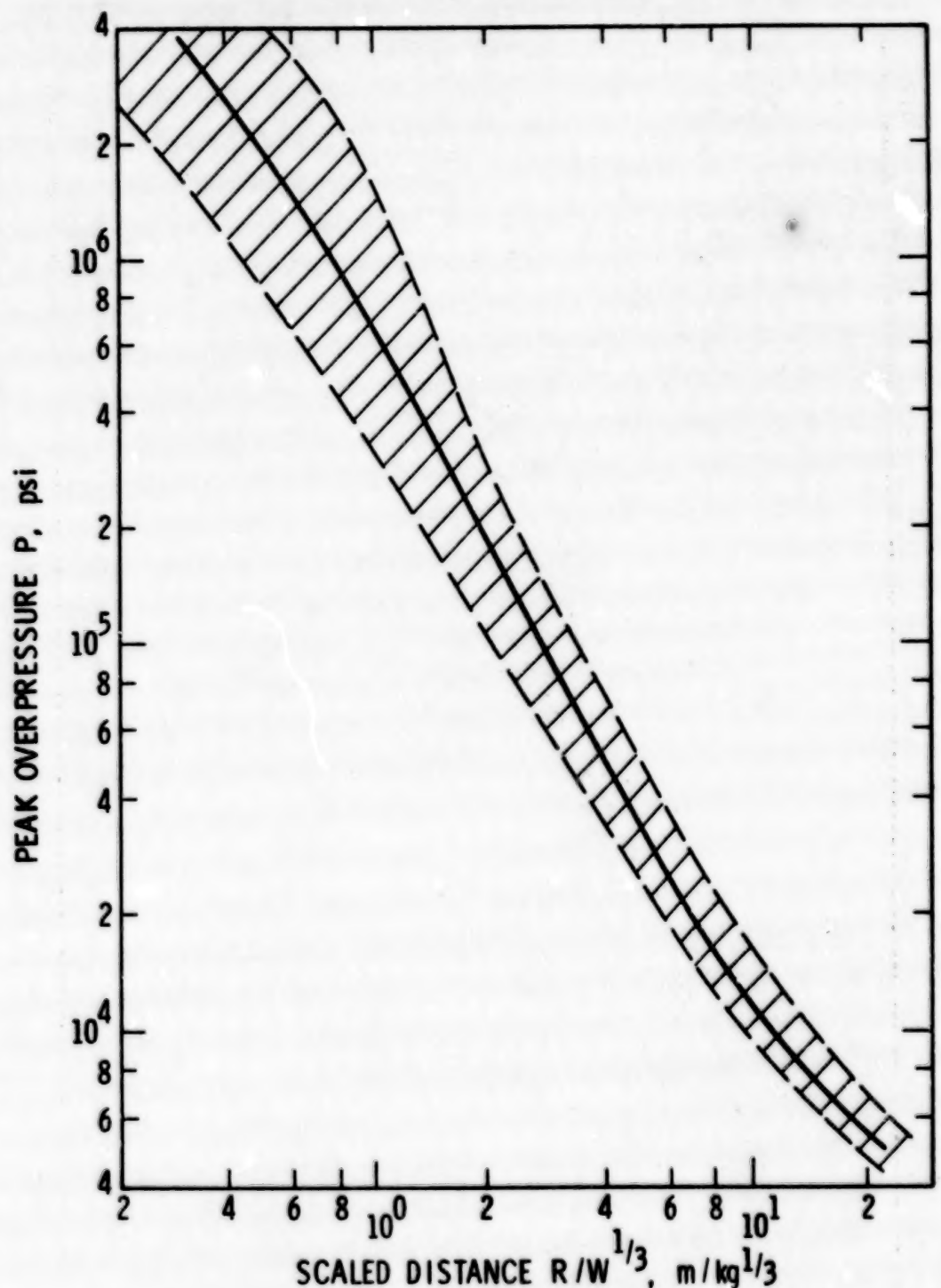
Figure 2-10. Pressure vs Scaled Distance. LO₂/RP-1 Propellant; CBM Failure Mode.



$$(\text{psi-sec/lb} \frac{1}{m} = \text{Pa} \cdot \text{s/kg} \frac{1}{3} \times 1.114 \times 10^{-4})$$

$$(\text{ft/lb} \frac{1}{m} = \text{m/kg} \frac{1}{3} \times 2.521)$$

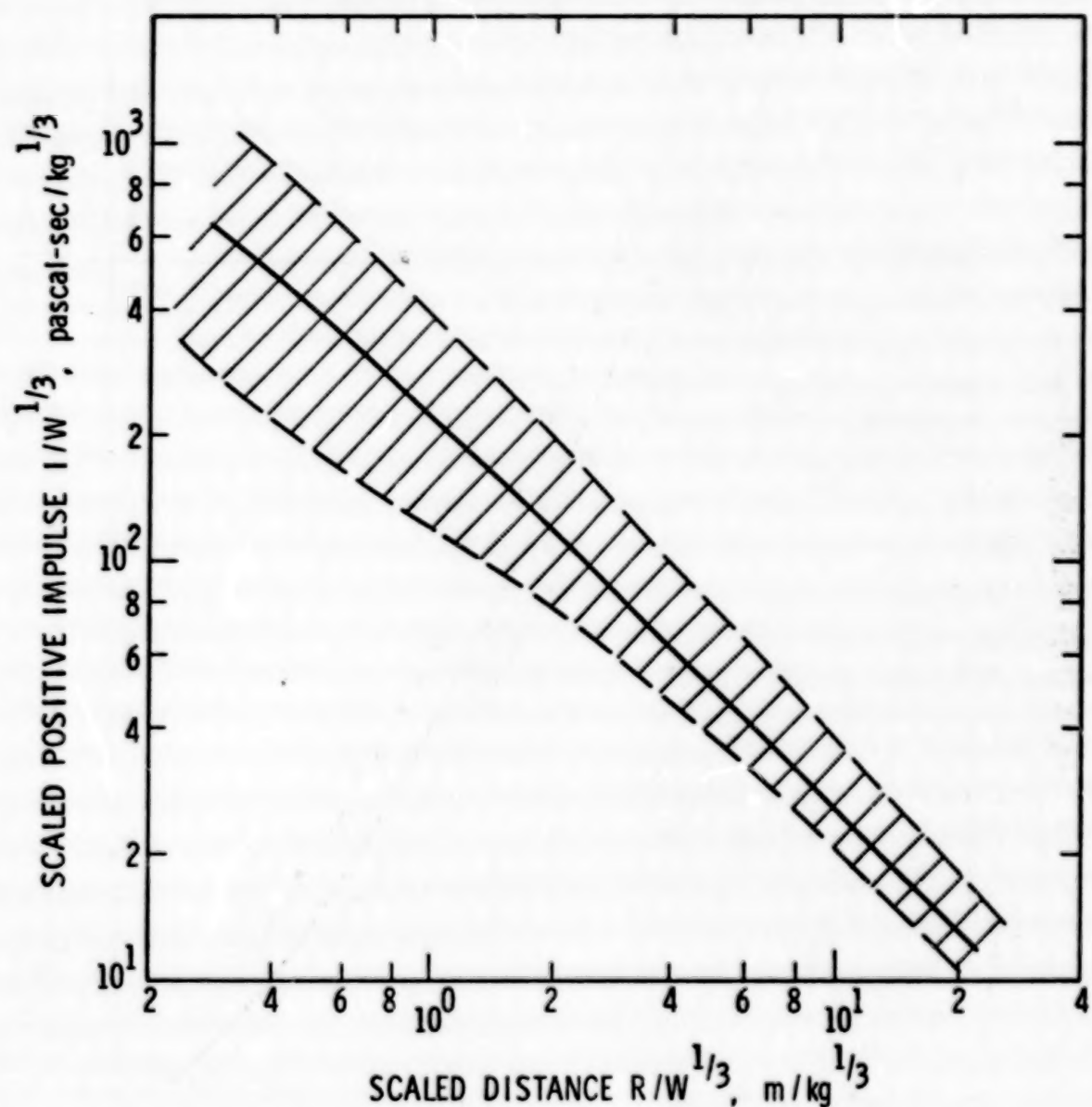
Figure 2-11. Scaled Positive Impulse vs Scaled Distance.
 $\text{LO}_2/\text{RP-1}$ Propellant; CBM Failure Mode.



$$(\text{psi} = \text{Pa} \times 1.450 \times 10^{-4})$$

$$(\text{ft/lb} \frac{1}{\text{m}} = \text{m/kg} \frac{1}{\text{m}} \times 2.521)$$

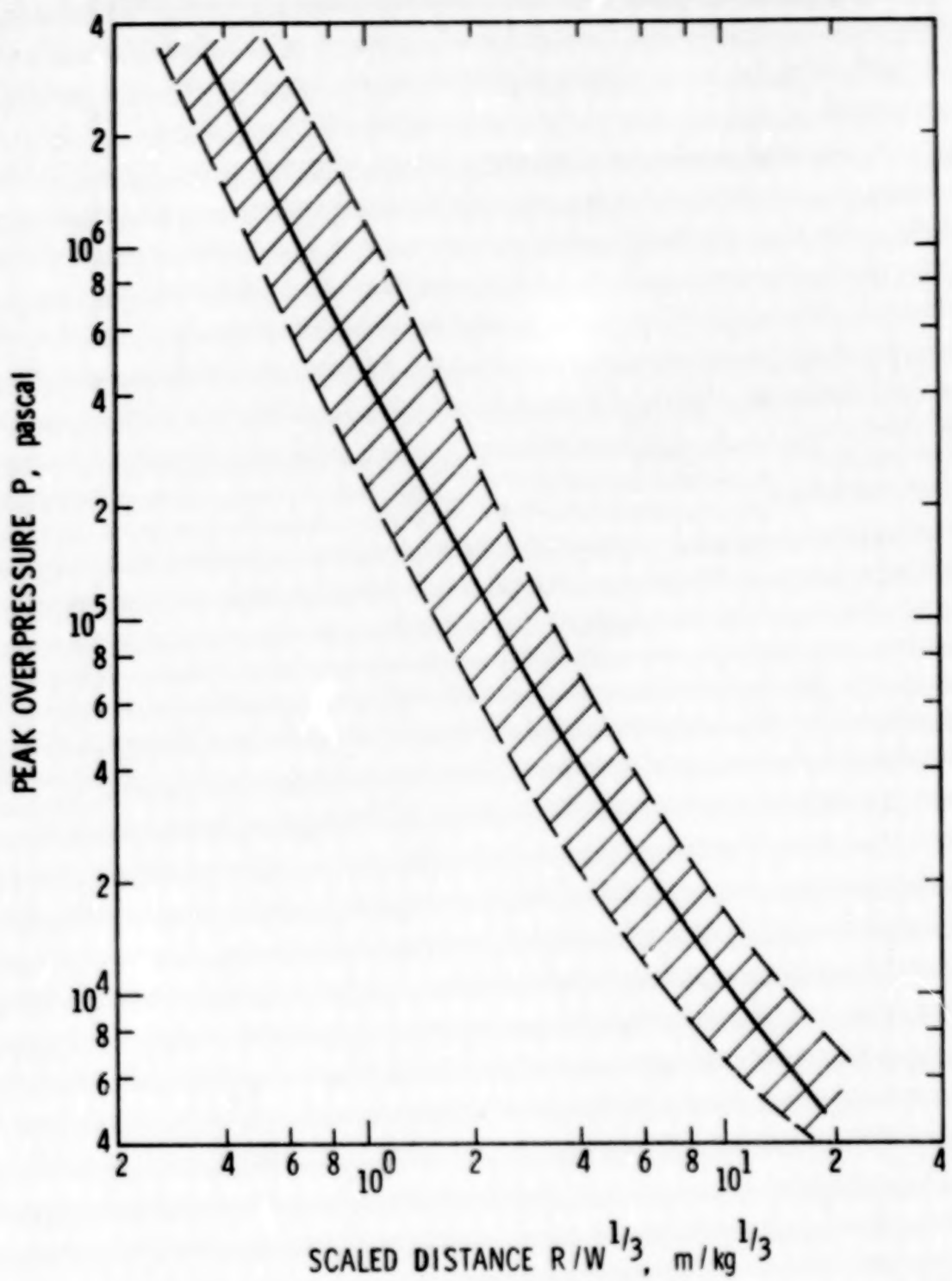
Figure 2-12. Pressure vs Scaled Distance. $\text{LO}_2/\text{RP-1}$ Propellant; CBGS and HVI Failure Modes.



$$(\text{psi-sec/lb}_m^{1/3} = \text{Pa} \cdot \text{s}/\text{kg}^{1/3} \times 1.114 \times 10^{-4})$$

$$(\text{ft/lb}_m^{1/3} = \text{m/kg}^{1/3} \times 2.521)$$

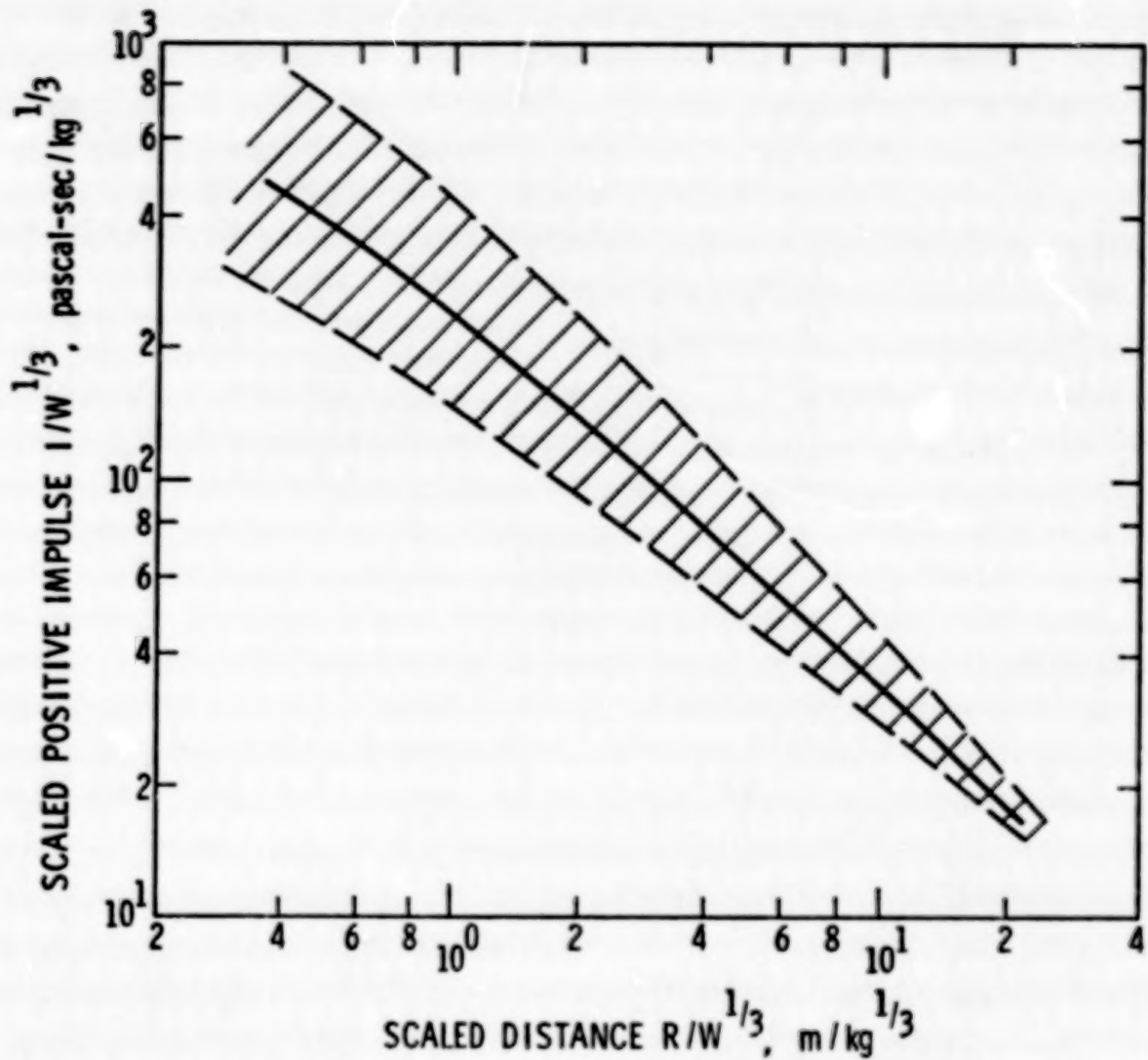
Figure 2-13. Scaled Positive Impulse vs Scaled Distance.
 $\text{LO}_2/\text{RP-1}$ Propellant; CBGS and HVI Failure Modes.



$$(\text{psi} = \text{Pa} \times 1.450 \times 10^{-4})$$

$$(\text{ft/lb}^{1/3}_{\text{m}} = \text{m/kg}^{1/3} \times 2.521)$$

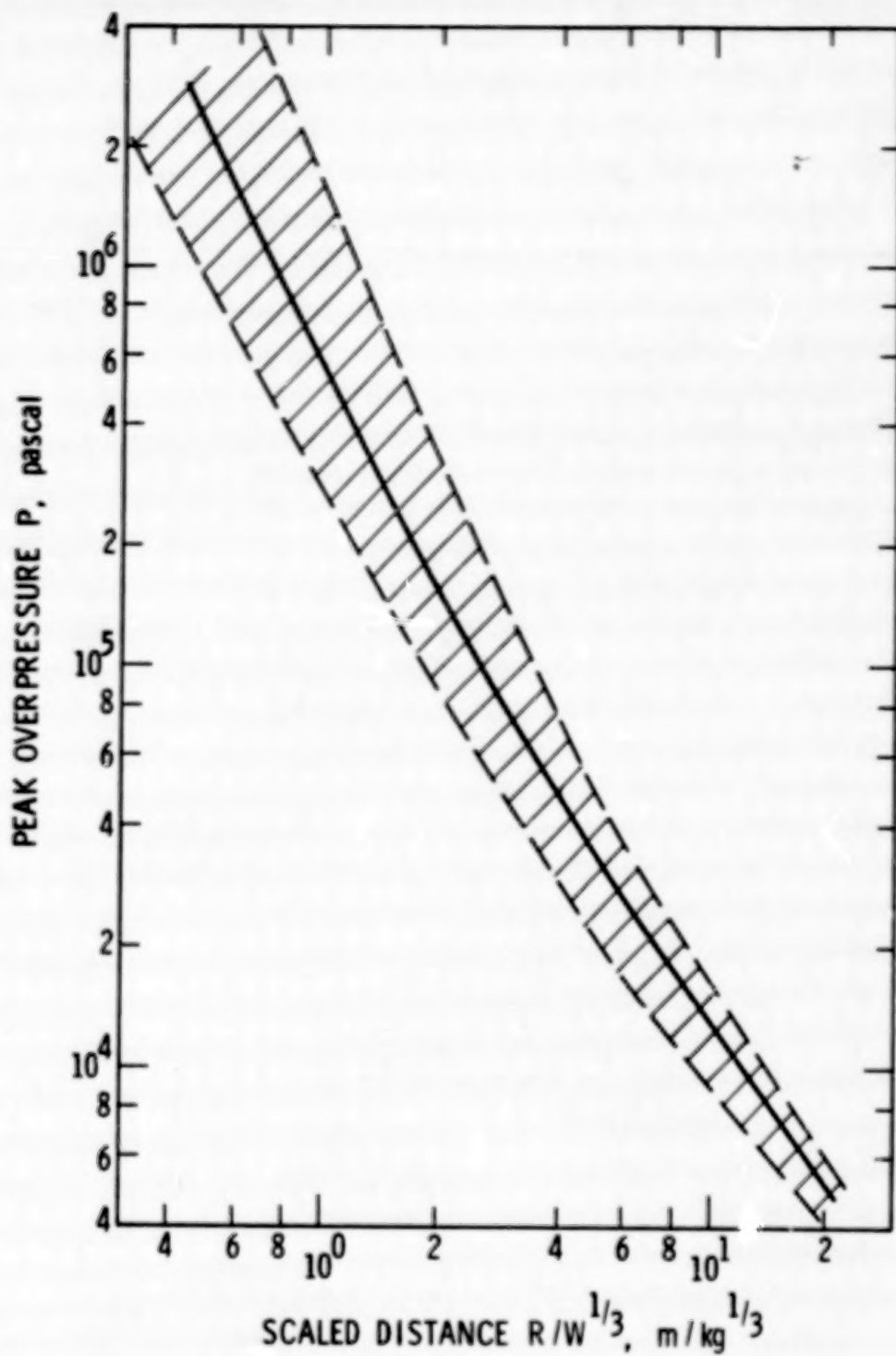
Figure 2-14. Pressure vs Scaled Distance. LO₂/LH₂ Propellant; CBM Failure Mode.



$$(\text{psi-sec/lb} \frac{1}{m} = \text{Pa} \cdot \text{s/kg} \frac{1}{m} \times 1.114 \times 10^{-4})$$

$$(\text{ft/lb} \frac{1}{m} = \text{m/kg} \frac{1}{m} \times 2.521)$$

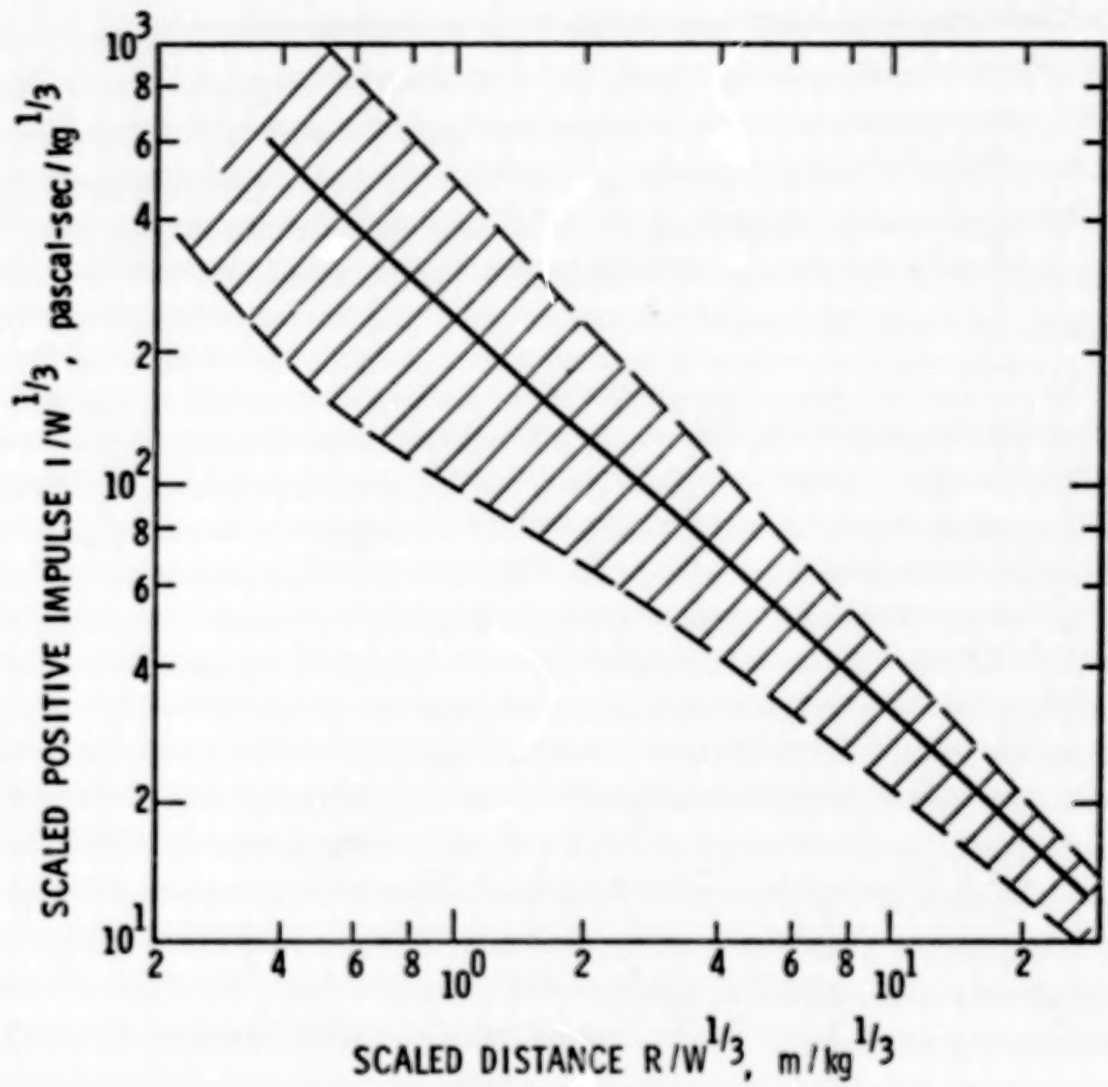
Figure 2-15. Scaled Positive Impulse vs Scaled Distance.
 LO_2/LH_2 Propellant; CBM Failure Mode.



$$(\text{psi} = \text{Pa} \times 1.450 \times 10^{-4})$$

$$(\text{ft/lb}_{\text{m}}^{1/3} = \text{m/kg}^{1/3} \times 2.521)$$

Figure 2-16. Pressure vs Scaled Distance. LO₂/LH₂ Propellant; CBGS and HVI Failure Modes.



$$(\text{psi-sec/lb}_m^{1/3} = \text{Pa} \cdot \text{s}/\text{kg}^{1/3} \times 1.114 \times 10^{-4})$$

$$(\text{ft/lb}_m^{1/3} = \text{m/kg}^{1/3} \times 2.521)$$

Figure 2-17. Scaled Positive Impulse vs Scaled Distance.
 LO_2/LH_2 Propellant; CBGS and HVI Failure Modes.

2-2.3 Examples for Determining Peak Side-On Overpressure and Specific Impulse

The problems which follow are continuations of some of the example problems started in Chapter I, Section 1-1.3.

Example 1: (Continuation of Example 1 of Chapter I, Section 1-1.3)

Propellant-Hypergolic

Combined mass of propellant and oxidizer-10,000 kg (22,000 lb_m)

Failure mode - CBM

Standoff distance R (assumption) - 50 m (164 ft)

Solution:

(1) Terminal yield Y = 0.8% (See Example 1 of Chapter I, Section 1-1.3).

$$(2) W = W_T \times \frac{Y}{100\%}$$

$$W = 10,000 \text{ kg} \times \frac{0.8\%}{100\%}$$

$$W = 80 \text{ kg (176 lb}_m)$$

$$(3) \text{ Scaled distance } R/W^{1/3} = 50 \text{ m}/(80 \text{ kg})^{1/3} = 12 \text{ m/kg}^{1/3}$$

(4) Table 2-1 indicates:

Acquire P, peak pressure, from Figure 2-7.

Acquire I/W^{1/3}, scaled impulse, from Figure 2-8.

$$(5) \text{ From Figure 2-7, } P = 8.2 \times 10^4 \text{ Pa (11.89 psi)}$$

$$(6) \text{ From Figure 2-8, } I/W^{1/3} = 27 \text{ Pa} \cdot \text{s/kg}^{1/3}$$

$$(7) I = \left(\frac{I}{W^{1/3}} \right) (W^{1/3}) = 116 \text{ Pa} \cdot \text{s (1.682} \times 10^{-2} \text{ psi} \cdot \text{sec)}$$

Example 2: (Continuation of Example 4 of Chapter I, Section 1-1.3)

Propellant and oxidizer = LO₂/RP-1

Combined mass of propellant and oxidizer-150,000 kg
(330,000 lb_m)

Failure mode - CBGS

Impact velocity (assumption) - 10/m.s (32.8 ft/sec)

Ignition time (assumption) - 0.5 seconds

Standoff distance (assumption) - 100 m (328 ft)

Solution:

(1) Terminal yield $Y = 6.25\%$ (See Example 4 of Chapter I, Section 1-1.3 for calculations)

$$(2) W = W_T \times \frac{Y}{100\%}$$

$$W = 150,000 \text{ kg} \times \frac{6.25\%}{100\%}$$

$$W \approx 9375 \text{ kg (20,600 lb}_m)$$

$$(3) \text{ Scaled distance } R/W^{1/3} = 100 \text{ m}/(9375)^{1/3} = 4.7 \text{ m/kg}^{1/3}$$

(4) Table 2-1 indicates:

Acquire P , peak pressure from Figure 2-12.

Acquire $I/W^{1/3}$, scaled impulse from Figure 2-13.

(5) From Figure 2-12, $P = 3.8 \times 10^4 \text{ Pa (5.5 psi)}$

(6) From Figure 2-13, $I/W^{1/3} = 55 \text{ Pa} \cdot \text{s}/\text{kg}^{1/3}$

$$(7) I = \left(\frac{I}{W^{1/3}} \right) (W^{1/3}) = 1160 \text{ Pa} \cdot \text{s (0.168 psi-sec)}$$

Example 3: (Continuation of Example 5 of Chapter I, Section 1-1.3)

Propellant and oxidizer - LO₂/LH₂

Combined mass of propellant and oxidizer - 10,000 kg (22,000 lb_m)

Failure mode - HVI

Impact velocity (assumption) - 40 m/s (131 ft/sec)

Type of surface impacted - hard

Standoff distance (assumption) - 100 m (328 ft)

Solution:

(1) Terminal yield $Y = 30\%$ (See Example 5 of Chapter I, Section 1-1.3 for calculations)

$$(2) \quad W = W_T \times \frac{Y}{100\%}$$

$$W = 10,000 \text{ kg} \times \frac{30\%}{100\%}$$

$$W = 3000 \text{ kg (6600 lb}_m)$$

$$(3) \quad \text{Scaled distance } R/W^{1/3} = 100 \text{ m}/(3000 \text{ kg})^{1/3} = 6.9 \text{ m/kg}^{1/3}$$

(4) Table 2-1 indicates:

Acquire P , peak pressure, from Figure 2-16.

Acquire $I/W^{1/3}$, scaled impulse, from Figure 2-17.

$$(5) \quad \text{From Figure 2-16, } P = 2.2 \times 10^4 \text{ Pa (3.19 psi)}$$

$$(6) \quad \text{From Figure 2-17, } I/W^{1/3} = 45 \text{ Pa} \cdot \text{s}/\text{kg}^{1/3}$$

$$(7) \quad I = \frac{I}{W^{1/3}} \quad (W^{1/3}) = 649 \text{ Pa} \cdot \text{s} (9.41 \times 10^{-2} \text{ psi-sec})$$

2-3 Pressure Waves From Gas Vessel Bursts

Application to spherical vessels will be discussed first.

2-3.1 Overpressures for Various Gases and Initial Conditions

The overpressure versus distance relationship for a bursting gas vessel is strongly dependent upon the pressure, temperature, and ratio of specific heats of the gas in the vessel. For high pressures and temperatures, relative to the air outside the vessel, the overpressure behavior is much like that of a blast wave from a high explosive. On the \bar{P}_s versus \bar{R} graph (Figure 2-18), the curves for higher pressures and temperature are located near the high explosive curve. The curves for lower pressures and temperatures lie farther from the high explosive curve.

The procedure for relating overpressures and distance from the source of a gas vessel burst is the following: Determine the starting overpressure and distance. Locate this point on a \bar{P}_s versus \bar{R} graph. (Figure 2-18). Follow the nearest curve on this graph for the overpressure versus distance behavior. Choose the \bar{R} of interest, and read \bar{P}_s from the proper curve. Alternatively, one can choose a value for \bar{P}_s and locate the corresponding \bar{R} .

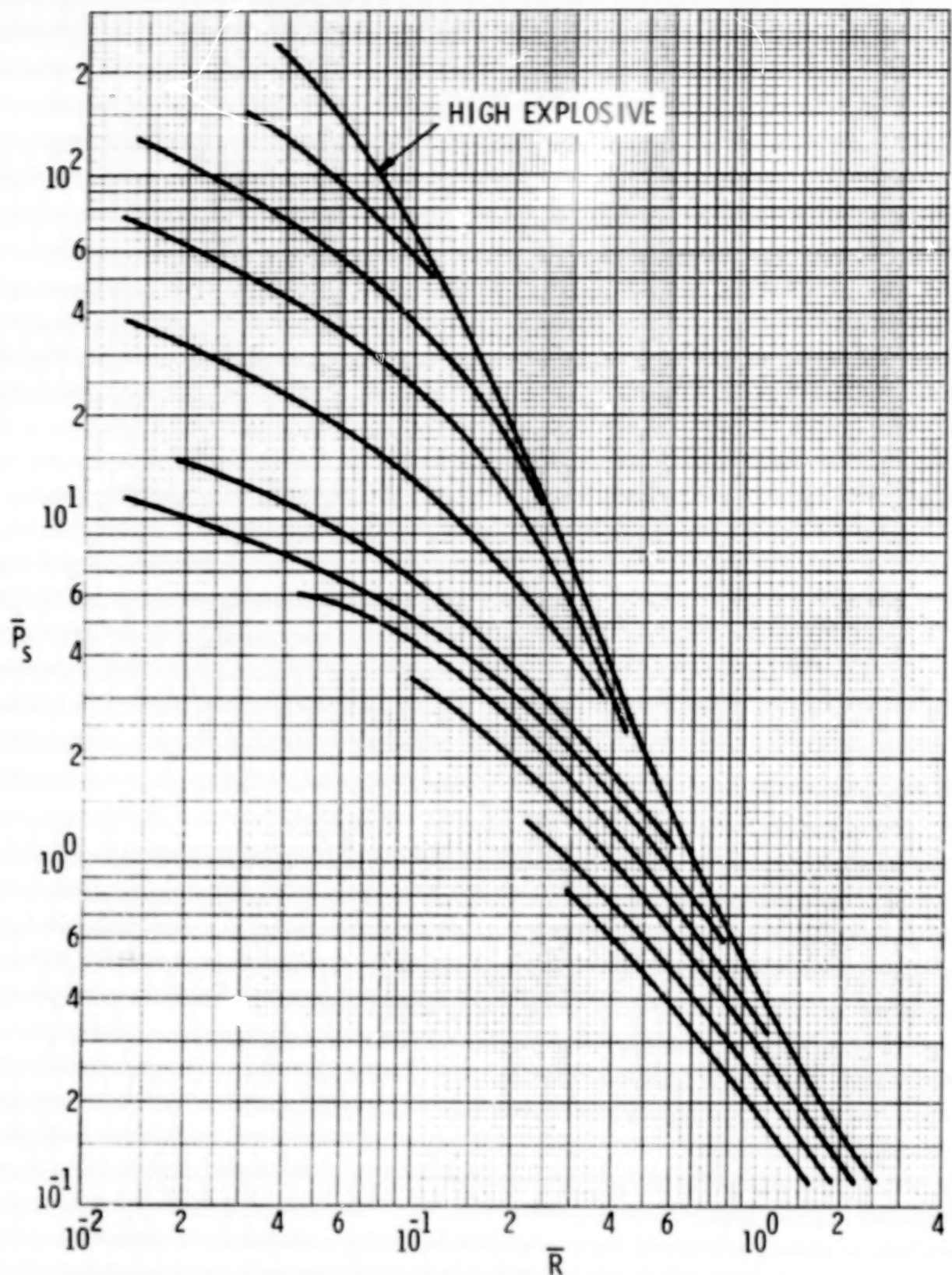


Figure 2-18. \bar{P}_s vs \bar{R} for Overpressure Calculations.

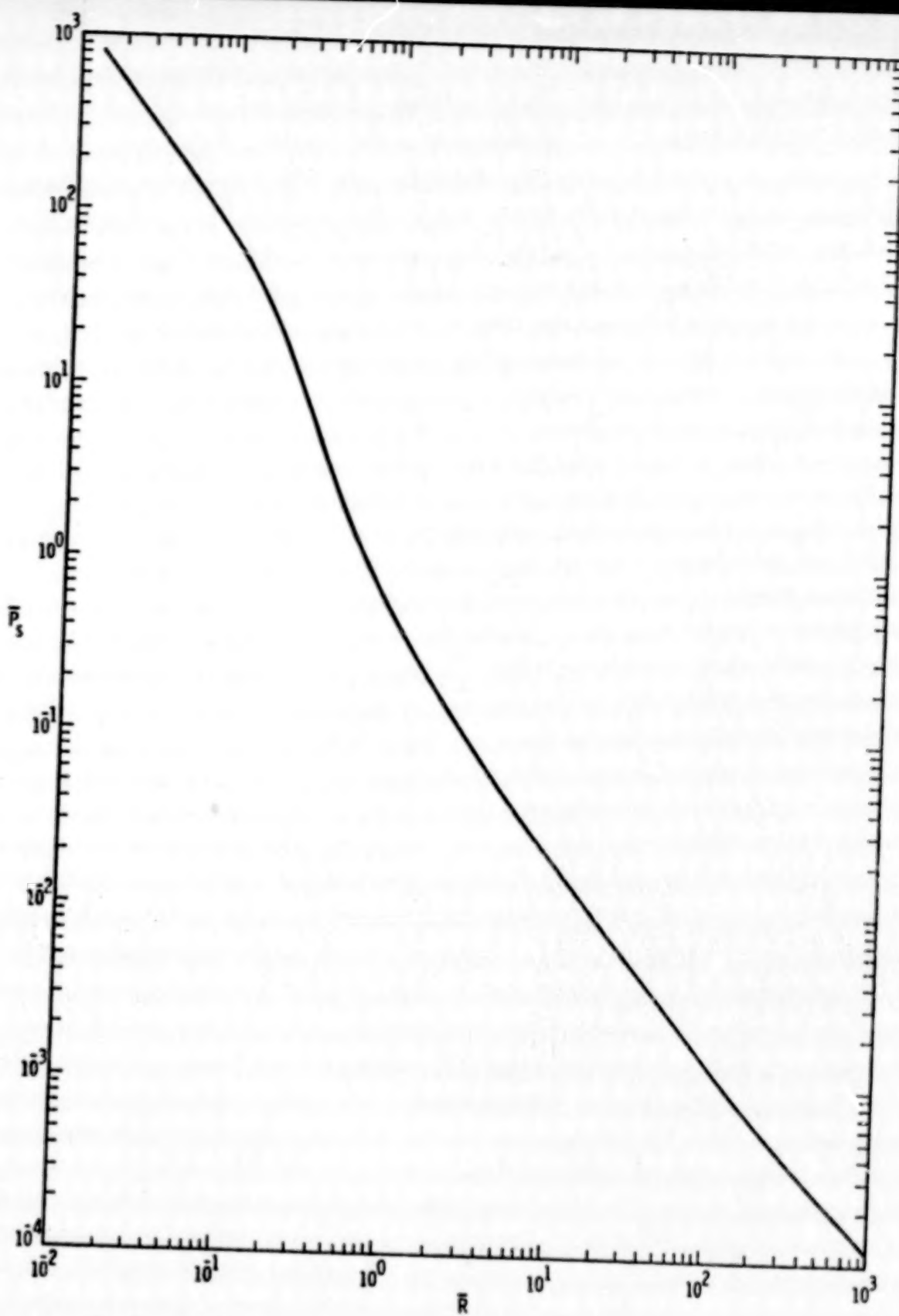


Figure 2-19. \bar{P}_s vs \bar{R} for Pentolite

For \bar{R} greater than about 2, Figure 2-19, \bar{P}_s versus \bar{R} for pentolite (a high explosive)⁽⁶⁾ can be used as an upper limit for P_s .

For a given p_1/p_a , T_1/T_a , and γ_1 , \bar{P}_{so} , the nondimensional starting shock overpressure, can be read from one of the graphs in Figures 2-20 and 2-21. For diatomic gases, such as air, O_2 , and H_2 , let γ_1 equal 1.4. For monatomic gases such as He, let $\gamma_1 = 1.667$.

The nondimensional starting dimensional starting distance \bar{R}_o is

$$\bar{R}_o = \frac{1}{\left[\frac{4\pi}{3} \left(\frac{p_1}{p_a} - 1 \right) \frac{V_i}{\gamma_1 - 1} \right]^{1/3}} \quad (2-11)$$

Locate \bar{R}_o and \bar{P}_{so} on the graph of \bar{P}_s versus \bar{R} as in Figure 2-22. This is the starting point. Follow the nearest curve for the \bar{P}_s versus \bar{R} behavior. The \bar{P}_s versus \bar{R} curves in Figure 2-18 are accurate to about $\pm 20\%$.

To determine the overpressure at a given distance, first compute \bar{R} .

$$\bar{R} = \frac{r}{\left[\left(\frac{p_1}{p_a} - 1 \right) V_i \right]^{1/3}} \quad (2-12)$$

where r is the distance from the center of the vessel, and V_i is the volume of the vessel before it bursts.

Then, read \bar{P}_s from the proper curve. Compute the overpressure:

$$\bar{P}_s = \frac{p_s - p_a}{p_a}, \text{ then } p_s - p_a = \bar{P}_s p_a. \text{ The quantity } p_s - p_a \text{ is}$$

the overpressure.

To determine the distance at which a given overpressure will be observed, compute \bar{P}_s from the given $p_s - p_a$:

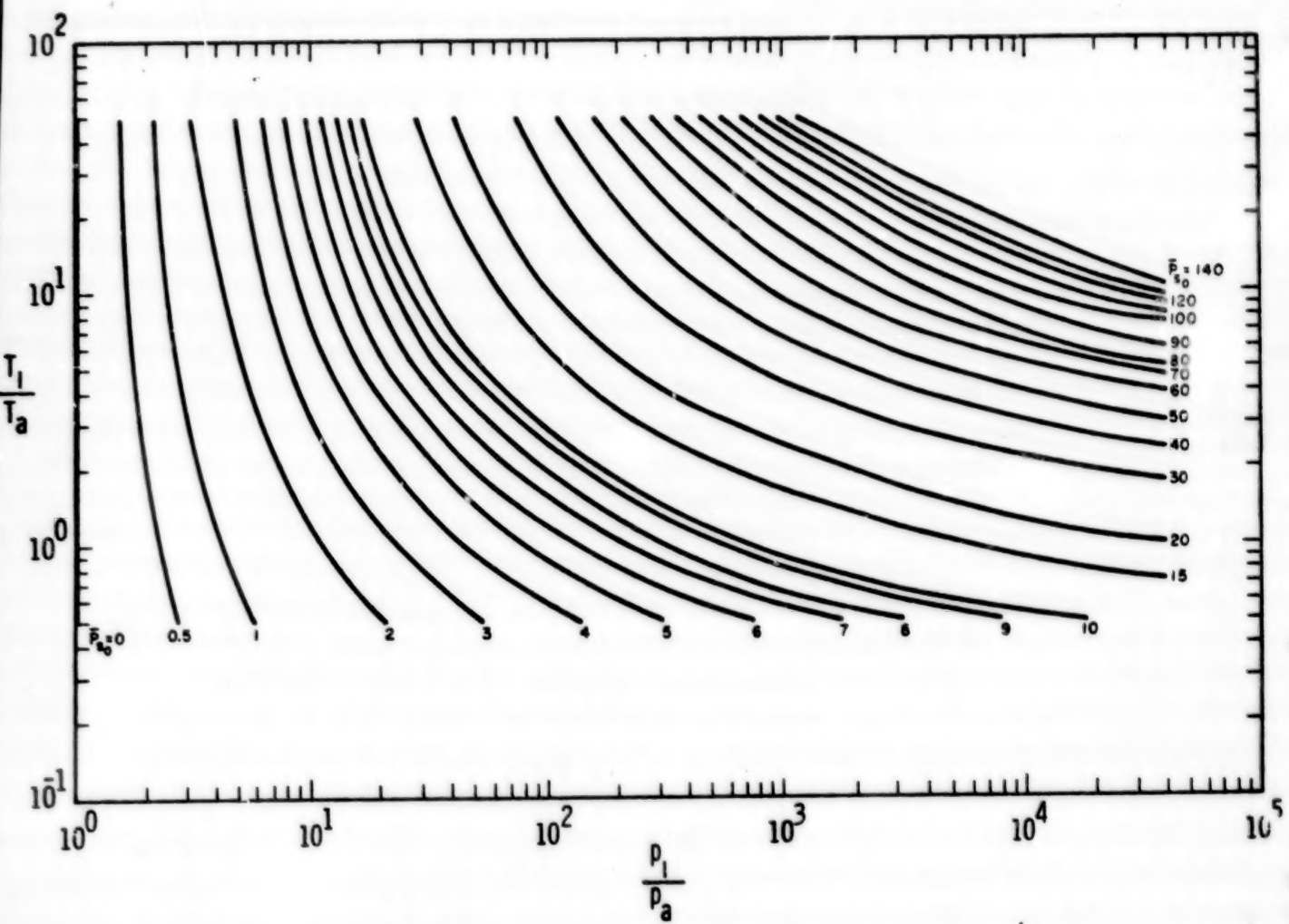


Figure 2-20. Kernel Temperature vs Kernel Pressure
for Constant \bar{P}_{s0} , $\gamma_1 = 1.4$

60

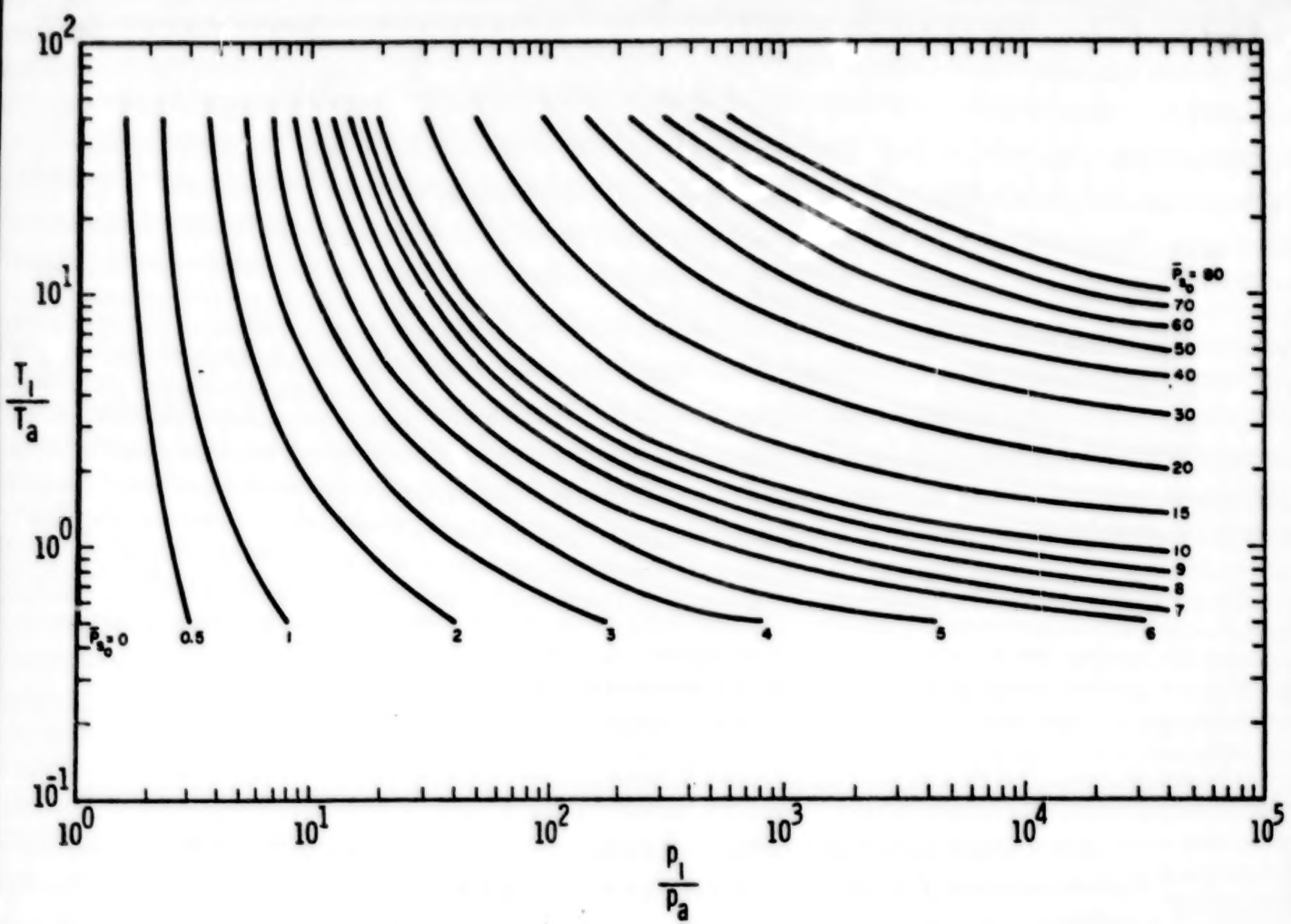


Figure 2-21. Kernel Temperature vs Kernel Pressure
for Constant Values of \bar{P}_{s0} , $\gamma_1 = 1.667$

(6)

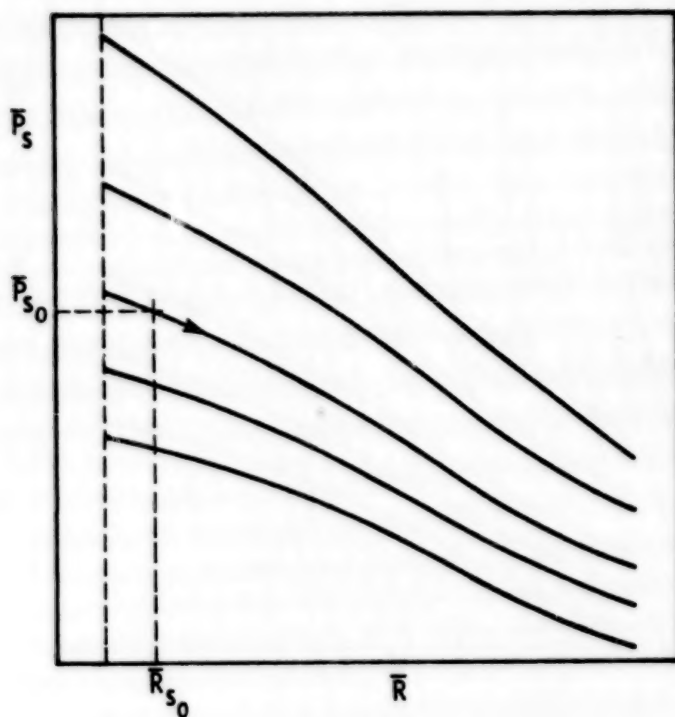


Figure 2-22. Location of Starting Point on Graph of \bar{P}_s vs \bar{R}

$$\bar{P}_s = \frac{P_s - P_a}{P_a} \quad (2-13)$$

Read \bar{R} from the proper curve, and calculate r :

$$\bar{R} = \frac{r}{\left[\left(\frac{P_1}{P_a} - 1 \right) V_i \right]^{1/3}} \quad \text{then} \quad (2-14)$$

$$r = \bar{R} \left[\left(\frac{P_1}{P_a} - 1 \right) V_i \right]^{1/3} \quad (2-15)$$

2-3.2 Specific Impulses for Various Gases and Initial Conditions

For the burst of a pressure vessel, the \bar{I} versus \bar{R} relationship in Figure 2-23 or 2-24 should be used. For \bar{R} in the range of 10^{-1} to 10^0 , the \bar{I} versus \bar{R} curve in Figure 2-24 is more convenient. This is an enlargement of part of Figure 2-23. These curves are accurate to about $\pm 25\%$. For a given distance, \bar{R} is calculated, and \bar{I} is read from Figure 2-23 or 2-24. Then I is calculated. Alternatively, one can choose a maximum acceptable specific impulse and find the minimum distance at which the specific impulse is less than this value.

Example:

A spherical pressure vessel of radius 1.0 m (3.3 ft) containing air ($\gamma_1 = 1.4$) bursts in a standard sea level atmosphere. The inside gas pressure is 1.013×10^6 Pa (147 psi) and the temperature is 300 K (80°F). There are no reflecting surfaces nearby. Find the peak overpressure and specific impulse at a distance of 5.0 m (16.4 ft) from the source.

Solution for peak overpressure:

\bar{R}_o and \bar{R} for the distance of interest are calculated. \bar{P}_{so} , the starting peak overpressure, is obtained from Figure 2-20. The correct curve is located in Figure 2-18 and P_s is read from the graph for the \bar{R} of interest.

$$\bar{R}_o = \frac{1}{\left[\frac{\frac{4\pi}{3} \left(\frac{P_1}{P_a} - 1 \right)}{\gamma_1 - 1} \right]^{1/3}} =$$
(2-16)

$$\frac{1}{\left[\frac{\frac{4\pi}{3} \left(\frac{1.013 \times 10^6 \text{ Pa}}{1.013 \times 10^5 \text{ Pa}} - 1 \right)}{1.4 - 1} \right]^{1/3}} = 0.2197$$

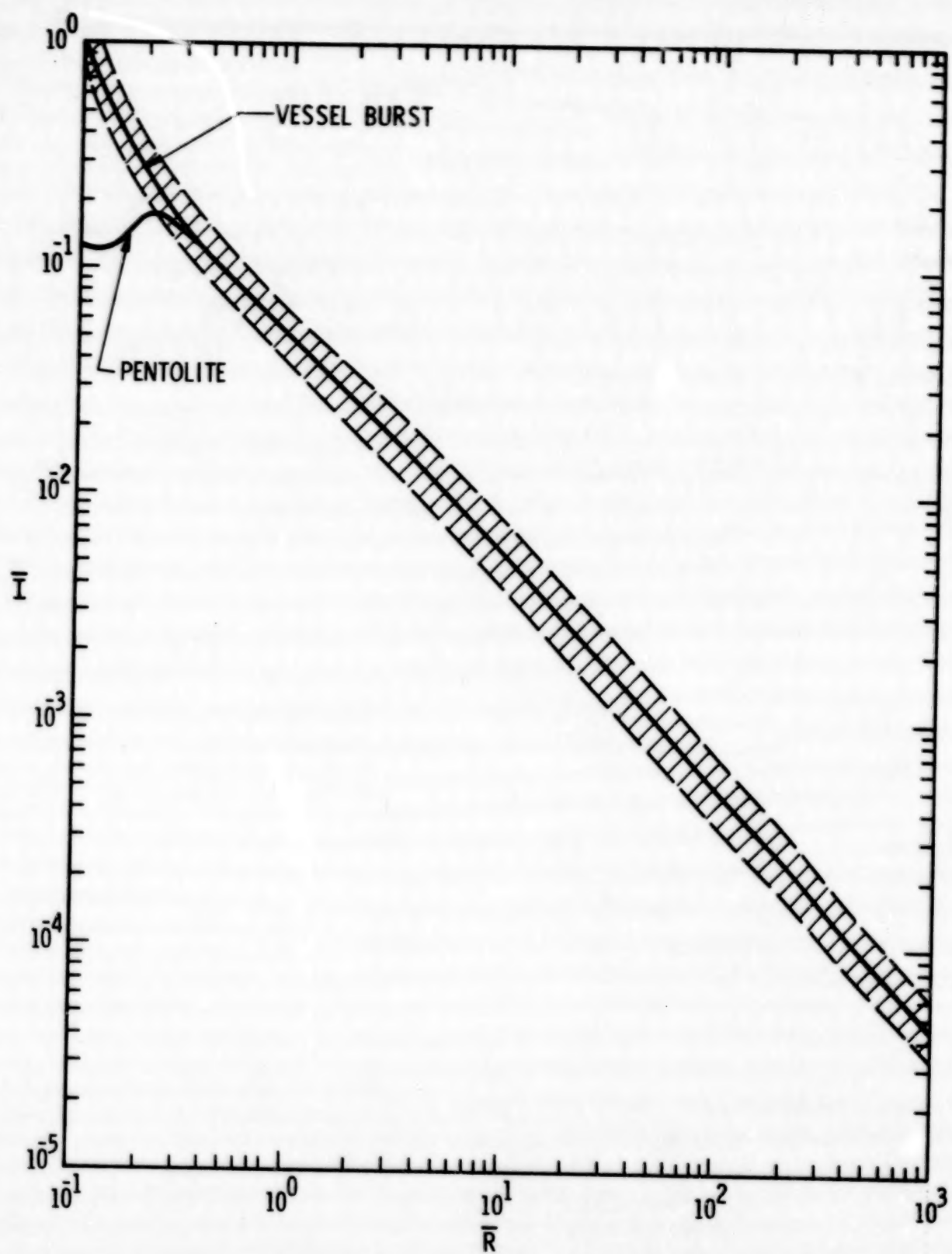


Figure 2-23. \bar{I} vs \bar{R} for Pentolite and Gas Vessel Bursts

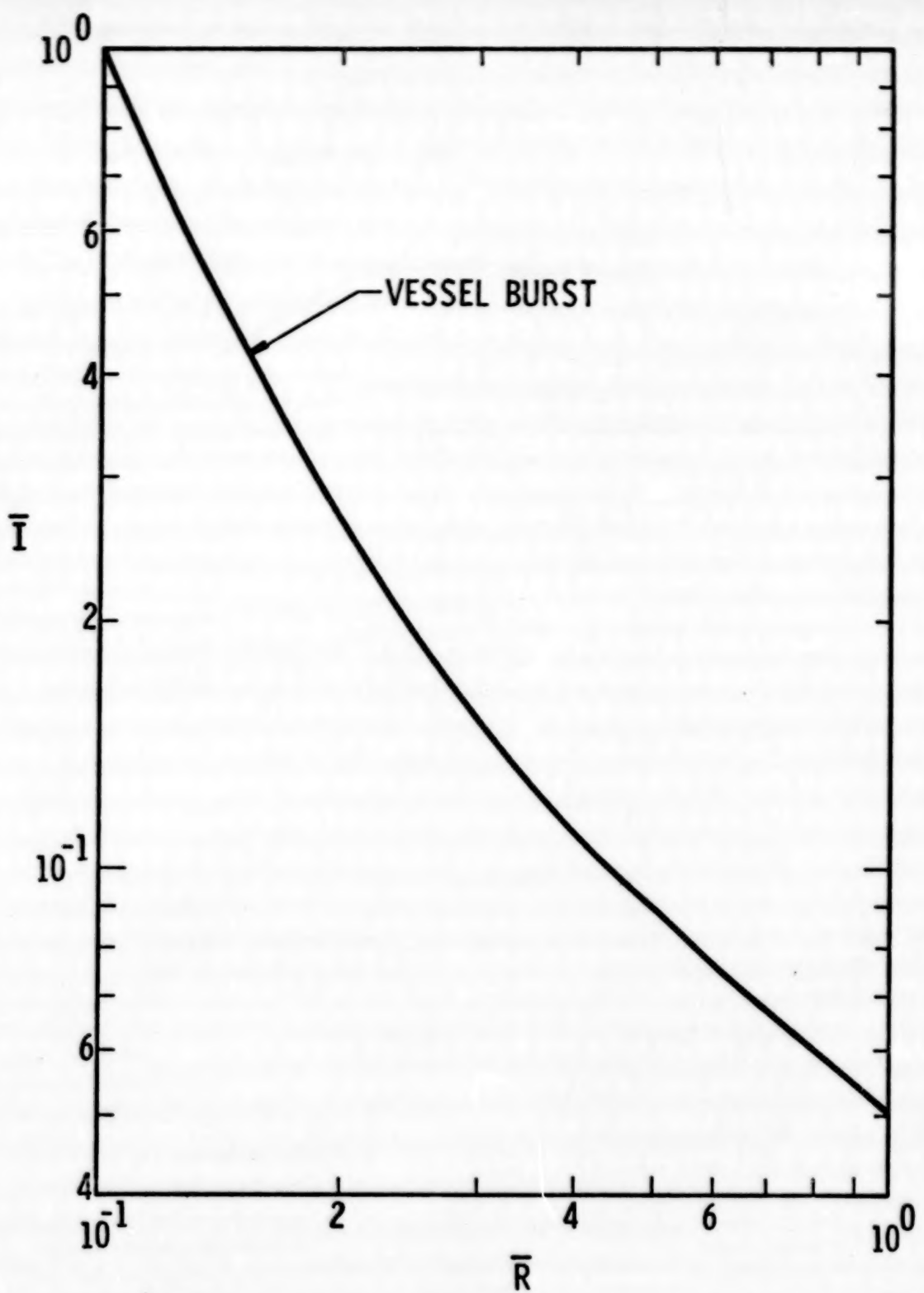


Figure 2-24. \bar{I} vs \bar{R} for Gas Vessel Bursts, Small \bar{R}

$$\bar{R} \text{ (at } r = 5.0 \text{ m)} = \left[\frac{\frac{4\pi r_o}{3}}{\left(\frac{P_1}{P_a} - 1 \right) \frac{\gamma_1 - 1}{r}} \right]^{1/3} =$$

(2-17)

$$\left[\frac{\frac{4\pi}{3}}{\left(\frac{1.013 \times 10^6 \text{ Pa}}{1.013 \times 10^5 \text{ Pa}} - 1 \right) \frac{1.4 - 1}{5.0 \text{ m} / 1.0 \text{ m}}} \right]^{1/3} = 1.099$$

For $P_1/P_a = 10$ and $T_1/T_a = 1$, $\bar{P}_{so} \approx 1.7$ (Figure 2-20). Looking at Figure 2-18, this point $(\bar{R}_o, \bar{P}_{so})$ falls near the third curve from the bottom. Following this curve, for $\bar{R} = 1.099$, $\bar{P}_s = 0.26$.

Since $\bar{P}_s = \frac{P_s - P_a}{P_a}$, $P_s - P_a = \bar{P}_s P_a = (0.26)(1.013 \times 10^5 \text{ Pa}) = 2.6 \times 10^4 \text{ Pa (3.77 psi)}$.

Solution for specific impulse:

The \bar{R} of interest has been calculated above. Read \bar{I} for this \bar{R} from Figure 2-23.

For $\bar{R} = 1.099$, $\bar{I} = 0.046$ (Figure 2-23).

$$\text{Since } \bar{I} = \frac{\bar{I} a_a}{P_a^{2/3} E^{1/3}}, \quad I = \bar{I} \frac{P_a^{2/3} E^{1/3}}{a_a}. \quad (2-18)$$

$$E = \left(\frac{P_1 - P_a}{\gamma_1 - 1} \right) \quad V_i = \left(\frac{1.013 \times 10^6 \text{ Pa} - 1.013 \times 10^5 \text{ Pa}}{1.4 - 1} \right)$$

(2-19)

$$\times \frac{4\pi}{3} (1.0 \text{ m})^3 = 9.55 \times 10^6 \text{ J}$$

$$I = \frac{(0.046)(1.013 \times 10^5 \text{ Pa})^{2/3} (9.55 \times 10^6 \text{ J})^{1/3}}{331 \text{ m/s}} = 64 \text{ Pa} \cdot \text{s}$$

(2-20)

$$(9.28 \times 10^{-3} \text{ psi} \cdot \text{sec})$$

2-3.3 Cylindrical Vessel

For a cylindrical vessel, given the length L and the diameter D , use its volume ($V_i = \frac{\pi D^2}{4} L$) in the equations above, performing the calculations as for a spherical vessel. After \bar{P}_s and \bar{I} have been determined, further corrections are necessary. For \bar{R} less than about 0.3, the calculated overpressure should be multiplied by a factor of 4 or 5. For \bar{R} near 1.0, the factor is 1.6. For \bar{R} greater than about 3.5, multiply the calculated overpressure by about 1.4. For \bar{R} less than about 0.3, the calculated specific impulse should be doubled. For \bar{R} near 1.0, the factor is about 1.1. For \bar{R} greater than about 1.6, no correction to the specific impulse is necessary. The difference between spherical and cylindrical vessel bursts is only known qualitatively. Therefore these corrections are very crude.

2-3.4 Ground Burst

The method described above is to be used for gas vessel bursts far from any reflecting surfaces. If there is a reflecting surface adjacent to the gas vessel, such as with a gas vessel on the ground, multiply V_i , the volume of the vessel, by a factor of 2. Use this new V_i in the calculations. Also, once \bar{P}_s has been calculated, increase it by 100% for \bar{R} less than about 1, and by 10% for \bar{R} greater than 1. After \bar{I} has been calculated, increase it by 60% for \bar{R} less than about 1. There is little effect for longer distances. Only qualitative effects are known, and therefore these corrections are very crude.

LIST OF REFERENCES

1. Fletcher, R. F., "Liquid-Propellant Explosions," Jour. of Space-craft and Rockets, 5, 10, pp 1227-1229, October 1968.
2. Willoughby, A. B., C. Wilton and J. Mansfield, "Liquid Propellant Explosive Hazards, Final Report-December 1968, Vol. I - Technical Documentary Report," AFRPL-TR-68-92, URS-652-35, URS Research Co., Burlingame, California.
3. Willoughby, A. B., C. Wilton and J. Mansfield, "Liquid Propellant Explosion Hazards, Final Report-December 1968, Vol. II - Test Data," AFRPL-TR-68-92, URS 652-35, URS Research Co., Burlingame, California.
4. Willoughby, A. B., C. Wilton and J. Mansfield, "Liquid Propellant Explosion Hazards, Final Report-December 1968, Vol. III - Prediction Methods," AFRPL-TR-68-92, URS 652-35, URS Research Co., Burlingame, California.
5. Strehlow, R. A., and W. E. Baker, "The Characterization and Evaluation of Accidental Explosions," Tech. Rep. AAE 75-3, Aero & Astr. Eng. Dept., U. of Ill., Urbana, Ill., June 1975 (also NASA CR 134779).
6. Baker, Wilfred E., Explosions in Air, University of Texas Press, Austin, Texas, May 1973.
7. Glasstone, Samuel (ed.), The Effects of Nuclear Weapons, U. S. AEC., 1962.
8. Kinney, Gilbert Ford, Explosive Shocks in Air, The Macmillan Co., New York, 1962
9. Cole, R. H., Underwater Explosions, Dover Publications, Inc., 1965.
10. Baker, W. E., V. B. Parr, R. L. Bessey and P. A. Cox, "Assembly and Analysis of Fragmentation Data for Liquid Propellant Vessels," NASA CR-134538, NASA Lewis Research Center, January 1974.

11. Kingery, C. N. and B. F. Pannill, "Peak Overpressure versus Scaled Distance for TNT Surface Burst (Hemispherical Charges)," BRL Memo Report No. 1518, Aberdeen Proving Ground, Maryland, April 1964, AD 443102.

APPENDIX II.A

GAS VESSEL BURST

2A-1. Nondimensional Parameters

A model analysis was performed for the pressurized gas-filled vessel burst. The following dimensionless parameters were obtained:⁽¹⁾

$$\bar{I} = \frac{\frac{I_a}{a}}{\frac{p_a^{2/3}}{E} \frac{1/3}{}} \quad \text{specific impulse} \quad (2A-1)$$

$$\bar{P}_s = \frac{p_s - p_a}{p_a} \quad \text{peak shock overpressure} \quad (2A-2)$$

$$\bar{R} = \frac{r p_a^{1/3}}{E^{1/3}} \quad \text{distance} \quad (2A-3)$$

2A-2. Source of Data

The data which were used in the shock overpressure and specific impulse calculations were generated numerically by a finite-difference computer program in which the one-dimensional (spherical coordinates) unsteady equations of conservation of mass, momentum, and energy in Lagrangian form are solved for a perfect gas. Artificial viscosity is used to smooth the shock waves.⁽²⁾

Previously, other investigators have used numerical methods to calculate the flow field variables after the burst of a pressurized sphere. Huang and Chou used the Hartree method of characteristics with Rankine-Hugoniot jump conditions across the shocks.⁽³⁾ Boyer, et al., used a numerical program similar to the one used here and compared their results to experimental data obtained by breaking glass spheres pressurized with air, He, and SF₆.⁽⁴⁾ Their values of nondimensional impulse versus distance fit in well with those calculated here.

Table 2A-1 gives the initial conditions of the cases that were run to generate the data used in this analysis.

TABLE 2A-1. INITIAL CONDITIONS FOR PRESSURE SPHERE BURSTS

<u>Case</u>	$\frac{P_1}{P_a}$	$\frac{T_1}{T_a}$	γ_1
1	5	0.5	1.4
2	5	2.54	1.4
3	5	10	1.4
4	5	50	1.4
5	10	0.5	1.4
6	10	50	1.4
7	100	0.5	1.4
8	100	50	1.4
9	150	50	1.4
10	500	50	1.4
A	94.49	1.0	1.4
B	94.49	1.167	1.2
C	94.49	0.84	1.667
11	37000	0.5	1.4
12	37000	5	1.4
13	37000	10	1.4
14	1000	1	1.4
15	1000	4	1.667
16	1000	0.5	1.4
17	5	5	1.4
18	22	1	1.4 (Ref. 4)

2A-3. Overpressure Calculation

The \bar{P}_s versus \bar{R} data were plotted for several sets of initial conditions, and it was found that the \bar{P}_s versus \bar{R} curves for high pressure bursts pass through the curves for lower pressures (see Figure 2A-1). (There is some crossing of the curves, but some of this is due to inaccuracy in the computer program). Therefore, if a number of curves were generated for high vessel pressures and various temperatures, the \bar{P}_s versus \bar{R} behavior for bursts at lower pressures could be determined by finding the starting point (\bar{R}_{q_0} , \bar{P}_{s0}) of a lower pressure burst and following the nearest \bar{P}_s versus \bar{R} curve.⁽⁵⁾ The curves in Figure 2-18 of the text were drawn based upon the curves in Figure 2A-1 of the appendix. Their uncertainty should not be assumed to be less than about $\pm 20\%$.

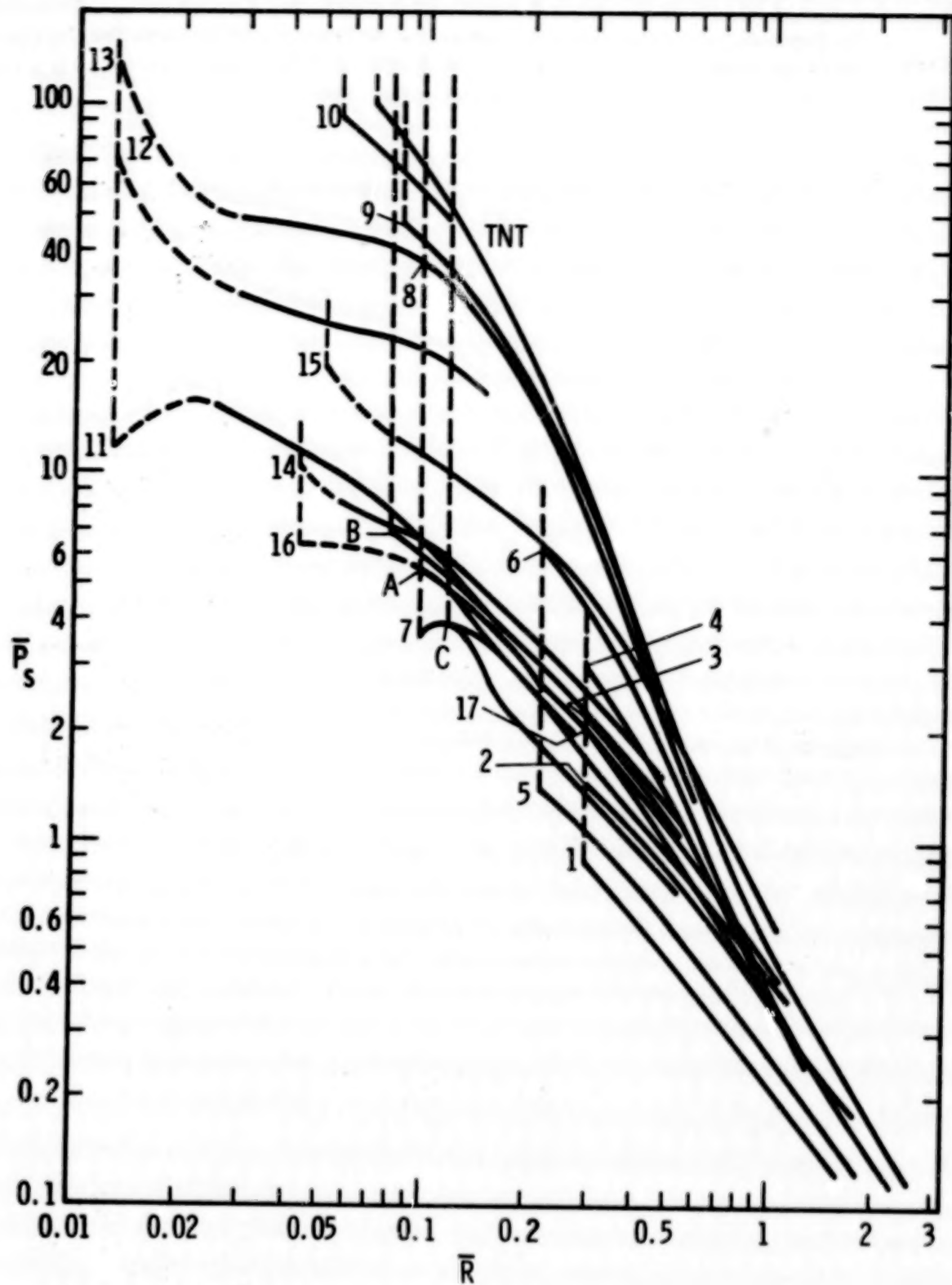


Figure 2A-1. \bar{P}_s vs \bar{R}

The starting distance \bar{R}_o corresponds to the surface of the vessel before it bursts, where $(r/r_o) = 1$.

$$\bar{R} = \frac{r}{\left[\left(\frac{p_1}{p_a} - 1 \right) \frac{V_i}{\gamma_1 - 1} \right]^{1/3}} = \frac{r}{\left[\left(\frac{p_1}{p_a} - 1 \right) \frac{\frac{4\pi r_o^3}{3}}{\gamma_1 - 1} \right]^{1/3}} = \quad (2A-4)$$

$$\frac{r}{\left[\left(\frac{p_1}{p_a} - 1 \right) \frac{\frac{4\pi}{3}}{\gamma_1 - 1} \right]^{1/3}}$$

$$\text{because } V_i = \frac{4\pi r_o^3}{3}. \quad (2A-5)$$

$$\text{Then } \bar{R}_o = \frac{1}{\left[\left(\frac{p_1}{p_a} - 1 \right) \frac{\frac{4\pi}{3}}{\gamma_1 - 1} \right]^{1/3}} \quad (2A-6)$$

\bar{P}_{so} is obtained by use of the shock tube equation: (6)

$$\frac{p_1}{p_a} = \frac{p_s}{p_a} \left[1 - \frac{(\gamma_1 - 1)(a/a_1)(p_s/p_a - 1)}{\sqrt{2\gamma_a} \sqrt{2\gamma_a + (\gamma_a + 1)(p_s/p_a - 1)}} \right]^{\frac{-2\gamma_1}{\gamma_1 - 1}} \quad (2A-7)$$

where $\frac{a}{a_1} = \sqrt{\frac{\gamma_a}{\gamma_1} \frac{T_a}{T_1}}$, and $\gamma_a = 1.4$. For a given $\frac{p_1}{p_a}$, $\frac{T_1}{T_a}$, and γ_1 , this equation must be solved iteratively for $\frac{p_s}{p_a}$. Then $\bar{P}_{so} = \frac{p_s}{p_a} - 1$.

The $\frac{P_1}{P_a}$ versus $\frac{T_1}{T_a}$ versus \bar{P}_{so} graphs (Figures 2-20 and 2-21 in the text) were obtained from this equation.

2A-4 Impulse Calculation

Specific impulse is calculated as $I = \int^+ (p - p_a) dt$, where + denotes the positive phase of the pressure wave. See Figure 2A-2.

The \bar{I} versus \bar{R} data were plotted for several sets of initial conditions (Figure 2A-3). For \bar{R} less than about 0.5, the behavior is not clear, and a maximum \bar{I} was chosen for the \bar{I} versus \bar{R} relationship in Figure 2-23 of the text. For \bar{R} greater than about 0.5, all of the curves lie within about 25% of the high explosive (pentolite) curve. The pentolite curve⁽⁷⁾ was therefore chosen as the best \bar{I} versus \bar{R} curve in this region.

2A-5 Effect of Cylindrical Geometry

This analysis can be used for bursts for cylindrically shaped pressure vessels if the volume V_i is known. The cylinder is treated as an "equivalent sphere" with same energy as the given cylinder.

Besides the energy in the vessel, its orientation with respect to the target is important. Qualitative relationships between \bar{P}_s and \bar{I} and the angle between the location of the target and the longitudinal axis of the vessel can be observed from the high explosive data in Reference 8. However, this angular orientation is usually unknown, and the "worst case" must be assumed. Then, the peak overpressure will be greater than that calculated for a spherical vessel for all \bar{R} . The specific impulse would also be greater in the near field.

2A-6 Effect of Reflecting Surface (Burst at Ground Level)

In this analysis, it was assumed that the vessel burst occurs far away from any reflecting surface. To apply this to a burst occurring on the ground, assume that twice as much energy is released, implying that the volume of the vessel is doubled. The reason for this is illustrated in Figure 2A-4. In (a), all of the energy is released above the reflecting ground surface. In (b) one-half of the energy is released above the reflecting ground surface, and one-half of the energy is released below. For a point P located above the ground surface to experience the same blast wave, the energy in vessel B must be twice the energy in vessel A. For the same pressure and ratio of specific heats of the gas, the volume of vessel B must be twice the vessel A. The situation in (b) is chosen because the analysis requires a spherically symmetric flow field.

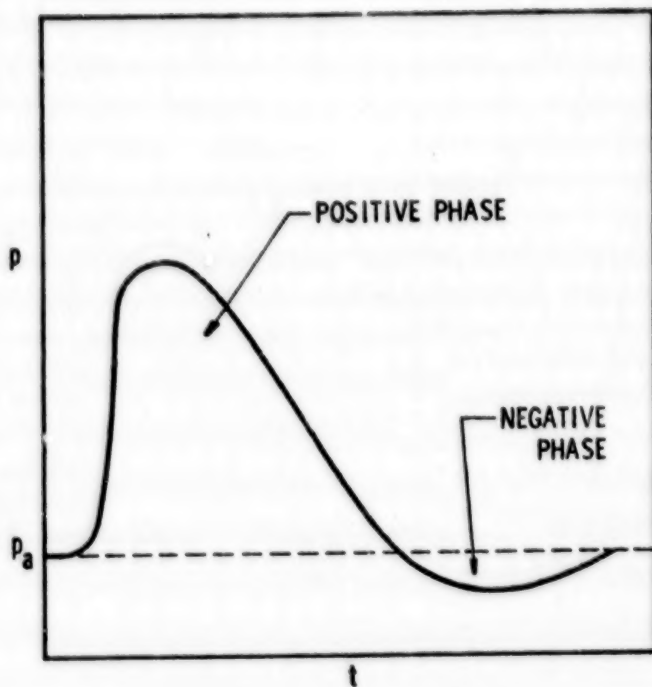


Figure 2A-2. p vs t

In addition to the effect upon the effective energy released, the presence of the ground surface must be accounted for in another way. Data in Reference 8 indicate that the peak overpressure should also be doubled near the source of the burst, and this factor should be decreased to unity in the far field. Those tests were conducted with high explosives, and, thus, only allow a qualitative description for pressure bursts, but it can be concluded that the overpressure would be greater for a sphere burst on the ground than would be expected from initial source energy considerations alone. The specific impulse would also be higher, at least in the near field.

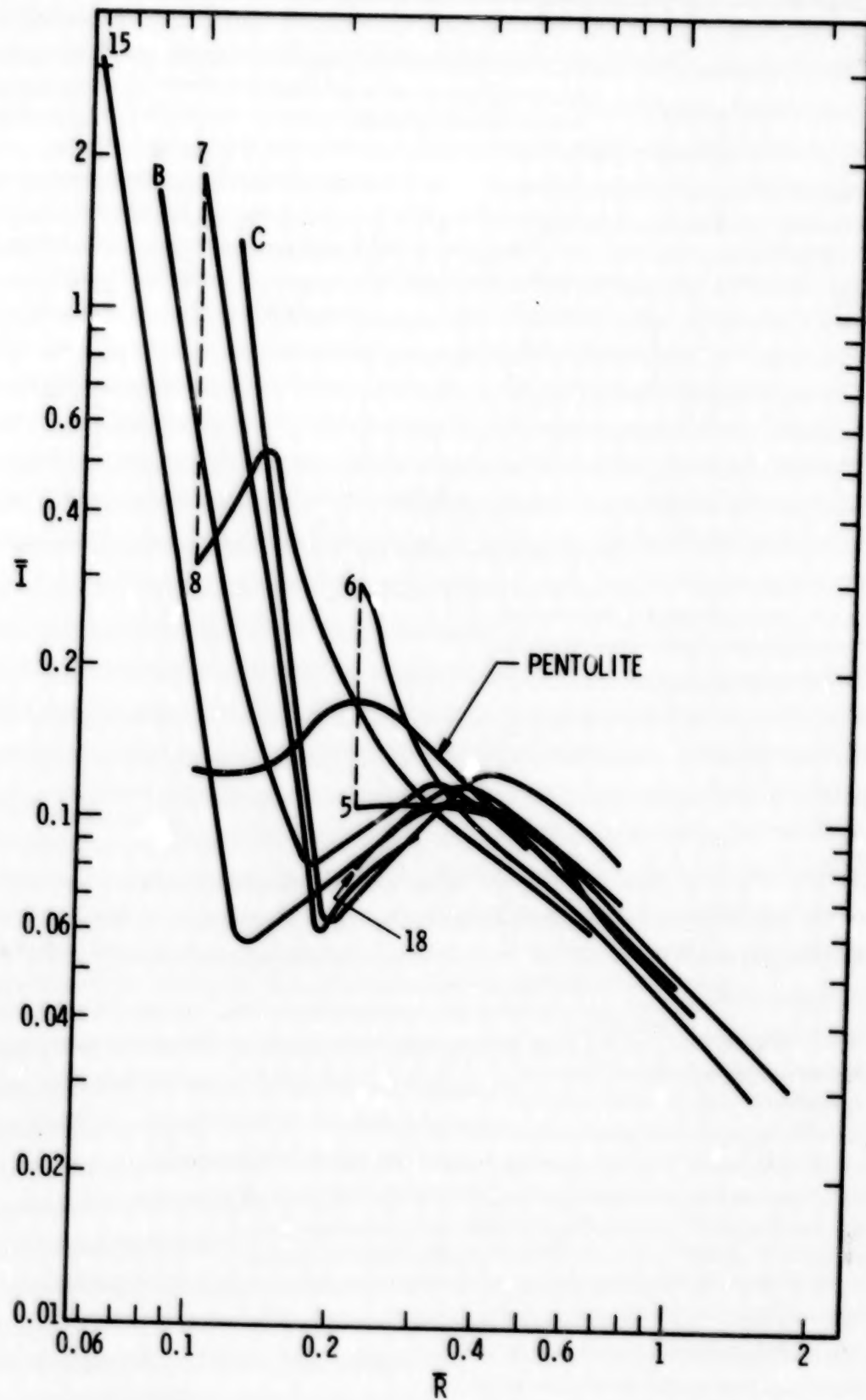
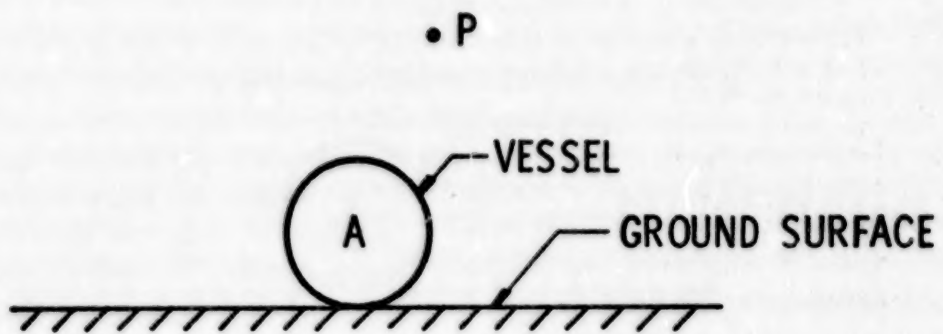
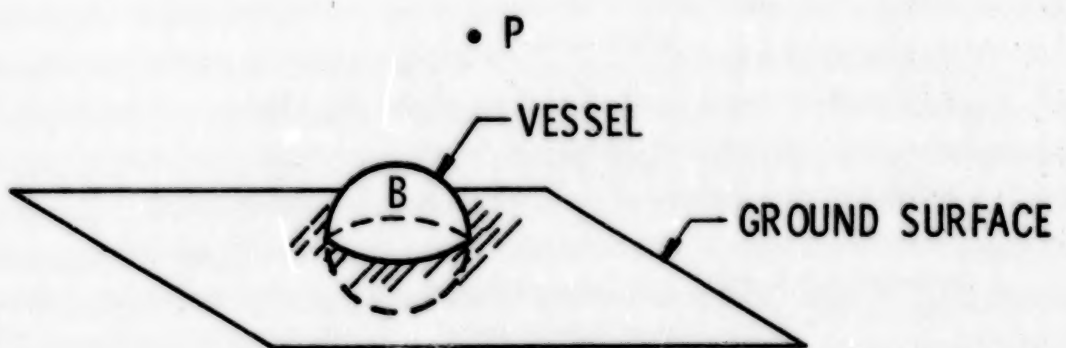


Figure 2A-3. \bar{I} vs \bar{R}



(a) Spherical vessel setting on ground surface



(b) Spherical vessel bisected by ground plane

Figure 2A-4. Assumed Spherical Geometry

LIST OF REFERENCES

1. Strehlow, Roger A., "Accidental Non-Ideal Explosions," Progress Report NASA NSG 3008, December 6, 1974.
2. Oppenheim, A. K., "Elementary Blast Wave Theory and Computations," Paper #I, Proceedings of the Conference on Mechanisms of Explosion and Blast Waves, J. Alstor, ed., Sponsored by the Joint Technical Coordinating Group for Air Launched Non-Nuclear Ordnance Working Party for Explosives, November 1973.
3. Huang, S. L., and P. C. Chou, "Calculations of Expanding Shock Waves and Late-Stage Equivalence," Drexel Institute of Technology Report 125-12, April 1968.
4. Boyer, D. W., H. L. Brode, I. I. Glass and J. G. Hall, "Blast from a Pressurized Sphere," UTIA Report No. 48, January 1958.
5. Ricker, Randall Edward, "Blast Waves from Bursting Pressurized Spheres," Department of Aeronautical and Astronautical Engineering, Master of Science Thesis, University of Illinois at Urbana-Champaign, May 1975.
6. Liepmann, H. W., and A. Roshko, Elements of Gasdynamics, John Wiley and Sons, Inc., New York, 1967.
7. Baker, Wilfred E., Explosions in Air, University of Texas Press, Austin, Texas, 1973.
8. Reisler, Ralph E., Louis Giglio-Tos, and George D. Teal, "Air Blast Parameters from Pentolite Cylinders Detonated on the Ground," BRL Memorandum Report No. 2471, April 1975.

SYMBOLS

a	speed of sound
D	diameter of cylinder
E	energy in pressure vessel
I	specific impulse
\bar{I}	nondimensional specific impulse
L	length of cylinder
p	pressure
\bar{P}_s	nondimensional overpressure
\bar{P}_{so}	starting nondimensional overpressure
r	distance from center of vessel
R	radius of sphere
\bar{R}	nondimensional distance
\bar{R}_o	nondimensional starting distance
r_o	radius of spherical vessel
t	time
T	temperature
V_i	volume of vessel before burst
γ	ratio of specific heats
θ	decay constant of pressure-time curve

SUBSCRIPTS

a	ambient conditions
s	behind shock wave
l	inside vessel before burst

CHAPTER III

EFFECTS OF PRESSURE WAVES

3-1 Damage Estimates to Structures

Previous sections have shown how to predict the peak free field side-on overpressure P_s and side-on impulse i_s at various locations around an accidental explosion. In this section, we show how to relate these two loading parameters to structural damage to buildings and vehicles in the vicinity. Before this discussion proceeds, the reader must decide what constitutes damage. For example, is breakage of glass and some damage to ceilings an acceptable or unacceptable level of damage? Or, can you accept minor structural damage with partitions distorted and joinery wrenched from fittings? On the other hand, might the target structure be dangerous to inhabit with the roof partially or totally collapsed, at least partial damage to one or more external walls, and some failed load-bearing structural members? Or, can one tolerate the building being 50% to 75% completely demolished? There is no one answer to what level of damage is acceptable. The engineer must decide for himself. If buildings are or can be inhabited by many people, the levels of damage should perhaps be low, while greater damage to individual dwellings could be tolerated.

Because different modes of response (or types of damage) must be considered, various solutions must be considered. The first solution deals with glass breakage. It yields a procedure for predicting the threshold of breakage of glass of various thickness and spans. The second solution is a curve fit to bomb damage data compiled by the British at the end of World War II. Although this curve fit was developed for a standard dwelling, it is also used for factories, main offices, and/or main engineering shops without introducing significant error. Three different empirical pressure versus impulse diagrams will be presented--the first is for minor structural damage involving wrenched joints and partitions, the second is for major structural damage with load bearing members at least partially destroyed, and the third is for 50% to 75% of the building demolished. These results yield general guidelines when accurate structural details are unknown. The third solution is for overturning a bus, truck, mobile home, missile on the launch pad, or other marginally stable target subject to toppling. The fourth and fifth solutions are for the initiation of yielding (the start of permanent deformation) in either beam or plate structural components. The beam elements can have

various support conditions. Plate elements can be either simply-supported* or clamped. These generalized solutions can be applied whenever the response of a structure looks critical and structural details are known in sufficient detail to override the second empirical solution based upon bombs damaging British residences. These generalized beam and plate solutions can be applied to many types of structures: cranes, frames, powerline towers, and components of houses and buildings. Each of the solutions will now be presented.

3-1.1 Breakage of Glass

The threshold applied pressure P_r for breaking glass can be determined from Equation (3-1).

$$\frac{P_r X^2}{\sigma_y h^2} = \frac{\left[1.0 + 3.08 \left(\frac{X}{Y} \right)^2 + \left(\frac{X}{Y} \right)^4 \right]}{8.68 \left[0.79 + 0.11 \left(\frac{X}{Y} \right)^2 + 0.79 \left(\frac{X}{Y} \right)^4 \right]^{1/2}} \quad (3-1)$$

where

σ_y = yield stress of glass [use Equation (3-2)]

h = thickness of glass

X = short half span

Y = long half span

P_r = threshold applied maximum reflected pressure

(The equation is valid for any self-consistent set of dimensions). Equation (1-1) works for either sheet or plate glass. The yield stress σ_y for glass, however, is not a simple material property, as in steel or other metals. The strength of glass is related to flaws which are both statistical in nature and a function of thickness. Although a complete theory of the kinematics of flaw behavior is not possible, the effective yield point for glass can be approximated by Equation (3-2).

*Simple support boundary conditions imply restriction of displacements at the boundaries, but no restraint on rotations.

$$[\sigma_y (\text{Pa})] [h(\text{m})] = 1.00 \times 10^{+6} \left(\frac{\text{N}}{\text{m}} \right) \quad (3-2)$$

The parameter P_r in Equation (3-1) is the peak applied load, and not the side-on free field overpressure P_s . For weak shocks with $P_s < 10 \text{ kPa}$ that strike a wall head-on, P_r equals $2.0 P_s$. For all shocks with flow parallel to a wall, P_r equals P_s . In general, the ratio P_r/P_s is a complex function of both shock strength P_s and the angle of incidence α . Figure 3-1 can be used to estimate P_r from P_s and α under ambient sea level atmospheric conditions. An α of 90° in Figure 3-1 means that the flow is parallel to the wall. All pressures in Figure 3-1 and this analysis are overpressures and not absolute pressures.

To illustrate the use of this solution, assume that a building has glass windows with panes that are 1.0 by 1.5×0.01 meters (3.28 by 4.92 by 0.0328 ft). Equation (3-2) indicates that the yield stress σ_y equals 10^{+8} Pa ($1.43 \times 10^4 \text{ psi}$). Because the aspect ratio X equals 0.6666,

Equation (3-1) gives a scaled applied load $\left(\frac{P_r X^2}{\sigma_y h^2} \right)^Y$ of 0.296. Sub-

stituting for σ_y , X , and h in the scaled applied load yields an applied pressure P_r of 2960 Pa (0.424 psi). Because this is a weak applied load, glass will begin to break in walls facing an accident whenever P_s

exceeds $\frac{P_r}{2}$ or 1480 Pa (0.212 psi). If the building has no glass in the walls facing the accident, but has glass in side walls, breakage will begin whenever P_s exceeds P_r or at 2960 Pa (0.424 psi).

The derivations of Equation (3-1) and (3-2) are presented in Appendix 3A. Equation (3-1) is a special case of a plate equation from subsequent sections: a brittle, simply-supported plate in the quasi-static loading realm. Experimental test data from static tests in the literature are also presented in Appendix 3A to demonstrate the validity of this solution. Figure 3-1 comes from curve fits to high-pressure data described in Reference 1.

3-1.2 Empirical Blast Damage Curves for Buildings

Figure 3-2 shows three different isodamage lines plotted as curves of side-on, free-field impulse versus side-on maximum overpressure. The basis for these curves is British data from enemy bombing in World War II plus records of explosions dating from 1871. Although this relationship was developed for the average British dwelling

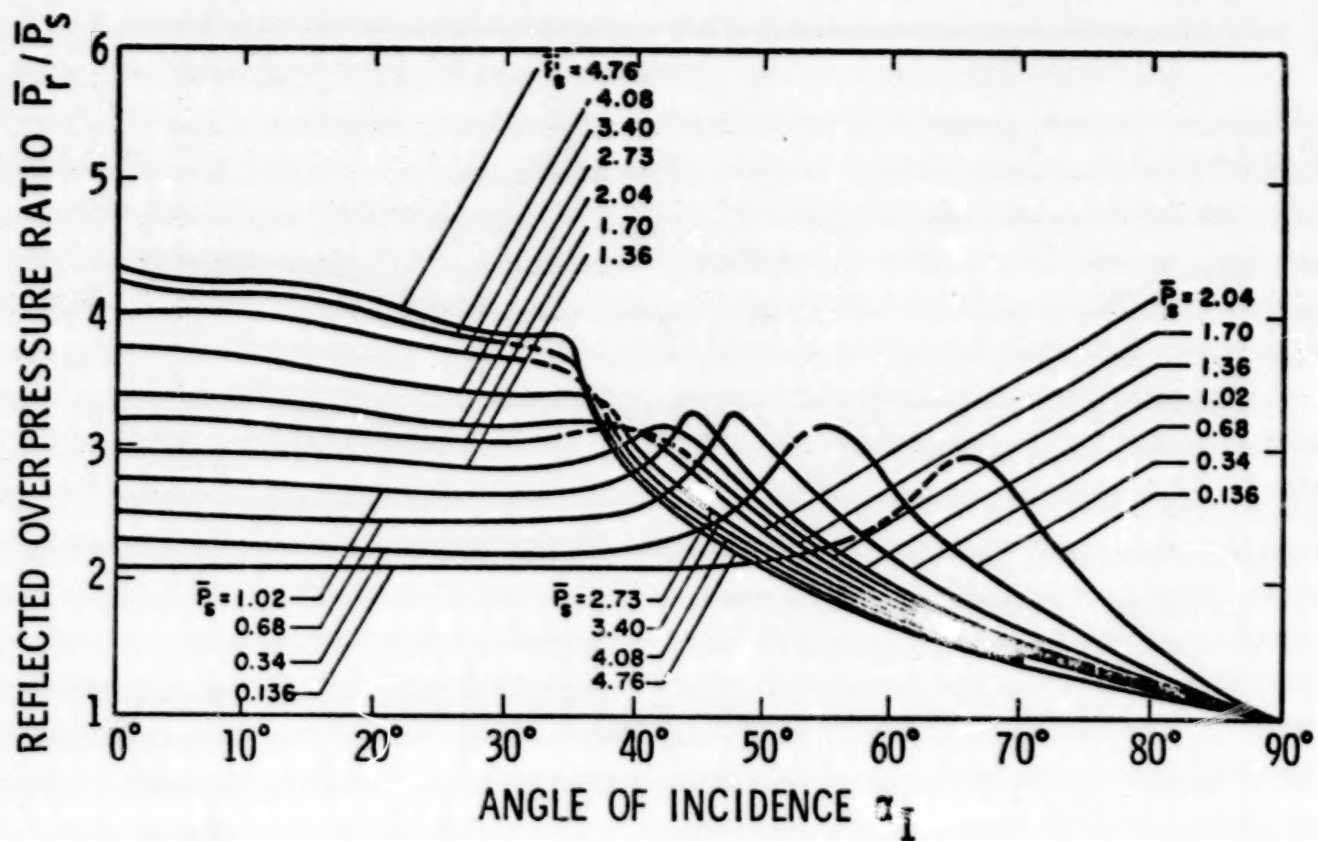


Figure 3-1. Reflected Overpressure Ratio as Function
of Angle of Incidence for Various Side-on
Overpressures

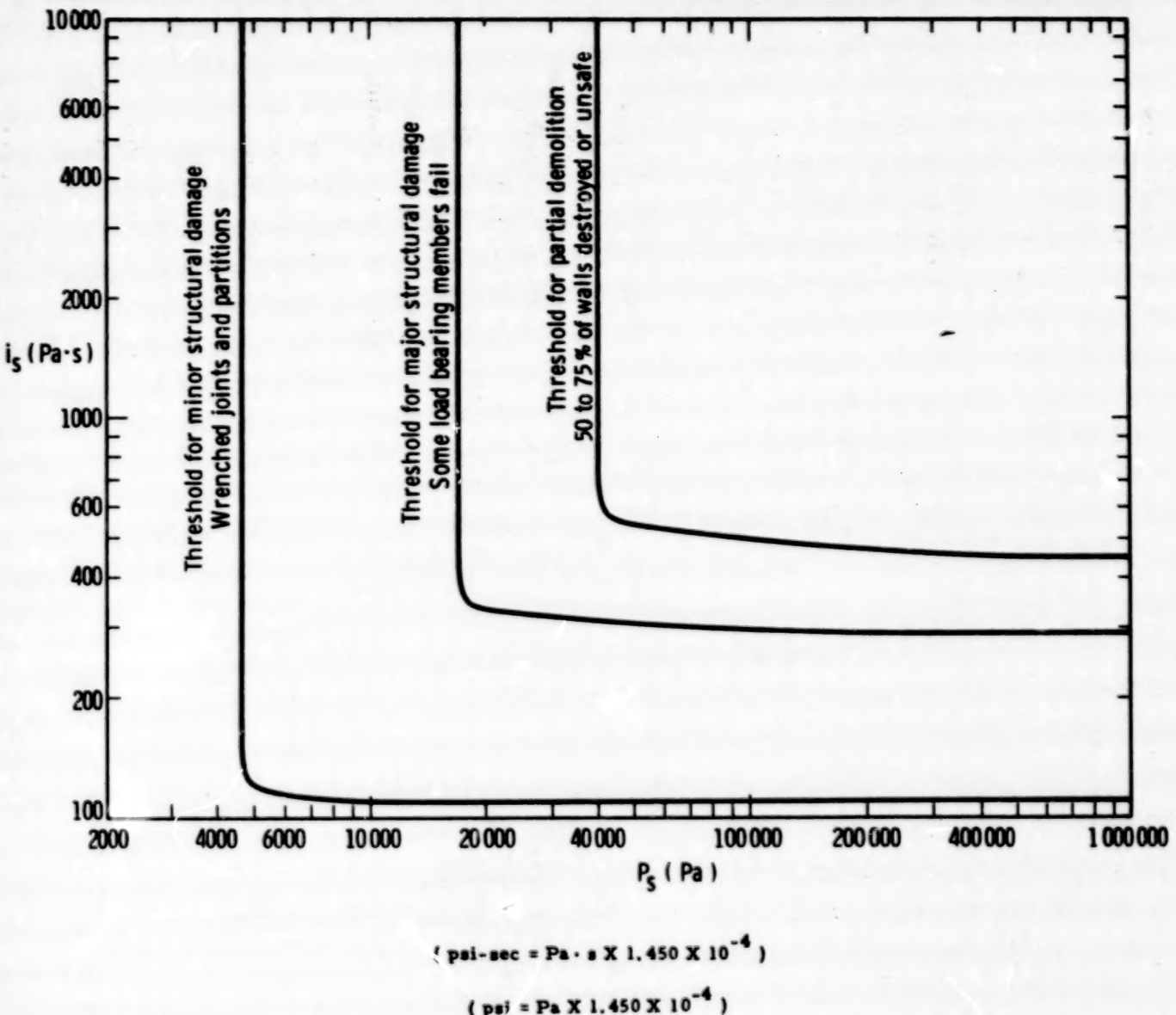


Figure 3-2. Pressure vs Impulse Diagram for Building Damage

house, it also works well for factories, main offices, and main engineering workshops. Reference 2 presents this relationship as a quantity-distance equation (charge weight versus standoff equation); however, we have modified the results so they can be presented as a pressure versus impulse diagram (a P-i diagram). Notice that as the level of damage increases, the pressures and impulses required to create the increased damage also increase. For pressures and impulses less than those shown in Figure 3-2, the specified magnitude of damage should not be obtained. The three levels of damage shown in Figure 3-2 are for minor structural damage, major structural damage, and partial demolition. By minor structural damage, we mean that glass has been broken, joints are wrenched, and partitions are out of some fittings. Major structural damage implies that the roof is partially or totally damaged, at least one external wall is partially damaged, and some load-bearing partitions or members have been destroyed. The term "partial demolition" implies that 50% to 75% of external brickwork or walls have been destroyed or rendered unsafe.

The British present an additional threshold for breakage of glass which we do not show in Figure 3-2. Most modern windows have larger spans and are often thinner than the standard window sizes associated with houses built in the 20's and 30's. The preceding analysis should be used if glass breakage constitutes serious damage. In addition, Jarrett presents a fifth contour for complete demolition. We do not present this contour because it is too extreme; a building suffering from partial demolition is uninhabitable and would have to be leveled.

Naturally, contours as presented in Figure 3-2 are approximations. These approximations suffice for large variations in structural types because the loads are also approximations. If a hardened structure or atypical building exists, damage can be better estimated by subdivision into its component plate and beam type elements. After a building has been subdivided into components, equations presented in subsequent sections can be applied to determine loads for initiating fracture in brittle structures and permanent deformation in ductile structures. These subsequent analysis procedures are more difficult to use than the graphical relationships shown in Figure 3-2; however, if they are properly applied, they can supplant Figure 3-2.

To illustrate the use of Figure 3-2, consider several illustrative examples. For example, suppose the free field blast conditions were P_s equal to 10 kPa (1.45 psi), i_s equal to 200 Pa·s (0.0290 psi-sec), then minor structural damage should be expected, but not major structural damage. On the other hand, if P_s equaled 50 kPa (7.25 psi) and i_s equaled 1000 Pa·s (0.145 psi-sec), partial demolition should be expected.

Finally, if P_s equaled 700 Pa (0.101 psi) and i_s equaled 70 Pa·s (0.0101 psi·sec), no damage should be expected unless the previous analysis indicated that glass would break.

3-1.3 Overturning

Trucks, buses, mobile homes, missiles on the launch pad, and various other objects can be damaged because they overturn when enveloped by a blast wave from an accidental explosion. To determine if a target overturns, we use two different graphs. The first graph, Figure 3-3, allows us to calculate the total average specific impulse i_t imparted to the target. The second graph, Figure 3-4, allows us to calculate the average specific impulse i_0 that is the threshold of overturning. If i_t imparted to the target exceeds i_0 , the target should overturn; however, if i_t is less than i_0 , the loading is insufficient to overturn the target. Both Figures 3-3 and 3-4 are nondimensional, so any self-consistent set of units can be used. The scaled total impulse imparted to a target

$$\left(\frac{a_o i}{p_o H} \right)$$
 in Figure 3-3 is a function of the scaled free-field pressure

$$P_s / p_o$$
 and the scaled free-field impulse $\left(\frac{a_o C_D i_s}{p_o H} \right)$ where p_o is

ambient atmospheric pressure, a_o is ambient sound velocity, P_s is side-on free-field overpressure, i_s is free-field side-on impulse, H is the smaller of either the target height or target width, and C_D is an air drag coefficient. For typical trucks, buses and other vehicles, H is the total height h of the vehicle. For missiles or other tall narrow objects, H is the diameter of the missile. The air drag coefficient C_D varies between 1.2 for streamlined cylindrical bodies to 1.8 for long rectangular shapes. In Figure 3-4 the scaled threshold impulse for just overturning an object is presented as a function of scaled target height

$$\left(\frac{h}{b} \right)$$
 and scaled c.g. location $\left(\frac{h_{cg}}{h} \right)$, where h is the total height

of the target, h_{cg} is the height of the c.g. location, h_{cp} is the height for the center of pressure, A is the presented target area, b is the vehicle track width or depth of target base, g is the acceleration of gravity, m is the total mass of the target, and i_0 is the threshold impulse. The analysis assumes that the target is not initially tilted, the c.g. is located at $\left(\frac{b}{2} \right)$ and the mass is uniformly distributed throughout the target. Use of these graphs to obtain answers is best presented through illustrative example.

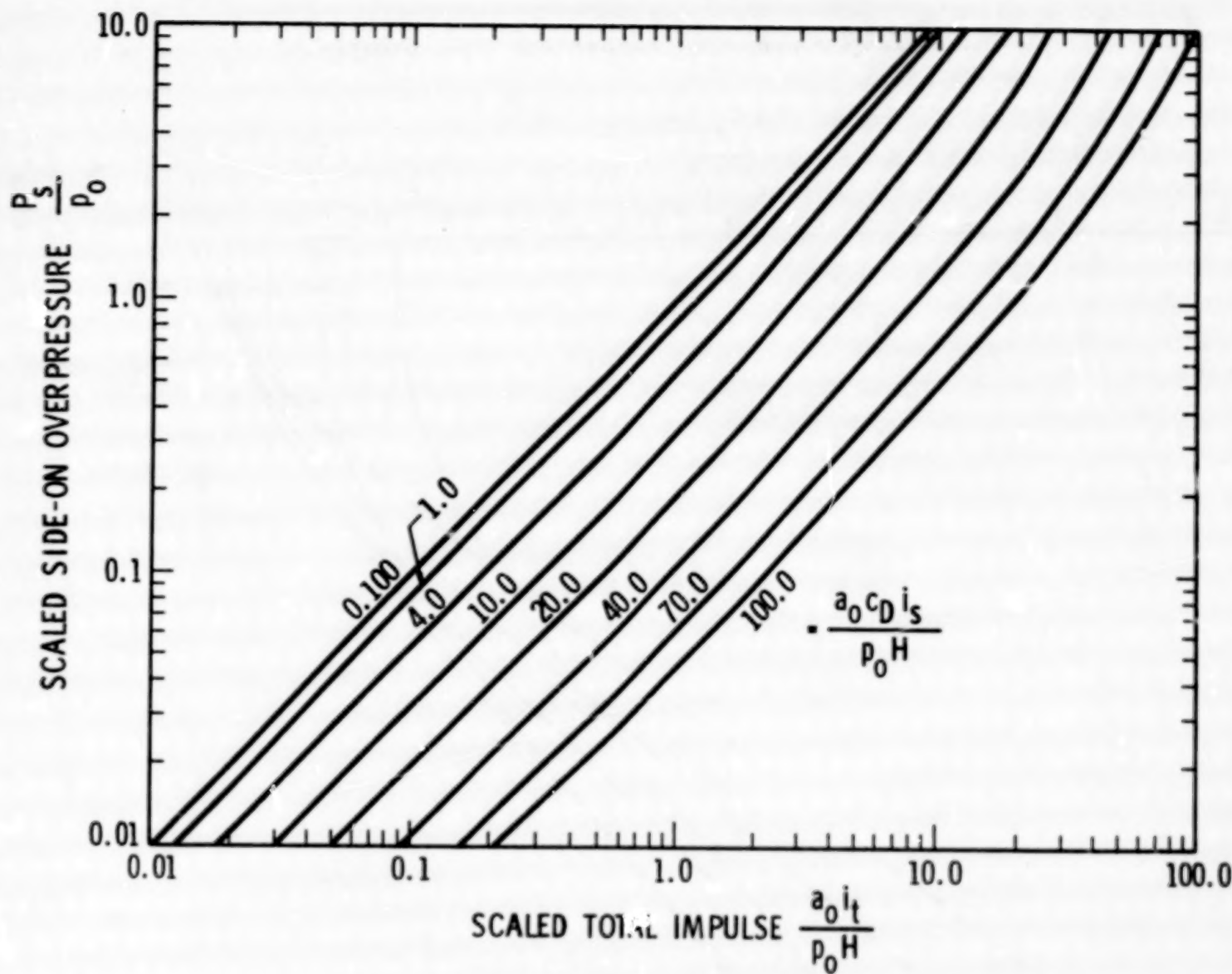


Figure 3-3. Specific Impulse Imparted to a Target
Which Might Overturn

TABLE OF CONTENTS

	<u>Page</u>
INTRODUCTION	1 1/A12
I. ESTIMATES OF EXPLOSIVE YIELD	8 1/B5
1-1 Explosive Yield as a Function of Propellant Type and Accident Conditions	8 1/B5
1-2 Explosive Yield as a Function of Fluid Type and Initial Conditions for Gas Vessel Bursts	26 1/C9
List of References	29 1/C12
II. CHARACTERISTICS OF PRESSURE WAVES	31 1/C14
2-1 General	31 1/C14
2-2 Pressure Waves from Propellant Explosions	40 1/D9
2-3 Pressure Waves from Gas Vessel Bursts	56 1/E11
List of References	68 1/F9
II. A GAS VESSEL BURST	70 1/F11
2A-1 Nondimensional Parameters	70 1/F11
2A-2 Source of Data	70 1/F11
2A-3 Overpressure Calculation	71 1/F12
2A-4 Impulse Calculation	74 1/G1
2A-5 Effect of Cylindrical Geometry	74 1/G1
2A-6 Effect of Reflecting Surface (Burst at Ground Level)	74 1/G1
List of References	78 1/G5
Symbols	79 1/G6

TABLE OF CONTENTS (Cont'd)

		<u>Page</u>
III.	EFFECTS OF PRESSURE WAVES	80 1/G7
3-1	Damage Estimates to Structures	80 1/G7
3-2	Injury Estimates to Humans	99 2/B3
	List of References	125 2/D1
III.A	STRUCTURAL RESPONSE	128 2/D4
3A-1	Overshoot Analysis	128 2/D4
3A-2	Development of Beam Equations	134 2/D10
3A-3	Development of Plate Equations	142 2/E4
3A-4	Development of Membrane Equations	153 2/F1
	List of References	158 2/F6
III.B	PRESSURE/IMPULSE COMBINATIONS PRODUCING LUNG DAMAGE	159 2/F7
	List of References	169 2/G3
III.C	PRESSURE/IMPULSE COMBINATIONS PRODUCING LOSS OF HEARING	171 2/G5
	List of References	175 2/G9
III.D	PRESSURE/IMPULSE COMBINATIONS PRODUCING WHOLE-BODY DISPLACEMENT AND SUBSEQUENT DAMAGE TO THE HEAD AND BODY	176 2/G10
	List of References	190 3/B1
IV.	CHARACTERISTICS OF FRAGMENTS	191 3/B2
4-1	General	191 3/B2
4-2	Methods for Estimating Fragment Initial Velocities for Spheres and Cylinders Bursting into Many Fragments	191 3/B2

TABLE OF CONTENTS (Cont'd)

	<u>Page</u>
4-3 Estimate of Initial Velocities of Fragments from Spheres and Cylinders Bursting into Two Equal Halves	218 3/D1
4-4 Determination of Appurtenance Velocity	228 3/D11
4-5 Methods for Computing Fragment Ranges and Impact Conditions	240 3/E9
4-6 Fragment Mass Distribution	279 4/All
4-7 Probability of Fragment Arrival Versus Range	286 4/B4
List of References	292 4/B10
IV. A METHODS FOR ESTIMATING FRAGMENT INITIAL VELOCITIES	293 4/B11
List of References	315 4/D5
IV. B COMPARISON OF EXPERIMENTAL RESULTS WITH CODE PREDICTIONS	316 4/D6
List of References	318 4/D8
IV. C ESTIMATE OF INITIAL VELOCITIES OF FRAGMENTS FROM SPHERES AND CYLINDERS BURSTING INTO TWO EQUAL HALVES	319 4/D9
List of References	354 4/G2
IV. D ESTIMATION OF VELOCITIES ATTAINED BY APPURTENANCES SUBJECTED TO BLAST LOADING	355 4/G3
List of References	377 5/B2
IV. E ANALYSES FOR FRAGMENT TRAJECTORIES	378 5/B3
List of References	401 5/C12

TABLE OF CONTENTS (Cont'd)

	<u>Page</u>
IV.F STATISTICAL FITTING TO FRAGMENT DATA	402 5/C13
4F-1 Derivation of Figures 4-46 Through 4-49	402 5/C13
4F-2 Derivation of Figure 4-50	402 5/C13
4F-3 Rationale for Averaging Fragment Mass Distribution for Events 3, 4, and 5	403 5/C14
4F-4 Fragment Mass Distributions for Gas Vessel Bursts	406 5/D3
4F-5 Rationale for Averaging Fragment Mass Distributions for Tanks A and B and Tanks D and E	412 5/D9
4F-6 Derivation of Figure 4-57, Fragment Distance Versus Percent Yield for Propellant Explosions	413 5/D10
4F-7 Derivation of Simulated Fragment Range Distribution for Gas Vessel Bursts	415 5/D12
4F-8 Rationale for Combining Simulated Range Distribution for Tanks A and B and for Tanks D and E	423 5/E6
List of References	424 5/E7
V. EFFECTS OF FRAGMENTS	425 5/E8
5-1 Damage Estimates to Structures and Facilities	425 5/E8
5-2 Damage Estimates to People from Secondary Fragments	433 5/F2
List of References	442 5/F11
V.A EFFECTS OF FRAGMENTS ON STRUCTURES	444 5/F13
List of References	446 5/G1

TABLE OF CONTENTS (Concl'd)

	<u>Page</u>
V. B DAMAGE ESTIMATES TO PEOPLE FROM SECONDARY FRAGMENTS	447 5/G2
5B-1 Penetrating Fragments	447 5/G2
5B-2 Nonpenetrating Fragments	455 5/G10
List of References	456 5/G11
VI. RISK ASSESSMENT AND INTEGRATED EFFECTS	458 5/G13
6-1 Risk Assessment	458 5/G13
6-2 Prediction of Relative Blast and Fragment Effects	461 6/A7
List of References	507 6/D11
VII. DISCUSSION OF RESULTS	508 6/D12
VIII. CONCLUSIONS	511 6/E1
IX. RECOMMENDATIONS	513 6/E3
LIST OF SYMBOLS	516 6/E6
CONVERSION FACTORS	523 6/E13
GLOSSARY OF TERMS	525 6/F1
BIBLIOGRAPHY	528 6/F4

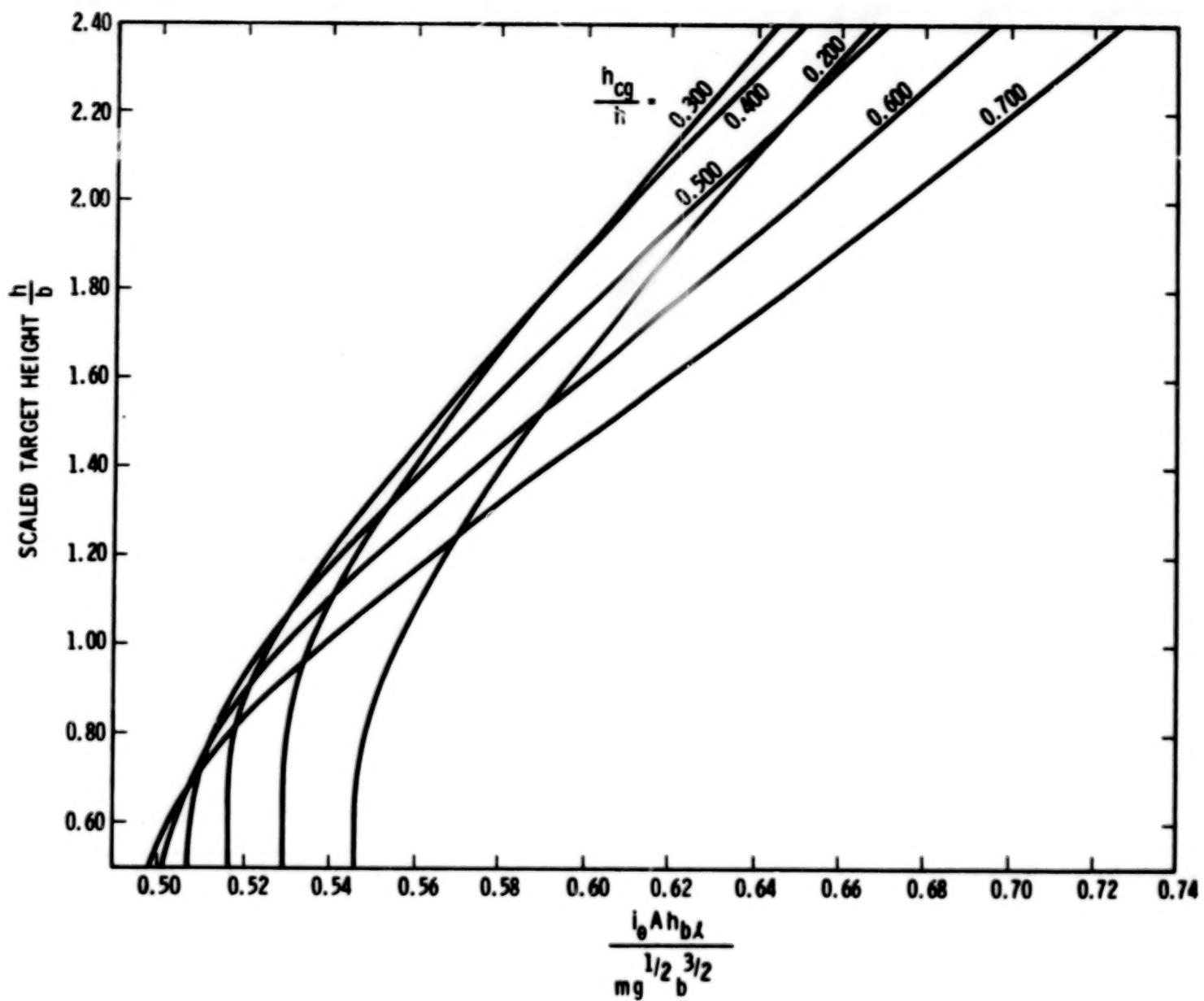


Figure 3-4. Impulse for Threshold of Overturning

Presume that a 2-1/2 ton truck is located such that the free-field pressure P_s equals 310 kPa (43.5 psi) and the free-field impulse i_s equals 1210 Pa·s (0.170 psi·sec). Such a vehicle has a height of 2.93 m (9.61 ft) a c.g. height of 1.37 m (4.49 ft), a vehicle track width of 1.77 m (5.81 ft), a cross-sectional area of 14.8 m^2 (159 ft^2) and a mass of 5430 kg ($1.19 \times 10^4 \text{ lb}_m$). If we assume that the drag coefficient equals 1.8, that atmospheric pressure is 101 kPa (14.7 psi) and that the velocity of sound in air is 329 m/sec (1079 ft/sec), then the scaled free-field pressure (P_s/p_o) is 3.06 and the scaled free-field impulse $\left(\frac{a_o C_D i_s}{p_o H}\right)$ is 2.41. Enter-

ing Figure 3-3 gives a scaled applied impulse $\left(\frac{a_o i_t}{p_o H}\right)$

of 3.93. Multiplying the scaled impulse by p_o and by H and dividing it by a_o then gives the applied specific impulse i_t of 3,547 Pa·s (0.498 psi·sec). This numerical value for i_t must be compared to i_{θ} obtained from

Figure 3-4. First the scaled target height $\left(\frac{h}{b}\right)$ and

scaled c.g. location $\left(\frac{h_{cg}}{h}\right)$ must be calculated. They equal 1.65 and 0.468, respectively. Entering Figure 3-4

yields a scaled critical threshold impulse $\left(\frac{i_{\theta} A h_{b\ell}}{m g^{1/2} b^{3/2}}\right)$

of 0.585. Multiplying the scaled impulse by m , $g^{1/2}$, and $b^{3/2}$ plus dividing by A and $h_{b\ell}$ (which is assumed to equal half the total height of the vehicle) yields the critical threshold impulse i_{θ} of 1081 Pa·s (0.113 psi·sec). Because the example has an applied impulse i_t that is greater than the critical threshold impulse i_{θ} (3547 Pa·s or 0.498 psi·sec), we would predict that the vehicle should overturn. This illustrative example described an actual experiment included in test data from Appendix 3A. The vehicle did overturn, as predicted.

The equation shown graphically in Figure 3-3 is:

$$\frac{a_o i_t}{P_o H} = \frac{1.47 \left(\frac{P_s}{P_o} \right) \left(\frac{a_o C_D i_s}{P_o H} \right)}{\left[7.0 + \left(\frac{P_s}{P_o} \right) \right]} +$$

$$\frac{\left[1.0 + \frac{3 \left(\frac{P_s}{P_o} \right)}{\left[7.0 + \left(\frac{P_s}{P_o} \right) \right]} \right] \left(\frac{P_s}{P_o} \right)}{\left[1.0 + 0.857 \left(\frac{P_s}{P_o} \right) \right]^{1/2}} \quad (3-3)$$

The equation shown graphically in Figure 3-4 is:

$$\frac{i_{\theta} A h b l}{m g^{1/2} b^{3/2}} = \left\{ \left[\frac{2}{3} + \frac{h^2}{6b^2} + \frac{2h^2}{b^2} \left(\frac{h_{cg}}{h} \right)^2 \right] x \right.$$

$$\left. \left[-\sqrt{\frac{1}{4} + \left(\frac{h^2}{b^2} \right) \left(\frac{h_{cg}}{h} \right)^2} - \left(\frac{h}{b} \right) \left(\frac{h_{cg}}{h} \right) \right] \right\}^{1/2} \quad (3-4)$$

Both equations are derived in Appendix 3A. In addition, experimental test data are used in Appendix 3A to demonstrate the validity of this solution.

3-1.4 Response of Beam Type Elements

Figure 3-5 is a load versus impulse diagram for the initiation of permanent deformation in beam-type structural elements. Three different curves are shown for simply-supported, clamped-clamped, or cantilever boundary conditions. Any self-consistent set of units can be used in Figure 3-5, as both ordinate and abscissa are nondimensional. The ordinate $\left(\frac{i b h \sqrt{E}}{\sigma_y \sqrt{\rho I A}} \right)$ is a scaled applied impulse, and the abscissa,

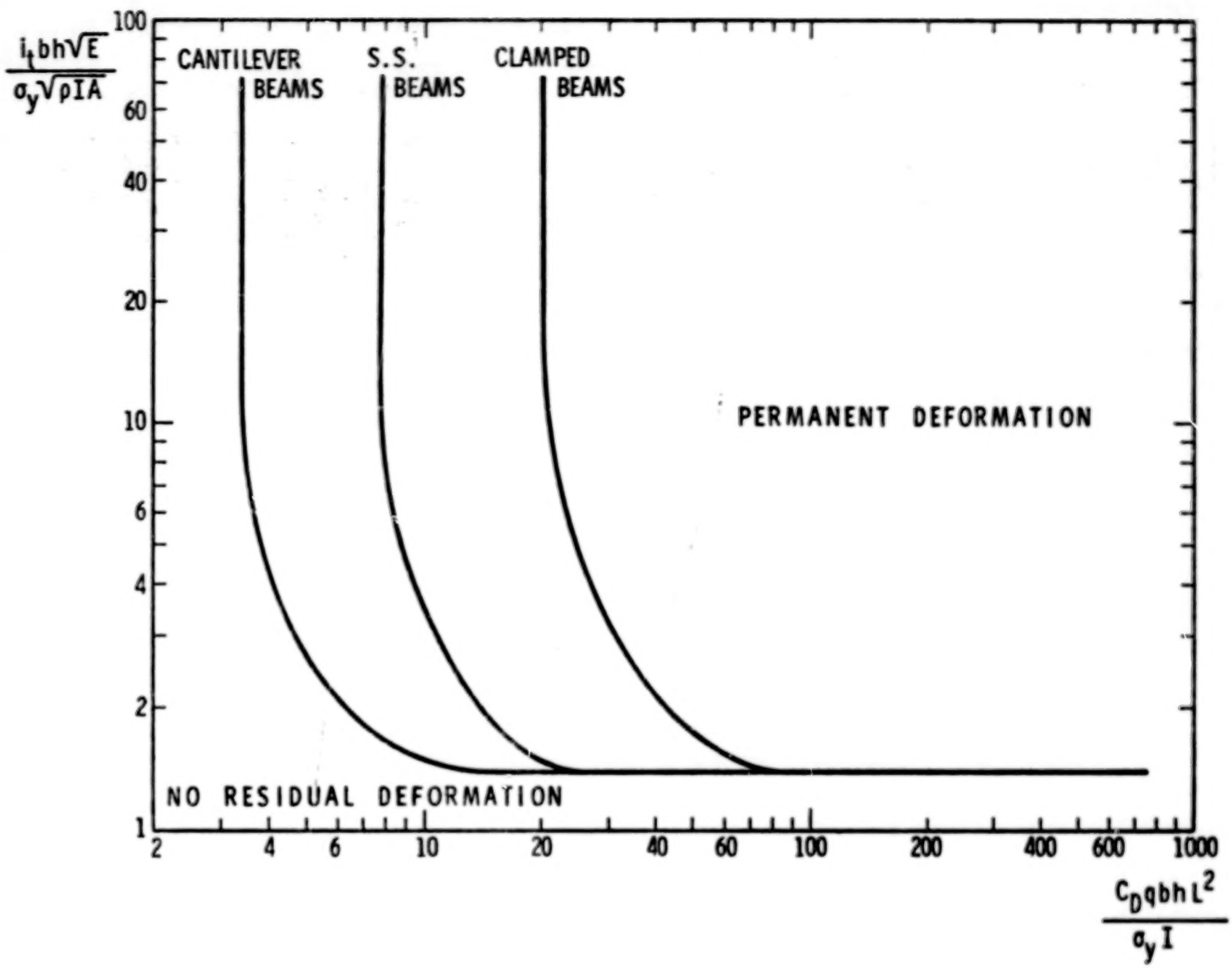


Figure 3-5. Normalized Load-Impulse Diagram for Beams

$$\left(\frac{C_D q b h L^2}{\sigma_y I} \right) \quad \text{is a scaled applied maximum drag pressure, where } i_t$$

is specific impulse, b is beam width, h is beam thickness, E is modulus of elasticity, σ_y is the yield stress, ρ is beam density, I is the second moment of area, A is the cross-sectional area, C_D is a drag coefficient, q is the drag pressure, and L is the beam length. If the applied impulses and pressures are greater than the threshold ones, the beam will permanently deform, but if the impulses and pressures are less than the threshold ones, no permanent deformation will occur. The quantities b , h , E , σ_y , ρ , I , A , and L are all straightforward beam properties. the loads i_t and $C_D q$ are loads imparted to the beam which must be computed from free-field pressure P_s and impulse i_s . If a beam is open so the blast can diffract around it, the drag pressure q is given by:

$$q = \left(\frac{1}{2} \right) \rho_1 u_1^2 \quad (3-5)$$

where

$$\frac{\rho_1}{\rho_0} = \frac{(\gamma - 1) + (\gamma + 1)}{(\gamma + 1) + (\gamma - 1)} \cdot \frac{\left(\frac{P_0 + P_s}{P_0} \right)}{\left(\frac{P_0 + P_s}{P_0} \right)}$$

$$\frac{u_1}{U} = \frac{2 \left(\frac{P_s}{P_0} \right)}{(\gamma - 1) + (\gamma + 1) \left(1 + \frac{P_s}{P_0} \right)}$$

$$\frac{U}{a_0} = \left\{ \frac{1}{2\gamma} \left[(\gamma - 1) + (\gamma + 1) \left(1 + \frac{P_s}{P_0} \right) \right] \right\}^{1/2}$$

and

p_0 = ambient atmospheric pressure

γ = ratio of specific heats for air (about 1.4)

a_0 = ambient speed of sound in air

ρ_0 = ambient mass density of air

The drag coefficient C_D for most beams should equal 1.8. To compute the applied impulse i_t for a beam in the open, use Figure 3-3 with H equal to the beam width b .

If the beam equations are being used as a strip out of a very long plate such that shock cannot diffract around it, then the peak reflected pressure P_r should be substituted for $(C_D q)$ and the reflected impulse i_r should be used for i_t . Figure 3-1 can be used to calculate P_r from the side-on pressure P_s and angle of incidence α . Peak reflected impulse i_r can also be estimated from this same figure. The ratio

$\left(\frac{i_r}{i_s}\right)$ equals the ratio $\left(\frac{P_r}{P_s}\right)$ as found in Figure 3-1, for all practical purposes.

We will now illustrate the use of this analysis with an illustrative problem:

Consider a simply-supported 8 WF 20 steel beam with a 10.0 m (32.8 ft) span, made of 1015/1018 steel, and located in a free-field blast of $P_s = 40 \text{ kPa}$ (5.62 psi) and $i_s = 450 \text{ Pa} \cdot \text{s}$ (0.0632 psi-sec). This particular beam has a $\sigma_y = 3.17 \times 10^{18} \text{ Pa}$ ($4.45 \times 10^4 \text{ psi}$), $E = 2.07 \times 10^{11} \text{ Pa}$, $\rho = 7845 \text{ kg/m}^3$ (0.284 lb_m/in³), $h = 0.207 \text{ m}$ (0.679 ft), $A = 0.00379 \text{ m}^2$ (0.0409 ft²), $b = 0.134 \text{ m}$ (0.440 ft), and $I = 2.88 \times 10^{-5} \text{ m}^4$ ($3.34 \times 10^{-3} \text{ ft}^4$). If this beam is unconfined and under sea level ambient atmospheric conditions where $\rho_0 = 1.225 \text{ kg/m}^3$ ($4.43 \times 10^{-5} \text{ lb}_m/in^3$), $p_0 = 1.01 \times 10^5 \text{ Pa}$ (14.7 psi), $a_0 = 329 \text{ m/sec}$ (1079 ft/sec) and $\gamma = 1.4$, then the definitions for Equation (3-5) yield $U = 381 \text{ m/sec}$ (1250 ft/sec), $u_1 = 80.5 \text{ m/sec}$ (264 ft/sec), $\rho_1 = 1.553 \text{ kg/m}^3$ ($5.61 \times 10^{-5} \text{ lb}_m/in^3$). Substituting in Equation (3-5) gives a drag pressure q of 5032 Pa (0.730 psi). The scaled pressure $\left(\frac{C_D q b h L^2}{\sigma_y I}\right)$ for a drag coefficient of 1.8 then

equals 2.752. Before computing the impulse i_t , the scaled quantities $\left(\frac{P}{P_0}\right)$ and $\left(\frac{a C_i}{P_0 H}\right)$ are found to equal 0.396 and 19.7, respectively. Figure 3-3 then gives a scaled applied impulse $\left(\frac{a i}{P_0 H}\right)$ of 1.95 or applied impulse i_t of 80.2 Pa·s (0.0113 psi-sec).

The scaled impulse $\left(\frac{i_t b h \sqrt{E}}{\sigma_y \sqrt{\rho I A}}\right)$ in Figure 3-5 is found to equal 0.109. Because both the scaled applied pressure and scaled applied impulse are less than the thresholds for yielding a simply-supported beam in Figure 3-5, these blast loads will not cause permanent deformation in a simply-supported 8 WF 20 beam with a 10.0 meter (32.8 ft) span.

The equations for the beam solutions are derived in Appendix 3A. In addition, experimental test data on aluminum cantilever beams are used to demonstrate that the asymptotes to these solutions properly predict elastic strains.

3-1.4 Response of Plate Elements

Figure 3-6 is a load versus impulse diagram for the initiation of permanent deformation or fracture in plate type structural elements, and Figure 3-7 is this diagram for membrane type elements. If a plate is clamped around its boundaries, both solutions must be evaluated; the correct answer is the one which gives the largest applied pressure P_r or impulse i_r . If a plate has simply-supported boundaries such that the edges are not restrained against membrane forces, the only solution which should be considered is the bending one, Figure 3-6. Any self-consistent set of units can be used with the figures, as all coordinates

are nondimensional. In both figures, the ordinate $\left(\frac{\sqrt{E} i}{i_r \sigma_y h \sqrt{\rho h}}\right)$

is a scaled applied impulse and the abscissa, either

$$\left(\frac{P X^2}{i_p \sigma_y^2}\right)$$

in Figure 3-6 or

$$\left(\frac{\sqrt{E} P X}{i_p \sigma_y^{3/2} h}\right)$$

in Figure 3-7,

is a scaled applied maximum pressure where i_r is the applied impulse,

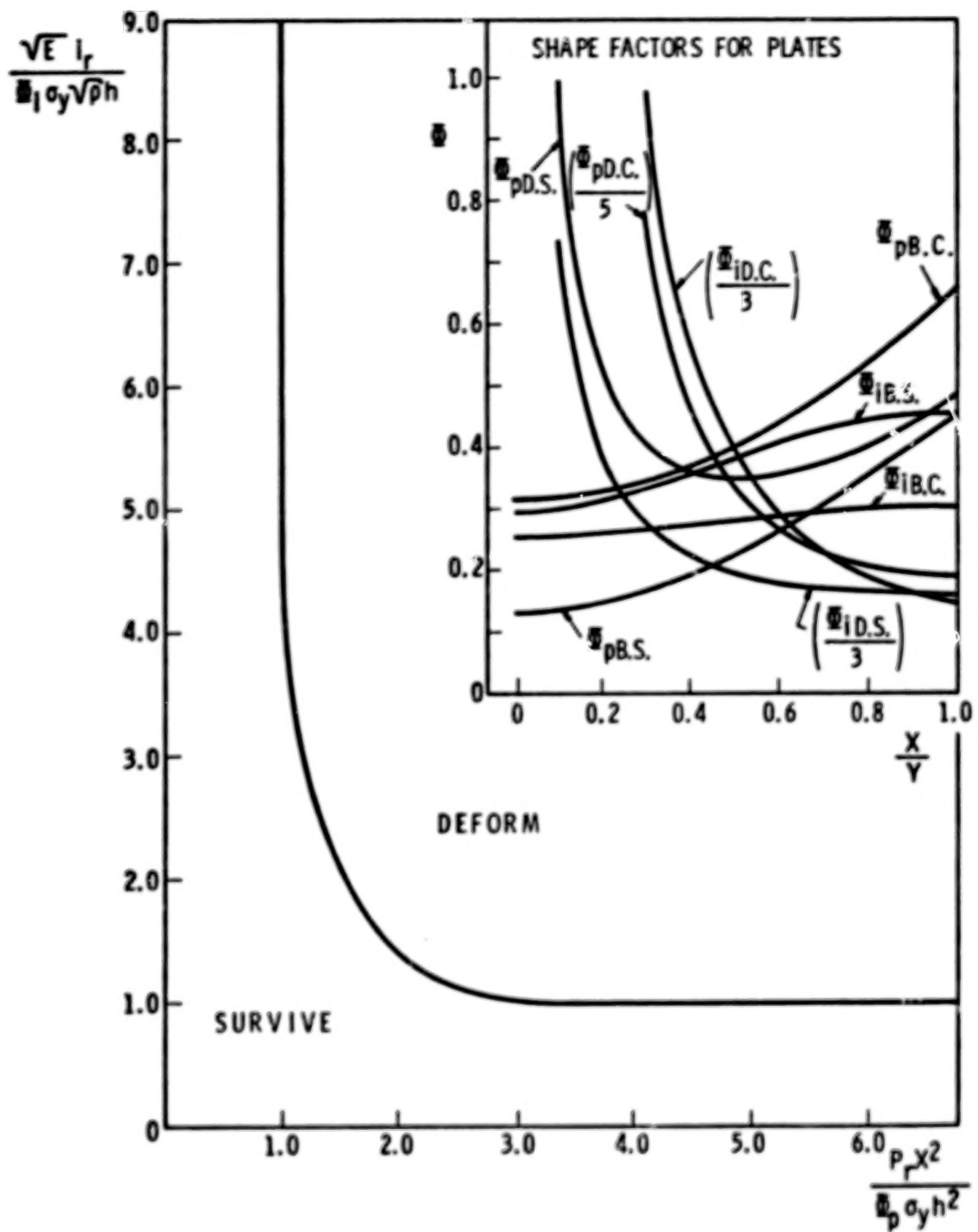


Figure 3-6. Normalized Load Impulse Diagram for Plates

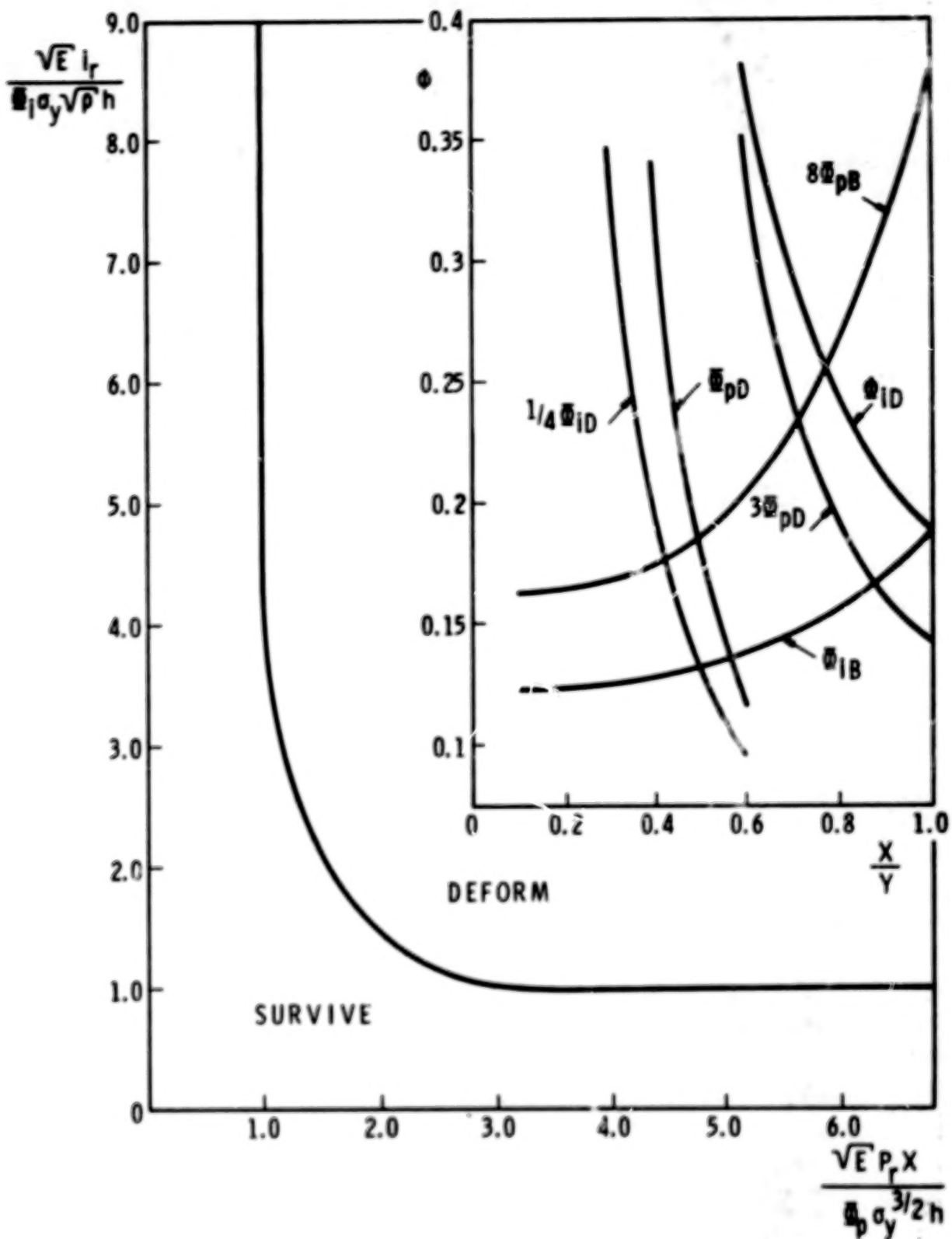


Figure 3-7. Normalized Load Impulse Diagram for Membranes

P_r is the applied pressure, E is the modulus of elasticity, σ_y is the yield stress of the plate, ρ is the density, h is plate or membrane thickness, X is the short half-span, Y is the long half-span, and ϕ_p and ϕ_i are pressure and impulse shape factors. The shape factors are functions of plate aspect ratio $(\frac{X}{Y})$. The four shape factors with a p subscript are pressure shape factors ϕ_p , whereas those with an i subscript are impulse ones ϕ_i . The other subscripts denote whether a plate is simply-supported with a brittle material (B.S.), or simply-supported with a ductile material (D.S.). Once plate material characteristics, boundary conditions and aspect ratio have been specified, the appropriate pair of shape factors for pressure and impulse can be chosen from the inserts in Figures 3-6 and 3-7. In many of the shape factor curves, ϕ has been either multiplied or divided by a constant so all shape factor functions could be presented on the same curve. For example, the factor ϕ_{pB} in Figure 3-7 equals the ordinate divided by eight. After shape factors have been chosen, the applied loads can be compared to threshold ones to determine if permanent deformation occurs. If P_r and i_r exceed the threshold values, the plate or membrane fractures if brittle or permanently deforms if ductile; otherwise, no permanent deformation should occur.

In using Figures 3-6 and 3-7, the pressures and impulses of importance are peak reflected ones and not free-field side-on ones. This means that Figure 3-1 must be used to obtain the ratio $\left(\frac{P_r}{P_s}\right)$ and also $\left(\frac{i_r}{i_s}\right)$ from α and P_s .

We will illustrate the use of Figures 3-6 and 3-7 with an example:

Assume that a 20 m by 30 m (65.6 ft by 98.4 ft) plate, 0.050 m (0.164 ft) thick can be either simply-supported or clamped, made of 1015/1018 steel and is placed facing a blast wave with $P_s = 40 \text{ kPa}$ (5.62 psi) and $i_s = 700 \text{ Pa} \cdot \text{s}$ (0.0983 psi-sec). This material is ductile and has a $\sigma_y = 3.17 \times 10^{11} \text{ Pa}$ ($4.45 \times 10^4 \text{ psi}$), and $E = 2.07 \times 10^{11} \text{ Pa}$ ($2.90 \times 10^7 \text{ psi}$). First Figure 3-1 must be used to obtain the reflection factor relating P_r to P_s and i_r to i_s . For a normal encounter ($\alpha = 0^\circ$), Figure 3-1 gives a reflection factor of 2.4, thus making the applied loads $P_r = 96 \text{ kPa}$ (13.5 psi) and $i_r = 1680 \text{ Pa} \cdot \text{s}$ (0.236 psi-sec). Next Figures 3-6 and 3-7 must be used to determine the

threshold pressures and impulses. For a simply-supported plate with an aspect ratio $(\frac{X}{Y})$ of 0.666 as in this problem, the shape factors $\Phi_{pDS} = 0.368$ and $\Phi_{iDS} = 0.513$. For bending in a clamped plate, $\Phi_{pDC} = 1.20$ and $\Phi_{iDC} = 0.75$, and for membrane action in a clamped plate, $\Phi_{pD} = 0.090$ and $\Phi_{iD} = 0.320$. Now the pressure and impulse asymptotes can be calculated for the initiation of damage in Figures 3-6 and 3-7.

The threshold pressure P_r for a simply-supported plate equals

$$\left(\frac{\Phi_{pDS} \sigma_y h^2}{X^2} \right) \text{ or } 2916 \text{ Pa (0.410 psi), and the threshold impulse equals } \left(\frac{\sqrt{\rho} h \sigma_y \Phi_{iDS}}{\sqrt{E}} \right) \text{ or } 1583 \text{ Pa}\cdot\text{s (0.222 psi-sec).}$$

Because both the threshold pressure and threshold impulse for initiation of damage are less than the applied loads, a simply-supported plate would exhibit permanent residual deformation. Both the membrane and bending solutions must be reviewed for a clamped plate. The clamped threshold

$$\text{bending pressure equals } \left(\frac{\Phi_{pDC} \sigma_y h^2}{X^2} \right) \text{ or } 9.51 \text{ kPa (1.34 psi), and the threshold membrane pressure equals } \left(\frac{\Phi_{pD} \sigma^{3/2} h}{\sqrt{E} X} \right)$$

or 5.58 kPa (0.784 psi). Both of these thresholds are exceeded by the applied pressure of 96 kPa (13.5 psi). The clamped

$$\text{threshold bending impulse equals } \left(\frac{\sqrt{\rho} h \sigma_y \Phi_{iDC}}{\sqrt{E}} \right) \text{ or } 2134 \text{ Pa}\cdot\text{s, and the threshold membrane impulse equals } \left(\frac{\sqrt{\rho} h \sigma_y \Phi_{iD}}{\sqrt{E}} \right)$$

or 987 Pa·s (0.139 psi-sec). Although the threshold membrane impulse is exceeded by the applied impulse of 1680 Pa·s (0.236 psi-sec), the clamped plate should survive because the bending threshold impulse exceeds the applied impulse. In other words, the clamped plate survives because the applied impulse is less than the threshold impulse in Figure 3-6.

The equations giving the asymptotes in Figures 3-6 and 3-7 are all derived in Appendix 3A. The breakage of glass solution which has already been presented is the equation for brittle material bending of a simply-supported plate loaded by a long-duration pressure. All pressure data for glass breakage have been essentially static tests. If dynamic pressure pulses are short enough that the response of a glass plate is in the impulse critical loading realm, the glass breakage solutions presented earlier may fail to apply. Under these circumstances, a glass solution should be possible

by substituting appropriate properties into Figure 3-6 for a brittle material. This glass solution is not advocated for general use, as it has not yet been substantiated with test results.

3-1.5 General

Approximate procedures have been presented whereby glass breakage, overturning of objects, generalized structural damage, damage to beam-like elements, and damage to plate-like structural elements can be estimated. Should an investigator have available finite-element or finite-difference computer codes, make either full-scale tests or appropriate model tests to determine if a structure is damaged, then these specific analyses can be used to supercede these approximate techniques. Any code or method of assessing damage should be modified and updated as advancements are made or as new test data become available.

3-2 Injury Estimates to Humans

3-2.1 Introduction

Literature concerning the harmful effects of blast has been published as early as 1768 by Zhar.⁽³⁾ However, knowledge of the mechanisms of blast damage to humans was extremely incomplete until World War I, when the physics of explosions were better understood. Since that time, numerous authors have contributed considerable time and effort in the study of blast damage mechanisms and blast pathology. Each accident situation has its own unique environment with trees, buildings, hills and various other topographical conditions which may dissipate the energy of the blast wave or reflect it and amplify its effect on an individual. Because of these different variational factors involved in an explosion-human body receiver situation, only a simplified and limited set of blast damage criteria will be included in this document. The human body "receiver" will be assumed to be standing in the free-field on flat and level ground when contacted by the blast wave. Excluding certain reflected wave situations, this is the most hazardous body exposure condition. Air-blast effects will also be subdivided into two major categories: direct (primary) blast effects and indirect blast effects.⁽⁴⁾

3-2.1.1 Direct Blast Effects

Direct or primary blast effects are associated with changes in environmental pressure due to the occurrence of the air blast. Mammals are sensitive to the incident, reflected and dynamic overpressures, the rate of rise to peak overpressure after arrival of the blast wave, and the duration of the blast wave.⁽⁴⁾ Specific impulse of the blast wave also

plays a major role.^(5, 6) Other parameters which determine the extent of blast injury are the ambient atmospheric pressure, the size and type of animal and possibly age. Parts of the body where there are the greatest differences in density of adjacent tissues are the most susceptible to primary blast damage.^(4, 7, 8) Thus, the air-containing tissues of the lungs are more susceptible to primary blast than any other vital organ.⁽⁹⁾ The ear, although not a vital organ, is the most sensitive. This organ responds to energy levels as low as 10^{-12} watts/m²⁽¹⁰⁾ or pressures approximately 2×10^{-5} Pa (2.9×10^{-9} psi). This small force causes an excursion of the eardrum a distance less than the diameter of a single hydrogen molecule.⁽¹⁰⁾

Pulmonary injuries directly or indirectly cause many of the pathophysiological effects of blast injury.⁽¹¹⁾ Injuries include pulmonary hemorrhage and edema,^(4, 11) rupture of the lungs,⁽³⁾ air-embolic insult to the heart and central nervous system,⁽⁴⁾ loss of respiratory reserve⁽⁴⁾ and multiple fibrotic foci, or fine scars, of the lungs.⁽¹²⁾ Other harmful effects are rupture of the eardrums and damage to the middle ear, damage to the larynx, trachea, abdominal cavity, spinal meninges and radicles of the spinal nerves and various other portions of the body.⁽³⁾

3-2. 1. 2 Indirect Blast Effects

Indirect blast effects can be subdivided into three major categories:⁽⁴⁾ secondary effects, tertiary effects and miscellaneous effects.

Secondary effects involve impact by missiles from the detonating device itself or from objects located in the nearby environment which are accelerated after interaction with the blast wave (appurtenances). Characteristics which affect the extent of damage done to a human due to impingement of fragments include the mass, velocity, shape, density, cross-sectional area and angle of impact.⁽⁴⁾ Pathophysiological effects include skin laceration, penetration of vital organs, blunt trauma, skull and bone fracture.⁽¹³⁾

Tertiary effects involve whole-body displacement and subsequent decelerative impact.⁽⁴⁾ In this case, the blast pressures and winds interact with the body in such a manner that it is essentially picked up and translated. Damage can occur during the accelerating phase or during decelerative impact.⁽¹⁴⁾ The extent of injury due to decelerative impact is by far the more significant⁽¹⁵⁾ and is determined by the velocity change at impact, the time and distance over which deceleration occurs, the type of surface impacted and the area of the body involved.⁽⁴⁾ When the human body is exposed to such acceleration or decelerative impact, the head is the most vulnerable to mechanical injury as well as the best protected area.⁽¹⁶⁾ In addition to injury to the head, vital internal organs can be damaged and bones can be broken as a result of

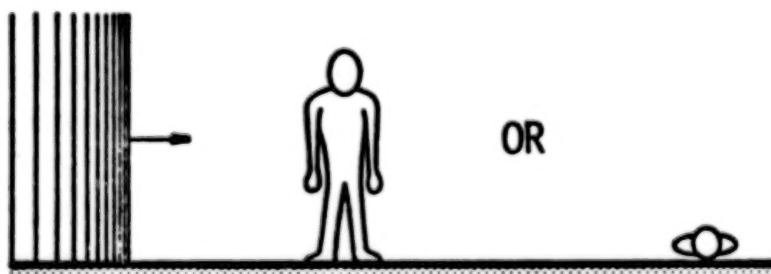
decelerative impact. The impact velocity required to produce a certain percentage of skull fractures is usually less than the impact velocity required to produce the same percentage total body (randomly oriented) impact lethality. (4, 13, 17) Since skull fracture is a very serious injury, this document will concern itself with skull fracture and total body decelerative impact onto hard surfaces.

Miscellaneous blast effects such as dust and thermal damage are of little significance for conventional blast materials⁽⁴⁾ and will not be considered in this document.

3-2.2 Pressure/Impulse Combinations Producing Lung Damage

Lung damage is a rather serious primary blast injury and has been studied for many years by many researchers. The damage criteria for lung damage presented in this chapter were developed from the results of many years of research conducted by the Lovelace Foundation for Medical Education and Research in Albuquerque, New Mexico. (6, 8) Since the Lovelace Foundation survivability curves were presented in terms of pressure and duration, they had to be modified so that they would be readily applicable in this document. The development of the Lovelace Foundation curves and the modification of these curves for applicability to this handbook can be found in References 4 and 6 and Appendix 3B, respectively. The interested reader should examine these areas for additional information. Only the results, as they apply directly to this handbook, are presented here.

Exposure of the human body target to propellant or bursting gas vessel air blast damage will be assumed to be in the free-field (remote from obstacles and on a flat and level terrain) with the long axis of the body perpendicular to the blast winds and the subject facing in any direction (see Figure 3-8). Pulmonary blast damage for this situation can be



LONG AXIS OF BODY PERPENDICULAR TO BLAST WINDS, SUBJECT FACING ANY DIRECTION

Figure 3-8. Subject in the Free-Field (Refs. 4 and 6)

shown to depend upon a scaled peak incident overpressure \bar{P}_s and a scaled specific impulse \bar{I}_s (see References 4 and 6 and Appendix 3B).

\bar{P}_s and \bar{I}_s are determined as follows:

$$\bar{P}_s = P_s / p_0 \quad (3-6)$$

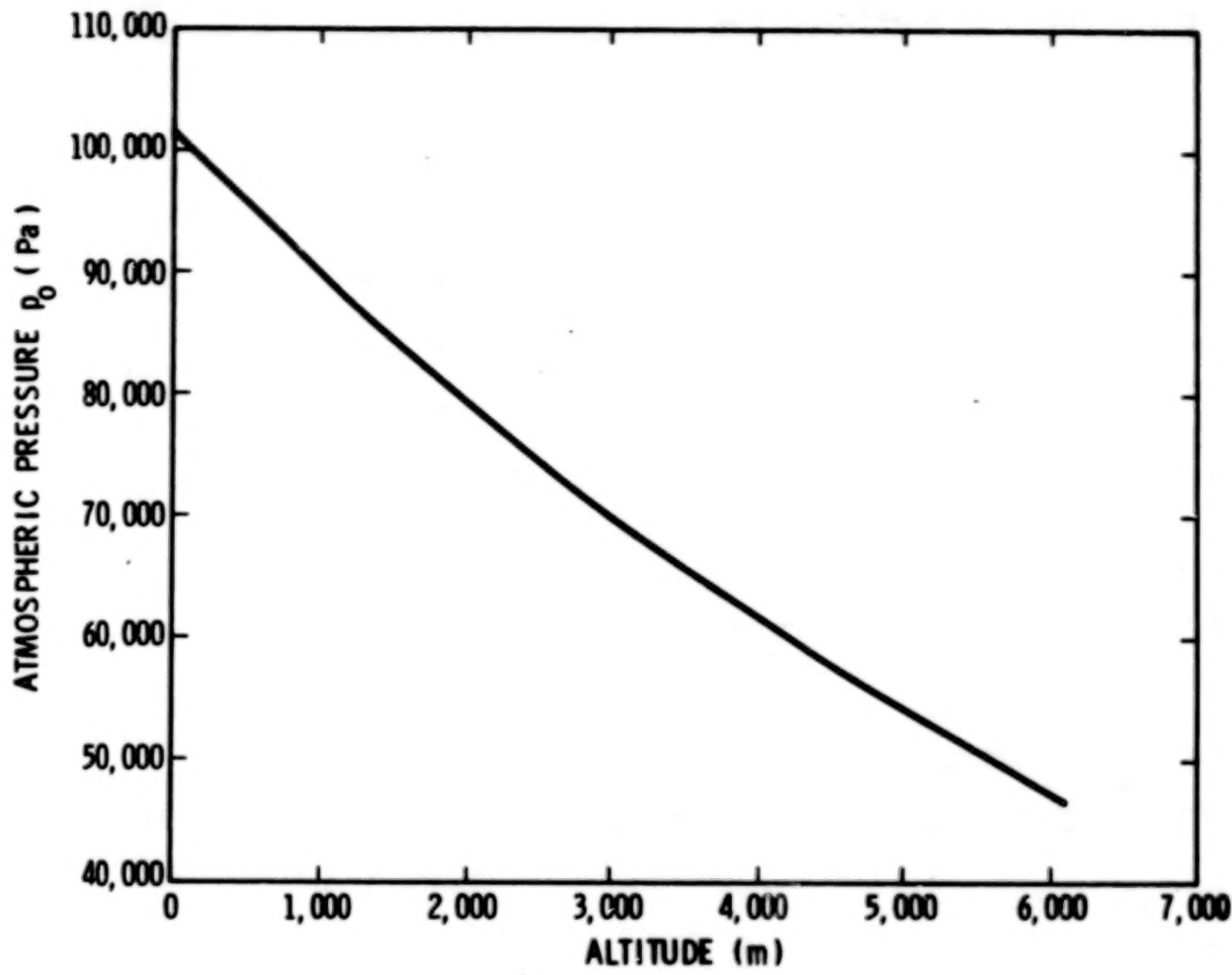
where P_s is peak incident overpressure (Pa) and p_0 is ambient atmospheric pressure

$$\bar{I}_s = \frac{I_s}{p_0^{1/2} m^{1/3}} \quad (3-7)$$

where m is the mass of the human body receiver in kilograms.

Figure 3-9 graphically depicts the manner in which ambient atmospheric pressure decreases with increasing altitude above sea level.⁽¹⁸⁾ The value for mass used in the scaling is determined by the demographic composition of the particular area under investigation. It is recommended that 5 kg (11 lb_m) be used for babies, 25 kg (55 lb_m) for small children, 55 kg (121 lb_m) for adult women, and 70 kg (154 lb_m) for adult males. The smallest bodies in this case are the most susceptible to pulmonary blast injury. Therefore, if the lightest individuals are expected to be free from possible lung damage at a particular scaled distance (see Chapter II) from the explosion, then the heavier individuals are also free from lung damage at the same scaled distance.

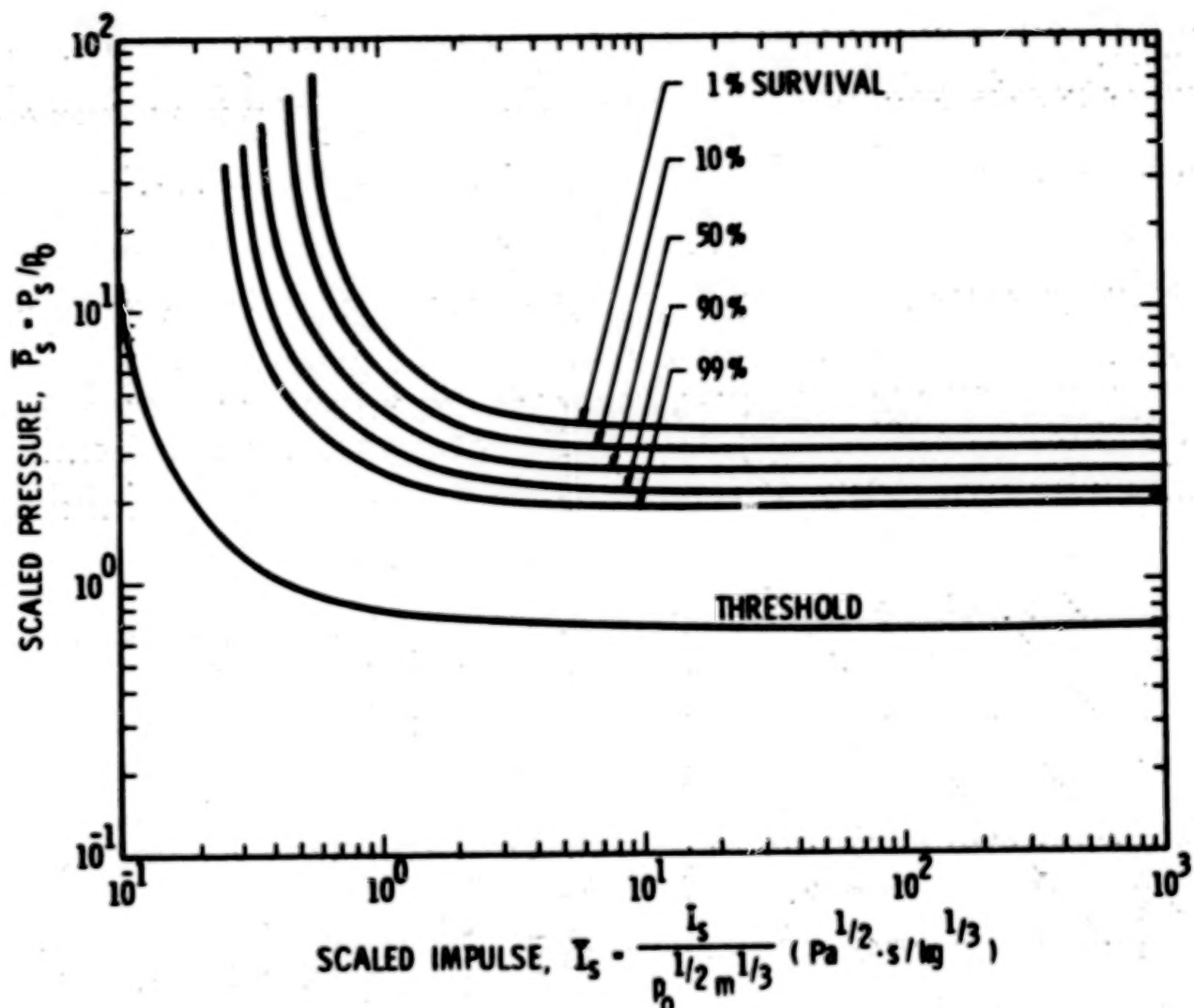
The scaled survival curves predicted for men applicable to free-field situations where the long axis of the body is perpendicular to the direction of propagation of the blast wave (see Figure 3-8) are shown in Figure 3-10. A word of explanation concerning the curves on the graphs may be helpful. The graph indicates that lower values of both scaled incident overpressure and scaled specific impulse are less harmful to the exposed individual than higher values. That is, as scaled pressure and impulse increase, survivability decreases within certain bounds demonstrated by the asymptotic limits of the curves in the figure. In short, to be assured that there is a minimal amount of lung damage from accidental blasts, the calculated scaled pressure and scaled impulse (using the lowest relevant value for mass) at the scaled distance being investigated should fall below the threshold lung damage curve on Figure 3-3. The method for assessing lung damage is as follows:



$$(\text{psi} = \text{Pa} \times 1.450 \times 10^{-4})$$

$$(\text{ft} = \text{m} \times 3.281)$$

Figure 3-9. Atmospheric Pressure vs Altitude Above
Sea Level (Ref. 16)



$$(\text{psi}^{1/2} \text{ sec}^{1/3} / \text{lb}_m^{1/3} = \text{Pa}^{1/2} \cdot \text{s}^{1/3} \times 9.253 \times 10^{-3})$$

104

Figure 3-10. Survival Curves for Lung Damage to Man

- (1) Determine peak incident overpressure P (or P_s) and specific impulse I (or I_s) at an appropriate distance from the particular propellant or gas vessel explosion situation under consideration using methods described in Chapters I and II.
- (2) Determine ambient atmospheric pressure (Figure 3-9).
- (3) Calculate scaled incident overpressure \bar{P}_s from Equation (3-6):

$$\bar{P}_s = P_s / p_0$$

- (4) Decide on the mass (in kg) of the lightest human to be exposed at this location.
- (5) Calculate scaled specific impulse \bar{I}_s from Equation (3-7):

$$\bar{I}_s = \frac{I_s}{p_0^{1/2} m^{1/3}}$$

- (6) Locate P_s and I_s on Figure 3-10 and determine if these values are in an acceptable risk area.*

3-2.3 Pressure/Impulse Combination Producing Loss of Hearing

The ear is a delicate receiver of acoustical energy and is very susceptible to damage from "fast" rising pressure waves. Damage to the middle and inner ear is especially severe because of its often permanent nature. (10) Although eardrum rupture is less severe, it is often used for the assessment of ear injury. Permanent ear damage, however, can occur without eardrum rupture, and in some cases rupture of the eardrum inhibits more serious injury. (10)

The ear injury criteria presented in this chapter are based primarily on the conclusions of reports written by Hirsch, (10) White, (4) and Ross, et al. (19) Modifications, however, needed to be made so that

*Regions below a particular curve in the figure denote more survival (less damage risk) than that which is represented by the curve.

their results would be readily adaptable to this document. Appendix 3C contains the development of the ear damage curves which follow, and the interested reader is encouraged to examine the appendix for a better understanding of the nature of ear damage.

The ear damage curves shown in Figure 3-11 represent, in increasing severity of damage, temporary threshold shift (TTS), threshold for eardrum rupture, and 50% eardrum rupture of those exposed. Temporary threshold shift represents the case where 90% of those exposed to a blast wave advancing at normal angle of incidence to the ear are not likely to suffer an excessive degree of hearing loss. The threshold for eardrum rupture curve is the location below which no ruptured ears are expected to occur and the 50% eardrum rupture curve is the location at which 50% of ears exposed are expected to rupture.

The method for assessing ear damage is as follows:

- (1) Determine peak incident overpressure P (or P_s) and specific impulse I (or I_s) at an appropriate distance from the particular propellant or gas vessel explosion situation under consideration using methods described in Chapters I and II.
- (2) Locate P_s and I_s on Figure 3-11 and determine if these values are in an acceptable risk area.*

3-2.4 Pressure/Impulse Combinations Producing Whole Body Displacement and Subsequent Damage to the Head and Body

A blast wave can interact with the human body in such a manner that it is grossly translated. Although injury can occur during the accelerative phase as well as the decelerative phase, the extent of injury due to decelerative impact, especially against a hard surface, is the more significant.⁽¹⁵⁾ Damage criteria can be established for various portions of the body but it is beneficial to establish two major injury categories. The head is the most vulnerable, yet best protected, portion of the body to mechanical injury during decelerative impact.⁽¹⁶⁾ Impact characteristics producing certain percentages of skull fracture are therefore viable damage criteria. It is also instructive to note impact characteristics which produce certain percentages of expected lethaliities from randomly

*Regions below a particular curve in the figure denote less damage risk than that which is represented by the curve.

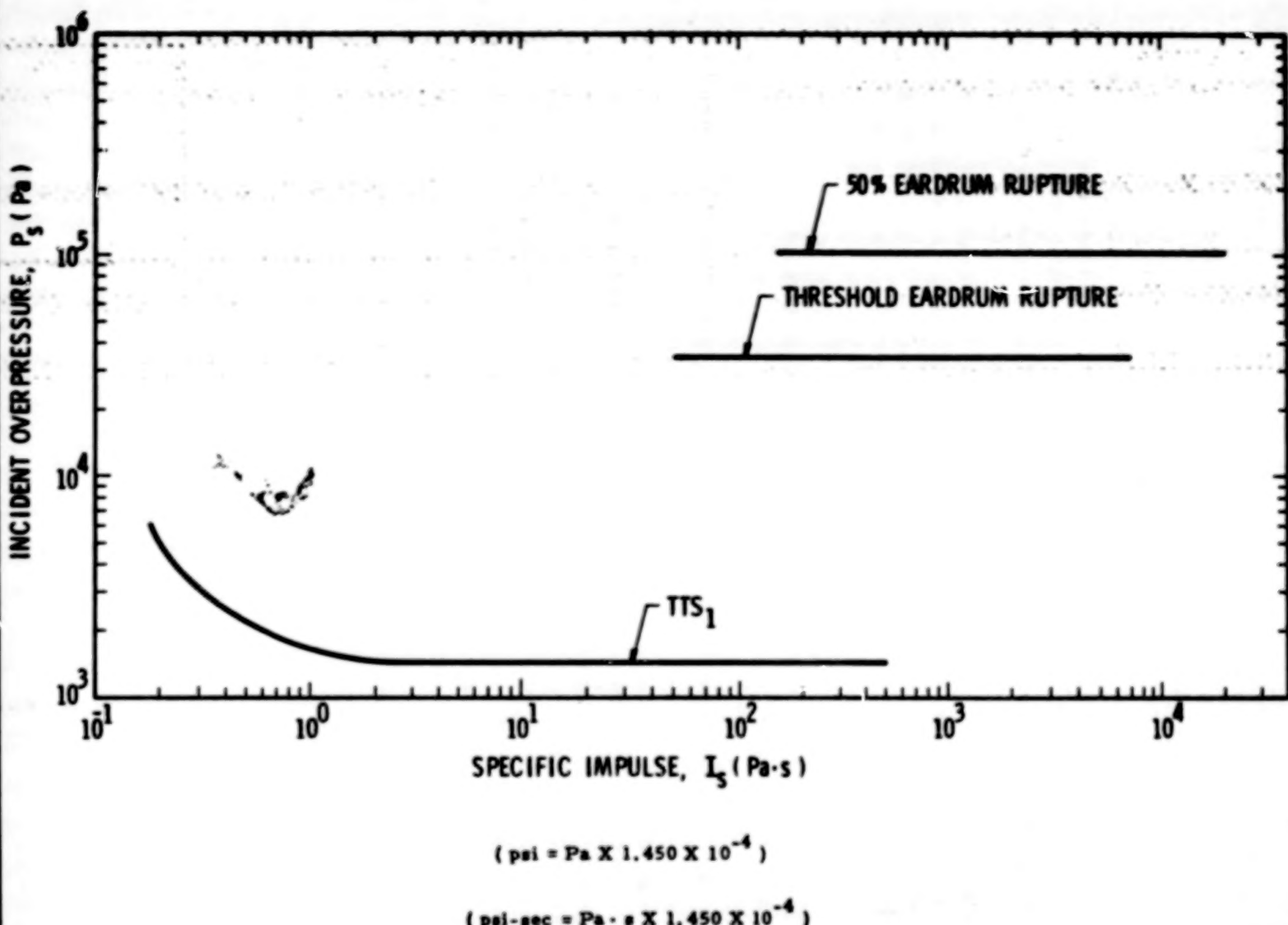


Figure 3-11. Human Ear Damage Curves for Blast Waves Arriving at Normal Angle of Incidence

oriented whole body impact. Death often ensues, in the latter case, as a result of damage to the central nervous system, large blood vessels or liver. (13)

A complete development of the tertiary blast (decelerative impact) damage criteria and pressure-impulse translation velocity curves can be found in Appendix 3D. The curious reader is encouraged to examine this appendix and related appendices for more information on the subject. Only the results which are readily applicable to the determination of the potential threat of whole body displacement damage are presented here.

For reasons explained in the appendix, expected translation damage to man can be expressed in terms of impact velocity. These critical velocities for skull fracture and total body displacement damage are shown in Tables 3-1 and 3-2, respectively. To make these tables readily applicable to this document, pressure-impulse combinations required to produce the specified critical human body displacement velocities given in the tables were calculated and scaled to eliminate mass dependency (see Appendix 3D). Figures 3-12 through 3-15 contain the pressure-scaled impulse combinations required to produce the velocities for various expected percentages of skull fracture (see Table 3-1) at sea level and 2000 m (6560 ft), 4000 m (13,100 ft) and 6000 m (19,700 ft) altitude above sea level. The curves are presented at different altitude conditions because translation was found to vary with atmospheric pressure and the speed of sound in air, both of which vary with altitude. Figures 16 through 19 contain the pressure-scaled impulse combinations required to produce the velocities for various expected percentages of lethality (see Table 3-2) at the four altitudes mentioned above. The procedure for determining the amount of potential tertiary blast (whole-body displacement) damage is as follows:

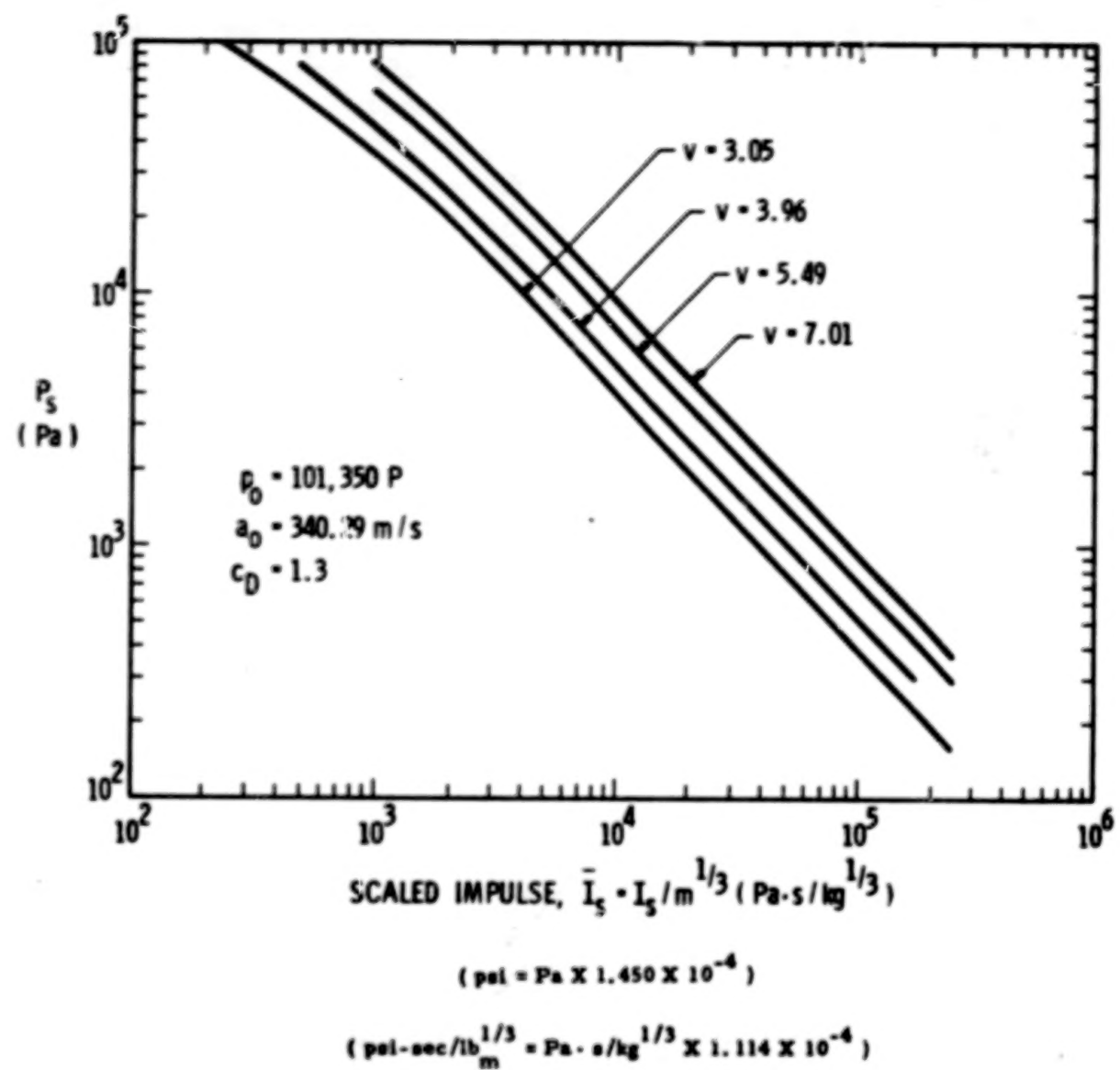
- (1) Determine peak incident overpressure P (or P_g) and specific impulse I (or I_g) at an appropriate distance from the particular propellant or gas vessel explosion situation under consideration using methods described in Chapters I and II.
- (2) Determine the lightest representative mass of an exposed human at this location and calculate $I_g / m^{1/3}$.

**TABLE 3-1. CRITERIA FOR TERTIARY DAMAGE
(DECELERATIVE IMPACT) TO THE HEAD**
(From References 2, 11 and 18)

<u>Skull Fracture Tolerances</u>	<u>Related Impact Velocity</u> <u>m/s (ft/sec)</u>
mostly "safe"	3.05 (10)
threshold	3.96 (13)
50%	5.49 (18)
near 100%	7.01 (23)

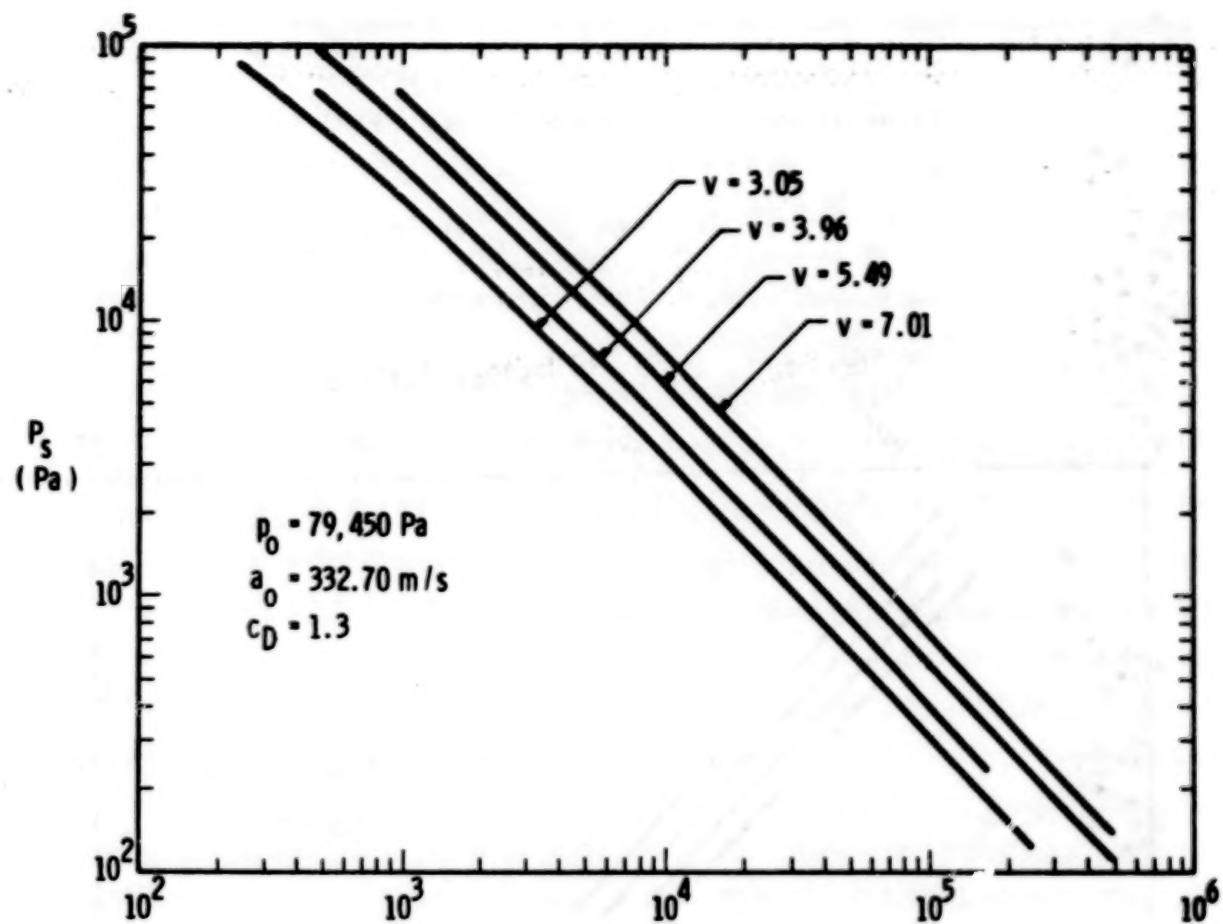
**TABLE 3-2. CRITERIA FOR TERTIARY DAMAGE INVOLVING
TOTAL BODY IMPACT**

<u>Total Body Impact Tolerance</u>	<u>Related Impact Velocity</u> <u>m/s (ft/sec)</u>
mostly "safe"	3.05 (10)
lethality threshold	6.40 (21)
lethality 50%	16.46 (54)
lethality near 100%	42.06 (138)



//O

Figure 3-12. Skull Fracture, 0 m Altitude



$$(\text{psi} = \text{Pa} \times 1.450 \times 10^{-4})$$

$$(\text{psi}\cdot\text{sec/lb}_m^{1/3} = \text{Pa}\cdot\text{s}/\text{kg}^{1/3} \times 1.114 \times 10^{-4})$$

Figure 3-13. Skull Fracture, 2000 m Altitude

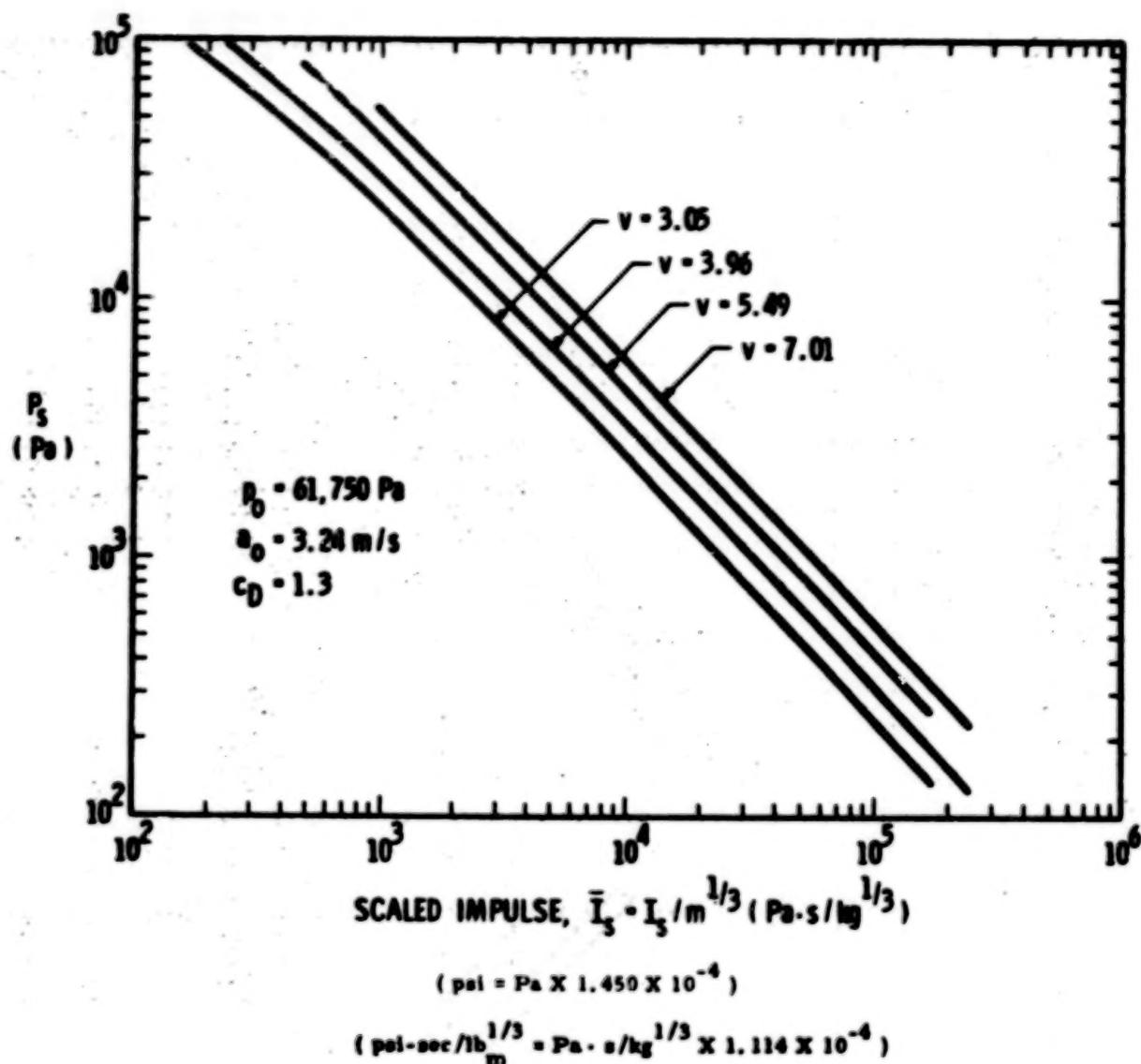
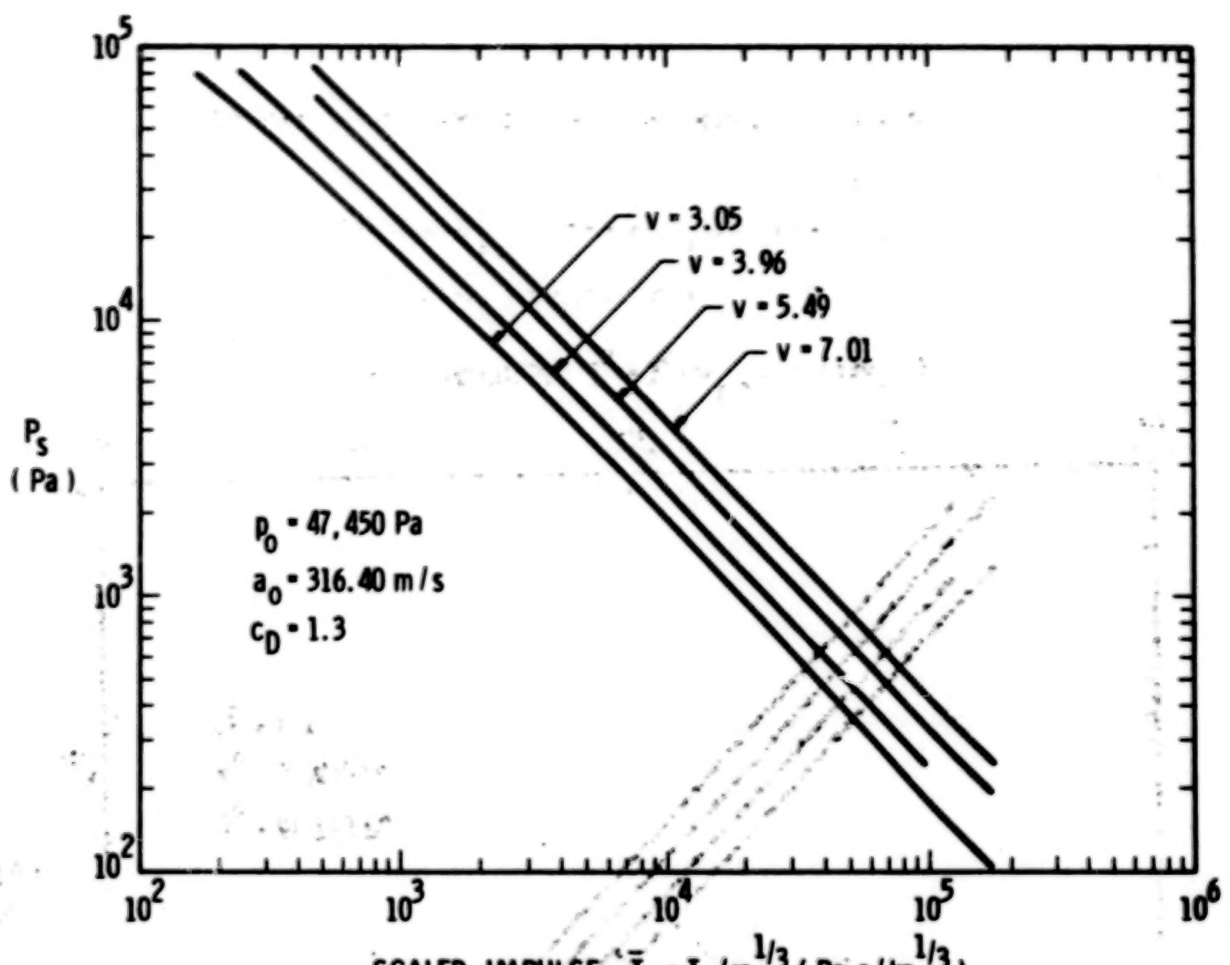


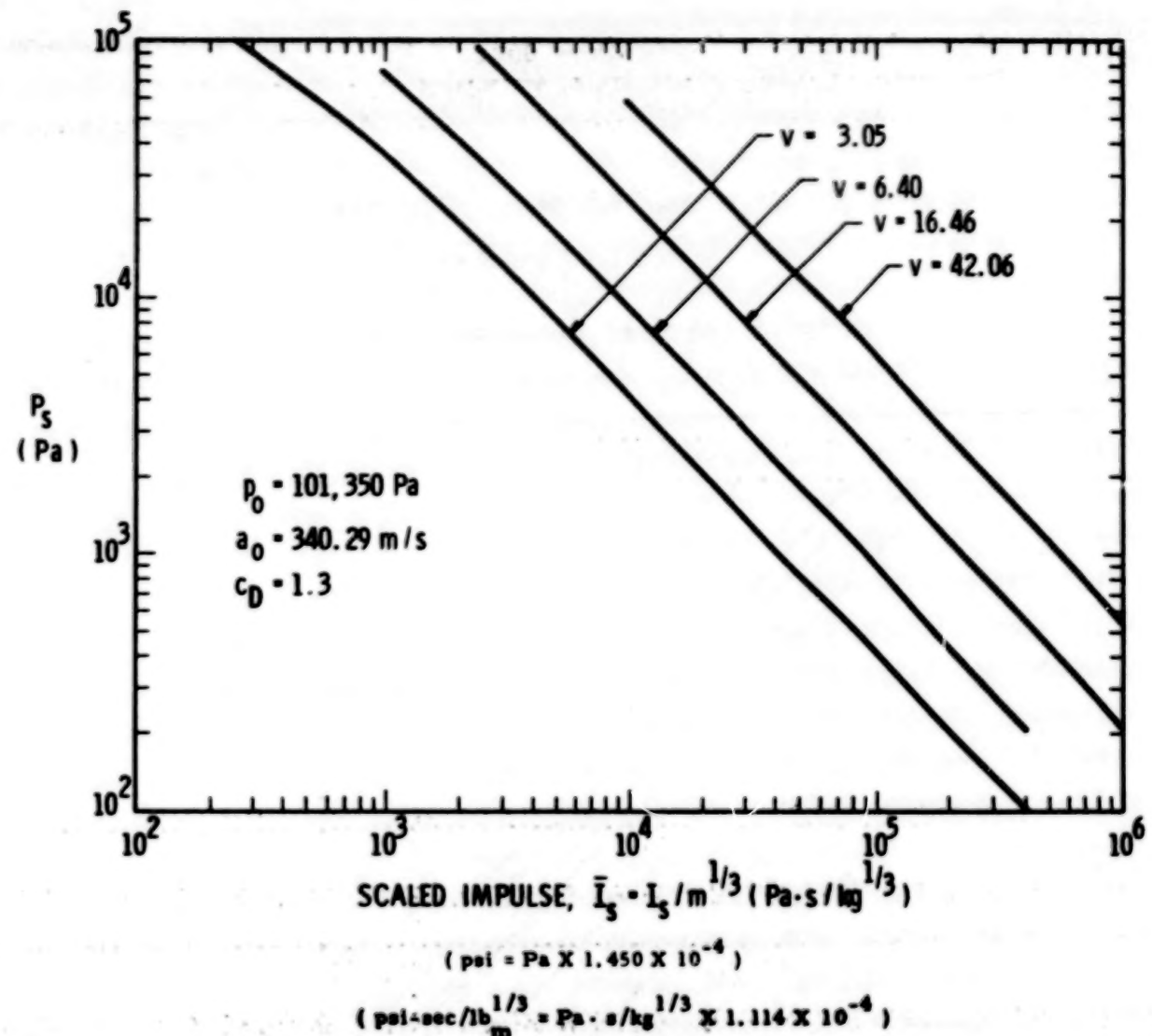
Figure 3-14. Skull Fracture, 4000 m Altitude



$$(\text{psi} = \text{Pa} \times 1.450 \times 10^{-4})$$

$$(\text{psi}\cdot\text{sec/lb/in}^{1/3} = \text{Pa}\cdot\text{s}/\text{kg}^{1/3} \times 1.114 \times 10^{-4})$$

Figure 3-15. Skull Fracture, 6000 m Altitude



114

Figure 3-16. Lethality from Whole Body Translation,
0 m Altitude

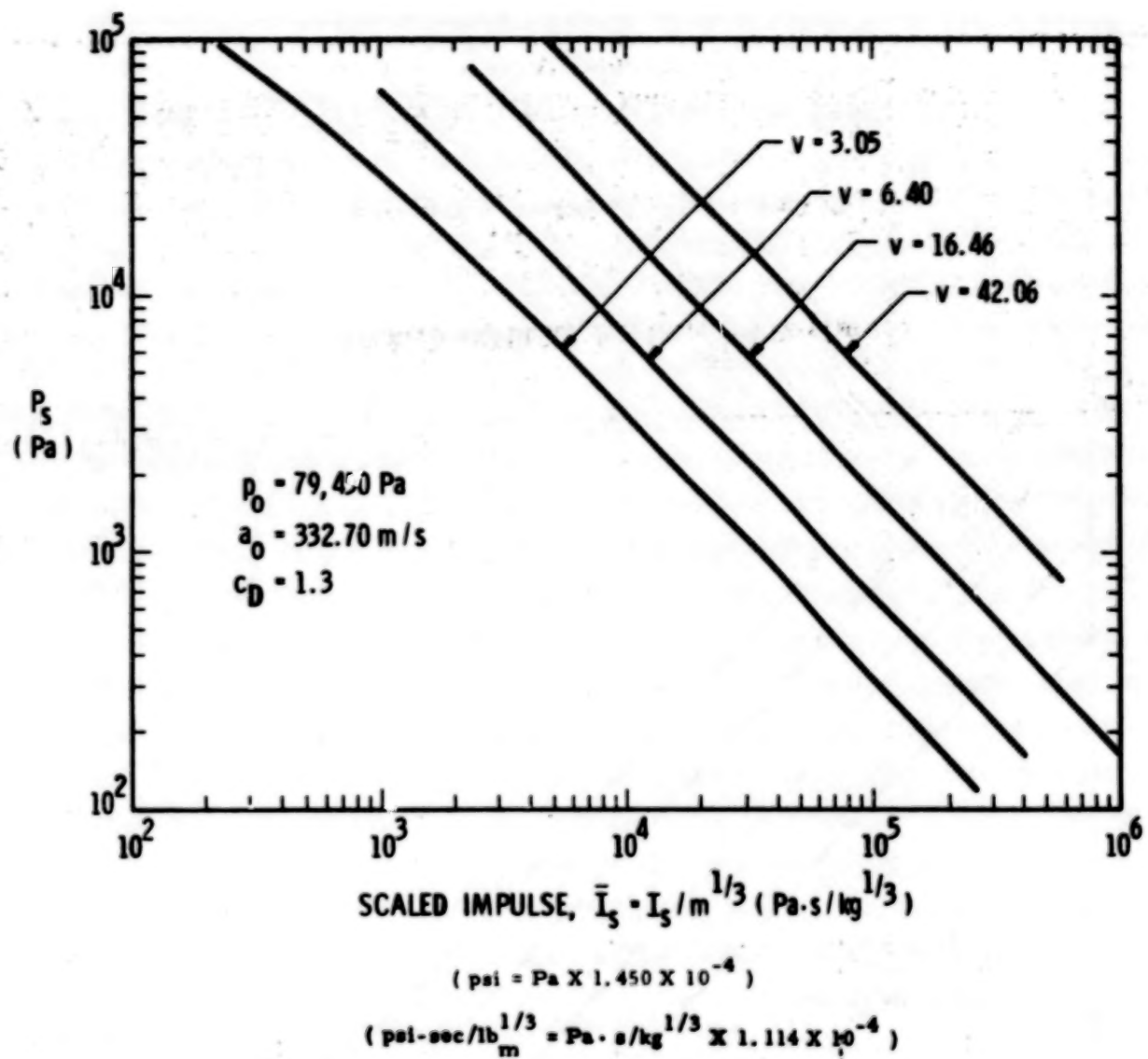


Figure 3-17. Lethality from Whole Body Translation,
2000 m Altitude

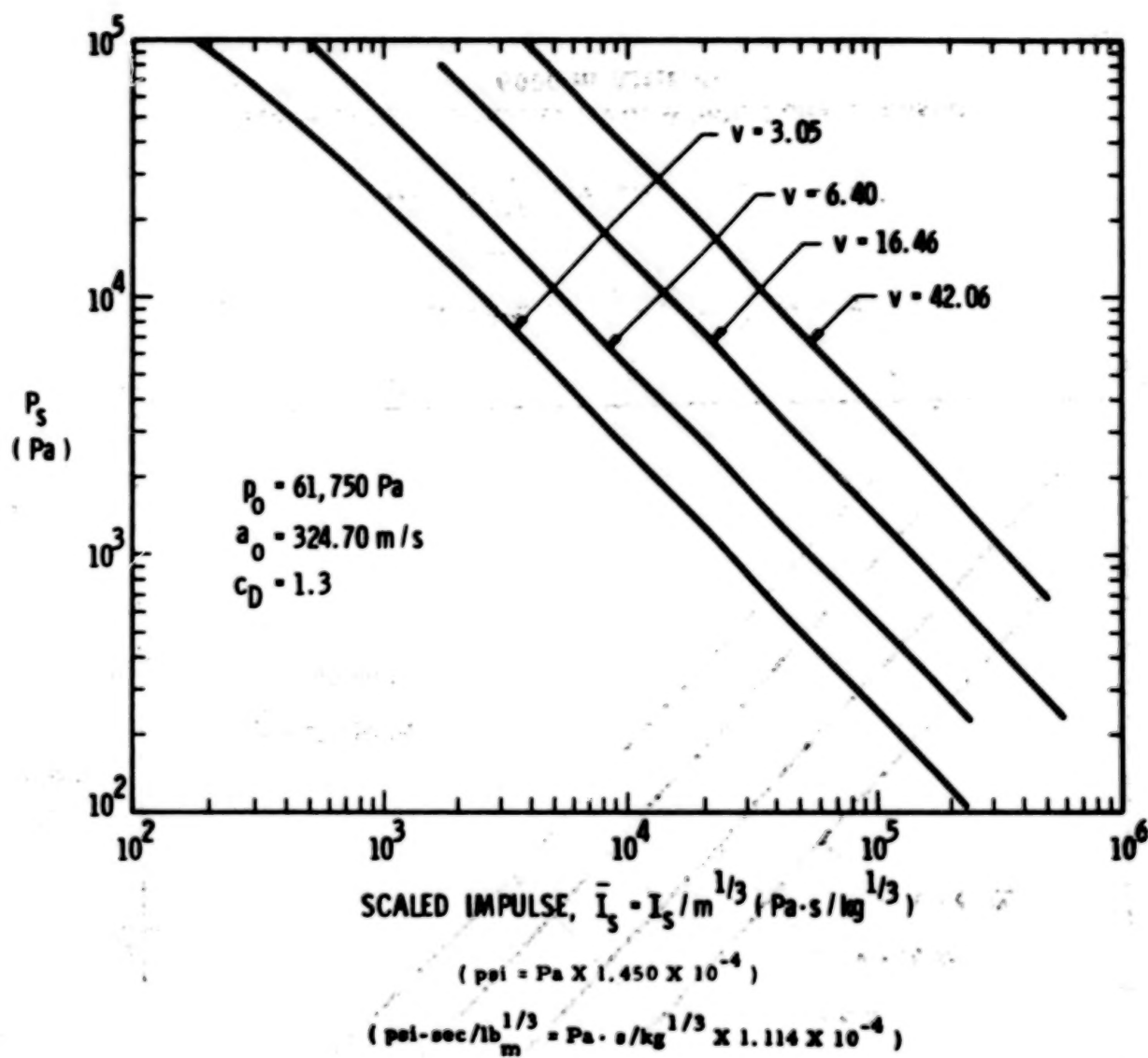


Figure 3-18. Lethality from Whole Body Translation,
4000 m Altitude

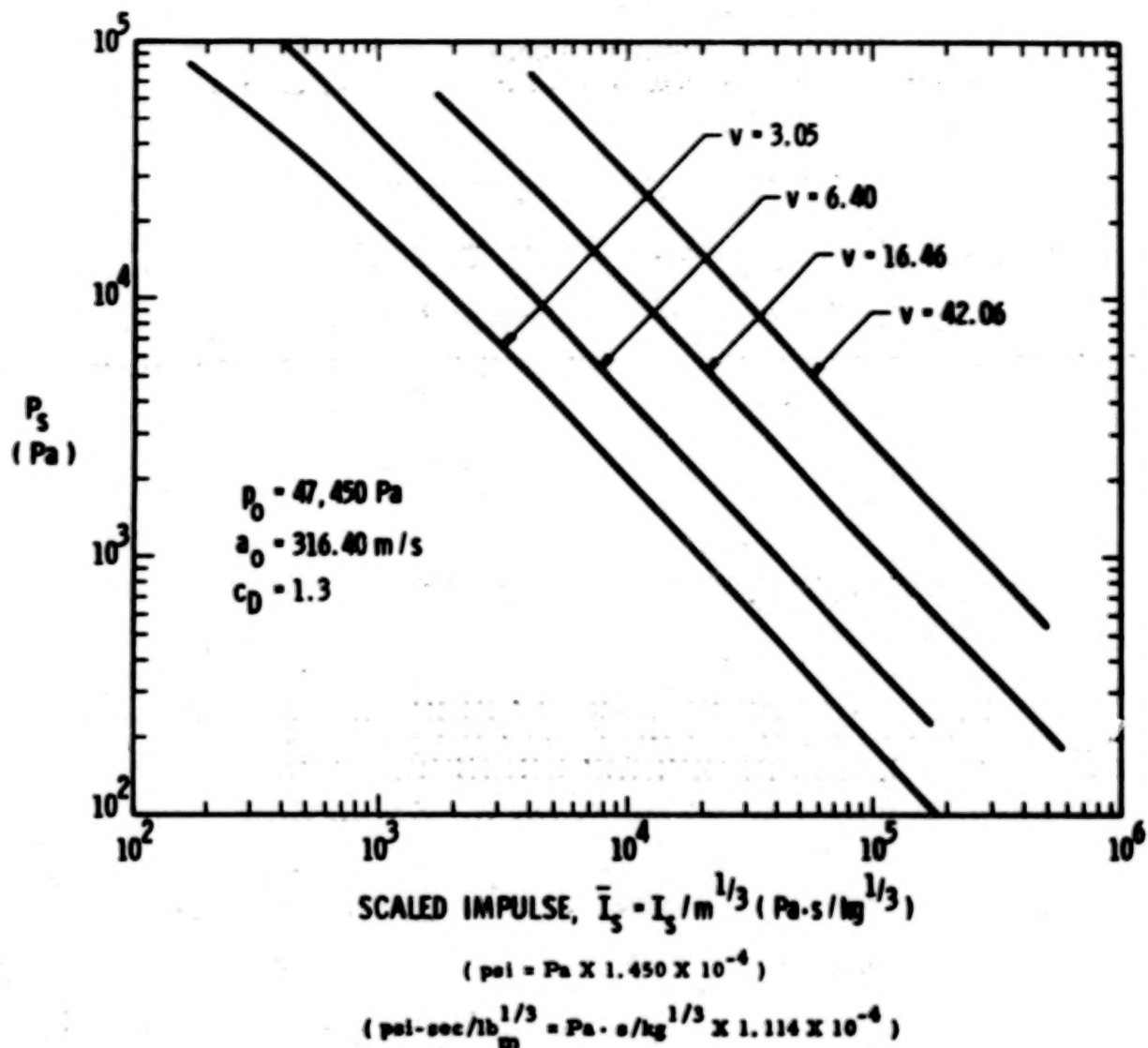


Figure 3-19. Lethality from Whole Body Translation,
6000-m Altitude

- (3) Determine the atmospheric pressure or altitude at the blast location and locate the position of the pressure-scaled impulse ($I_g/m^{1/3}$) combination on the appropriate graph of Figures 3-12 through 3-15 for percent skull fracture or Figures 3-16 through 3-19 for percent lethality from whole body impact. Determine if this pressure-scaled impulse combination is in an acceptable risk area.*

3-2.5 Summary of Potential Damage to the Human Body Due to Pressure Waves

This section has been added to expedite the determination of the effects of pressure waves on the human body. Table 3-3 contains a summary of the different body damage conditions and associated damage criteria discussed in Sections 1 through 4. The procedures for determining the potential hazards to the human body from pressure waves are as follows:

- (1) Determine peak incident overpressure P (or P_s) and specific impulse I (or I_g) at an appropriate distance from the particular propellant or gas vessel explosion situation under consideration using methods described in Chapters I and II.
- (2) Determine ambient atmospheric pressure (Figure 3-9 or footnote "‡" of Table 3-3).
- (3) Calculate the graph axis values P_s/p_0 , $I_g/p_0 m^{1/3}$ and $I_g/m^{1/3}$ (see Table 3-3) using the smallest (or most likely) mass in an anticipated exposed human being.
- (4) Using Table 3-3, locate the figures corresponding to the different potential damage conditions for the human body exposed to pressure waves in the free-field.
- (5) Locate the appropriate graph axis values [see Table 3-3 and (3) above] on the relevant graphs and determine if these values are in an acceptable risk area.†

* Regions below a particular curve in the figures denote less damage risk than that which is represented by the curve.

† Regions below a particular curve in the figures denote more survival (less damage risk) than that which is represented by the curve.

TABLE 3-3. SUMMARY OF POTENTIAL DAMAGE TO THE HUMAN BODY DUE TO PRESSURE WAVES

<u>Condition</u>	<u>Appropriate Figure Numbers*</u>	<u>Axes of Figure[†]</u>
Lung Damage	3-10	P_s/P_o versus $I_s/P_o^{1/2} m^{1/3}$
Ear Damage	3-11	P_s versus I_s
Skull Impact Damage	3-12, 3-13, 3-14, or 3-15 [‡]	P_s versus $I_s/m^{1/3}$
Whole Body Impact Damage	3-16, 3-17, 3-18, or 3-19 [‡]	P_s versus $I_s/m^{1/3}$

* Regions below a particular curve in a figure denote less damage risk than that which is represented by the curve.

[†] where P_s is peak incident overpressure (P) in Pa

I_s is impulse (I) in Pa·s

m is mass of the body in kg

P_o is atmospheric pressure in Pa (see Figure 3-9)

[‡] Choice of figure number depends on ambient atmospheric pressure (or height above sea level). That is, for pressure (altitude):

101,350 Pa (0 m)	- Figures 3-12 and 3-16
79,450 Pa (2000 m)	- Figures 3-13 and 3-17
61,750 Pa (4000 m)	- Figures 3-14 and 3-18
47,450 Pa (6000 m)	- Figures 3-15 and 3-19

3-2.6 Examples for Determining the Expected Damage to Human Beings from Pressure Waves

The problems which follow assume that the peak incident over-pressure P (or P_{u}) and specific impulse I (or I_s) were predetermined using the methods of Chapters I and II.

Example 1:

- (1) Pressure and impulse at a particular standoff distance are assumed to be the following:

$$P = 2.03 \times 10^6 \text{ Pa (294 psi)}$$

$$I = 6.56 \times 10^3 \text{ Pa} \cdot \text{s (0.951 psi-sec)}$$

- (2) Suppose the explosion occurs at sea level. Then, from footnote "‡" of Table 3-3.

$$P_0 = 1.0135 \times 10^5 \text{ Pa (14.7 psi)}$$

$$(3) \frac{P}{P_0} = \frac{2.03 \times 10^6 \text{ Pa}}{1.0135 \times 10^5 \text{ Pa}} = 2.00 \times 10^1$$

If one anticipates that only 70 kg (154 lb_m) adults are exposed, then

$$\frac{I_s}{P_0^{1/2} m^{1/3}} = \frac{6.56 \times 10^3 \text{ Pa} \cdot \text{s}}{(1.014 \times 10^5 \text{ Pa})^{1/2} (70 \text{ kg})^{1/3}} =$$

$$5.00 \frac{\text{Pa}^{1/2} \cdot \text{s}}{\text{kg}^{1/3}}$$

$$\frac{I_s}{m^{1/3}} = \frac{6.56 \times 10^3 \text{ Pa} \cdot \text{s}}{(70 \text{ kg})^{1/3}} = 1.592 \times 10^3 \frac{\text{Pa} \cdot \text{s}}{\text{kg}^{1/3}}$$

- (4) From Table 3-3, the appropriate figures for the various damage conditions at 1.0135×10^5 Pa (14.7 psi) atmospheric pressure are:

Lung Damage - Figure 3-10

Ear Damage - Figure 3-11

Skull Impact Damage - Figure 3-12

Whole Body Impact Damage - Figure 3-16

- (5) Locating the appropriate graph axis values on the proper figures gives the following results:

Lung Damage - less than 1% survivability

Ear Damage - much greater than 50% eardrum rupture

Skull Impact Damage - near 100% skull fracture

Whole Body Impact Damage - not able to be determined precisely from graph but expected to be near 100% lethality.

Example 2: Note: This example is a continuation of Example 2 of Chapter II, Section 2-2

- (1) Pressure and impulse were determined to be the following:

$$P = 3.8 \times 10^4 \text{ Pa (5.51 psi)}$$

$$I = 1.16 \times 10^3 \text{ Pa} \cdot \text{s (0.168 psi-sec)}$$

- (2) Suppose the explosion occurs at an altitude of 4000 m (13,100 ft) then, from footnote "e" of Table 3-3,

$$P_0 = 6.175 \times 10^4 \text{ Pa (8.96 psi)}$$

$$(3) \frac{P_s}{P_0} = \frac{3.8 \times 10^4 \text{ Pa}}{6.175 \times 10^4 \text{ Pa}} = 6.2 \times 10^{-1}$$

If one anticipates that the lightest people exposed to an explosion are approximately 55 kg (121 lb_m) women, then

$$\frac{I_s}{p_0^{1/2} m^{1/3}} = \frac{1.16 \times 10^3 \text{ Pa}\cdot\text{s}}{(6.175 \times 10^4 \text{ Pa})^{1/2} (55 \text{ kg})^{1/3}} =$$

$$1.23 \frac{\text{Pa}^{1/2} \cdot \text{s}}{\text{kg}^{1/3}}$$

$$\frac{I_s}{m^{1/3}} = \frac{1.16 \times 10^3 \text{ Pa}\cdot\text{s}}{(55 \text{ kg})^{1/3}} = 3.05 \times 10^2 \frac{\text{Pa}\cdot\text{s}}{\text{kg}^{1/3}}$$

- (4) From Table 3-3, the appropriate figures for the various damage conditions at $6.175 \times 10^4 \text{ Pa}$ (8.96 psi) atmospheric pressure are:

Lung Damage - Figure 3-10

Ear Damage - Figure 3-11

Skull Impact Damage - Figure 3-14

Whole Body Impact Damage - Figure 3-18

- (5) Locating the appropriate graph axis values on the proper figures give the following results:

Lung Damage - slightly under threshold lethality

Ear Damage - slightly above threshold eardrum rupture

Skull Impact Damage - slightly under the curve for mostly "safe" from skull fracture

Whole Body Impact Damage - slightly under the curve for mostly "safe" from lethality.

Example 3: Note: This example is a continuation of Example 3 of Chapter II, Section 2-2

- (1) Pressure and impulse were determined to be the following:

$$P = 2.2 \times 10^4 \text{ Pa (3.19 psi)}$$

$$I = 6.49 \times 10^2 \text{ Pa} \cdot \text{s (0.0941 psi-sec)}$$

- (2) Suppose the explosion occurs at sea level. Then, from footnote "t" of Table 3-3,

$$P_0 = 1.0135 \times 10^5 \text{ Pa (14.7 psi)}$$

$$(3) \frac{P}{P_0} = \frac{2.2 \times 10^4 \text{ Pa}}{1.0135 \times 10^5 \text{ Pa}} = 2.2 \times 10^{-1}$$

If one anticipates that the lightest people exposed to the explosion are 25 kg (55 lb_m) children, then

$$\frac{\frac{I}{s}}{P_0^{1/2} m^{1/3}} = \frac{6.49 \times 10^2 \text{ Pa} \cdot \text{s}}{(1.0135 \times 10^5 \text{ Pa})^{1/2} (25 \text{ kg})^{1/3}} = \\ 6.97 \times 10^{-1} \frac{\text{Pa}^{1/2} \cdot \text{s}}{\text{kg}^{1/3}}$$

$$\frac{\frac{I}{s}}{m^{1/3}} = \frac{6.49 \times 10^2 \text{ Pa} \cdot \text{s}}{(25 \text{ kg})^{1/3}} = 2.22 \times 10^2 \frac{\text{Pa} \cdot \text{s}}{\text{kg}^{1/3}}$$

- (4) From Table 3-3, the appropriate figures for the various damage conditions at $1.0135 \times 10^5 \text{ Pa (14.7 psi)}$ atmospheric pressure are:

Lung Damage - Figure 3-10

Ear Damage - Figure 3-11

Skull Impact Damage - Figure 3-12

Whole Body Impact Damage - Figure 3-16

- (5) Locating the appropriate graph axis values on the proper figures gives the following results:

Lung Damage - no significant lung damage

Ear Damage - just below threshold eardrum
rupture

Skull Impact Damage - no expected skull fracture
body injury.

Whole Body Impact Damage - no significant whole
body injury.

LIST OF REFERENCES

1. Glasstone, Samuel, Editor, "The Effects of Nuclear Weapons," prepared by U. S. Atomic Energy Commission for U. S. Department of Defense, Revised Edition, February 1964, pp. 147.
2. Jarrett, D. E., "Derivation of the British Explosive Safety Distances," Annals of the New York Academy of Sciences, Vol. 152, Art. 1, October 1968, pages 32 and 33.
3. Burenin, P. I., "Effect of Shock Waves," Final Report on Contract NASA-2485, Techtran Corporation, March 1974.
4. White, Clayton S., "The Scope of Blast and Shock Biology and Problem Areas in Relating Physical and Biological Parameters," Annals of the New York Academy of Sciences, Vol. 152, Art. 1, October 1968, pp. 89+.
5. White, Clayton S., Robert K. Jones, Edward G. Damon, E. Royce Fletcher, and Donald R. Richmond, "The Biodynamics of Air-blast," Technical Report to Defense Nuclear Agency, DNA 2738T, Lovelace Foundation for Medical Education and Research, July 1971. AD 734208.
6. Richmond, Donald R., Edward G. Damon, E. Royce Fletcher, I. Gerald Bowen, and Clayton S. White, "The Relationship Between Selected Blast-Wave Parameters and the Response of Mammals Exposed to Air Blast," Annals of the New York Academy of Sciences, Vol. 152, Art. 1, October 1968, pp. 103+.
7. Damon, Edward G., John T. Yelverton, Ulrich C. Luft, Kabby Mitchell, Jr., and Robert K. Jones, "The Acute Effects of Air Blast on Pulmonary Function in Dogs and Sheep," Technical Progress Report to Defense Atomic Support Agency, DASA 2461, Lovelace Foundation for Medical Education and Research, March 1970. AD 709972.
8. Bowen, I. G., E. R. Fletcher, D. R. Richmond, "Estimate of Man's Tolerance to the Direct Effects of Air Blast," Technical Report to Defense Atomic Support Agency, DASA 2113, Lovelace Foundation for Medical Education and Research, October 1968. AD 693105.

9. Damon, Edward G., Donald R. Richmond, E. Royce Fletcher, and Robert K. Jones, "The Tolerance of Birds to Airblast," Final Report to Defense Nuclear Agency, DNA 3314F, Lovelace Foundation for Medical Education and Research, July 1974. AD 785259.
10. Hirsch, Frederic G., "Effects of Overpressure on the Ear-A Review," Annals of the New York Academy of Sciences, Vol. 152, Art. 1, October 1968, pp. 147+.
11. Damon, Edward G., Ernest A. Henderson, and Robert K. Jones, "The Effects of Intermittent Positive Pressure Respiration on Occurrence of Air Embolism and Mortality Following Primary Blast Injury," Technical Report to Defense Nuclear Agency, DNA 2989F, Lovelace Foundation for Medical Education and Research, January 1973. AD 754448.
12. Damon, Edward G., John T. Yelverton, Ulrich C. Luft, and Robert K. Jones, "Recovery of the Respiratory System Following Blast Injury," Technical Progress Report to Defense Atomic Support Agency, DASA 2580, Lovelace Foundation for Medical Education and Research, October 1970. AD 718369.
13. Clemedson, Carl-Johan, Gustav Hellström, and Sten Lingren, "The Relative Tolerance of the Head, Thorax, and Abdomen to Blunt Trauma," Annals of the New York Academy of Sciences, Vol. 152, Art. 1, October 1968, pp. 187+.
14. Hirsch, Arthur E., "The Tolerance of Man to Impact," Annals of the New York Academy of Sciences, Vol. 152, Art. 1, October 1968, pp. 168+.
15. Glasstone, Samuel, The Effects of Nuclear Weapons, U. S. Government Printing Office, Revised Edition, April 1962.
16. von Gierke, Henning E., "On the Dynamics of Some Head Injury Mechanisms," Aerospace Medical Research Laboratories, Wright-Patterson Air Force Base, Ohio, 1971. AD 728885.
17. White, Clayton S., I. Gerald Bowen, Donald R. Richmond, and Robert L. Corsbie, "Comparative Nuclear Effect of Biomedical Interest," CEX-58.8, Civil Effects Study, U. S. Atomics Energy Commission, January 1971.

18. Champion, K. S. W., W. J. O'Sullivan, Jr., and Sidney Jeweles, U. S. Standard Atmosphere, 1962, U. S. Government Printing Office, Washington, D. C., December 1962.
19. Ross, R., et al, "Criteria for Assessing Hearing Damage Risk from Impulse-Noise Exposure," Human Engineering Laboratory, Aberdeen Proving Ground, Maryland, August 1967. AD 666-206.
20. White, Clayton S., "The Nature of the Problems Involved in Estimating the Immediate Casualties from Nuclear Explosions," Civil Effects Test Operations, U. S. Atomic Energy Commission, July 1971, DR-1886.

APPENDIX III: A

STRUCTURAL RESPONSE

Various structural response solutions have been presented. This appendix gives the development of some of those relationships and data used to substantiate their validity. Response solutions developed elsewhere are referenced, rather than rederived.

3A-1 Overturning Analysis

Consider any rigid target such as a truck which can be struck from the side with a blast pulse. The natural rocking period of this object can closely be approximated as an inverted pendulum, and is very long, on the order of seconds. So, the response for any energy release less than that of a nuclear weapon is in the impulsive loading realm. We will determine if the structure overturns by comparing the impulse imparted to the target to the threshold impulse necessary to just overturn the object.

First compute the threshold specific impulse i_0 . If the target has a total height h , presented area A , a width b , a center of gravity (c.g) height off the ground h_{cg} , a center of pressure h_{cp} , mass m , and a gravitational field of g , then the threshold work W_k to raise the c.g. to brink of toppling is:

$$W_k = mg \left(\sqrt{\frac{b^2}{4} + h_{cg}^2} - h_{cg} \right) \quad (3A-1)$$

If mass is fairly uniformly distributed throughout the body, the mass moment of inertia about the c.g. is approximately given by:

$$J_{cg} = \frac{m}{12} (b^2 + h^2) \quad (3A-2)$$

Transferring this mass moment of inertia from the c.g. to the point of overturning gives:

$$J = m \left(\frac{b^2}{3} + \frac{h^2}{12} + h_{cg}^2 \right) \quad (3A-3)$$

Assume toppling with no sliding. The rotational kinetic energy initially imparted to the body KE equals $(1/2)J\omega^2$ where ω is the initial angular velocity. Substituting for J and equating KE to W_k gives, after some manipulation:

$$\omega = \sqrt{2g} \frac{\sqrt{\sqrt{\frac{b^2}{4} + h_{cg}^2} - h_{cg}}}{\sqrt{\frac{b^2}{3} + \frac{h^2}{12} + h_{cg}^2}} \quad (3A-4)$$

By applying conservation of angular momentum, one can write:

$$i_\theta Ah_{bl} = J\omega \quad (3A-5)$$

Substituting for J and ω plus rearranging terms finally yields:

$$\frac{i_\theta Ah_{bl}}{mg^{1/2} b^{3/2}} = -\sqrt{\left[\frac{2}{3} + \frac{h^2}{6b^2} + \frac{2h^2}{b^2} \left(\frac{h_{cg}^2}{h^2}\right)\right] \left[-\sqrt{\frac{1}{4} + \frac{h^2}{b^2} \left(\frac{h_{cg}^2}{h^2}\right)} - \frac{h}{b} \left(\frac{h_{cg}}{h}\right)\right]} \quad (3A-6)$$

Equation (3A-6) is the relationship plotted as Figure 3-4.

Next we must compute the impulse i_s imparted to the target. This total impulse is made up of the sum of a diffracted phase of loading and a drag phase of loading. A free-field blast pressure history can be approximated by

$$p(t) = P_s \left(1 - \frac{t}{T}\right) e^{-t/T} \quad (3A-7)$$

where T is the positive duration. Integrating Equation (3A-7) from zero to T yields the side-on impulse i_s or, conversely, the duration T if P_s and i_s are specified

$$T = ei_s / P_s \quad (3A-8)$$

Actually we are more interested in the drag pressure q than free-field pressures. A transient drag pressure history is closely approximated by:

$$q(t) = q \left(1 - \frac{t}{T}\right)^2 e^{-2t/T} \quad (3A-9)$$

Integrating Equation (3A-9) gives a drag impulse i_q of:

$$i_q = \frac{qT}{4} \left(1 - \frac{1}{e^2}\right) \quad (3A-10)$$

Finally to express i_q as a function of P_s and i_s , we must write q as a function of P_s . This relationship is given by:

$$q = \frac{5C_D P_s^2}{2(7P_0 + P_s)} \quad (3A-11)$$

where C_D is a drag coefficient. Substituting Equation (3A-11) for Equation (3A-9) and Equation (3A-8) for T into Equation (3A-10) gives the desired drag impulse i_q as a function of P_s and i_s .

$$i_q = \frac{1.47 (P_s/P_0)}{(7.0 + P_s/P_0)} (C_D i_s) \quad (3A-12)$$

Next, the diffracted impulse i_r must be estimated. This equals:

$$i_r = \frac{P H}{2U} \quad (3A-13)$$

where U is shock front velocity, P_r is the peak reflected pressure, and H is the smaller of either vehicle height h or vehicle length L . Expressions for U and P_r must also be written as function of P_s . These are given by:

$$\left(\frac{U}{a_0}\right)^2 = 1.0 - 0.857 \frac{P_s}{P_0} \quad (3A-14)$$

and

$$\frac{P_r}{P_s} = 2.0 + \frac{6 P_s}{7 P_o + P_s} \quad (3A-15)$$

where a_0 is the speed of sound in air ahead of the shock. Substituting Equation (3A-14) and (3A-15) into Equation (3A-13) then yields:

$$i_r = \sqrt{\frac{1.0 + \frac{3 P_s / P_o}{(7 + P_s / P_o)}}{1.0 + 0.857 (P_s / P_o)}} \frac{P_s H}{a_0} \quad (3A-16)$$

But, i_r is the sum of i_s and i_t . Hence after adding together Equations (3A-12) and (3A-16) plus dividing through by $\frac{P_o H}{a_0}$ we get:

$$\frac{a_i}{P_o H} = \frac{1.47(P_s / P_o) \left(\frac{a_o C_D i_s}{P_o H} \right)}{(7.0 + P_s / P_o)} + \frac{\left[1.0 + \frac{3 P_s / P_o}{(7.0 + P_s / P_o)} \right] (P_s / P_o)}{\sqrt{1.0 + 0.857 (P_s / P_o)}} \quad (3A-17)$$

Equation (3A-17) is the relationship plotted in Figure 3-3.

Various tests have been conducted which can be used to demonstrate the validity of this solution.

Johnson, Mayerhofer, and Schuman⁽¹⁾ describe a series of experiments in which 76.2 mm, 152 mm, 228 mm, and 305 mm diameter cylinders all of the same height (1.555 m), same mass (26.99 kg), same c.g. location (9.695 in), and essentially the same effective depth of target base were placed in blast fields of various intensities. The target bases were larger than the cylinder diameters. The distance from the center of the cylinder to the pivot point (which equals half of b) was 0.203 m, (0.667 ft). Because all shapes are cylinders, a single drag coefficient of 1.2 can be used for all targets. Table 3A-1 summarizes these test data.

TABLE 3A-1
OVERTURNING CYLINDER TEST DATA

<u>Reference</u>	<u>Target</u>	<u>P_s (kPa)</u>	<u>i_s (Pa · s)</u>	<u>A(m²)</u>	<u>Response</u>
<u>Diameter, mm</u>					
76.2		51.7	4,826	0.1185	over
76.2		27.5	3,447	0.1185	stood
76.2		6.89	1,138	0.1185	stood
152		34.4	3,999	0.2370	over
152		20.6	2,896	0.2370	stood
152		6.89	1,138	0.2370	stood
228		34.4	3,999	0.3554	over
228		20.6	2,896	0.3554	stood
228		6.89	1,138	0.3554	stood
305		34.4	3,999	0.4740	over
305		20.6	2,896	0.4740	over
305		6.89	1,138	0.4740	stood

These data can be cast into nondimensional format to determine if overturning is properly predicted. Because all cylinders have a smaller diameter than height, the parameter H equals the diameter D in these tests. Table 3A-2 presents in tabular form the calculations which are required. First, the scaled free-field pressures and impulses must be calculated as in the second and third columns of Table 3A-2. Then the scaled impulse applied to the target (a_i/p_D) is calculated from Figure 3-3. If column 4 is multiplied by $(p_D h_b / a mg^{1/2} b^{3/2})$, then a scaled applied load is created which can be compared to the scaled threshold impulse. Because h, b, and h_b are constant in all experiments, the quantities h/b and h_b/h equal 3.83 and 1.71 respectively in all tests, and the scaled threshold impulse from Figure 3-4 is constant in all experiments. Whenever $(i_t A_h b^{1/2} / mg^{1/2} b^{3/2})$ is greater than $(i_g A_h b^{1/2} / mg^{1/2} b^{3/2})$, we predict overturning in Table 3A-2; otherwise, we predict that the cylinders remain upright. As can be seen in Table 3A-2, all but two of the predictions are correct. The two which did not agree were close to the limit values.

There are other overturning data in References 2 and 3, where busses, a camper, and a truck were exposed to air blast waves and either severely rocked or overturned. Table 3A-3 summarizes experimental conditions for test on five different vehicles described in these two sources. The same type of calculations must be made as were performed on the cylinders. These computations are summarized in Table 3A-4. The second and third

TABLE 3A-2

OVERTURNING CALCULATIONS FOR CYLINDERS

Reference Target Dia- meter, mm	$\frac{P_s}{P_o}$	$\frac{a_o C_D l_s}{P_o D}$	$\frac{a_l}{P_o D}$	$\frac{l_s A h_{b_f}}{mg^{1/2} b^{3/2}}$	$\frac{l_g A h_{b_f}}{mg^{1/2} b^{3/2}}$	Response	Properly Predicted
76.2	0.510	246.7	25.14	2.48	1.302	over	yes
76.2	0.272	176.2	9.96	0.985		stood	yes
76.2	0.068	58.2	0.89	0.088		stood	yes
152	0.340	102.2	7.30	3.25		over	yes
152	0.204	74.0	3.28	1.46		stood	no
152	0.068	29.1	1.03	0.460		stood	yes
228	0.340	68.2	4.98	4.436		over	yes
228	0.204	49.4	2.26	2.012		stood	no
228	0.068	19.4	0.34	0.304		stood	yes
305	0.340	51.1	3.82	6.04		over	yes
305	0.204	37.0	1.74	2.76		over	yes
305	0.068	14.5	0.27	0.432	1.302	stood	yes

TABLE 3A-3

VEHICLE OVERTURNING TEST DATA

Vehicle	P_s (Pa)	l_s (Pa · s)	C_D	h (m)	h_{cg} (m)	b (m)	$A(m^2)$	$m(kg)$	Response
NWC Bus 1959 Bluebird 44 passenger	58,500	964	1.8	3.05	1.02	2.14	25.7	7,040	Severe rocking
3/4 Ton Dodge 1953 camper NWC Test	63,400	1,070	1.8	2.13	0.915	1.68	7.65	2,260	Severe rocking loss camper
Dial Pack Test 1951 Reo Bus 55 Passenger	48,200	4,480	1.8	2.67	0.965	2.14	18.0	5,630	Severe rocking
Dial Pack Test 1957 GMC Bus 20 Passenger	11,700	1,860	1.8	2.38	0.853	1.76	11.1	2,960	Little or no damage
NWL Test 2 1/2 ton truck	310,000	1,210	1.8	2.93	1.37	1.77	14.8	5,430	Overturned

columns are the scaled overpressures and impulses in the free-field. By using the loads, the applied scaled impulses are obtained as in the fourth column from Figure 3-4. Multiplying this applied load by $(p_0 h A_h / a mg^{1/2} b^{3/2})$ then gives a scaled applied load in the fifth column which can be compared with the scaled threshold impulse in the eighth column.

TABLE 3A-4
OVERTURNING CALCULATIONS FOR VEHICLES

<u>Vehicle</u>	$\frac{P_s}{P_0}$	$\frac{s_{CDs}}{P_0 h}$	$\frac{s_t}{P_0 h}$	$\frac{t^{AH}_{bl}}{m s^{1/2} b^{3/2}}$	$\frac{h}{b}$	$\frac{h_{cg}}{h}$	$\frac{V^{AH}_{th}}{m s^{1/2} b^{3/2}}$	Overtur	Properly Predicted
44 Pass. Bus	0.578	1.85	0.792	0.447	1.43	0.333	0.568	no	yes
Camper	0.627	2.93	0.981	0.415	1.27	0.428	0.546	no	yes
55 Pass. Bus	0.477	9.85	1.40	0.502	1.25	0.363	0.544	no	yes
20 Pass. Bus	0.116	4.57	0.224	0.103	1.36	0.358	0.553	no	yes
2 1/2 Ton Truck	3.07	2.41	3.93	2.08	1.65	0.670	0.585	yes	yes

To determine the threshold overturning impulse, (h/b) and (h_{cg}/h) are computed as in the sixth and seventh columns of Table 3A-4. Figure 3-4 is then used to obtain the scaled threshold overturning impulse as in the eighth column. If the fifth column of Table 3A-4 exceeds the eighth column, then we predict vehicle overturning; otherwise, the vehicles do not overturn. As can be seen in Table 3A-4, the response of all vehicles is properly predicted.

3A-2 Development of Beam Equations

The development of both the beam equations in this section and the plate equations in the next section closely follow a procedure advocated by Westine and Baker⁽⁴⁾. These solutions are energy ones which yield residual conditions, but not transient time histories of response. Basically the procedure being followed is:

- (1) assume a deformed shape for the structural element which is consistent with boundary conditions,
- (2) calculate the strain energy stored in the structural element because of this deformed shape,
- (3) compute the kinetic energy imparted to the structural element because of this deformed shape,

- (4) compute the maximum possible work performed as the peak applied load displaces with the assumed deformed shape,
- (5) obtain the impulsive loading realm asymptote by equating the strain energy to the kinetic energy, and
- (6) obtain the quasi-static loading realm asymptote by equating the maximum possible work to the strain energy.

This procedure was followed in making estimates for structural response in elastic simply-supported beams, cantilever beams, and clamped-clamped beams. One derivation will be presented to indicate the method; results will be given for other boundary conditions. Assume that the deformed shape for a simply-supported beam is given by:

$$w = w_0 \cos \frac{\pi x}{L} \quad (3A-18)$$

where L is the total span
 w_0 is the deflection at mid-span
 w is the deflection anywhere in the beam
 x is the coordinate system with its origin at mid-span that locates one's position on the beam.

Substituting into the small deflection moment-curvature relationship yields, after differentiating Equation (3A-18) twice,

$$M = -EI \frac{d^2 w}{dx^2} = -\frac{\pi^2 w_0 EI}{L^2} \cos \frac{\pi x}{L} \quad (3A-19)$$

where M is the moment at some location in the beam
 E is the modulus of elasticity
 I is the second moment of area

But, the strain energy U is obtained from:

$$U = \frac{1}{2} \int_0^{L/2} \frac{M^2 dx}{2EI} \quad (3A-20)$$

After performing the required integration:

$$U = \frac{\frac{4}{\pi} w_0^2 EI}{4 L^3} \quad (3A-21)$$

The kinetic energy KE equals the summation over the beam of half of a differential mass times the initial velocity squared. If one uses conservation of momentum to determine the initial velocity, kinetic energy is given by

$$KE = \sum_{beam} \frac{1}{2} m v_0^2 = \int_0^L \frac{1}{2} (\rho A dx) \left(\frac{i b dx}{\rho A dx} \right)^2 \quad (3A-22)$$

where ρ = beam mass density
 A = beam cross sectional area
 b = beam width
 i = applied specific impulse

After performing the required integration:

$$KE = \frac{i^2 b^2 L}{2 \rho A} \quad (3A-23)$$

The work W_k imparted to the beam is obtained by summing over the surface the peak pressure p times the deflection w times the area $b dx$. After substituting the assumed deformed shape for w , this summation is given by:

$$W_k = \sum_{beam} p w b dx = 2 p w_0 b \int_0^{L/2} \cos \frac{\pi x}{L} dx \quad (3A-24)$$

After performing the required integration:

$$W_k = \frac{2}{\pi} p w_0 b L \quad (3A-25)$$

The equation of the deflection asymptote in the impulsive loading realm is obtained by equating KE to U to obtain:

$$\frac{i^2 b^2 L}{2 \rho A} = \frac{\frac{4}{\pi} w_0^2 EI}{4 L^3} \quad (3A-26)$$

Or,

$$\frac{ibL}{\sqrt{\rho EI A}} = \frac{\pi^2}{\sqrt{2}} \left(\frac{w_o}{L} \right) \quad \begin{cases} \text{S. S. beam} \\ \text{impulsive realm} \end{cases} \quad (3A-27)$$

But the maximum strain ϵ_{max} is given by:

$$\epsilon_{max} = \frac{\sigma_{max}}{E} = \frac{M_{max} h}{2 EI} \quad (3A-28)$$

The maximum moment in Equation (3A-19) occurs when the $\cos(\pi x)/L$ equals 1.0. Substituting Equation (3A-27) into Equation (3A-19) for w/L , and Equation (3A-19) when maximized into Equation (3A-28), then gives:

$$\epsilon_{max} = \frac{1}{\sqrt{2}} \frac{ibh}{\rho EI A} \quad (3A-29)$$

If we wish to prevent yielding, the impulse asymptote is finally obtained by setting $\epsilon_{max} = \sigma_y/E$, where σ_y is the yield stress, and rearranging terms to obtain:

$$\frac{\frac{ibh\sqrt{E}}{\sigma_y\sqrt{\rho I A}}}{\sqrt{2}} = \sqrt{2} \quad \begin{cases} \text{S. S. beam} \\ \text{impulsive asymptote} \end{cases} \quad (3A-30)$$

This asymptote is the one plotted in Figure 3-5 for simply-supported beams. The asymptote for the quasi-static realm is obtained by equating W_k to U to obtain:

$$\frac{2}{\pi} \rho w_o b L = \frac{\frac{4}{\pi} w_o^2 E}{2 L^3} \quad (3A-31)$$

Or,

$$\frac{\rho b L^3}{EI} = \frac{\pi^5}{8} \left(\frac{w_o}{L} \right)^2 \quad \begin{cases} \text{S. S. beam} \\ \text{quasi-static realm} \end{cases} \quad (3A-32)$$

Substituting Equation (3A-32) into Equation (3A-19) and Equation (3A-19) into Equation (3A-28) then gives:

$$\epsilon_{\max} = \frac{4 p b h L^2}{\pi^3 E I} \quad (3A-33)$$

Setting $\epsilon_{\max} = \sigma_y/E$ and rearranging terms finally gives the quasi-static loading realm asymptote:

$$\frac{p b h L^2}{\sigma_y I} = \frac{\pi^3}{4} \quad \left\{ \begin{array}{l} \text{S. S. beam} \\ \text{quasi-static asymptote} \end{array} \right\} \quad (3A-34)$$

This equation is the other asymptote plotted in Figure 3-5 for simply-supported beams. The curved transition between the asymptotes was obtained by exercising personal judgement to draw in a curve. This transition is similar to an analytic curve for a single-degree-of-freedom linear oscillator. The same procedures are also used to determine asymptotes and solutions for cantilever and clamped beams.

The assumed deformed shape for a cantilever beam is:

$$w = w_0 \left(1 - \cos \frac{\pi x}{2L} \right) \quad (3A-35)$$

where w_0 is the tip deformation
 L is the total span
 w is the deformation anywhere in the beam
 x is the reference coordinate with an origin at the root of the beam

This gives

$$\frac{i b L}{\sqrt{\rho E I A}} = \frac{\pi^2}{4\sqrt{2}} \left(\frac{w_0}{L} \right) \quad \left\{ \begin{array}{l} \text{cantilever beam} \\ \text{impulsive realm} \end{array} \right\} \quad (3A-36)$$

and

$$\epsilon_{\max} = \frac{1}{\sqrt{2}} \frac{i b h}{\sqrt{\rho E I A}} \quad (3A-37)$$

If we limit the maximum strain to yielding, the cantilever impulsive loading realm asymptote is obtained:

$$\frac{i b h \sqrt{E}}{\sigma_y \sqrt{\rho I A}} = \sqrt{2} \quad \left\{ \begin{array}{l} \text{cantilever beam} \\ \text{impulsive asymptote} \end{array} \right\} \quad (3A-38)$$

This is the asymptote plotted in Figure 3-5. Equating the work to U gives the quasi-static loading realm asymptote:

$$\frac{p b L^3}{E I} = \frac{5}{64(\pi - 2)} \left(\frac{w_o}{L} \right) \quad \left\{ \begin{array}{l} \text{cantilever beam} \\ \text{quasi-static realm} \end{array} \right\} \quad (3A-39)$$

The maximum moment is the root of the cantilever beam. Substituting moment from Equation (3A-28) gives:

$$\epsilon_{max} = \frac{8(\pi - 2)}{\pi^3} \frac{p b h L^2}{E I} \quad (3A-40)$$

After limiting the strain to yielding, the cantilever quasi-static loading realm asymptote is obtained:

$$\frac{p b h L^2}{\sigma_y I} = \frac{\pi^3}{8(\pi - 2)} \quad \left\{ \begin{array}{l} \text{cantilever beam} \\ \text{quasi-static asymptote} \end{array} \right\} \quad (3A-41)$$

This is the other cantilever beam asymptote plotted in Figure 3-5. The transition was faired in the same manner as for simply-supported beams.

The last beam solution is for clamped beams. The strain energy in a clamped beam can be estimated by realizing that a clamped beam is equivalent to two simply-supported beams fastened end-to-end as in Figure (3A-1).

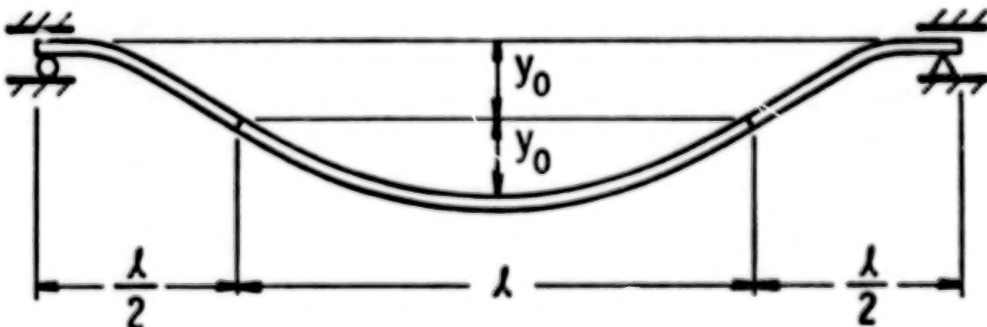


Figure 3A-1. Geometry of a Clamped Beam

The resulting impulsive realm equation is:

$$\frac{ibL}{\sqrt{\rho EI A}} = \pi^2 \sqrt{2} \left(\frac{w_o}{L} \right) \quad \left. \begin{array}{l} \text{clamped beam} \\ \text{impulsive realm} \end{array} \right\} \quad (3A-42)$$

After limiting the maximum strain to yielding, we have:

$$\frac{ibh\sqrt{E}}{\sigma_y \sqrt{\rho I A}} = \sqrt{2} \quad \left. \begin{array}{l} \text{clamped beam} \\ \text{impulsive asymptote} \end{array} \right\} \quad (3A-43)$$

This is the asymptote plotted in Figure 3-5. It is identical to the simply-supported beam impulsive asymptote.

Equating the work W_k to the strain energy U gives the quasi-static loading realm asymptote:

$$\frac{pbL^3}{EI} = 2\pi^4 \left(\frac{w_o}{L} \right) \quad \left. \begin{array}{l} \text{clamped beam} \\ \text{quasi-static realm} \end{array} \right\} \quad (3A-44)$$

Or, after limiting the strain to yielding:

$$\frac{pbhL^2}{\sigma_y I} = 2\pi^2 \quad \left. \begin{array}{l} \text{clamped beam} \\ \text{quasi-static asymptote} \end{array} \right\} \quad (3A-45)$$

This asymptote is the final one plotted in Figure 3-5.

As proof that this approach predicts elastic strains in cantilever beams, we will use test data on rectangular aluminum beams in the impulsive realm as reported by Baker, et al⁽¹⁵⁾, and unpublished data on rectangular steel beams in the quasi-static realm obtained by J. D. Day. Substituting $bh^3/12$ for I and bh for A in Equation (3A-37) yields the following equation for elastic strain at the root of a rectangular cantilever beam in the impulsive loading realm. This equation is plotted in

$$\epsilon = 2.45 \frac{i}{h\sqrt{\rho E}} \quad (3A-46)$$

Figure (3A-2) and compared to Baker's test data on 6061-T6 beams of

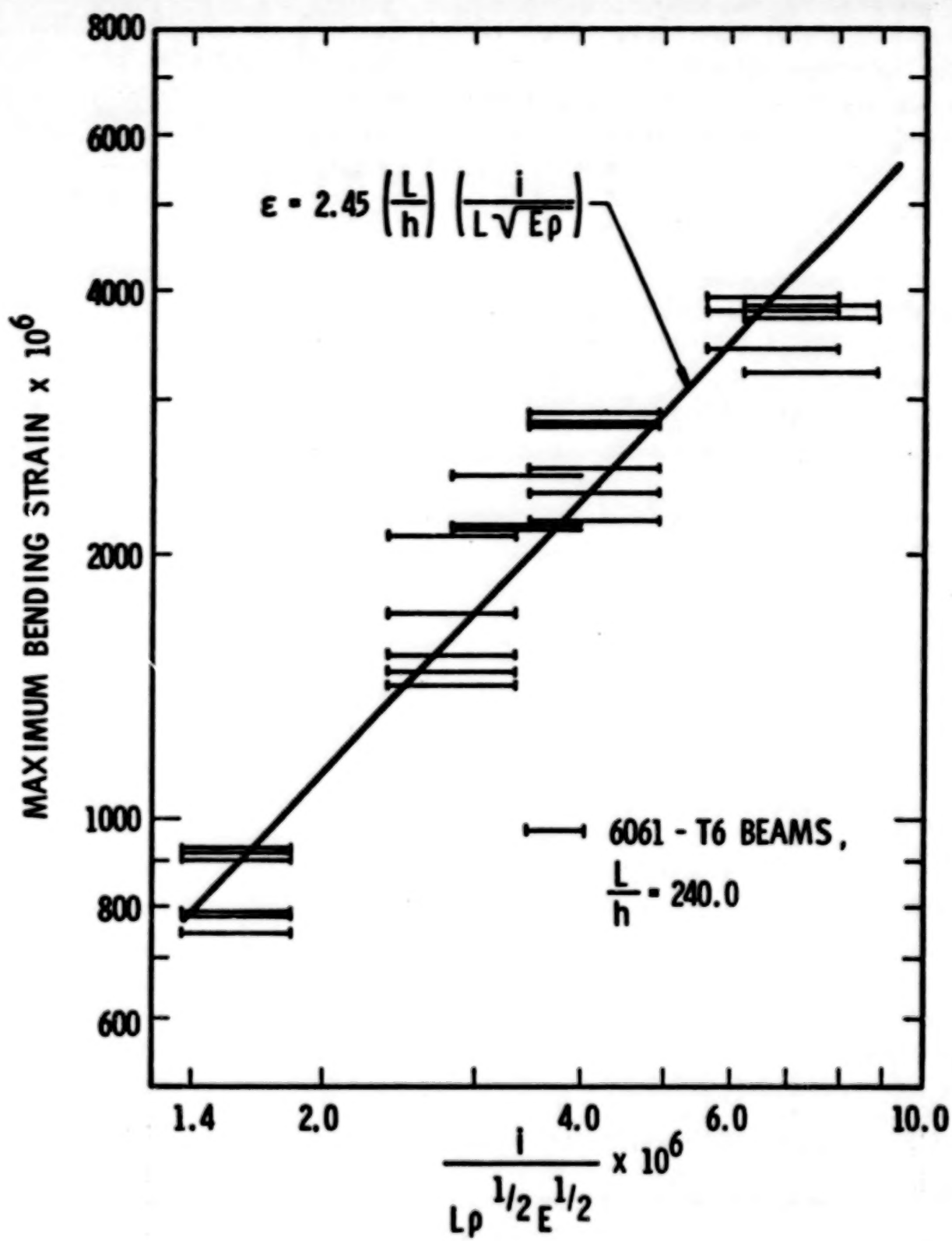


Figure 3A-2. Elastic Response of Cantilevers,
Impulsive Loading Realm

thickness 1.30 mm (0.051 in) and length 0.305 m (12.0 in). Bars rather than points are plotted as data because the applied impulse was calculated from charge weight and standoff relationships rather than measured. These bars begin and end with upper and lower limits for different techniques of estimating the loading. As can be seen, correlation is excellent.

Substituting $C_D q$ for p and $bh^3/12$ for I in Equation (3A-40) yields an expression for computing elastic root strains in cantilever rectangular beams in the quasi-static loading realm.

$$\epsilon = 3.534 \left(\frac{L}{h} \right)^2 \left(\frac{C_0 q}{E} \right) \quad (3A-47)$$

In Table 3A-5, Day's unpublished data on steel cantilevers which are 0.1524 m x 0.019 m x 0.019 m (6 in. x 0.75 in. x 0.75 in.) show that measured strains and calculated ones correlate well.

TABLE 3A-5
STRAINS AT ROOT OF CANTILEVER BEAMS
IN THE QUASI-STATIC REALM

<u>Test No.</u>	<u>P_s (kPa)</u>	<u>q (kPa)</u>	<u>Experimental $\epsilon \times 10^{+6}$</u>	<u>Calculated $\epsilon \times 10^{+6}$</u>
1	60	12	23.2	23.6
2	60	12	22.9	23.4
3	72	17	32.5	32.5
4	111	38	80.4	73.5
5	143	60	141.0	117.5

Although test data are not presented on beams with other boundary conditions, they should correlate also because the principles are identical and only the boundary conditions change.

3A-3 Development of Plate Equations

The same procedures are used to develop plate solutions as were used for beam solutions except that biaxial states of stress and the development of yield lines must be considered. For a simply-supported plate we assume a deformed shape given by

$$w = w_0 \cos \frac{\pi x}{2X} \cos \frac{\pi y}{2Y} \quad (3A-48)$$

where X and Y are half spans

x and y use the coordinate system whose origin is the middle of a plate

w_0 is the midspan deflection

w is the deflection at any x, y position

The strains are given in a bending plate by:

$$\epsilon_{xx} = -z \frac{\partial^2 w}{\partial x^2}, \quad \epsilon_{yy} = -z \frac{\partial^2 w}{\partial y^2}, \quad \text{and} \quad \epsilon_{xy} = 2z \frac{\partial^2 w}{\partial x \partial y} \quad (3A-49)$$

The strain energy U per unit volume under a biaxial state of stress is:

$$\frac{U}{\text{vol}} = \int_{\text{strains}} \left(\frac{E}{2} \epsilon_{xx}^2 + G \epsilon_{xy}^2 + \frac{E}{2} \epsilon_{yy}^2 \right) \quad (3A-50)$$

where E = modulus of elasticity

$$G = \text{shear modulus} = \frac{E}{2(1+\nu)}$$

Differentiating Equation (3A-48), substituting in the strain relationships, and squaring yields

$$\epsilon_{xx}^2 = \frac{\pi^2 w_0^2 z^2}{16 X^4} \cos^2 \left(\frac{\pi x}{2X} \right) \cos^2 \left(\frac{\pi y}{2Y} \right) \quad (3A-51a)$$

$$\epsilon_{yy}^2 = \frac{\pi^2 w_0^2 z^2}{16 Y^4} \cos^2 \left(\frac{\pi x}{2X} \right) \cos^2 \left(\frac{\pi y}{2Y} \right) \quad (3A-51b)$$

$$\epsilon_{xy}^2 = \frac{\pi^4 w_0^2 z^2}{4 X^2 Y^2} \sin^2 \left(\frac{\pi x}{2X} \right) \sin^2 \left(\frac{\pi y}{2Y} \right) \quad (3A-51c)$$

Substituting for G in Equation (3A-50), 0.3 for v , and Equation (3A-51) yields a triple integral for the strain energy. Performing the required integration and collecting terms eventually yields:

$$U = \frac{\pi^4}{6(4)^3} \frac{Ew_0^2 h^3}{XY} \left[\left(\frac{Y}{X}\right)^2 + 3.08 + \left(\frac{X}{Y}\right)^2 \right] \quad (3A-52)$$

The kinetic energy imparted to the plate is easily determined. It equals:

$$KE = \sum_{\text{plate}} \frac{m}{2} v_0^2 = 4 \int_0^X \int_0^Y \left[\frac{i^2 (dx)^2 (dy)^2}{2 \rho h (dx)(dy)} \right] = 2i^2 \frac{XY}{\rho h} \quad (3A-53)$$

Equating KE to U gives the impulsive loading realm asymptote of:

$$\frac{w_0}{Y} = \frac{16\sqrt{3}}{\pi^2 \left[\left(\frac{Y}{X}\right)^2 + 3.08 + \left(\frac{X}{Y}\right)^2 \right]^{1/2}} \left(\frac{iX}{\sqrt{\rho E} h^2} \right)$$

The strains are maximum in the center of a simply-supported plate and at its outer fibers; i.e., at $\cos \pi x/2\pi = 1.0$, $\cos \pi y/2Y = 1.0$, and $z = h/2$ where

$$\epsilon_{xx_{\max}} = \frac{\pi^2}{8} \left(\frac{h}{X} \right) \left(\frac{Y}{X} \right) \left(\frac{w_0}{Y} \right) \quad (3A-55a)$$

$$\epsilon_{yy_{\max}} = \frac{\pi^2}{8} \left(\frac{h}{Y} \right) \left(\frac{w_0}{Y} \right) \quad (3A-55b)$$

$$\epsilon_{xy} = 0 \quad (3A-55c)$$

Substituting for w_0/Y then gives:

$$\epsilon_{xx_{max}} = \frac{2\sqrt{3}}{\left[1.0 + 3.08 \left(\frac{X}{Y}\right)^2 + \left(\frac{X}{Y}\right)^4\right]^{1/2}} \left(\frac{i}{\sqrt{\rho E h}} \right) \quad (3A-56a)$$

$$\epsilon_{yy_{max}} = \frac{2\sqrt{3}}{\left[1.0 + 3.08 \left(\frac{Y}{X}\right)^2 + \left(\frac{Y}{X}\right)^4\right]^{1/2}} \left(\frac{i}{\sqrt{\rho E h}} \right) \quad (3A-56b)$$

But, in a plate, stress is related to elastic strain through Hooke's Law:

$$\sigma_{xx} = \frac{E}{(1 - \nu^2)} \left(\epsilon_{xx} + \nu \epsilon_{yy} \right) \quad (3A-57a)$$

$$\sigma_{yy} = \frac{E}{(1 - \nu^2)} \left(\epsilon_{yy} + \nu \epsilon_{xx} \right) \quad (3A-57b)$$

Hence substituting for strains yields:

$$\frac{\sigma_{xx_{max}}}{E} = \left(\frac{3.81 i}{\sqrt{\rho E h}} \right) \left[\frac{0.3 + \left(\frac{Y}{X}\right)^2}{1.0 + 3.08 \left(\frac{Y}{X}\right)^2 + \left(\frac{Y}{X}\right)^4} \right]^{1/2} \quad (3A-58a)$$

$$\frac{\sigma_{yy_{max}}}{E} = \left(\frac{3.81 i}{\sqrt{\rho E h}} \right) \left[\frac{1.0 + 0.3 \left(\frac{Y}{X}\right)^2}{1.0 + 3.08 \left(\frac{Y}{X}\right)^2 + \left(\frac{Y}{X}\right)^4} \right]^{1/2} \quad (3A-58b)$$

Next we need a yield criterion for a biaxial state of stress. If we use the Huber-Hencky-Mises distortion energy yields criterion,

$$(\sigma_{yy} - \sigma_{zz})^2 + (\sigma_{zz} - \sigma_{xx})^2 + (\sigma_{xx} - \sigma_{yy})^2 = 2 \sigma_y^2 \quad (3A-59)$$

where σ_y is the yield stress under unaxial loading.

In Equation (3A-59) σ_{zz} equals zero; hence Equation (3A-59) becomes:

$$\left(\frac{\sigma_{yy}}{E}\right)^2 - \left(\frac{\sigma_{yy}}{E}\right) \left(\frac{\sigma_{xx}}{E}\right) + \left(\frac{\sigma_{xx}}{E}\right)^2 = \left(\frac{\sigma_y}{E}\right)^2 \quad (3A-60)$$

Substituting Equations (3A-58) in Equation (3A-60) and gathering terms finally yields the impulsive loading realm asymptote for a simply-supported plate:

$$\left(\frac{3.81\sqrt{E}i}{\sigma_y \sqrt{\rho} h}\right) = \left[\frac{1.0 + 3.08 \left(\frac{X}{Y}\right)^2 + \left(\frac{X}{Y}\right)^4}{0.79 + 0.11 \left(\frac{X}{Y}\right)^2 + 0.79 \left(\frac{X}{Y}\right)^4} \right]^{1/2} \begin{cases} \text{brittle S.S. plate} \\ \text{impulsive asymptote} \end{cases} \quad (3A-61)$$

This is the asymptote plotted in Figure 3-6 for a brittle simply-supported plate in the impulsive realm. The i function in Figure 3-6 accounts for the effects of the (X/Y) aspect ratio and any numerical constants. A simply-supported plate is assumed to fail by shattering upon reaching yield anywhere in the plate.

Even though a ductile plate has reached yield at its center, this plate will neither rupture nor deform plastically. Before permanent plastic deformation can be observed, a ductile plate must form a collapse mechanism by the creation of yield lines. This behavior gives a ductile material more energy absorbing capabilities than its brittle counterpart. It is very difficult to extend this solution to an elastic-plastic one; however, we will do it by ignoring any localized plastic behavior so the elastic solution can be extended. Although this approach is not rigorous, it is used to obtain acceptable engineering answers. In a simply-supported plate the yield lines which originate at the center eventually propagate out toward the plate corners. After reaching the corners, the plate collapses. In the corners at $x = X/2$ and $y = Y/2$, no normal stresses exist. Collapse is caused by shear stresses reaching the appropriate yield condition. In the corner, the shear stress is given by:

$$\epsilon_{xy} = \frac{\frac{\pi^2}{2} z w_0}{XY} \quad (3A-62)$$

Substituting $h/2$ for z and Equation (3A-54) for w_0/Y yields:

$$\epsilon_{xy} = \frac{4\sqrt{3} i}{h\sqrt{\rho E} \left[\left(\frac{Y}{X}\right)^2 + 3.08 + \left(\frac{X}{Y}\right)^2 \right]^{1/2}} \quad (3A-63)$$

The yield criterion for shear requires that $\tau_y = \sigma_y/\sqrt{3}$. Setting this yield stress equal to $G\epsilon_{xy}$ and rearranging terms finally yields:

$$\frac{\sqrt{E} i}{\sigma_y \sqrt{\rho h}} = \frac{1+v}{6} \left[\left(\frac{Y}{X}\right)^2 + 3.08 + \left(\frac{X}{Y}\right)^2 \right]^{1/2} \left\{ \begin{array}{l} \text{ductile S.S.} \\ \text{plate} \\ \text{impulsive} \\ \text{asymptote} \end{array} \right\} \quad (3A-64)$$

This is the asymptote plotted in Figure 3-6 for a ductile, simply-supported plate in the impulsive loading realm.

Before the quasi-static asymptotes can be calculated for a simply-supported plate, the maximum possible work must be estimated. This work W_k is given by the integral:

$$W_k = 4 \int_0^X \int_0^Y p w dx dy = 4 p w_0 \int_0^X \int_0^Y \cos \frac{\pi x}{2X} \cos \frac{\pi y}{2Y} dx dy = \frac{16}{\pi^2} p w_0 XY \quad (3A-65)$$

Equating W_k to U gives the quasi-static loading realm asymptote of:

$$\frac{w_0}{Y} = \frac{6(4)^5 p X^2 Y}{\pi^6 E h^3 \left[\left(\frac{Y}{X}\right)^2 + 3.08 + \left(\frac{X}{Y}\right)^2 \right]} \quad (3A-66)$$

Substituting Equation (3A-66) into the strain Equation (3A-55) and using Hooke's Law gives:

$$\frac{\sigma_{xx_{max}}}{E} = \frac{8.68 \left(\frac{P}{E}\right) \left(\frac{Y^2}{h^2} + 0.3 \frac{X^2}{h^2} \right)}{\left[\left(\frac{Y}{X}\right)^2 + 3.08 + \left(\frac{X}{Y}\right)^2 \right]} \quad (3A-67a)$$

$$\frac{\sigma_{yy_{max}}}{E} = \frac{8.68 \left(\frac{P}{E}\right) \left(\frac{X^2}{h^2} + 0.3 \frac{Y^2}{h^2} \right)}{\left[\left(\frac{Y}{X}\right)^2 + 3.08 + \left(\frac{X}{Y}\right)^2 \right]} \quad (3A-67b)$$

Finally use of Equation (3A-60) as a yield criterion, substitution of Equation (3A-67) into Equation (3A-60) and algebraically rearranging terms gives the quasi-static loading realm asymptote for brittle fracture in a simply-supported plate.

$$\frac{8.68 p X^2}{\sigma_y h^2} = \frac{1.0 + 3.08 \left(\frac{X}{Y}\right)^2 + \left(\frac{X}{Y}\right)^4}{0.79 + 0.11 \left(\frac{X}{Y}\right)^2 + 0.79 \left(\frac{X}{Y}\right)^4}^{1/2} \left\{ \begin{array}{l} \text{brittle S. S.} \\ \text{plate} \\ \text{quasi-static} \\ \text{asymptote} \end{array} \right\} \quad (3A-68)$$

As in the impulsive loading realm, the ductile plate in the quasi-static loading realm is assumed to form a collapse mechanism when the shears in the corners reach yield. The shear stress in the corners is given by Equation (3A-62) in both loading realms. Substituting $h/2$ for z and Equation (3A-66) for w_0/Y gives:

$$\epsilon_{xy} = \frac{3(4)^5 p XY}{2\pi^4 E h^2 \left[\left(\frac{Y}{X}\right)^2 + 3.08 + \left(\frac{X}{Y}\right)^2 \right]^2} \quad (3A-69)$$

Finally, setting the shear yield stress $\sigma_y/\sqrt{3}$ equal to $[E/2(1+v)]\epsilon_{xy}$, substituting Equation (3A-69) for ϵ_{xy} , and rearranging terms yields the asymptote for ductile, simply-supported plates in the quasi-static loading realm.

$$\frac{\rho X^2}{\sigma_y h^2} = 0.09524 \left[\left(\frac{Y}{X} \right)^2 + 3.08 \left(\frac{X}{Y} \right) + \left(\frac{X}{Y} \right)^3 \right] \begin{cases} \text{ductile S.S.} \\ \text{plate} \\ \text{quasi-static} \\ \text{asymptote} \end{cases}$$

(3A-70)

This asymptote is also plotted in Figure 3-6, with the right hand side of the equation the Φ_{pDS} function.

Next, clamped plates were evaluated using the same approach. The assumed deformed shape for a clamped plate is given by:

$$w = \frac{w_0}{4} \left(1 + \cos \frac{\pi x}{X} \right) \left(1 + \cos \frac{\pi y}{Y} \right) \quad (3A-71)$$

The strains and the strain energy are still given by Equation (3A-49) and (3A-50), respectively. Manipulating as before, we get

$$U = \frac{2\pi^4}{(4)^4} \frac{E w_0^2 h^3}{XY} \left[\left(\frac{Y}{X} \right)^2 + 1.026 + \left(\frac{X}{Y} \right)^2 \right] \quad (3A-72)$$

The kinetic energy KE is independent of the deformed shape and is therefore the same in both clamped and simply-supported plates. Equating KE to U gives the impulsive loading realm asymptote of:

$$\frac{w_0}{Y} = \frac{16}{\pi^2 \left[\left(\frac{Y}{X} \right)^2 + 1.026 + \left(\frac{X}{Y} \right)^2 \right]^{1/2}} \sqrt{\frac{i X}{\rho E} h^2} \quad (3A-73)$$

Using methods identical to the previous ones, we get

$$\frac{4.40\sqrt{E} i}{\sigma_y \sqrt{\rho} h} = \left[\frac{1.0 + 1.026 \left(\frac{X}{Y} \right)^2 + \left(\frac{X}{Y} \right)^4}{0.79 + 0.11 \left(\frac{X}{Y} \right)^2 + 0.79 \left(\frac{X}{Y} \right)^4} \right]^{1/2} \begin{cases} \text{brittle clamped} \\ \text{plate} \\ \text{impulsive} \\ \text{asymptote} \end{cases}$$

(3A-74)

This asymptote was used in Figure 3-6 for a brittle clamped plate.

For a ductile material, no failure occurs until a yield line forms an ellipse close to the edge of the clamped plate. We have assumed that this yield line is finally completed when the location $y = Y$ and $x = 0$ yields.

Based on this assumption, our procedure gives:

$$\frac{4.40\sqrt{E_i}}{\sigma_y \sqrt{\rho} h} = \left[1.265 + 1.30 \left(\frac{Y}{X} \right)^2 + 1.265 \left(\frac{Y}{X} \right)^4 \right]^{1/2} \left\{ \begin{array}{l} \text{ductile clamped} \\ \text{plate} \\ \text{impulsive} \\ \text{asymptote} \end{array} \right\}$$

(3A-75)

This equation is also found in Figure 3-6.

The work W_k imparted to a clamped plate is given by the integral.

$$W_k = 4 \int_0^X \int_0^Y p w dx dy =$$

(3A-76)

$$pw_o \int_0^X \int_0^Y (1 + \cos \frac{\pi x}{X})(1 + \cos \frac{\pi y}{Y}) dx dy = pw_o XY$$

Equating W_k to U and manipulating gives the quasi-static loading realm asymptote of:

$$\frac{w_o}{Y} = \frac{(4)^4 p X^2 Y}{2 \pi^4 E h^3 \left[\left(\frac{Y}{X} \right)^2 + 1.026 + \left(\frac{X}{Y} \right)^2 \right]} \quad (3A-77)$$

Proceeding as before, we obtain the quasi-static asymptote for the initiation of brittle failure in a clamped plate.

$$\frac{3.55 p X^2}{\sigma_y h^2} = \frac{1.0 + 1.026 \left(\frac{X}{Y}\right)^2 \left(\frac{X}{Y}\right)^4}{\left[0.79 + 0.11 \left(\frac{X}{Y}\right)^2 + 0.79 \left(\frac{X}{Y}\right)^4\right]^{1/2}} \begin{cases} \text{brittle clamped} \\ \text{plate} \\ \text{quasi-static} \\ \text{asymptotic} \end{cases}$$

(3A-78)

This asymptote is plotted in Figure 3-6. A ductile clamped plate will not form a collapse mechanism until yielding occurs at $y = Y$ and $x = 0$. Our procedure gives

$$\frac{3.55 p X^2}{\sigma_y h^2} = 1.125 \left(\frac{X}{Y}\right)^2 + 1.155 + 1.125 \left(\frac{Y}{X}\right)^2 \begin{cases} \text{ductile clamped} \\ \text{plate} \\ \text{quasi-static} \\ \text{asymptote} \end{cases}$$

(3A-79)

Some experimental data can be compared with this solution. Willoughby, et al.⁽⁶⁾ describe 32 experimental tests on simply-supported brick walls. The walls were 2.436 m (8 ft) high by 3.654 m (12 ft) wide, had a thickness of 0.203 m (8 in), modulus of elasticity of 8.96 GPa (1.3×10^6 psi) and yield stress of 1.20 MPa (174 psi) as measured statically in flexural beam experiments. Because brick and mortar are fairly brittle materials, the appropriate Φ function is Φ_{PBS} which for an aspect ratio of 0.6166 equals 0.292. The loadings in these tests were all long-duration simulations of nuclear explosions, which infers that the loading is in the quasi-static realm. Setting $P X^2 / \sigma_y h^2$ equal to Φ_{PBS} and substituting for σ_y , X (half span), and h give a reflected pressure to initiate cracking of 9722 Pa (1.41 psi). All 32 tests in a shock tube resulted in cracked walls. The reflected pressures in their tests all ranged from 20.7 kPa to 703 kPa (3.00 psi to 102 psi), which are all greater than the predicted threshold.

This solution can also be extended to the breakage of glass panels. Basically a pane of glass is a brittle, simply-supported panel with flaws. So, Figure 3-6 applies, provided Φ_{IBS} and Φ_{PBS} are used. If we assume that durations of loading are long relative to response time, the loading is quasi-static and the results are as given by Equation (3-1). An additional consideration with glass is that its yield point depends upon flaws and is not a material characteristic independent of plate thickness. Glass has lower breaking stress as thickness grows greater because of increased likelihood of flaws. Equation (3-2) was used to interrelate yield stress and plate thickness. This relationship can be developed approximately from the definition for stress intensity factor in bending. A bending stress intensity factor is given by:

$$K_I = \frac{6.0M g\left(\frac{a}{h}\right)}{(h - a)^{3/2}} \quad (3A-80)$$

where K_I is the stress intensity factor ($N/m^{3/2}$)

a is the crack length (m)

M is the elastic section modulus, $\frac{\sigma_y h^2}{6}$ (N)

g is function (-)

Substituting into Equation (3A-80) and rearranging terms gives:

$$\frac{K_I}{\sigma_y h^{1/2}} = \frac{g\left(\frac{a}{h}\right)}{\left(1 - \frac{a}{h}\right)^{3/2}} \quad (3A-81)$$

Or in functional format

$$\frac{\sigma_y h^{1/2}}{K_I} = \Psi\left(\frac{a}{h}\right) \quad (3A-82)$$

If the function $\Psi\left(\frac{a}{h}\right)$ is given by

$$\Psi\left(\frac{a}{h}\right) = \text{const } \left(\frac{a}{h}\right)^{1/2} \quad (3A-83)$$

then Equation (3-2) follows when the stress intensity factor K_I and the length of crack a are taken as constants.

$$\sigma_y h = \text{constant} \quad (3A-84)$$

Equation (3-2) is Equation (3A-84) with the constant evaluated. Reference 7 contains a compilation of experimental test data in which various investigators loaded square and rectangular glass panels of different thickness with long duration pressures until they broke. Figure 3A-3 shows these test data for different aspect ratio glass panes. The straight line in Figure 3A-3

is Equation (3-1) plotted so it can be compared to these test results. The scatter is large; nevertheless, this comparison demonstrates that Equation (3-1) results in answers of the correct magnitude.

3A-4 Development of Membrane Equations

Figure 3-7 is a solution for membrane behavior. Energy solutions are used in its development similar to those used in the development of plate solutions. We begin by assuming a deformed shape.

$$w = w_0 \cos \frac{\pi x}{2X} \cos \frac{\pi y}{2Y} \quad (3A-85)$$

In a membrane, the strains can be approximated by:

$$\epsilon_{xx} = 1/2 \left(\frac{\partial w}{\partial x} \right)^2, \quad \epsilon_{yy} = 1/2 \left(\frac{\partial w}{\partial y} \right)^2, \quad \text{and} \quad \epsilon_{xy} = \frac{\partial w}{\partial x} \cdot \frac{\partial w}{\partial y} \quad (3A-86)$$

The strain energy per unit volume is still given by Equation (3A-50).

Differentiating Equation (3A-50) and substituting it into the strain equations give:

$$\epsilon_{xx} = \frac{\pi^2}{8} \frac{w_0^2}{X^2} \sin^2 \frac{\pi x}{2X} \cos^2 \frac{\pi y}{2Y} \quad (3A-87a)$$

$$\epsilon_{yy} = \frac{\pi^2 w_0^2}{8 Y^2} \cos^2 \frac{\pi x}{2X} \sin^2 \frac{\pi y}{2Y} \quad (3A-87b)$$

$$\epsilon_{xy} = \frac{\pi^2 w_0^2}{16 XY} \sin \frac{\pi x}{2X} \sin \frac{\pi y}{2Y} \quad (3A-87c)$$

Substituting Hooke's Law and integrating gives

$$u = \frac{9\pi^2}{2048} \frac{E w_0^4 h}{XY} \left[\left(\frac{Y}{X} \right)^2 + 0.3422 + \left(\frac{X}{Y} \right)^2 \right] \quad (3A-88)$$

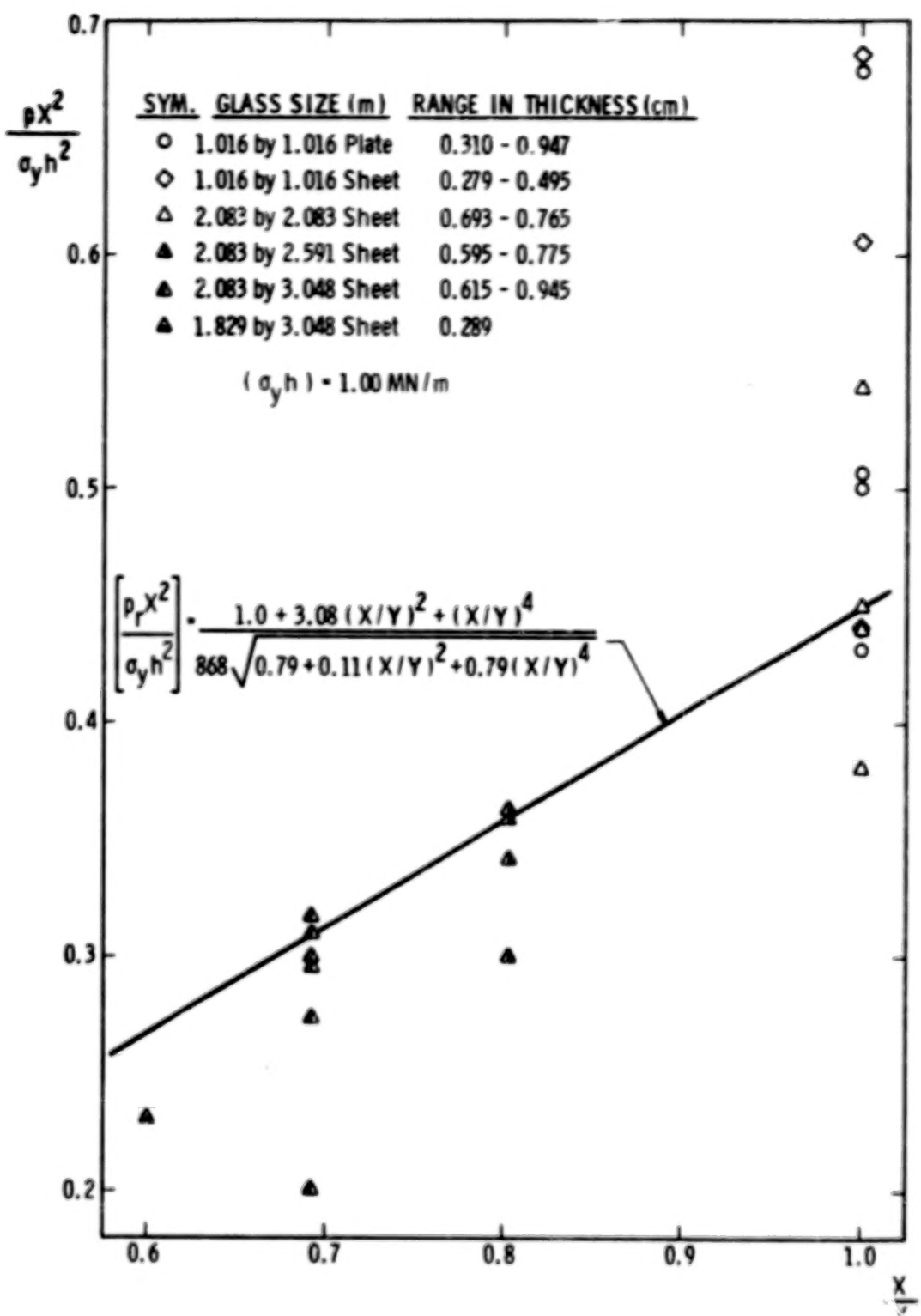


Figure 3A-3. Scaled Glass Breakage

Because the assumed deformed shape for the membrane is the same as that for the simply-supported plate, the kinetic energy KE is given by Equation (3A-53) and the work Wk by Equation (3A-65). Equating KE to U gives the impulsive loading realm asymptote of:

$$\frac{w_o}{X} = \frac{8}{\sqrt{3\pi}} \left[\left(\frac{Y}{X} \right)^2 + 0.3422 + \left(\frac{X}{Y} \right)^2 \right]^{1/4} \left(\frac{i^2}{\rho E h^2} \right)^{1/4} \quad (3A-89)$$

For a brittle material, ϵ is a maximum at the edge, $x = X$ and $y = 0$, where

$$\epsilon_{xx} = \frac{\pi^2}{8} \left(\frac{w_o}{X} \right)^2 = \frac{8\pi i Y}{3\sqrt{\rho E} h X} \left[\left(\frac{Y}{X} \right)^2 + 0.3422 + \left(\frac{X}{Y} \right)^2 \right]^{1/2} \quad (3A-90a)$$

$$\epsilon_{yy} = 0 \quad (3A-90b)$$

$$\epsilon_{xy} = 0 \quad (3A-90c)$$

Using these, Hooke's Law, and the yield criterion, we get:

$$\frac{8.183 \sqrt{E} i}{\sqrt{\rho} \sigma_y h} = \left[1.0 + 0.3422 \left(\frac{X}{Y} \right)^2 + \left(\frac{X}{Y} \right)^4 \right]^{1/2} \begin{cases} \text{brittle membrane} \\ \text{impulsive} \\ \text{asymptote} \end{cases} \quad (3A-91)$$

In a similar manner, the ductile membrane does not develop a yield surface until yielding occurs at $x = 0$ and $y = Y$ to complete the formation of a collapse mechanism. The ductile asymptote can therefore be written from the brittle one, provided X and Y are interchanged in Equation (3A-91). This manipulation is possible because of the symmetry in plate geometry. The impulsive loading realm asymptote for a ductile material is then given by:

$$\frac{8.183 \sqrt{E} i}{\sqrt{\rho} \sigma_y h} = \left[1.0 + 0.3422 \left(\frac{Y}{X} \right)^2 + \left(\frac{Y}{X} \right)^4 \right]^{1/2} \begin{cases} \text{ductile mem-} \\ \text{brane} \\ \text{impulsive} \\ \text{asymptote} \end{cases} \quad (3A-92)$$

The quasi-static asymptotes are obtained, as before, by equating the work W_k to U :

$$\frac{w_o}{X} = \left\{ \frac{37.38 p Y^2}{E X h \left[\left(\frac{Y}{X} \right)^2 + 0.3422 + \left(\frac{X}{Y} \right)^2 \right]} \right\}^{1/3} \quad (3A-93)$$

Substituting into the strain equations, Equations (3A-87), at $x = X$ and $y = 0$ gives:

$$\epsilon_{xx} = \frac{\frac{\pi}{8} \frac{w_o^2}{X^2}}{= \frac{\pi (37.38)^{2/3} \left(\frac{p Y^2}{E X h} \right)^{2/3}}{8 \left[\left(\frac{Y}{X} \right)^2 + 0.3422 + \left(\frac{X}{Y} \right)^2 \right]^{2/3}}} \quad (3A-94a)$$

$$\epsilon_{yy} = 0 \quad (3A-94b)$$

$$\epsilon_{xy} = 0 \quad (3A-94c)$$

Again using Hooke's Law and the yield criterion, we get:

$$49.46 \left(\frac{E^{1/2} p X}{\sigma_y^{3/2} h} \right) = \left[1.0 + 0.3422 \left(\frac{X}{Y} \right)^2 + \left(\frac{X}{Y} \right)^4 \right] \left\{ \begin{array}{l} \text{brittle membrane} \\ \text{quasi-static asymptote} \end{array} \right\} \quad (3A-95)$$

The ductile material asymptote can be written by inspection from the brittle material asymptote by making use of the same symmetry as was used in the impulsive loading realm. Interchanging X and Y and rearranging terms gives:

$$49.46 \left(\frac{E^{1/2} p X}{\sigma_y^{3/2} h} \right) = \left[\left(\frac{X}{Y} \right) + 0.3422 \left(\frac{Y}{X} \right) + \left(\frac{Y}{X} \right)^3 \right] \left\{ \begin{array}{l} \text{ductile membrane} \\ \text{quasi-static asymptote} \end{array} \right\} \quad (3A-96)$$

All of these asymptotes are plotted in Figure 3-7 with the function accounting for all aspect ratios. The transition between loading realms is a sketched-in estimate that closely approximates the appropriate transition for a single-degree-of-freedom linear oscillator.

LIST OF REFERENCES

1. Johnson, O. T., R. D. Mayerhofer, and W. J. Schuman, Jr., Effect of Blast Upon Simulated and Actual Missiles (Project 1.4 Operation Snow Ball) (U), BRL Memorandum Report #1655, May 1965.
2. Custard, George C. and John Thayer, Target Response to Explosive Blast, Falcon R & D Co. Contract No. DAHC04-69-C-0095 with Armed Services Explosive Safety Board, September 1970.
3. Soper, W. G., Modeling Laws Related To Target Vulnerability, U. S. Naval Weapons Lab Memorandum No. T-9/67, Dahlgren, Virginia, August 1967 (CONFIDENTIAL).
4. Westine, P. S. and W. E. Baker, "Energy Solutions For Predicting Deformations In Blast Loaded Structures," 16th Annual Explosives Safety Seminar, Hollywood, Florida, September 24-26, 1975.
5. Baker, W. E., W. O. Ewing, Jr., and J. W. Hanna, Laws For Large Elastic Response And Permanent Deformation of Model Structures Subjected To Blast Loading, BRL Report No. 1060, December 1958.
6. Willoughby, A. B., C. Wilton, B. L. Gabrielson, and J. V. Zaccor, Loading, Structural Response, and Debris Characteristics of Wall Panels, U.R.S. Contract No. 11618 (6300A-250) with Office of Civil Defense, Final Report, July 1969, AD 693 792.
7. Iverson, J. H., Summary of Existing Structures Evaluation, Part II: Window, Glass and Applications, Stanford Research Institute Contract No. OCD-DAHC20-67-C-0136 with Office of Civil Defense, December 1968.

APPENDIX III. B

PRESSURE/IMPULSE COMBINATIONS PRODUCING LUNG DAMAGE

Portions of the body where there are great differences in density of adjacent tissues are the most susceptible to blast injury.^(1, 2, 3) The lungs, which contain numerous air sacs, or alveoli, are less dense than surrounding tissues and are therefore very sensitive to blast injury. Because of their relatively low density, the air sacs of the lungs are compressed by the implosion of the abdominal and chest walls and upward motion of the diaphragm after interaction with the blast wave. Within tolerable limits of pressure magnitude and rate of increase in external pressure, the body is able to compensate for the rise in external pressure by body wall motion and increases in internal pressure. However, when the inward motion of the body wall is excessively rapid and severe, there is marked distortion of the thoracic organs, including the lungs, causing hemorrhage into airways and shearing and extension of the lungs along and around the relatively "stiff" major bronchi and pulmonary arteries.⁽⁴⁾ Depending upon the severity and extensiveness of mass hemorrhage and arterial air embolism, death can ensue within a short period.

Investigators have taken two basic approaches in studying the reaction of the body to external forces. Von Gierke,^(5, 6, 7, 8, 9, 10) Kaleps,⁽⁹⁾ Carmichael,⁽¹⁰⁾ and Fletcher⁽¹¹⁾ have studied the possibility of producing biodynamic models which simulate the reaction-response characteristics of the human body. Von Gierke's model is basically mechanical involving springs, masses and damping mechanisms, while Fletcher's model is fluid-mechanical involving springs, masses, damping mechanisms and gases. Other authors, including many individuals at the Lovelace Foundation for Medical Education and Research in Albuquerque, New Mexico, have analyzed the results of experiments involving laboratory animals and have extrapolated their results, using certain basic assumptions, to the human animal. Since the information acquired by this latter group directly lends itself to the formulation of lethality (or survivability) curves for humans subjected to primary blast damage, their results, with slight modification, will be used extensively.

Bowen, et al.,⁽³⁾ and White, et al.,⁽⁴⁾ have developed pressure versus duration lethality curves for humans which are especially amenable to this document. Some of the major factors which determine the extent of damage from the blast wave are the characteristics of the blast wave, ambient atmospheric pressure, and the type of animal target, including its mass and geometric orientation relative to the blast wave and nearby

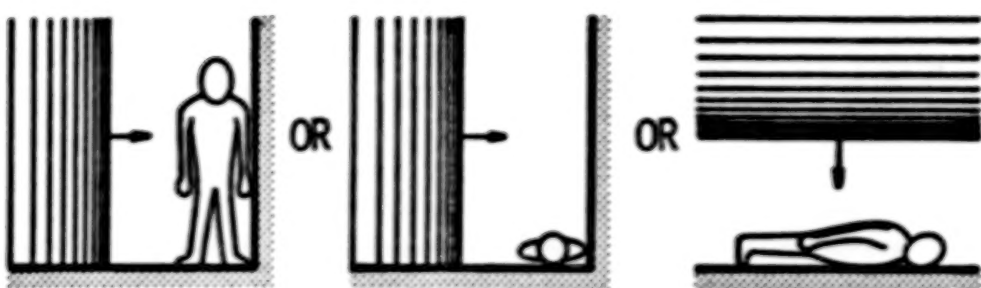
objects.⁽⁴⁾ Although Richmond⁽¹²⁾ and later White,⁽⁴⁾ both from the Lovelace Foundation, discuss the tendency of the lethality curves to approach iso-pressure lines for "long" duration blast waves, their lethality curves demonstrate dependence on pressure and duration alone. Since impulse, or more properly, specific impulse, is dependent on pressure as well as duration, pressure-impulse lethality or survivability curves may be more appropriate. The tendency for pressure-impulse lethality curves to approach asymptotic limits is also very aesthetically appealing from a mathematical point of view. Also, since both pressure and specific impulse at a specified distance from a propellant explosion can be calculated directly using methods described in Chapters I and II, it is especially appropriate that pressure-impulse lethality (or survivability) curves be developed for this document.

The human target orientation positions which required the lowest incident pressure-impulse combinations for a specified amount of damage to the human body are standing or lying very near a flat reflecting surface with the incident blast wave approaching the wall at a normal angle of incidence (see Figure 3B-1). However, the complexities involved with the shape and type of reflecting surface, the incident angle of the blast wave, and the proximity of the human body target to the reflecting surface are much too involved for this document. Also, the fact that there may not be a suitable reflecting surface near an individual exposed to a propellant explosion blast wave precludes the use of lethality (survivability) curves based on reflection from proximate surfaces. The next most sensitive human body orientation is exposure to the blast wave in the free field with the long axis of the body perpendicular to the blast winds with the subject facing in any direction (see Figure 3B-2). This position is a likely body exposure orientation and will be assumed in this document to be the position of victims exposed to primary blast damage from propellant explosions.

Researchers at Lovelace^(3,4) produced scaling laws for pressure and duration effects on animals. It is, therefore, necessary to develop a consistent scaling law for impulse. Simplifying Lovelace's scaling laws in such a manner that only the human species or large animals are considered, one is able to arrive at the following relationships or scaling laws:

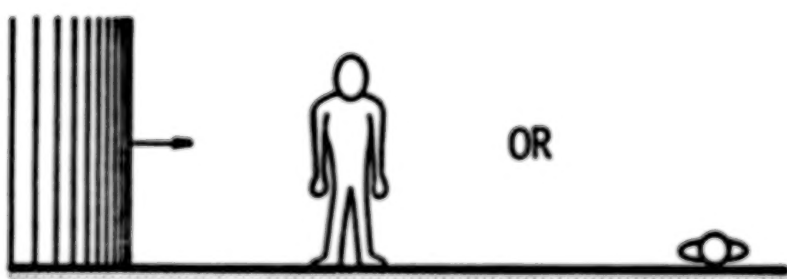
- (1) The effect of incident overpressure is dependent on the ambient atmospheric pressure. That is,

$$\bar{P}_s = \frac{P_s}{P_0} \quad (3B-1)$$



THORAX NEAR A REFLECTING SURFACE WHICH IS PERPENDICULAR TO BLAST WINDS, SUBJECT FACING ANY DIRECTION.

Figure 3B-1. Thorax Near a Reflecting Surface Which Is Perpendicular to Blast Winds, Subject Facing Any Direction



LONG AXIS OF BODY PERPENDICULAR TO BLAST WINDS, SUBJECT FACING ANY DIRECTION

Figure 3B-2. Long Axis of Body Perpendicular to Blast Winds, Subject Facing Any Direction

where

\bar{P}_s is scaled incident peak overpressure

P_s is peak incident overpressure

P_0 is ambient atmospheric pressure

(2) The effect of blast wave positive duration is dependent on ambient atmospheric pressure and the mass of the human target. That is,

$$\bar{T} = \frac{T P_0^{1/2}}{m^{1/3}} \quad (3B-2)$$

where

\bar{T} is scaled positive duration

T is positive duration

m is mass of human body

(3) Impulse I_s can be approximated by

$$I_s = \left(\frac{1}{2}\right) P_s T \quad (3B-3)$$

Equation (3B-3) assumes a triangular wave shape and is conservative, from an injury standpoint, for "long" duration blast waves which approach square wave shapes because it underestimates the specific impulse required for a certain percent lethality. It is also a close approximation for "short" duration blast waves which characteristically have a short rise time to peak overpressure and an exponential decay to ambient pressure, the total wave shape being nearly triangular. After these considerations are taken into account, Equation (3B-3) appears to be a conservative estimate for specific impulse which readily meets the needs of this document. Applying the blast scaling developed at the Lovelace Foundation for peak overpressure and positive duration to specific impulse determined by Equation (3B-3), one can arrive at a scaling law for specific impulse:

$$\bar{I}_s = \left(\frac{1}{2}\right) \bar{P}_s \bar{T} \quad (3B-4)$$

where

\bar{I}_s is scaled specific impulse

From Equations (3B-1), (3B-2), and (3B-4),

$$\bar{I}_s = \left(\frac{1}{2}\right) \frac{\bar{P}_s \bar{T}}{\bar{P}_o^{1/2} m^{1/3}} \quad (3B-5)$$

or from Equation (3B-3)

$$\bar{I}_s = \frac{\bar{I}_s}{\bar{P}_o^{1/2} m^{1/3}} \quad (3B-6)$$

Thus, as indicated by Equation (3B-6), scaled specific impulse I_s is dependent on ambient atmospheric pressure and the mass of the human target.

As mentioned earlier, the air blast damage survivability curves constructed by researchers at the Lovelace Foundation^(3, 4) are based on incident overpressure and duration. It was therefore necessary, for our applications, to modify the survival curves for man applicable to free-stream situations where the long axis of the body is perpendicular to the direction of propagation of the blast wave so that the axes of the graph would be scaled incident overpressure and scaled specific impulse. To do this, it was necessary to determine the pressure and duration combinations which produced each survivability curve, calculate scaled incident overpressure and scaled specific impulse using Equations (3B-1) and (3B-5) above, and reconstruct the survivability curves accordingly. These reconstructed curves are shown in Figure 3-10. It should be noted that these curves represent percent survivability, and higher scaled pressure and scaled impulse combinations allow fewer survivors. Presenting the curves in this fashion is advantageous since they apply to all altitudes with different atmospheric pressures and all masses (or sizes) of human bodies. Peak incident overpressure and specific impulse for different propellant explosions and failure modes can also be easily determined using methods previously described in Chapters I and II of this document and can be scaled using Equations (3B-1) and (3B-6). The proper ambient atmospheric pressure to use for the scaling can be acquired from Figure 3-9, which shows

how atmospheric pressure decreases with increasing altitude above sea level.⁽¹³⁾ The value for mass used in the scaling is determined by the demographic composition of the particular area under investigation. It is recommended that 5 kg (11 lb_m) be used for babies, 25 kg (55 lb_m) for small children, 55 kg (121 lb_m) for adult women, and 70 kg (154 lb_m) for adult males. It should be noticed that the smallest bodies in this case are the most susceptible to injury.

It is often beneficial to compare experimental results with theoretical predictions. Using some of the Lovelace Foundation data,⁽³⁾ it is possible to make some comparison. Unfortunately, the Lovelace data include maximum reflected overpressure and not incident overpressure. White, et al.,⁽⁴⁾ mentions that the Lovelace Foundation's pressure versus duration survivability curves, on which the scaled pressure versus scaled impulse survivability curves presented here are based, were determined by using a "biological-equivalent dose." When the body is exposed to the air blast in the free-field with its long axis perpendicular to the direction of travel of the blast wave, the biological-equivalent dose was taken to be the incident plus the dynamic pressure. When the body is exposed to air blast from a reflecting surface, the biological-equivalent dose was taken to be the reflected pressure. Thus, for the purpose of using the available experimental data involving reflected overpressures for the free-field situation involving incident overpressures, the reflected overpressures are "biologically equivalent" to incident plus dynamic overpressures. That is,

$$\bar{P}_r = \bar{P}_s + \bar{Q} \quad (3B-7)$$

where

\bar{P}_r is scaled reflected overpressure

\bar{P}_s is scaled incident overpressure

\bar{Q} is scaled dynamic pressure.

It is relatively easy to determine the scaled incident overpressure in the free-field which is biologically equivalent to scaled peak reflected overpressure near a reflecting surface. From Baker's⁽¹⁴⁾ tables, combinations of scaled incident overpressures and scaled dynamic pressures at various scaled distances can be acquired. Scaled incident overpressure versus the sum of scaled incident overpressure plus scaled dynamic pressure (or biologically equivalent scaled peak reflected overpressure) can then be plotted (see Figure 3B-3).

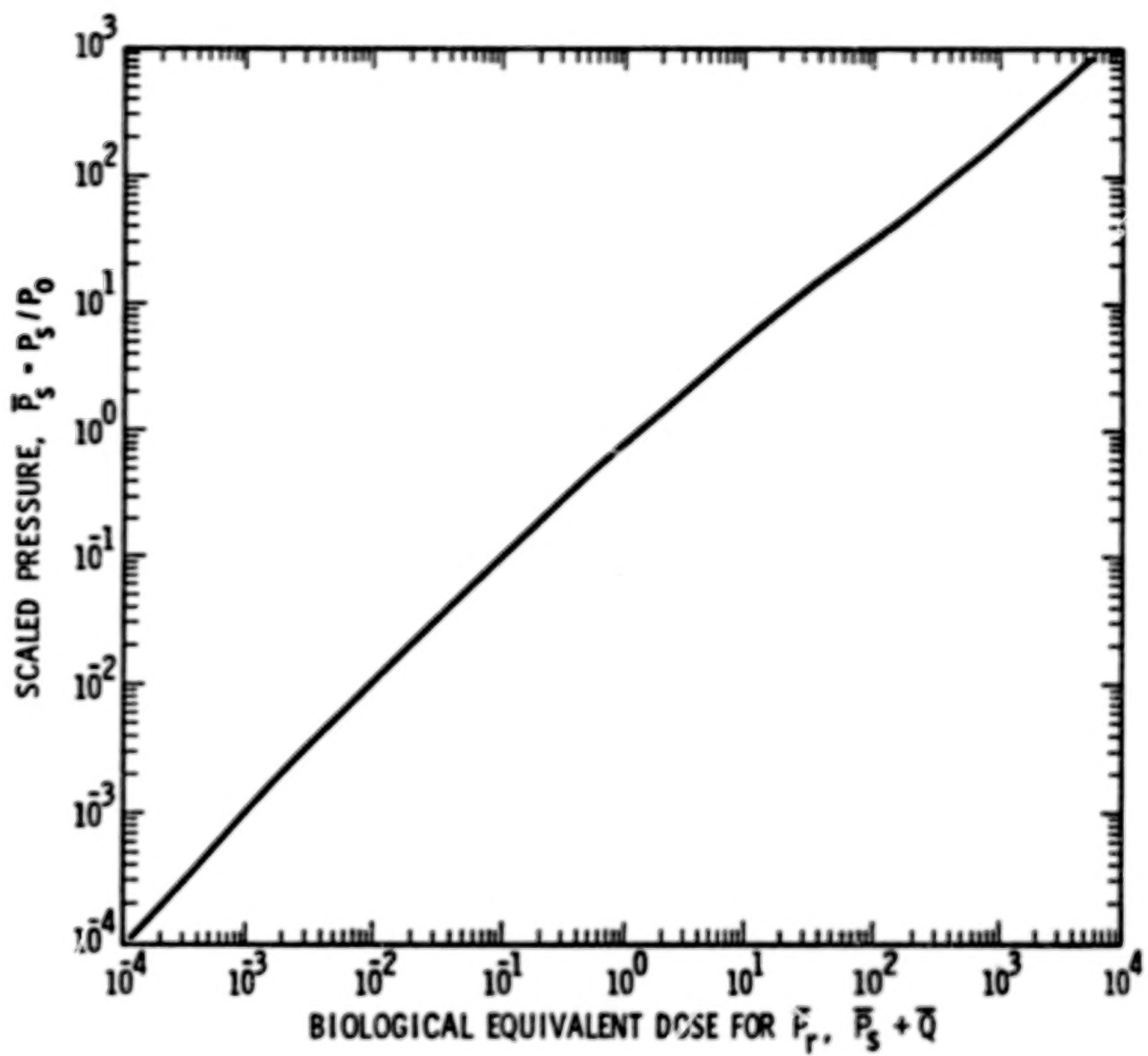
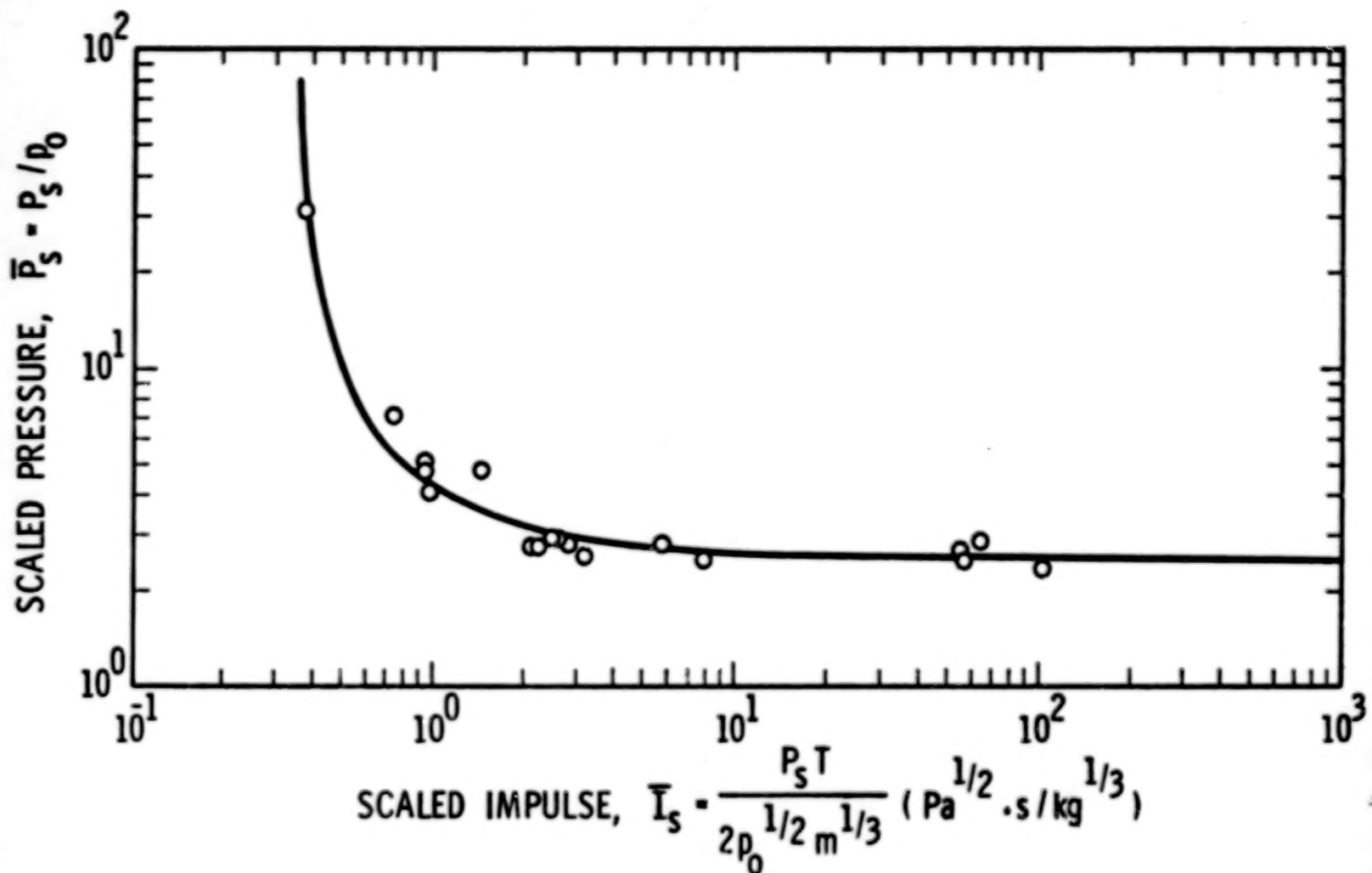


Figure 3B-3. Blast Pressures for Predicting Blast Lethality

Work performed at the Lovelace Foundation indicated that burros, monkeys, sheep, swine, goats, dogs, cats, and steers have a biological response to air blast which is similar to that of humans.^(3,4) Using some of the data accumulated by the Lovelace Foundation⁽³⁾ for the species mentioned above, Figure 3B-3, and Equations (3B-1) and (3B-5), it is possible to calculate scaled peak incident overpressure P_s and scaled specific impulse I_s for approximately 50 percent lethality (or 50% survivability). The relevant data and calculated scaled incident peak overpressure and scaled specific impulses are summarized in Table 3B-1. Calculated values are plotted on Figure 3B-4 with the 50-percent survivability curve (from Figure 3-10 for comparison. The correlation between the predicted curve and experimental data is excellent, thus allowing a certain degree of confidence to the survivability curves predicted for man.

TABLE 3B-1. EXPERIMENTAL DATA FOR PRIMARY
BLAST DAMAGE TO ANIMALS

Species	Group No. N	Mass m (kg)	Scaled Peak Reflected Overpressure P_r	Duration t (sec)	Ratio of Animals Dying Within 24 Hrs To Those Exposed (~ 50%)	Scaled Peak Incident Overpressure P_s	Scaled Specific Impulse I_s $(P_0)^{1/2} (m)^{1/3}$
Cat	73	1.98	3.658	0.3740	4/8	2.35	100.66
Monkey	77	6.00	9.317	0.0038	2/4	4.80	1.44
	80	5.40	4.608	0.1230	3/5	2.80	28.23
Dog	88	15.40	7.858	0.0040	3/6	4.10	0.97
	90	18.30	4.958	0.0158	5/9	2.90	2.50
	91	18.60	4.492	0.0152	5/9	2.75	2.27
	96	17.20	4.067	0.0226	2/4	2.55	3.21
	101	16.10	4.058	0.0556	3/7	2.50	7.92
	108	15.40	4.008	0.4000	6/10	2.49	57.58
Goat	113	20.80	9.250	0.0038	3/5	4.79	0.952
	114	21.10	9.833	0.00372	3/5	4.95	0.953
	117	22.80	4.800	0.0172	2/4	2.90	2.53
	121	21.20	4.617	0.0398	4/8	2.80	5.79
	125	16.80	4.742	0.4000	3/5	2.85	64.02
	126	20.30	4.283	0.4000	4/10	2.65	55.88
Sheep	130	52.60	110.833	0.000308	2/5	32.00	0.378
	137	59.20	16.417	0.0029	4/8	7.00	0.749
	142	54.80	4.508	0.210	6/10	2.75	21.87
Steer	150	176.00	3.550	0.184	5/10	2.30	10.86



168

Figure 3B-4. 50 Percent Survival Curve for Man, Long Axis of Body Perpendicular to Direction of Blast Wave Propagation (Refs. 3 and 4)

LIST OF REFERENCES

1. White, Clayton S., "The Scope of Blast and Shock Biology and Problem Areas in Relating Physical and Biological Parameters," Annals of the New York Academy of Sciences, Vol. 152, Art. 1, October 1968, pp. 89-102.
2. Damon, Edward G., Donald R. Richmond, E. Royce Fletcher, and Robert K. Jones, "The Tolerance of Birds to Airblast," Final Report to Defense Nuclear Agency, DNA 3314F, Lovelace Foundation for Medical Education and Research, July 1974. AD 785-259.
3. Bowen, I. E., E. R. Fletcher, and D. R. Richmond, "Estimate of Man's Tolerance to the Direct Effects of Air Blast," Technical Report to Defense Atomic Support Agency, DASA 2113, Lovelace Foundation for Medical Education and Research, October 1968. AD 693-105.
4. White, Clayton S., Robert K. Jones, Edward G. Damon, E. Royce Fletcher, and Donald R. Richmond, "The Biodynamics of Airblast," Technical Report to Defense Nuclear Agency, DNA 2738T, Lovelace Foundation for Medical Education and Research, July 1971. AD 734-208.
5. von Gierke, Henning E., "Dynamic Characteristics of the Human Body," Aerospace Medical Research Laboratory, Wright-Patterson Air Force Base, Ohio, 1973. AD 769-022.
6. von Gierke, Henning E., "Man to Model, or Model to Man," Aerospace Medical Research Laboratory, Wright-Patterson Air Force Base, Ohio, 1971. AD 771-670.
7. von Gierke, Henning E., "Biodynamic Models and Their Applications," Aerospace Medical Research Laboratory, Wright-Patterson Air Force Base, Ohio, 1971. AD 736-985.
8. von Gierke, Henning E., "Mechanical Behavior of Biological Systems," Aerospace Medical Research Laboratory, Wright-Patterson Air Force Base, Ohio, September 1967. AD 758-963.
9. Kaleps, Ints, and Henning E. von Gierke, "A Five-Degree-of-Freedom Mathematical Model of the Body," Aerospace Medical Research Laboratory, Paper No. 8, Wright-Patterson Air Force Base, Ohio. AD 740-445

10. Carmichael, J. B., Jr., and Henning E. von Gierke, "Biodynamic Applications Regarding Isolation of Humans from Shock and Vibration," Aerospace Medical Research Laboratory, Wright-Patterson Air Force Base, Ohio, September 1973. AD 770-316.
11. Fletcher, E. R., "A Model to Simulate Thoracic Responses to Air Blast and to Impact," Aerospace Medical Research Laboratory, Paper No. 1, Wright-Patterson Air Force Base, Ohio, December, 1971. AD 740-438.
12. Richmond, Donald R., Edward G. Damon, E. Royce Fletcher, I. Gerald Bowen, and Clayton S. White, "The Relationship Between Selected Blast Wave Parameters and the Response of Mammals Exposed to Air Blast," Annals of the New York Academy of Sciences, Vol. 152, Art. 1, October 1968, pp. 103-121.
13. Champion, K. S. W., W. J. O'Sullivan, Jr., and Sidney Teweles, "U. S. Standard Atmosphere, 1962," U. S. Government Printing Office, Washington, D. C., December 1962.
14. Baker, Wilfred E., Explosions in Air, University of Texas Press, Austin, Texas, 1973.

APPENDIX III.C

PRESSURE/IMPULSE COMBINATIONS PRODUCING LOSS OF HEARING

The ear is an organ system which converts sound waves into nerve impulses. It responds to a band of frequencies ranging from 20 Hz to 20,000 Hz. This highly sensitive organ can respond to energy levels as low as 10^{-12} watt/m², which causes the eardrum to deflect less than the diameter of a single hydrogen molecule.⁽¹⁾ Not being able to respond faithfully to pulses having periods less than 0.3 millisecond, it attempts to do so by making a single large excursion.⁽¹⁾ It is this motion which can cause injury to the ear.

The human ear is divided into the external, middle, and inner ear. The external ear amplifies the overpressure of the sound wave by approximately 20 percent and detects the location of the source of sound.⁽¹⁾ Rupture of the eardrum, or tympanic membrane, which separates the external ear from the middle ear, has captured most of the attention of clinicians although it is not the most severe type of ear injury. The eardrum and ossicles of the middle ear transfer acoustical energy from the external ear to the inner ear where mechanical energy is finally converted into the electrical energy of the nerve impulse. The middle ear is an impedance matching device as well as an amplification stage. The middle ear contains two dampers: the stapedius muscle and associated ligaments which limit the vibration of the stapes when subjected to intense signals, and the tensor tympani muscle and its adjoining ligaments which limit the vibration of the eardrum. The first damper is the most important. These dampers have a reflex time of approximately 0.005 to 0.01 second,⁽¹⁾ which is longer than "fast" rising air blasts. The manner in which the malleus and incus are linked allows far more resistance to inward displacement than to outward displacement. However, if the eardrum ruptures after inward displacement during positive phase of loading of the blast wave, the malleus and incus are less likely to displace as far outward during the negative phase of loading of the blast wave as they would if the eardrum remained intact. In this case, eardrum rupture could be beneficial. The maximum overpressure and its rise time, however, control the characteristics of the negative phase and is therefore of prime importance.⁽¹⁾ Rupture of the eardrum thus becomes a good measure of serious ear damage.

Unfortunately, the state-of-the-art for predicting eardrum rupture is not as well developed as that for predicting lung damage from blast waves. A direct relationship, however, has been established between the percentage of ruptured eardrums and maximum overpressure. Examining data from

Vadala,⁽²⁾ Henry⁽³⁾ and Reider,⁽⁴⁾ Hirsh⁽¹⁾ constructed a graph similar to that shown in Figure 3C-1 and concluded that 50 percent of exposed eardrums rupture at 103 kPa (15 psi). White⁽⁵⁾ supports this conclusion for "fast" rising overpressures with durations of 0.003 second to 0.4 second occurring at ambient atmospheric pressure of 101 kPa (14.7 psi). Hirsch⁽¹⁾ also concluded that threshold eardrum rupture for "fast" rising overpressures is 34.5 kPa (5 psi), which is also supported by White⁽⁵⁾ for the range of duration and at the atmospheric pressure mentioned above.

At lower overpressures than those required to rupture eardrums, a temporary loss of hearing can occur. Ross, et al.,⁽⁶⁾ have produced a graph of peak overpressure versus duration for temporary threshold shift (TTS). Below the limits of the graph, a majority (75 percent at least) of those exposed are not likely to suffer excessive hearing loss. According to Ross, et al.,⁽⁶⁾ their curves should be lowered 10 dB to protect 90 percent of those exposed, lowered 5 dB to allow for a normal angle of incidence of the blast wave, and increased 10 dB to allow for occasional impulses. In sum, to assure protection to 90 percent of those exposed and to allow for normal incidence to the ear (the worst exposure case) of an occasional air blast, their curves should be lowered 5 dB.

Limits for eardrum rupture and temporary threshold shift, as presented above, are dependent on peak incident overpressure and duration. Since specific impulse is dependent upon the duration of the blast wave and since both peak incident overpressure and specific impulse at a specified distance from a propellant explosion can be calculated directly using methods described in Chapters I and II, it is especially appropriate that pressure-impulse ear damage curves be developed for this document from the pressure-duration curves. Assuming a triangular shape for the blast wave allows for simple calculations which are conservative from an injury standpoint. That is, "long" duration blast waves approach square wave shapes, and hence specific impulse required to produce a certain amount of ear damage is underestimated, while "short" duration blast waves are essentially triangular in shape. Thus, specific impulse I_s can be approximated by Equation (3C-1).

$$I_s = \left(\frac{1}{2}\right) P_s T \quad (3C-1)$$

where

P_s is peak incident overpressure.

The ear damage criteria presented in Figure 3-11 were developed from the criteria for eardrum rupture developed by Hirsch⁽¹⁾ and White⁽⁵⁾

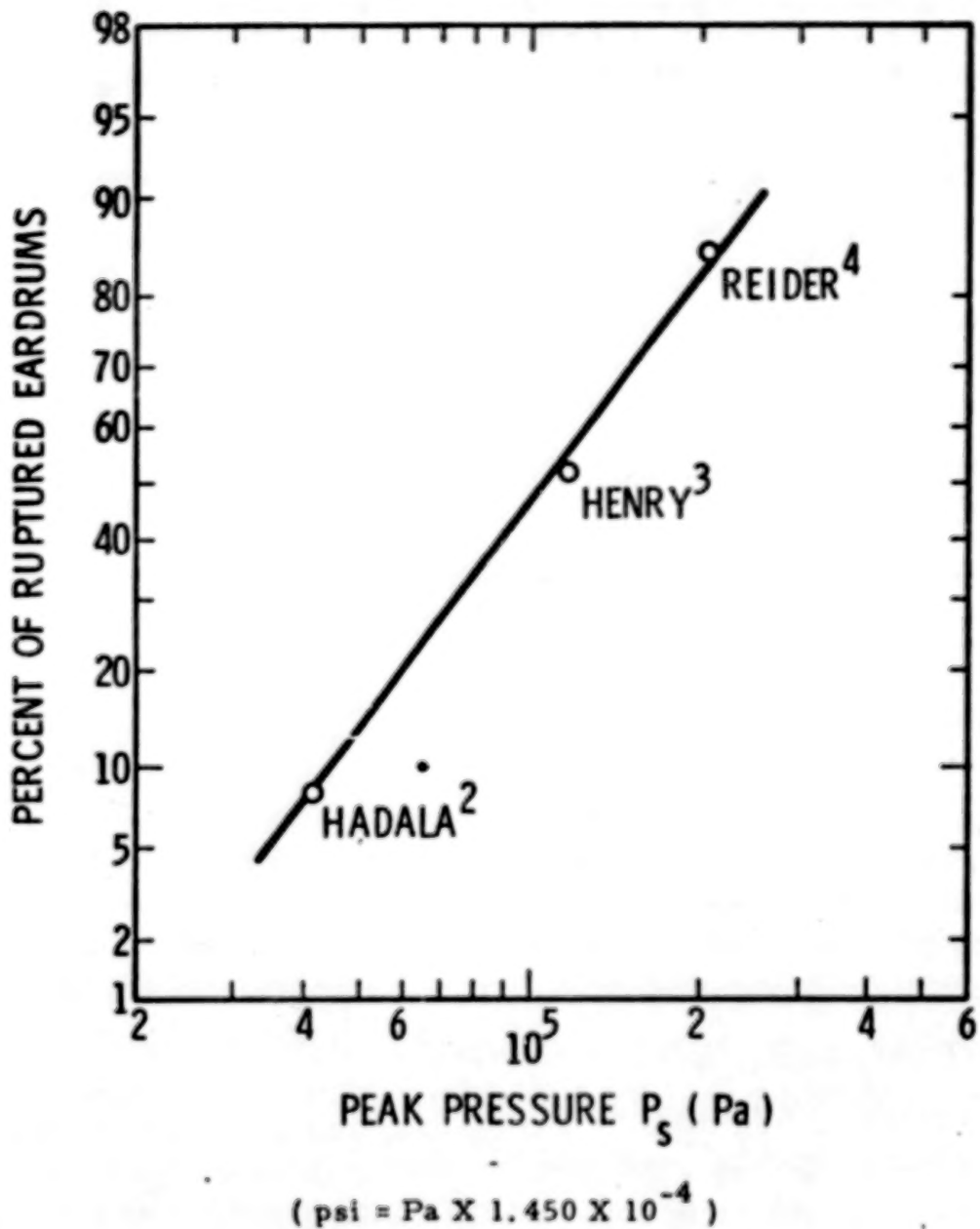


Figure 3C-1. Percent Eardrum Rupture Vs Overpressure

and from the criteria for temporary threshold shift developed by Ross, et al.(6) Equation (3C-1) was used to calculate specific impulse, and temporary threshold shift represents the case where 90 percent of those exposed to a blast wave advancing at normal angle of incidence to the ear are not likely to suffer an excessive degree of hearing loss.

LIST OF REFERENCES

1. Hirsch, Frederic G., "Effects of Overpressure on the Ear--A Review," Annals of the New York Academy of Sciences, Vol. 152, Art. 1, October 1968, pp. 147+.
2. Vadala, A. J., "Effects of Gun Explosions on the Ear and Hearing Mechanism," Milit. Surg. 66, 1930, pp. 710-822.
3. Henry, G. A., "Blast Injuries of the Ear," Laryngoscope 55, 1945, pp. 663-672.
4. Reider, H. L., Personal communication by Hirsch⁽¹⁾ concerning data from two industrial explosions, Los Alamos Scientific Laboratory, Los Alamos, New Mexico.
5. White, Clayton S., "The Scope of Blast and Shock Biology and Problem Areas in Relating Physical and Biological Parameters," Annals of the New York Academy of Sciences, Vol. 152, Art. 1, October 1968, pp. 89+.
6. Ross, R., et al., "Criteria for Assessing Hearing Damage Risk from Impulse-Noise Exposure," Human Engineering Laboratory, Aberdeen Proving Ground, Maryland, August 1967. AD 666-206.

APPENDIX III. D

PRESSURE/IMPULSE COMBINATIONS PRODUCING WHOLE-BODY DISPLACEMENT AND SUBSEQUENT DAMAGE TO THE HEAD AND BODY

During whole-body displacement, blast overpressures and impulses interact with the body in such a manner that it is essentially picked up and translated. Tertiary blast damage involves this whole-body displacement and subsequent decelerative impact.⁽¹⁾ Bodily damage can occur during the accelerating phase or during decelerative impact.⁽²⁾ The extent of injury due to decelerative impact is the more significant,⁽³⁾ however, and is determined by the velocity change at impact, the time and distance over which deceleration occurs, the type of surface impacted, and the area of the body involved.⁽¹⁾

Although the head is the most vulnerable portion of the body to mechanical injury during decelerative impact, it is also the best protected.⁽⁴⁾ Because of the delicate nature of the head, many may feel that translation damage criteria should be based on skull fracture or concussion. However, since body impact position is likely to be randomly oriented after translation, others may feel that this factor should be taken into account in determining expected amounts of impact damage. In an effort to satisfy proponents of each point of view, both types of impact, essentially head foremost and random body impact orientation, will be considered.

Because of the many parameters involved in decelerative impact, a few assumptions will be made. First of all, translation damage will be assumed to occur during decelerative impact with a hard surface, the most damaging case.⁽³⁾ Another assumption is that, since impact onto only hard surfaces is being considered, translation damage will depend only on impact velocity. That is, impacting only one type of surface precludes the need for considering change in velocity of the body during impact. This assumption, however, is not entirely valid when one considers that the compressibility of various portions of the body can vary considerably.

White^(1,5) and Clemedson, et al.,⁽⁶⁾ agree that the tentative criteria for tertiary damage (decelerative impact) to the head should be those presented in Table 3D-1. White's⁽⁵⁾ recently revised criteria for tertiary damage due to total body impact are summarized in Table 3D-2. It is beneficial to note that the mostly "safe" velocity criteria for each type of impact condition are identical.

In order to make these conclusions useful to this document, it is necessary to establish the pressure and impulse combinations which are required to translate human bodies and propel them at the critical velocities presented in Tables 3D-1 and 3D-2. This can readily be done by modifying the appurtenance computer program developed for Chapter IV and making a few assumptions about the characteristics of the human body.

TABLE 3D-1. CRITERIA FOR TERTIARY DAMAGE
(DECELERATIVE IMPACT) TO THE HEAD
(FROM REFS. 1, 5, 6)

<u>Skull Fracture Tolerance</u>	Related Impact Velocity m/s (ft/sec)	
Mostly "safe"	3.05	(10)
Threshold	3.96	(13)
50 percent	5.49	(18)
Near 100 percent	7.01	(23)

TABLE 3D-2. CRITERIA FOR TERTIARY DAMAGE
INVOLVING TOTAL BODY IMPACT

<u>Total Body Impact Tolerance</u>	Related Impact Velocity m/s (ft/sec)	
Mostly "safe"	3.05	(10)
Lethality threshold	6.40	(21)
Lethality 50 percent	16.46	(54)
Lethality near 100 percent	42.06	(138)

Hoerner⁽⁷⁾ concludes that the human body is similar in aerodynamic shape to a cylinder with length-to-diameter ratio between 4 and 7. For calculating translation velocity, the average 5.5 will be used, and the human target will be assumed to be standing and facing the blast wave in the free-field. Hoerner also estimates that, in the standing position, man's drag coefficient is between 1.0 and 1.3. Since the higher drag coefficient allows higher velocities for any pressure-impulse blast wave combination, a value of 1.3 for drag coefficient will be used. This should allow a certain margin of safety in the calculation. The average density of a human is approximately the same as that of water, and it is beneficial to consider four body masses, the approximate mass depending upon the location of an anticipated explosion. These masses are 5 kg (11 lb_m) for babies, 25 kg (55 lb_m) for children, 55 kg (121 lb_m) for women, and 70 kg (154 lb_m) for men. Appropriate comparable cylinder diameters making the assumptions stated above are 0.10 m (3.28 ft), 0.18 m (0.59 ft), 0.23 m (0.75 ft), and 0.25 m (0.82 ft), respectively. Atmospheric pressure and speed of sound, which are used in the velocity calculations, vary with altitude as shown in Figures 3-9 and 3D-1. Sea level, 2000 m (6560 ft), 4000 m (13,100 ft), and 6000 m (19,700 ft) altitudes are convenient intervals and were chosen in exercising the computer program.

A listing of this computer program is shown in Figure 3D-2. Explanations of variables are given in comments throughout the listing. A better understanding of the appurtenance velocity calculation and a listing of the original appurtenance computer program can be acquired from Chapter IV and its associated appurtenance appendix.

As mentioned above, the computer program is used to determine the pressure-impulse combinations required to impart seven different translation velocities (four for skull fracture and four for total body impact, one velocity being the same for both) to four different masses at four different altitudes. If the results are divided into skull fracture and total body impact damage with four velocities represented on each pressure versus impulse graph, 32 graphs are required (2 damage conditions X 4 masses X 4 altitudes). Because of this, a scaling relationship was developed to reduce the total number of graphs.

In an effort to form a scaling relationship, consider the interaction of a blast wave with an object as shown in Figure 3D-3. As the wave strikes the object, a portion is reflected from the front face, and the remainder diffracts around the object. In the diffraction process, the incident wave front closes in behind the object, greatly weakened locally, and a pair of trailing vortices is formed. Rarefaction waves sweep across the front face, attenuating the initial reflected blast pressure. After passage of the front, the body is immersed in a time-varying flow field. Maximum pressure on the front face during this "drag" phase of loading is the stagnation pressure.

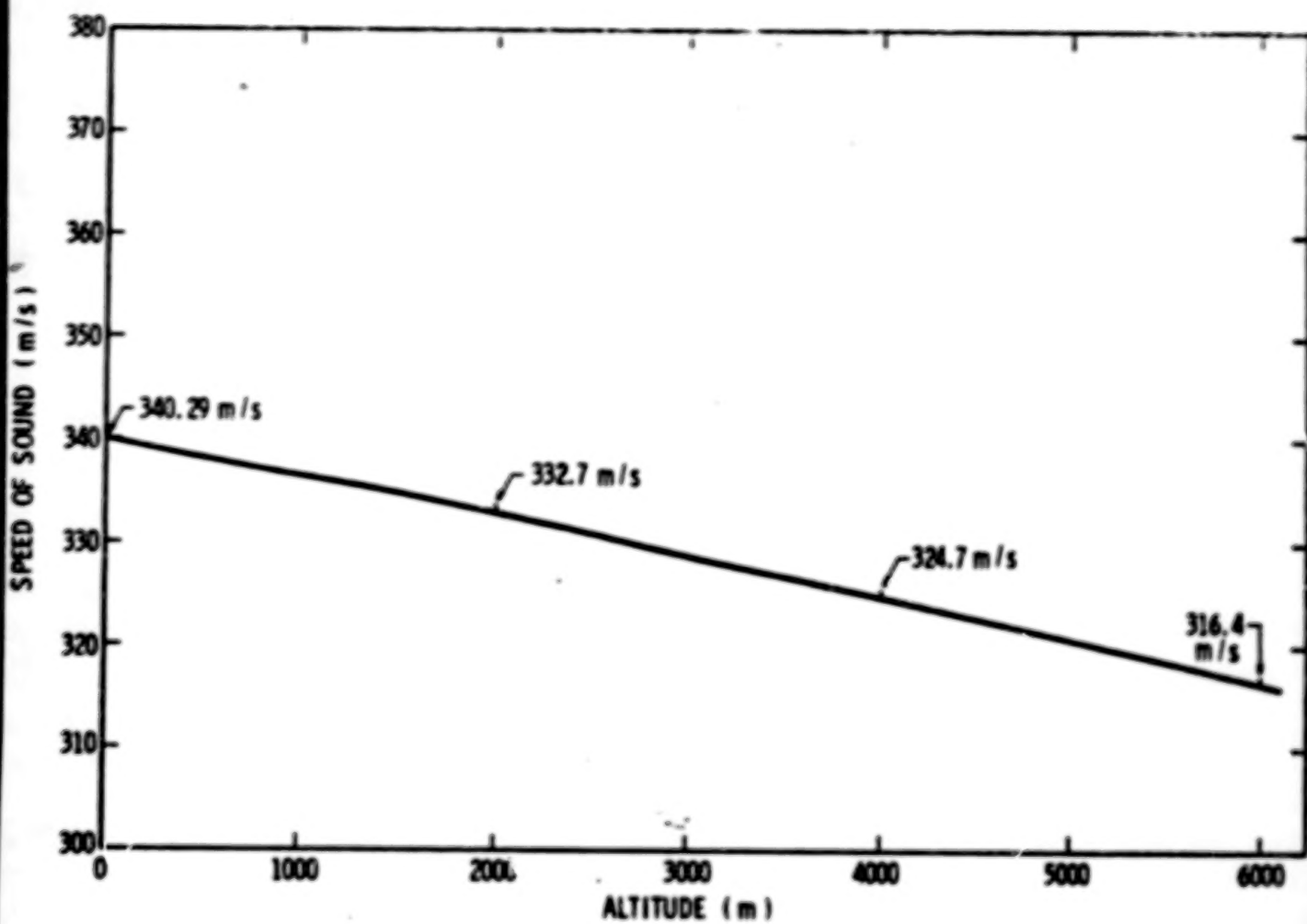


Figure 3D-1. Variation of Speed of Sound with Altitude

PROGRAM SVELAP(INPUT,OUTPUT)

THIS PROGRAM DETERMINES THE BLAST OVERPRESSURES AND IMPULSES REQUIRED TO PROPEL A SPECIFIED APPURTENANCE AT A SPECIFIED VELOCITY.
SVELAP OR S-VEL-AP IS A CODE NAME DESIGNATING--SPECIFIC VELOCITY APPURTENANCE,

```
DIMENSION PB(30),BB(30),PI(50),P(50),PBH(5),UB(5),OB(5),PRR(5),XXT  
13(7),XXXT3(7,50),PP(7,50),PPI(7,50),XT3(50),PPP1(7,50)  
INTEGER FIND,HA  
REAL IGRAL  
  
READ IN CURVES FOR PBAR VS. B AND  
PBAR VS. UBAR,OBAR,PBAR  
PO = ATMOSPHERIC PRESSURE  
AO = SPEED OF SOUND  
X = DIST. FROM FRONT OF OBJECT TO LOCATION OF LARGEST MEAN  
PRESENTED AREA  
H = MINIMUM TRANSVERSE (TO SHOCK WAVE) DIST. AT LOCATION OF  
LARGEST MEAN PRESENTED AREA  
CD = DRAG COEFFICIENT  
A = MEAN PRESENTED AREA  
TM = OBJECT MASS  
HA, 1 = OBJECT IN AIR  
2 = OBJECT ON GROUND  
PI = IMPULSE  
P = PRESSURE  
XXT3 = CONSTANT VELOCITY  
  
READ 400,(PB(I),BB(I),I=1,21)  
READ 401,(PBH(I),UB(I),OB(I),PRR(I),I=1,5)  
READ 120,HA  
READ 120,H  
READ 130,(PI(I),I=1,5)  
READ 120,N  
READ 110,(XXT3(I),I=1,7)  
DO 10 LL=1,4  
READ 100,PO,AO  
DO 10 LH=1,4  
READ 110,X,H,CD,A,TH  
DO 11 I=1,7  
DO 11 J=1,5  
DO 10 K=1,N  
FIND=1  
P(1)=0.001  
IF(K,EO,1) GO TO 12  
P(K)=10.*P(K-1)  
12 PBAR=P(K)/PO  
CALL PARAB(B,PBAR,PO,BB)  
IF(B,EO,0,0) GO TO 30  
TBPT(J)=H/(P(K)*(1.0-(1.0-EXP(-B))/B)))  
IF(PBAR,GT,3.5) GO TO 305  
PBARH=2.0*PBAR+3.0*PBAR**2.0/4.0  
OBAR=5.0/2.0*PBAR**2.0/(7.0+PBAR)  
UBAR=SQRT(1.0+b,0*PBAR/7.0)
```

Figure 3D-2. Human Body Appurtenance Computer Program

TABLE OF CONTENTS

	<u>Page</u>
INTRODUCTION	1 1/A12
I. ESTIMATES OF EXPLOSIVE YIELD	8 1/B5
1-1 Explosive Yield as a Function of Propellant Type and Accident Conditions	8 1/B5
1-2 Explosive Yield as a Function of Fluid Type and Initial Conditions for Gas Vessel Bursts	26 1/C9
List of References	29 1/C12
II. CHARACTERISTICS OF PRESSURE WAVES	31 1/C14
2-1 General	31 1/C14
2-2 Pressure Waves from Propellant Explosions	40 1/D9
2-3 Pressure Waves from Gas Vessel Bursts	56 1/E11
List of References	68 1/F9
II. A GAS VESSEL BURST	70 1/F11
2A-1 Nondimensional Parameters	70 1/F11
2A-2 Source of Data	70 1/F11
2A-3 Overpressure Calculation	71 1/F12
2A-4 Impulse Calculation	74 1/G1
2A-5 Effect of Cylindrical Geometry	74 1/G1
2A-6 Effect of Reflecting Surface (Burst at Ground Level)	74 1/G1
List of References	78 1/G5
Symbols	79 1/G6

TABLE OF CONTENTS (Cont'd)

		<u>Page</u>
III.	EFFECTS OF PRESSURE WAVES	80 1/G7
3-1	Damage Estimates to Structures	80 1/G7
3-2	Injury Estimates to Humans	99 2/B3
	List of References	125 2/D1
III.A	STRUCTURAL RESPONSE	128 2/D4
3A-1	Overturning Analysis	128 2/D4
3A-2	Development of Beam Equations	134 2/D10
3A-3	Development of Plate Equations	142 2/E4
3A-4	Development of Membrane Equations	153 2/F1
	List of References	158 2/F6
III.B	PRESSURE/IMPULSE COMBINATIONS PRODUCING LUNG DAMAGE	159 2/F7
	List of References	169 2/G3
III.C	PRESSURE/IMPULSE COMBINATIONS PRODUCING LOSS OF HEARING	171 2/G5
	List of References	175 2/G5
III.D	PRESSURE/IMPULSE COMBINATIONS PRODUCING WHOLE-BODY DISPLACEMENT AND SUBSEQUENT DAMAGE TO THE HEAD AND BODY	176 2/G10
	List of References	190 3/B1
IV.	CHARACTERISTICS OF FRAGMENTS	191 3/B2
4-1	General	191 3/B2
4-2	Methods for Estimating Fragment Initial Velocities for Spheres and Cylinders Bursting into Many Fragments	191 3/B2

TABLE OF CONTENTS (Cont'd)

	<u>Page</u>
4-3 Estimate of Initial Velocities of Fragments from Spheres and Cylinders Bursting into Two Equal Halves	218 3/D1
4-4 Determination of Appurtenance Velocity	228 3/D11
4-5 Methods for Computing Fragment Ranges and Impact Conditions	240 3/E9
4-6 Fragment Mass Distribution	279 4/All
4-7 Probability of Fragment Arrival Versus Range	286 4/B4
List of References	292 4/B10
IV.A METHODS FOR ESTIMATING FRAGMENT INITIAL VELOCITIES	293 4/B11
List of References	315 4/D5
IV.B COMPARISON OF EXPERIMENTAL RESULTS WITH CODE PREDICTIONS	316 4/D6
List of References	318 4/D8
IV.C ESTIMATE OF INITIAL VELOCITIES OF FRAGMENTS FROM SPHERES AND CYLINDERS BURSTING INTO TWO EQUAL HALVES	319 4/D9
List of References	354 4/G2
IV.D ESTIMATION OF VELOCITIES ATTAINED BY APPURTEANCES SUBJECTED TO BLAST LOADING	355 4/G3
List of References	377 5/B2
IV.E ANALYSES FOR FRAGMENT TRAJECTORIES	378 5/B3
List of References	401 5/C12

TABLE OF CONTENTS (Cont'd)

	<u>Page</u>
IV.F STATISTICAL FITTING TO FRAGMENT DATA	402 5/C13
4F-1 Derivation of Figures 4-46 Through 4-49	402 5/C13
4F-2 Derivation of Figure 4-50	402 5/C13
4F-3 Rationale for Averaging Fragment Mass Distribution for Events 3, 4, and 5	403 5/C14
4F-4 Fragment Mass Distributions for Gas Vessel Bursts	406 5/D3
4F-5 Rationale for Averaging Fragment Mass Distributions for Tanks A and B and Tanks D and E	412 5/D9
4F-6 Derivation of Figure 4-57, Fragment Distance Versus Percent Yield for Propellant Explosions	413 5/D10
4F-7 Derivation of Simulated Fragment Range Distribution for Gas Vessel Bursts	415 5/D12
4F-8 Rationale for Combining Simulated Range Distribution for Tanks A and B and for Tanks D and E	423 5/E6
List of References	424 5/E7
V. EFFECTS OF FRAGMENTS	425 5/E8
5-1 Damage Estimates to Structures and Facilities	425 5/E8
5-2 Damage Estimates to People from Secondary Fragments	433 5/F2
List of References	442 5/F11
V.A EFFECTS OF FRAGMENTS ON STRUCTURES	444 5/F13
List of References	446 5/G1

TABLE OF CONTENTS (Concl'd)

	<u>Page</u>
V. B DAMAGE ESTIMATES TO PEOPLE FROM SECONDARY FRAGMENTS	447 5/G2
5B-1 Penetrating Fragments	447 5/G2
5B-2 Nonpenetrating Fragments	455 5/G10
List of References	456 5/G11
VI. RISK ASSESSMENT AND INTEGRATED EFFECTS	458 5/G13
6-1 Risk Assessment	458 5/G13
6-2 Prediction of Relative Blast and Fragment Effects	461 6/A7
List of References	507 6/D11
VII. DISCUSSION OF RESULTS	508 6/D12
VIII. CONCLUSIONS	511 6/E1
IX. RECOMMENDATIONS	513 6/E3
LIST OF SYMBOLS	516 6/E6
CONVERSION FACTORS	523 6/E13
GLOSSARY OF TERMS	525 6/F1
BIBLIOGRAPHY	528 6/F4

```

      GO TO 307
305 CALL PARUQP(PBAR,UBAR,QBAR,PBARR)
      IF(UBAR,EQ,0,0) GO TO 30
307 PR=PBARR*PO
      Q=QBAR*PO
      U=UBAR*A0
      T1=X/U
      IF(MA,EQ,1) GO TO 308
      T2=4.0*M/U+T1
      GO TO 309
308 T2=2.0*M/U+T1
309 CONTINUE
      IF(T2.GT.T) GO TO 30
      GO TO 31
30 XT3(K)=0.0
      GO TO 16
31 DT2=0*(1.0-T2/T)**2.0*EXP(-B*T2/T)
      CD0=CD*DT2/PR
      TL=(T2-CD0*T1)/(1.0-CD0)
      APR=PR*TL/2.0
      ACDO=CD*DT2*(TL-T2)/2.0
      B1=(2.0/B)-(2.0/B**2.0)=1.0
      T3=T
      EXPT3=CD*0*T*EXP(-B*T3/T)/B
      TIMET3=(2.0*T3/T)-(2.0*T3/(B*T))-(T3/T)**2.0
      EXPT2=CD*0*T*EXP(-B*T2/T)/B
      TIMET2=(2.0*T2/T)-(2.0*T2/(B*T))-(T2/T)**2.0
      IGRL=(EXPT3*(TIMET3+B1))-(EXPT2*(TIMET2+B1))
      XT3(K)=A/TM*(APR+IGRL-ACDO)
      IF(K,EQ,1) GO TO 10
      IF(ABS(XXT3(I)-XT3(K)),LE,0.005) GO TO 16
      IF(FIND,EQ,2) GO TO 13
      IF(XXT3(I),GT,XT3(K)) GO TO 10
      FIND=2
14 P(K+1)=P(K)
      P(K)=P(K-1)+(P(K+1)-P(K-1))/2.0
      GO TO 12
13 IF(XT3(K),GT,XXT3(I)) GO TO 14
      P(K-1)=P(K)
      P(K)=P(K-1)+(P(K+1)-P(K-1))/2.0
      GO TO 12
10 CONTINUE
16 XXT3(I,J)=XT3(K)
      PP(I,J)=P(K)
      PPI(I,J)=PI(J)
      PPPI(I,J)=PI(J)/(TM*(1./3.))
11 CONTINUE

      PRINT OUT RESULTS
      XXT3=CONSTANT VELOCITY
      XXT3=CALCULATED VELOCITY
      PPI=IMPLUSE
      PP=PRESSURE
      PPPI=PPI/(TM*(1./3.))

      IF(MA,EQ,2) GO TO 400
      PRINT 499,PO,A0,X,M,CD,A,TM

```

Figure 3D-2. (Cont'd)

```

GO TO 401
400 PRINT 500,P0,A0,X,H,CD,A,TH
401 PRINT 501
DO 20 I=1,7
DO 20 J=1,M
500 PRINT 502,XXT3(I),XXXT3(I,J),PPI(I,J),PP(I,J),PPPI(I,J)
18 CONTINUE
400 FORMAT(6F12,0)
401 FORMAT(16F5,2)
100 FORMAT(2F15.5)
110 FORMAT(5F15.5)
120 FORMAT(I2)
130 FORMAT(8F10,2)
444 FORMAT(1H1,5HPO = ,E12.5,/,6H AD = ,E12.5,/,6H X = ,E12.5,/,
16H H = ,E12.5,/,6H CD = ,E12.5,/,6H A = ,E12.5,/,6H TM = ,E12.5,
2/,20H APPURTEANCE IN AIR)
500 FORMAT(1H1,5HPO = ,E12.5,/,6H AD = ,E12.5,/,6H X = ,E12.5,/,
16H H = ,E12.5,/,6H CD = ,E12.5,/,6H A = ,E12.5,/,6H TM = ,E12.5,
2/,23H APPURTEANCE ON GROUND)
501 FORMAT(1H1,4X,5H XXT3,6X,6H XXXT3,7X,4H PPI,4X,3H PP,8X,5H PPPI)
502 FORMAT(1H ,SE12,5)
STOP
END

```

SUBROUTINE PARAMB(B,PBAR,PB,BB)

DIMENSION PB(30),BB(30)

REAL B,PBAR

IF(PBAR.LE.PB(21)) GO TO 20

B=0.0

GO TO 11

20 DO 10 I=1,21

IF(PBAR.EQ.PB(I)) GO TO 9

K=I+1

PBARX0=ABS(PB(K)-PB(I))

PBARX=ABS(PBAR-PB(I))

IF (PBARX.GT.PBARX0) GO TO 10

B=(BB(K)-BB(I))/(PB(K)-PB(I))*(PBAR-PB(I))+BB(I)

GO TO 11

9 B=BB(I)

GO TO 11

10 CONTINUE

11 RETURN

END

Figure 3D-2. (Cont'd)

```

SUBROUTINE PARUQP(PBAR,UBAR,QBAR,PBARR,PBR,UB,QB,PBR)
DIMENSION PBB(5),UB(5),QB(5),PBR(5)
REAL PBAR,UHAR,QHAR,PBARR
IF(PBAR.LE.PBR(5)) GO TO 20
UBAR=QBAR=PBARR=0.0
GO TO 11
20 DO 10 I=1,5
IF (PBAR.EQ.PBB(I)) GO TO 9
K=I+1
PBx0=ABS(PBB(K)-PBB(I))
PRX=ABS(PBAR-PBB(I))
IF (PRX.GT.PBx0) GO TO 10
UHAR=(UB(K)-UB(I))/(PBB(K)-PBB(I))*(PBAR-PBB(I))+UB(I)
QBAR=(QB(K)-QB(I))/(PBB(K)-PBB(I))*(PBAR-PBB(I))+QB(I)
PBARR=(PBR(K)-PBR(I))/(PBB(K)-PBB(I))*(PBAR-PBB(I))+PBR(I)
GO TO 11
9 UHAR=UB(I)
QBAR=QB(I)
PBARR=PBR(I)
GO TO 11
10 CONTINUE
11 RETURN
END

```

Figure 3D-2. (Concl'd)

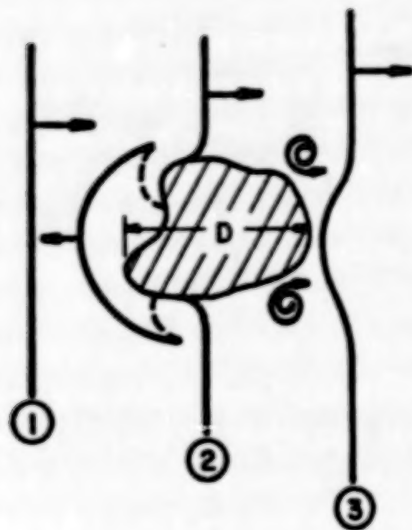


Figure 3D-3. Interaction of Blast Wave with Irregular Object

To determine the momentum imparted to the body from the blast wave, it is necessary to consider both the diffracted phase of loading and the drag phase of loading.

Side-on overpressure is often expressed as a function of time by the modified Friedlander equation: (8)

$$p(t) = P_s \left(1 - \frac{t}{T}\right) e^{-bt/T} \quad (3D-1)$$

where

P_s is peak side-on overpressure

T is the duration of the positive phase of the blast wave

b is a dimensionless time constant.

Integrating this equation gives specific impulse

$$I_s = \frac{P_s T}{b} \left[1 - \frac{(1 - e^{-b})}{b} \right] \quad (3D-2)$$

Diffracted specific impulse I_r can be approximated by

$$I_r = \frac{P_r}{2} \Delta t \quad (3D-3)$$

where

P_r is peak reflected pressure

Δt is length of time for the blast load to reach P_r after initial interaction with the blast wave

or

$$I_r = \frac{P_r}{2} \frac{d}{U} \quad (3D-4)$$

where

d is effective diameter of human

U is shock front velocity

Shock front velocity can be expressed as

$$\left(\frac{U}{a_0}\right)^2 = 1 + \frac{6}{7} \frac{P_s}{P_0} \quad (3D-5)$$

where

a_0 is the speed of sound

P_s is peak side-on overpressure

P_0 is ambient atmospheric pressure

For shocks of intermediate to weak strengths ($P_s/P_0 \leq 3.5$):⁽⁸⁾

$$\frac{P_r}{P_s} = 2 \left(\frac{P_s}{P_0} \right) + \frac{3}{4} \left(\frac{P_s}{P_0} \right)^2 \quad (3D-6)$$

Thus, from Equations (3D-4), (3D-5), and (3D-6),

$$I_x = \frac{\left[\left(\frac{P_s}{P_0} \right) + \frac{3}{8} \left(\frac{P_s}{P_0} \right)^2 \left(\frac{P_s d}{a_0} \right) \right]}{\sqrt{1 + \frac{6}{7} \left(\frac{P_s}{P_0} \right)}} \quad (3D-7)$$

The time history of drag pressure, slightly modified from Glasstone,⁽³⁾ is

$$q(t) = Q \left(1 - \frac{t}{T} \right)^2 e^{-bt/T} \quad (3D-8)$$

where

Q is peak drag pressure.

Integrating Equation (3D-8) with respect to time over the time interval from 0 to T , drag specific impulse I_q becomes:

$$I_q = \left(\frac{QT}{b} \right) \left[1 - \frac{2}{b} + \frac{2}{b^2} (1 - e^{-b}) \right] \quad (3D-9)$$

From Baker,⁽⁸⁾ peak drag pressure (for $P_s/P_0 \leq 3.5$) can be determined by

$$Q = \frac{5}{2} C_D \frac{P_s^2}{(7 P_0 + P_s)} \quad (3D-10)$$

where

C_D is the drag coefficient for the human body.

Solving Equation (3D-2) for T and inserting Equation (3D-10) into Equation (3D-9):

$$I_q = \frac{5}{2} \frac{\left(\frac{P_s}{P_0} \right)}{\left[7 + \left(\frac{P_s}{P_0} \right) \right]} C_D I_s \left[\left(-\frac{2}{b} \right) + \left(\frac{b}{e^{-b} + b - 1} \right) \right] \quad (3D-11)$$

Specific impulse is the integral of pressure with respect to time, while impulse is the integral of force with respect to time, pressure being force per unit area. Total momentum imparted to the body is equivalent to total impulse i_T :

$$i_T = m V \quad (3D-12)$$

where

m is the mass of the body

V is velocity

or

$$m V = (I_r + I_q) (5.5 d^2) \quad (3D-13)$$

where

$(5.5 d^2)$ is the assumed cross-sectional area of the body.

Substituting Equations (3D-11) and (3D-17) into (3D-13) and rearranging terms produces

$$\frac{a_0 m V}{5.5 d^3 p_0} = \frac{\left[\left(\frac{P_s}{p_0} \right) + \left(\frac{3}{8} \right) \left(\frac{P_s}{p_0} \right)^2 \right] \left(\frac{P_s}{p_0} \right)}{\sqrt{1 + \left(\frac{6}{7} \right) \left(\frac{P_s}{p_0} \right)}} + \frac{(2.5) \left(\frac{P_s}{p_0} \right)}{\left[7 + \left(\frac{P_s}{p_0} \right) \right]} \\ \left[\left(-\frac{2}{b} \right) + \left(\frac{b}{e^{-b} + b - 1} \right) \right] \frac{a_0 C_D I_s}{p_0 d} \quad (3D-14)$$

which is a nondimensional equation. If one assumes that the density of man is the same as the density of water ρ_w and that the shape of man can be approximated by a cylinder with a length-to-diameter ratio of 5.5, then mass becomes

$$m = \rho_w \frac{\pi d^2}{4} (5.5 d) \quad (3D-15)$$

or

$$d = \left(\frac{4m}{5.5\pi\rho_w} \right)^{1/3} \quad (3D-16)$$

Substituting Equation (3D-16) into (3D-14) and rearranging terms, one can obtain

$$\frac{\pi\rho_w a_0 V}{4p_0} = \frac{\left[\left(\frac{P_s}{P_0} \right) + \left(\frac{3}{8} \right) \left(\frac{P_s}{P_0} \right)^2 \right] \left(\frac{P_s}{P_0} \right)}{\sqrt{1 + \left(\frac{6}{7} \right) \left(\frac{P_s}{P_0} \right)}} + \frac{(2.5) \left(\frac{P_s}{P_0} \right)}{\left[7 + \left(\frac{P_s}{P_0} \right) \right]} \\ \left[\left(-\frac{2}{b} \right) + \left(\frac{b}{e^{-b} + b - 1} \right) \right] \frac{a_0 C_D I_s}{P_0} \left(\frac{5.5\pi}{4} \right)^{1/3} \frac{\rho_w}{m^{1/3}} \quad (3D-17)$$

Thus,

$$\left(\frac{\rho_w a_0 V}{P_0} \right) = f \left(\frac{P_s}{P_0}, \frac{C_D a_0 I_s \rho_w^{1/3}}{P_0 m^{1/3}} \right) \quad (3D-18)$$

Equation (3D-18) demonstrates a nondimensional functional dependence. Dimensionally, for constant values of ρ_w , a_0 , and p_0 , Equation (3D-18) becomes

$$V = f \left(P_s, \frac{I_s}{m^{1/3}} \right) \quad (3D-19)$$

Thus, after calculating the pressure and impulse combinations required to translate an individual of a certain mass at a specific potentially hazardous velocity, it is beneficial to plot the calculations on a graph of P_s versus $(I_s/m^{1/3})$. By doing this, pressure-impulse combinations needed to propel different body masses at the predetermined velocity can be acquired directly from the graph, assuming that the density and length-to-diameter ratios of the body are the same. Hence, eight graphs (2 damage conditions X 4 altitudes), instead of the previously mentioned 32 graphs (2 damage conditions X 4 masses X 4 altitudes), are required to identify

the pressure-impulse combinations which will produce the human translation velocities specified in Tables 3D-1 and 3D-2 for any mass human body within the limits of the aforementioned assumptions. The results are plotted in Figures 3-12 through 3-19.

It is a very simple matter to use the graphs to determine if there exists a potential threat due to whole body translation and subsequent decelerative impact on a hard surface. An example will demonstrate the procedure.

Suppose a propellant blast occurs at sea level ($p_0 = 101 \text{ kPa}$). The closest people to the blast are several adult males with an approximate mass of 70 kg (154 lb_m). Using methods established in Chapters I and II for calculating pressure and impulse, it is determined that these humans are exposed to an incident overpressure of 1600 Pa (0.232 psi) and a specific impulse of 20 kPa·s (2.90 psi-sec). Scaled impulse ($I_s/m^{1/3}$) is then 4850 Pa·s/kg^{1/3}. Examining Figures 3-12 and 3-16 indicates that the point (1600 Pa, 4850 Pa·s/kg^{1/3}) lies below the threshold curves for skull fracture and for whole body impact, respectively. Since the point is below the curves, no skull fracture or death is expected from whole body displacement. It should be kept in mind that the curves cannot be extended for impulses lower than those shown on the graph, and thus the graphs are somewhat limited since they do not appear to be asymptotic.

LIST OF REFERENCES

1. White, Clayton S., "The Scope of Blast and Shock Biology and Problem Areas in Relating Physical and Biological Parameters," Annals of the New York Academy of Sciences, Vol. 152, Art. 1, October 1968, pp. 89+.
2. Hirsch, Arthur E., "The Tolerance of Man to Impact," Annals of the New York Academy of Sciences, Vol. 152, Art. 1, October 1968, pp. 168+.
3. Glasstone, Samuel, The Effects of Nuclear Weapons, U. S. Government Printing Office, Revised Edition, April 1962.
4. von Gierke, Henning E., "On the Dynamics of Some Head Injury Mechanisms," Aerospace Medical Research Laboratories, Wright-Patterson Air Force Base, Ohio, 1971. AD 728-885.
5. White, Clayton S., "The Nature of the Problems Involved in Estimating the Immediate Casualties from Nuclear Explosions," CEX-71.1, Civil Effects Study, U. S. Atomic Energy Commission, July 1971.
6. Clemedson, Carl-Johan, Gustav Hellström, and Sten Lindgren, "The Relative Tolerance of the Head, Thorax, and Abdomen to Blunt Trauma," Annals of the New York Academy of Sciences, Vol. 152, Art. 1, October 1968, pp. 187+.
7. Hoerner, Sighard F., Fluid-Dynamic Drag, Published by the Author, Midland Park, New Jersey, 1958.
8. Baker, Wilfred E., Explosions in Air, University of Texas Press, Austin, Texas, May 1973.

CHAPTER IV

CHARACTERISTICS OF FRAGMENTS

4-1 General

The fragments generated during accidental explosions of the types covered in this workbook can come from several sources. They can be pieces of the exploding vessels themselves, or pieces of wreckage from an impact which also results in an explosion, or nearby objects (appurtenances) accelerated by the blast waves from the explosion. The methods of prediction given in this chapter allow one first to estimate initial fragment velocities for various types of accident and geometry of vessel or explosion source. Next, predictions can be made of fragment ranges and impact conditions using initial velocities as inputs. Finally, fragment mass distributions can be predicted in a statistical sense for several classes of accidental explosion.

The various graphs and equations used to generate predictions of fragment characteristics are the result of exercise of a number of computer programs, and fits to experimental data. A number of appendices are included in the chapter to describe the computer programs, statistical analyses, and other supporting information.

4-2 Methods for Estimating Fragment Initial Velocities for Spheres and Cylinders Bursting into Many Fragments

4-2.1 Spherical Gas Vessels

The following is the deterministic technique for predicting initial fragment velocities for fragments emanating from containment vessels of spherical geometry. This technique requires that you know the external radius of the spherical confinement vessel, the thickness of the wall of the spherical confinement vessel, the density of the confinement vessel material, and the internal gas pressure at burst. The present figures allow this technique to be used for gases whose properties are similar to air and helium.

The first step in the procedure is to calculate a mass ratio consisting of the mass of a volume of gas equal to the internal volume of the sphere at standard temperature and pressure, divided by the mass of the confinement vessel. The equation for calculating this mass ratio is given in each of the examples in terms of the radius of the spherical confinement vessel, the thickness of the vessel walls, and the density of the gas and vessel material, respectively.

The second step in this procedure is to calculate a pressure ratio which is the pressure of the internal gas at the time the confinement vessel bursts divided by atmospheric pressure. Having obtained the mass ratio and the pressure ratio, a value for initial velocity ratio \bar{v} can be obtained from Figures 4-1 through 4-8, which constitutes Step 3 in the procedure. The figure used to look up the value of \bar{v} depends upon whether air or helium is considered and the radius of the confinement vessel. Since figures are not generated for all possible vessel radii, it is necessary to consult the figure with a radius value that is nearest to the radius of the confinement vessel considered. Since plots are not given in the figures for all possible mass ratios, it is also necessary to read values for \bar{v} from the plots for mass ratios having values most nearly above and below the mass ratio considered. The appropriate value for \bar{v} can then be obtained by the method of linear interpolation as in Step 4 of the examples. Once the velocity ratio value has been obtained for the specific case considered, it can be multiplied by the appropriate speed of sound at ambient conditions for the gas considered to obtain the initial fragment velocity.

Examples 1 through 3 illustrate how this procedure may be used to obtain initial fragment velocities from bursting spheres. Fragment velocities from bursting cylinders are discussed in the next section with examples. Example 1 is the calculation for a case in which some experimental data have been obtained to verify the results, as is Example 2. Discussion of experimental results which verify the code used to generate Figures 4-1 through 4-8 is given in Appendix 4A. Example 3 is taken from a proposed case where a Centaur pressure tank is overpressurized with helium.

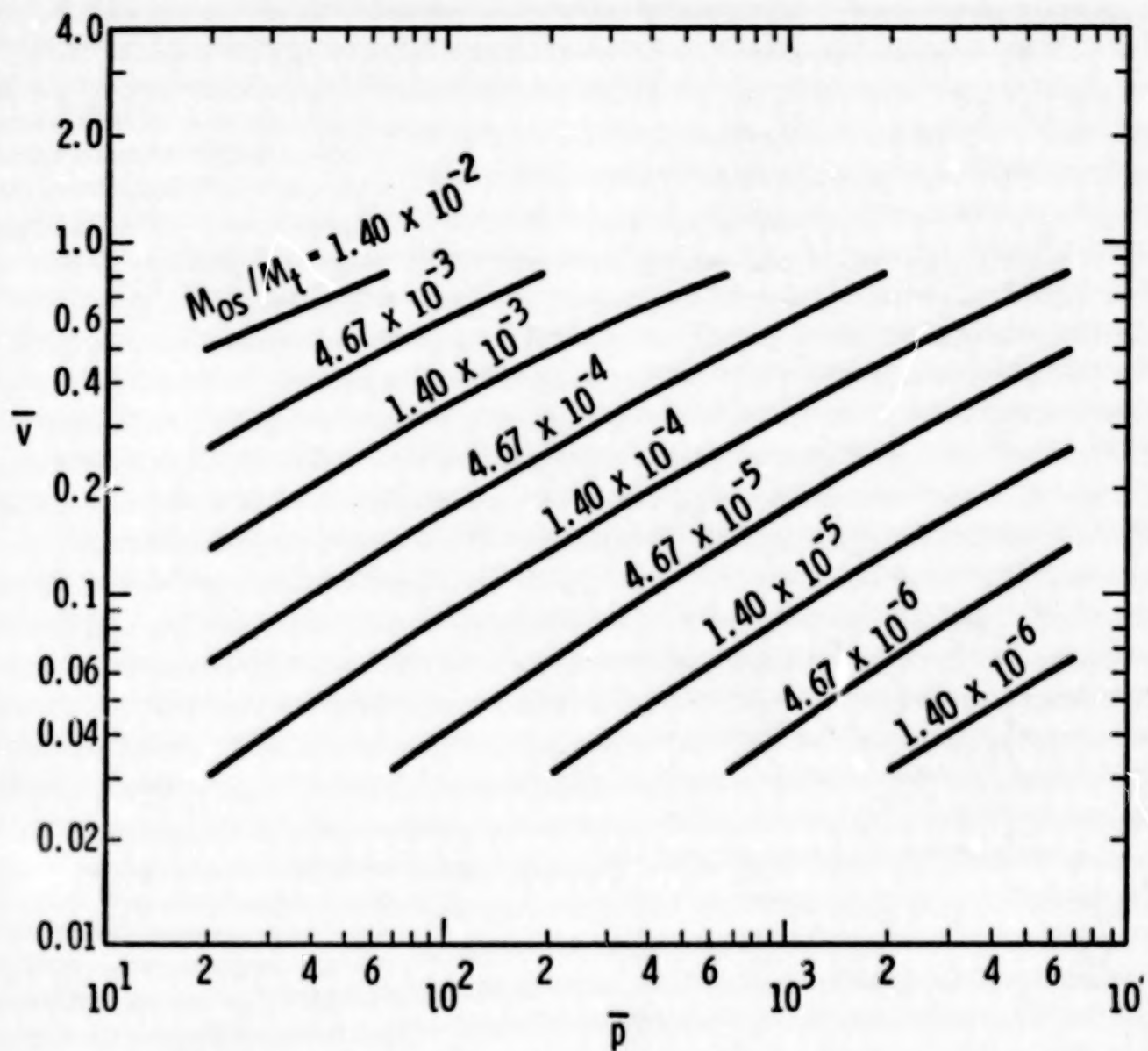
The procedure illustrated here for estimating initial fragment velocities from bursting pressurized confinement vessels was made possible by the generation of Figures 4-1 through 4-8 from the computer code SPHER. This code and the theory behind it are discussed in the appendices. A similar code used to generate Figures 4-9 through 4-16 for cylindrical confinement vessels was generated from a code CYLIN. This code is also discussed in the appendices.

Example 1. For Spheres

Assume: A spherical containment vessel of glass

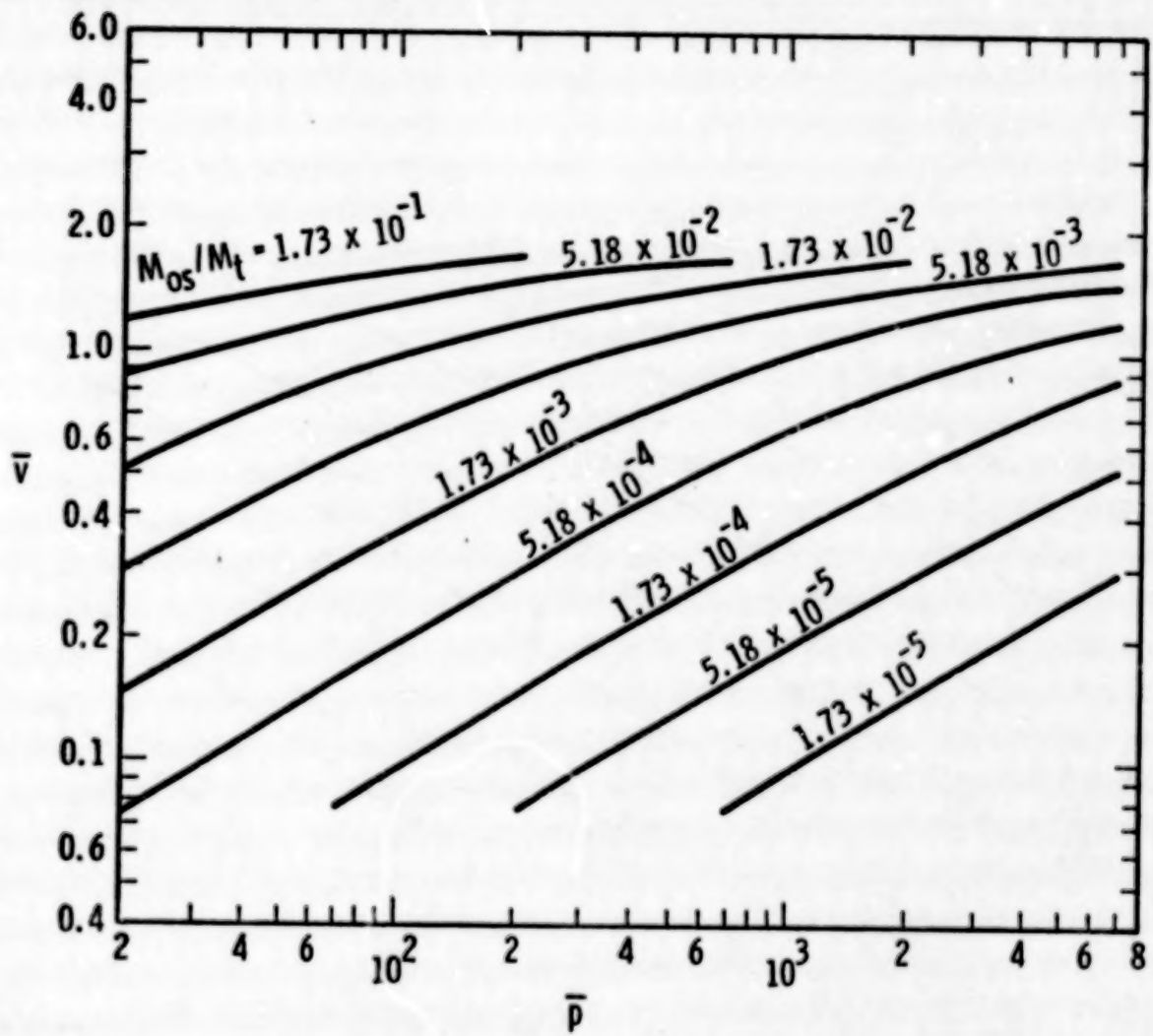
R = 0.0245 m (1 in.) internal radius of sphere

t = 0.001 m (3.94×10^{-2} in.) glass wall thickness



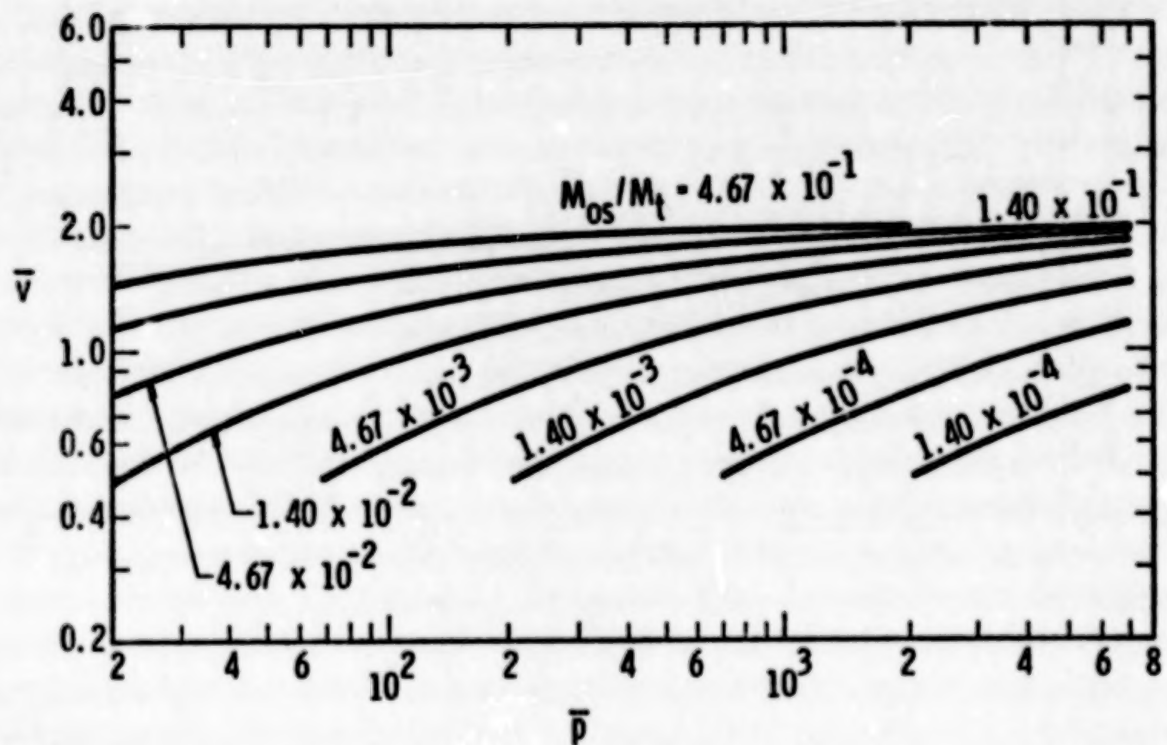
$$a_{os} = 331 \text{ m/s}$$

Figure 4-1. Fragment Velocities for Contained Air
in a Sphere of Radius 0.0762 m



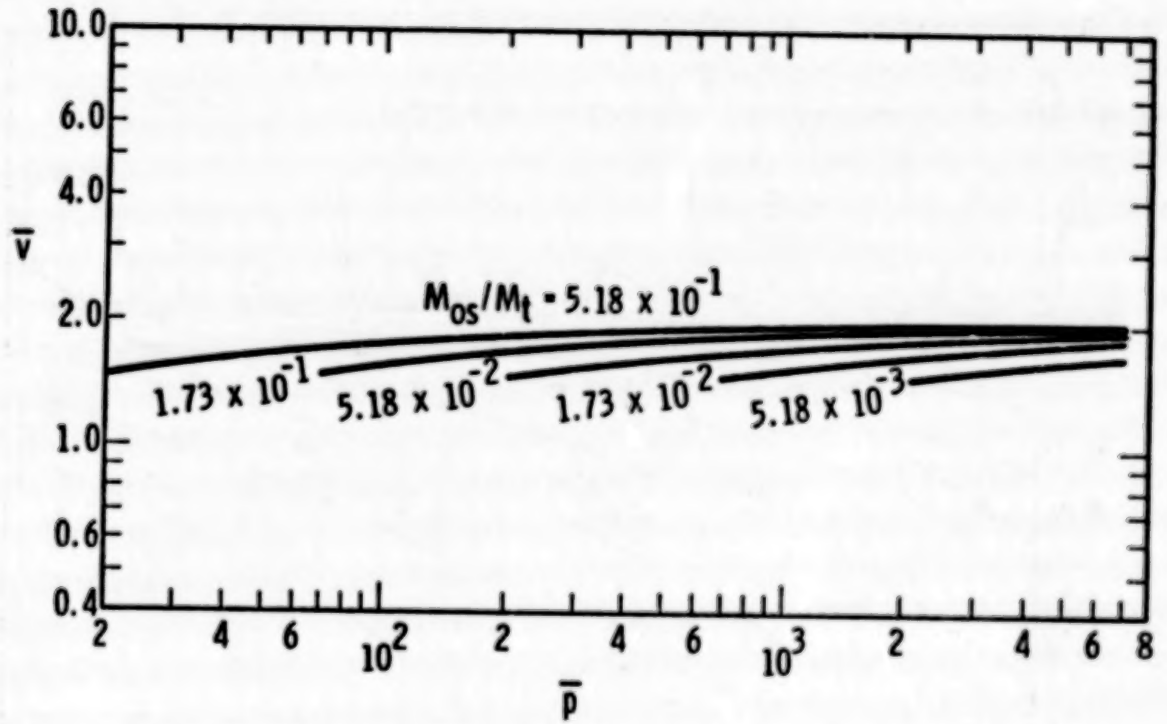
$$a_{os} = 331 \text{ m/s}$$

Figure 4-2. Fragment Velocities for Contained Air
in a Sphere of Radius 0.254 m



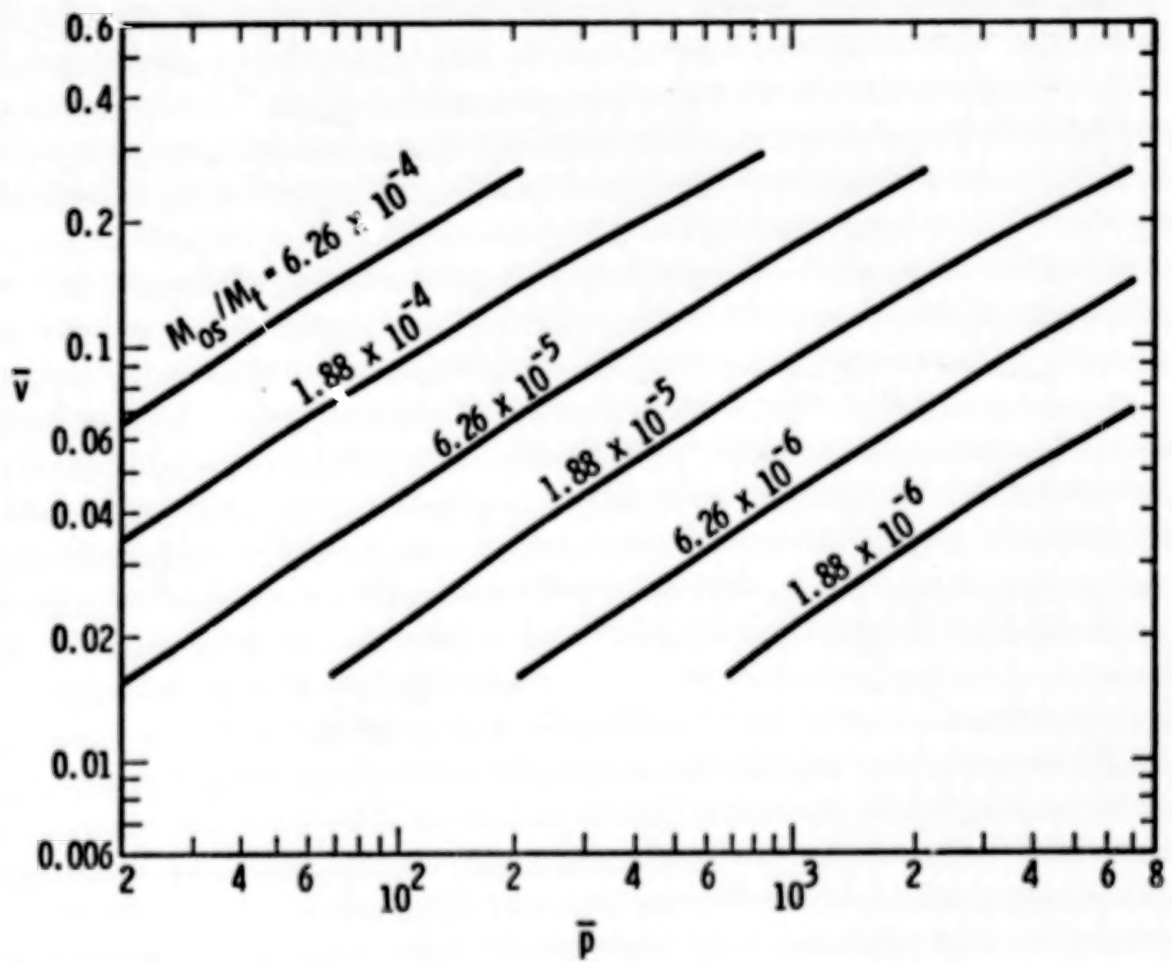
$$a_{os} = 331 \text{ m/s}$$

Figure 4-3. Fragment Velocities for Contained Air
in a Sphere of Radius 0.762 m



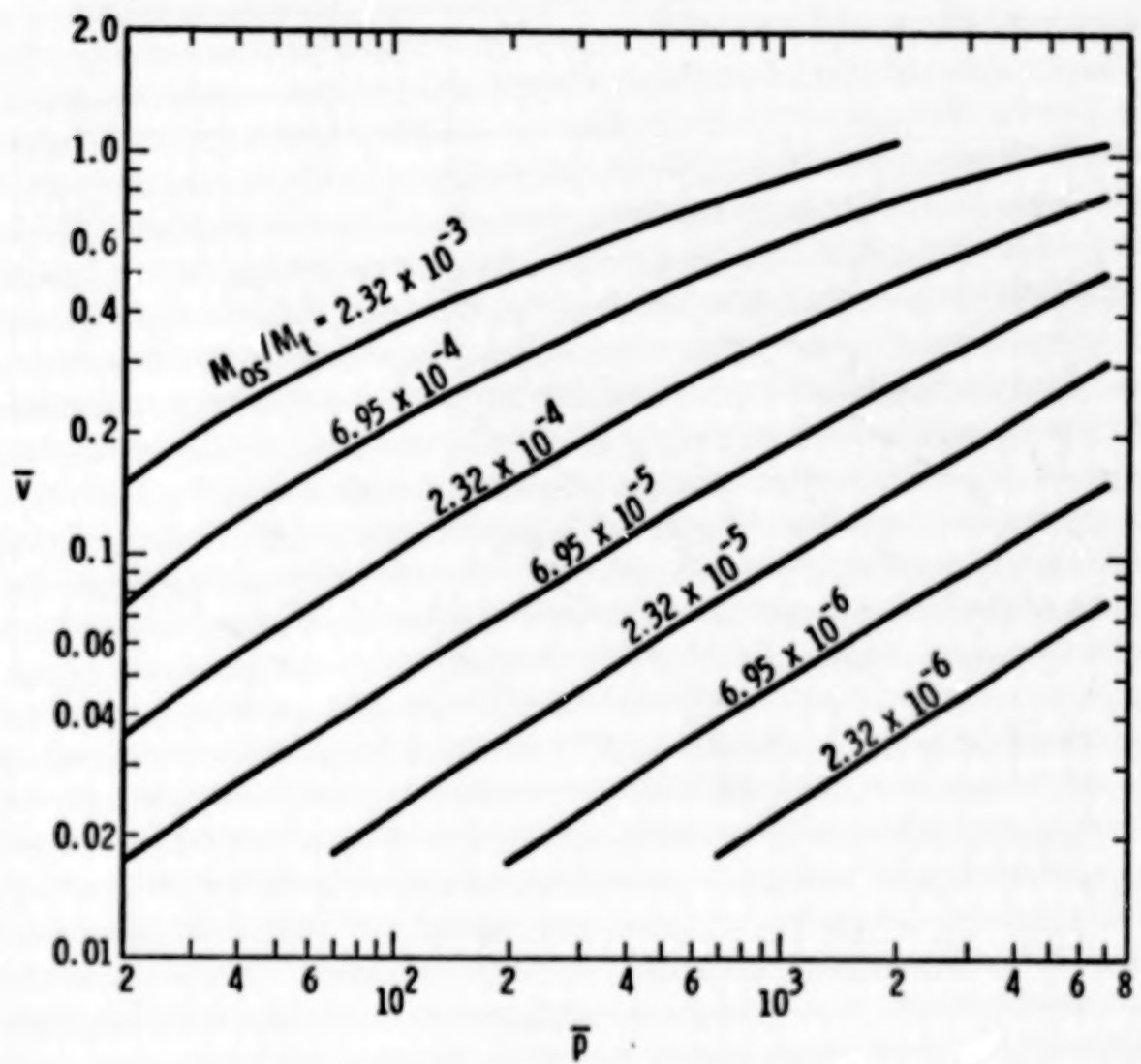
$$a_0 = 331 \text{ m/s}$$

**Figure 4-4. Fragment Velocities for Contained Air
in a Sphere of Radius 2.54 m**



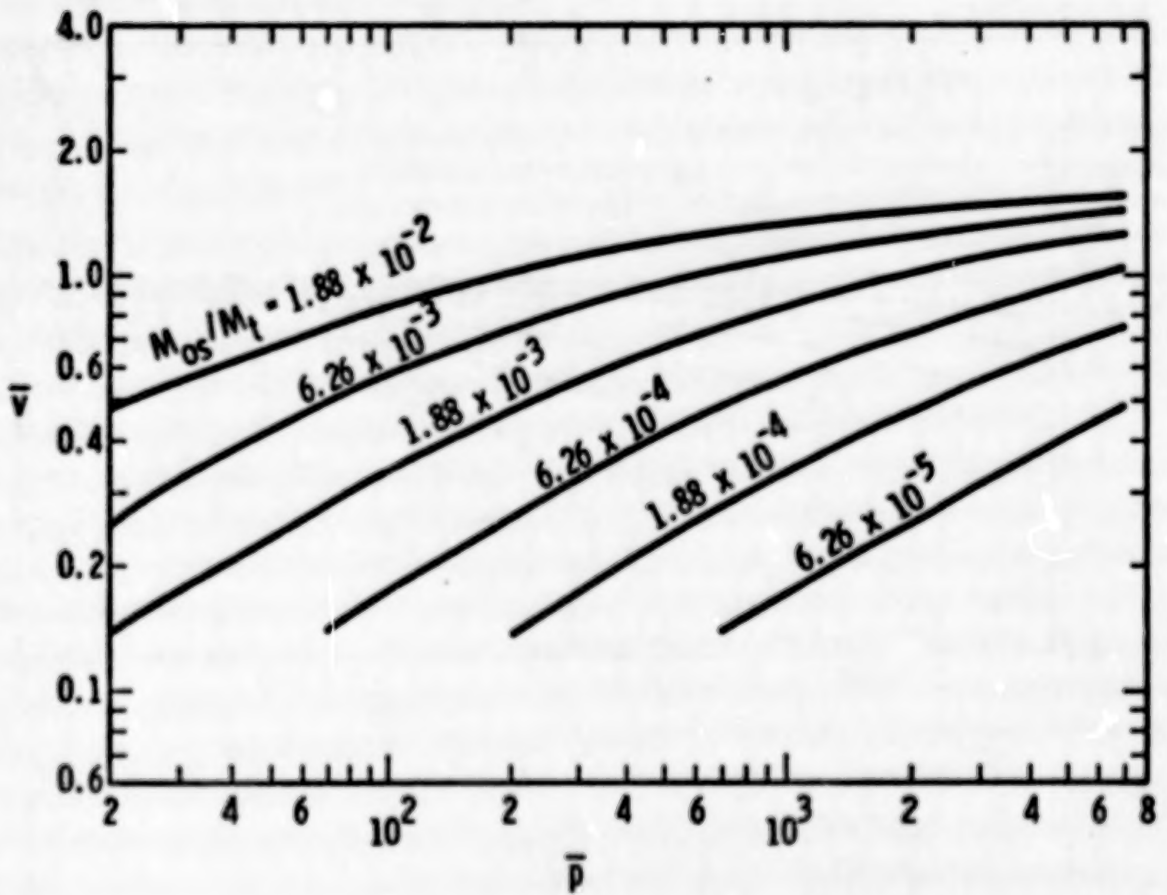
$$a_{os} = 963 \text{ m/s}$$

Figure 4-5. Fragment Velocities for Contained He
in a Sphere of Radius 0.0762 m



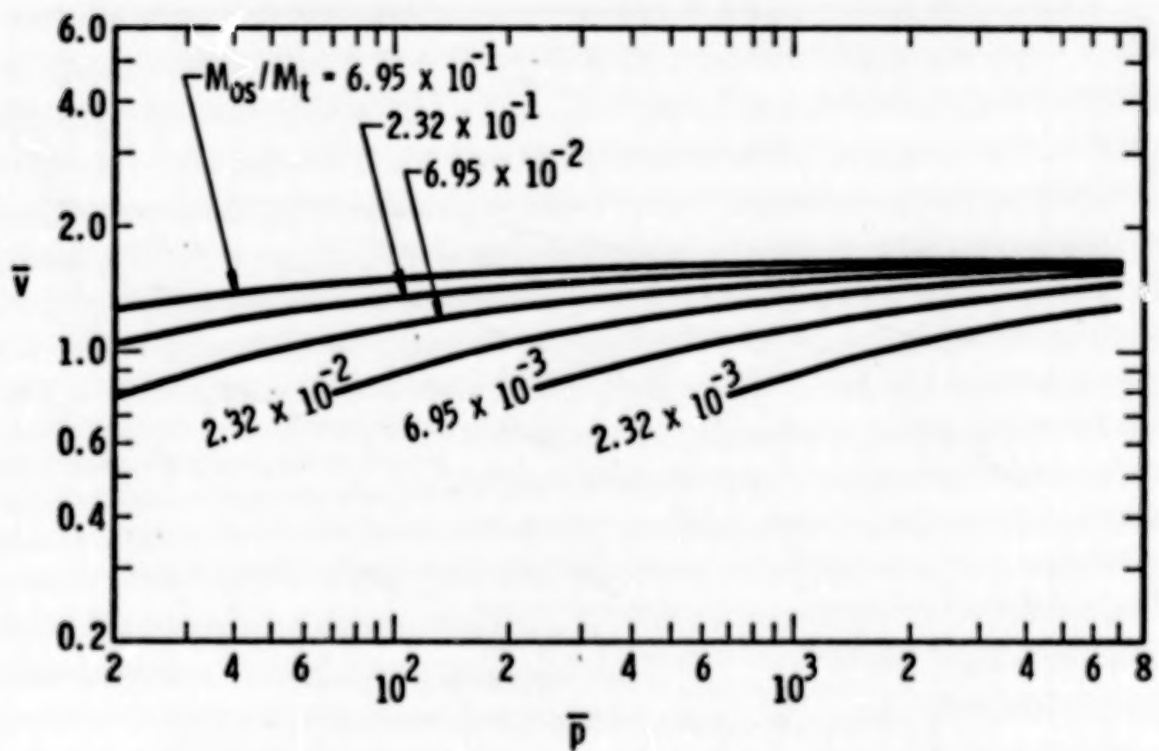
$$a_{os} = 963 \text{ m/s}$$

Figure 4-6. Fragment Velocities for Contained He
in a Sphere of Radius 0.254 m



$$a_{os} = 963 \text{ m/s}$$

Figure 4-7. Fragment Velocities for Contained He
in a Sphere of Radius 0.762 m



$$a_{os} = 963 \text{ m/s}$$

Figure 4-8. Fragment Velocities for Contained He
in a Sphere of Radius 2.54 m

Burst from internal air pressure

$$P_o = 2.25 \times 10^6 \text{ Pa (326 psi)}$$

Step 1. Calculate mass ratio M_{os}/M_t from equation

$$\frac{M_{os}}{M_t} = \frac{R^3 \rho_{air}}{[R^3 - (R-t)^3] \rho_{glass}}$$

From assumptions $R = 0.0254 \text{ m}$

$$t = 0.001 \text{ m}$$

From density tables $\rho_{air} = 1.293 \text{ kg/m}^3$, at standard temperature and pressure.

$$\rho_{glass} = 2600 \text{ kg/m}^3$$

Therefore,

$$\frac{M_{os}}{M_t} = \frac{(1.293)(0.0254)^3}{[(0.0254)^3 - (0.0254 - 0.001)^3] (2600)} = 4.38 \times 10^{-3}$$

Step 2. Calculate pressure ratio \bar{p} from equation

$$\bar{p} = \frac{P_o}{1.01 \times 10^5}$$

$$\text{From assumption } P_o = 2.25 \times 10^6 \text{ Pa}$$

Therefore,

$$\bar{p} = \frac{2.25 \times 10^6}{1.01 \times 10^5} = 22.21$$

Step 3. From Figure 4-1, for a vessel of radius closest to the vessel considered containing air, find \bar{V} for the M_{os}/M_t ratio

most nearly above and below the value of Step 1 for the \bar{p} of Step 2. This is:

$$\text{at } \bar{p} = 22.2$$

$$M_1 = (M_{os}/M_t) \text{ below} = 1.40 \times 10^{-3}, \quad \bar{V}_1 = 0.140$$

$$M_2 = (M_{os}/M_t) \text{ Step 1} = 4.38 \times 10^{-3}, \quad \bar{V}_2 = ?$$

$$M_3 = (M_{os}/M_t) \text{ above} = 4.67 \times 10^{-3}, \quad \bar{V}_3 = 0.266$$

Step 4. Find \bar{V}_2 by linear interpolation from the equation

$$\bar{V}_2 = (\bar{V}_3 - \bar{V}_1) \left(\frac{M_2 - M_1}{M_3 - M_1} \right) + \bar{V}_1 =$$

$$\bar{V}_2 = (0.266 - 0.140) \left(\frac{4.38 - 1.40}{4.67 - 1.40} \right) + 0.140 = 0.255$$

Step 5. Multiply \bar{V}_2 by the a_{os} value given in Figure 4-1 to obtain the initial fragment velocity

$$V_i = \bar{V}_2 \cdot a_{os} = (0.255) (3.31 \times 10^2 \text{ m/s}) = 84.4 \text{ m/s}$$

The initial fragment velocity is 84.4 m/s (277 ft/sec).

Note: This example was run using code SPHER, the code used to generate Figure 4-1, for the specific data assumed. The results gave a $V_i = 80.2 \text{ m/s}$ (263 ft/sec) compared to our result of 84.4 m/s (277 ft/sec) obtained from the figure. This gives some indication of the interpolation error and error in reading numbers from the figure which can be expected.

This particular example was taken from the data of D. W. Boyer, et al.,⁽¹⁾ who performed experiments in which glass spheres of various dimensions were burst under internal gas pressure. For this particular sphere dimension and gas pressure, the experimental data showed fragments had an average initial fragment velocity of 75.6 m/s (248 ft/s). Our value obtained from the tables is about 10% higher than this.

A comparison of other data from the tests by Boyer with fragment velocities obtained from code SFHER or the tables generated from code SPHLR is given in Appendix 4A.

Example 2. For Spheres

Assume: A spherical containment vessel of glass

$$R = 0.0254 \text{ m (1 in.) internal radius of sphere}$$

$$t = 0.001 \text{ m } (3.94 \times 10^{-2} \text{ in.}) \text{ glass wall thickness}$$

Burst from internal helium (He) pressure

$$P_o = 2.25 \times 10^6 \text{ Pa (326 psi)}$$

Step 1. Calculate mass ratio M_{os}/M_t from equation

$$\frac{M_{os}}{M_t} = \frac{R^3 \rho_{He}}{[R^3 - (R - t)^3] \rho_{glass}}$$

From assumptions: $R = 0.0254 \text{ m}$

$$t = 0.001 \text{ m}$$

From density tables: $\rho_{He} = 0.1785 \text{ kg/m}^3$ at STP

$$\rho_{glass} = 2600 \text{ kg/m}^3$$

Therefore,

$$\frac{M_{os}}{M_t} = \frac{(0.1785)(0.0254)^3}{[(0.0254)^3 - (0.0254 - 0.001)^3] (2600)} = 6.05 \times 10^{-4}$$

Step 2. $\bar{p} = 22.2$ (same as in Example 1)

Step 3. From Figure 4-5, for a vessel of radius closest to the vessel considered containing He, find \bar{V} for the M_{os}/M_t ratio most nearly above and below the value of Step 1 for the \bar{p} of Step 2.

at $\bar{p} = 22.2$

$$M_1 = (M_{os}/M_t) \text{ below} = 1.88 \times 10^{-4}, \quad \bar{v}_1 = 0.036$$

$$M_2 = (M_{os}/M_t) \text{ Step 1} = 6.05 \times 10^{-4}, \quad \bar{v}_2 = ?$$

$$M_3 = (M_{os}/M_t) \text{ above} = 6.26 \times 10^{-4}, \quad \bar{v}_3 = 0.068$$

Step 4. Find \bar{v}_2 by linear interpolation from the equation

$$\bar{v}_2 = (\bar{v}_3 - \bar{v}_1) \left(\frac{M_2 - M_1}{M_3 - M_1} \right) + \bar{v}_1$$

$$\bar{v}_2 = (0.068 - 0.036) \left(\frac{6.05 - 1.88}{6.26 - 1.88} \right) + 0.036$$

$$= 0.066$$

Step 5. Multiply v_2 by the a_{os} value in Figure 4-5 to obtain the initial fragment velocity

$$v_i = \bar{v}_2 \cdot a_{os} = (0.066) (9.63 \times 10^2 \text{ m/s}) = 64.0 \text{ m/s}$$

The initial fragment velocity is 64 m/s (210 ft/sec)

Example 3, For Spheres

Assume: A Centaur pressurant tank

$$V = 0.121 \text{ m}^3 (7361 \text{ in}^3) \text{ volume of tank}$$

$$t = 0.0046 \text{ m (0.181 in.) titanium wall thickness}$$

Burst from internal He pressure

$$P_o = 2.07 \times 10^7 \text{ Pa (3000 psi)}$$

Step 1. Calculate mass ratio M_{os}/M_t from equation

$$\frac{M_{os}}{M_t} = \frac{R^3 \rho_{He}}{[R^3 - (R - t)^3] \rho_{titanium}}$$

from assumptions

$$V = \frac{4}{3} \pi R^3 = 0.121 \text{ m}^3$$

Therefore

$$R = \left[\frac{(3)(0.121)}{4\pi} \right]^{1/3} \text{ m}$$

$$R = 0.307 \text{ m} = 30.7 \text{ cm}$$

$$t = 0.0046 \text{ m}$$

From density tables

$$\rho_{He} = 0.1785 \text{ kg/m}^3 \text{ at STP}$$

$$\rho_{Ti} = 4500 \text{ kg/m}^3$$

Therefore,

$$\frac{M_{os}}{M_t} = \frac{(0.307)^3 (0.1785)}{[(0.307)^3 - (0.307 - 0.0046)^3] (4500)} = 8.96 \times 10^{-4}$$

Step 2. Calculate pressure ratio \bar{p} from equation

$$p = \frac{P_o}{1.01 \times 10^5}$$

from assumption

$$P_o = 2.07 \times 10^7 \text{ Pa}$$

Therefore,

$$\bar{p} = \frac{2.07 \times 10^7}{1.01 \times 10^5} = 205$$

Step 3. From Figure 4-6, for a vessel of radius closest to the vessel considered containing He, find \bar{V} for the M_{os}/M_t ratio most nearly above and below the value of Step 1 for the \bar{p} value of Step 2. This is:

$$\text{at } \bar{p} = 205$$

$$M_1 = (M_{os}/M_t) \text{ below} = 6.95 \times 10^{-4}, \quad \bar{V}_1 = 0.30$$

$$M_2 = (M_{os}/M_t) \text{ Step 1} = 8.96 \times 10^{-4}, \quad \bar{V}_2 = ?$$

$$M_3 = (M_{os}/M_t) \text{ above} = 2.32 \times 10^{-3}, \quad \bar{V}_3 = 0.49$$

Step 4. Find \bar{V}_2 by linear interpolation from equation

$$\bar{V}_2 = (\bar{V}_3 - \bar{V}_1) \left(\frac{M_2 - M_1}{M_3 - M_1} \right) + \bar{V}_1$$

$$V_2 = (0.49 - 0.30) \left(\frac{8.96 - 6.95}{23.2 - 6.95} \right) + 0.30$$

$$= 0.32 \text{ m/s}$$

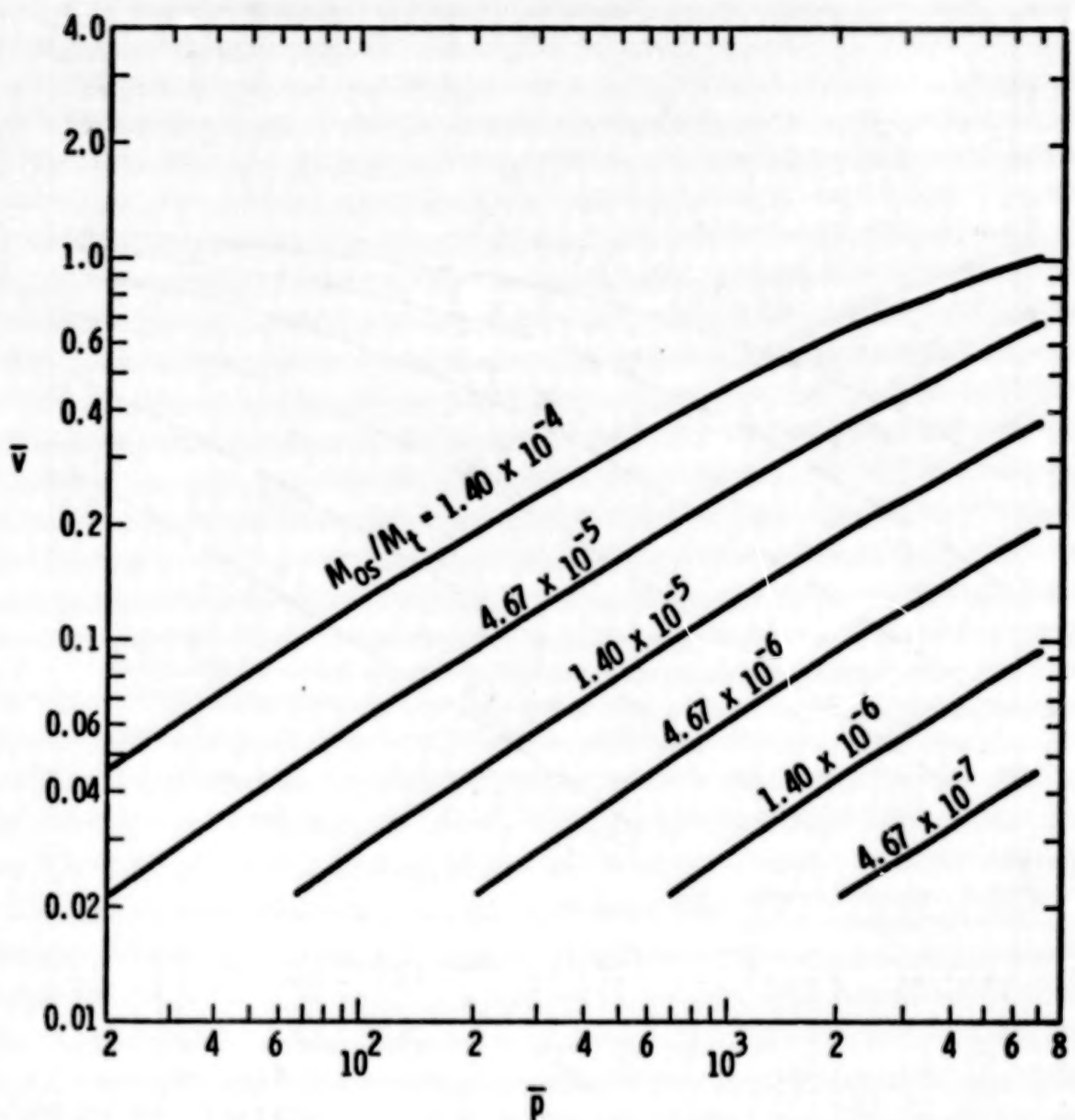
Step 5. Multiply V_2 by the a_{os} value given in Figure 4-6 to obtain the initial fragment velocity.

$$V_i = \bar{V}_2 \cdot a_{os} = (0.32) (963 \text{ m/s}) = 311 \text{ m/s}$$

The initial fragment velocity is 311 m/s (1022 ft/s).

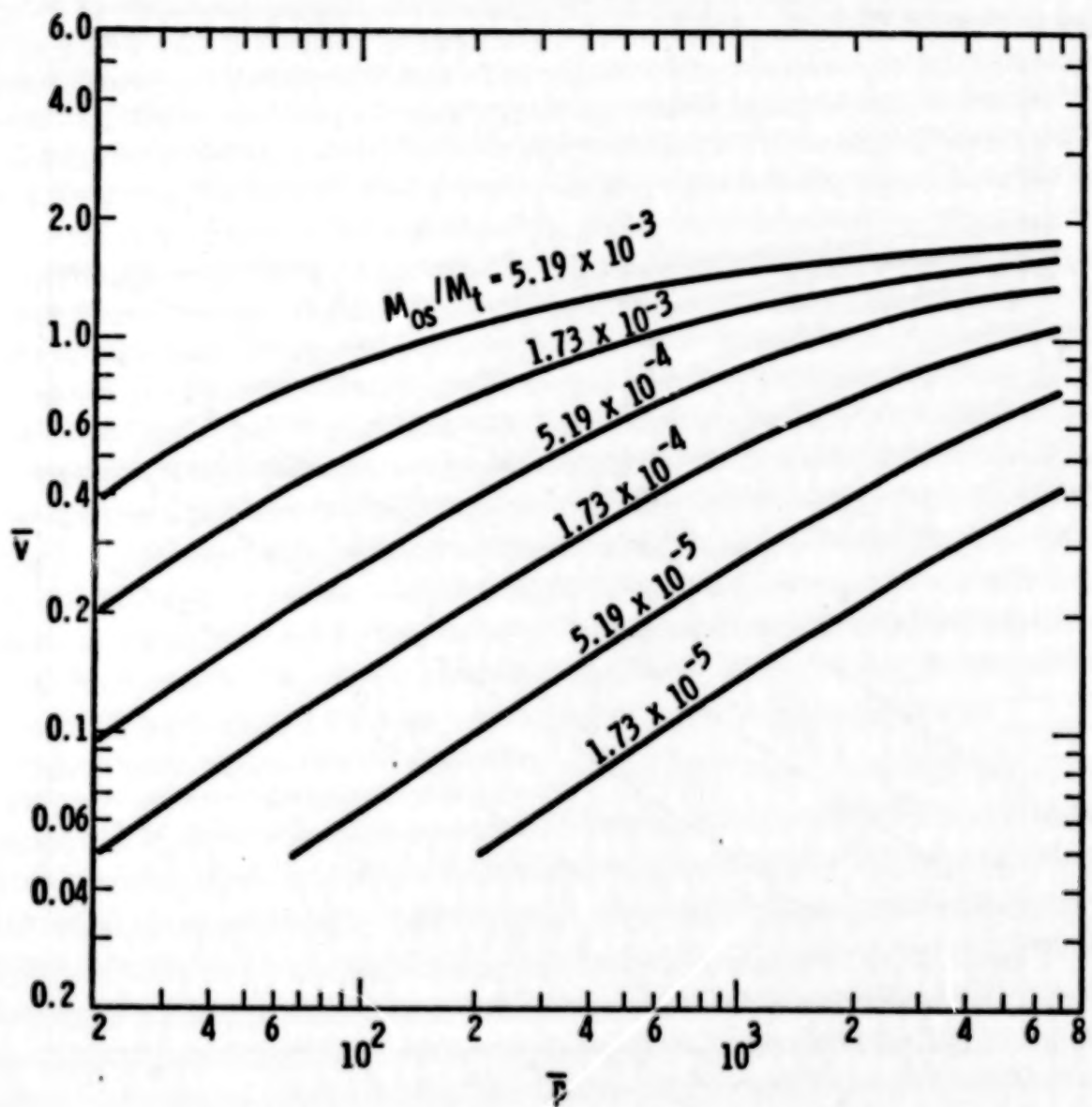
4-2.2 Cylindrical Gas Vessels

The following deterministic procedure may be used to estimate initial fragment velocities emanating from containment vessels of cylindrical configuration. Figures 4-9 through 4-16 may be used to estimate initial fragment velocities for a broad spectrum of burst pressures and confinement vessel dimensions. Figures 4-9 through 4-12



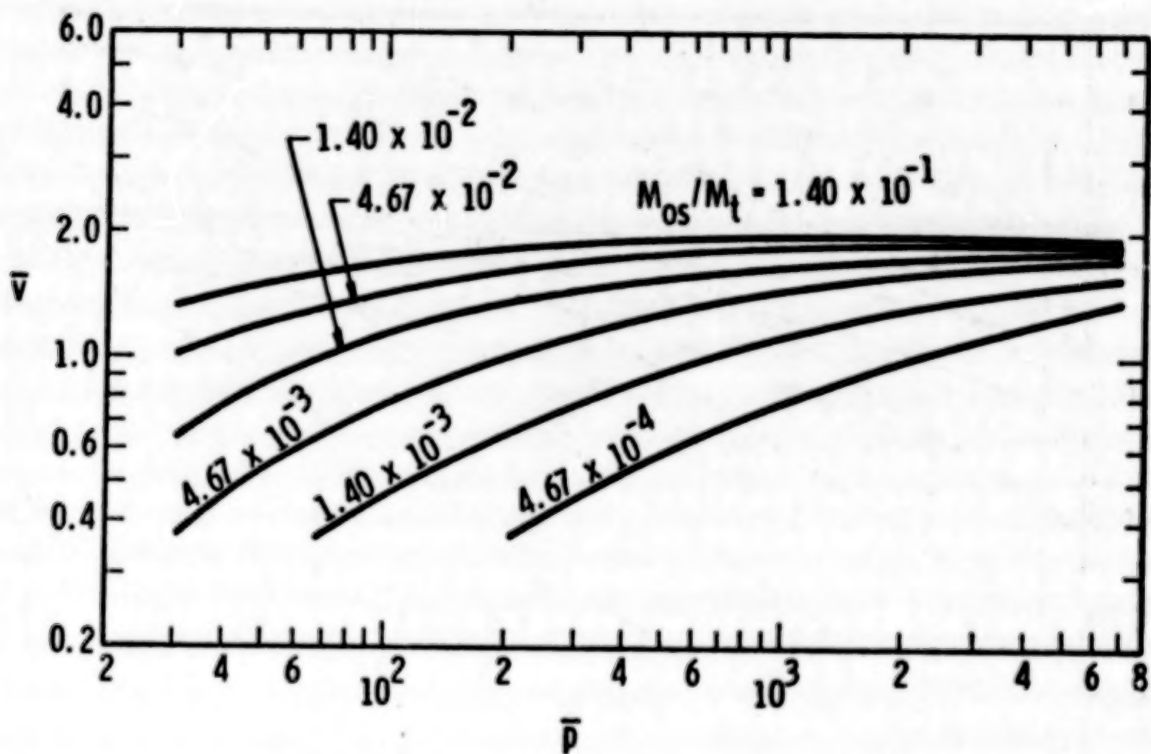
$$a_{os} = 331 \text{ m/s}$$

Figure 4-9. Fragment Velocities for Contained Air
in a Cylinder of Radius 0.0762 m



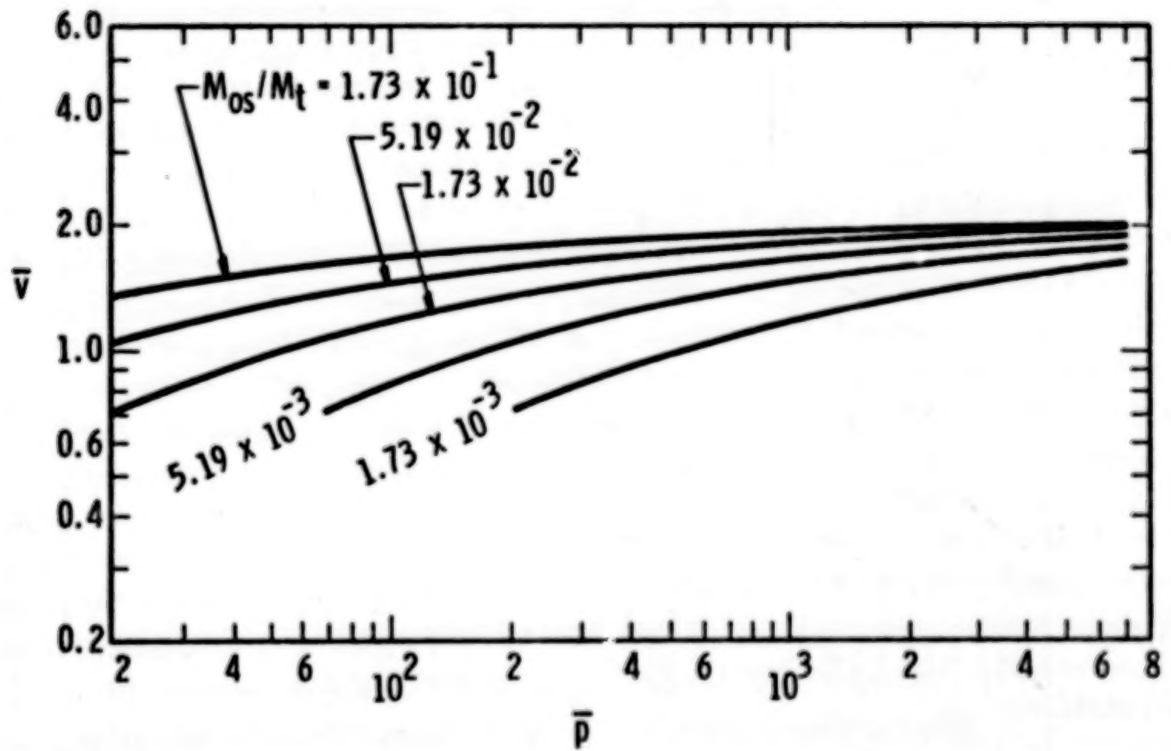
$$a_{os} = 331 \text{ m/s}$$

Figure 4-10. Fragment Velocities for Contained Air
in a Cylinder of Radius 0.254 m



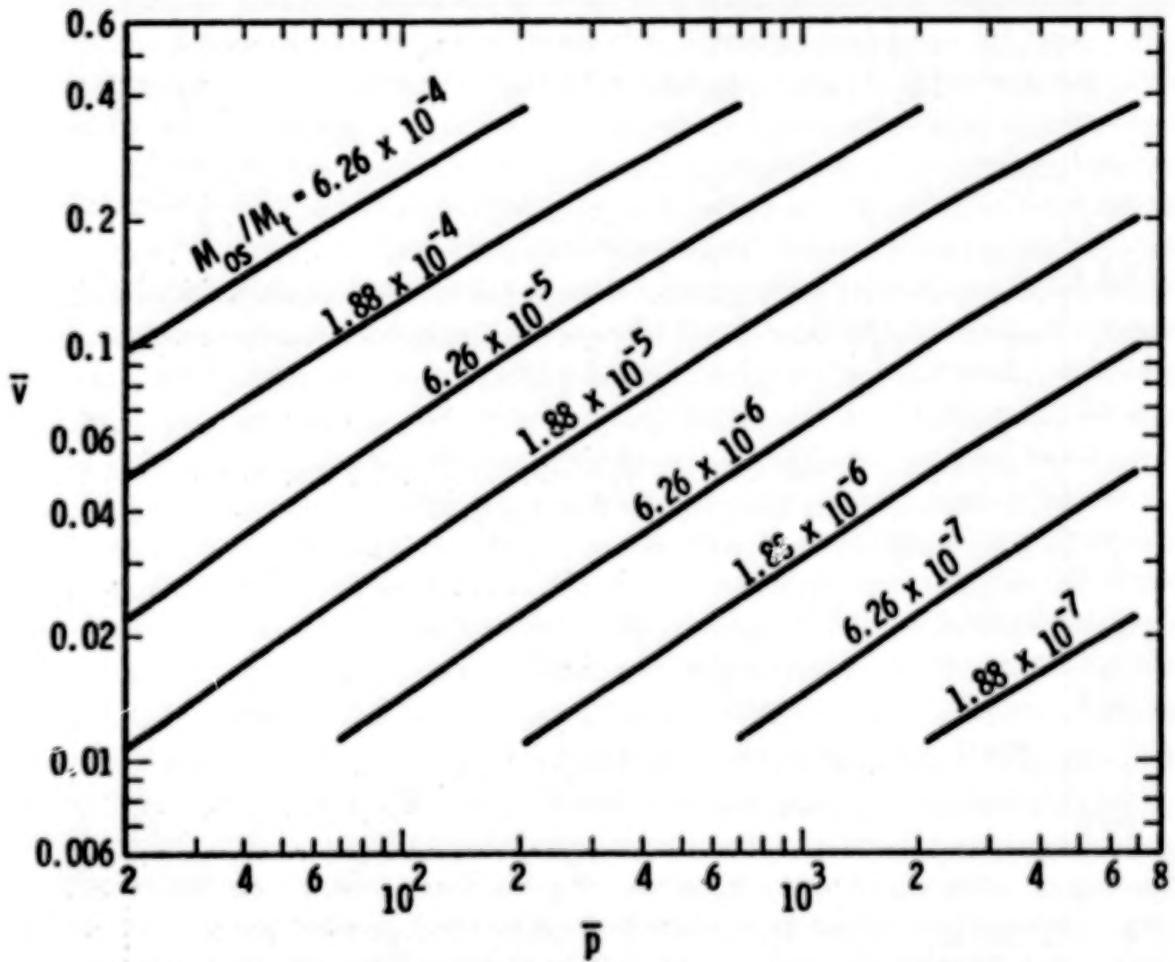
$$a_{os} = 331 \text{ m/s}$$

Figure 4-11. Fragment Velocities for Contained Air
in a Cylinder of Radius 0.762 m



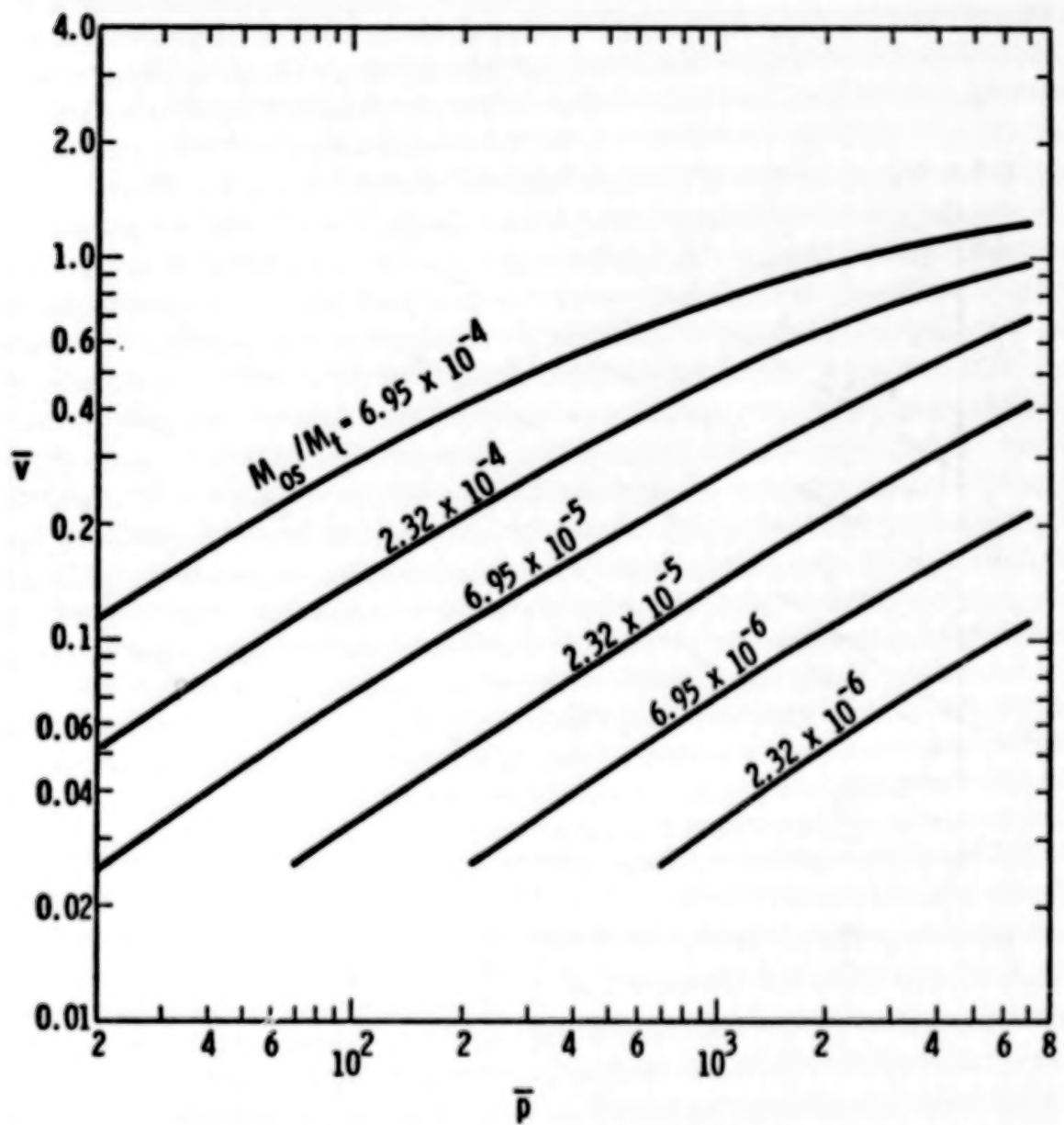
$$a_{os} = 331 \text{ m/s}$$

Figure 4-12. Fragment Velocities for Contained Air
in a Cylinder of Radius 2.54 m



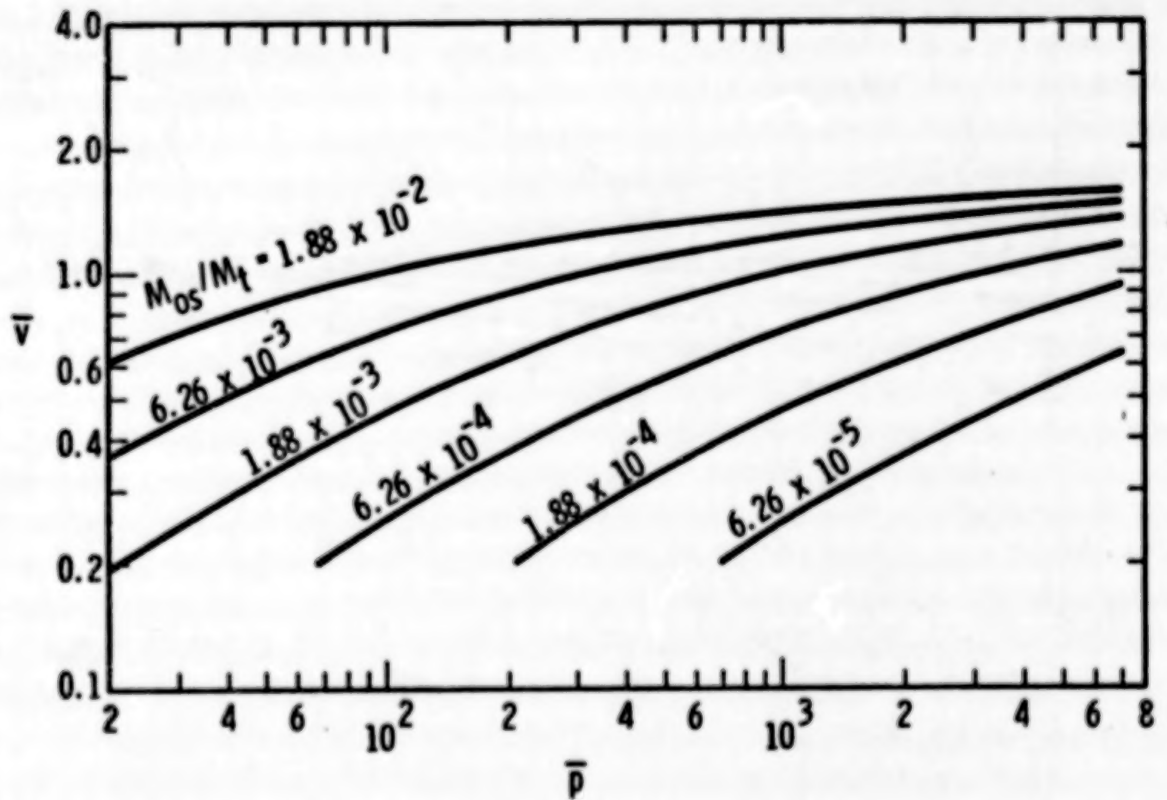
$$a_{os} = 963 \text{ m/s}$$

Figure 4-13. Fragment Velocities for Contained He
in a Cylinder of Radius 0.0762 m



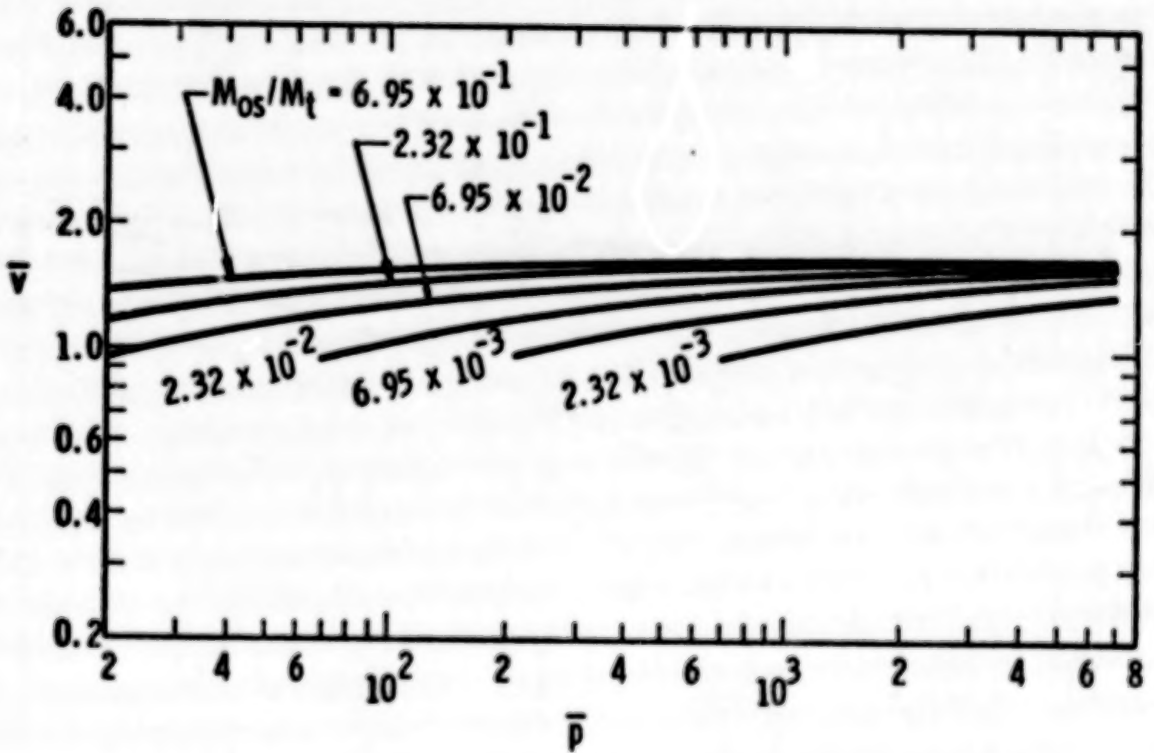
$$a_{c.s.} = 963 \text{ m/s}$$

Figure 4-14. Fragment Velocities for Contained He
in a Cylinder of Radius 0.254 m



$$a_{os} = 963 \text{ m/s}$$

**Figure 4-15. Fragment Velocities for Contained He
in a Cylinder of Radius 0.762 m**



$$a_{0s} = 963 \text{ m/s}$$

Figure 4-16. Fragment Velocities for Contained He
in a Cylinder of Radius 2.54 m

may be used for estimating initial fragment velocities for a confined gas with properties similar to air. Figures 4-13 through 4-16 may be used for estimating initial fragment velocities for a confined gas whose properties are similar to helium. The code used to generate these figures (code CYLIN) is described in Appendix 4A. It should be pointed out that because of the two-dimensional nature of the analysis, the effects of the cylinder ends are not taken into account. The length of the cylinder thus does not affect results and is immaterial so long as the properties of the cylinder per unit length are known.

Example 1 below demonstrates how the initial velocity of fragments emanating from a bursting containment vessel may be obtained through the use of the figures. In this example, a steel cylinder approximately 2 feet in diameter and having wall thickness of approximately a quarter of an inch is assumed to burst at 10^4 psi from the pressure of confined air. It should be noted that all calculations are done using standard SI units. It should also be noted that the tank mass is nondimensionalized in the figures by the use of a ratio with the mass of the confined gas at standard temperature and pressure. Example 2 is a calculation for the initial fragment velocities emanating from a cylinder similar to that of Example 1, which bursts under pressurization from helium gas. The method for calculating fragment velocities shown in these examples for cylinders is the same as those for spheres with the exception of a different equation for calculating the mass ratio and the use of the different figures to obtain \bar{v} as a function of \bar{p} and the mass ratio.

Examples 1. For Cylinders

Assume:

A cylindrical confinement vessel

$t = 0.005 \text{ m} (-0.025 \text{ in.})$ steel wall thickness

$R = 0.30 \text{ m} (-12.0 \text{ in.})$ radius of tank

Bursts from internal air pressure

$P_o = 7.00 \times 10^7 \text{ Pa} (-10^4 \text{ psi})$

Step 1. Calculate mass ratio M_{os}/M_t from equation

$$\frac{M_{os}}{M_t} = \frac{R^2 \rho_{air}}{[R^2 - (R - t)^2] \rho_{steel}}$$

from assumptions

$$R = 0.030 \text{ m}$$

$$t = 0.005 \text{ m}$$

from density tables

$$\rho_{\text{air}} = 1.293 \text{ kg/m}^3 \text{ at STP}$$

$$\rho_{\text{steel}} = 7800 \text{ kg/m}^3$$

Therefore,

$$\frac{M_{os}}{M_t} = \frac{(1.293)(0.30)^2}{(7800)(0.30^2 - 0.295^2)} \\ = 5.01 \times 10^{-3}$$

Step 2. Calculate pressure ratio \bar{p} from equation

$$\bar{p} = \frac{P_0}{1.01 \times 10^5}$$

from assumptions

$$P_0 = 7.0 \times 10^7 \text{ Pa}$$

$$\bar{p} = \frac{7.0 \times 10^7}{1.01 \times 10^5} = 693$$

Step 3. From Figure 4-10 for a vessel of radius closest to the vessel considered, find V for M_{os}/M_t ratio most nearly above and below the value of Step 1 for the \bar{p} of Step 2. This is:

$$\bar{p} = 693$$

$$M_1 = (M_{os}/M_t) \text{ below} = 1.73 \times 10^{-3}, \quad \bar{V}_1 = 1.05$$

$$M_2 = (M_{os}/M_t)_2 = 5.01 \times 10^{-3}, \quad \bar{V}_2 = ?$$

$$M_3 = (M_{os}/M_t) \text{ above} = 5.19 \times 10^{-3}, \quad \bar{V}_3 = 1.38$$

Step 4. Find \bar{V}_2 by linear interpolation from equation

$$\bar{V}_2 = (\bar{V}_3 - \bar{V}_1) \left(\frac{M_2 - M_1}{M_3 - M_1} \right) + \bar{V}_1$$

$$\bar{V}_2 = (1.38 - 1.05) \left(\frac{5.01 - 1.73}{5.19 - 1.73} \right) + 1.05 = 1.36$$

Step 5. Multiply V_2 by the a_{os} value given in the figure to obtain the initial fragment velocity

$$V_i = \bar{V}_2 \cdot a_{os} = (1.36) (3.31 \times 10^2 \text{ m/s}) = 451 \text{ m/s}$$

The initial fragment velocity is 451 m/s (1480 ft/sec).

Example 2. For Cylinders

Assume same conditions as Example 1, but the vessel contains helium.

Step 1. Calculate mass ratio M_{os}/M_t from equation

$$\frac{M_{os}}{M_t} = \frac{R^2 \rho_{He}}{[R^2 - (R - t)^2] \rho_{steel}}$$

$$\rho_{helium} = 0.1785 \text{ kg/m}^3 \text{ at STP}$$

Other values as in Example 1.

$$\frac{M_{os}}{M_t} = \frac{(0.1785)(0.30)^2}{(7800)(0.30^2 - 0.295^2)} = 6.92 \times 10^{-4}$$

Step 2. Same as in Example 1, $\bar{p} = 693$.

Step 3. From Figure 4-14 for a tank of radius closest to the tank considered find \bar{V} for M_{os}/M_t ratio most nearly above and below the value of Step 1 for the \bar{p} of Step 2. This is

$$M_1 = (M_{os}/M_t) \text{ below} = 2.32 \times 10^{-4}, \quad \bar{V}_1 = 0.41$$

$$M_2 = (M_{os}/M_t) \text{ } = 6.92 \times 10^{-4}, \quad \bar{V}_2 = ?$$

$$M_3 = (M_{os}/M_t) \text{ above} = 6.95 \times 10^{-4}, \quad \bar{V}_3 = 0.67$$

Step 4. Find \bar{V}_2 by linear interpolation from equation

$$\bar{V}_2 = (\bar{V}_3 - \bar{V}_1) \left(\frac{M_2 - M_1}{M_3 - M_1} \right) + \bar{V}_1$$

$$\bar{V}_2 = (0.67 - 0.41) \left(\frac{6.92 - 2.32}{6.95 - 2.32} \right) + 0.41 = 0.67$$

Step 5. Multiply V_2 by the a_{os} value given in the figure to obtain the initial fragment velocity

$$V_i = \bar{V}_2 a_{os} = (0.67)(963 \text{ m/s})$$

$$= 645 \text{ m/s}$$

The initial fragment velocity is 645 m/s (2120 ft/sec).

4-3 Estimate of Initial Velocities of Fragments from Spheres and Cylinders Bursting into Two Equal Halves

The method developed by Taylor and Price⁽²⁾ for calculating velocities of fragments from bursting spherical reservoirs was modified to provide velocity calculations for fragments from both cylindrical and spherical gas vessels. The development of the necessary equations, the numerical iteration method used to simultaneously solve the resulting

differential equations, the computer program and results of the analysis are all explained in considerable depth for the interested reader in Appendix 4C. Only assumptions and conclusions necessary for determining fragment velocities are included here.

The assumptions relevant to the calculation of fragment velocity in this section follow. More complete listing of assumptions are contained in Appendix 4C, but only essential elements are contained here. The pertinent assumptions upon which conclusions which follow are based are:

- (1) The vessel with gas under pressure breaks into two equal halves along a plane perpendicular to the cylindrical axis, and the two container fragments are driven in opposite directions.
- (2) The thickness of the containment vessel is uniform.
- (3) The containment vessel has hemispherical end caps.
- (4) Vessels are made of Titanium or Titanium alloys (material used for containment vessels in flight-weight vehicles) and has a length-to-diameter (L/D) ratio of 10.0.
- (5) Contained gases are either air, carbon dioxide (CO_2) or hydrogen (H_2).

The summarized calculations are presented in nondimensionalized units in order to condense and simplify the determination of fragment velocity. The pertinent nondimensional (unitless) relations are defined as follows:

- (1) Nondimensional pressure

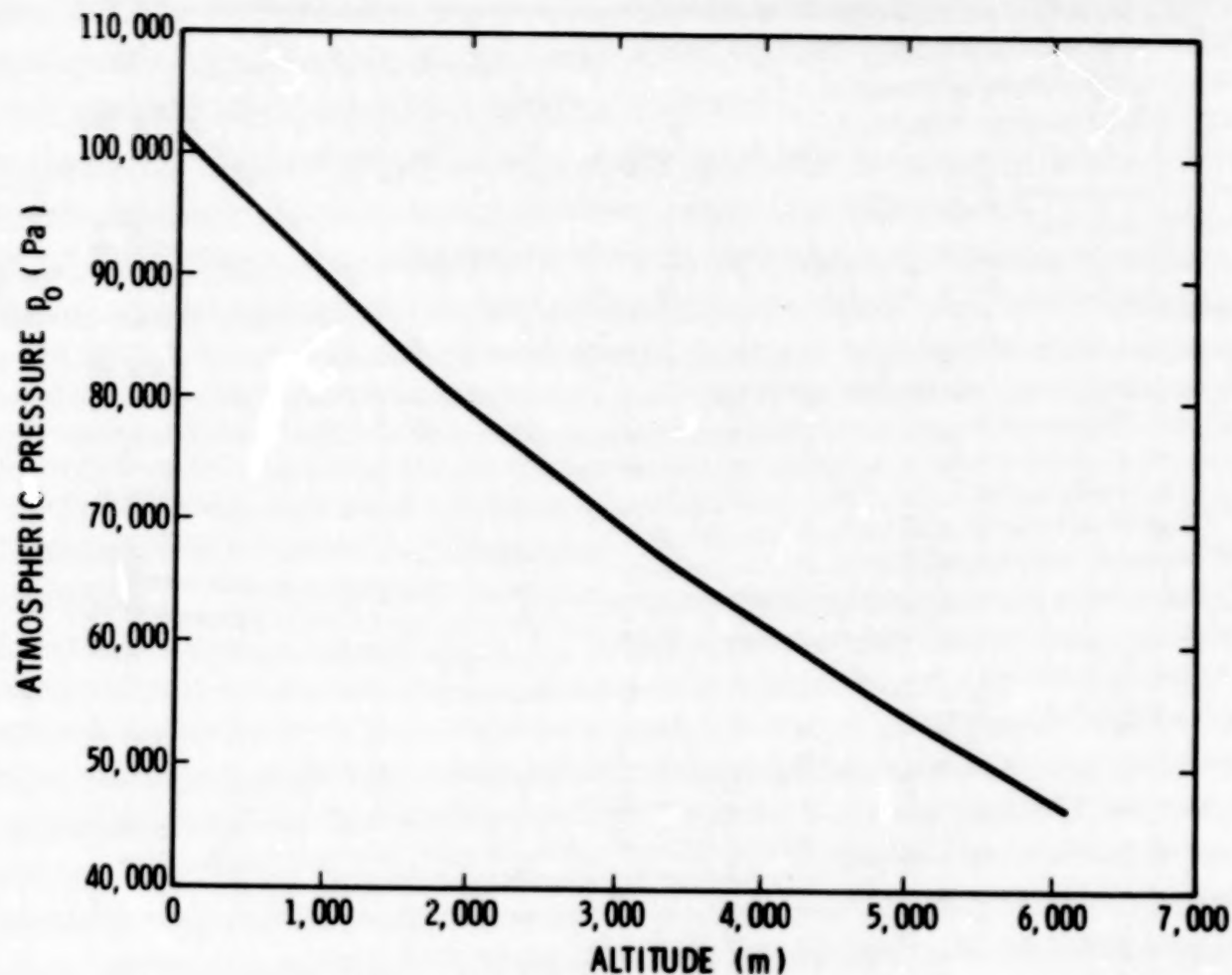
\bar{P} = initial pressure/atmospheric pressure (or P/p_0) where the change in atmospheric pressure p_0 with altitude is shown in Figure 4-17.

- (2) Nondimensional thickness

h/D = cylinder thickness/cylinder diameter

- (3) Nondimensional length

L/D = total length/cylinder diameter



$$(\text{psi} = \text{Pa} \times 1.450 \times 10^{-4})$$

$$(\text{ft} = \text{m} \times 3.281)$$

220

Figure 4-17. Atmospheric Pressure vs Altitude

(4) Nondimensional velocity

\bar{V} = final velocity/sound speed of gas (or V/a_0) where V is the velocity of the fragment and a_0 is sound speed.

The sound speeds a_0 for the gases mentioned are:

Air - 344 m/s (13 550 in/sec)

CO_2 - 258 m/s (10 150 in/sec)

H_2 - 1270 m/s (50 000 in/sec)

Figures 4-18 through 4-20 contain plots of \bar{V} versus \bar{P} for air, carbon dioxide and hydrogen gases, respectively, the L/D ratios being held constant at 10.0 and as many as three curves, one for each h/D ratio (0.001, 0.01 and 0.1), being plotted on a single figure. Nondimensional velocity and pressure combinations for intermediate values of h/D can be approximated from these figures. Figure 4-21 contains a plot of \bar{V} versus L/D. It should be noted that, for high nondimensional pressures ($\bar{P} \approx 4080$), \bar{V} is essentially independent for values of L/D from 1.0 (sphere) to 10.0.

The procedure for determining the velocity of fragments consisting of halves of spheres or cylinders made of Titanium or Titanium alloys and containing air, carbon dioxide or hydrogen gas under pressure, is as follows:

(1) Determine atmospheric pressure p_0 (see Figure 4-17).

(2) Calculate nondimensional pressure \bar{P} :

$$\bar{P} = P/p_0$$

(3) Calculate nondimensional thickness h/D.

(4) Calculate nondimensional length L/D.

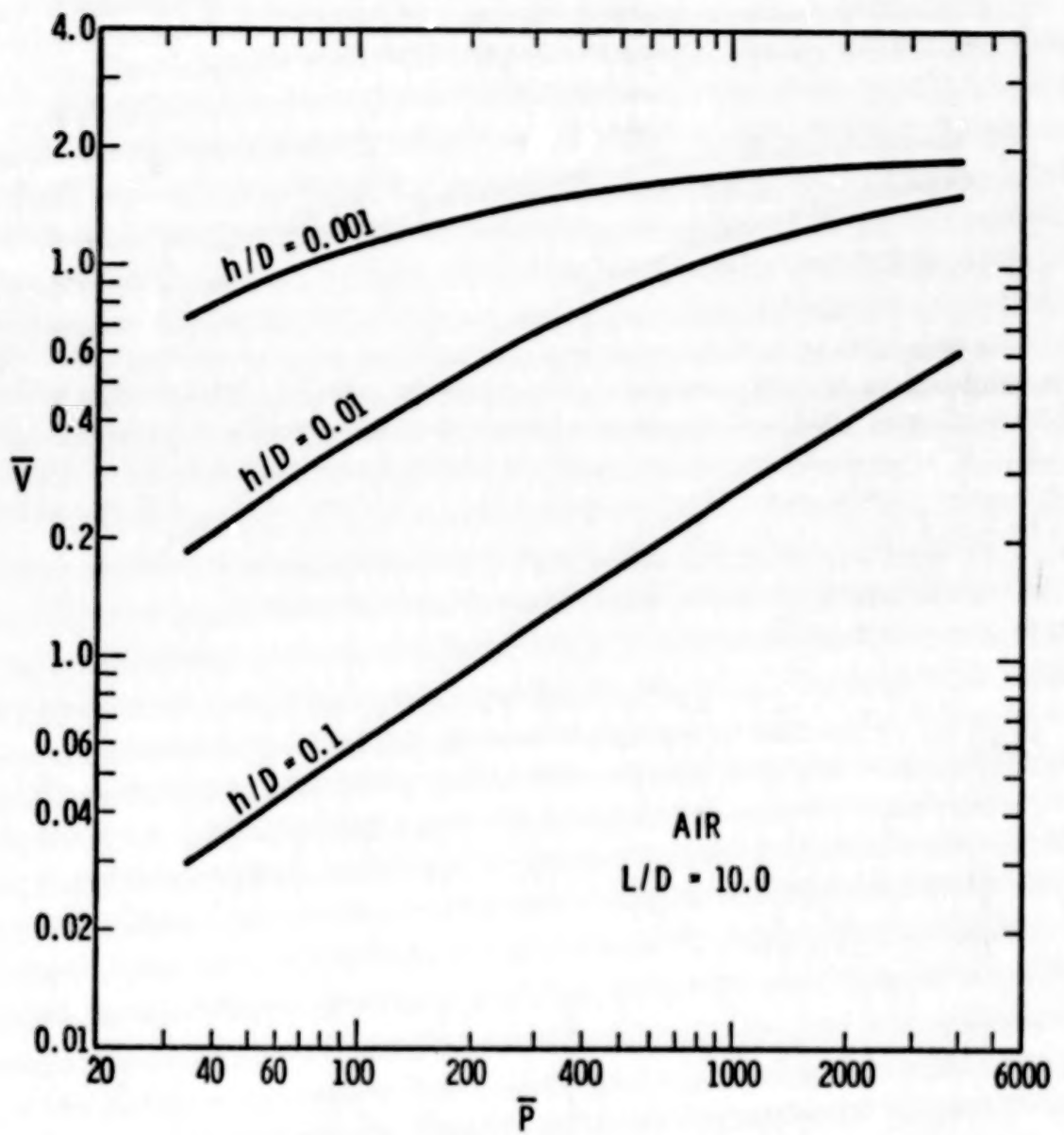


Figure 4-18. Nondimensional Velocity Vs Nondimensional Pressure for Vessels Containing Air

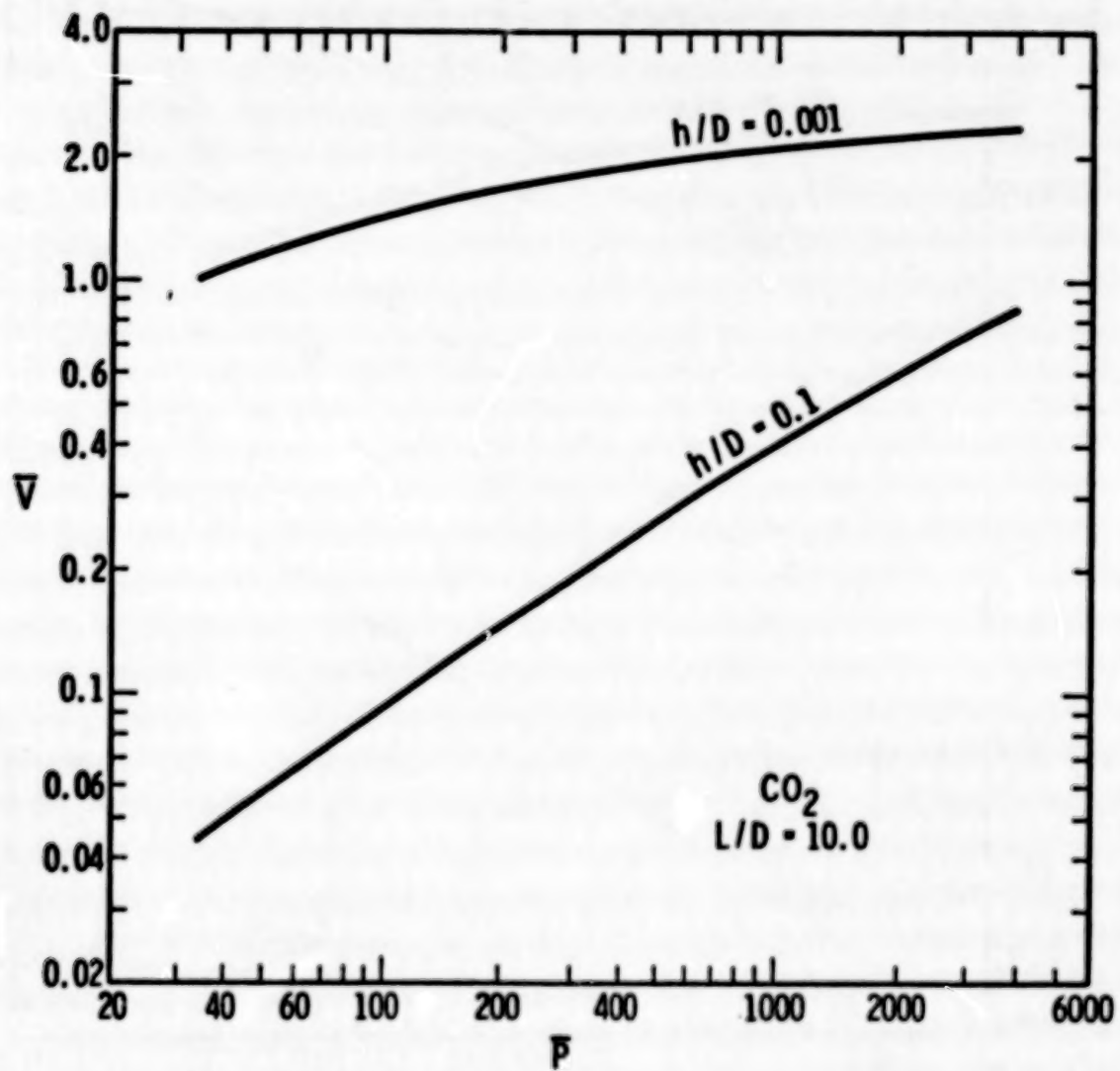


Figure 4-19. Nondimensional Velocity Vs Nondimensional Pressure for Vessels Containing CO_2

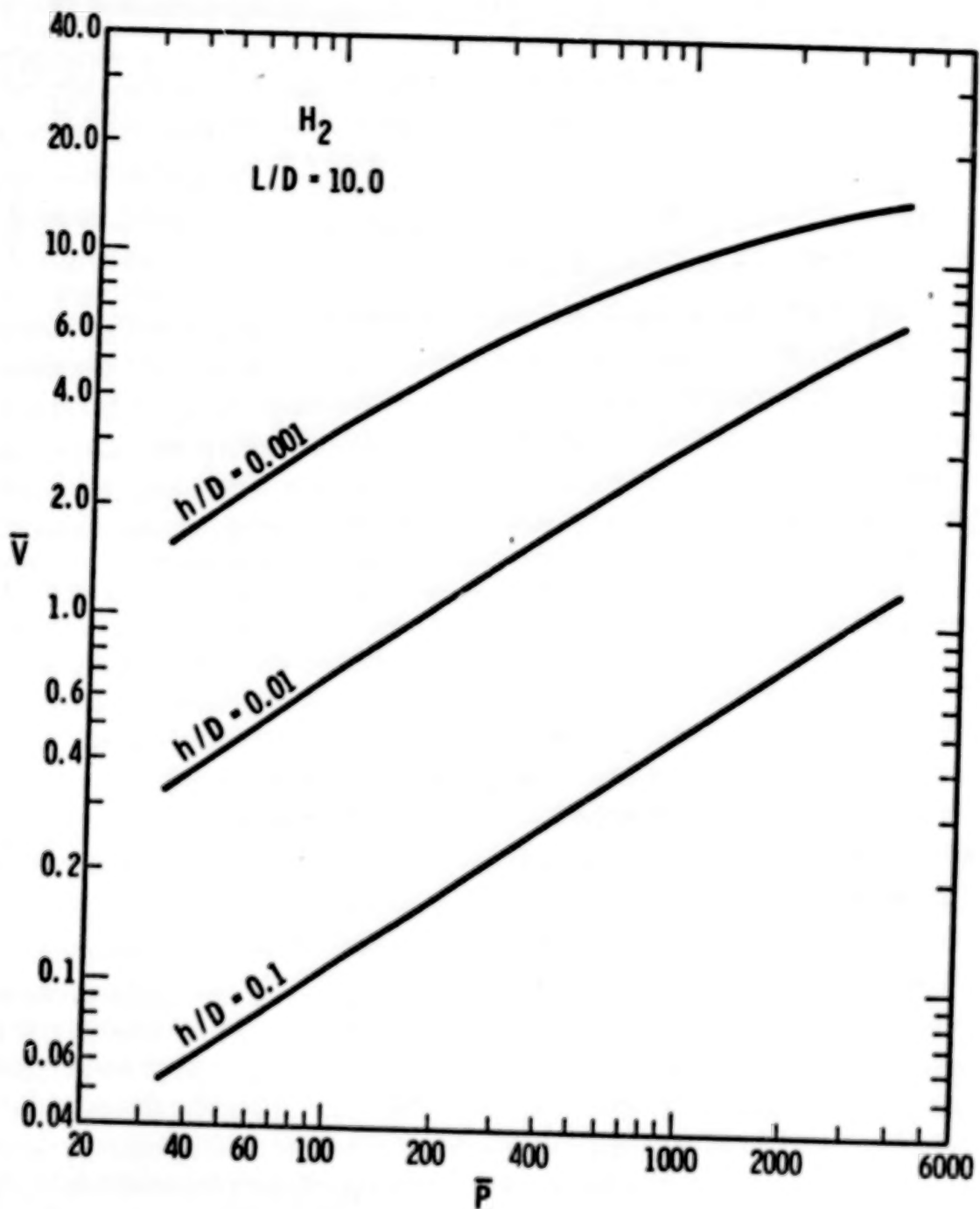


Figure 4-20. Nondimensional Velocity Vs Nondimensional Pressure for Vessels Containing H_2

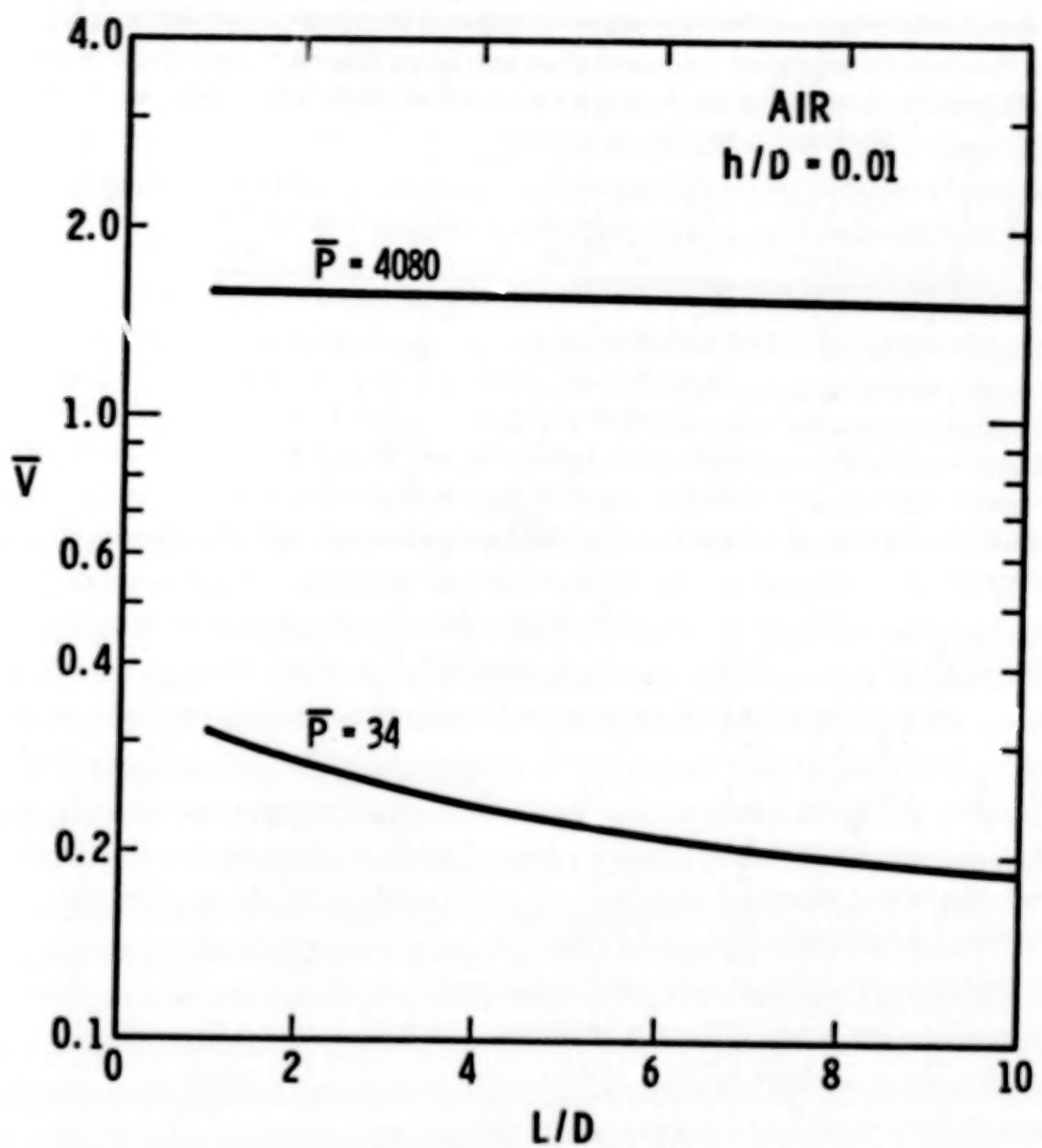


Figure 4-21. Nondimensional Velocity Vs Length-to-Diameter (L/D) Ratio

- (5) For L/D equal to 10.0, * choose the appropriate figure of Figures 4-18, 4-19 or 4-20 which relate to contained gases of air, carbon dioxide (CO_2) and hydrogen (H_2), respectively, and choose the curve with proper h/D value. Positions of curves for intermediate h/D values can be interpolated.
- (6) Knowing the gas, h/D and \bar{P} , find \bar{V} from the figure and calculate velocity V (m/s):

$$V = \bar{V} a_0$$

where a_0

344 m/s (air)
258 m/s (CO_2)
1270 m/s (H_2)

Some examples will help clarify the procedure for calculating fragment velocity.

Example 1:

A pressure vessel made of a Titanium alloy is cylindrical in shape with hemispherical end caps. The vessel is 5 m (16.4 ft) long and 0.5 m (1.64 ft) outside diameter. Its thickness is uniform and is 0.005 m (0.197 in). Contained gas is air at a pressure of $1.0135 \times 10^7 \text{ Pa}$ ($1.47 \times 10^3 \text{ psi}$). The vessel is located at sea level. If the vessel splits into two halves along a plane perpendicular to the cylindrical axis, what are the expected velocities of each of the two fragments?

Solution:

- (1) From Figure 4-17,

$$p_0 = 1.0135 \times 10^5 \text{ Pa (14.7 psi)}$$

- (2) Nondimensional pressure \bar{P} :

* Extreme caution should be taken when L/D ratios differ from 10.0. Figure 4-21 is a graphical representation of \bar{V} versus L/D varying from 1.0 to 10.0. Accurate values of \bar{V} cannot be determined for values of L/D less than 10.0 and for gases, values of \bar{P} and h/D ratios which are not contained in Figure 4-21.

$$\bar{P} = \frac{P}{P_0} = \frac{1.0135 \times 10^7 \text{ Pa}}{1.0135 \times 10^5 \text{ Pa}} = 100$$

- (3) Nondimensional thickness L/D:

$$L/D = \frac{(0.005 \text{ m})}{0.5 \text{ m}} = 0.01$$

- (4) Nondimensional length L/D:

$$L/D = \frac{5\text{m}}{0.5 \text{ m}} = 10.0$$

- (5) The center curve of Figure 4-18 is the appropriate curve for air, L/D of 10.0, and h/D of 0.01.

- (6) From Figure 4-18 and \bar{P} of 100, one finds that

$$V \approx 0.36$$

or

$$V = (0.36) (344 \text{ m/s}) \approx 124 \text{ m/s (407 ft/sec)}$$

Example 2:

Same as Example 1, except let P be $3.45 \times 10^6 \text{ Pa}$ (500 psi) and length of the vessel be 1 m (3.28 ft).

Solution:

$$(1) P_0 = 1.0135 \times 10^5 \text{ Pa (see Example 1)}$$

$$(2) \bar{P} = \frac{3.45 \times 10^6 \text{ Pa}}{1.0135 \times 10^5 \text{ Pa}} \approx 34$$

$$(3) h/D = 0.01 \text{ (see Example 1)}$$

$$(4) L/D = \frac{1\text{m}}{0.5 \text{ m}} = 2$$

- (5) Since L/D is not 10.0, Figures 4-18, 4-19, and 4-20 cannot be used. Normally, the fragment velocity could not

be calculated from the information in this chapter. However, Figure 4-21 applies for contained air, h/D of 0.01 and \bar{P} of 34, and can be used.

- (6) From Figure 4-21:

$$V \approx .28$$

or

$$V = (.28) (344 \text{ m/s}) \approx 96 \text{ m/s (315 ft/sec)}$$

Example 3:

Same as Example 1 except hydrogen is the contained gas.

Solution:

- (1) $p_0 = 1.0135 \times 10^5 \text{ Pa}$ (see Example 1)
- (2) $P = 100$ (see Example 1)
- (3) $h/D = 0.01$ (see Example 1)
- (4) $L/D = 10.0$ (see Example 1)
- (5) The center curve of Figure 4-20 is the appropriate curve for hydrogen, L/D of 10.0, and h/D of 0.01.
- (6) - From Figure 4-20 and \bar{P} of 100 one finds that

$$V \approx (0.7)$$

or

$$V \approx (0.7) (1270 \text{ m/s}) \approx 890 \text{ m/s (2900 ft/sec)}$$

4-4 Determination of Appurtenance Velocity

The method used here to calculate appurtenance velocity is an extension of work performed by Baker, et al. (3). Appendix 4D contains the development of the basic equations as well as a listing of the computer program used to generate nondimensional velocity curves as a function of nondimensional pressure and nondimensional impulse. The interested reader is encouraged to examine the appendix for a better understanding

of the interaction of appurtenances with blast waves. In order to arrive at values for appurtenance velocity, however, it is not necessary to refer to the appendix since all of the curves and equations required to calculate velocity are contained in this section. It is beneficial, however, to keep in mind that the method used for calculating the velocity of an appurtenance assumes that the appurtenance behaves as a rigid body, that none of the energy in the blast wave is absorbed in breaking the appurtenance loose from its moorings or deforming it elastically or plastically, and that gravity effects are ignored during the acceleration phase of the motion.

The velocity of an appurtenance can be determined from a nondimensional velocity which depends on nondimensional pressure and nondimensional impulse. In functional format

$$\frac{M V a_0}{P_0 A (K H + X)} = f \left(\frac{P_s}{P_0}, \frac{C_D I_s a_0}{P_s (K H + X)} \right) \quad (4-1)$$

↑ ↑ ↑
 nondimensional nondimensional nondimensional
 velocity \bar{V} pressure \bar{P}_s impulse \bar{I}_s

where M is the total mass of the appurtenance

V is the velocity of the appurtenance

a_0 is the velocity of sound in air

P_0 is atmospheric pressure

A is the mean presented area of the appurtenance

K is a nondimensional constant which is 4 for appurtenances on the ground and 2 for appurtenances in the air,

H is the minimum transverse distance of the mean presented area

X is the distance from the front of the object to the location of its largest cross-sectional area

P_s is peak incident overpressure

C_D is the drag coefficient

and

I_s is the peak incident specific impulse

The variables can be classified into three major categories:

- (1) static environmental variables (a_0 , p_0)
- (2) blast wave variables (P_s , I_s)
- (3) appurtenance variables (M , V , A , K , H , X , C_D)

The static environmental variables, sound speed a_0 and atmospheric pressure p_0 , vary with altitude or location above sea level. This altitude dependency is shown in Figures 4-22 and 4-23. The blast wave variables, peak incident overpressure P_s and specific impulse I_s at specific standoff distances (i.e., distance from center of the explosion to the center of the appurtenance) can be determined from Chapters I and II of this handbook. Appurtenance variables are all associated with the object which may be propelled after interaction with the blast wave. The method for determining the velocity V will be discussed later. The choice of total mass M depends on the volume and density of the object, and non-dimensional constant K depends on its position. Representative values for drag coefficient C_D can be acquired from Figure 4-24. The mean presented area A of the appurtenance depends on its shape. It is the largest projected area of the appurtenance facing the approaching blast wave. The transverse distance H is the minimum dimension of the largest cross-sectional area of the object facing the blast wave. The length X is the distance from the point of the appurtenance which first interacts with the blast wave to the plane containing the largest cross-sectional area facing the approaching blast wave. For objects which have a flat face facing the blast wave, which is also the location of the plane with the largest cross-sectional area, X equals zero ($X = 0$). Figure 4-25 helps explain the meaning of the various appurtenance variables.

Figure 4-26 is a graphical representation of Equation (1) for various values of nondimensional velocity. The procedure for calculating appurtenance velocity V follows. Care, however, should be taken when interpolating between curves and extending curves. Estimates made by extending the curves to lower nondimensional impulses are especially hazardous.

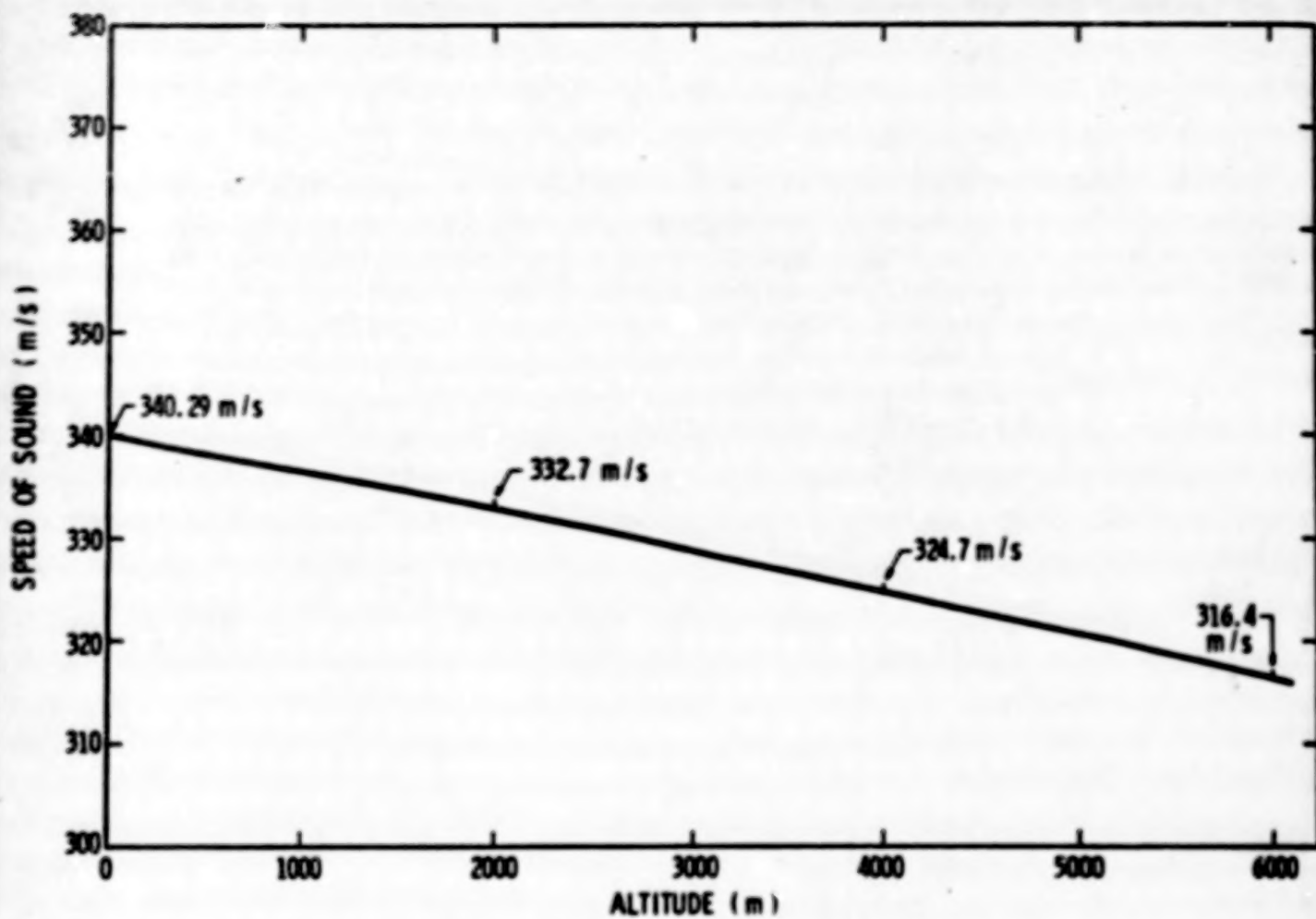
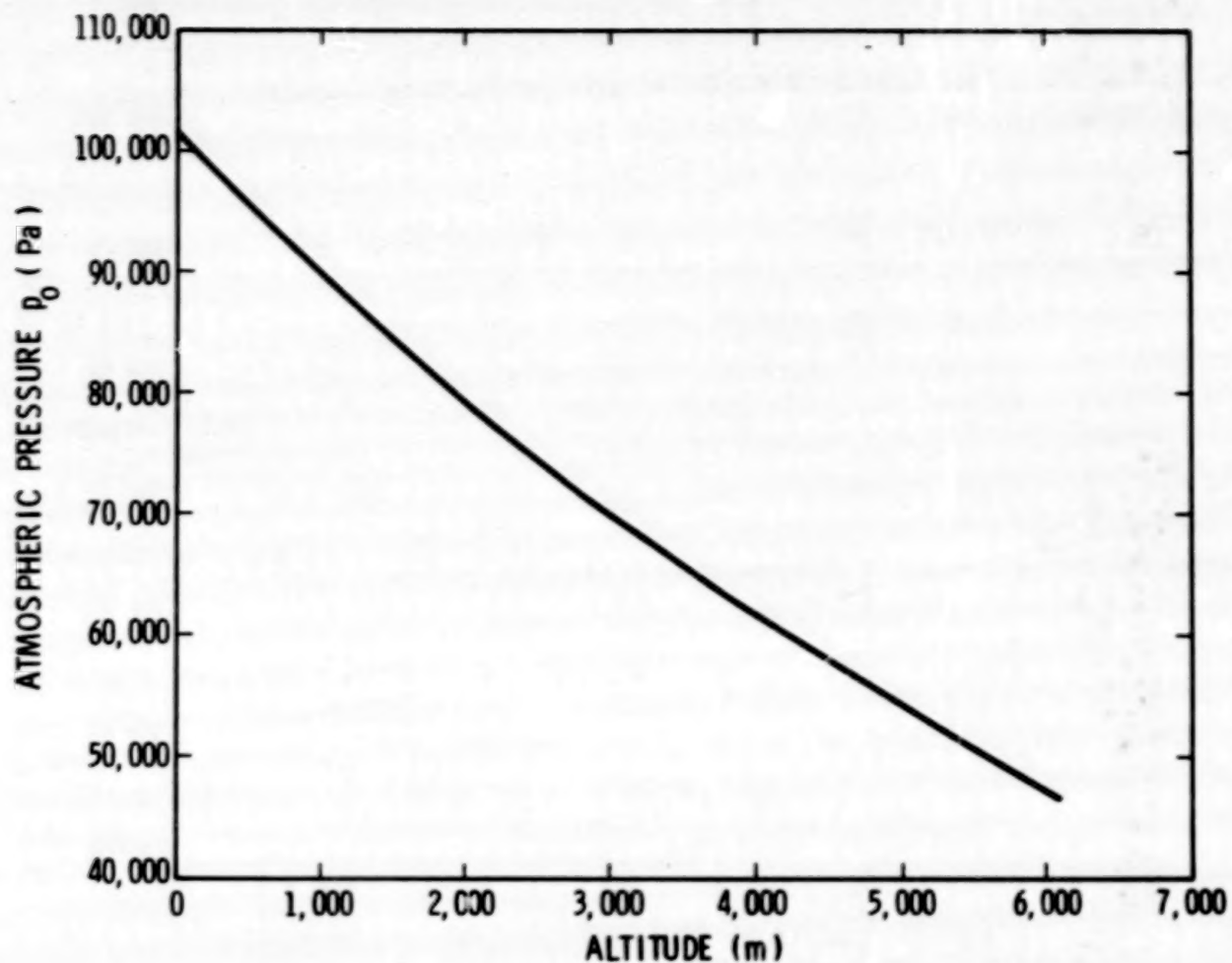


Figure 4-22. Speed of Sound Vs Altitude

231



$$(\text{psi} = \text{Pa} \times 1.450 \times 10^{-4})$$

$$(\text{ft} = \text{m} \times 3.281)$$

Figure 4-23. Atmospheric Pressure vs Altitude

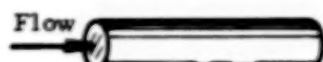
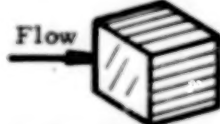
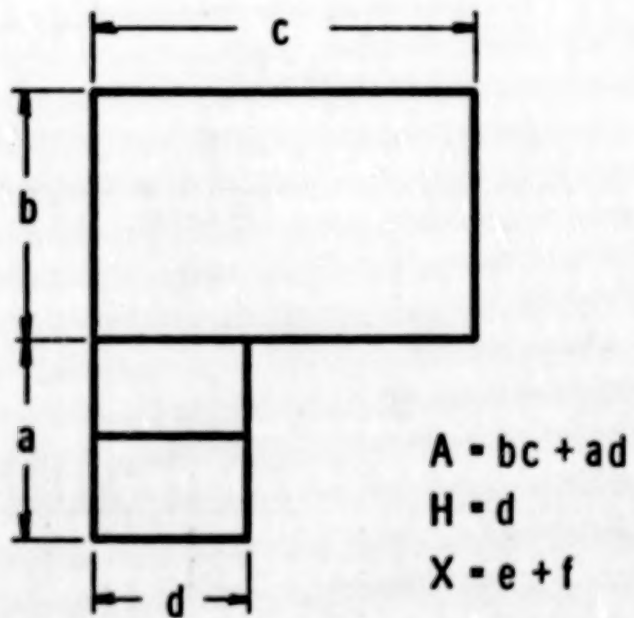
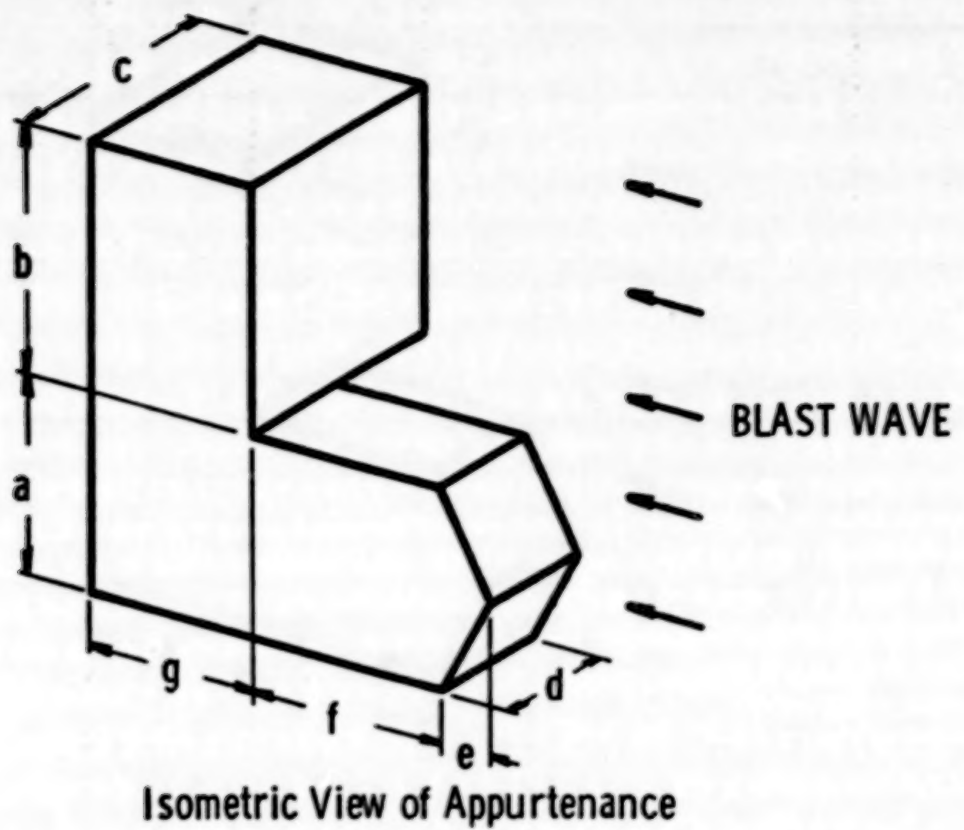
SHAPE	SKETCH	C_D
Right Circular Cylinder (long rod), side-on		1.20
Sphere		0.47
Rod, end-on		0.82
Disc, face-on		1.17
Cube, face-on		1.05
Cube, edge-on		0.80
Long Rectangular Member, face-on		2.05
Long Rectangular Member, edge-on		1.55
Narrow Strip, face-on		1.98

Figure 4-24. Drag Coefficients, C_D , of Various Shapes



Front View of Appurtenance

Figure 4-25. Pictorial Explanation of Appurtenance Variables

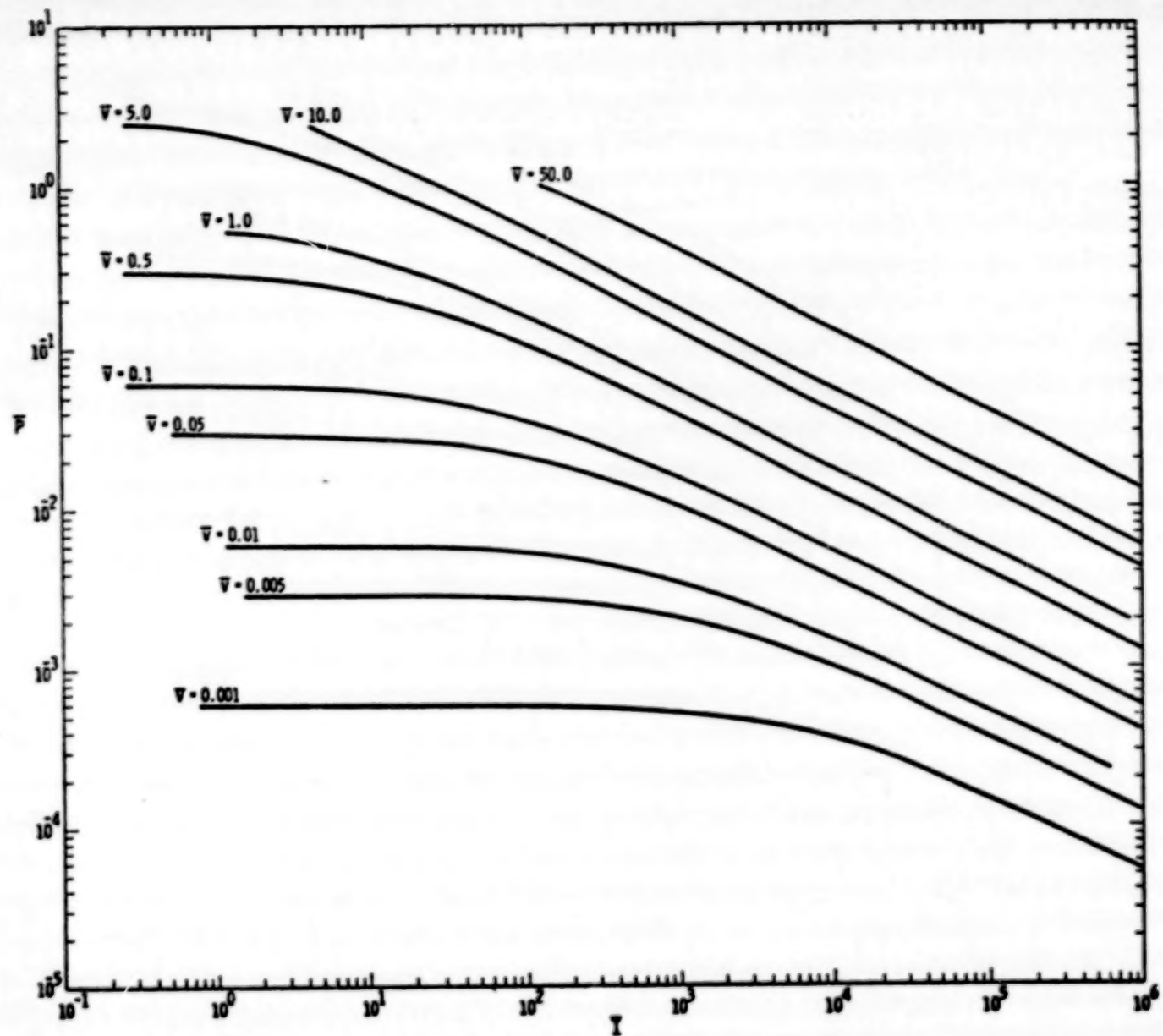


Figure 4-26. Nondimensional Appurtenance Velocity \bar{V} as a Function of Nondimensional Pressure \bar{P} and Nondimensional Impulse I

- (1) Determine static environment variables, speed of sound a_0 (m/s) and atmospheric pressure p_0 (Pa), from Figures 4-22 and 4-23, respectively.
- (2) Determine blast wave variables, peak incident overpressure P_s (Pa) and specific impulse I_s (Pa· s), from Chapters I and II.
- (3) Determine appurtenance variables:
 - (a) M - total mass in kilograms
 - (b) A - mean presented area in square meters
 - (c) K - dimensionless constant which equals 4 for appurtenances on the ground and 2 for appurtenances in the air
 - (d) H - minimum transverse distance of the mean presented area in meters
 - (e) X - distance from the front of the appurtenance to the location of its largest cross-sectional area in meters
 - (f) C_D - nondimensional drag coefficient of the appurtenance (see Figure 4-24)

- (4) Calculate nondimensional pressure \bar{P} where

$$\bar{P}_s = \frac{P_s}{p_0}$$

- (5) Calculate nondimensional impulse \bar{I}_s where

$$\bar{I}_s = \frac{C_D I_s a_0}{\bar{P}_s (K H + X)}$$

- (6) Find the location of the point (\bar{I}_s, \bar{P}_s) on the graph in Figure 4-26 and estimate a value for nondimensional velocity \bar{V} from the curves of constant nondimensional velocity.

(7) Calculate appurtenance velocity V (in m/s) where

$$\bar{V} = \frac{M V a_o}{P_o A (KH + X)}$$

and thus

$$V = \frac{\bar{V} P_o A (KH + X)}{M a_o}$$

Some examples will clarify the procedure.

Example 1:

Assume that an explosion occurs at sea level. A cubical cement block with a side facing the blast front is located at such a distance from the source of the explosion that it is exposed to an incident peak overpressure P_s of 1.4×10^5 Pa (20.3 psi) and an incident specific impulse I_s of 1.9×10^4 Pa·s (2.76 psi-sec). The density of the cement block is 1.792×10^3 kg/m³ (0.647 lb_m/in³).

Solution:

(1) Static environmental variables:

$$a_o = 340 \text{ m/s}$$

$$P_o = 1.0135 \times 10^5 \text{ Pa}$$

(2) Blast wave variables:

$$P_s = 1.0 \times 10^5 \text{ Pa}$$

$$I_s = 1.9 \times 10^4 \text{ Pa.s}$$

(3) Appurtenance variables:

(a) $M = \text{density} \times \text{volume}$

$$= 1.792 \times 10^3 \text{ kg/m}^3 \times (2.5 \text{ m})^3$$

$$= 2.8 \times 10^4 \text{ kg}$$

(b) $A = (2.5 \text{ m})^2$

$$A = 6.25 \text{ m}^2$$

(c) Appurtenance is on the ground. Therefore,

$$K = 4$$

(d) $H = 2.5 \text{ m}$

(e) $X = 0 \text{ m}$ since the portion of block facing the blast wave is flat.

(f) Drag coefficient from Figure 4-24

$$C_D = 1.05$$

(4) Nondimensional pressure

$$\bar{P}_s = \frac{P_s}{P_0} = \frac{1.0 \times 10^5 \text{ Pa}}{1.0135 \times 10^5 \text{ Pa}} = 0.99$$

(5) Nondimensional impulse

$$\bar{I}_s = \frac{C_D I_s a_0}{P_s (KH + X)} = \frac{(1.05)(1.9 \times 10^4)(340)}{(1.0 \times 10^5)[(4)(2.5) + (0)]} = 6.8$$

(6) From Figure 4-26, the point (\bar{I}_s, \bar{P}_s) or $(6.8, 0.99)$ is located very close to the $\bar{V} = 5.0$ line

(7) Appurtenance velocity

$$V = \frac{\bar{V} P_0 A (KH + X)}{M a_0}$$

$$V = \frac{(5)(1.0135 \times 10^5)(6.25)[(4)(2.5) + (0)]}{(2.8 \times 10^4)(340)} =$$

$$3.3 \text{ m/s (10.8 ft/sec)}$$

Example 2:

Assume an upright cylindrical pole weighing 10.0 kg (22 lb_m) with radius of 0.01 m (0.0328 ft) and length of 4 m (13.1 ft) is subjected to the same blast parameters as mentioned in Example 1. The blast is incident on the curved portion of the pole.

Solution:

(1) Static environmental variables:

$$a_0 = 340 \text{ m/s}$$

$$p_0 = 1.0135 \times 10^5 \text{ Pa}$$

(2) Blast wave variables:

$$P_s = 1.0 \times 10^5 \text{ Pa}$$

$$I_s = 1.9 \times 10^4 \text{ Pa} \cdot \text{s}$$

(3) Appurtenance variables:

(a) $M = 10.0 \text{ kg}$

(b) $A = 2 \times \text{radius} \times \text{length}$

$$A = (2)(0.01)(4)$$

$$A = 0.08 \text{ m}^2$$

(c) $K = 4$

(d) $H = 2r = (2)(0.01) = 0.02 \text{ m}$

(e) $X = r = 0.01 \text{ m}$

(f) $C_D = (\text{from Figure 4-24}) = 1.20$

(4) $\bar{P}_s = \frac{P_s}{P_0} = \frac{1.0 \times 10^5}{1.0135 \times 10^5} \approx 0.99$

$$(5) \quad \bar{I}_s = \frac{C_D I_s a_0}{P_s (KH + X)} = \frac{(1.20)(1.9 \times 10^4)(340)}{(1.0 \times 10^5)[(4)(0.02) + (0.01)]}$$

$$= 8.61 \times 10^2$$

(6) Figure 4-26, the point (\bar{I}_s, \bar{P}_s) or $(861, 0.99)$ is located above the $\bar{V} = 50.0$ line at a location where one might expect $\bar{V} \approx 200$.

(7) Appurtenance velocity

$$V = \frac{\bar{V} P_0 A (KH + X)}{M a_0}$$

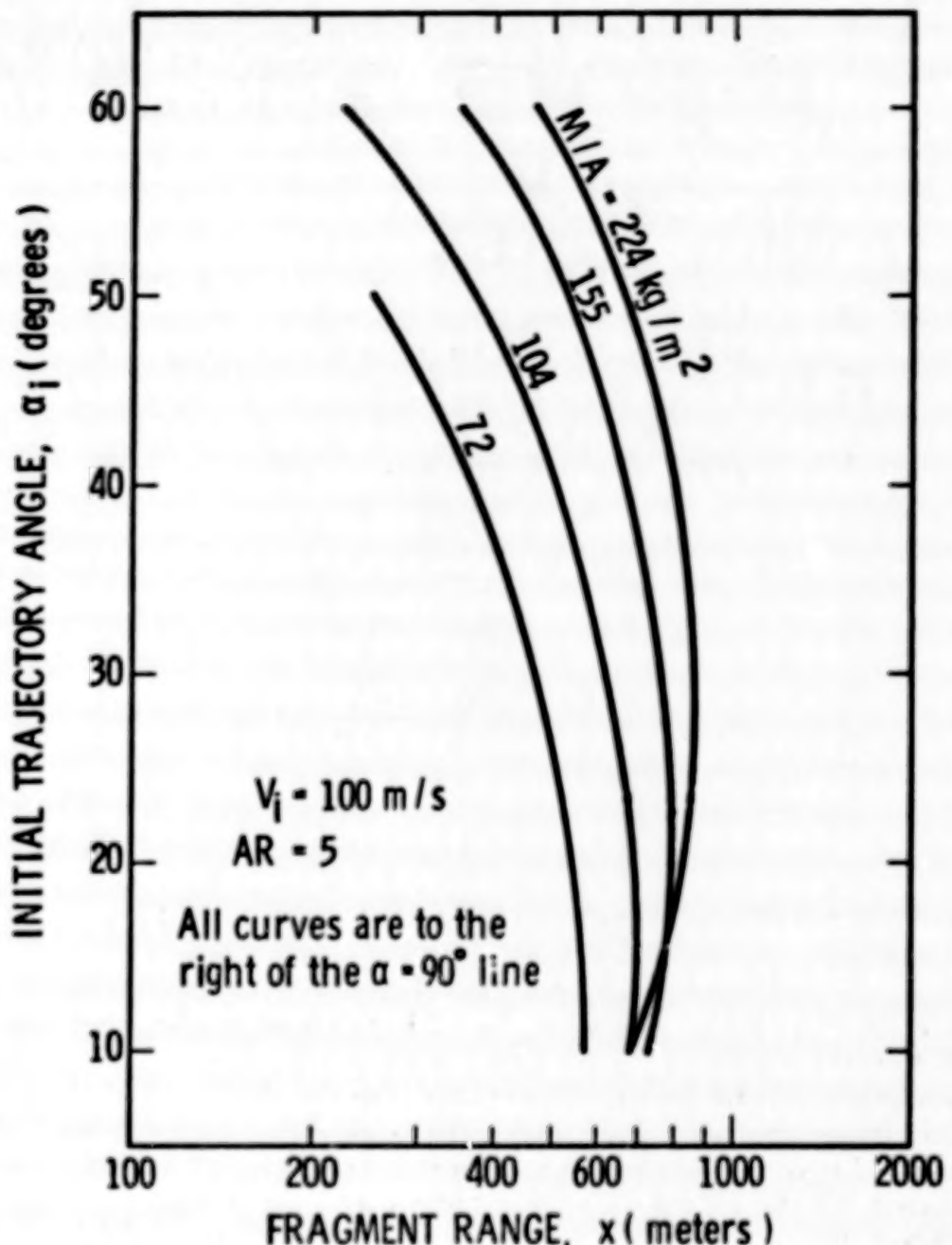
$$V \approx \frac{(200)(1.0135 \times 10^5)(0.08)[(4)(0.02) + (0.01)]}{(10)(340)}$$

$$V \approx 42.9 \text{ m/s (141 ft/sec)}$$

4-5 Methods for Computing Fragment Ranges and Impact Conditions

Two methods have been developed to estimate the range and terminal velocities of fragments. They depend on the fragment shapes. In the first method, the fragment is assumed to have a disc shape with a diameter at least five times greater than the thickness of the fragment. For these fragments lift effects are taken into consideration. A second method may be used where fragments are "chunky" shaped. These fragments may be represented by a sphere or cube where no single linear dimension can be said to be very much greater than any other. For these fragments lift forces are neglected and only drag forces are considered.

To estimate fragment ranges, the following techniques may be used based on Figures 4-27 through 4-36 which have been generated by computer codes. The codes (FRISB and TRAJE) and their underlying analysis are discussed in Appendix 4E. To determine fragment terminal velocities, data must be input to the codes themselves.



(ft = m X 3.281)

Figure 4-27. Disc Fragment Range for
 $V_i = 100 \text{ m/s}$, $AR = 5$

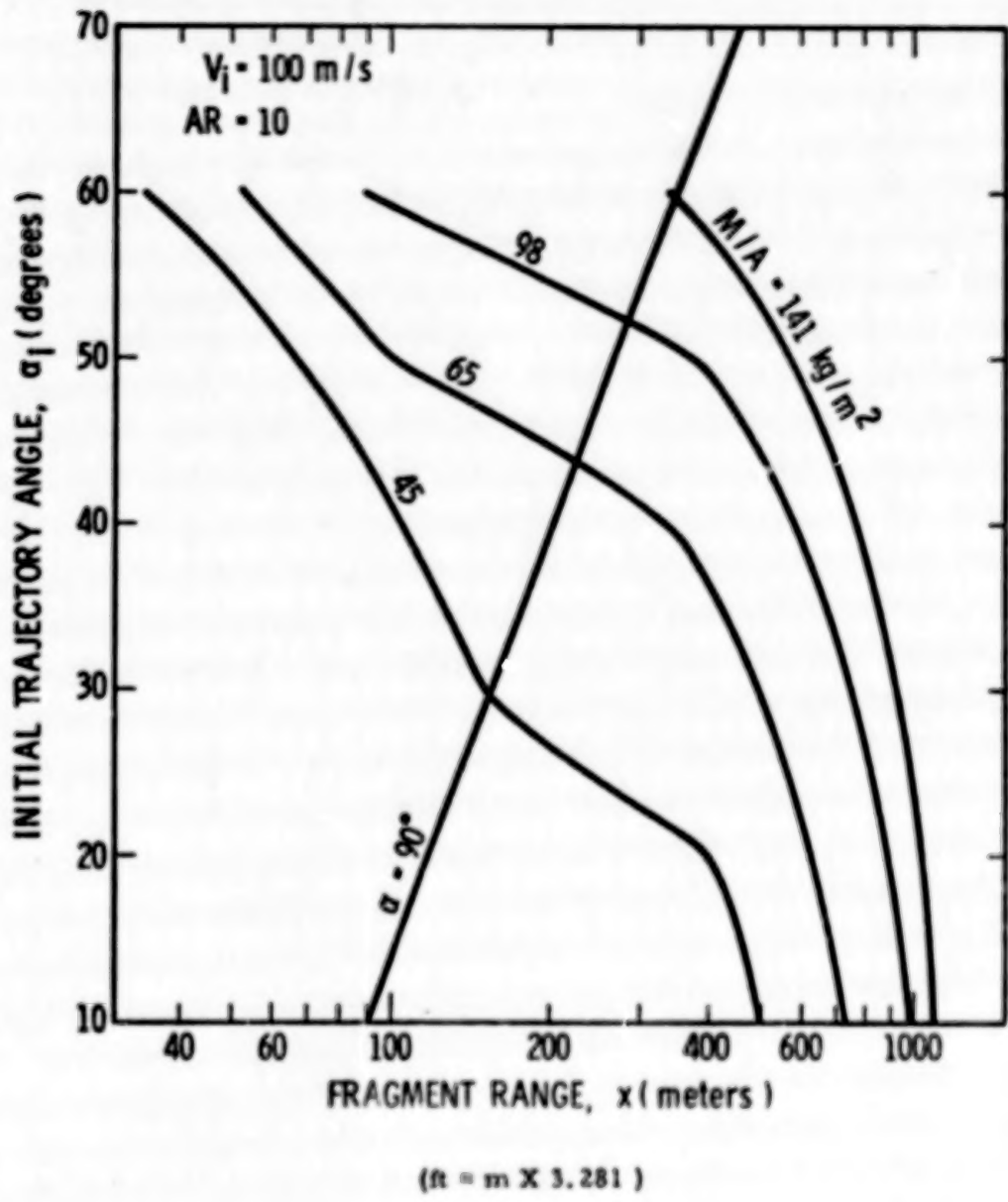


Figure 4-28. Disc Fragment Range for
 $V_i = 100 \text{ m/s}, AR = 10$

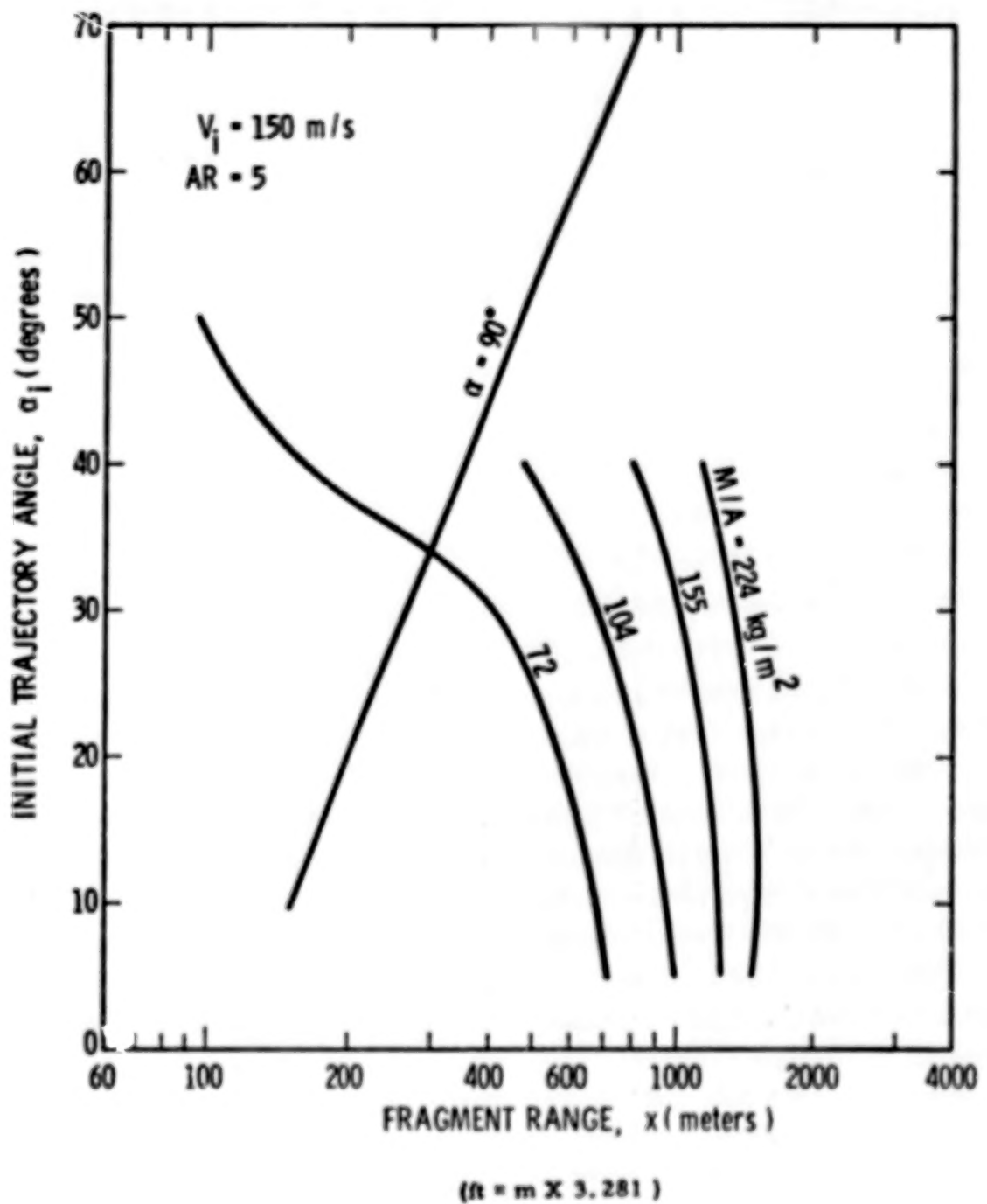


Figure 4-29. Disc Fragment Range for
 $V_i = 150 \text{ m/s}$, $AR = 5$

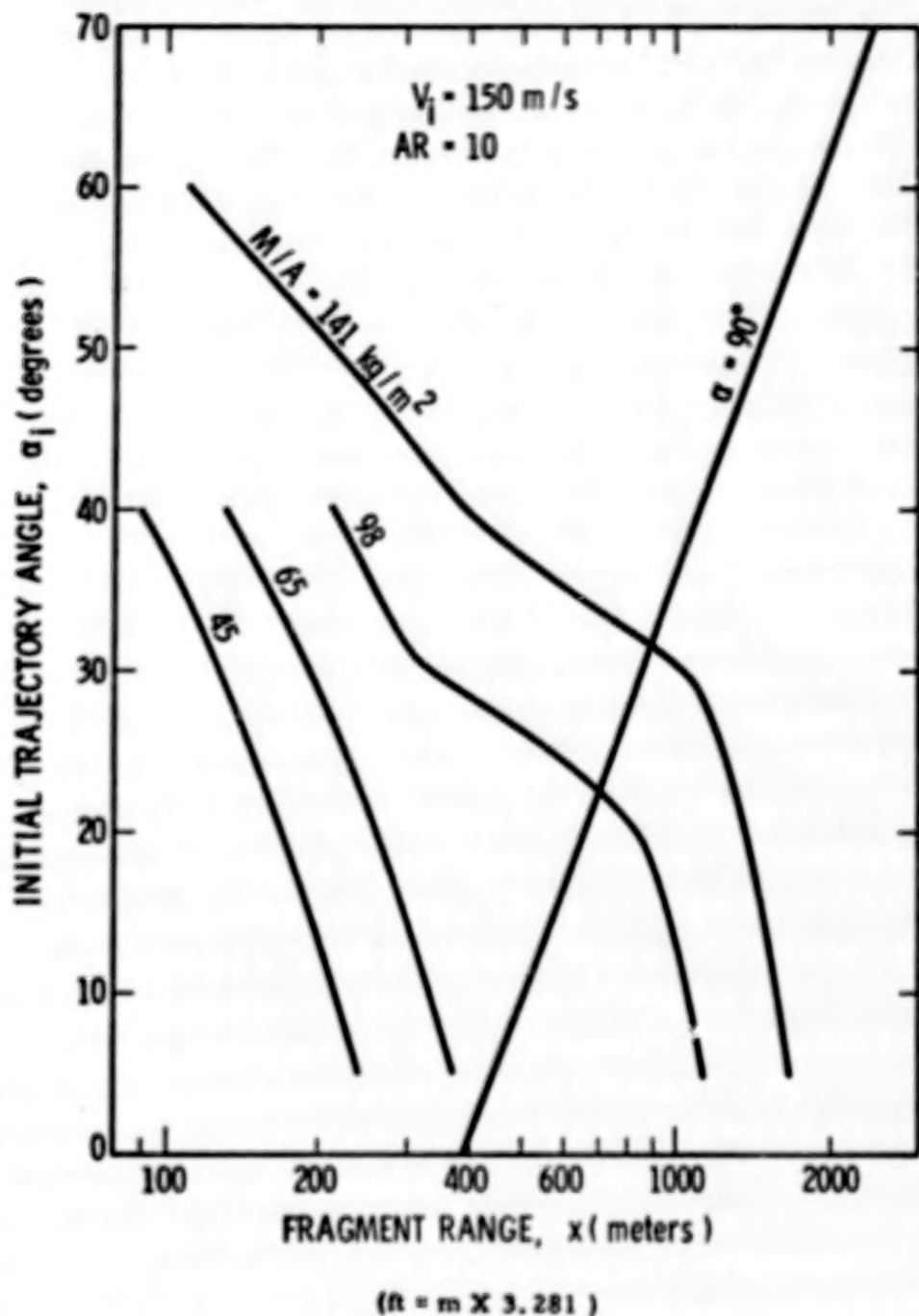


Figure 4-30. Disc Fragment Range for
 $V_i = 150 \text{ m/s}$, $AR = 10$

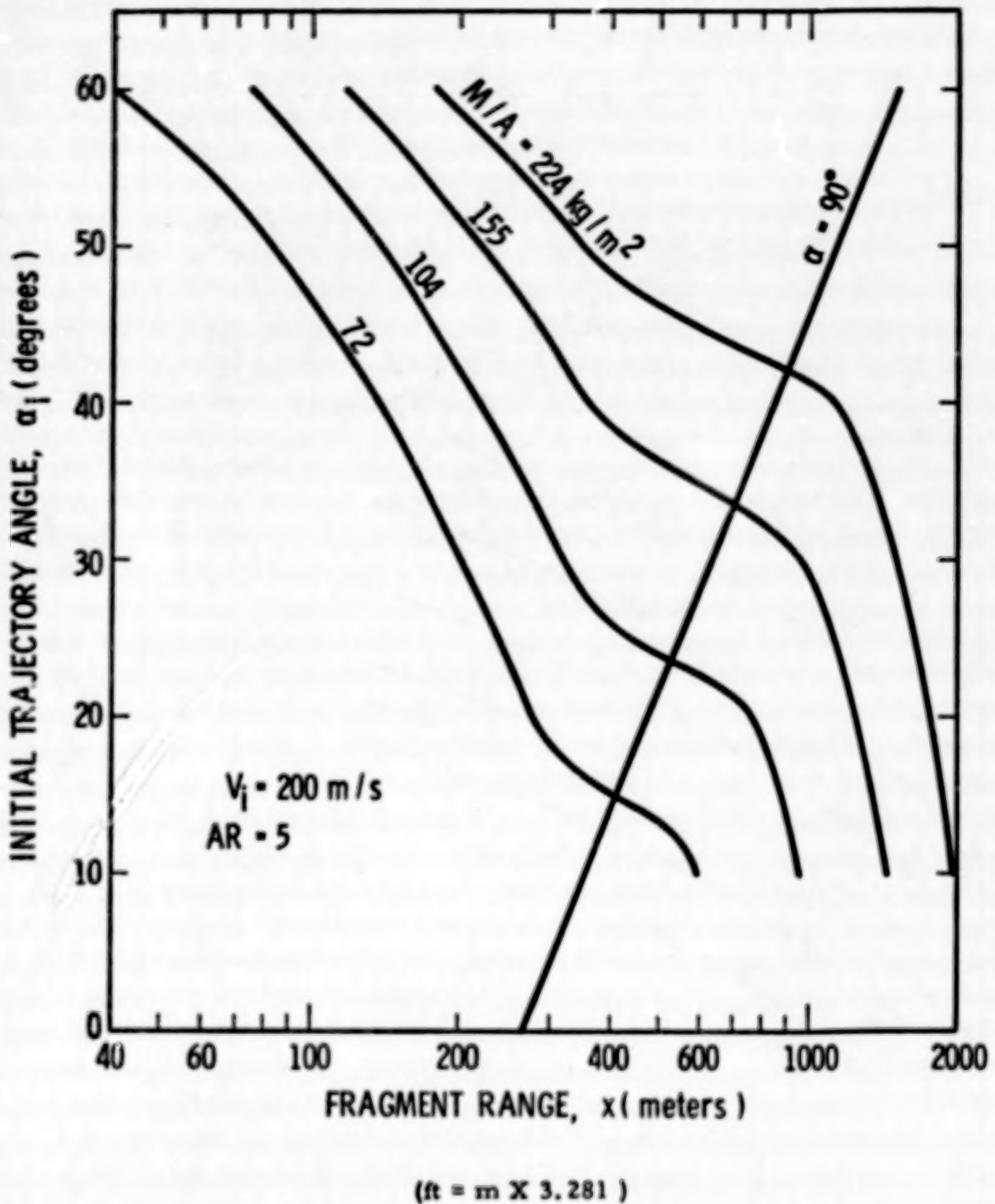


Figure 4-31. Disc Fragment Range for
 $V_i = 200 \text{ m/s}, AR = 5$

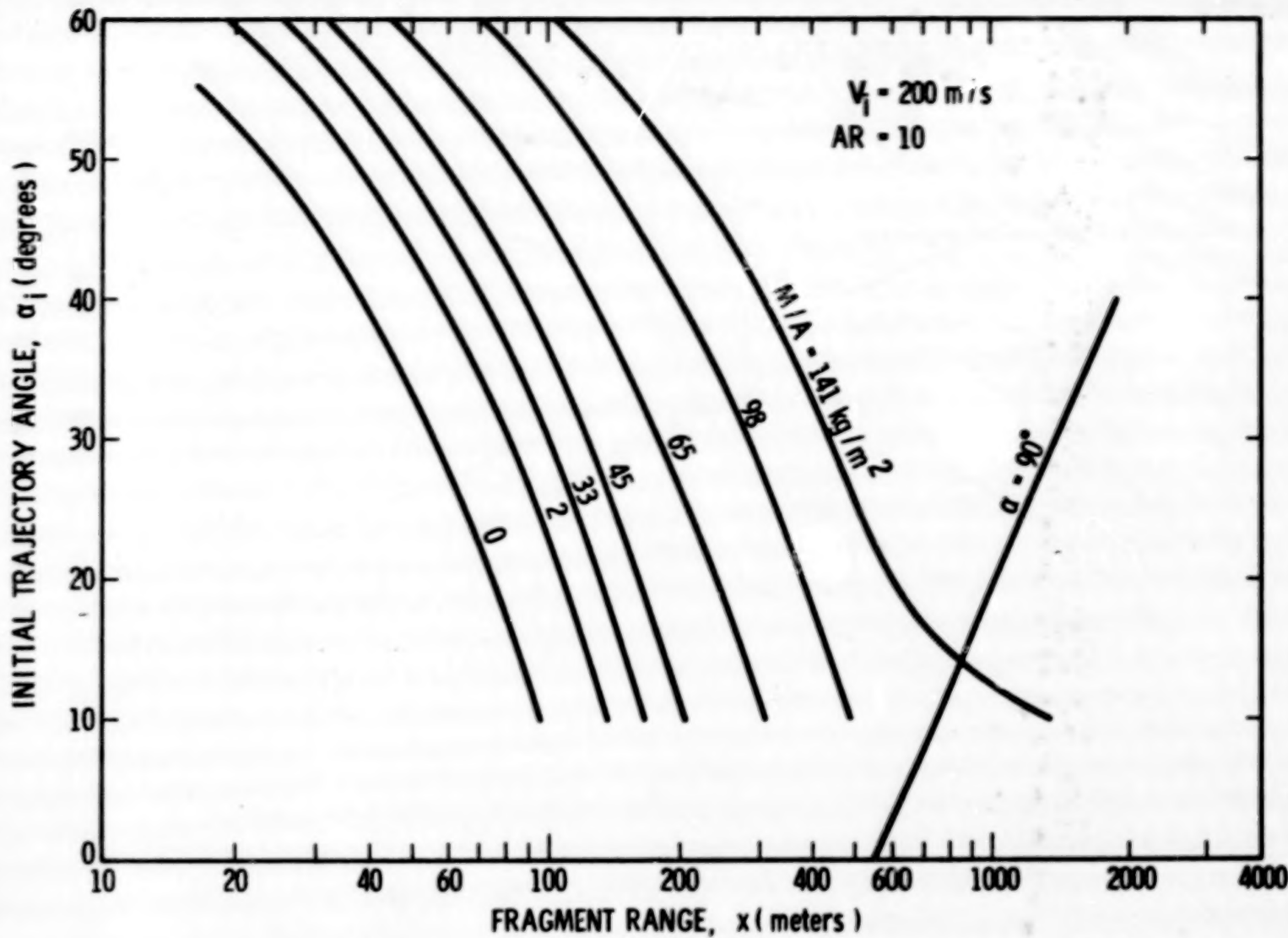


Figure 4-32. Disc Fragment Range for
 $V_i = 200 \text{ m/s}$, $AR = 10$

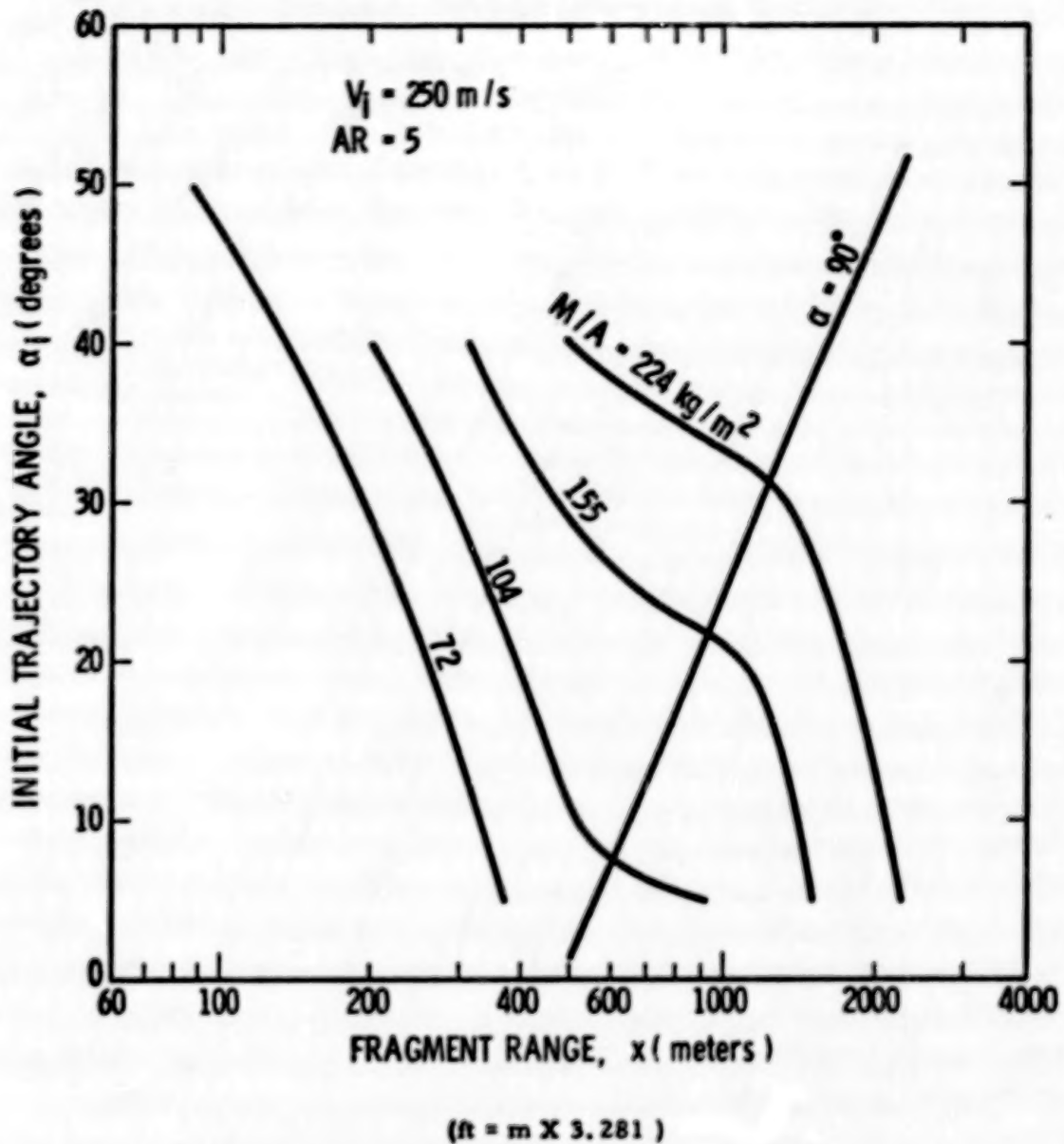


Figure 4-33. Disc Fragment Range for
 $V_i = 250 \text{ m/s}$, $AR = 5$

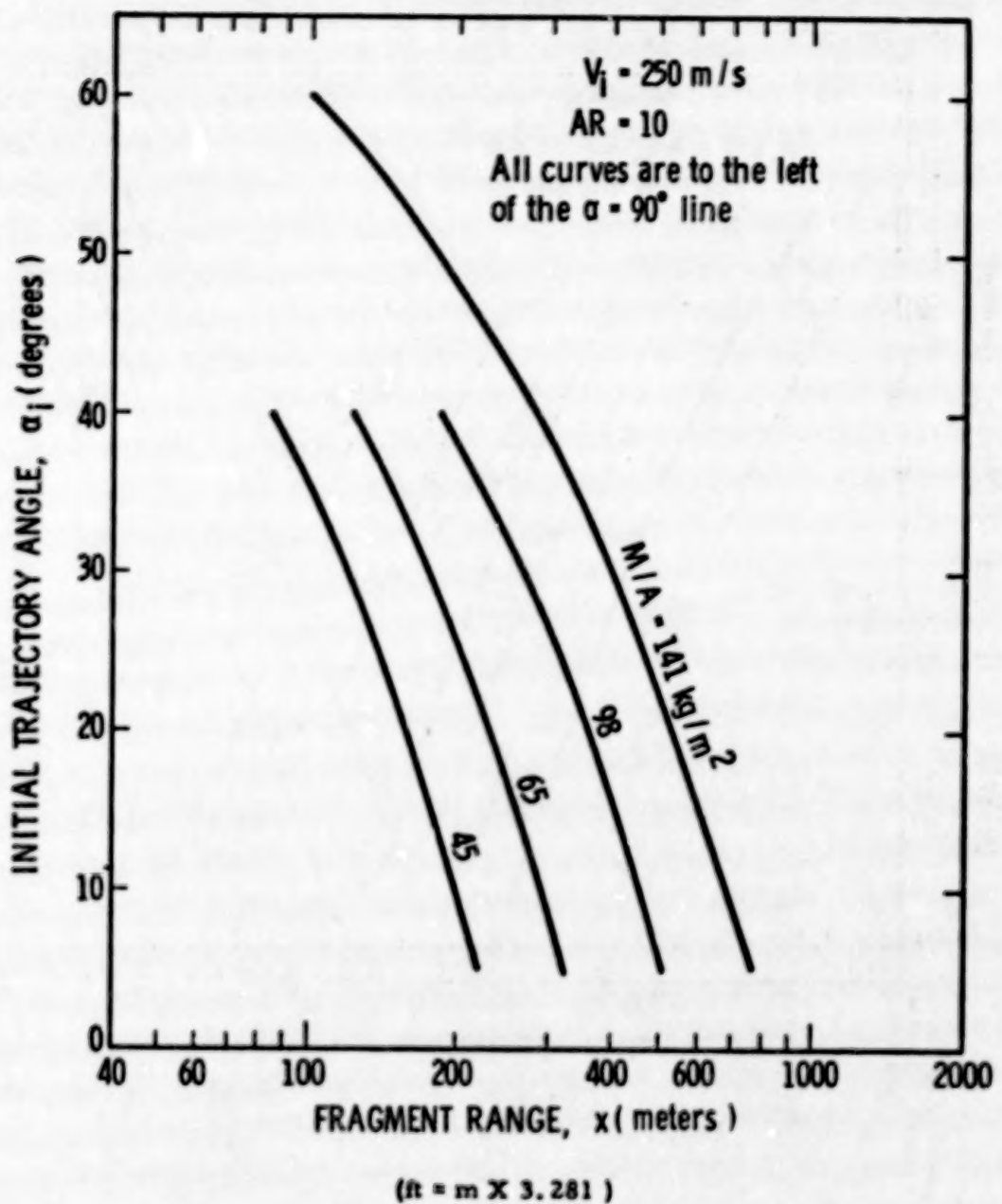


Figure 4-34. Disc Fragment Range for
 $V_i = 250 \text{ m/s}$, $AR = 10$

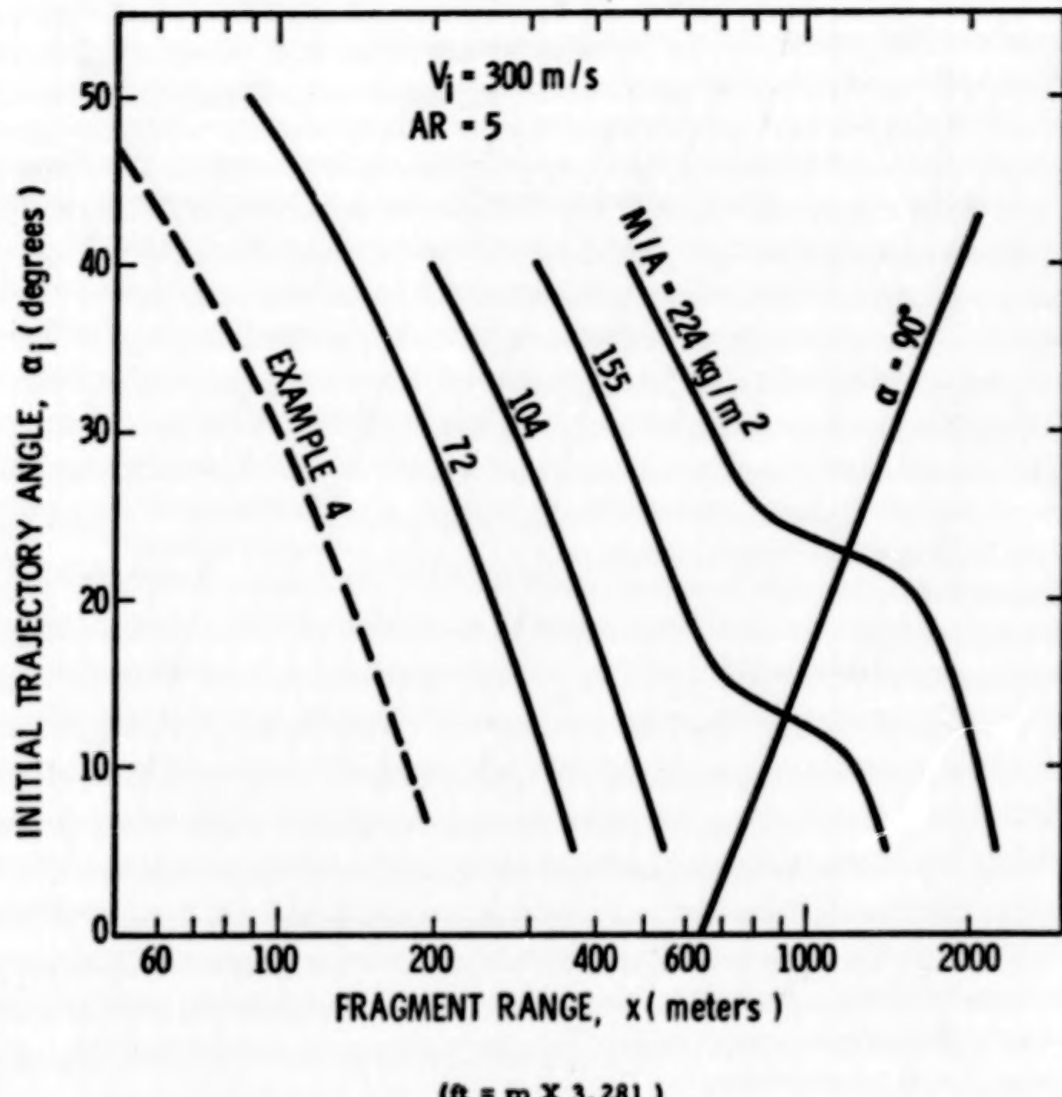


Figure 4-35. Disc Fragment Range for
 $V_i = 300 \text{ m/s}$, $AR = 5$

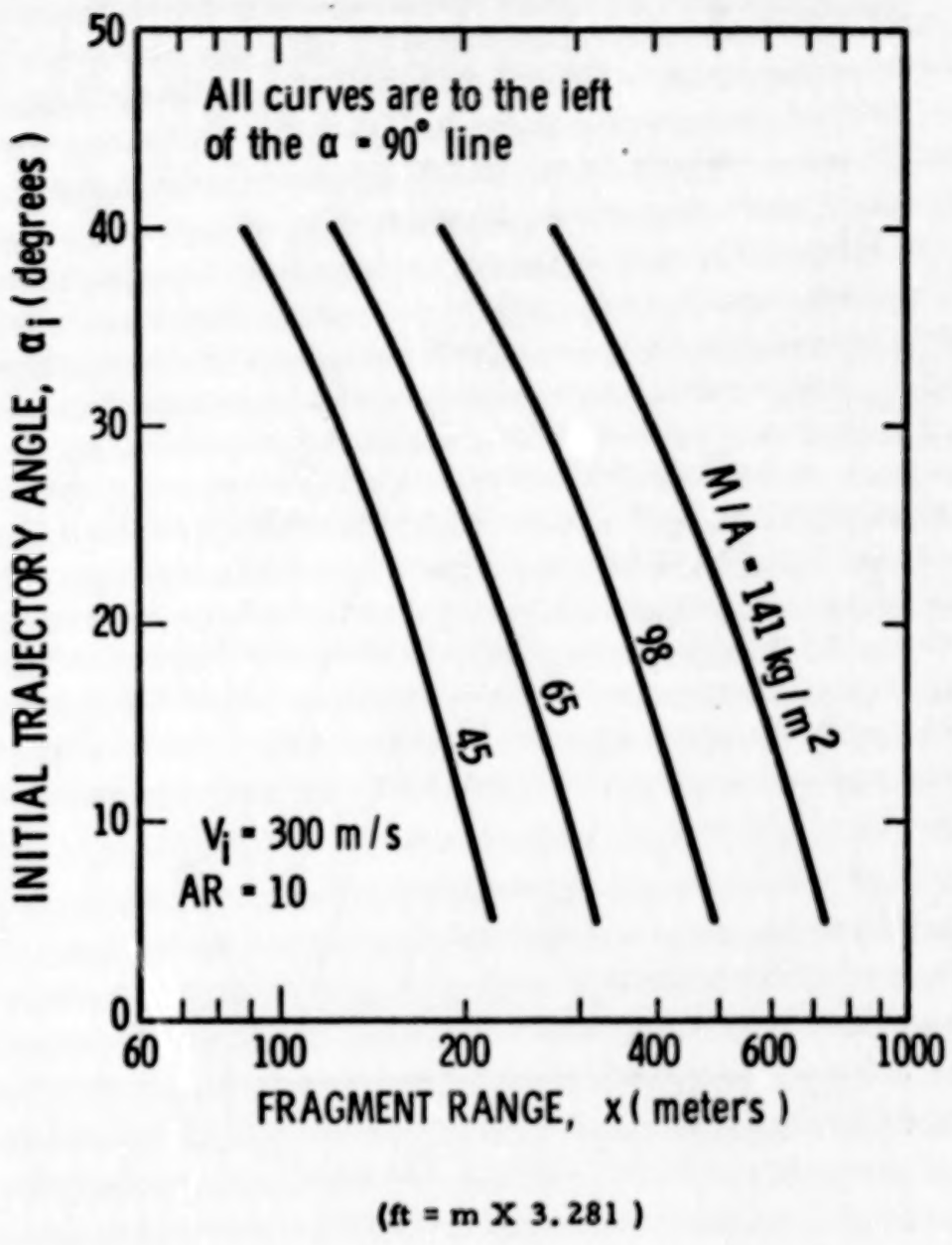


Figure 4-36. Disc Fragment Range for
 $V_i = 300 \text{ m/s}$, $AR = 10$

4-5.1 Lifting Fragments

Where fragments from bursting vessels are determined to be disc shaped, the fragment could conceivably fly or lift in much the same manner as a Frisbee. If this occurs the fragment may go further than one without lift. A computer program (FRISB) was written to determine the trajectory of a flying disc generated by an explosion. Details of the FRISB code are shown in Appendix 4E.

Several independent variables govern the flight of a disc fragment. To determine the effects of these variables on the fragment trajectory, a number of sample cases were analyzed by the FRISB code. A list of the input variables for the sample cases is presented in Table 4-1. Plots of maximum range versus initial trajectory angle are shown for those values of the independent variables in Figures 4-27 through 4-36. These graphs may be used to predict the maximum range of fragments having similar properties.

The following information must be known about the fragment to calculate its range using the figures:

1. initial fragment velocity - V_i (m/s)
2. mass of the fragment - M (kg)
3. diameter of the fragment - d (m)
4. thickness of the fragment - t (m)
5. planform or top surface area of fragment - A (m^2)
6. initial trajectory angle of the fragment - α_i (rad)

The procedure for determining fragment range is:

- Step 1. calculate the aspect ratio, $AR = d/t$, for the fragment
- Step 2. calculate the mass to area ratio M/A for the fragment
- Step 3. locate the graph for the assumed value of V_i and AR , and select the curve for the calculated value of the mass to area ratio, M/A
- Step 4. locate the point on the curve for the initial trajectory angle α_i and read the corresponding maximum range.

TABLE 4-1. PROGRAM FRISB TEST CASES

These cases were run for the
following initial velocities:

Lift and Drag Coefficients

$$V_i = 100 \text{ m/s}$$

$$C_L = .32 \quad C_D = .85$$

$$V_i = 150 \text{ m/s}$$

$$V_i = 200 \text{ m/s}$$

$$V_i = 250 \text{ m/s}$$

$$V_i = 300 \text{ m/s}$$

<u>Fragment Aspect Ratio AR</u>	<u>Fragment Area A - m²</u>	<u>Fragment Mass M - kg</u>	<u>Fragment Initial Trajectory Angle α_i - deg.</u>
5	0.0139	1	10
	0.0139	1	20
	0.0139	1	30
	0.0139	1	40
	0.0139	1	50
	0.0139	1	60
10	0.022	1	10
	0.022	1	20
	0.022	1	30
	0.022	1	40
	0.022	1	50
	0.022	1	60
5	0.0289	3	10
	0.0289	3	20
	0.0289	3	30
	0.0289	3	40
	0.0289	3	50
	0.0289	3	60

TABLE 4-1. (cont'd)

<u>Fragment Aspect Ratio AR</u>	<u>Fragment Area A - m²</u>	<u>Fragment Mass M - kg</u>	<u>Fragment Initial Trajectory Angle α_i - deg.</u>
10	0.0461	3	10
	0.0461	3	20
	0.0461	3	30
	0.0461	3	40
	0.0461	3	50
	0.0461	3	60
5	0.0645	10	10
	0.0645	10	20
	0.0645	10	30
	0.0645	10	40
	0.0645	10	50
	0.0645	10	60
10	0.102	10	10
	0.102	10	20
	0.102	10	30
	0.102	10	40
	0.102	10	50
	0.102	10	60
5	0.134	30	10
	0.134	30	20
	0.134	30	30
	0.134	30	40
	0.134	30	50
	0.134	30	60

TABLE 4-1. (cont'd)

Fragment Aspect Ratio AR	Fragment Area A - m ²	Fragment Mass M - kg	Fragment Initial Trajectory Angle α _i - deg.
10	0.213	30	10
	0.213	30	20
	0.213	30	30
	0.213	30	40
	0.213	30	50
	0.213	30	60

Since there are an infinite number of possible combinations of the independent variables, the graphs presented must be limited to particular values. However, most of the curves are parallel for varying values of the independent variables M/A, AR and V, allowing estimations to be made for fragments that are not represented by the curves presented. The procedure for this extrapolation is explained in Examples 3 and 4.

Example 1:

Determine the maximum range of a disc shape fragment assuming the following properties: $V_i = 100 \text{ m/s}$ (328 ft/sec), Mass = 1 kg (2.2 lb_m), Area = 0.0139 m^2 (0.150 ft²), $d = 0.25 \text{ m}$ (0.820 ft), $t = 0.05 \text{ m}$ (0.164 ft), and the initial trajectory of the fragment at $t = 0$ was $\alpha_i = 30^\circ$.

- Step 1. First determine the value of the aspect ratio for the fragment $AR = d/t = 0.25/0.05 = 5$.
- Step 2. Determine the value of the mass to area ratio for the fragment $M/A = 1/0.0139 = 72$.
- Step 3. From Figure 4-27, which is the figure for $V_i = 100 \text{ m/s}$ and $AR = 5$ (which are given), it can be seen that the maximum range of the fragment is 465 meters (1530 ft).

Example 2:

Determine the maximum range of a disc shaped fragment assuming the following properties: $V_i = 300 \text{ m/s}$ (984 ft/sec), Mass = 1 kg (2.2 lb_m), Area = 0.0139 m^2 (0.150 ft²), $d = 0.25 \text{ m}$ (0.820 ft), $t = 0.05 \text{ m}$ (0.169 ft), and $\alpha_i = 30^\circ$.

Step 1. Same as Example 1.

Step 2. Same as Example 1.

Step 3. From Figure 4-35 for $V_i = 300 \text{ m/s}$ and AR = 5, the maximum range is 188 meters (617 ft). But this particular point lies to the left of the straight line marked, $\alpha_i = 90^\circ$. This line indicates that all events to the left of this line resulted in the fragment attaining a completely vertical flight. At this point it was assumed that all lift and stability were lost and the fragment fell straight to the ground. All events to the right of the line indicate a "normal" flight. The $\alpha_i = 90^\circ$ line is present only where the initial velocities and/or trajectory angles were sufficient to cause a vertical trajectory.

Example 3:

Determine the maximum range of a disc-shape fragment assuming the following properties: $V_i = 230 \text{ m/s}$ (755 ft/sec), Mass = 18.6 kg (40.9 lb_m), $A = 0.155 \text{ m}^2$ (1.67 ft²), $d = 0.444 \text{ m}$ (1.46 ft), $t = 0.0444 \text{ m}$ (0.146 ft), and $\alpha_i = 30^\circ$.

Step 1. Calculate the aspect ratio for the fragment from the assumed data. $AR = 0.444/0.0444 = 10$.

Step 2. Calculate the mass to area ratio for the fragment from the assumed data. $M/A = 18.6/0.155 = 120$.

Step 3. Since no graph exists for $V_i = 230 \text{ m/s}$ we must interpolate using the graphs for $V_i = 200$ and $V_i = 250 \text{ m/s}$, $AR = 10$.

A curve for $M/A = 120$ also does not exist so an interpolation procedure must also be used here. The curve for both graphs and all values of M/A are essentially parallel so it will only be necessary to determine one point at the correct M/A and V_0 to construct the curve for all values of α_i . At $\alpha_i = 30^\circ$ for $M/A = 98$ and 141 for both $V_i = 200$ and

$V_i = 250$ (Figure 4-32 and 4-34) read the values of range.

$$V_i = 200 \text{ m/s}$$

$$V_i = 250 \text{ m/s}$$

$$\alpha_i = 30^\circ$$

$$\alpha_i = 30^\circ$$

$$M/A = 98 \text{ Range} = 283 \text{ m}$$

$$M/A = 98 \text{ Range} = 265 \text{ m}$$

$$M/A = 141 \text{ Range} = 440 \text{ m}$$

$$M/A = 141 \text{ Range} = 400 \text{ m}$$

Step 4. For each velocity find the range for $M/A = 120$ by interpolating between $M/A = 98$ and $M/A = 141$. For $V_i = 200 \text{ m/s}$:

$$\text{Range Difference } 440 - 283 = 157 \text{ m}$$

$$M/A \text{ Difference } 141 - 98 = 43 \text{ kg/m}^2$$

$$\text{or } \frac{157}{43} = 3.65 \text{ m/(kg/m}^2\text{)}$$

The difference between value of nearest curve and required value of M/A is:

$$141 - 120 = 21 \text{ kg/m}^2$$

The amount of change in the range for this increment is:

$$21 \text{ kg/m}^2 (3.65) \text{ m/(kg/m}^2\text{)} = 77 \text{ m}$$

The range at $M/A = 120$ will therefore be

$$440 \text{ m} - 77 = 363 \text{ m}$$

Similarity for $V_i = 250 \text{ m/s}$

$$440 - 265 = 135$$

$$141 - 98 = 43$$

$$135/43 = 3.13 \text{ m/(kg/m}^2\text{)}$$

$$(21)(3.13) = 66 \text{ m}$$

$$440 - 66 = 334 \text{ m}$$

With these values of range curves for $M/A = 120$ can be constructed by drawing the curves parallel to the curve for other values of M/A and through these values of range at $\alpha_i = 30^\circ$.

Step 5. With these values of range for $M/A \approx 120$, interpolate for the correct velocity of $V_i = 230 \text{ m/s}$.

Difference in range for $V_i = 200 \text{ m/s}$ and $V_i = 250 \text{ m/s}$ is $363 - 334 \text{ m} = 29 \text{ m}$

The velocity difference is $250 - 200 = 50 \text{ m/s}$.

The change in range per 1 m/sec change in velocity is

$$\frac{29 \text{ m}}{50 \text{ m/sec}} = .58 \text{ m/(m/s)}$$

The change in range from 200 to 230 m/s is:
 $(30)(.58) = 17 \text{ m}$

Since the range is decreasing with increasing velocity, the range for $M/A = 120$, $V_i = 230 \text{ m/s}$ will be: $363 - 17 = 346 \text{ m (1140 ft)}$.

A curve can be constructed to give the values of range at other values of α_i using the procedure described in Step 4.

Example 4:

Determine the maximum range of a disc-shape fragment assuming the following properties: $V_i = 448 \text{ m/s (1470 ft/sec)}$, $M = 0.0495 \text{ kg (0.109 lb}_m)$, $A = 0.00129 \text{ m}^2 (0.0139 \text{ ft}^2)$, $d = 0.40 \text{ m (1.31 ft)}$, $t = 0.0919 \text{ m (0.30 ft)}$ and $\alpha_i = 15^\circ$.

Step 1. Calculate the aspect ratio for the fragment from the assumed data. $AR = 0.40/0.0919 = 4.4$.

Step 2. Calculate the mass to area ratio for the fragment from the assumed data. $M/A = 38.4$.

Step 3. Since no graph exists for a $V_i = 448 \text{ m/s}$ and an $AR = 4.4$ we must choose Figure 4-35 for $V_i = 300 \text{ m/s}$, $AR = 5$ to obtain an approximation for range. There is no curve in Figure 4-35 for which $M/A = 38$ but the curves are parallel and evenly spaced. Between $M/A = 72$ and $M/A = 104$ at $\alpha_i = 40^\circ$ there is a difference in

range of 60 meters or $\frac{60}{104 - 72} = 1.88 \frac{\text{m}}{\text{kg/m}^2}$.

From $M/A = 104$ to $M/A = 155$ at $\alpha_i = 40^\circ$, there is a difference in range of 110 meters or $\frac{110}{155 - 104} =$

$2.16 \frac{\text{m}}{\text{kg/m}^2}$. This is an average of about $2 \frac{\text{m}}{\text{kg/m}^2}$

It is required to construct a curve for $M/A = 38 \text{ kg/m}^2$. The nearest curve to this value is $M/A = 72$ for a difference of $72 - 38 = 34 \text{ kg/m}^2$. The value of the range for $M/A = 38$ at 40° should be about 70 meters. Construct a curve through this point and parallel to the other curves. The range for $\alpha_i = 15^\circ$ is then read as 155 meters (509 ft).

This particular case was checked by substitution of the assumed data into the FRISB code (described in Appendix 4E). The maximum range predicted by the code was 142 meters which is about 8% lower than the curve approximation.

Several cases where the initial conditions did not match a particular graph were checked in this manner to determine the accuracy of the approximation. The error ranged from 5% to 80%. The greatest errors occurred when trying to predict the range for values of $(M/A) < 20$. These checks indicate that although the predictions from interpolation are crude, they provide a means of obtaining a rough order of magnitude for the fragment range, when gross extrapolations are required.

The FRISB code may also be used to predict the trajectory of a fragment that generates no lift as does the TRAJE code. A value of $C_L = 0$ is input into FRISB for this computation. The code can also be used to predict the trajectory of a fragment that is long and thin and spins like a helicopter rotor blade. The input involved for the use of this feature is presented in Appendix 4E along with a discussion of the analysis procedure.

4-5.2 Drag Fragments

Some fragments are shaped such that no one linear dimension is significantly greater than any other. The maximum range for such fragments (i.e., chunky fragments, fragments which can be approximated by a cube or sphere) can be obtained using the technique to be described.

Required input data are the initial velocity, V_i , of the fragment, a characteristic area A of the fragment (which can be generated as shown

below), the mass of the fragment, and an initial trajectory angle or spectrum of initial trajectory angles, α_i . Typical steps in the procedure for calculating the maximum range from Figures 4-37 through 4-45 are the following:

Step 1. Find the characteristic area of the fragment:

(a) from the equation

$$A = V^{2/3}$$

where V is the fragment volume. V may be obtained from the mass of the fragment, M , and its density, ρ , from the equation

$$V = M/\rho$$

(b) from the projected area of the fragment if it has three-dimensional symmetry or can be nearly approximated by a solid of three-dimensional symmetry (i. e., a sphere or a cube).

Step 2. Calculate the mass area ratio for the fragment, M/A .

Step 3. Consult Figures 4-37 through 4-45 to find the figure for a V_i and A value most nearly equal that of the fragment considered. Linear interpolation can be used where necessary (see example problems).

Step 4. Read the maximum range from the figure for the M/A of Step 2 and the initial trajectory angles considered.

For a more precise range calculation the computer code, TRAJE, used to generate these figures may be used along with the input data for the fragment.

Example 1. For Drag Fragments

Assume: A nearly spherical shaped fragment that can be approximated by a sphere of radius $R = 0.0584$ m (0.192 ft) having an initial velocity of 200 m/s (656 ft/sec) and made out of steel. Find the maximum range expected for any initial trajectory angle.

Step 1. The characteristic area of the fragment is, by method (a)

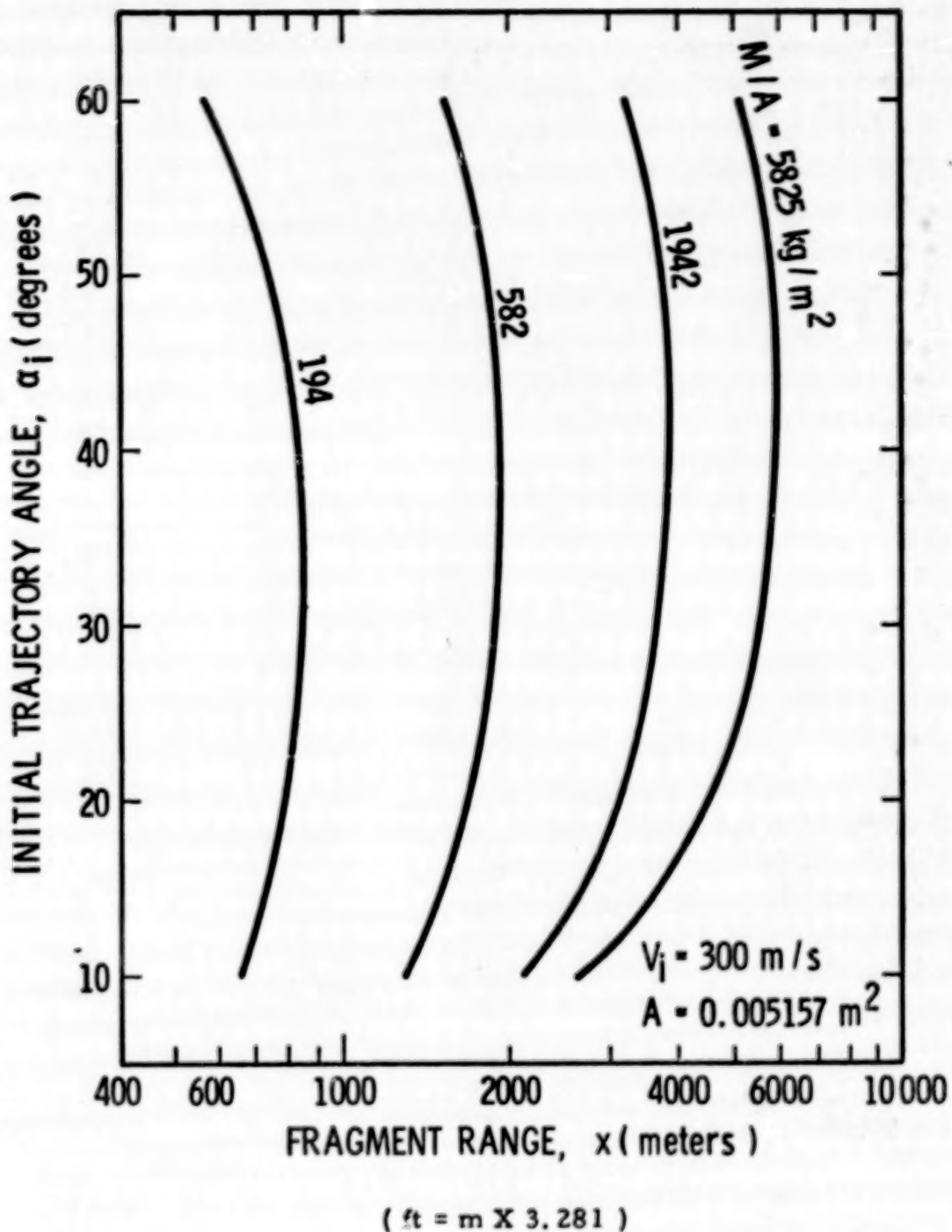


Figure 4-37. Fragment Range for Drag Fragments,
 $V_i = 300 \text{ m/s}, A = 0.005157 \text{ m}^2$

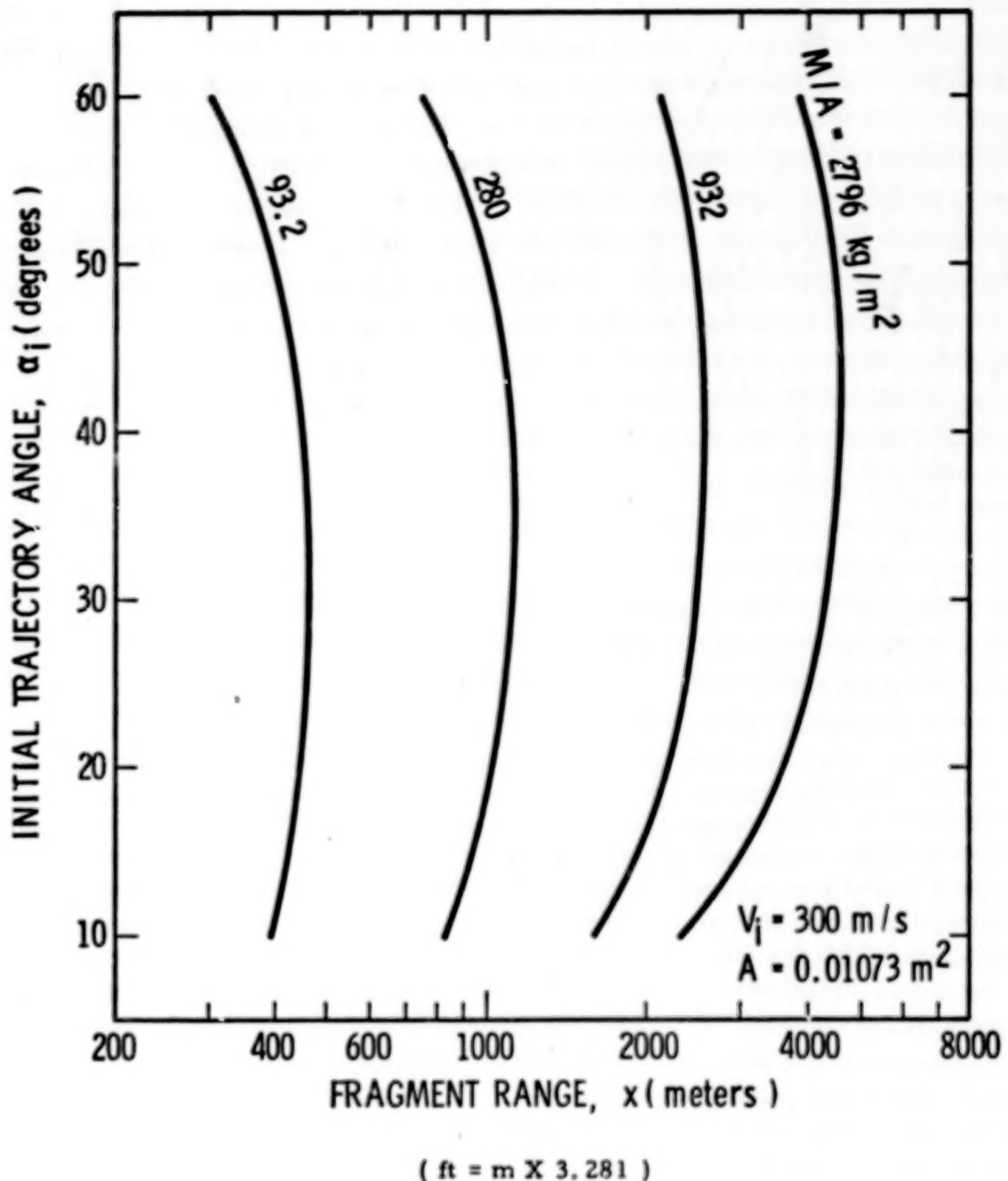


Figure 4-38. Fragment Range for Drag Fragments,
 $V_i = 300 \text{ m/s}$, $A = 0.0173 \text{ m}^2$

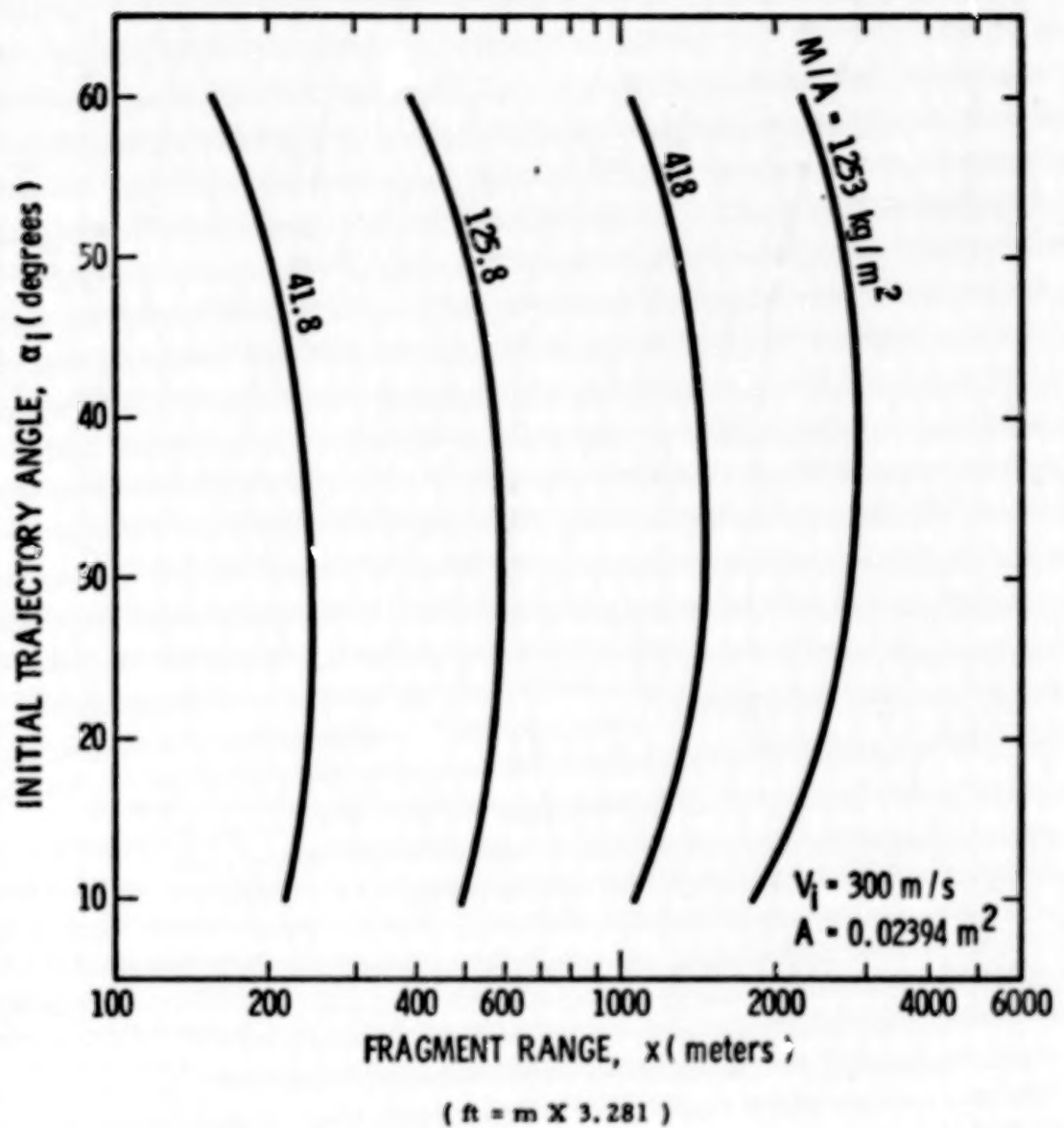


Figure 4-39. Fragment Range for Drag Fragments,
 $V_i = 300 \text{ m/s}$, $A = 0.02394 \text{ m}^2$

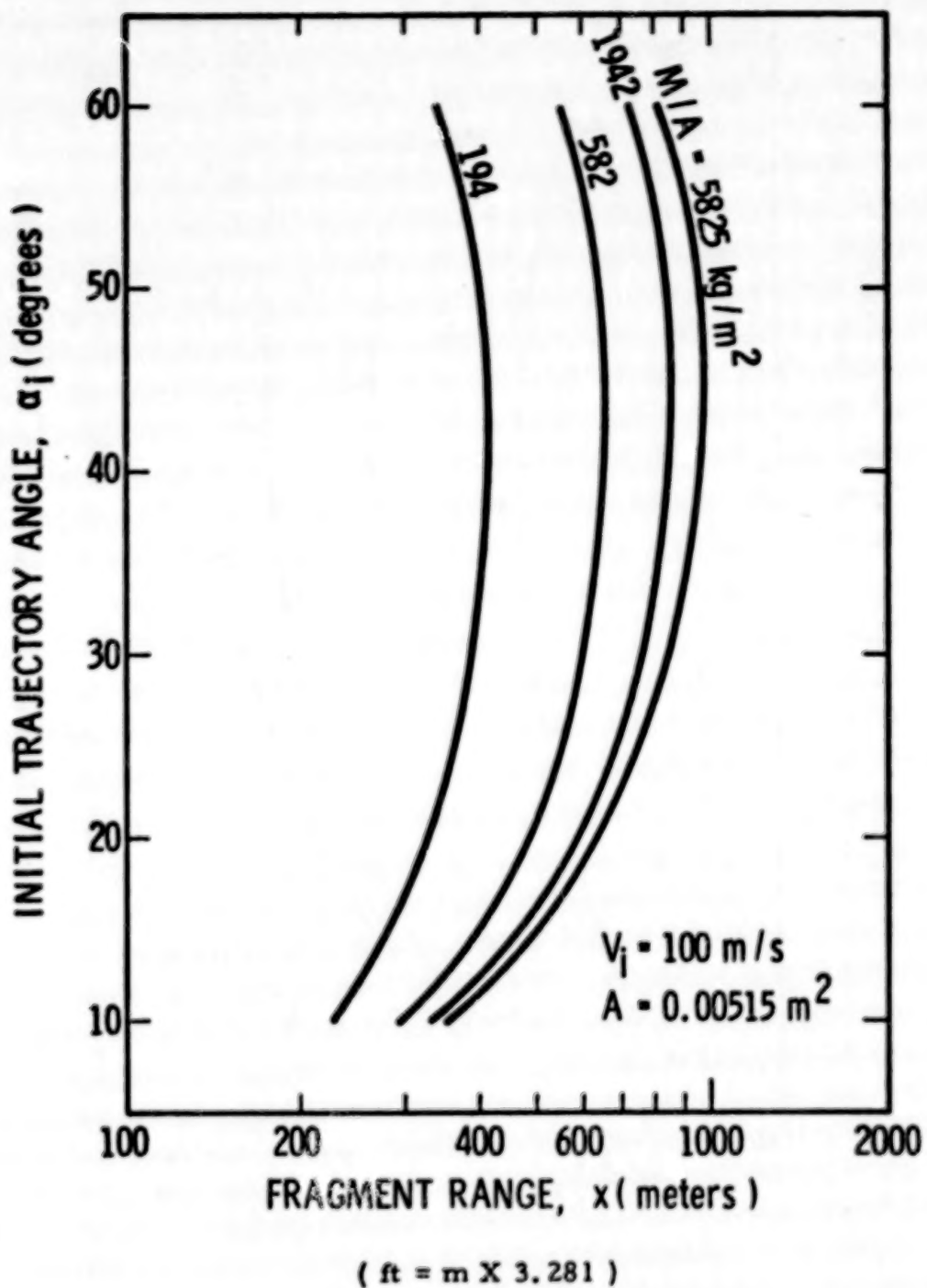


Figure 4-40. Fragment Range for Drag Fragments,
 $V_i = 100 \text{ m/s}$, $A = 0.00515 \text{ m}^2$

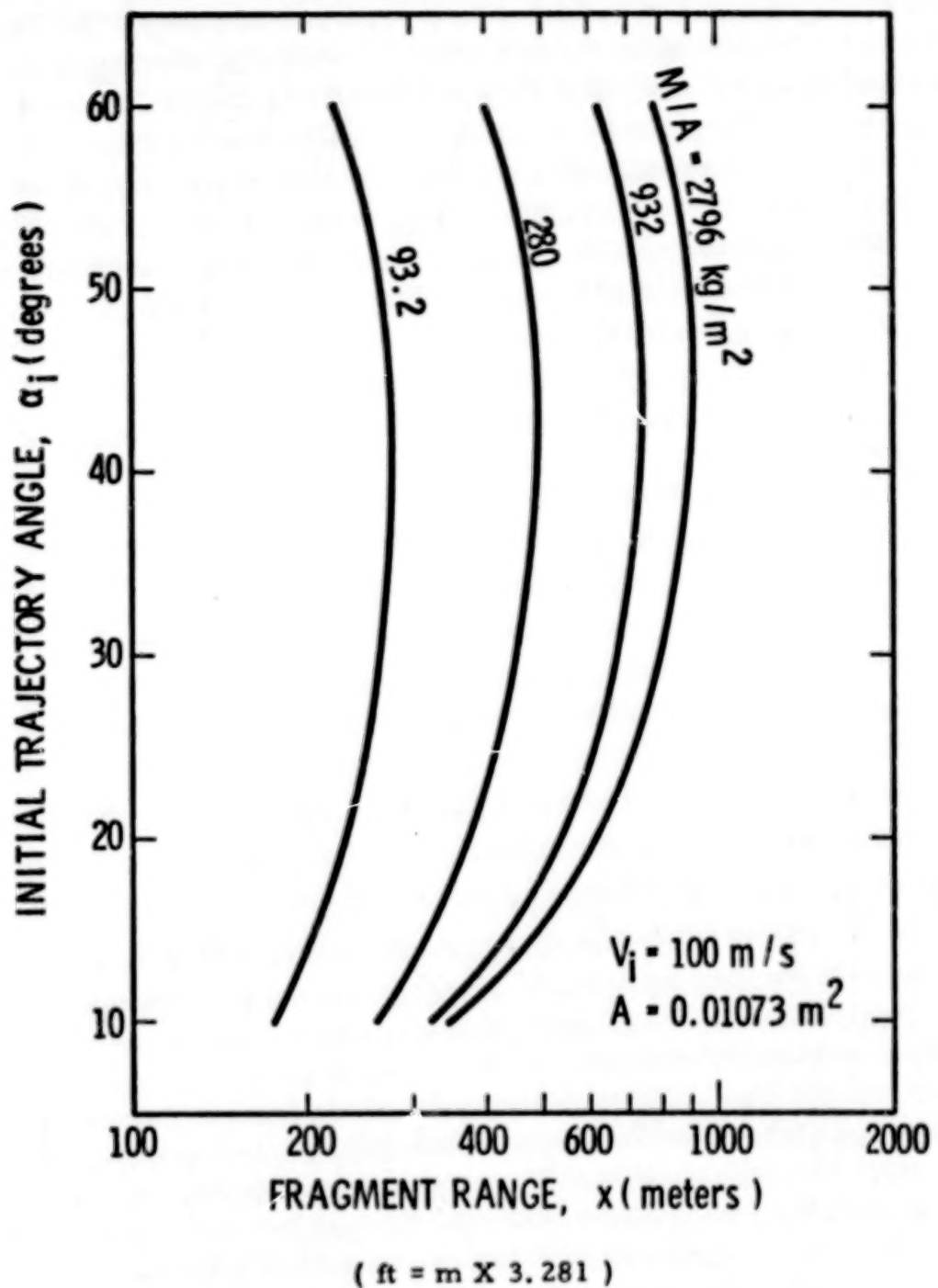


Figure 4-41. Fragment Range for Drag Fragments,
 $V_i = 100 \text{ m/s}$, $A = 0.01073 \text{ m}^2$

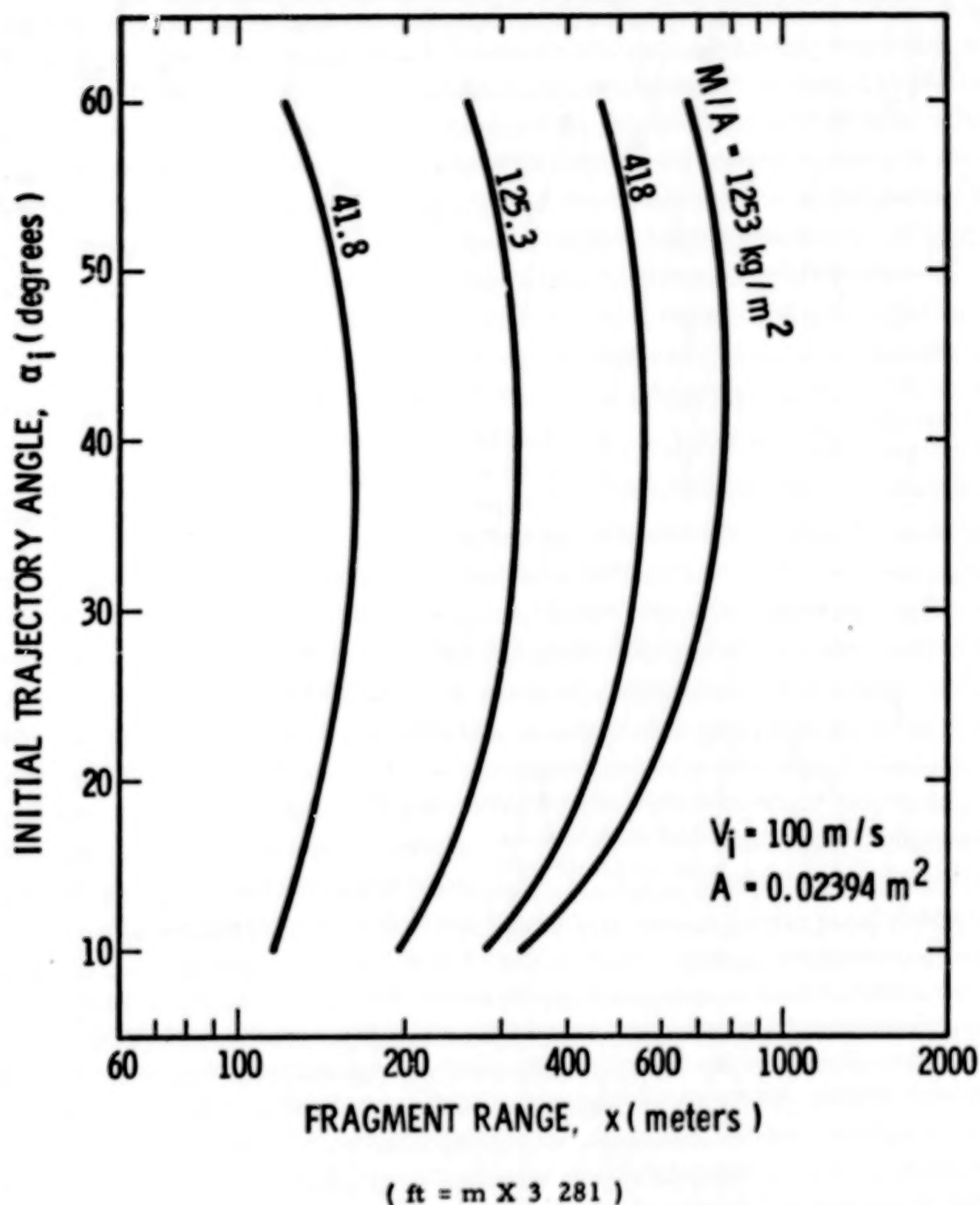


Figure 4-42. Fragment Range for Drag Fragments,
 $V_i = 100 \text{ m/s}, A = 0.02394 \text{ m}^2$

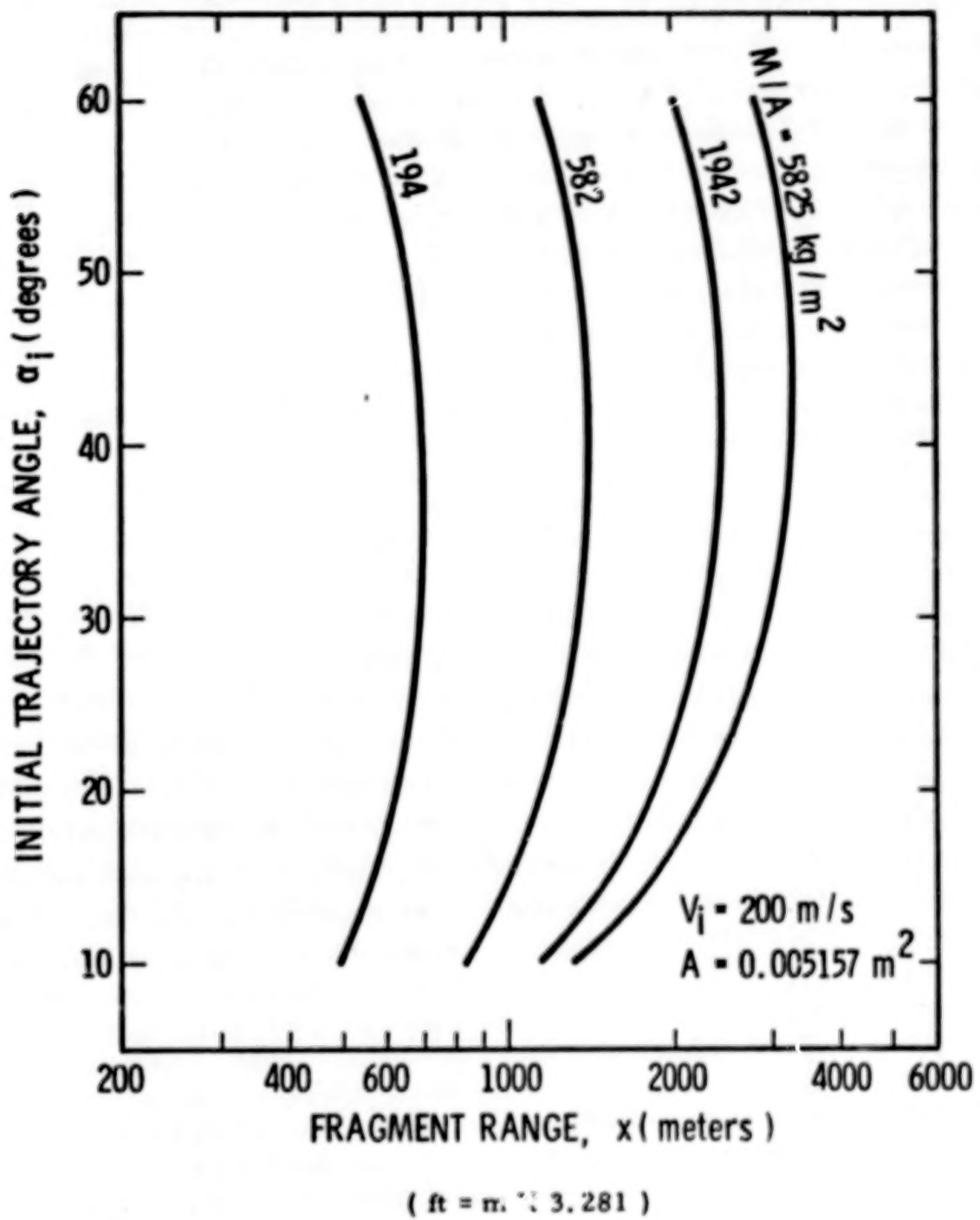


Figure 4-43. Fragment Range for Drag Fragments,
 $V_i = 200 \text{ m/s}$, $A = 0.005157 \text{ m}^2$

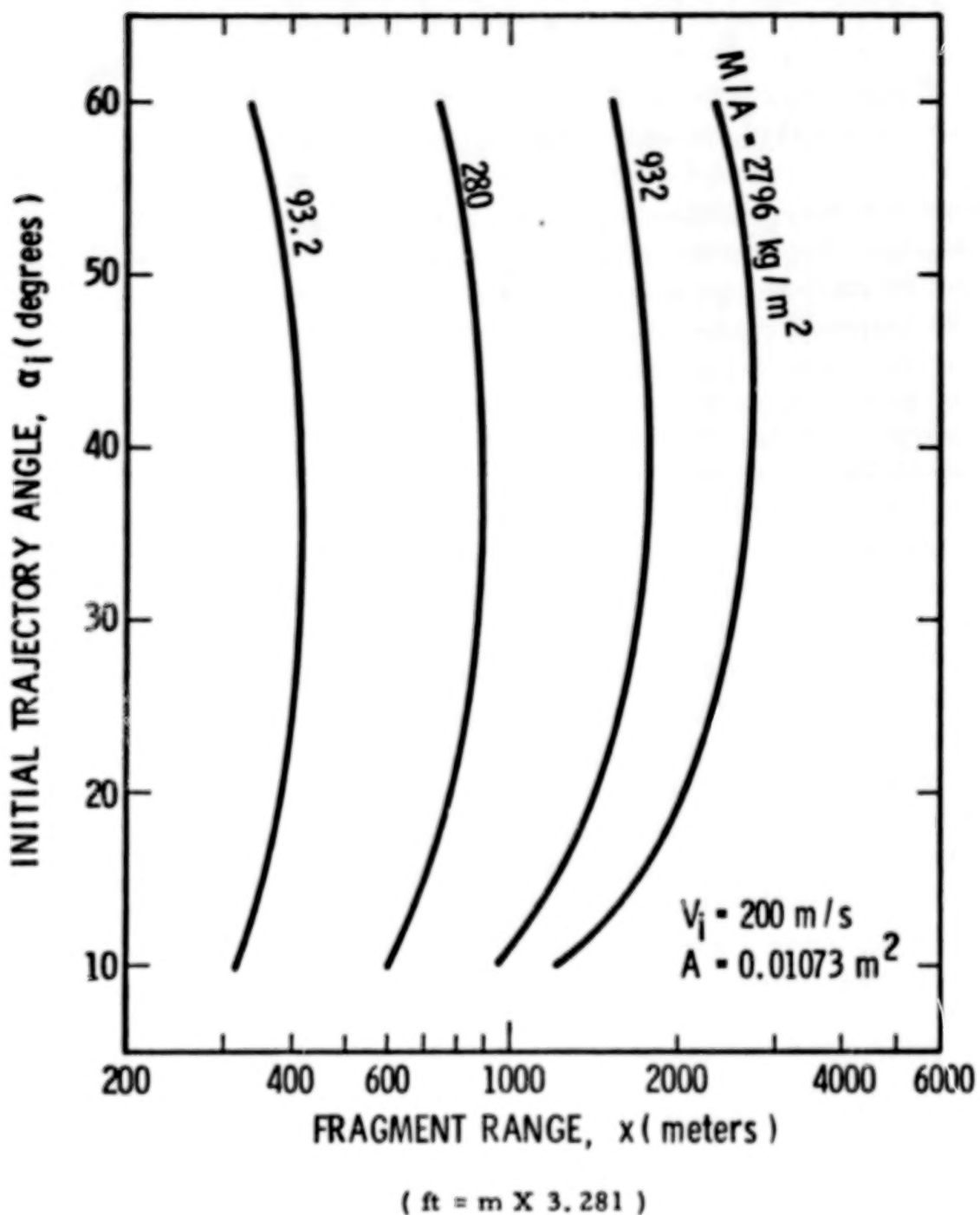


Figure 4-44. Fragment Range for Drag Fragments,
 $V_i = 200 \text{ m/s}$, $A = 0.01073 \text{ m}^2$

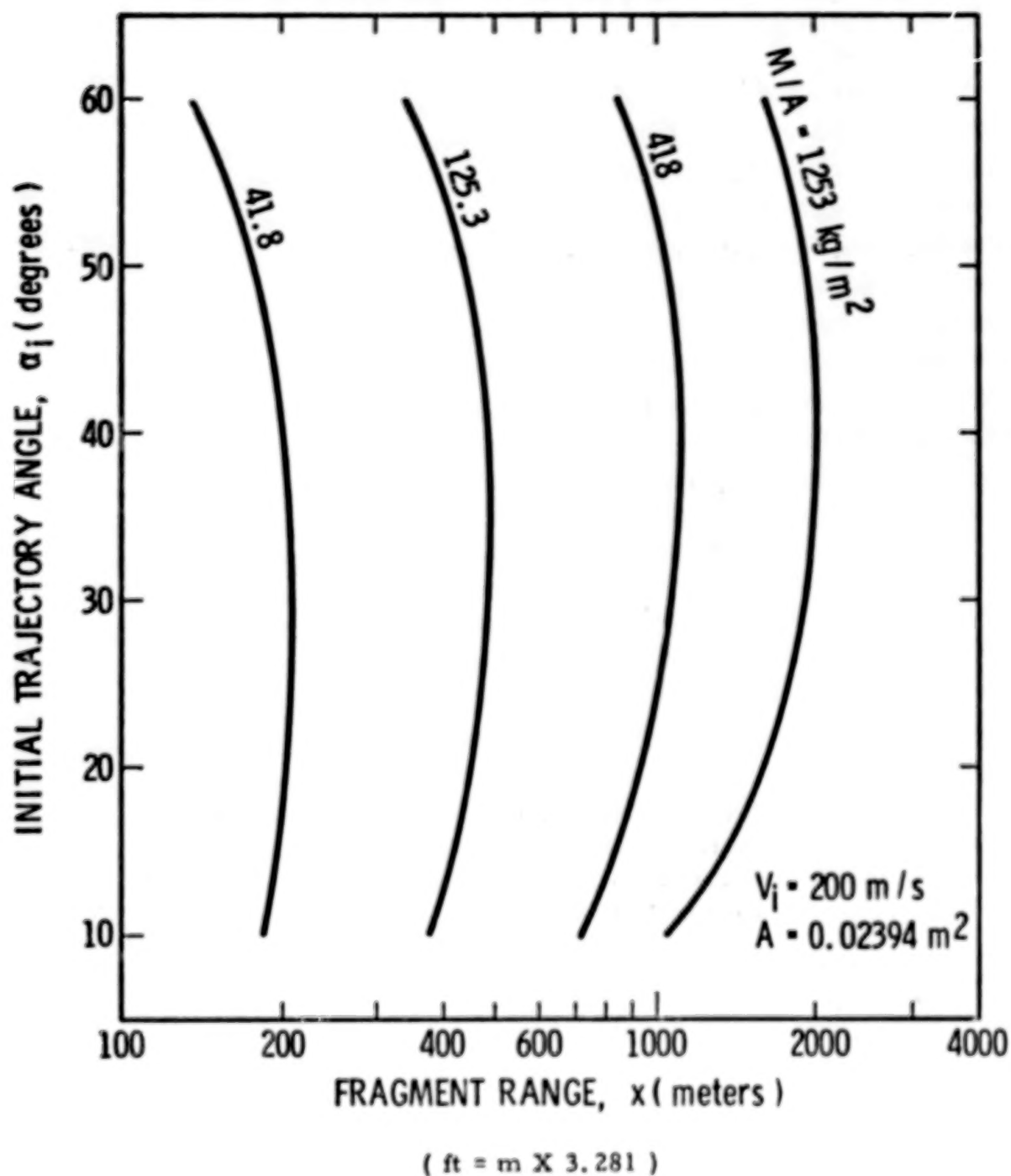


Figure 4-45. Fragment Range for Drag Fragments,
 $V_i = 200 \text{ m/s}, A = 0.02394 \text{ m}^2$

$$A_1 = [(4/3)\pi R^3]^{2/3} = 2.60 R^2 = 0.00887 \text{ m}^2$$

by method (b)

$$A_2 = \pi R^2 = 0.0107 \text{ m}^2$$

Step 2. Calculate the mass area ratio for the fragment where

$$M = \rho V = (4/3) \pi R^3$$

For a sphere

$$\rho_{\text{steel}} = 7800 \text{ kg/m}^3$$

therefore

$$M = (7800) (4/3) (\pi) (0.0584)^3 = 6.51 \text{ kg}$$

using A_2 from Step 1,

$$M/A_2 = 6.51/0.0107 = 608 \text{ kg/m}^2$$

Step 3. The given V_1 of 200 m/s and $A_2 = 0.0107 \text{ m}^2$ corresponds to values for Figure 4-44. From this figure it can be seen that the maximum range for a fragment having an M/A of 932 kg/m^2 is $x_3 = 1800 \text{ m}$ and for an M/A of 280 kg/m^2 is $x_1 = 900 \text{ m}$.

Step 4. By linear interpolation for our M/A of 608 kg/m^2

$$m_1 = M/A = 280 \text{ kg/m}^2 \quad x_1 = 900 \text{ m}$$

$$m_2 = M/A = 608 \text{ kg/m}^2 \quad x_2 = ?$$

$$m_3 = M/A = 932 \text{ kg/m}^2 \quad x_3 = 1800 \text{ m}$$

$$x_2 = (x_3 - x_1) \frac{(m_2 - m_1)}{(m_3 - m_1)} + x_1$$

$$\begin{aligned} x_2 &= (1800 - 900) \frac{(608 - 280)}{(932 - 280)} + 900 \\ &= 1352 \text{ m (4,430 ft)} \end{aligned}$$

Example 2. For Drag Fragments

Assume: A chunky aluminum fragment of a mass of approximately 1.20 kg (2.64 lb_m) and an initial velocity of 250 m/s (820 ft/sec). Find the maximum range expected for any initial trajectory angle.

Step 1. The characteristic area of the fragment is, by method (a)

$$A = (M/\rho)^{2/3}$$

from density tables

$$\rho_{Al} = 2700 \text{ kg/m}^3$$

therefore

$$A = (1.20/2700)^{2/3} = 5.83 \times 10^{-3} \text{ m}^2$$

Step 2. M is given as M = 1.2 kg taking A from Step 1, thus

$$M/A = \frac{1.2}{5.83 \times 10^{-3}} = 206 \text{ kg/m}^2$$

Step 3. A conservative value for the range will be obtained by using data from Figures 4-40 and 4-43 for a fragment of characteristic area $5.16 \times 10^{-3} \text{ m}^2$ which is slightly less than the area of the fragment considered, calculated in Step 1.

From Figure 4-43, for a fragment having $V_i = 200 \text{ m/s}$ we may obtain a maximum range for $M/A \approx 206 \text{ kg/m}^2$ by linear interpolation from the maximum ranges, x, for M/A ratios most nearly greater and less than $M/A = 206 \text{ kg/m}^2$:

$$m_1 = M/A = 194 \text{ kg/m}^2 \quad x_1 = 700 \text{ m}$$

$$m_2 = M/A = 206 \text{ kg/m}^2 \quad x_2 = ?$$

$$m_3 = M/A = 582 \text{ kg/m}^2 \quad x_3 = 1400 \text{ m}$$

$$x_2 = (x_3 - x_1) \frac{(m_2 - m_1)}{(m_3 - m_1)} + x_1 = (1400 - 700) \frac{(206 - 194)}{(582 - 194)} +$$

700

$$x_2 = 720 \text{ m}$$

From Figure 4-37, for a fragment having a $V_i^2 = 300 \text{ m/s}$ we may obtain a maximum range for $M/A = 206 \text{ kg/m}^2$ by linear interpolation as in the previous paragraph.

$$m_1' = M/A = 194 \text{ kg/m}^2 \quad x_1' = 850 \text{ m}$$

$$m_2' = M/A = 206 \text{ kg/m}^2 \quad x_2' = ?$$

$$m_3' = M/A = 582 \text{ kg/m}^2 \quad x_3' = 1920 \text{ m}$$

$$x_2' = (1920 - 850) \frac{(206 - 194)}{(582 - 194)} + 850 = 880 \text{ m}$$

Step 4. Interpolating for a $V_i^2 = 250 \text{ m/s}$ between the values found for $V_i^2 = 200 \text{ m/s}$ and 300 m/s

$$x_2' = (x_2' - x_2) \frac{(250 - 200)}{(300 - 200)} + x_2$$

$$= (880 - 720) 1/2 + 720$$

$$\approx 800 \text{ m}$$

A conservative value for range for this fragment is 800 m (2600 ft).

Example 3. For Drag Fragments

Assume: A titanium alloy fragment with a mass of 3.12 kg (6.84 lb_m) initial velocity of 125 m/s (410 ft/sec). Find its maximum range for any initial trajectory angle.

Step 1. $A = (M/\rho_{Ti})^{2/3}$

since

$$\rho_T = 4460 \text{ kg/m}^3$$

$$A = \left(\frac{3.12}{4460}\right)^{2/3} = 7.0 \times 10^{-3} \text{ m}^2$$

Step 2. $M/A = \frac{3.12}{7.0 \times 10^{-3}} = 395 \text{ kg/m}^2$

Step 3. For a conservative value for range use Figures 4-40 and 4-43 for an $A = 5.15 \times 10^{-3} \text{ m}^2$ which is less than the area of the fragment considered. From Figure 4-40,

for $V_i = 100 \text{ m/s } A = 5.15 \times 10^{-3} \text{ m}^2 \text{ M/A} = 194 \text{ kg/m}^2 \text{ } X_1 = 420 \text{ m}$

for $V_i = 100 \text{ m/s } A = 5.15 \times 10^{-3} \text{ m}^2 \text{ M/A} = 582 \text{ kg/m}^2 \text{ } X_3 = 660 \text{ m}$

therefore, interpolating as in the previous examples for an $M/A = 395 \text{ kg/m}^2$

for $V_i = 100 \text{ m/s } A = 5.15 \times 10^{-3} \text{ m}^2 \text{ M/A} = 395 \text{ kg/m}^2 \text{ } X_2 = 544 \text{ m}$

From Figure 4-43, similarly

$$\text{for } V_i = 200 \text{ m/s } A = 5.15 \times 10^{-3} \text{ m}^2 \text{ M/A} =$$

$$395 \text{ kg/m}^2 \quad X_2' = 1062 \text{ m}$$

interpolating for a V_i of 125 m/s

$$V_i = 125 \text{ m/s } A = 5.15 \times 10^{-3} \text{ m}^2 \text{ M/A} =$$

$$395 \text{ kg/m}^2 \quad X_2'' = 673 \text{ m}$$

Thus a conservative value for the range would be 673 m (2210 ft).

4-5.3 For Cylindrical Propellant Tanks

Data from initial velocity measurements of fragments from Project PYRO experiments (Reference 3) were used to derive an estimate of the fragment initial velocity distribution. For medium percent yields (5 to 15%), Figures 4-46 and 4-47 present the fragment initial velocity distributions for LO_2/LH_2 , and $\text{LO}_2/\text{RP-1}$ respectively, confined in a cylindrical missile (CBM). For medium percent yields (5 to 15%) Figures 4-48 and 4-49 show the fragment initial velocity distributions for LO_2/LH_2 and $\text{LO}_2/\text{RP-1}$ respectively confined by the ground surface (CBGS). In the CBGS tests, the missiles were allowed to fall back to the pad. In the CBM tests, the bulkheads between the LO_2 and LH_2 were ruptured, allowing the liquids to mix inside the missile.

Figures 4-46 through 4-49 can be used to estimate the percentage of fragments which will have an initial velocity, U_i , equal to or less than a particular U_i .

For example, if we wished to estimate the percentage of fragments which would have an initial velocity equal to or less than 1,000 m/s (3280 ft/sec) for a LO_2/LH_2 CBM case, we would refer to Figure 4-46 and on the initial velocity axis (abscissa) at 1,000 m/s go upward to the intersection with the line. Then, at the intersection point read the percentage value from the ordinate, which is 95.5%. Conversely, if we wanted to know what initial velocity 90% of the fragments would not exceed, we would enter the chart on the 90% line, go over the intersection with the curve and read downward to the initial velocity axis the value 680 m/s (2230 ft/sec).

Figure 4-50 is a plot of fragment initial velocity versus yield (%) for LO_2/LH_2 CBM tests listed on page 86 of Reference 3. A 95th percentile has been included based on the same standard deviation as the

TABLE OF CONTENTS

	<u>Page</u>
INTRODUCTION	1 1/A12
I. ESTIMATES OF EXPLOSIVE YIELD	8 1/B5
1-1 Explosive Yield as a Function of Propellant Type and Accident Conditions	8 1/B5
1-2 Explosive Yield as a Function of Fluid Type and Initial Conditions for Gas Vessel Bursts	26 1/C9
List of References	29 1/C12
II. CHARACTERISTICS OF PRESSURE WAVES	31 1/C14
2-1 General	31 1/C14
2-2 Pressure Waves from Propellant Explosions	40 1/D9
2-3 Pressure Waves from Gas Vessel Bursts	56 1/E11
List of References	68 1/F9
II. A GAS VESSEL BURST	70 1/F11
2A-1 Nondimensional Parameters	70 1/F11
2A-2 Source of Data	70 1/F11
2A-3 Overpressure Calculation	71 1/F12
2A-4 Impulse Calculation	74 1/G1
2A-5 Effect of Cylindrical Geometry	74 1/G1
2A-6 Effect of Reflecting Surface (Burst at Ground Level)	74 1/G1
List of References	78 1/G5
Symbols	79 1/G6

TABLE OF CONTENTS (Cont'd)

		<u>Page</u>
III.	EFFECTS OF PRESSURE WAVES	80 1/G7
3-1	Damage Estimates to Structures	80 1/G7
3-2	Injury Estimates to Humans	99 2/B3
	List of References	125 2/D1
III.A	STRUCTURAL RESPONSE	128 2/D4
3A-1	Overturning Analysis	128 2/D4
3A-2	Development of Beam Equations	134 2/D10
3A-3	Development of Plate Equations	142 2/E4
3A-4	Development of Membrane Equations	153 2/F1
	List of References	158 2/F6
III.B	PRESSURE/IMPULSE COMBINATIONS PRODUCING LUNG DAMAGE	159 2/F7
	List of References	169 2/G3
III.C	PRESSURE/IMPULSE COMBINATIONS PRODUCING LOSS OF HEARING	171 2/G5
	List of References	175 2/G9
III.D	PRESSURE/IMPULSE COMBINATIONS PRODUCING WHOLE-BODY DISPLACEMENT AND SUBSEQUENT DAMAGE TO THE HEAD AND BODY	176 2/G10
	List of References	190 3/B1
IV.	CHARACTERISTICS OF FRAGMENTS	191 3/B2
4-1	General	191 3/B2
4-2	Methods for Estimating Fragment Initial Velocities for Spheres and Cylinders Bursting into Many Fragments	191 3/B2

TABLE OF CONTENTS (Cont'd)

		<u>Page</u>
4-3	Estimate of Initial Velocities of Fragments from Spheres and Cylinders Bursting into Two Equal Halves	218 3/D1
4-4	Determination of Appurtenance Velocity	228 3/D11
4-5	Methods for Computing Fragment Ranges and Impact Conditions	240 3/E9
4-6	Fragment Mass Distribution	279 4/A11
4-7	Probability of Fragment Arrival Versus Range	286 4/B4
	List of References	292 4/B10
IV.A	METHODS FOR ESTIMATING FRAGMENT INITIAL VELOCITIES	293 4/B11
	List of References	315 4/D5
IV.B	COMPARISON OF EXPERIMENTAL RESULTS WITH CODE PREDICTIONS	316 4/D6
	List of References	318 4/D8
IV.C	ESTIMATE OF INITIAL VELOCITIES OF FRAGMENTS FROM SPHERES AND CYLINDERS BURSTING INTO TWO EQUAL HALVES	319 4/D9
	List of References	354 4/G2
IV.D	ESTIMATION OF VELOCITIES ATTAINED BY APPURTENANCES SUBJECTED TO BLAST LOADING	355 4/G3
	List of References	377 5/B2
IV.E	ANALYSES FOR FRAGMENT TRAJECTORIES	378 5/B3
	List of References	401 5/C12

TABLE OF CONTENTS (Cont'd)

	<u>Page</u>
IV. F STATISTICAL FITTING TO FRAGMENT DATA	402 5/C13
4F-1 Derivation of Figures 4-46 Through 4-49	402 5/C13
4F-2 Derivation of Figure 4-50	402 5/C13
4F-3 Rationale for Averaging Fragment Mass Distribution for Events 3, 4, and 5	403 5/C14
4F-4 Fragment Mass Distributions for Gas Vessel Bursts	406 5/D3
4F-5 Rationale for Averaging Fragment Mass Distributions for Tanks A and B and Tanks D and E	412 5/D9
4F-6 Derivation of Figure 4-57, Fragment Distance Versus Percent Yield for Propellant Explosions	413 5/D10
4F-7 Derivation of Simulated Fragment Range Distribution for Gas Vessel Bursts	415 5/D12
4F-8 Rationale for Combining Simulated Range Distribution for Tanks A and B and for Tanks D and E	423 5/E6
List of References	424 5/E7
V. EFFECTS OF FRAGMENTS	425 5/E8
5-1 Damage Estimates to Structures and Facilities	425 5/E8
5-2 Damage Estimates to People from Secondary Fragments	433 5/F2
List of References	442 5/F11
V.A EFFECTS OF FRAGMENTS ON STRUCTURES	444 5/F13
List of References	446 5/G1

TABLE OF CONTENTS (Concl'd)

	<u>Page</u>
V. B DAMAGE ESTIMATES TO PEOPLE FROM SECONDARY FRAGMENTS	447 5/G2
5B-1 Penetrating Fragments	447 5/G2
5B-2 Nonpenetrating Fragments	455 5/G10
List of References	456 5/G11
VI. RISK ASSESSMENT AND INTEGRATED EFFECTS	458 5/G13
6-1 Risk Assessment	458 5/G13
6-2 Prediction of Relative Blast and Fragment Effects	461 6/A7
List of References	507 6/D11
VII. DISCUSSION OF RESULTS	508 6/D12
VIII. CONCLUSIONS	511 6/E1
IX. RECOMMENDATIONS	513 6/E3
LIST OF SYMBOLS	516 6/E6
CONVERSION FACTORS	523 6/E13
GLOSSARY OF TERMS	525 6/F1
BIBLIOGRAPHY	528 6/F4

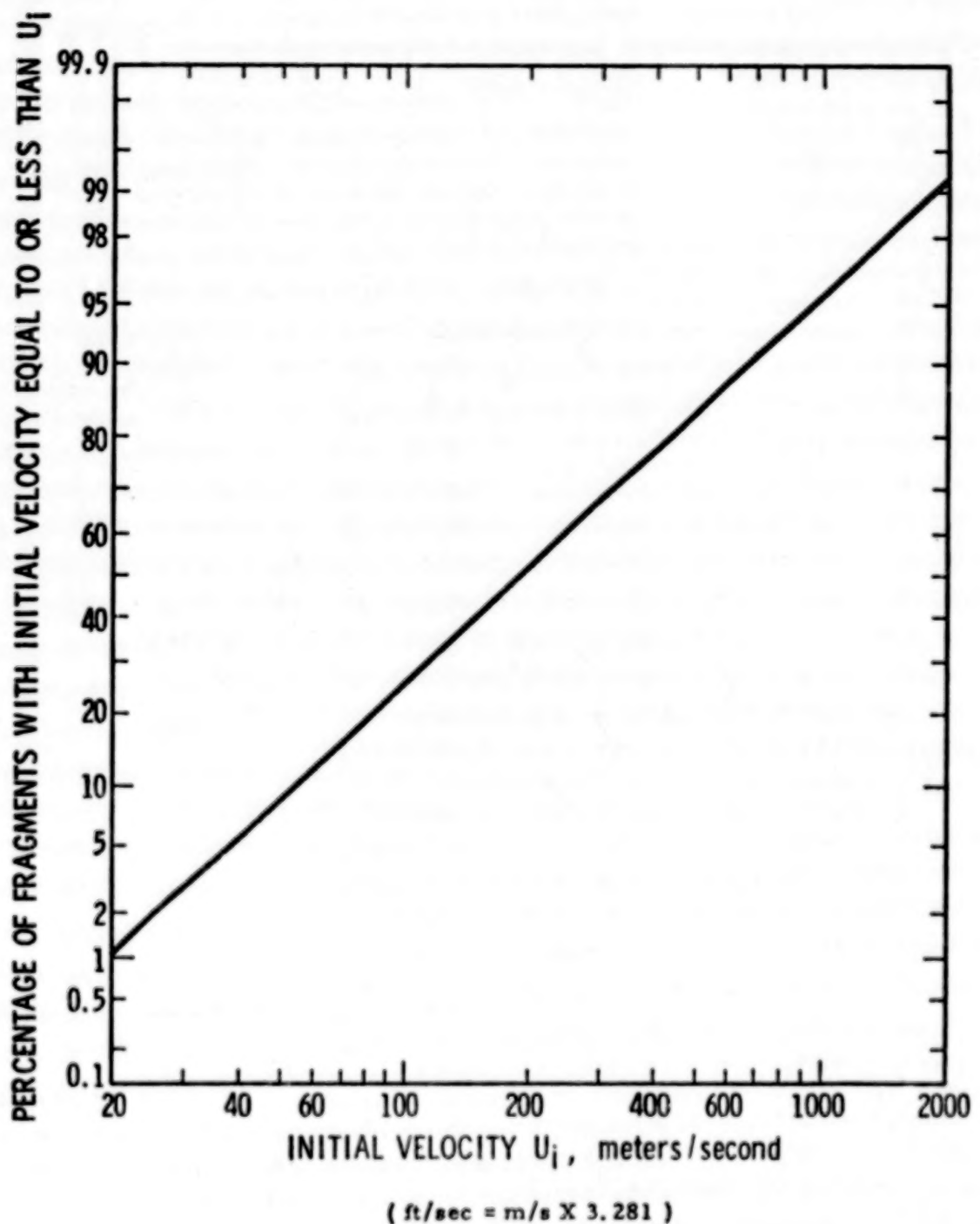


Figure 4-46. Initial Velocity Distribution,
CBM, LO_2/LH_2

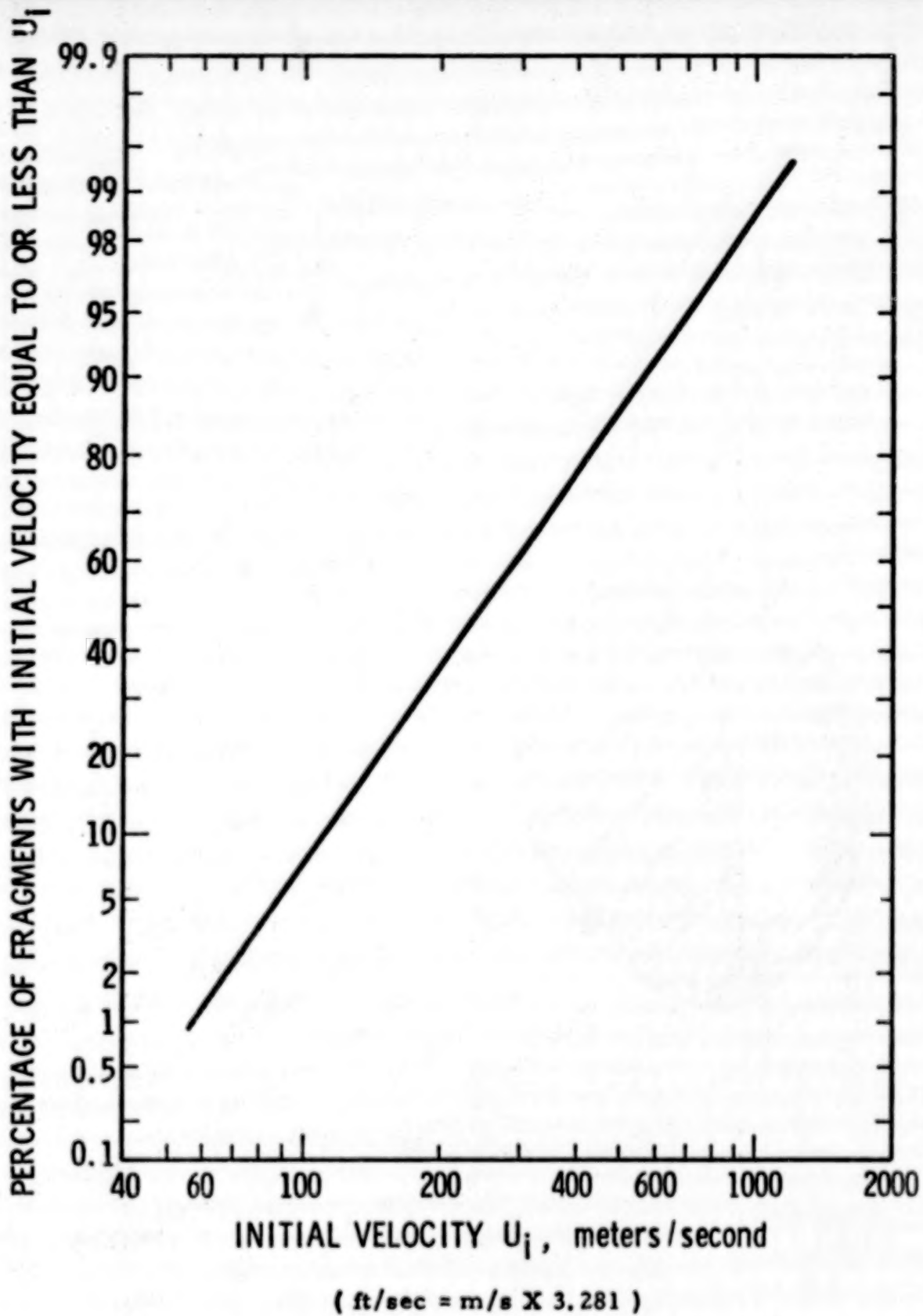


Figure 4-47. Initial Velocity Distribution,
CBM, LO₂/(RP-1)

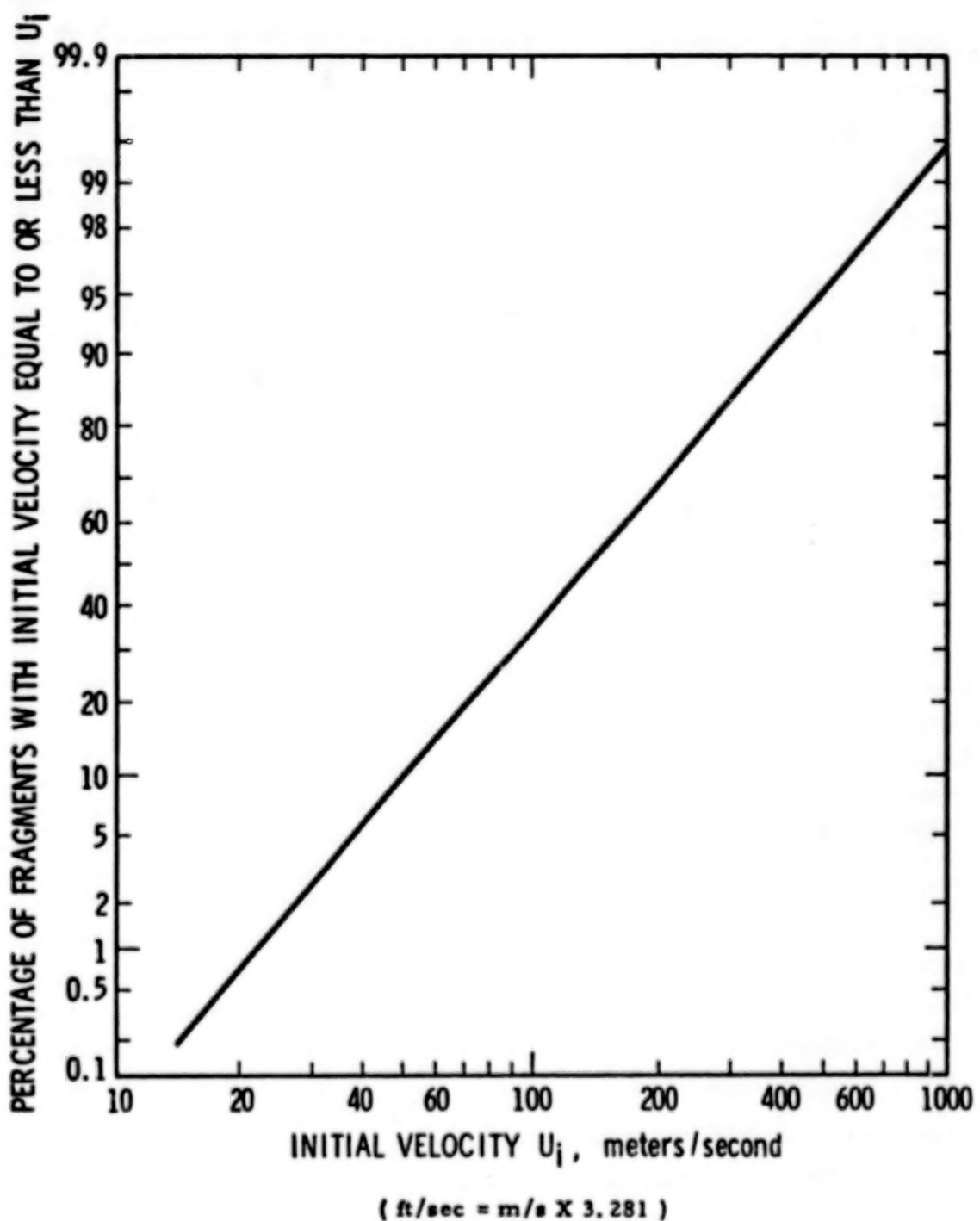


Figure 4-48. Initial Velocity Distribution,
CBGS, LO_2/LH_2

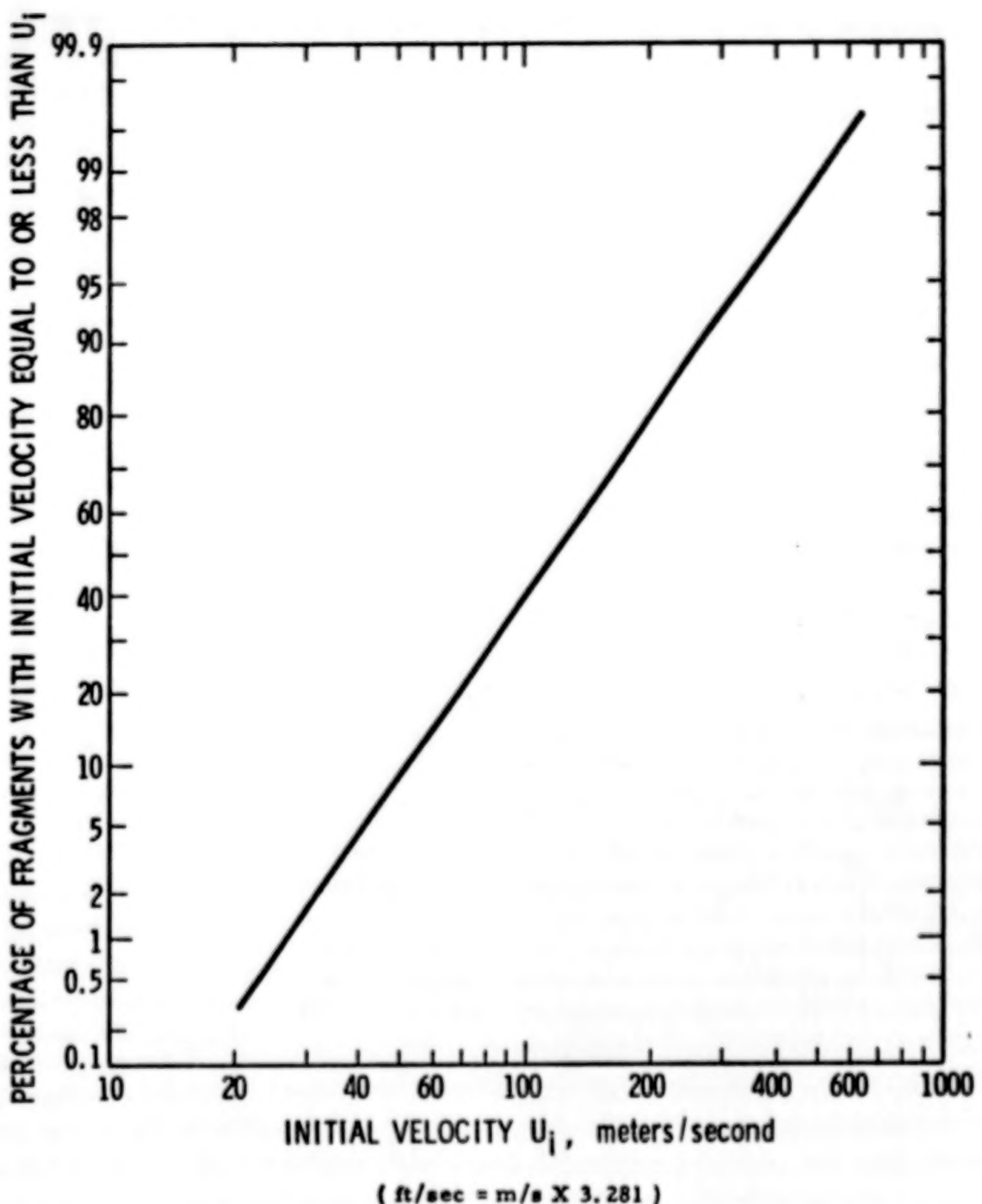


Figure 4-49. Initial Velocity Distribution,
CBGS, LO_2 /(RP-1)

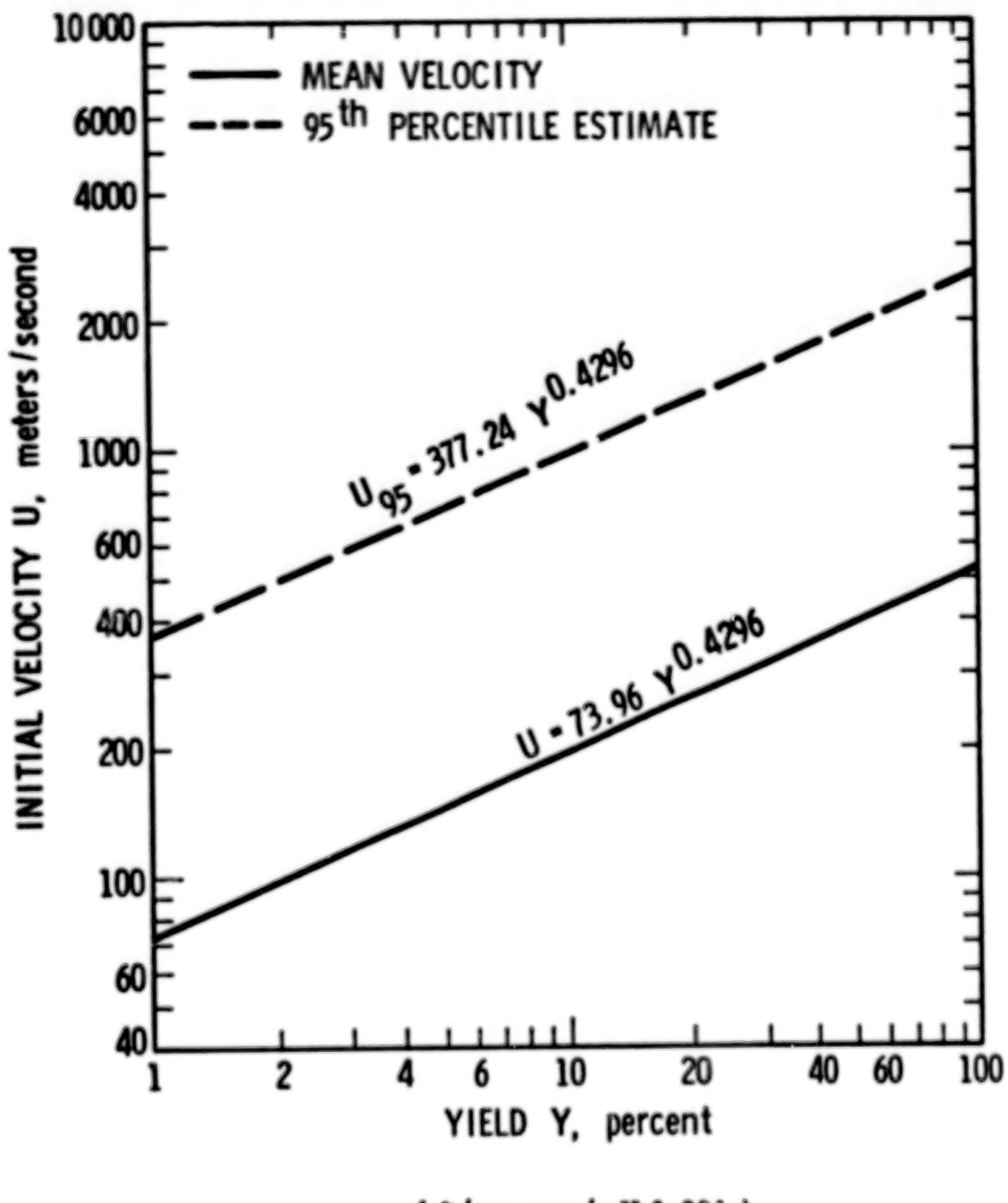


Figure 4-50. Initial Velocity Vs Yield,
CBM, LO₂/LH₂

distribution shown in Figure 4-46. From Figure 4-50, for a yield of 50%, we would expect that 95% of the fragments would have an initial velocity of 1900 m/s (6230 ft/sec) or less.

Details on the derivation of Figure 4-46 through 4-50 are given in Appendix 4F, Sections 4F-1 and 4F-2.

4-6 Fragment Mass Distribution

4-6.1 Propellant Explosions

From the data in Reference 3, the fragment mass (weight) followed log normal distributions. That is, the logarithms of the fragment masses followed a normal or Gaussian distribution.

Figure 4-51 and 4-52 present the fragment mass (W_i) distribution for two events taken from Reference 3. These were termed Events 1 and 2, and were Saturn IV confined-by-missile (CBM) explosions. Event 1 had a percent yield of 5%, and Event 2 a yield of 1.1%.

Figure 4-53 is an average of the distribution of Events 3, 4, and 5 from Reference 3. These events were spill tests using three tanks on 120 radials with $\text{LO}_2/\text{LH}_2/\text{RP-1}$, and mixing on the ground (CBGS). The rationale for averaging the distribution of these events is given in Appendix 4F.

These charts can be used in the same manner as Figures 4-46 through 4-50 are used for fragment initial velocity.

4-6.2 Gas Vessel Bursts

In experiments by Pittman, (Reference 4), five tanks (two cylinders and three spheres) were ruptured by increasing pressurization until rupture. The tanks were made of the same material (Ti 6 Al 4V alloy) with an ultimate stress (σ_u) of 1.05 GPa (150,000 psi). Pertinent data and calculated parameters for four of the tanks are given in Table 4-2, where \bar{W} is the geometric mean fragment mass, $W(T)$ is the tank weight, P is the burst pressure, and E_0 is the energy of detonation of 1 gram of TNT or 4190 J. It is interesting to note that the ratio [$W/W(T)$] doubles while the ratio (P/σ_u) changes by an order of magnitude. As shown in Appendix 4F, the fragment mass follows a log normal distribution. That is, the logarithms of the fragment masses follow a normal or Gaussian distribution.

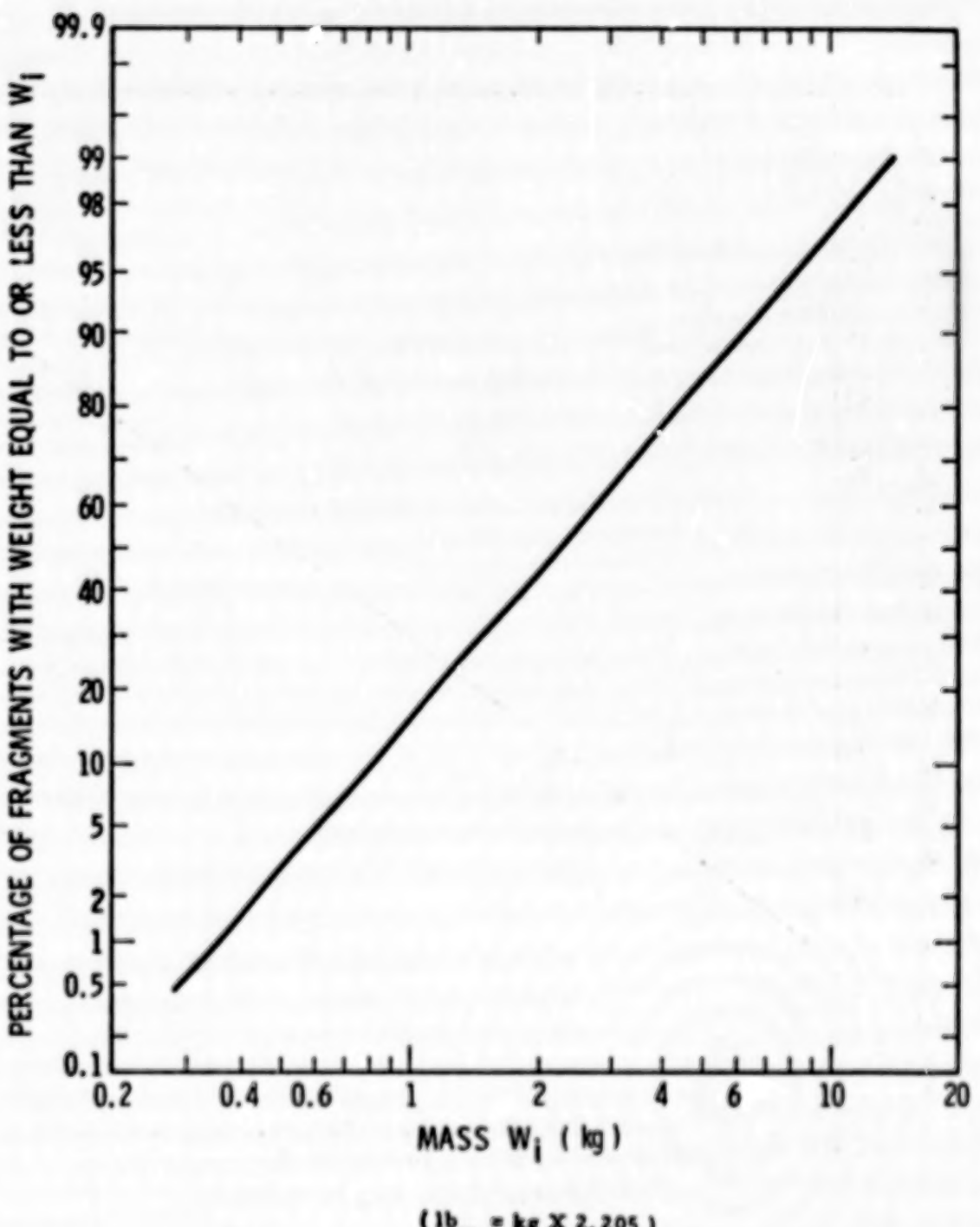


Figure 4-51. Fragment Mass Distribution from S IV CBM,
 LO_2/LH_2 , 5% Yield

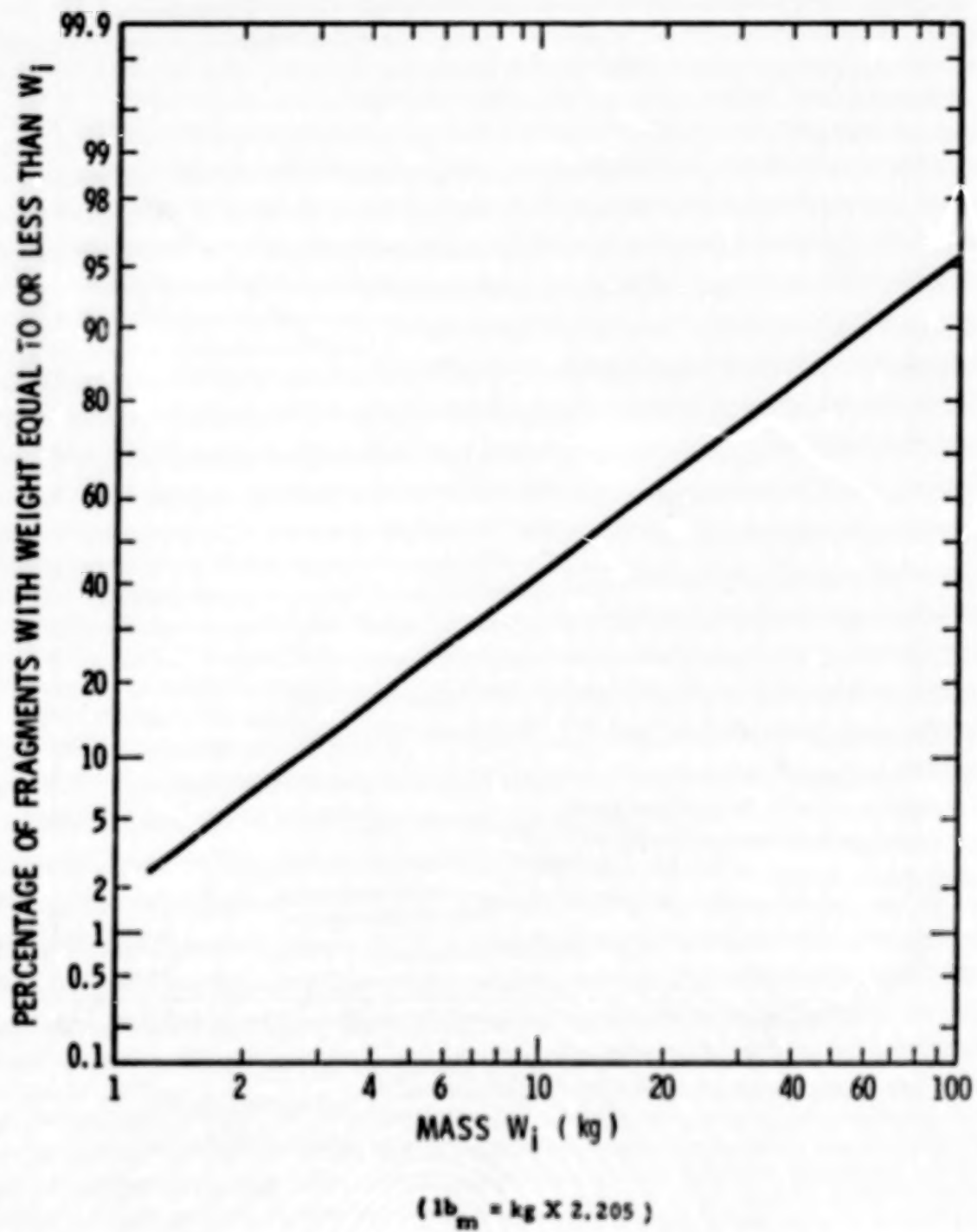


Figure 4-52. Fragment Mass Distribution from S IV CBM,
 $\text{LO}_2 / \text{LH}_2$, 1.1% Yield

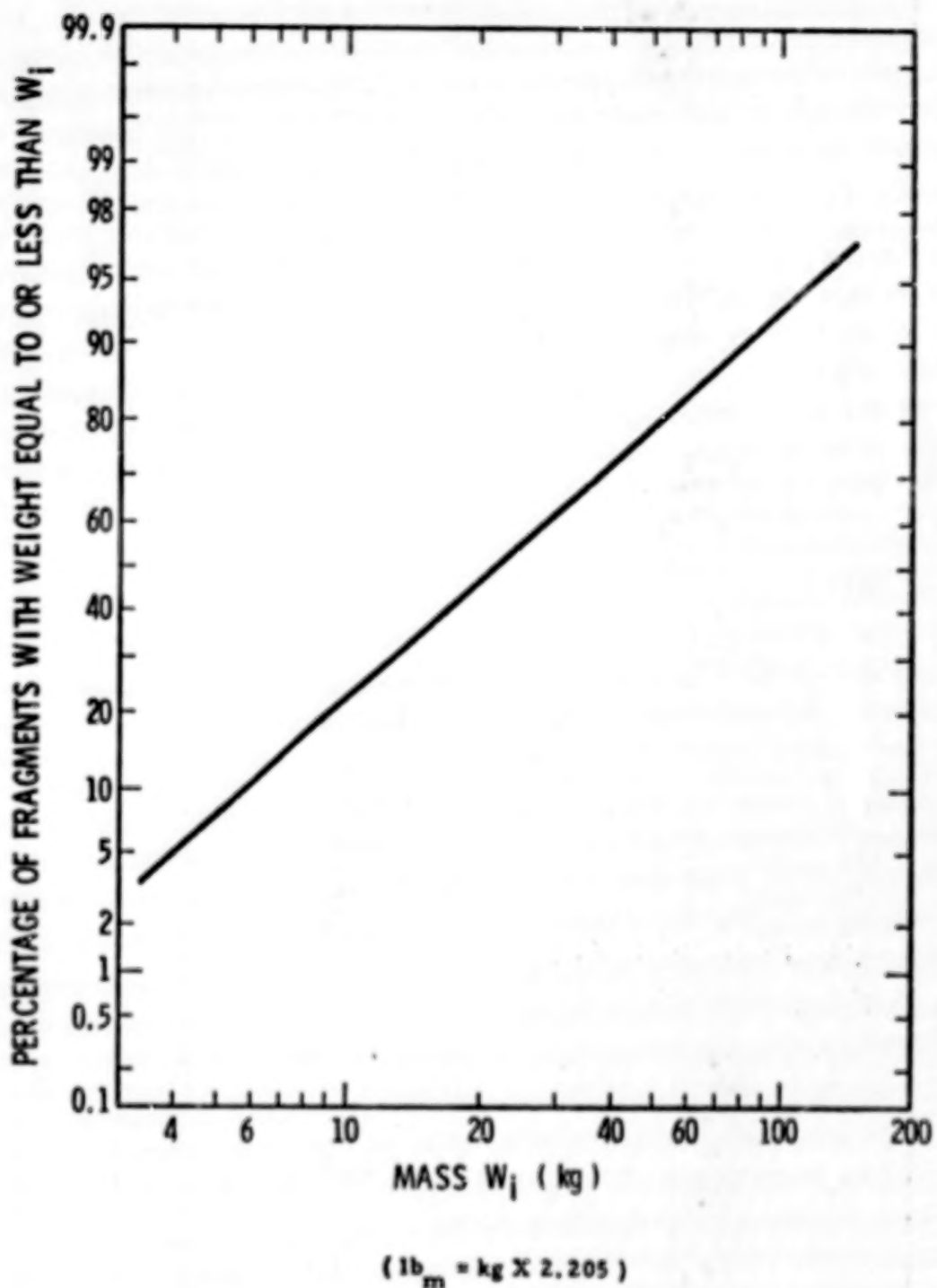


Figure 4-53. Average of Events 3, 4 and 5, Fragment Mass Distribution, CBGS

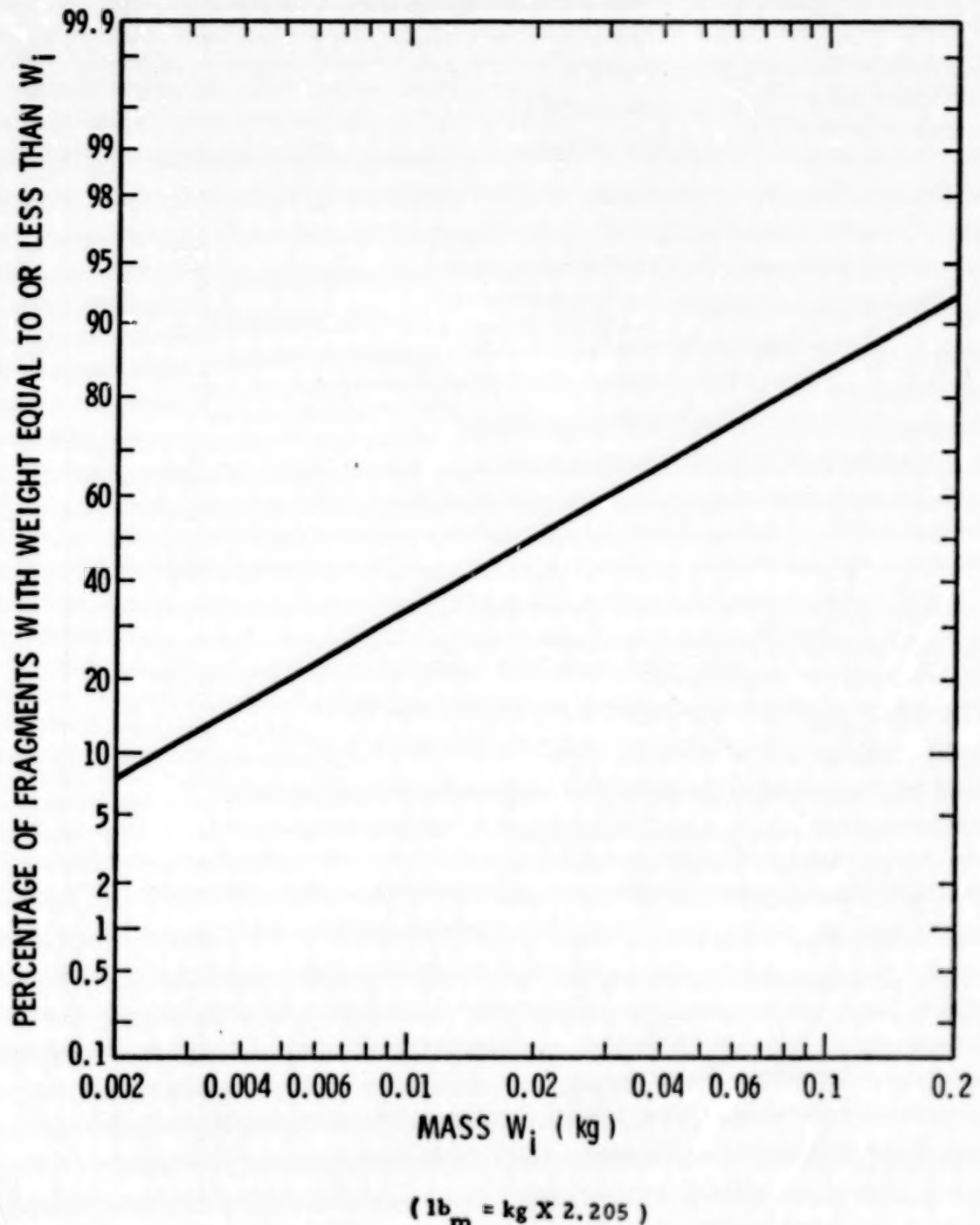


Figure 4-54. Fragment Mass Distribution for Small Cylinders, $V \approx 0.05 m^3$, $P \approx 4.2 MPa$

TABLE 4-2. PARAMETERS OF BURSTING TANKS

Tank #	Burst Pressure (P) MPa	Volume m ³	Mean Frag. Mass (W) kg	\bar{W} $W_{(T)}$	$\frac{P}{\sigma_u}$	$\frac{PV}{E_0}$
A	4.309	0.038	0.0195	0.00505	0.0042	39
B	4.137	0.048	0.0206	0.00444	0.0040	47
D	55.160	0.170	0.713	0.00917	0.0533	2,238
E	56.050	0.170	0.795	0.00964	0.0542	2,274

Tests for significant differences in means were made for Tanks A and B and for Tanks D and E. As shown in Appendix 4F no significant difference was found, so the fragment mass distributions of Tanks A and B and of Tanks D and E were averaged. These average distributions are shown in Figures 4-54 and 4-55. These figures can be used for fragment mass estimation in the same manner as Figures 4-46 through 4-50 are used for fragment initial velocity estimation.

Figure 4-56 is a plot of normalized yield (PV/E_0) versus mean fragment mass (W) for the four tanks. Two of the four points are clustered at each end of the range shown in Figure 4-56. Thus, the response in the middle of the range is still unknown. That is, the relationship of \bar{W} to PV/E_0 may not be linear on a log-log-scale. Data points in the mid-ranges are needed to confirm or deny the linear relationship.

With the risks described above, one can estimate mean fragment mass for any decided ratio of PV/E_0 up to 3 kg. One could then estimate the 90th percentile of the distribution (that value of fragment mass which would equal or exceed the mass of 90% of the fragments) by using the estimate of the standard deviation (S) from the average of Tanks D and E (1.695). An example follows:

For a burst pressure (P) of 10^8 Pa (14 000 psi) and a tank volume of 0.80 m^3 (2.83 ft^3)

$$PV = (.080)(10^8) = 8 \times 10^6$$

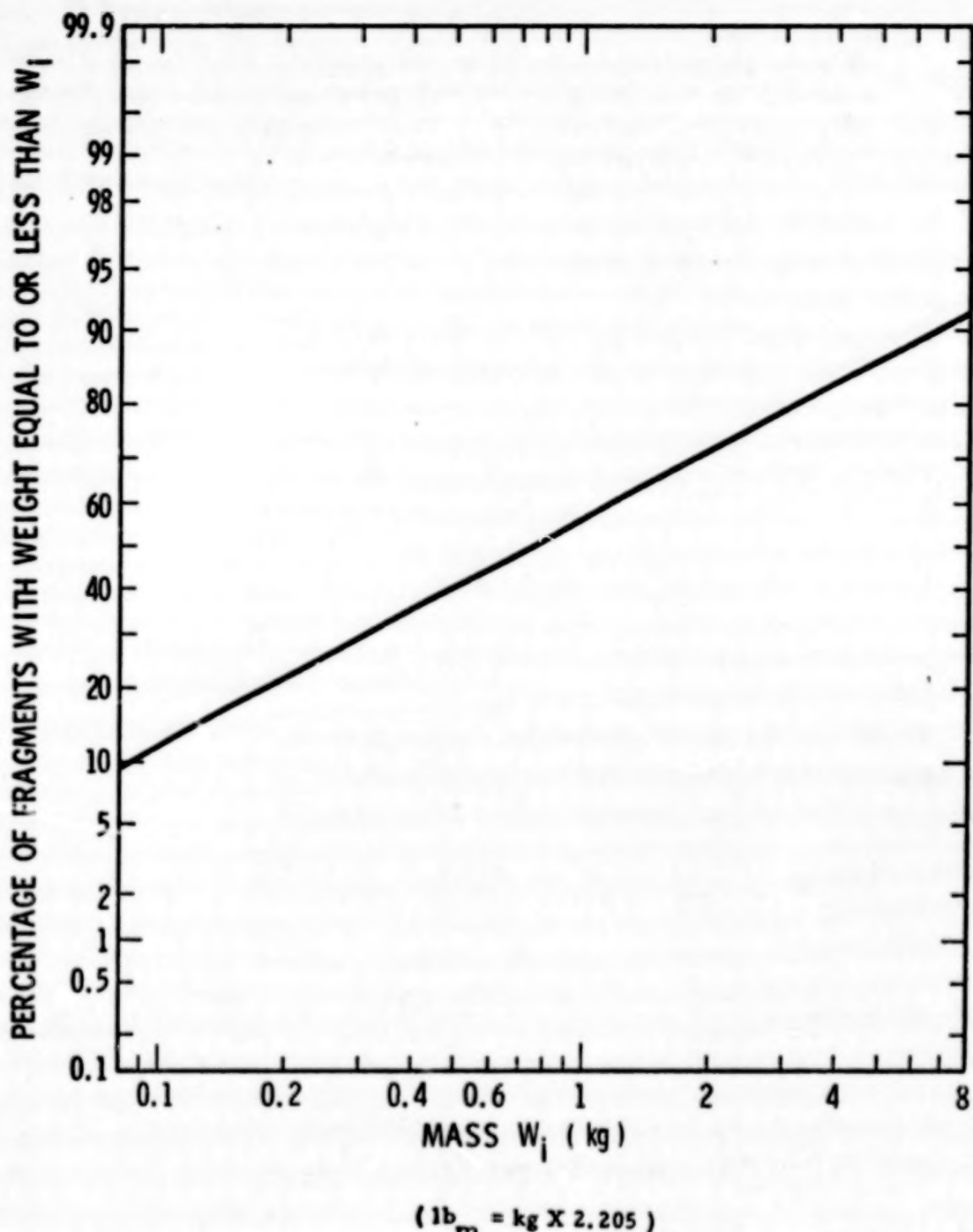


Figure 4-55. Fragment Mass Distribution for Titanium Alloy Spheres, $V \approx 0.170 \text{ m}^3$, $P \approx 55 \text{ MPa}$

$$\frac{PV}{E_0} = \frac{8,000,000}{4190} = 1900$$

Entering the chart (Figure 4-56) on the abscissa of 1900, reading up to the intersection of the line and over the ordinate, a value of 0.56 kg is obtained for mean fragment mass. Any Percentile (P_p) value of fragment mass can then be estimated by the formula:

$$P_p = \exp (\ln \bar{W} + K s),$$

where \bar{W} is the mean mass, s is the estimate for the standard deviation, and k is a value from the normal distribution table. Typical values are shown in Table 4-3.

For the 90th percentile,

$$\begin{aligned} P_{90} &= \exp [\ln 0.56 + 1.28 \cdot 1.695] \\ &= \exp (1.590) = 4.903 \text{ kg (10.79 lb}_m\text{)} \end{aligned}$$

Thus, one would expect that 90% of the fragments would have a mass equal to or less than 4.903 kg (10.79 lb_m).

TABLE 4-3. VALUES OF k OF PERCENTILES
OF THE NORMAL DISTRIBUTION

Percentile	99	95	90	80	70
k	2.33	1.65	1.28	0.84	0.53

4-7 Probability of Fragment Arrival Versus Range

4-7.1 Propellant Explosions

From Reference 3, Figure 4-57 is a representation of fragment distance versus percent yield, with a 95 percent confidence interval. The derivation of this figure is explained in Appendix 4F.

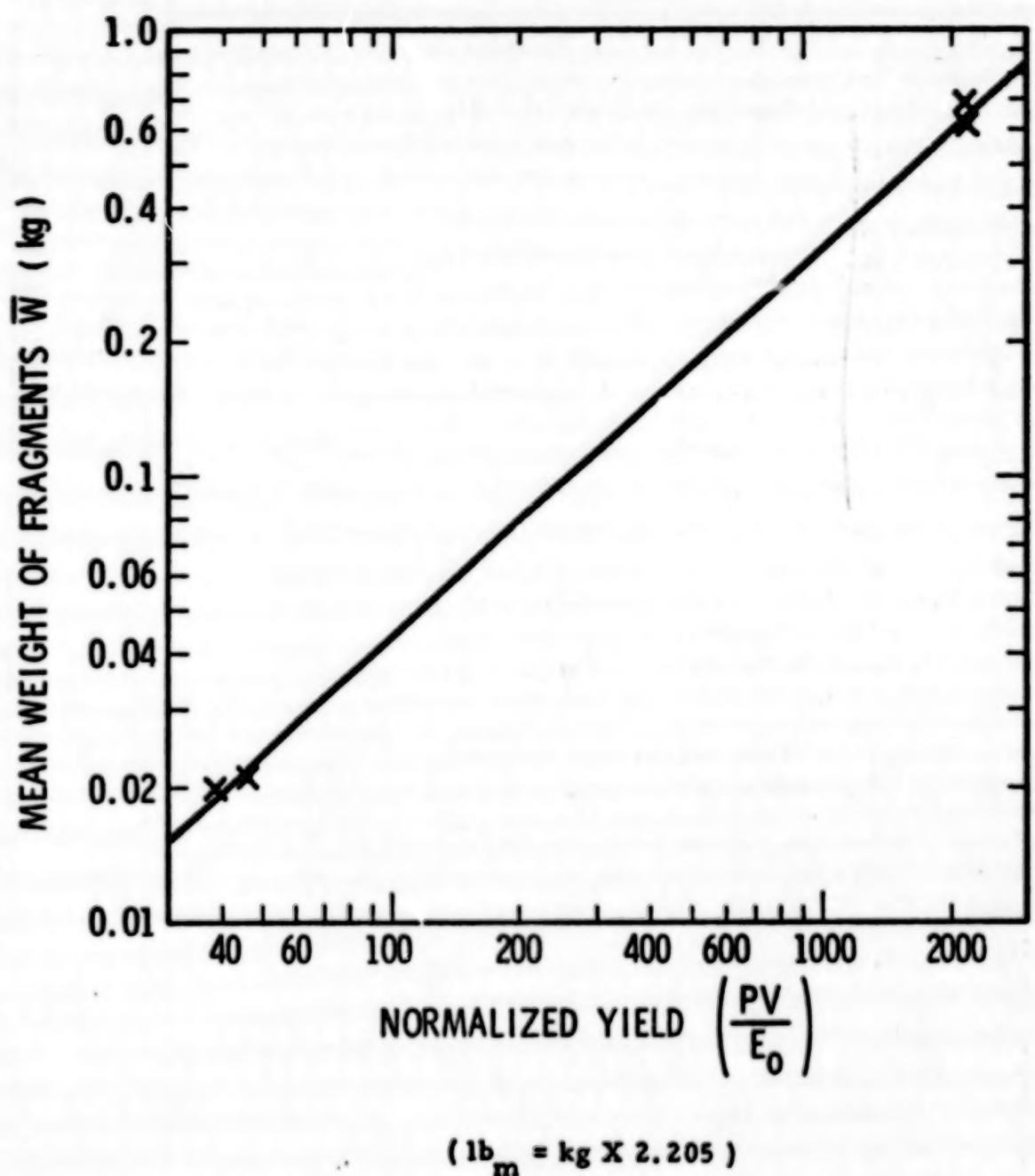


Figure 4-56. Normalized Yield Vs Mean Fragment Mass
for Bursting Tanks

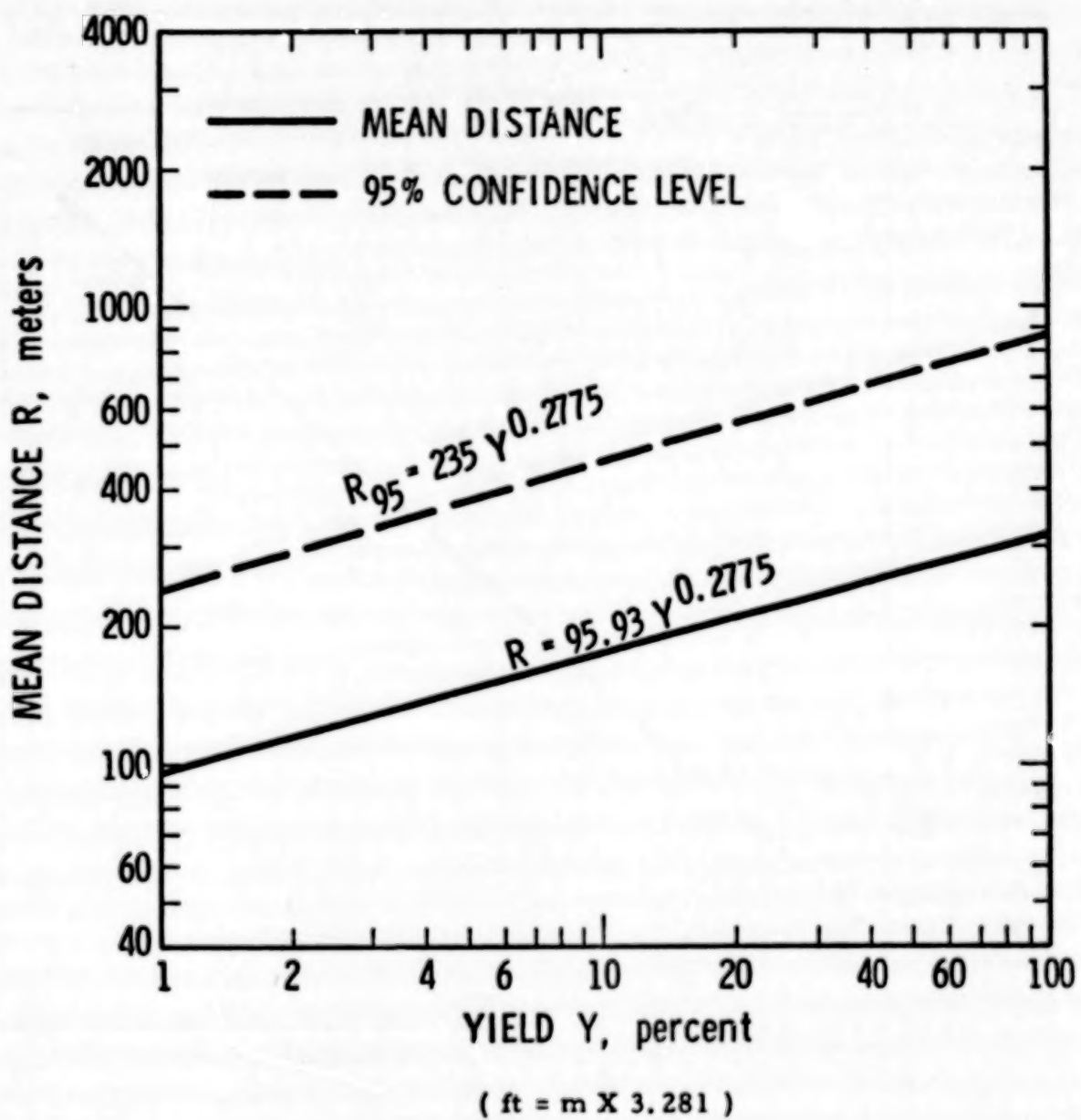


Figure 4-57. Fragment Range Vs Yield, Propellant Explosions

Figure 4-57 can be used to estimate the mean distance of a fragment range for any given yield (percent). Also, one can obtain a 95% confidence level on maximum distance. For example, given a yield of 20%, one would expect that 95% or more of the fragments would fall within 560 meters of the explosion center.

4-7.2 Gas Vessel Bursts

In the experiment by Pittman (Reference 4), the fragments from the bursting tanks were partially contained in a circular area with a 20 foot radius with 8 ft high walls on the perimeter. Thus, the data on the fragment range was severely biased.

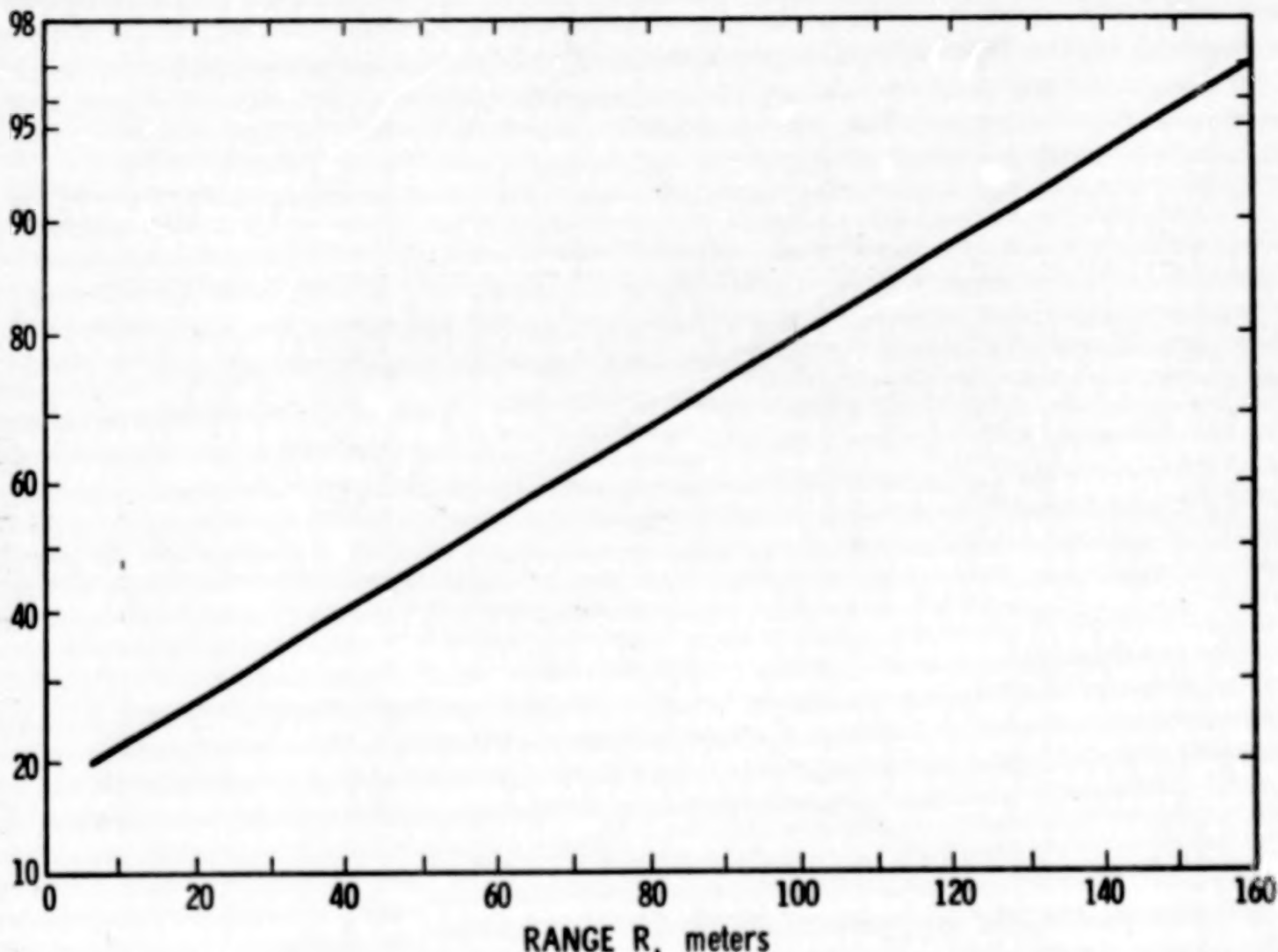
However, by exercising the computer programs (Appendix 4E) for fragment range as a function of fragment mass, drag, and flight angle, a distribution of fragment ranges was obtained for each of four tanks. These distributions were well fitted to members of the normal of Gaussian family.

Then, "t" tests for significant difference in mean ranges for Tanks A and B and for Tanks D and E were made. In the statistical sense, there were no significant differences in means between Tanks A and B, and between Tanks D and E.

Figures 4-58 and 4-59 present these simulated fragment range distributions for Tanks A and B and for Tanks D and E respectively. These charts can be used to estimate fragment range for similar gas vessels.

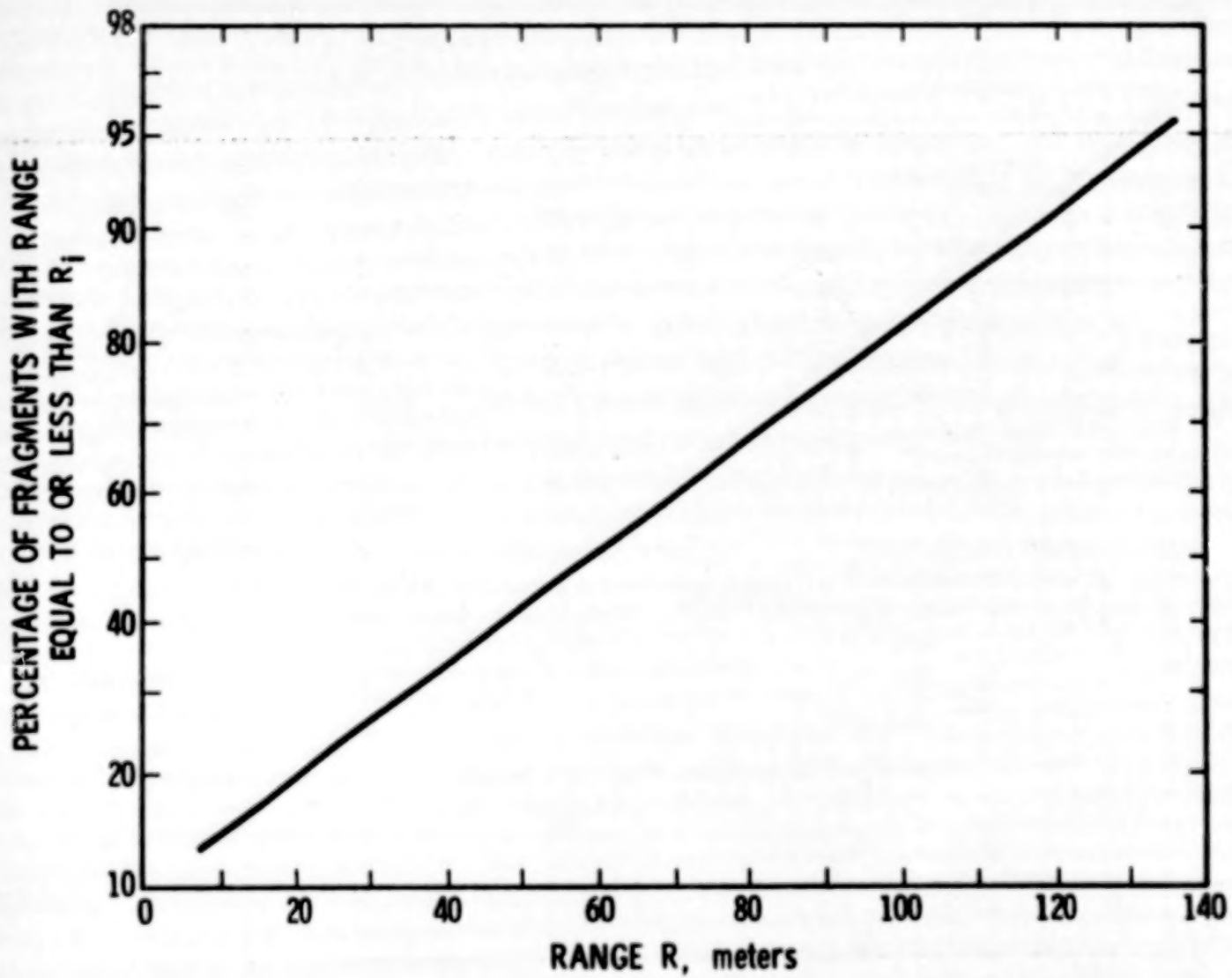
Complete details on the derivation of the simulated fragment range, goodness of fit tests, and "t" tests are given in Appendix 4F.

PERCENTAGE OF FRAGMENTS WITH RANGE
EQUAL TO OR LESS THAN R_i



(ft = m X 3.281)

290
Figure 4-58. Fragment Range Distribution for Small
Cylinders, $V = 0.05$ m, $P = 4.2$ MPa



(ft = m X 3.281)

Figure 4-59. Fragment Range Distribution for Spheres.
 $V = 0.170 \text{ m}^3$, $P = 55 \text{ MPa}$

LIST OF REFERENCES

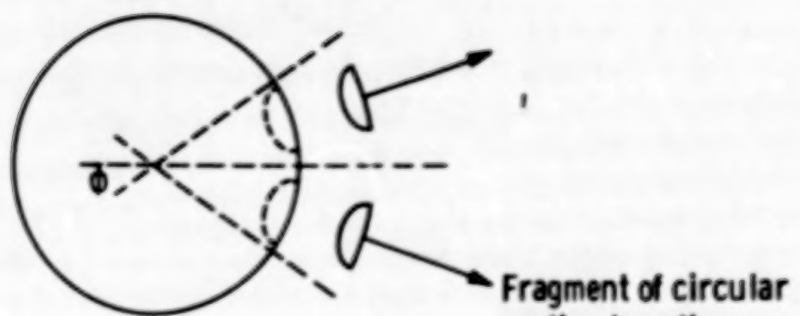
1. Boyer, D. W., H. L. Brode, I. I. Glass, and J. G. Hall, Blast From a Pressurized Sphere, UTIA Report No. 48, Institute of Aerophysics, University of Toronto, 1958.
2. Taylor, D. B. and C. F. Price, "Velocities of Fragment From Bursting Gas Reservoirs," ASME Transactions, Journal of Engineering for Industry, November 1971.
3. Baker, W. E., V. B. Parr, R. L. Bessey, and P. A. Cox, "Assembly and Analysis of Fragmentation Data for Liquid Propellant Vessels," NASA Report CR-134538, January 1974.
4. Pittman, J. F., "Blast and Fragment Hazards From Bursting High Pressure Tanks", Naval Ordnance Laboratory Report NOLTR 72-102, May 1972.

APPENDIX IV.A

METHODS FOR ESTIMATING FRAGMENT INITIAL VELOCITIES

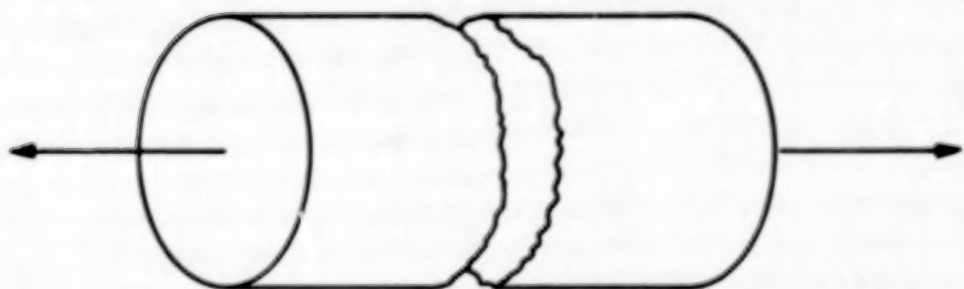
Figure 4A-1 shows the conceptual models used in analyzing bursting confinement vessels to obtain estimates of initial fragment velocities. The spherical confinement vessel case has been discussed in References 1 and 2. For this case the sphere is conceived of as fragmenting into n fragments of circular projection, and the fragments travel in a radial direction without tumbling. The energy of the confined gas is partitioned between the kinetic energy of the fragment, the energy of the gas escaping between the cracks between the fragments as they are formed, and the energy of the expansion of the internal gas. The equations of motion for the fragments are developed in Reference 2, and a computer code SPHER has been developed for the solution of these nonlinear differential equations describing the fragment motion. Solution of the differential equations is accomplished by use of Runge-Kutta integration techniques. Program SPHER appears at the end of this appendix with a description of the input-output variables.

Figure 4A-1 also shows the conceptualization of a cylinder fragmenting into n fragments. For this case, the fragments are considered to be strips which move radially from the center of the cylinder. Motion of the cylinder ends is not considered. Figure 4A-2 shows the geometric parameters of the cylinder used in the analysis. A cylinder of length L and radius R is assumed to burst into n strip fragments of width d and thickness th . A cross-section of each strip is a segment of the cross-section of the cylinder having a segment height of h and segment diameter d . In the following analysis, the projected area of each fragment is obtained from the surface area and the initial subtended angle of the fragment at the center of the cylinder, with the result being Equation (4A-11). The area of a crack about any fragment at any time is obtained by assuming the cracks only form lengthwise along the cylinder, and by obtaining an equation for the width of these cracks in terms of the initial radius of the cylinder and the radial distance r , the fragment has traveled at any time, t . The equation for fragment area is given in Equation (4A-14). One of the differential equations of motion derived on the basis of an adiabatic gas expansion and radial motion of the fragments is the same for this analysis as it was for the sphere, as are the general equations used for nondimensionalization; see Equation (4A-15). A second differential equation, Equation (4A-35), is obtained from the perfect gas assumption, an equation for the mass flow of gas through the cracks formed between the fragments [Equation (4A-19)], and cylinder geometry considerations. Values for the nondimensional constants are also obtained through these considerations and are given in Equations (4A-36) and (4A-37).

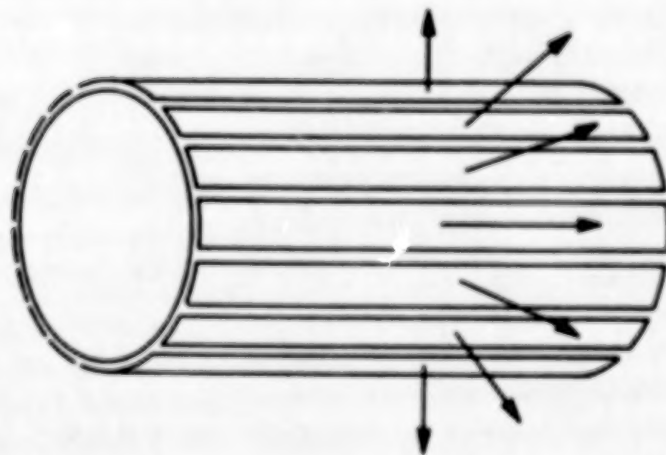


a. n - Fragment sphere

Fragment of circular
section traveling
radially

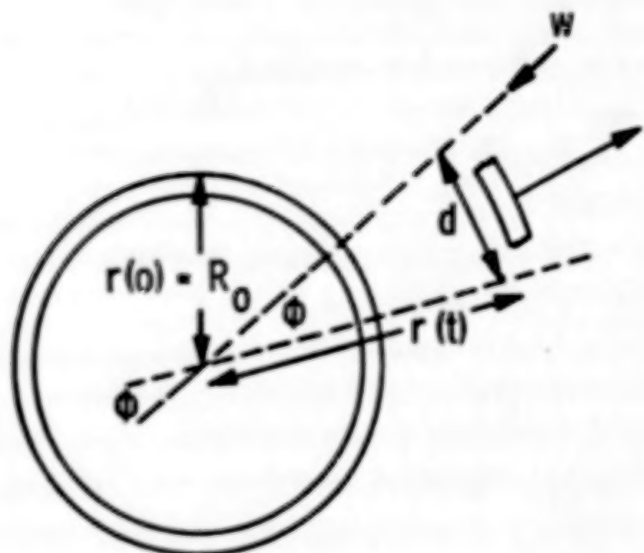


b. 2-Fragment cylinder

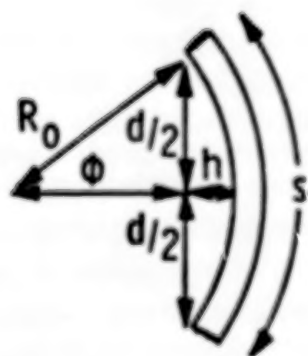


c. n - Fragmenting cylinder

Figure 4A-1. Conceptual Models of Bursting
Confinement Vessels



a. Cylinder cross section



b. Strip fragment cross section

Figure 4A-2. Geometric Parameters for a Fragmenting Cylinder

This analysis does not take into account the stored energy (strain energy) in the walls of the container immediately prior to burst. The strain energy for the spherical containment vessel case can be shown to be given approximately by:

$$SE = 2 \pi R^2 h (1 - v)^2 \frac{\sigma_y^2}{E} \quad (4A-1)$$

where

σ_y = the stress in the container wall

SE = the strain energy stored in the vessel

R = the sphere radius before burst

h = the sphere wall thickness

v = Poisson's ratio for the material

E = the bulk modulus for the material

This equation may be written:

$$SE = \pi R^4 P^2 \frac{(1 - v)^2}{(2 Eh)} \quad (4A-2)$$

where P is the pressure of the confined gas, by substitution of the approximate relation,

$$2h\sigma_y = RP \quad (4A-3)$$

The stored energy in the confined gas is

$$GE = \frac{4\pi PR^3}{3(\gamma - 1)} \quad (4A-4)$$

Thus, the ratio, e, of the strain to stored energy is

$$e = \frac{3RP(\gamma - 1)(1 - v)^2}{8hE} \quad (4A-5)$$

For a steel container pressurized with air having $R/h \leq 100$,

$$\begin{aligned}
 e &= 1.45 \times 10^{-3} P \text{ (kg/cm}^2\text{)} \\
 &\approx 1.03 \times 10^{-4} P \text{ (psi)} \\
 &\approx 1.48 \times 10^{-8} P \text{ (Pa)}
 \end{aligned}$$

Thus, even for this very high radius-to-thickness ratio, pressure would have to exceed 10^6 Pa to produce significant strain energy (1%) relative to the total energy available. We therefore conclude that, as a rule, strain energy can be neglected. This is emphatically not true when the vessel rupture process is similar to that of a high explosive bomb casing burst, where considerable expansion of the case occurs before rupture (up to 1.8 radii).

A computer code for the simultaneous solution of nonlinear differential equations [Equations (4A-15) and (4A-35)] (CYLIN) has been developed. This code, similar to code SPHER, uses the Runge-Kutta integration technique for the solution of the differential equations. The code, along with definitions for its input and output parameters, is given at the end of the appendix. Figures 4A-3 and 4A-4 show comparative results from the two computer codes. Figure 4A-4 shows the maximum fragment velocities predicted for spheres and cylinders of equivalent volume as a function of the number of fragments assumed. For all cases, the value for maximum fragment velocity becomes a constant when more than about 10 to 30 fragments are assumed. In general, for equal volumes and radii, the sphere fragment velocities are less than the cylinder fragment velocities. This may be because of the assumption that no energy is used in accelerating the ends of the cylinders. Thus, more energy is available for the fragments formed from the cylindrical wall. Figure 4A-3 gives comparative results for maximum fragment velocities for the two geometric cases versus mass ratio for gases of various specific heat ratios. Again, the predicted cylindrical velocities are higher than that of the spherical velocities.

Some empirical verification of the results from program SPHER is given in Appendix IV.B. Very little data are available, however, to verify this analysis. Although there are data available for fragment velocities from cylindrical confinement vessels, most of these data are from bursting artillery shells. The processes involved in the fragmentation of these shells are so dynamic that the shell may expand up to twice its diameter before cracks are formed between the fragments. Our analysis would not be applicable to this kind of event. Our analysis assumes a relatively brittle confinement vessel which does not expand significantly prior to the time that cracks are formed between the fragments. This would be the case for confinement vessels which are slowly pressurized, as opposed to the highly dynamic situation existing when a high explosive is detonated internal to the confinement vessel.

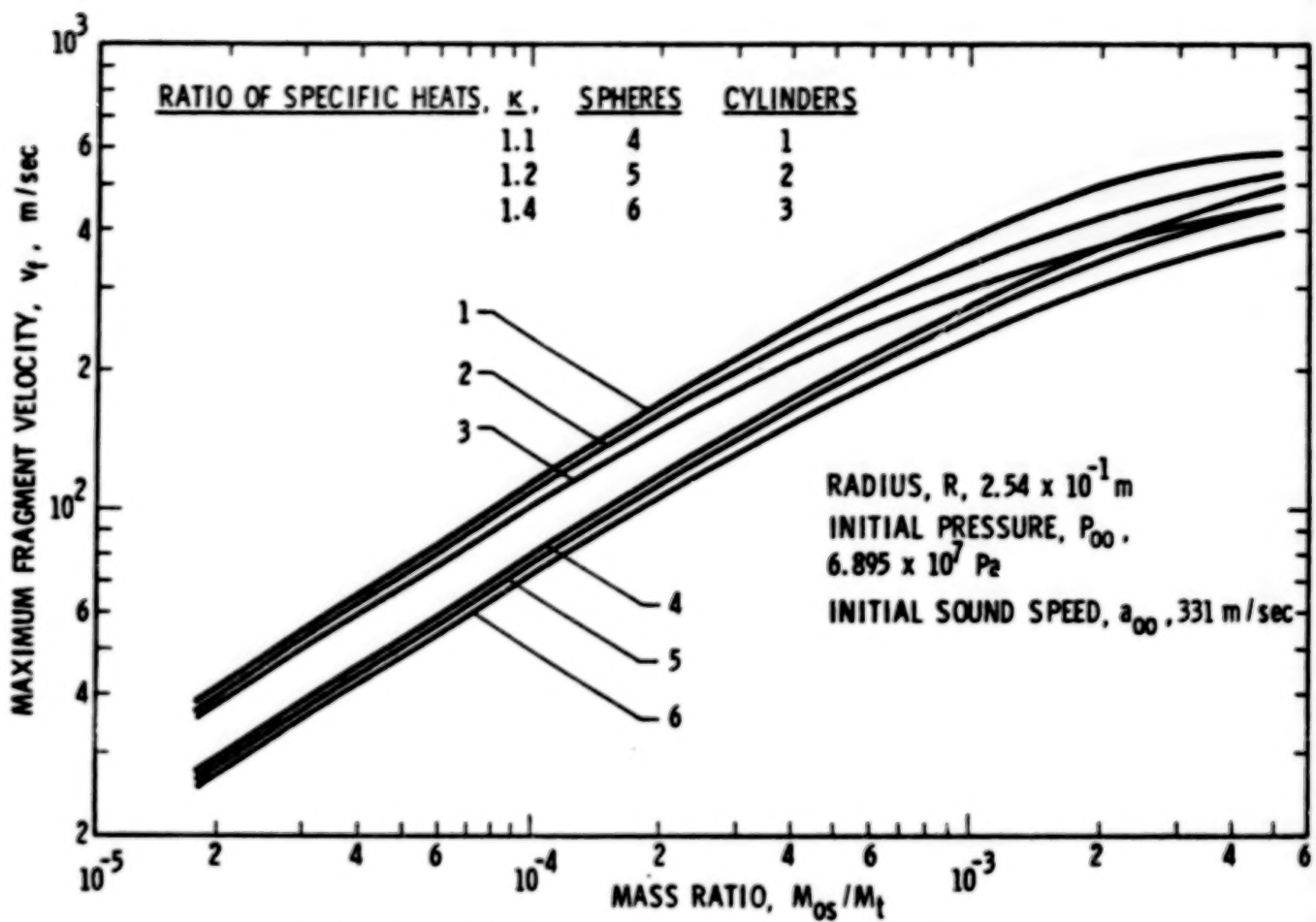


Figure 4A-3. Maximum Fragment Velocity as a Function of Mass Ratio for Spheres and Cylinders of Equivalent Volume

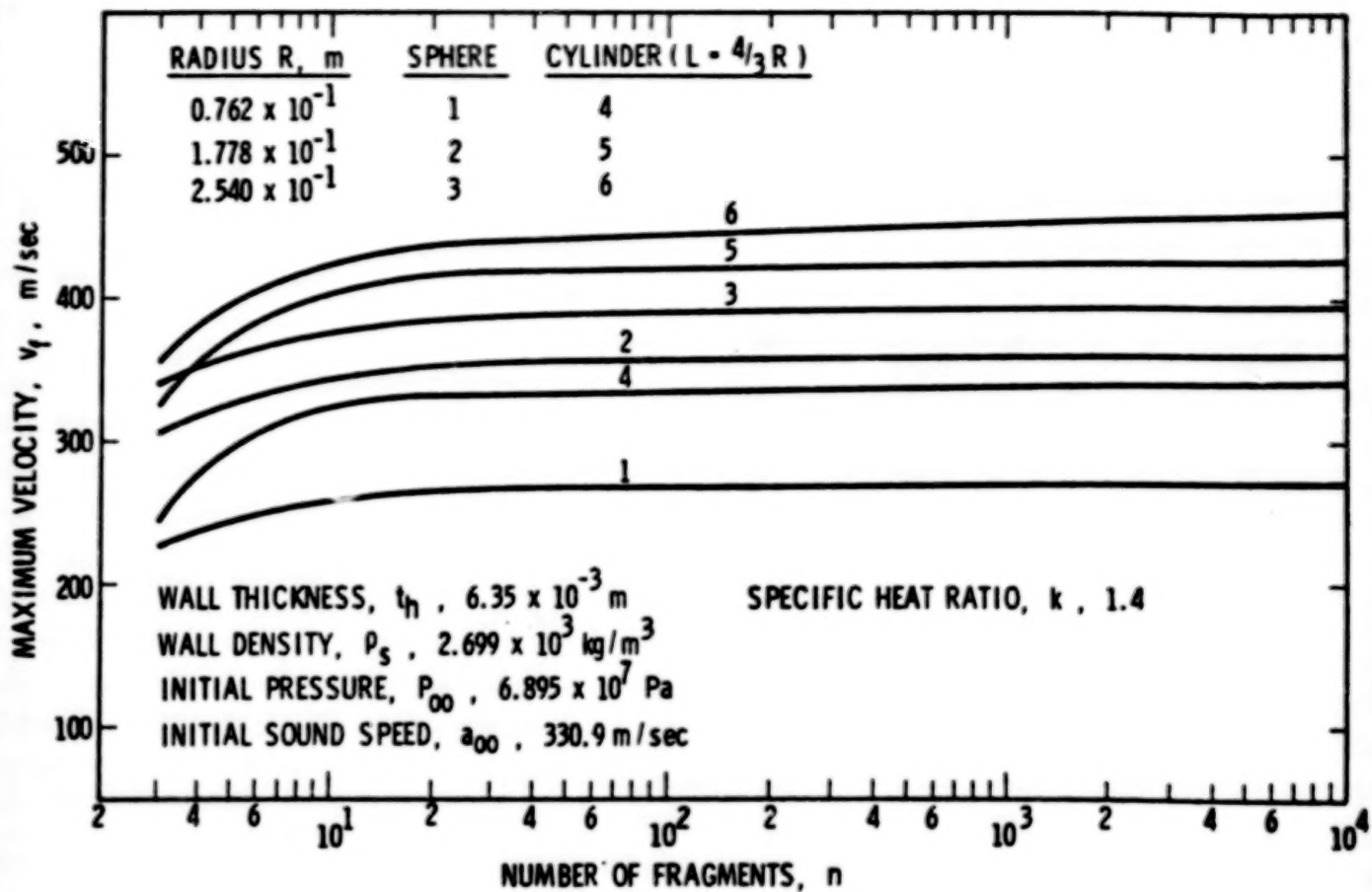


Figure 4A-4. Maximum Fragment Velocity as a Function of Number of Fragments for Equivalent Volume Cylinders and Spheres

299

Analysis for a Cylindrical Shell Fragmenting Into Strip Fragments

Variable List:

- A - term in Equation (4A-16)
- A_f - fragment area
- a_{∞} - sound speed in confined gas, $\tau = 0$
- a_* - critical sound speed in mass flow equation
- B - term in Equation (4A-16)
- C - term in Equation (4A-16)
- D - term in Equation (4A-16)
- d - width of fragment segment
- F - fragment projected area
- g - nondimensionalized displacement of a fragment
- h - segment height (see Figure 4A-2)
- k - mass flow rate coefficient
- L - cylinder length
- M - mass of contained gas at any instant, τ
- M_f - fragment mass
- M_t - cylindrical shell mass
- n - number of fragments
- P - crack perimeter about a fragment
- P_* - nondimensionalized pressure
- P_0 - pressure of confined gas at any instant, τ

- P_{∞} - initial pressure of confined gas
- R - initial cylinder radius
- r - fragment displacement at any instant, τ
- s - segment length
- T_0 - temperature of confined gas at any instant, τ
- t_h - shell thickness
- V_0 - volume of confined gas at any instant, τ
- V_s - volume of shell material
- w - crack width
- x - nondimensionalizing constant for displacement
- α - nondimensional constant
- β - nondimensional constant
- θ - nondimensionalizing constant for time
- θ - angle subtended at the center of the cylinder by a fragment
 $\tau = 0$
- κ - ratio of specific heats for confined gas
- ρ_0 - confined gas density at any instant, τ
- ρ_* - critical density of gas in mass flow equation
- ρ_s - density of shell material
- τ - time
- ξ - nondimensionalized time

Prime denotes derivatives with respect to ξ .

From considerations of the cylinder geometry (see Figure 4A-2):

$$M_t = \rho_s V_s = \pi \rho_s L \left[(R + t_h)^2 - R^2 \right] \quad (4A-6)$$

$$A_f = \frac{2\pi RL}{n} \quad (4A-7)$$

$$F = L \cdot d = L \cdot 2 \left[R^2 - (R - h)^2 \right]^{1/2} \quad (4A-8)$$

From Figure 4A-2:

$$A_f = L \cdot S, \quad S = \frac{\theta}{2\pi} \cdot 2\pi R = \theta R, \quad \theta = \cos^{-1}\left(\frac{R-h}{R}\right)$$

Therefore,

$$A_f = L \cdot R \cdot \cos^{-1}\left(\frac{R-h}{R}\right) \quad (4A-9)$$

From Equations (4A-6) and (4A-9),

$$h = R \left(1 - \cos \frac{2\pi}{n} \right) \quad (4A-10)$$

From Equations (4A-10) and (4A-8),

$$F = 2L \cdot R \left[1 - \left(\cos \frac{2\pi}{n} \right)^2 \right]^{1/2} \quad (4A-11)$$

The crack area at any time τ for fragment i is

$$(Pw)_i = 2L \cdot w \quad (4A-12)$$

From Figure 4A-2, it may be seen that

$$w = \theta [r(\tau) - R] = \frac{2\pi}{n} [r(\tau) - R] \quad (4A-13)$$

From Equations (4A-12) and (4A-13),

$$(Pw)_i = \frac{4\pi L}{n} \cdot [r(\tau) - R] = \frac{4\pi L \cdot R}{n} \left(\frac{r(\tau)}{R} - 1 \right) \quad (4A-14)$$

From Reference 2, Equations (4A-19), (4A-20), and (4A-21),

$$g'' = n P_* \left[1 - \frac{(g')^2}{(P_*)^{\kappa-1/\kappa}} \right]^{\kappa/\kappa-1}$$

$$x = \frac{M_t a_{oo}^2}{F P_{oo}} \left(\frac{2}{\kappa-1} \right)^{1/2} \quad (4A-15)$$

$$\theta = \frac{M_t a_{oo}}{F P_{oo}} \left(\frac{2}{\kappa-1} \right)^{1/2}$$

From differentiation of the ideal gas equation,

$$\frac{d P_o(\tau) / d \tau}{P_o(\tau)} = \frac{1}{\rho_o(\tau) V_o(\tau)} \frac{d M(\tau)}{d \tau} + \frac{1}{T_o(\tau)} \frac{d T_o(\tau)}{d \tau}$$

$$= \frac{1}{V_o(\tau)} \frac{d V_o(\tau)}{d \tau} \quad (4A-16)$$

$$A = B + C - D$$

Using the variable changes $P_o(\tau) = P_{oo} \cdot P'_*(\xi)$ t $\tau = \theta \xi$, term A becomes

$$A = \frac{1}{\theta} \frac{P'_*(\xi)}{P'_*(\xi)} \quad (4A-17)$$

and using these variable changes with the ideal gas law, term C becomes

$$C = \frac{1}{\theta} \frac{\kappa-1}{\kappa} \frac{P'_*}{P'_*} \quad (4A-18)$$

The confined gas mass flow rate through the cracks is [from Equation (4A-12), Reference 2]

$$\frac{d M(\tau)}{d \tau} = - k \rho_* a_* P_w \quad (4A-19)$$

The total crack area is

$$P_w = \sum (P_w)_i = n(P_w)_i$$

and from Equations (4A-14) and (4A-19)

$$\frac{dM(\tau)}{d\tau} = -k \rho_* a_* 4\pi L \cdot R \left(\frac{r(\tau)}{R} - 1 \right) \quad (4A-20)$$

But from the cylindrical geometry

$$V_o(\tau) = \pi r^2(\tau) \cdot L \quad (4A-21)$$

Thus, from Equations (4A-16), (4A-20) and (4A-21), term B becomes

$$\begin{aligned} B &= \frac{1}{\rho_o(\tau) V_o(\tau)} \frac{dM(\tau)}{d\tau} \\ &= \frac{1}{\rho_o(\tau) \cdot \pi r^2(\tau) \cdot L} \cdot \left[-k \rho_* a_* 4\pi L \cdot R \left(\frac{r(\tau)}{R} - 1 \right) \right] \\ &= -\frac{4k \rho_* a_* R}{\rho_o(\tau)} \left[\frac{1}{R r(\tau)} - \frac{1}{r^2(\tau)} \right] \end{aligned} \quad (4A-22)$$

From standard one-dimensional flow relationships

$$\rho_* = \rho_o(\tau) \left(\frac{2}{\kappa + 1} \right)^{1/\kappa - 1} \quad (4A-23)$$

$$a_* = a_o(\tau) \left(\frac{2}{\kappa + 1} \right)^{1/2}$$

Assuming an adiabatic gas expansion

$$a_o(\tau) = a_{oo} P_*^{\kappa-1/2\kappa}$$

and nondimensionalizing displacement and time

$$r(\tau) = X g(\xi) \quad \tau = \theta \xi \quad (4A-24)$$

we obtain from Equations (4A-22), (4A-23) and (4A-24)

$$B = -4k \left(\frac{2}{\kappa+1} \right)^{1/\kappa-1} \left(\frac{2}{\kappa+1} \right)^{1/2} a_{oo} P_*^{\kappa-1/2\kappa} R \left[\frac{1}{R X g(\xi)} - \frac{1}{X^2 g(\xi)^2} \right] \quad (4A-25)$$

$$= \frac{-4ka_{oo}P_*^{\kappa-1/2\kappa}R \left(\frac{2}{\kappa+1} \right)^{\kappa+1/2(\kappa-1)}}{X^2 g^2(\xi)} \left[\frac{Xg(\xi)}{R} - 1 \right] \quad (4A-26)$$

From Equation (4A-16)

$$D = \frac{1}{V_o(\tau)} \frac{dV_o(\tau)}{d\tau} \quad (4A-27)$$

Differentiating Equation (4A-21) gives

$$\frac{dV_o(\tau)}{d\tau} = \frac{d\pi r^2(\tau) \cdot L}{d\tau} = \pi L \cdot 2r(\tau) \cdot \frac{dr(\tau)}{d\tau} \quad (4A-28)$$

Thus,

$$D = \frac{1}{V_o(\tau)} \frac{dV_o(\tau)}{\tau} = \frac{2}{r(\tau)} \frac{dr(\tau)}{d\tau} \quad (4A-29)$$

Changing the variable with Equation (4A-24), term D becomes

$$D = \frac{2}{X g(\xi)} \frac{X}{\theta} g'(\xi) = \frac{2}{\theta} \frac{g'(\xi)}{g(\xi)} \quad (4A-30)$$

From Equations (4A-16), (4A-17), (4A-18), (4A-26), and (4A-30),

$$\frac{1}{\theta} \frac{P'_*}{P_*} = \frac{4ka_{oo}P_*^{\kappa-1/2\kappa}R \left(\frac{2}{\kappa+1} \right)^{\kappa+1/2(\kappa-1)}}{X^2 g^2} \left(\frac{X}{R} \cdot g - 1 \right)$$

(continued)

$$+ \frac{1}{\theta} \left(\frac{\kappa - 1}{\kappa} \right) \frac{P'_*}{P_*} - \frac{2}{\theta} \frac{g'}{g} \quad (4A-31)$$

$$\frac{P'_*}{\theta \kappa P_*} = \frac{4 k a_{oo} P_*^{\kappa-1/2\kappa} R \left(\frac{2}{\kappa+1} \right)^{\kappa+1/2(\kappa-1)}}{X^2 g^2} - \left(\frac{X}{R} g - 1 \right) - \frac{2}{\theta} \frac{g'}{g} \quad (4A-32)$$

Multiplying through Eq. (4A-32) by $\theta \kappa g^2$

$$\begin{aligned} \frac{P'_*}{P_*} g^2 &= - \frac{4 k \kappa \theta a_{oo} g \left(\frac{2}{\kappa+1} \right)^{\kappa+1/2(\kappa-1)}}{X} P_*^{\kappa-1/2\kappa} \\ &+ \frac{\theta 4 k \kappa a_{oo} R \left(\frac{2}{\kappa+1} \right)^{\kappa+1/2(\kappa-1)}}{X^2} P_*^{\kappa-1/2\kappa} - 2 \kappa g g' \end{aligned} \quad (4A-33)$$

From Equation (4A-15),

$$\begin{aligned} \frac{\theta}{X} &= \frac{1}{a_{oo}} \left(\frac{2}{\kappa-1} \right)^{-1/2} \\ \frac{\theta}{X} &= \frac{F^2 P_{oo}^2}{M_t^2 a_{oo}^4} \left(\frac{2}{\kappa-1} \right)^{-2} \cdot \frac{M_t a_{oo}}{F P_{oo}} \left(\frac{2}{\kappa-1} \right)^{1/2} \\ &= \frac{F P_{oo}}{M_t^3 a_{oo}^3} \left(\frac{2}{\kappa-1} \right)^{-3/2} \end{aligned} \quad (4A-34)$$

Assume constants α and β such that Equation (4A-33) becomes

$$\frac{P'_*}{P_*} g^2 = [-\alpha g + \alpha \beta] P_*^{\kappa-1/2\kappa} - 2 \kappa g g' \quad (4A-35)$$

Then from Equations (4A-33), (4A-34), and (4A-35),

$$\alpha = 4 \kappa \kappa a_{\infty} \left(\frac{2}{\kappa + 1} \right)^{(\kappa+1)/2(\kappa-1)} \cdot \frac{1}{a_{\infty}} \left(\frac{2}{\kappa - 1} \right)^{-1/2} \quad (4A-36)$$

$$= 4 \kappa \kappa \left(\frac{2}{\kappa + 1} \right)^{(\kappa+1)/2(\kappa-1)} \left(\frac{2}{\kappa - 1} \right)^{-1/2} \quad (4A-37)$$

$$\beta = 4 \kappa \kappa a_{\infty} R \left(\frac{2}{\kappa + 1} \right)^{(\kappa+1)/2(\kappa-1)} \cdot \frac{F P_{\infty}}{M_t a_{\infty}^3} \left(\frac{2}{\kappa - 1} \right)^{-3/2}$$

$$\cdot \frac{1}{4 \kappa \kappa \left(\frac{2}{\kappa + 1} \right)^{(\kappa+1)/2(\kappa-1)} \left(\frac{2}{\kappa - 1} \right)^{-1/2}}$$

$$\beta = R \left(\frac{2}{\kappa - 1} \right)^{-1} \frac{F P_{\infty}}{M_t a_{\infty}^2} \quad (4A-38)$$

Differential Equations (4A-15) and (4A-35) are solved simultaneously by code CYLIN using the Runge-Kutta integration technique for initial conditions

$$g(0) = \frac{R}{X} \quad P_g(0) = 1.0 \quad \text{and} \quad g'(0) = 0$$

Since M_t and F are both proportional to L , M_t/F is independent of the cylinder length. Thus, length L drops out of the equations for β , X , and θ ; i.e., the cylinder length does not enter into the solution for Equations (4A-15) and (4A-35).

Computer Codes CYLIN and SPHER

The following computer codes were used to solve the simultaneous nonlinear differential equations for motion of many fragments emanating from bursting confinement vessels of cylindrical and spherical configuration. These codes were used to generate the data for the method of deterministic fragment initial velocity calculations given in the text of the workbook.

PROGRAM VARIABLE DEFINITIONS FOR CODES
SPHER AND CYLIN

<u>Program Variable</u>	<u>Definition</u>	<u>SI</u>	<u>Units</u>
			<u>English</u>
CAP1	Ratio of specific heats of gas	--	--
AO	Sound speed	m/s	in/sec
PO	Initial pressure	Pa	psi
RR	Cylinder radius	m	in.
CL	Cylinder length	m	in.
EL	End length	m	in.
CT	Cylinder thickness	m	in.
ET	End thickness	m	in.
DEN	Density	kg/m ³	lb _f /in ^{3*}
VO	Volume	m ³	in ³
TM	Total mass of confinement vessel	kg	lb _f ^{**}
FN	Number of fragments (always two)	--	--
FK	Gas discharge coefficient	--	--
AH	Time interval of iteration	--	--
XMAX	Maximum time of iteration	--	--
PERI	Perimeter (calculated)	m	in.
FF	Area of cross section to which force is applied (calculated)	m ²	in ²
XX	Characteristic dimension (calculated)	m	in.

* lb_f indicates English weight measurement of pounds of force. Sea level gravitation is assumed.

<u>Program Variable</u>	<u>Definition</u>	<u>SI</u>	<u>Units</u>	<u>English</u>
THETA	Characteristic time (calculated)	s	s	
A1	Dimensionless mass parameter	--	--	
B1	Dimensionless geometry parameter	--	--	
NEND	Branching constant. If zero, program stops. If > 1, program continues.	--	--	
G1	distance to initial velocity	m	in.	
G2	initial fragment velocity	m/s	ft/sec	
G3	initial fragment acceleration	m/s ²	in/sec ²	
G4	final explosive product mixture pressure	Pa	psi	
T1	time to initial velocity	s	s	
PI	the constant, π	none	none	
CAP2	the quantity $(1 - \kappa)/\kappa$	none	none	
CAP3	the quantity $-1/\kappa$	none	none	
CAP4	the quantity $(3\kappa - 1)/2\kappa$	none	none	
CQ	normalized initial fragment displacement from center of sphere	none	none	
X	normalized time	none	none	
Y(2)	normalized velocity	none	none	
Y(3)	normalized pressure	none	none	
Y(1)	normalized fragment displacement	none	none	
NA	number of differential equations to be solved	none	none	
F(1), F(2), F(3)	differential equations solved			
TT	normalized time	none	none	
PS	normalized pressure	none	none	

```

PROGRAM SPHER (INPUT,OUTPUT,TAPE1 =OUTPUT,TAPE2 =INPUT)
DIMENSION F(),Y(3),W1(3),W2(3),PS(200),TT(200)
310 FORMAT (3E10.5)
312 FORMAT (4E10.3)
314 FORMAT (2E10.3)
315 FORMAT (3/,20H GAS CHARACTERISTICS,/,,7H KAPPA=,E10.3,
11SH SOUND SPEED=,E10.3,7H IN/SEC,/,,10H PRESSURE ,E10.3,9H PSI,
12/,23H VESSEL CHARACTERISTICS,/,,8H RADIUS=,E10.3,5H INS.,
18H MASS=,E10.3,16H LBS,-SEC,SG./IN,/,,18H NO. OF FRAGMENTS=,
1E10.3,2/)
319 FORMAT (3/,13H FINAL VALUES,/,,6H TIME=,E10.3,4H SEC,/,
11DH DISTANCE=,E10.3,9H INS,/,,10H VELOCITY=,E10.3,7H FT/SEC,/,
114H ACCELERATION=,E10.3,10H IN/SEC-SEC,/,,10H PRESSURE=,E10.3,
14H PSI)
320 FORMAT (52H CHARACTERISTICS OF MOTION OF FRAGMENTS (NORMALIZED)
1,2/,10H T-NORM,9X,1HG,10X,2HG!,7X,3HG!!,,/)
321 FORMAT ( /,22H PRESSURE (NORMALIZED),/,,4X,7H T-NORM,bX,
16HP=NORM,,/)
322 FORMAT (14H INITIAL CONDITIONS,/,,6H X(0)=,E10.4,7H G(0)=,E10.4,
18H G'(0)=,E10.4,9H P-NORM=,E10.4,2/)
502 FORMAT (/,8HTOO MUCH)
600 FORMAT (I2)
3001 FORMAT (E10.3)
500 JJ=0
READ (2,310) CAP1,A0,PO
READ (2,312) FN,RR,TM,FK
READ (2,314) AH,XMAX
READ (2,600) NEND
GO TO 551
550 PO=PO/10,
AH=1.0E-5
551 CONTINUE
#WRITE (1,315) CAP1,A0,PO,RR,TM,FN
PI= 3.1415926535
FF=4.*PI*(RR**2)*(1./FN)-(1./FN**2))
XX=TM*(A0**2,0)*(2.0/(CAP1-1.))/(FF*PO)
THETA=TM*A0*((2.0/(CAP1-1.0))**0.5)/(FF*PO)
CAP2=(1.00-CAP1)/CAP1
CAP3=-1.0/CAP2
CAP4=(3.0*CAP1-(1.0))/(2.0*CAP1)
A1=3.*FK*CAP1*((2.0/(CAP1+1.0))**((CAP1+1.0)/(2.0*(CAP1+1.0))))*
1*((2.0/(CAP1-1.0))**-0.5)
B1=((RR)**2)*((2.0/(CAP1-1.0))**-2)*(FF*PO)**2)/
1*((TM**2)*(A0**4))
C0=RR/XX
X=0.0
Y(1)=C0
Y(2)=0.0
Y(3)=1.0
YT=0.0
YTT=0.0
#WRITE (1,322) X,Y(1),Y(2),Y(3)
NA=3
F(1)=Y(2)
F(2)=FN*Y(3)*((1.00-(Y(2)**2,0)*(Y(3)**2*CAP2))**CAP3)
F(3)=((Y(1)**3)*(Y(3)**2*CAP4)*(A1*B1-A1*(Y(1)**2)))*
13.*CAP1*(Y(2)*Y(3)/Y(1))

```

```

FP=F(2)
30 S=RKLDEQ (NA,Y,F,X,AH,0)
50 F(1)=Y(2)
F(2)=FN*Y(3)*((1.00-(Y(2)**2.0)*(Y(3)**CAP2))**CAP3)
F(3)=((Y(1)**3)*(Y(3)**CAP4)*(A1*B1-A1*(Y(1)**2)))*
13.*CAP1*(Y(2)*Y(3)/Y(1))
IF (S-1.) 40,30,40
40 CONTINUE
F2T=(F2-F(2))/F2
F2T=ABS(F2T)
IF (F2T=.10) 700,700,701
700 AH=3,0*AH
701 CONTINUE
JJ=JJ+1
IF (JJ=200) 504,503,503
504 CONTINUE
TT(JJ)=X
PS(JJ)=Y(3)
YT=(Y(2)-YT)/Y(2)
YT=Y(2)
IF (YT=.001) 10,10,41
41 CONTINUE
GO TO 30
10 CONTINUE
T1=THETA*X
G1=XX*Y(1)-XX*CO
G2=XX/THETA*(Y(2))
G2=G2/12.0
G3=(XX/(THETA)**2.0)*F(2)
G4=PO*Y(3)
WRITE (1,319) T1,G1,G2,G3,G4
IF (PO=10000,) 552,552,550
552 IF (NEND=1) 501,500,500
503 CONTINUE
WRITE (1,502)
501 STOP
END

```

```

PROGRAM CYLIN (INPUT,OUTPUT,TAPE1 =OUTPUT,TAPE2 =INPUT)
DIMENSION F(3),Y(3),W1(3),W2(3),PS(200),TT(200)
310 FORMAT (3E10,5)
312 FORMAT (4E10,3)
314 FORMAT (2E10,3)
315 FORMAT (3/,20H GAS CHARACTERISTICS,/,7H KAPPA=E10,3,
11SH SOUND SPEED=E13,5,7H IN/SEC,/,10H PRESSURE ,E10,3,4H PSI,
12/,23H VESSEL CHARACTERISTICS,/,8H RADIUS=E10,3,5H INS.,
18H MASS=E10,3,16H LBS.=SEC,SQ./IN,/,18H NO. OF FRAGMENTS=,
1E10,3,2/)
319 FORMAT (3/,13H FINAL VALUES,/,6H TIME=E10,3,4H SEC,7,
110H DISTANCE=E10,3,4H INS,/,10H VELOCITY=E10,3,7H FT/SEC,/,1
114H ACCELERATION=E10,3,10H IN/SQ-SEC,/,10H PRESSURE=E10,3,
14H PSI)
320 FORMAT (5PH CHARACTERISTICS OF MOTION OF FRAGMENTS (NORMALIZED)
1,2/,10H T-NORM,4X,1HG,10X,2HG!,7X,3HG!!,,/)
321 FORMAT ( /,22H PRESSURE (NORMALIZED),/,4X,7H T-NORM,6X,
16HP=NORM,,)
322 FORMAT (19H INITIAL CONDITIONS,/,6H X(0)=,E10,4,7H G(0)=,E10,4,
18H G'(0)=,E10,4,9H P-NORM=,E10,4,2/)
324 FORMAT ( /,12H CYL LENGTH=,E10,3)
502 FORMAT ( /,8HTOO MUCH)
600 FORMAT (I2)
3001 FORMAT (E10,3)
500 JJ=0
READ (2,310) CAP1,A0,PO
READ (2,312) FN,RR,TM,FK
READ(2,3001) GNL
READ (2,314) AH,XMAX
READ (2,600) NEND
GO TO 551
550 PO=PO/10,
AH=1.0E-5
551 CONTINUE
WRITE (1,324) GNL
WRITE (1,315) CAP1,A0,PO,RR,TM,FN
PI= 3.1415926535
FF=2.*GNL*RR*((1.-(COS(2.*PI/FN))**2 ))**0.5
XX=TM*(A0**2.0)*(2.0/(CAP1-1.))/(FF*PO)
THETA=TM*A0*((2.0/(CAP1-1.0))**0.5)/(FF*PO)
CAP2=(1.00-CAP1)/CAP1
CAP3=-1.0/CAP2
CAP4=(3.0*CAP1-(1.0))/(2.0*CAP1)
A1=4.00*FK*CAP1*((2.0/(CAP1+1.0))**((CAP1+1.0)/(2.0*(CAP1-1.0))))
1*((2.0/(CAP1-1.0))**0.5)
B1=RR*((2.0/(CAP1-1.0))**-1.0)*(FF*PO)/(TM*(A0**2.0))
CO=RR/XX
X=0.0
Y(1)=CO
Y(2)=0.0
Y(3)=1.0
YT=0.0
YTT=0.0
WRITE (1,322) X,Y(1),Y(2),Y(3)
NA=3
F(1)=Y(2)
F(2)=FN=Y(3)*((1.00-(Y(2)**2 )*(Y(3)**CAP2))**CAP3)

```

```

TERM2=2.*CAP1*(Y(2)*Y(3)/Y(1))
F(3)=((Y(1)**=2.)*(Y(3)**CAP4)*(A1*B1=A1*(Y(1))))=TERM2
F2=F(2)
30 S=RKLDEQ (NA,Y,F,X,AH,0)
50 F(1)=Y(2)
F(2)=FN=Y(3)=((1.00-(Y(2)**2.)*(Y(3)**CAP2))**CAP3)
TERM2=2.*CAP1*(Y(2)*Y(3)/Y(1))
F(3)=((Y(1)**=2.)*(Y(3)**CAP4)*(A1*B1=A1*(Y(1))))=TERM2
IF (S=1.) 40,30,90
90 CONTINUE
F2T=(F2-F(2))/F2
F2T=ABS(F2T)
IF (F2T=.10) 700,700,701
700 AH=1,5+AH
701 CONTINUE
JJ=JJ+1
IF (JJ=200) 504,503,503
504 CONTINUE
TT(JJ)=X
PS(JJ)=Y(3)
YTT=(Y(2)-YT)/Y(2)
YT=Y(2)
IF(YTT=.001) 10,10,91
91 CONTINUE
GO TO 30
10 CONTINUE
T1=THETA*X
G1=XX*Y(1)-XX*CO
G2=XX/THETA*(Y(2))
G2=G2/12.0
G3=(XX/(THETA)**2.0)*F(2)
G4=PO*Y(3)
WRITE (1,314) T1,G1,G2,G3,G4
IF (PO=10000,) 552,552,550
552 IF (NEND=1) 501,500,500
503 CONTINUE
WRITE (1,502)
501 STOP
END

```

```

FUNCTION RKLDEQ(N,Y,F,X,H,NT)
C D2 UCSD RKLDEQ RUNGE-KUTTA-GILL LINEAR DIFFERENTIAL EQUATION SOLVER F=63
C D2 UCSD RKLDEQ
C MODIFIED MAY 1963 (0 REMOVED FROM CALLING SEQUENCE)
C TEST OF ALGOL ALGORITHM
C DIMENSION Y(10),F(10),Q(10) RKLDG
C REAL X,H--INTEGER N,NT--COMMENT--BEGIN INTEGER I,J,L--REAL A
C NT=NT+1
C GO TO (1,2,3,4),NT RKLDG
C GO TO S(NT) RKLDG
1 DO 11 J=1,N RKLDG
11 Q(J)=0, RKLDG
A=.5 RKLDG
X=X+H/2, RKLDG
GO TO 5 RKLDG
2 A=.29289321881 RKLDG
GO TO 5 RKLDG
3 A=1.7071067812 RKLDG
X=X+H/2, RKLDG
GO TO 5 RKLDG
4 DO 41 I=1,N RKLDG
41 Y(I)=Y(I)+H*F(I)/6.+Q(I)/3., RKLDG
NT=0 RKLDG
RKLDEQ=2, RKLDG
GO TO 6 RKLDG
5 DO 51 L=1,N RKLDG
51 Y(L)=Y(L)+A*(H*F(L)+Q(L)) RKLDG
Q(L)=2.*A*H*F(L)+(1.-3.*A)*Q(L) RKLDG
RKLDEQ=1, RKLDG
6 CONTINUE RKLDG
RETURN RKLDG
END RKLDG

```

LIST OF REFERENCES

1. Baker, W. E., V. B. Parr, R. L. Bessey, and P. A. Cox, "Assembly and Analysis of Fragmentation Data for Liquid Propellant Vessels," NASA CR-134538, NASA Lewis Research Center, January 1974.
2. Bessey, R. L., "Fragment Velocities from Exploding Liquid Propellant Tanks," Shock and Vibration Bulletin, No. 44, August 1974, pp. 133-139.

APPENDIX IV. B

COMPARISON OF EXPERIMENTAL RESULTS WITH CODE PREDICTIONS

Some experimental data for initial fragment velocities from bursting containment vessels are available to check the predictions of fragment velocities from code SPHER. For example, D. W. Boyer, et al. (Reference 1) have measured fragment velocities from bursting glass spheres of various dimensions where the contained gas was air or helium (He). The text of the workbook, "Example 1 for Spheres," shows how the initial fragment velocity for one of these cases could be obtained from the tables. Table 4B-1 lists the data from the Boyer report and compares it with values obtained from Figures 4-1 through 4-8 of the workbook text, using the method demonstrated in the examples shown in the text. The data are also compared to values obtained by runs of code SPHER for the specific burst pressure and sphere geometries used in the experimental runs.

Results are within about 10% of one another for any of the methods used.

Table 4B-2 lists data for fragments from bursting titanium alloy spheres pumped up with nitrogen. The experimental data are from a report by Pittman (Reference 2). Pittman measured the velocities of fragments emanating from the spheres with breakwire and strobe photographic techniques. Code SPHER and the tables predict the velocities from the small diameter sphere within 10%. Velocities predicted for the larger diameter spheres are low by 15% where breakwire techniques were used to measure the fragment velocities. They agree well with the measured data where strobe photography was used to measure the fragment velocities.

TABLE 4B-1. INITIAL FRAGMENT VELOCITIES, V_i ,
FROM BURSTING GLASS SPHERES

$$(\rho = 2.6 \times 10^3 \text{ kg/m}^3)$$

Sphere Characteristics		Pressurizing Gas		Initial Fragment Velocities		
Radius cm	Wall Thickness cm	Type	Pressure Pa	V_i (Boyer)* m/s	V_i (Code) m/s	V_i (Tables) m/s
1.27	0.100	Air	2.25×10^6	51.8	51.5	57.6
2.54	0.100	"	" "	75.6	80.2	84.4
6.35	0.190	"	1.38×10^6	69.8	78.0	75.6
1.27	0.100	He	2.25×10^6	44.2	38.4	43.6
2.54	0.100	"	" "	79.4	61.6	64.0

* V_i values were obtained from Reference 1 by averaging measured values for similar cases from Table 1 of Reference 1 for the 1.27 and 2.54 cm radius spheres and by measurements from Figure 13 of Reference 1 for the 6.35 cm radius sphere.

TABLE 4B-2. INITIAL FRAGMENT VELOCITIES, V_i ,
FROM BURSTING TITANIUM ALLOY SPHERES

$$(\rho = 4.46 \times 10^3 \text{ kg/m}^3)$$

Sphere Characteristics		Pressurizing Gas		Initial Fragment Velocities		
Radius cm	Wall Thickness cm	Type	Pressure Pa	V_i (Pittman)* m/s	V_i (Code) m/s	V_i (Tables) m/s
11.7	0.274	N	5.51×10^7	366 ± 15	352	338
34.3	0.919	"	" "	342 ± 30^1	339	322
34.3	0.919	"	" "	426 ± 27^2	339	322
34.3	0.919	"	" "	448 ± 30^2	339	322

* Values taken from Reference 2.

¹This value was based on velocity measurements using a strobe photographic technique.

²These values were based on velocity measurements using breakwire measurement techniques.

LIST OF REFERENCES

1. Boyer, D. W., H. L. Brode, I. I. Glass, and J. G. Hall, "Blast from a Pressurized Sphere," UTIA Report No. 48, Institute of Aerophysics, University of Toronto, January 1958.
2. Fittman, J. F., "Blast and Fragment Hazards from Bursting High Pressure Tanks," Naval Ordnance Laboratory Report NOLTR 72-102, 17 May 1972.

APPENDIX IV. C

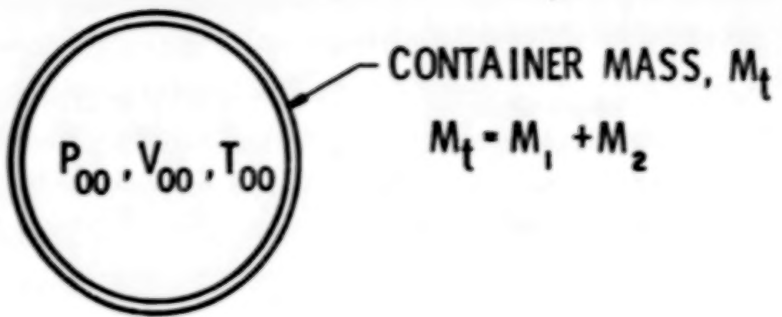
ESTIMATE OF INITIAL VELOCITIES OF FRAGMENTS FROM SPHERES AND CYLINDERS BURSTING INTO TWO EQUAL HALVES

The method developed by Taylor and Price⁽¹⁾ for calculating velocities of fragments from bursting spherical gas reservoirs was modified to provide velocity calculations for fragments from both cylindrical and spherical gas vessels. These modifications were primarily geometrical in nature and will be discussed in more detail in subsequent pages. To compute the velocity of fragments from bursting spheres or cylinders which contain gas under pressure, the following assumptions were made:

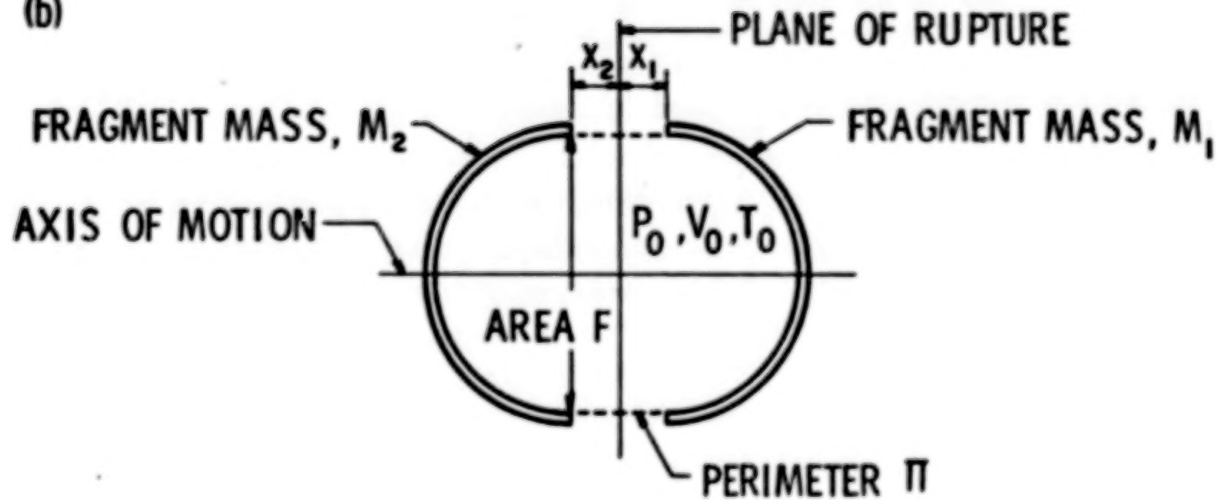
- (1) The vessel with gas under pressure breaks into two equal halves along a plane perpendicular to the cylindrical axis, and the two container fragments are driven in opposite directions.
- (2) Gas within the vessel obeys ideal gas laws.
- (3) Originally contained gas escapes from the vessel through the opening between the fragments into a surrounding vacuum. The escaping gas travels perpendicular to the direction of motion of the fragments with local sonic velocity.
- (4) Energy necessary to break the vessel walls is negligible compared to the total energy of the system.
- (5) Drag and lift forces are ignored since the distance the fragment travels before it attains its maximum velocity and the time it takes to attain its maximum velocity are too short for drag and lift forces to have a significant effect.

A schematic depicting the essential characteristics of the Taylor and Price solution for bursting spheres is shown in Figure 4C-1. Before accelerating into an exterior vacuum, the sphere has internal volume V_{00} and contains a perfect gas of adiabatic exponent (ratio of specific heats) K and gas constant R with initial pressure P_{00} and temperature T_{00} (Figure 4C-1a). At a time $\tau = 0$, rupture occurs along a perimeter Π , and the two fragments are propelled in opposite directions due to forces applied against the area F which is perpendicular to the axis of motion of the fragments (Figure 4C-1b). The mass of the two frag-

(a)



(b)



(c)

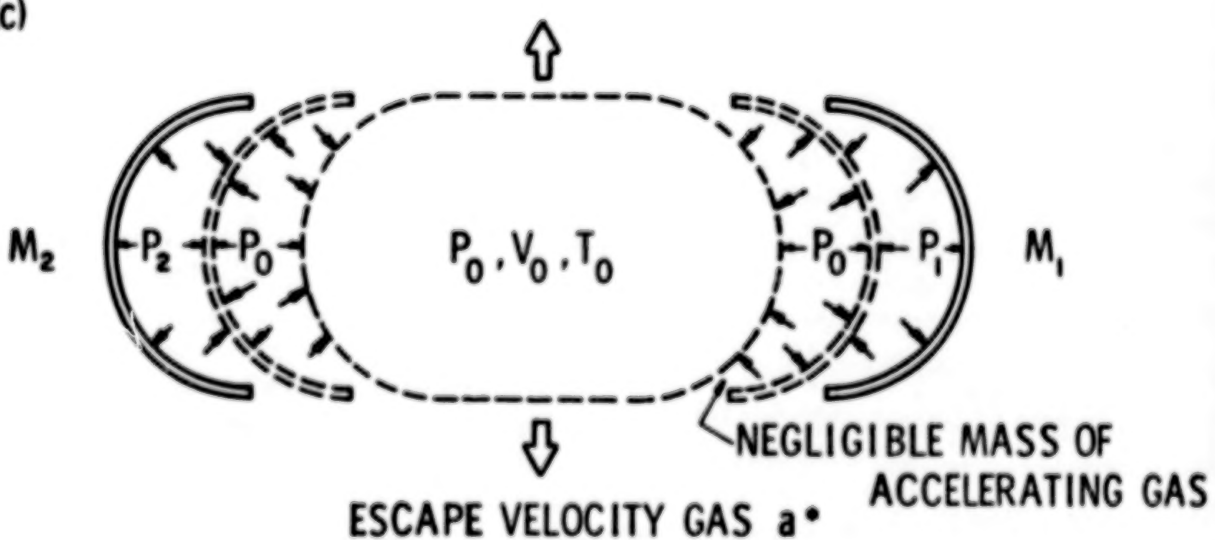


Figure 4C-1. Parameters for Sphere Bursting
into Two Halves

ments, M_1 and M_2 , is considered large relative to the mass of the remaining gas at elevated pressure (Figure 4C-1c).

As mentioned earlier, the Taylor and Price solution for calculating velocities of halves of bursting spheres was modified to predict velocities of halves of bursting cylinders. Figure 4C-2 contains the geometric parameters associated with cylindrical vessels. The generalized fragment velocity solution and subsequent computer program allow for computation of the velocity of half of the cylinder. The vessel is assumed to break into two equal halves along a plane perpendicular to its cylindrical axis. The cylinder can have spherical segment end caps or can have flat faces. The vessel has cylindrical radius r , cylindrical thickness C_t , end cap thickness E_t , cylindrical length C_L , and end cap length E_L beyond the cylindrical portion. When $C_t = C_L = 0$ and $E_L = r$, the containment vessel becomes a sphere, and the solution corresponds to that formulated by Taylor and Price. That is, a cylinder with hemispherical end caps with length-to-diameter (L/D) ratio of 1.0 is a sphere.

The Taylor and Price⁽¹⁾ solution, generalized to allow for cylindrical as well as spherical vessels, follows. The equations of motion and initial conditions of the two fragments are

$$M_1 \frac{d^2 x_1}{d\tau^2} = FP_1(\tau), \text{ with } x_1(0) = 0, \frac{dx_1(0)}{d\tau} = 0 \quad (4C-1)$$

$$M_2 \frac{d^2 x_2}{d\tau^2} = FP_2(\tau), \text{ with } x_2(0) = 0, \frac{dx_2(0)}{d\tau} = 0 \quad (4C-2)$$

where subscripts refer to each fragment and x_1 and x_2 are displacement distances and are taken along the axis of motion. To allow for cylindrical containment vessels, the cross sectional area F over which the force is applied becomes

$$F = \pi (r - C_t)^2 \quad (4C-3)$$

The equation of state for the unaccelerated gas remaining within the confinement of the container fragments is

$$P_o(\tau) V_o(\tau) = C(\tau) RT_o(\tau) \quad (4C-4)$$

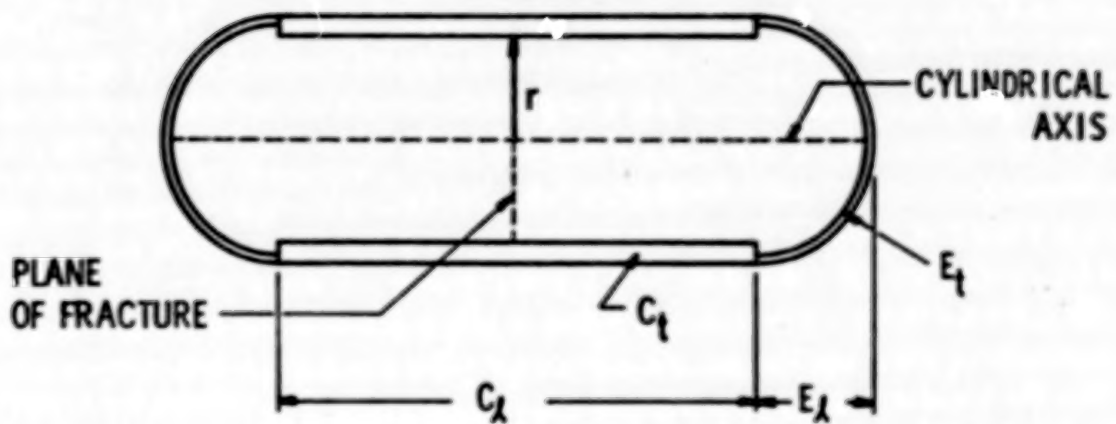


Figure 4C-2. Geometry of Cylindrical Vessels

where subscript 0 denotes reservoir conditions immediately after failure, R is the gas constant, P is pressure, V is volume, T is temperature and $C(\tau)$ is the mass of gas confined at high pressure as a function of time. The rate of change of the confined mass is

$$\frac{d C(\tau)}{d \tau} = -k \pi x a_* a_s \quad (4C-5)$$

where

$$x = x_1 + x_2 \quad (4C-6)$$

and k is the coefficient of discharge of the area between the fragments and a_* is the gas density at critical gas velocity a_* . The expression for perimeter π is the same as for spheres,

$$\pi = 2\pi r \quad (4C-7)$$

Gas density a_* and a_* are standard expressions

$$a_* = a_0(\tau) \left(\frac{2}{K+1} \right)^{1/(K-1)} \quad (4C-8)$$

$$a_* = a_0(\tau) \left(\frac{2}{K+1} \right)^{1/2}$$

where K is the adiabatic exponent (ratio of specific heats) for an ideal gas. The volume is assumed to be variable and can be described by

$$V_o(\tau) = V_{oo} + FX \quad (4C-9)$$

Nearly all of the gas is assumed to be accelerated with the fragments, with gas immediately adjacent to the fragments being accelerated to the velocity of the fragments. From simple-one-dimensional flow relationships,

$$P_1(\tau) = P_o(\tau) \left(1 - \left\{ \frac{K-1}{2[a_o(\tau)]^2} \right\} \left[\frac{dx_1(\tau)}{d\tau} \right]^2 \right)^{K/(K-1)} \quad (4C-10)$$

$$P_2(\tau) = P_o(\tau) \left(1 - \left\{ \frac{K-1}{2[a_o(\tau)]^2} \right\} \left[\frac{dx_2(\tau)}{d\tau} \right]^2 \right)^{K/(K-1)}$$

To generalize the solution, one can use the following nondimensional forms of the variables:

$$\text{Dimension: } x(\tau) = Xg(\xi), \quad x_1(\tau) = Xg_1(\xi), \quad x_2 = Xg_2(\xi)$$

$$\text{Time: } \tau = \theta \xi \quad (4C-11)$$

$$\text{Pressure: } P_o(\tau) = P_{oo} P_*(\xi)$$

From appropriate solutions and initial conditions:

$$\frac{dx_1(\tau)}{d\tau} = \frac{X}{\theta} g_1' , \quad \frac{dx_2(\tau)}{d\tau} = \frac{X}{\theta} g_2'$$

$$\frac{d^2 x_1(\tau)}{d\tau^2} = \frac{X}{\theta^2} g_1'' , \quad \frac{d^2 x_2(\tau)}{d\tau^2} = \frac{X}{\theta^2} g_2''$$

$$\frac{dP_0(\tau)}{d\tau} = \frac{P_{\infty}}{\theta} P_*' \quad (4C-12)$$

$$x_1(0) = x_2(0) = \frac{dx_1(0)}{d\tau} = \frac{dx_2(0)}{d\tau} = g_0(0) = g_2(0) = g_1'(0) = g_2'(0) = 0$$

$$P_*(0) = 1$$

where primes denote differentiation with respect to ξ . The pair of characteristic values for dimension X and time θ chosen by Taylor and Price are:

$$X = \frac{M_t a_{\infty}^2}{F P_{\infty}} \left(\frac{2}{K-1} \right) \quad (4C-13)$$

$$\theta = \frac{M_t a_{\infty}}{F P_{\infty}} \left(\frac{2}{K-1} \right)^{1/2}$$

The final derived equations contain two dimensionless groups which define the nature of the solutions, these are

$$\alpha = \frac{P_{\infty} V_{\infty}}{M_t a_{\infty}^2} \quad (4C-14)$$

$$\beta = k \left(\frac{2}{K+1} \right)^{\frac{K+1}{2(K-1)}} \left(\frac{2}{K-1} \right)^{1/2} \frac{V_{\infty}}{F^2}$$

Differences between the Taylor and Price solution for spheres and our solution for cylinders, with spherical caps being a special case of cylinders, occur in the determination of area F given by Equation (4C-3) and perimeter Π given in Equation (4C-7) where r is cylindrical radius (except for the special case of a sphere where r is spherical radius) instead of spherical radius. A difference also exists in the calculation of initial volume of the gas which, for the cylindrical case with spherical segment endcaps with one base, becomes

$$V_{\infty} = \pi \left\{ (r - C_t)^2 C_l + (E_l - E_t) \left[(r - E_t)^2 + 1/3 (E_l - E_t)^2 \right] \right\} \quad (4C-15)$$

for the adiabatic case,

$$\frac{P_o(\tau)}{P_{\infty}} = \left[\frac{P_o(\tau)}{P_{\infty}} \right]^K = \left[\frac{T_o(\tau)}{T_{\infty}} \right]^{\frac{K}{K-1}} = \left[\frac{a_o(\tau)}{a_{\infty}} \right]^{\frac{2K}{K-1}} \quad (4C-16)$$

Substitution of Equations (4C-10), (4C-12) through (4C-14), and (4C-16) into Equations (4C-1) and (4C-2) gives

$$\frac{M_1}{M_t} g_1'' = P_* \left[1 - \frac{g_1'^2}{(P_*) \frac{K-1}{K}} \right]^{\frac{K}{K-1}} \quad (4C-17)$$

$$\frac{M_2}{M_t} g_2'' = P_* \left[1 - \frac{g_2'^2}{(P_*) \frac{K-1}{K}} \right]^{\frac{K}{K-1}}$$

Differentiation of Equation (4C-4) and substitution of Equations (4C-5) through (4C-9) and (4C-11) and (4C-12) yields

$$\left[\left(\frac{K-1}{2} \right) \alpha + g \right] \frac{P_*'}{P_*} = - \frac{gK}{\alpha} g (P_*)^{\frac{2K}{K-1}} - Kg' \quad (4C-18)$$

Since fragment masses are equal ($M_1 = M_2 = M_t/2$), the equations for the motion of the two fragments become identical, with identical initial conditions and identical solutions so that $g_1 = g_2 = g/2$. Equations in Equation (4C-17) then reduce to

$$g'' = 4 P_* \left[1 - \frac{g'^2}{4(P_*) \frac{K-1}{K}} \right]^{\frac{K}{K-1}} \quad (4C-19)$$

Rearranging terms in Equation (4C-18) produces

$$P_*' = \frac{-\frac{gK}{a} g P_*^{\frac{2K}{2K-1}} - Kg' P_*}{\left(\frac{K-1}{2}\right)a + g} \quad (4C-20)$$

For initial conditions, $g(0) = 0$, $g'(0) = 0$, and $P_*(0) = 1$, nondimensional values of distance, velocity, acceleration and pressure as a function of time can be calculated by solving Equations (4C-19) and (4C-20) simultaneously using Runge Kutta method of numerical iteration. Dimensional values can then be calculated from

$$\tau = \theta \xi, \quad x_1(\tau) = \frac{Xg(\xi)}{2}, \quad x_1'(\tau) = \frac{X}{2\theta} g'(\xi), \quad (4C-21)$$

$$x_1''(\tau) = \frac{X}{2\theta^2} g''(\xi), \quad P_o(\tau) = P_{oo} P_*(\xi)$$

The computer program entitled/Frag 2/ was written in Fortran IV and exercised on a teletype tymshare terminal. The computer program is user-oriented and accepts either SI or English units and outputs either SI or English units. Rigorous English measure input is not used for length and mass measurements. Instead, inches are used instead of feet for length measurements and pounds-force (weight measure) are used instead of slugs for mass measurements in both input and output stages of the program since these units are commonly used in these types of measurements. The ratio of specific heats (K), speed of sound (a_{oo}), initial pressure (P_{oo}), external radius of the cylinder of sphere, and the discharge coefficient, chosen as 1.0 in all cases examined, are input parameters. The user has a choice of inputting cylinder length, end length, cylinder thickness, end thickness, and wall density; or volume, mass of the reservoir and cylinder thickness (see Table 4C-2). The

program also requires that a step size and limit be added to allow for the iteration process to begin and end. Nondimensional times are inputted for this purpose. The user has a choice of displaying nondimensional distance, velocity, acceleration and pressure as a function of nondimensional time and/or displaying dimensional distance, velocity, acceleration and pressure as a function of dimensional time. In all cases, final dimensional times, distance, velocity, acceleration and pressure are printed.

An explanation of the Runge-Kutta subroutine is contained in Table 4C-1. This is a standard computer library function which has nine arguments. After the Runge-Kutta subroutine explanation, one can find a list of the program variables, a listing of the program, and sample input and output in Table 4C-2.

TABLE 4C-1. RUNGE-KUTTA COMPUTER LIBRARY FUNCTION

FILE NAME: F16

SUBROUTINE RUNGE
NAME:

PURPOSE: This subroutine employs the Fourth Order Runge-Kutta Method to solve N simultaneous first-order ordinary differential equations by calculating successive values of Y according to the formula:

$$Y_{i+1} = Y_i + \frac{h}{6} (K_1 + 2K_2 + 2K_3 + K_4)$$

$$\text{where } K_1 = f(x_i, Y_i)$$

$$K_2 = f(x_i + \frac{h}{2}, Y_i + \frac{hK_1}{2})$$

$$K_3 = f(x_i + \frac{h}{2}, Y_i + \frac{hK_2}{2})$$

$$K_4 = f(x_i + h, Y_i + hK_3)$$

TABLE 4C-1. (cont'd)

METHOD:	The subroutine is called by the calling program five times in order to approximate successive $Y(I)$'s; the first time to initialize, the second time to calculate $K_1(I)$, the third time to calculate $K_2(I)$, the fourth time to calculate $K_3(I)$ and the fifth time to calculate $K_4(I)$. In addition, each time the subroutine is called, it calculates a new $Y(I)$ and a new $X(I)$ which are returned to the calling program where the functions (first-order differential equations) are evaluated with the new $X(I)$ and $Y(I)$. These values of the function are then returned to the subroutine where they are used as $K_1(I)$, $K_2(I)$, $K_3(I)$, or $K_4(I)$ and approximately accumulated to obtain $Y_{i+1}(I)$ in the 5 calls to the subroutine.
ARGUMENTS:	The subroutine RUNGE uses nine arguments: N, Y, F, X, H, M, SAVEY, PHI, K.
1.	The first argument, N, represents the number of simultaneous first-order ordinary differential equations to be solved.
2.	The second argument, Y, is the array name which the calling program uses to transmit the initial $Y(I)$ values for each differential equation. Upon completion of the 5 calls to RUNGE, $Y(I)$ will contain the new approximated values for the $Y_{i+1}(I)$'s.
3.	The third argument, F, is the array which contains the current values of the differential equations calculated by the main program, i. e., $F(J)$ contains the value of the Jth first-order differential equation.
4.	The fourth argument, X, represents the independent variable which should be initialized in the main program before calling RUNGE. RUNGE increments X by the stepsize H.
5.	The fifth argument, H, represents the step size for X.

TABLE 4C-1 (concl'd)

6. The sixth argument, M, indicates which of the five passes of the subroutine is to be executed. The main program must initialize this argument as 1. RUNGE then successively increments the variable by 1 up to 5.
7. The seventh argument, SAVY, is used within RUNGE and must be dimensioned in the calling program to be of size N.
8. The eighth argument, PHI, is also used internally by RUNGE, but must be dimensioned in the calling program to be of size N.
9. The ninth argument, K, is manipulated within RUNGE. K should be tested right after the call to RUNGE, in the calling program.

When $K = 1$, control should transfer to a set of code in the calling program which calculates new values for the first-order differential equations, $F(I)$, with the current values of X and $Y(I)$. Then RUNGE should be called again.

When $K = 2$, the approximation for $Y(I)$ is completed. Values for the $Y_{i+1}(I)$'s are stored in $Y(I)$ at this time, and normal flow of the calling program should resume.

LIMITATIONS

AND

COMMENTS:

1. The calling program must dimension SAVY and PHI.
2. The calling program must set $M = 1$ before calling RUNGE.
3. The calling program must set up the N first-order differential equation values in an array F to be passed through to RUNGE when the subroutine returns with $K = 1$.
4. The calling program must set up separate arrays if all X and Y values for the set of differential equations are to be saved, perhaps for plotting purposes.

TABLE 4C-2. COMPUTER PROGRAM ENTITLED/FRAG/
IN FORTRAN IV

Function: This program computes the velocity of a fragment from a bursting sphere or cylinder, with or without spherical segment end caps with one base, which contains gas under pressure. It is assumed that the vessel breaks into two equal halves along a plane perpendicular to the cylindrical axis. Distance, acceleration and residual pressure as a function of time are also computed.

Input-Output Considerations: The program accepts input in either SI or English units and can print output in SI or English units making any conversions needed internally. The program considers SI units of mass in kilograms, length in meters and time in seconds. The program considers English units of mass in pounds of force (weight measure used for convenience), length in inches and time in seconds. Input data are:

(A) Gas characteristics:

(CAP1) Adiabatic exponent (ratio of specific heats) for gas in the containment vessel.

(AO) Speed of sound in gas of vessel.

(PO) Initial pressure of gas in vessel.

(B) Vessel characteristics:

(RR) Cylinder radius

choice of

(ZN) = 1: (A) Cylinder length

(B) Length of end cap

(C) Cylinder thickness

(D) Thickness of end cap

(E) Wall density

TABLE 4C-2. (cont'd)

- (ZN) = 2: (A) Volume of containment vessel
(B) Mass of reservoir
(C) Cylinder thickness
- (C) Dynamic variables:
(FN) Number of fragments (always 2.)
(FK) Discharge coefficient (chosen to be 1.)
(AH) Nondimensional time increment for calculations
(XMAX) Maximum nondimensional time calculation.
- (D) Input/Output format:
(ZN2) Input units
1. = SI
2. = English
(ZN3) Output units
1. = SI
2. = English
(FN1) Display nondimensional dynamic variance
1. = Yes
2. = No
(FN2) Display dimensional dynamic variance
1. = Yes
2. = No
(FN3) Make range calculation always
2. (NO)

Variables: The definition and units of variables in this program follow.

TABLE 4C-2. (cont'd)

<u>Program Variable</u>	<u>Variable</u>	<u>Definition</u>	<u>SI</u>	<u>Units English</u>
FN2	--	if = 1., program displays normal time, distance, velocity, accelerations and pressure	--	--
FN3	--	(always 2.)	--	--
CL	C _l	cylinder length	m	in
EL	E _l	end length	m	in
CT	C _t	cylinder thickness	m	in
ET	E _t	end thickness	m	in
DEN	--	density	kg/m ³	lb-f/in ³ *
VOO	--	outside volume of vessel	m ³	in ³
VO	V _{oo}	internal volume of vessel	m ³	in ³
VOW	--	wall volume	m ³	in ³
TM	M _Z	total mass of reservoir	kg	lb-f*
PO1	--	unit conversion step for PO	--	--
RR1	--	unit conversion step for RR	--	--
CL1	--	unit conversion step for CL	--	--
EL1	--	unit conversion step for EL	--	--
CT1	--	unit conversion step for CT	--	--

* lb-f indicates English weight measurement of pounds of force. Sea level gravitation is assumed.

TABLE 4C-2. (cont'd)

<u>Program Variable</u>	<u>Variable</u>	<u>Definition</u>	<u>SI</u>	<u>Units English</u>
ET1	--	unit conversion step for ET	--	--
DEN1	--	unit conversion step for DEN	--	--
TM1	--	unit conversion step for TM	--	--
CAP1	K	ratio of specific heats of gas	--	--
A _o	a _{oo}	sound speed	m/s	in/sec
P _o	P _{oo}	initial pressure	Pa	psi
RR	r	cylinder radius	m	in
ZN1	--	if = 1., input is C _t , E _f , C _t , E _t , density of vessel (A, B, C, D, E in pro- gram)	--	--
		if = 2., input is V _{oo} , M _t , C _t (A, B, C in program)	--	--
ZN2	--	specifies input units 1. implies SI 2. implies English	--	--
ZN3	--	specifies output units 1. implies SI 2. implies English	--	--
FN	--	number of fragments (always 2)	--	--
FK	--	gas discharge coefficient		
AH	--	dimensionless time inter- val of iteration	--	--
SMAX	--	maximum dimensionless time of iteration	--	--

TABLE 4C-1, (cont'd)

<u>Program Variable</u>	<u>Variable</u>	<u>Definition</u>	<u>SI</u>	<u>Units English</u>
FN1	--	if = 1., program displays θ , $\dot{\theta}$, $\ddot{\theta}$, P_*	--	--
VO1	--	unit conversion step for VO	--	--
PERI	Π	perimeter (calculated)	m	in
FF	F	area of cross-section to which force is applied (calculated)	m^2	in^2
XX	X	characteristic dimension (calculated)	m^2	in^2
THETA	θ	characteristic time (calculated)	s	sec
CAP2	--	quantity $K/(K-1)$	--	--
CAP3	--	quantity $(3K-1)/2K$	--	--
CAP 4	--	quantity $(K+1)/2(K-1)$	--	--
A1	α	dimensionless parameter	--	--
B1	β	dimensionless geometry parameter	--	--
X	--	normalized time	--	--
Y(1)	--	normalized initial frag- ment displacement	--	--
Y(2)	--	normalized velocity	--	--
Y(3)	--	normalized pressure	--	--
F(1), F(2), F(3)	--	differential equations solved (see Equations 4C-19 and 4C-20)	--	--

TABLE 4C-2. (concl'd)

<u>Program Variable</u>	<u>Variable</u>	<u>Definition</u>	<u>SI</u>	<u>Units</u>
				<u>English</u>
TT	--	normalized time (output)	--	--
G	g	normalized distance (output)	--	--
GG	g'	normalized velocity (output)	--	--
GGG	g''	normalized acceleration (output)	--	--
PS	P*	normalized pressure (output)	--	--
T1	--	time (output)	s	sec
GL, FG1	--	distance (output)	m	in
G2, FG2	--	velocity (output)	m/s	in/sec
G3, FG3	--	acceleration (output)	m/s ²	in/sec ²
G4, FG4	--	pressure (output)	Pa	psi

TABLE 4C-2. (cont'd)

XTRAN
VER. JUL 13

```

*QED
*APPEND/FRAG2/
*/  

DIMENSION F(3),Y(3),W1(3),W2(3),PS(50),TT(50),G(50),GG(50),GGG(50)
3001 FORMAT (E10.3)
309 FORMAT (2/,45H READ IN KAPPA, SOUND SPEED, INITIAL PRESSURE)
310 FORMAT (3E10.5)
311 FORMAT (2/,19H IF PARAMETERS ARE:,,62H CYL. LENGTH, END LENGTH,
CYL. THICK., END THICK., WALL DENS.,,,,
5H ENTER 1,2/,40H VOLUME, MASS OF RESERVBIR, CYL. THICK.,,,,
5H ENTER 2)
312 FORMAT (5E10.4)
313 FORMAT (2/,36H READ IN TIME INTERVAL, MAXIMUM TIME)
314 FORMAT (2E10.3)
316 FORMAT (2/,48H DISPLAY NNDIMENSIONAL DYNAMIC VAR.? YES=1 NO=2)
317 FORMAT (2/,45H DISPLAY DIMENSIONAL DYNAMIC VAR.? YES=1 NO=2)
318 FORMAT (2/,35H MAKE RANGE CALCULATION? YES=1 NO=2)
320 FORMAT (52H CHARACTERISTICS OF MOTION OF FRAGMENTS (NORMALIZED)
,2/,3X,6HT-NORM,6X,1HG,9X,2HG*,6X,2HG",6X,6HP-NORM,/)
322 FORMAT (2/,19H INITIAL CONDITIONS,/,6H X(0)=,E10.4,7H G(0)=,E10.4,
5H G'(0)=,E10.4,9H P-NORM=,E10.4,2/)

895 FORMAT (2/,29H ENGLISH INPUT/ENGLISH OUTPUT,2/,4X,5H ITEM,6X,
14H ENGLISH UNITS,2/,6H KAPPA,9X,E10.4,/,12H SOUND SPEED,3X,E10.4,
7H IN/SEC,/,9H PRESSURE,6X,E10.4,4H PSI,/,7H RADIUS,6X,E10.4,
3H IN,/,7H VOLUME,6X,E10.4,6H CU IN,/,15H RESERVBIR MASS,E10.4,
4H LBF,/,12H CYL. THICK.,3X,E10.4,3H IN,/,13H NO. OF FRAGS,2X,E10.4)
896 FORMAT (2/,24H ENGLISH INPUT/SI OUTPUT,2/,4X,5H ITEM,6X,14H
ENGLISH UNITS,10X,9H SI UNITS,2/,6H KAPPA,9X,E10.4,14X,E10.4,/,
12H SOUND SPEED,3X,E10.4,7H IN/SEC,7X,E10.4,6H M/SEC,/,9H PRESSURE,
6X,E10.4,4H PSI,10X,E10.4,8H PASCALS,/,7H RADIUS,6X,E10.4,3H IN,11X,
E10.4,7H METERS,/,7H VOLUME,6X,E10.4,6H CU IN,8X,E10.4,10H CU METERS,
/,15H RESERVBIR MASS,E10.4,4H LBF,10X,E10.4,3H KG,/,12H CYL. THICK.,
3X,E10.4,3H IN,11X,E10.4,7H METERS,/,13H NO. OF FRAGS,2X,E10.4,
14X,E10.4)

897 FORMAT (2/,24H SI INPUT/ENGLISH OUTPUT,2/,4X,5H ITEM,6X,9H
SI UNITS 15X,14H ENGLISH UNITS,2/,6H KAPPA,9X,E10.4,14X,E10.4,/,12H
SOUND S) ED,3X,E10.4,6H M/SEC,8X,E10.4,7H IN/SEC,/,9H PRESSURE,6X,E10.4
,8H PASCALS,6X,E10.4,4H PSI,/,7H RADIUS,6X,E10.4,7H METERS,7X,
E10.4,3H IN,/,7H VOLUME,6X,E10.4,10H CU METERS,4X,E10.4,6H CU IN,/,
15H RESERVBIR MASS,E10.4,3H KG,11X,E10.4,4H LBF,/,12H CYL. THICK.,
3X,E10.4,7H METERS,7X,E10.4,3H IN,/,13H NO. OF FRAGS,2X,E10.4,
14X,E10.4)

898 FORMAT (2/,19H SI INPUT/SI OUTPUT,2/,4X,5H ITEM,6X,9H SI
UNITS,2/,6H KAPPA,9X,E10.4,/,12H SOUND SPEED,3X,E10.4,6H M/SEC,/,  

9H PRESSURE,6X,E10.4,8H PASCALS,/,7H RADIUS,6X,E10.4,7H METERS,/,  

7H VOLUME,6X,E10.4,10H CU METERS,/,11H TOTAL MASS,4X,E10.4,3H KG,  

/,12H CYL. THICK.,3X,E10.4,7H METERS,/,13H NO. OF FRAGS,2X,E10.4)

900 FORMAT (2/,24H READ IN CYLINDER RADIUS)
901 FORMAT (E10.5)
902 FORMAT (2/,15H READ IN VALUES)
903 FORMAT (5E10.5)
904 FORMAT (2/,46H READ IN NO. OF FRAGMENTS(2.), DISCHARGE CBEF.)
```

TABLE 4C-2. (cont'd)

905 FORMAT (2/, 28H INPUT UNITS? SI=1 ENGLISH=2)
 906 FORMAT (2/, 29H OUTPUT UNITS? SI=1 ENGLISH=2)
 907 FORMAT (2/, 19H SI INPUT/SI OUTPUT, 2/, 4X, 5H ITEM, 6X,
 9H SI UNITS, 2/, 6H KAPPA, 9X, E10.4, /, 12H SOUND SPEED, 3X, E10.4, 6H M/SEC,
 /, 9H PRESSURE, 6X, E10.4, 8H PASCALS, /,
 7H RADIUS, 8X, E10.4, 7H METERS, /, 12H CYL. LENGTH, 3X, E10.4, 7H METERS, /,
 11H END LENGTH, 4X, E10.4, 7H METERS, /, 12H CYL. THICK., 3X, E10.4,
 7H METERS, /, 11H END THICK., 4X, E10.4, 7H METERS, /, 13H WALL DENSITY,
 2X, E10.4, 8H KG/CU M, /, 15H RESERVOIR MASS,
 E10.4, 3H KG, /, 13H NO. OF FRAGS, 2X, E10.4)
 908 FORMAT (2/, 24H SI INPUT/ENGLISH OUTPUT, 2/, 4X, 5H ITEM, 6X, 9H SI
 UNITS, 15X, 14H ENGLISH UNITS, 2/, 6H KAPPA, 9X, E10.4, 14X, E10.4, /,
 12H SOUND SPEED, 3X, E10.4, 6H M/SEC, 8X, E10.4, 7H IN/SEC, /, 9H PRESSURE,
 6X, E10.4, 8H PASCALS, 6X, E10.4, 4H PSI, /, 7H RADIUS, 8X, E10.4, 7H METERS,
 7X, E10.4, 3H IN, /, 12H CYL. LENGTH, 3X, E10.4, 7H METERS, 7X, E10.4,
 3H IN, /, 11H END LENGTH, 4X, E10.4, 7H METERS, 7X, E10.4, 3H IN, /, 12H CYL.
 THICK., 3X, E10.4, 7H METERS, 7X, E10.4, 3H IN, /, 12H END THICK., 3X,
 E10.4, 7H METERS, 7X, E10.4, 3H IN)
 9081 FORMAT (13H WALL DENSITY, 2X, E10.4, 8H KG/CU M, 6X, E10.4,
 10H LBF/CU IN, /,
 15H RESERVOIR MASS, E10.4, 3H KG, 11X, E10.4, 4H LBF, /, 13H NO. OF FRAGS,
 2X, E10.4, 14X, E10.4)
 909 FORMAT (2/, 24H ENGLISH INPUT/SI OUTPUT, 2/, 4X, 5H ITEM, 6X, 14H
 ENGLISH UNITS, 10X, 9H SI UNITS, 2/, 6H KAPPA, 9X, E10.4, 14X, E10.4, /,
 12H SOUND SPEED, 3X, E10.4, 7H IN/SEC, 7X, E10.4, 6H M/SEC, /, 9H PRESSURE,
 6X, E10.4, 4H PSI, 10X, E10.4, 8H PASCALS, /, 7H RADIUS, 8X, E10.4, 3H IN,
 11X, E10.4, 7H METERS, /, 12H CYL. LENGTH, 3X, E10.4, 3H IN, 11X, E10.4,
 7H METERS, /, 11H END LENGTH, 4X, E10.4, 3H IN, 11X, E10.4, 7H METERS, /,
 12H CYL. THICK., 3X, E10.4, 3H IN, 11X, E10.4, 7H METERS, /, 12H END THICK.,
 3X, E10.4, 3H IN, 11X, E10.4, 7H METERS)
 9091 FORMAT (13H WALL DENSITY, 2X, E10.4, 10H LBF/CU IN, 4X,
 E10.4, 8H KG/CU M, /,
 15H RESERVOIR MASS, E10.4, 4H LBF, 10X, E10.4, 3H KG, /, 13H NO. OF FRAGS,
 2X, E10.4, 14X, E10.4)
 910 FORMAT (2/, 29H ENGLISH INPUT/ENGLISH OUTPUT, 2/, 4X, 5H ITEM, 6X,
 14H ENGLISH UNITS, 2/, 6H KAPPA, 9X, E10.4, /, 12H SOUND SPEED, 3X, E10.4,
 7H IN/SEC, /, 9H PRESSURE, 6X, E10.4, 4H PSI, /, 7H RADIUS, 8X, E10.4,
 3H IN, /, 12H CYL. LENGTH, 3X, E10.4, 3H IN, /, 11H END LENGTH, 4X, E10.4,
 3H IN, /, 12H CYL. THICK., 3X, E10.4, 3H IN, /, 12H END THICK., 3X, E10.4,
 3H IN, /, 13H WALL DENSITY, 2X, E10.4, 10H LBF/CU IN, /,
 15H RESERVOIR MASS, E10.4, 4H LBF, /, 13H NO. OF FRAGS,
 2X, E10.4)
 911 FORMAT (2/, 50H CHARACTERISTICS OF MOTION OF FRAGMENTS (SI UNITS),
 2/, 2X, 5H TIME, 5X, 6H DIST., 5X, 5H VEL., 4X, 7H ACCEL., 2X, 9H PRESSURE, /)
 912 FORMAT (2/, 55H CHARACTERISTICS OF MOTION OF FRAGMENTS
 (ENGLISH UNITS),
 2/, 2X, 5H TIME, 5X, 6H DIST., 5X, 5H VEL., 4X, 7H ACCEL., 2X, 9H PRESSURE, /)
 913 FORMAT (3/, 13H FINAL VALUES, /, 6H TIME=, E10.4, 4H SEC, /, 10H
 DISTANCE=, E10.4, 7H METERS, /, 10H VELOCITY=, E10.4, 6H M/SEC, /, 14H
 ACCELERATION=, E10.4, 9H M/SQ-SEC, /, 10H PRESSURE=, E10.4, 8H PASCALS)
 914 FORMAT (3/, 13H FINAL VALUES, /, 6H TIME=, E10.4, 4H SEC, /, 10H
 DISTANCE=, E10.4, 3H IN, /, 10H VELOCITY=, E10.4, 7H IN/SEC, /, 14H
 ACCELERATION=, E10.4, 10H IN/SQ-SEC, /, 10H PRESSURE=, E10.4, 4H PSI)

TABLE 4C-2. (cont'd)

```

JJ=0
WRITE (1,309)
READ (0,310) CAPI,A8,P8
WRITE (1,900)
READ (0,901) RR
WRITE (1,311)
READ (0,3001) ZN1
WRITE (1,902)
READ (0,903) A,B,C,D,E
WRITE (1,905)
READ (0,3001) ZN2
WRITE (1,906)
READ (0,3001) ZN3
WRITE (1,904)
READ (0,314) FN,FK
WRITE (1,313)
READ (0,314) AH,XMAX
WRITE (1,316)
READ (0,3001) FN1
WRITE (1,317)
READ (0,3001) FN2
WRITE (1,318)
READ (0,3001) FN3
IF (ZN1-1.0) 100,100,101
100 CL=A
EL=B
CT=C
ET=D
DEN=E
PI=3.1415926535
V20=PI*(RR*RR*CL+EL*RR*RR+EL*EL*EL/3.0)
V4=PI*((RR-CT)**2.0*CL+(EL-ET)*((RR-ET)**2.0+(EL-ET)**2.0/3.0))
V8=V20-V4
TM=DEN*V20
IF (ZN2.EQ.1.0.AND.ZN3.EQ.1.0) G8 T8 102
IF (ZN2.EQ.1.0.AND.ZN3.EQ.2.0) G9 T8 103
IF (ZN2.EQ.2.0.AND.ZN3.EQ.1.0) G8 T8 104
IF (ZN2.EQ.2.0.AND.ZN3.EQ.2.0) G8 T8 105
102 WRITE (1,907) CAPI,A8,P8,RR,CL,EL,CT,ET,DFN,TM,FN
G8 T8 106
103 A81=A8/0.0254
P81=P8*0.0254*0.0254/4.448222
RRI=RR/0.0254
CLI=CL/0.0254
ELI=EL/0.0254
CTI=CT/0.0254
ETI=ET/0.0254
DENI=(DEN/14.5939)*(9.80665/0.3048)*(0.0254**3.0)
TM1=TM/14.5939*(9.80665/0.3048)
WRITE (1,908) CAPI,CAPI,A8,A81,P8,P81,RR,RRI,CL,CLI,EL,ELI,CT,CTI,
ET,ETI
WRITE (1,9081) DEN,DENI,TM,TM1,FN,FN

```

TABLE 4C-2. (cont'd)

```

A0=A01
P0=P01
RR=RRI
CL=CLI
EL=ELI
CT=CTI
ET=ETI
DEN=DEN1/386.0886
TM=TM1/386.0886
V0=V0/0.0254**3.0
G8 T0 106
104 A01=A0*0.0254
P01=P0*4.448222/0.0254/0.0254
RRI=RR*0.0254
CLI=CL*0.0254
ELI=EL*0.0254
CTI=CT*0.0254
ETI=ET*0.0254
DEN1=DEN*(0.3048/9.80665)*14.5939/(0.0254**3.0)
TM1=TM*(0.3048/9.80665)*14.5939
WRITE (1,909) CAPI,CAPI,A0,A01,P0,P01,RR,RRI,CL,CLI,ELI,ELI,CT,CTI,
ET,ETI
WRITE (1,9091) DEN,DEN1,TM,TM1,FN,FN
A0=A01
P0=P01
RR=RRI
CL=CLI
EL=ELI
CT=CTI
ET=ETI
DEN=DEN1
TM=TM1
V0=V0*0.0254**3.0
G8 T0 106
105 WRITE (1,910) CAPI,A0,P0,RR,CL,EL,CT,ET,DEN,TM,FN
DEN=DEN/386.0886
TM=TM/386.0886
G8 T0 106
101 V0=A
TM=B
CT=C
PI=3.1415926535
IF(ZN2.EQ.1.0.AND.ZN3.EQ.1.0) G8 T0 95
IF(ZN2.EQ.1.0.AND.ZN3.EQ.2.0) G8 T0 94
IF(ZN2.EQ.2.0.AND.ZN3.EQ.1.0) G8 T0 93
IF(ZN2.EQ.2.0.AND.ZN3.EQ.2.0) G8 T0 92
95 WRITE(1,898) CAPI,A0,P0,RR,V0,TM,CT,FN
G8 T0 106

```

TABLE 4C-2. (cont'd)

```

94 A8I=A8/0.0254
P8I=P8*0.0254*0.0254/4.448222
RRI=RR/0.0254
V8I=V8/(0.0254)**3.0
TM1=(TM/14.5939)*(9.80665/0.3048)
CT1=CT/0.0254
WRITE(1,897) CAPI,CAPI,A8,A8I,P8,P8I,RR,RRI,V8,V8I,TM,TM1,CT,CT1,
FN,FN
A8=A8I
P8=P8I
RR=RRI
V8=V8I
TM=TM1/386.0886
CT=CT1
GO TO 106
93 A8I=A8*0.0254
P8I=P8*4.448222/0.0254/0.0254
RRI=RR*0.0254
V8I=V8*(0.0254)**3.0
TM1=TM*(0.3048/9.80665)*14.5939
CT1=CT*0.0254
WRITE(1,896) CAPI,CAPI,A8,A8I,P8,P8I,RR,RRI,V8,V8I,TM,TM1,CT,CT1,
FN,FN
A8=A8I
P8=P8I
RR=RRI
V8=V8I
TM=TM1
CT=CT1
GO TO 106
92 WRITE(1,895) CAPI,A8,P8,RR,V8,TM,CT,FN
TM=TM/386.0886
106 CONTINUE
PERI=2.0*PI*RR
FF=PI*(RR-CT)**2.0
XX=TM*A8*A8*(2.0/(CAPI-1.0))/(FF*P8)
THETA=TM*A8*((2.0/(CAPI-1.0))**0.5)/(FF*P8)
CAP2=CAPI/(CAPI-1.0)
CAP3=(3.0*CAPI-1.0)/(2.0*CAPI)
CAP4=(CAPI+1.0)/(2.0*(CAPI-1.0))
AI=P8*V8/(TM*A8*A8)
BI=FX*(2.0/(CAPI+1.0))**CAP4*((2.0/(CAPI-1.0))**0.5)*PERI*V8/(FF*FF)
X=0.0
Y(1)=0.0
Y(2)=0.0
Y(3)=1.0
WRITE (1,322) X,Y(1),Y(2),Y(3)
NA=3

```

TABLE 4C-2. (cont'd)

```

F(1)=Y(2)
F(2)=4.0*Y(3)*(1.0-Y(2)*Y(2)/(4.0*Y(3)**(1.0/CAP2)))*CAP2
F(3)=(-B1*CAPI/AI*Y(1)*Y(3)**CAP3-CAPI*Y(2)*Y(3))/((CAPI-1.0)/2.0*AI+
Y(1))
IF (FN1-1.0) 200,200,30
200 WRITE (1,320)
30 CALL RUNGE (NA,X,Y,F,AH,KA,W1,W2)
IF (KA-1) 40,50,40
50 F(1)=Y(2)
F(2)=4.0*Y(3)*(1.0-Y(2)*Y(2)/(4.0*Y(3)**(1.0/CAP2)))*CAP2
F(3)=(-B1*CAPI/AI*Y(1)*Y(3)**CAP3-CAPI*Y(2)*Y(3))/((CAPI-1.0)/2.0*AI+
Y(1))
G0 T0 30
40 IF (FN1-1.0) 45,45,201
45 WRITE (1,312) X,Y(1),Y(2),F(2),Y(3)
201 C0NTINUE
JJ=JJ+1
TT(JJ)=X
G(JJ)=Y(1)
GG(JJ)=Y(2)
GGG(JJ)=F(2)
PS(JJ)=Y(3)
IF (X-XMAX) 41,10,10
41 C0NTINUE
G0 T0 30
10 C0NTINUE
IF (FN2-1.0) 130,130,131
130 IF(ZN3-1.0) 108,108,109
108 WRITE(1,911)
G0 T0 110
109 WRITE(1,912)
110 D0 107 I=1,JJ
TI=THETA*TT(I)
GI=(XX*G(I))/2.0
G2=(XX/(2.0*THETA))*GG(I)
G3=XX/(2.0*THETA*THETA)*GGG(I)
G4=P0*PS(I)
107 WRITE(1,312) TI,GI,G2,G3,G4
131 FTI=THETA*X
FG1=(XX*Y(I))/2.0
FG2=(XX/(2.0*THETA))*Y(2)
FG3=XX/(2.0*THETA*THETA)*F(2)
FG4=P0*Y(3)
IF(ZN3-1.0) 111,111,112
111 WRITE(1,913) FTI,FG1,FG2,FG3,FG4
G0 T0 113
112 WRITE(1,914) FTI,FG1,FG2,FG3,FG4
113 C0NTINUE
IF (FN3-1.0) 204,204,205
204 C0NTINUE
205 C0NTINUE
END
*

```

TABLE 4C-2. (cont'd)

READ IN KAPPA, SBUND SPEED, INITIAL PRESSURE
1.67,6880.,500.

READ IN CYLINDER RADIUS
6.0

IF PARAMETERS ARE:
CYL. LENGTH, END LENGTH, CYL. THICK., END THICK., WALL DENS.,
ENTER 1

VOLUME, MASS OF RESERVOIR, CYL. THICK.,
ENTER 2

1

READ IN VALUES
0.0,6.0,0.012,0.012,0.1622

INPUT UNITS? SI=1 ENGLISH=2
2

OUTPUT UNITS? SI=1 ENGLISH=2
1

READ IN NO. OF FRAGMENTS(2.), DISCHARGE CREF.
2.,1.

READ IN TIME INTERVAL, MAXIMUM TIME
0.1,1.7

DISPLAY NONDIMENSIONAL DYNAMIC VAR.? YES=1 NO=2
1

DISPLAY DIMENSIONAL DYNAMIC VAR.? YES=1 NO=2
1

MAKE RANGE CALCULATION? YES=1 NO=2
2

TABLE 4C-2. (cont'd)

ENGLISH INPUT/SI OUTPUT

ITEM	ENGLISH UNITS	SI UNITS
KAPPA	.1670E+01	.1670E+01
SOUND SPEED	.6880E+04 IN/SEC	.1748E+03 M/SEC
PRESSURE	.5000E+03 PSI	.3447E+07 PASCALS
RADIUS	.6000E+01 IN	.1524E+00 METERS
CYL. LENGTH	.0000E+01 IN	.0000E+01 METERS
END LENGTH	.6000E+01 IN	.1524E+00 METERS
CYL. THICK.	.1200E-01 IN	.3048E-03 METERS
END THICK.,	.1200E-01 IN	.3048E-03 METERS
WALL DENSITY	.1622E+00 LBF/CU IN	.4490E+04 KG/CU M
RESERVOIR MASS	.8788E+00 LBF	.3986E+00 KG
NO. OF FRAGS	.2000E+01	.2000E+01

INITIAL CONDITIONS

$x(0) = .0000E+01$ $g(0) = .0000E+01$ $g''(0) = .0000E+01$ $p-norm = .1000E+01$

CHARACTERISTICS OF MOTION OF FRAGMENTS (NORMALIZED)

T-NORM	G	G"	G'''	P-NORM
.1000E+00	.1960E-01	.3845E+00	.3550E+01	.9765E+00
.2000E+00	.7434E-01	.6943E+00	.2619E+01	.9138E+00
.3000E+00	.1554E+00	.9116E+00	.1761E+01	.8293E+00
.4000E+00	.2543E+00	.1055E+01	.1151E+01	.7388E+00
.5000E+00	.3648E+00	.1149E+01	.7525E+00	.6516E+00
.6000E+00	.4831E+00	.1211E+01	.4952E+00	.5720E+00
.7000E+00	.6063E+00	.1251E+01	.3277E+00	.5015E+00
.8000E+00	.7329E+00	.1278E+01	.2171E+00	.4398E+00
.9000E+00	.8617E+00	.1296E+01	.1431E+00	.3864E+00
.1000E+01	.9919E+00	.1308E+01	.9316E-01	.3402E+00
.1100E+01	.1123E+01	.1315E+01	.5936E-01	.3003E+00
.1200E+01	.1255E+01	.1320E+01	.3658E-01	.2658E+00
.1300E+01	.1387E+01	.1323E+01	.2143E-01	.2359E+00
.1400E+01	.1519E+01	.1324E+01	.1163E-01	.2099E+00
.1500E+01	.1652E+01	.1325E+01	.5591E-02	.1873E+00
.1600E+01	.1784E+01	.1326E+01	.2174E-02	.1675E+00
.1700E+01	.1917E+01	.1326E+01	.5397E-03	.1502E+00
.1800E+01	.2050E+01	.1326E+01	.2697E-04	.1350E+00

TABLE 4C-2. (concl'd)

CHARACTERISTICS OF MOTION OF FRAGMENTS (SI UNITS)

TIME	DIST.	VEL.	ACCEL.	PRESSURE
.4804E-04	.1421E-02	.5804E+02	.1116E+07	.3367E+07
.9607E-04	.5391E-02	.1048E+03	.8230E+06	.3150E+07
.1441E-03	.1127E-01	.1376E+03	.5533E+06	.2859E+07
.1921E-03	.1844E-01	.1593E+03	.3618E+06	.2547E+07
.2402E-03	.2646E-01	.1735E+03	.2365E+06	.2246E+07
.2882E-03	.3503E-01	.1828E+03	.1556E+06	.1972E+07
.3363E-03	.4397E-01	.1889E+03	.1030E+06	.1729E+07
.3843E-03	.5315E-01	.1930E+03	.6821E+05	.1516E+07
.4323E-03	.6249E-01	.1956E+03	.4497E+05	.1332E+07
.4804E-03	.7193E-01	.1974E+03	.2928E+05	.1173E+07
.5284E-03	.8144E-01	.1985E+03	.1866E+05	.1035E+07
.5764E-03	.9100E-01	.1993E+03	.1150E+05	.9163E+06
.6245E-03	.1006E+00	.1997E+03	.6735E+04	.8132E+06
.6725E-03	.1102E+00	.1999E+03	.3655E+04	.7236E+06
.7205E-03	.1198E+00	.2001E+03	.1757E+04	.6456E+06
.7686E-03	.1294E+00	.2001E+03	.6831E+03	.5775E+06
.8166E-03	.1390E+00	.2001E+03	.1696E+03	.5179E+06
.8647E-03	.1486E+00	.2001E+03	.8476E+01	.4655E+06

FINAL VALUES

TIME= .8647E-03 SEC
 DISTANCE= .1486E+00 METERS
 VELOCITY= .2001E+03 M/SEC
 ACCELERATION= .8476E+01 M/SQ-SEC
 PRESSURE= .4655E+06 PASCALS

STOP

(SMAINS)205+1

+

-

The matrix of different initial conditions run on the computer is given in Table 4C-3. For these calculations, the containment vessel was chosen to be made of a titanium alloy since these alloys are often used for flight-weight containment vessels. Gases chosen were air, xenon (Xe), hydrogen (H_2), and carbon dioxide (CO_2). Table 4C-4 contains nondimensionalized input parameters and nondimensionalized final velocities. It should be noted that these nondimensional quantities are not the same as the dimensionless parameters generated in the program to calculate velocity. Rather, the nondimensional parameters in Table 4C-4 take the following form:

- (1) Nondimensional pressure \bar{P} = initial pressure/atmospheric pressure
- (2) Nondimensional thickness h/D = cylinder thickness/cylinder diameter
- (3) Nondimensional length L/D = total length/cylinder diameter
- (4) Nondimensional velocity \bar{V} = final velocity/sound speed of gas.

For all of the cases run, the following conditions hold:

- (1) All vessels were assumed to be made of titanium or a titanium alloy.
- (2) The thickness of the containment vessel is uniform.
- (3) All containment vessels have hemispherical endcaps.

Figures 4C-3 through 4C-5 contain plots of \bar{V} versus \bar{P} for h/d ratios of 0.001, 0.01 and 0.1, respectively, the L/D ratio being held constant at 10.0 and as many as three curves, one for each of the gases (CO_2 , air, H_2), being plotted on each figure. Figures 4-18 through 4-20 contain plots of V versus P for air, carbon dioxide and hydrogen gases, respectively, the L/D ratio being held constant at 10.0 and as many as three curves, one for each h/D ratio (0.001, 0.01, and 0.1) being plotted on a single figure. Figure 4-21 contains a plot of \bar{V} versus L/D ratio for air and a h/D ratio of 0.01. Two curves are plotted on this figure, one for each of two different initial gas pressures.

From the curves in the figures mentioned above, one can make a few conclusions.

TABLE 4C-3

INITIAL CONDITIONS

Containment Vessel Characteristics

$R = 6.0 \text{ in}$
 $\rho_g = 0.1622 \text{ lbf/in}^3$
 $N = 2.$
 $k = 1.0$

Sonic Velocities

Air - $13550 \text{ in/sec} = 344.17 \text{ m/s}$
Xe - $5880 \text{ in/sec} = 174.752 \text{ m/s}$
H₂ - $50000 \text{ in/sec} = 1270 \text{ m/s}$
CO₂ - $10150 \text{ in/sec} = 257.81 \text{ m/s}$

Run No.	L/D	Gas	γ	a_{∞} (in/sec)	P _{oo} (psi)	C _L (in)	E _L (in)	h/D	C _T (in)	E _T (in)
1	1.0	Air	1.4	13550	500	0.0	6.0	0.001	0.012	0.012
2					60000					
3					500					
4					60000					
5					500					
6					60000					
7		Xe	1.67	6880	500					
8					60000					
9					500					
10					60000					
11					500					
12					60000					
13	2.5	Air	1.4	13550	500	18.0	6.0	0.01	0.12	0.12
14					60000					
15	5.0	Air	1.4	13550	500	48.0	6.0	0.01	0.12	0.12
16					60000					
17	7.5	Air	1.4	13550	500	78.0	6.0	0.01	0.12	0.12
18					60000					
19	10.0	Air	1.4	13550	500	108.0	6.0	0.001	0.012	0.012
20					2000					
21					8000					
22					25000					
23					60000					
24					500					
25					2000					
26					8000					
27					25000					
28					60000					

TABLE 4C-3. (Cont'd)

<u>Run No.</u>	<u>L/D</u>	<u>Gas</u>	<u>γ</u>	<u>a_{oo} (in/sec)</u>	<u>P_{oo} (psi)</u>	<u>CL (in)</u>	<u>EL (in)</u>	<u>h/D</u>	<u>CT (in)</u>	<u>ET (in)</u>
29	10.0	Air	1.4	13550	500	108.0	6.0	0.1	1.2	1.2
30					2000					
31					8000					
32					25000					
33					60000					
34		H ₂	1.4	50000	500		0.001	0.012	0.012	
35					2000					
36					8000					
37					25000					
38					60000					
39					500		0.01	0.12	0.12	
40					2000					
41					8000					
42					25000					
43					60000					
44					500		0.01	1.2	1.2	
45					2000					
46					8000					
47					25000					
48					60000					
49		CO ₂	1.225	10150	500		0.001	0.012	0.012	
50					2000					
51					8000					
52					25000					
53					60000					
54					500		0.1	1.2	1.2	
55					2000					
56					8000					
57					25000					
58					60000					

TABLE 4C-4. NONDIMENSIONAL INPUT PARAMETERS
AND NONDIMENSIONAL VELOCITY

<u>Run No.</u>	<u>L/D</u>	<u>Gas</u>	<u>γ</u>	<u>Nondim. Pressure ($P_{\infty}/1 \text{ Atm.}$)</u>	<u>h/D</u>	<u>Nondim. Velocity (V/v_{∞})</u>	<u>Velocity (m/sec)</u>
1	1.0	Air	1.4	34.01	0.001	0.9519	327.6
2				4081.63		1.9066	656.2
3				34.01	0.01	0.3094	106.5
4				4081.63		1.5841	542.2
5				34.01	0.1	0.0527	18.3
6				4081.63		0.8406	289.3
7		Xe	1.67	34.01	0.001	1.1451	200.1
8				4081.63		1.6337	285.5
9				34.01	0.01	0.5734	100.2
10				4081.63		1.4918	260.7
11				34.01	0.1	0.1194	20.86
12				4081.63		1.0787	188.5
13	2.5	Air	1.4	34.01	0.01	0.2679	92.20
14				4081.63		1.5908	547.5
15	5.0	Air	1.4	34.01	0.01	0.2253	77.54
16				4081.63		1.5611	537.3
17	7.5	Air	1.4	34.01	0.01	0.2014	69.30
18				4081.63		1.5344	528.1
19	10.0	Air	1.4	34.01	0.001	0.7284	250.7
20				136.05		1.2128	417.4
21				544.22		1.5870	546.2
22				1700.68		1.7881	615.4
23				4081.63		1.9005	654.1
24				34.01	0.01	0.1851	63.72
25				136.05		0.4373	150.5
26				544.22		0.8792	302.6
27				1700.68		1.2703	437.2
28				4081.63		1.5129	520.7
29				34.01	0.1	0.0292	10.05
30				136.05		0.0731	25.16
31				544.22		0.1812	62.37
32				1700.68		0.3713	127.8
33				4081.63		0.6102	210.0

TABLE 4C-4. (Cont'd)

<u>Run No.</u>	<u>L/D</u>	<u>Gas</u>	<u>Y</u>	<u>Nondim. Pressure (P_{oo}/1 Atm.)</u>	<u>h/D</u>	<u>Nondim. Velocity (V/a_{oo})</u>	<u>Velocity (m/sec)</u>
34	10.0	H ₂	1.4	34.01	0.001	0.1561	198.2
35				136.05		0.3739	474.8
36				544.22		0.7847	996.6
37				1700.68		1.1850	1505.
38				4081.63	↓	1.4457	1836.
39				34.01	0.01	0.0333	42.35
40				136.05		0.0833	105.8
41				544.22		0.2054	260.8
42				1700.68		0.4159	528.2
43				4081.63	↓	0.6712	852.4
44				34.01	0.1	0.0052	6.550
45				136.05		0.0130	16.46
46				544.22		0.0325	41.30
47				1700.68		0.0691	87.74
48				4081.63	↓	0.1228	156.0
49		CO ₂	1.225	34.01	0.001	1.0081	259.9
50				136.05		1.5550	400.9
51				544.22		1.9600	505.3
52				1700.68		2.1958	566.1
53				4081.63	↓	2.3339	601.7
54				34.01	0.1	0.0440	11.35
55				136.05		0.1100	28.37
56				544.22		0.2711	69.90
57				1700.68		0.5446	140.4
58				4081.63	↓	0.8627	222.4

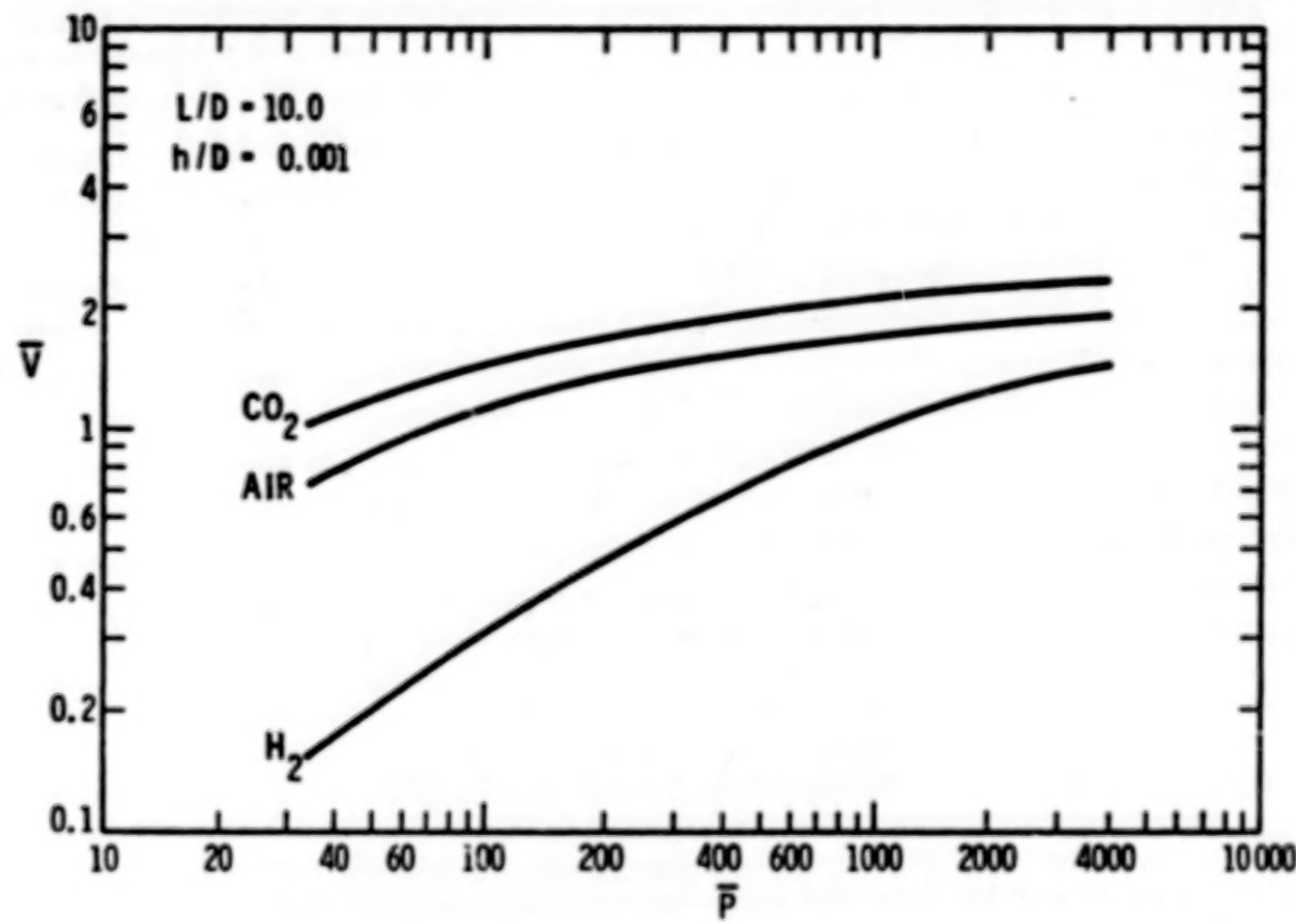


Figure 4C-3. Non dimensional Velocity Vs Nondimensional Pressure for Several Gases

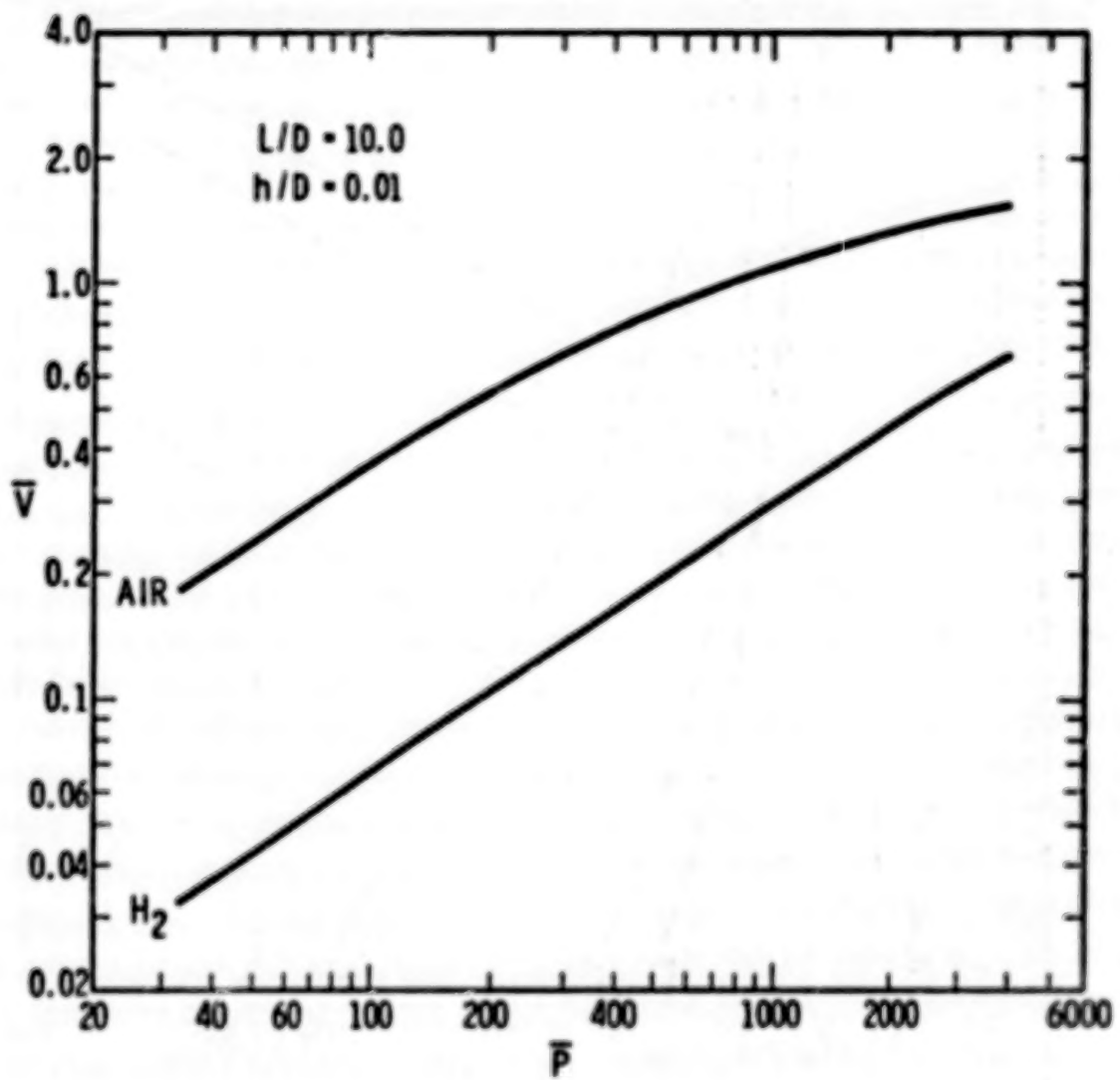


Figure 4C-4. Nondimensional Velocity Vs Nondimensional Pressure, $h/D = 0.01$

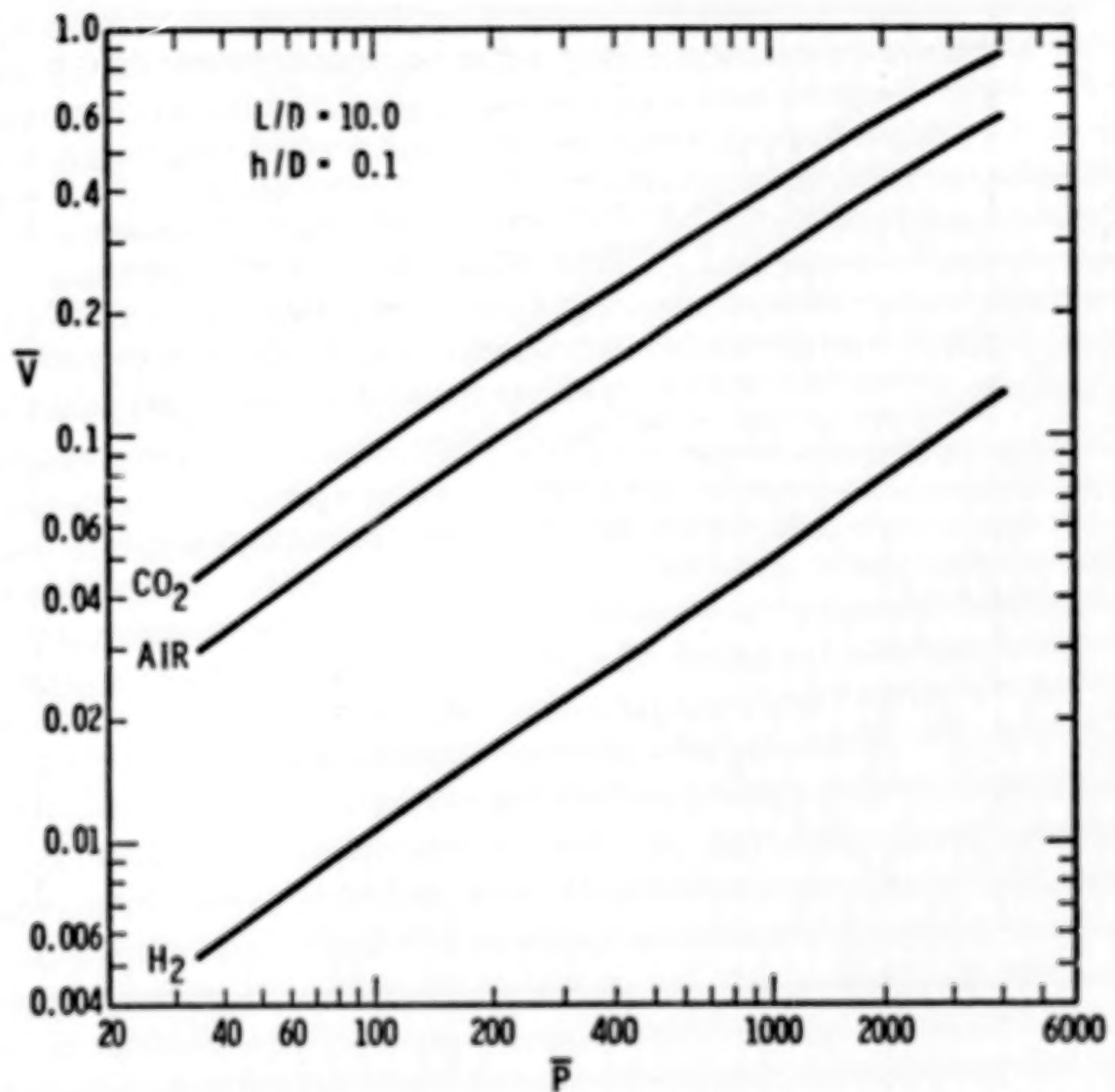


Figure 4C-5. Nondimensional Velocity Vs Nondimensional Pressure, $h/D = 0.1$

Conclusions

- (1) In all cases, fragment velocity increases as initial pressure increases, but at a decreasing rate.
- (2) Fragment velocities from vessels containing the heavier gases (and the lower sonic velocities) are higher than that for the lighter gases (and the higher sonic velocities) for the same initial pressure, L/D ratio and h/D ratio. The rate of change in velocity with increasing pressure, however, is greater for the lighter gases, and all the curves plotted appear to approach an asymptotic limit for a fixed h/D ratio (Figures 4C-3 through 4C-5).
- (3) Fragment velocities for thin-walled vessels (low h/D ratios) are higher than those for thick-walled vessels (high h/D ratios), for the same initial pressure, L/D ratio and gas. The rate of change in velocity with increasing pressure, however, is greater for the thick-walled vessels, and all the curves plotted appear to approach an asymptotic limit for a fixed gas (Figures 4-18 through 4-20).
- (4) For a fixed initial pressure, fragment velocities decrease with increasing L/D ratios. For higher initial pressures, however, the rate of decrease in the fragment velocity with increasing L/D ratios decreases (Figure 4-21).

LIST OF REFERENCES

1. Taylor, D. B., and C. F. Price, "Velocity of Fragments from Burst Gas Reservoirs," ASME Transactions, Journal of Engineering for Industry, November 1971.

APPENDIX IV.D

ESTIMATION OF VELOCITIES ATTAINED BY APPURTENANCES SUBJECT TO BLAST LOADING

The situation discussed here involves the interaction of appurtenances (nearby objects) with the blast wave from propellant or pressure vessel explosions. These objects can be parts of the launch tower, storage tanks, vehicles, and objects in or attached to the upper stages of the launch vehicle itself, or they can be tools, benches, chairs, and machinery in a shop area. The types of appurtenances depend upon the location of the explosion, and, for this reason, results in this appendix are presented in such a manner that velocities of essentially any conceivable appurtenance in the blast field can be calculated.

To be able to predict velocities to which appurtenances are accelerated by explosions, one must consider the interaction of blast waves with solid objects. Figure 4D-1⁽¹⁾ shows schematically, in three stages, the interaction of a blast wave with an irregular object. As the wave strikes the object, a portion is reflected from the front face, and the remainder diffracts around the object. In the diffraction process, the incident wave front closes in behind the object, greatly weakened locally, and a pair of trailing vortices is formed. Rarefaction waves sweep across the front face, attenuating the initial reflected blast pressure. After passage of the front, the body is immersed in a time-varying flow field. Maximum pressure on the front face during this "drag" phase of loading is the stagnation pressure.

To predict the effect of a blast wave on an appurtenance, it is necessary to examine the net transverse pressure on the object as a function of time. This loading, somewhat idealized, is shown in Figure 4D-2. After time of arrival t_a , the net transverse pressure rises linearly from zero to a maximum peak reflected pressure P_r in time $(T_1 - t_a)$. For an object with a flat face nearest the approaching blast wave, this time interval is zero. Pressure then falls linearly to drag pressure in time $(T_2 - T_1)$ and decays more slowly to zero in time $(T_3 - T_2)$.

Once the time history of net transverse pressure loading is known, the prediction of appurtenance velocity can be made. The basic assumptions are that the appurtenance behaves as a rigid body, that none of the energy in the blast wave is absorbed in breaking the appurtenance loose from its moorings or deforming it elastically or plastically, and that gravity effects can be ignored during this acceleration phase of the motion. The equation of motion of the object is then

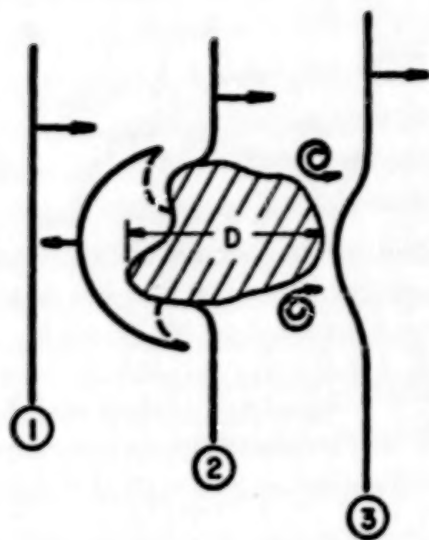


Figure 4D-1. Interaction of Blast Wave with Irregular Object

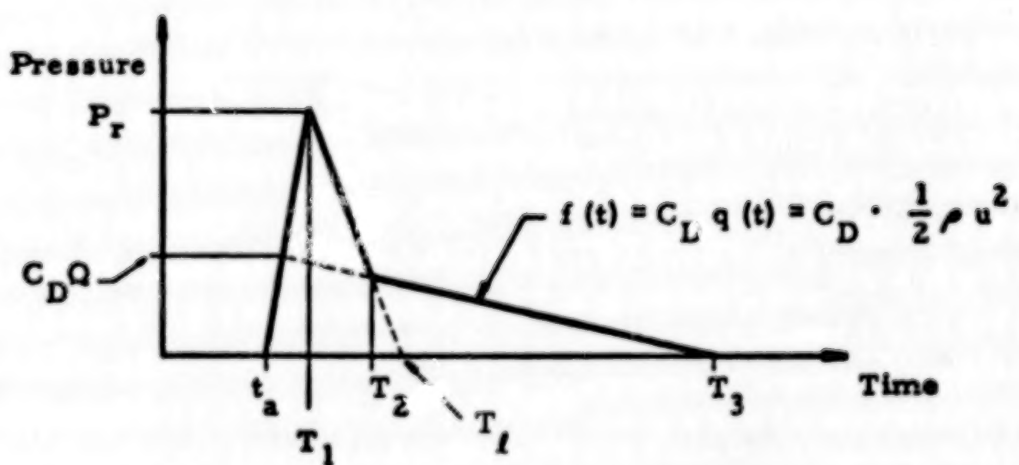


Figure 4D-2. Time History of Net Transverse Pressure on Object During Passage of a Blast Wave

$$A \dot{p}(t) = M \ddot{x} \quad (4D-1)$$

where

A = area of the object presented to the blast front

$p(t)$ = net transverse pressure according to Figure 4D-2

M = total mass of the object

x = displacement of the object (dots denote derivatives with respect to time)

The object is assumed to be at rest initially, so that

$$x(0) = 0, \dot{x}(0) = 0 \quad (4D-2)$$

Equation (4D-1) can be integrated directly. With use of the initial conditions, Equation (4D-2), this operation yields, for appurtenance velocity,

$$\dot{x}(T_3) = \frac{A}{M} \int_0^{(T_3 - t_a)} p(t) dt = \frac{A}{M} I_d \quad (4D-3)$$

where

I_d = total drag and diffraction impulse

The integration in Equation (4D-3) can be performed explicitly if the pressure time history is described by suitable mathematical functions, or performed graphically or numerically if $p(t)$ cannot be easily written in function form. In either case, Equation (4D-3) yields the desired result--a predicted velocity for an object. The integral in Equation (4D-3) is merely the area under the curve in Figure 4D-2.

The time history of drag pressure is the modified exponential with maximum given by

$$C_D Q = C_D \cdot \frac{1}{2} \rho_s u_s^2 \quad (4D-4)$$

where

C_D = steady-state drag coefficient for the object

Q = peak dynamic overpressure

ρ_s = peak density

u_s = peak particle velocity

The characteristics of the diffraction phase of the loading can be determined easily if the peak side-on overpressure P_s or the shock velocity u_s is known, together with the shape and some characteristic dimensions of the object. The peak amplitude of the drag phase $C_D Q$ can also be determined explicitly from P_s or u_s . The time history of the ensuing drag loading $C_D q(t)$, however, is quite difficult to predict accurately for propellant blasts or blasts from gas vessel explosions.

Side-on overpressure is often expressed as a function of time by the modified Friedlander equation. (2)

$$p(t) = P \left(\frac{1-t}{T} \right) e^{-bt/T} \quad (4D-5)$$

where

T = duration of the positive phase of the blast wave

Integrating this equation gives the impulse

$$I = \int_0^T p(t) dt = \frac{PT}{b} \left[1 - \frac{(1-e^{-b})}{b} \right] \quad (4D-6)$$

The dimensionless parameter b is called the time constant, is a function of shock strength, and is reported in Chapter 6 of Reference 2. It is plotted graphically in Figure 4D-3 for a range of shock strengths, \bar{P} , where

$$\bar{P} = \frac{P}{P_0} \quad (4D-7)$$

and P_0 is ambient air pressure. Ambient air pressure P_0 varies with altitude as shown in Figure 3-9. The peak reflected overpressure P_r and peak dynamic pressure Q are unique functions of P for a given ambient pressure P_0 . For shocks of intermediate to weak strengths, $\bar{P} \leq 3.5$, these functions are⁽²⁾

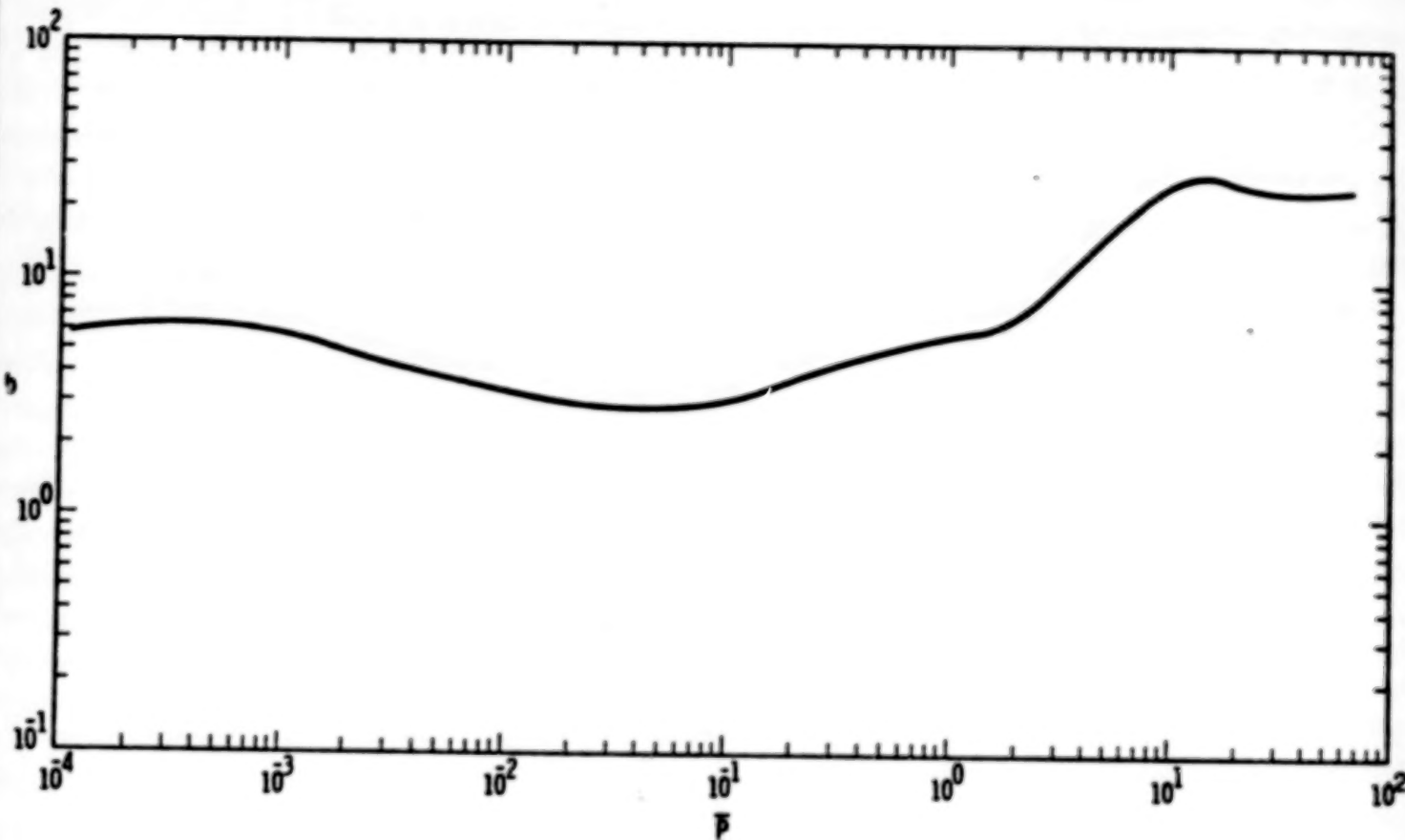


Figure 4D-3. Dimensionless Time Constant Vs
Nondimensional Overpressure

359

$$\bar{P}_r = 2\bar{P} + \frac{3\bar{P}^2}{4} \quad (4D-8)$$

and

$$\bar{Q} = \left(\frac{5}{2}\right) \frac{\bar{P}^2}{7 + \bar{P}} \quad (4D-9)$$

where

$$\bar{P}_r = \frac{\bar{P}_r}{P_0}, \quad \bar{Q} = \frac{Q}{P_0} \quad (4D-10)$$

For the time history of drag pressure, a good fit to experimental data for TNT is a slightly modified form of that employed by Glasstone, (3)

$$q(t) = Q \left(\frac{1-t}{T}\right)^2 e^{-bt/T} \quad (4D-11)$$

In order to estimate values for the time intervals shown in Figure 4D-2, it is necessary to obtain the shock front velocity U . This is a unique function of the shock strength \bar{P} and, for $\bar{P} \leq 3.5$, is given by(2)

$$\bar{U}^2 = 1 + \frac{6\bar{P}}{7} \quad (4D-12)$$

for

$$U = \bar{U} a_0 \quad (4D-13)$$

where

$$a_0 = \text{speed of sound in air}$$

The manner in which a_0 varies with altitude is shown in Figure 3D-1. For shock strengths \bar{P} greater than 3.5, \bar{P}_r , \bar{Q} and \bar{U} for Equations (4D-8), (4D-9), and (4D-12), respectively, can be approximated from tables in Chapter 6 of Reference 2. Methods for estimating $(T_1 - t_a)$ and $(T_2 - T_1)$ are given by Norris, et al. (4) and depend on the shock front velocity given above and the geometry of the appurtenance. The first time interval can be acquired from

$$(T_1 - t_a) = \frac{x}{U} \quad (4D-14)$$

where X is the distance from the front of the object to the plane facing the approaching blast wave which has the largest cross-sectional area. The latter time interval can be determined from

$$(T_2 - T_1) = \frac{4h}{U} \quad (4D-15)$$

for appurtenances on the ground and

$$(T_2 - T_1) = \frac{2h}{U} \quad (4D-16)$$

for appurtenances in the air, where H is the minimum transverse dimension of the largest mean presented area. Time interval $(T_3 - t_a)$ is equivalent to T and can be acquired by rearranging Equation (4D-6) giving

$$T = \frac{Ib}{P \left[1 - \frac{(1 - e^{-b})}{b} \right]} \quad (4D-17)$$

The integral in Equation (4D-3) is just the area under the curve in Figure 4D-2. Using the law of similar triangles, time interval $(T_1 - T_2)$ (see Figure 4D-2) can be obtained from

$$\frac{(T_f - T_2)}{(T_f - T_1)} = \frac{C_D q(T_2)}{P_r} \quad (4D-18)$$

Solving Equation (4D-18) for T_f ,

$$T_f = \frac{T_2 - \frac{C_D q(T_2)}{P_r} T_1}{1 - \frac{C_D q(T_2)}{P_r}} \quad (4D-19)$$

The total area under the curve in Figure 4D-2 is then

$$I_d = \text{Area}_{\text{Total}} = \text{Area}_{\Delta t_a P_r T_1} + C_D \int_{T_2}^{T_3} q(t) dt - \text{Area}_{\Delta T_2 [C_D q(T_2)] T_1} \quad (4D-20)$$

where $\Delta t_a P_r T_1$ represents the triangle with vertices t_a , P_r and T_1 , and $\Delta T_2 [C_D q(T_2)] T_1$ represents the triangle with vertices T_2 , $C_D q(T_2)$, and T_1 . The integral in Equation (4D-20) can be solved by substituting Equation (4D-11) for $q(t)$. Making similar substitutions and solving the integral, Equation (4D-20) becomes

$$I_d = \frac{P_r (T_f - t_a)}{2} + \left\{ \frac{C_D Q T}{b} e^{-(b/T)t} \left[\left(\frac{2t}{T} - \frac{2t}{bT} - \left(\frac{t}{T} \right)^2 \right) + \left(\frac{2}{b} - \frac{2}{b^2} - 1 \right) \right] \right\}_{t=T_4}^{t=T_3} - \frac{C_D Q}{2} \left(1 - \frac{T_2}{T} \right)^2 e^{-bT_2/T} (T_f - T_2) \quad (4D-21)$$

After substituting appropriate values for the variables and evaluating the middle portion of Equation (4D-21) over the time interval T_2 to T_3 , total drag and diffraction impulse I_d can be determined. Substituting total impulse I_d , the mean presented area A and total mass M of the object into Equation (4D-3), the maximum velocity of the appurtenance can be found.

Surely, this is a needlessly long procedure to follow every time an estimate of appurtenance velocity is required. In order to simplify the velocity calculation, Equation (4D-3) can be put into nondimensional form. This was done by substituting known environmental variables into Equations (4D-3) and (4D-21) and rearranging terms. After performing all of the substitutions, a tremendously long equation evolves, which reduces to the simple functional format

$$\frac{M V a_o}{p_o A (K H + X)} = f \left(\frac{P_s}{p_o}, \frac{C_D I_s a_o}{P_s (K H + X)} \right) \quad (4D-22)$$

where

M = mass of object

V = velocity of object

a_o = velocity of sound in air

p_o = atmospheric pressure

A = mean presented area of object

K = constant (4 if appurtenance is on the ground and 2 if appurtenance is in air)

H = minimum transverse dimension at location of largest presented area of object

X = distance from the front of object to location of largest cross-sectional area

P_s = peak incident overpressure

C_D = drag coefficient

I_s = peak incident specific impulse

The manner in which p_o and a_o vary with altitude is shown in Figures 3-9 and 3D-1, respectively. Representative values for drag coefficient C_D can be found in Figure 4D-4. Equation (4D-22) states that nondimensional appurtenance velocity is a function of nondimensional pressure and nondimensional impulse. A computer program was written to determine combinations of nondimensional pressures and impulses required to produce various nondimensional velocities. A graphical representation of the nondimensional pressure P_s and nondimensional impulse I_s combinations producing various values of nondimensional velocity V is shown in Figure 4D-5. Objects of various sizes and shapes, as shown in the key for symbols, were used as input into the program to test the nondimensional scaling law. As expected, all calculated points were near the appropriate nondimensional velocity curves. Thus, Figure 4D-5 can be used to calculate the velocity of any type of appurtenance. Care should be taken when interpolating between curves and extending curves. Estimates made by extending the curves to lower nondimensional impulses are especially hazardous. An example for calculating appurtenance velocity follows.

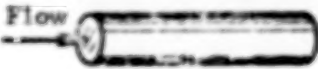
SHAPE	SKETCH	C_D
Right Circular Cylinder (long rod), side-on		1.20
Sphere		0.47
Rod, end-on		0.82
Disc, face-on		1.17
Cube, face-on		1.05
Cube, edge-on		0.80
Long Rectangular Member, face-on		2.05
Long Rectangular Member, edge-on		1.55
Narrow Strip, face-on		1.98

Figure 4D-4. Drag Coefficients, C_D , for Various Shapes

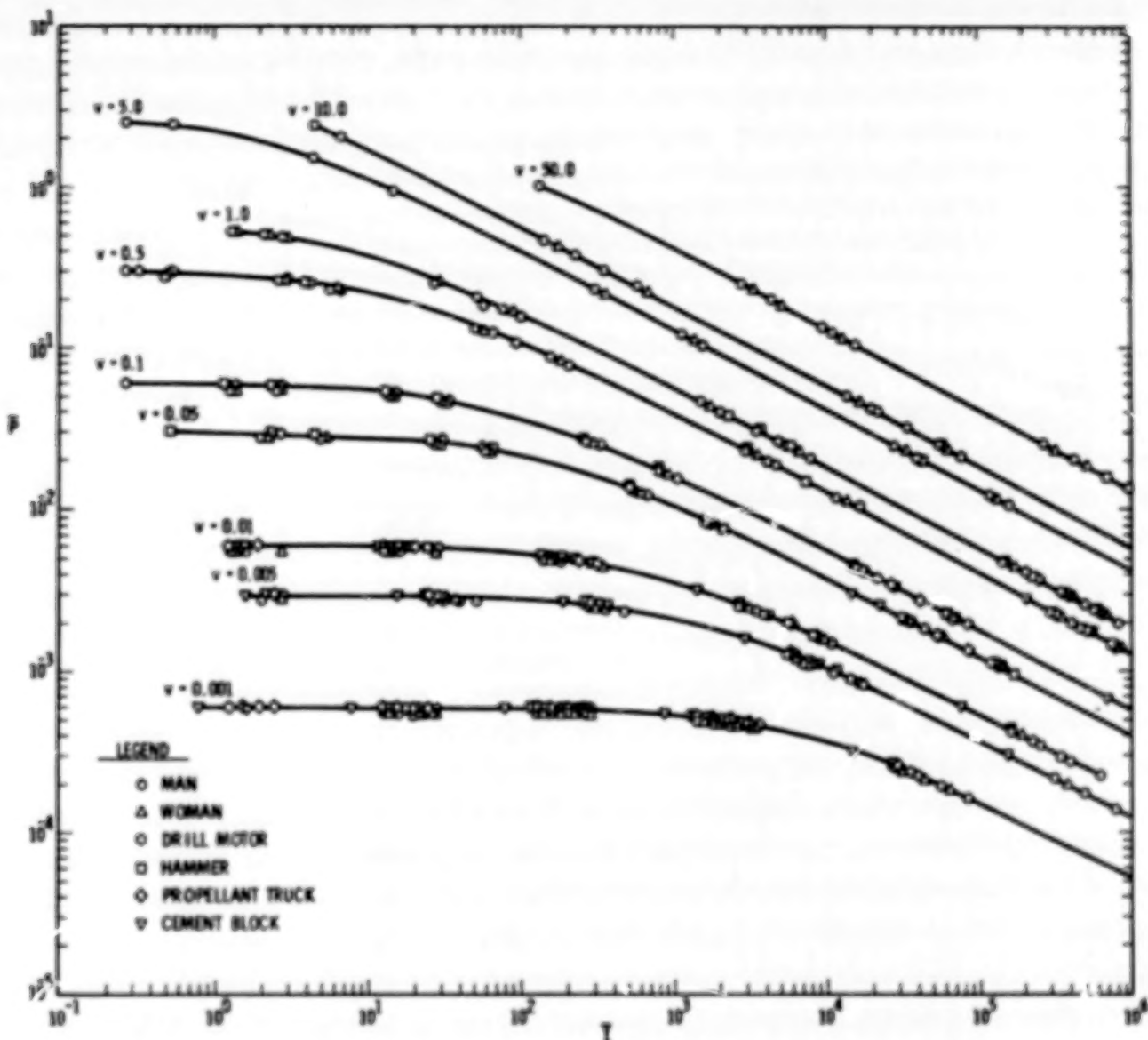


Figure 4D-5. Nondimensional Appurtenance Velocity \bar{V} as a Function of Nondimensional Pressure \bar{P}_s and Nondimensional Impulse \bar{I}

Example

Suppose a square cement block is subjected to an explosion. At the block it was determined that

$$P_s = 1.0 \times 10^5 \text{ Pa (14.5 psi)}$$

$$I_s = 1.9 \times 10^4 \text{ Pa} \cdot \text{s (2.756 psi-sec)}$$

The explosion occurs at sea level. Therefore,

$$P_0 = 1.0135 \times 10^5 \text{ Pa}$$

$$a_0 = 340 \text{ m/s (1115 ft/sec)}$$

The block has characteristics [see Equation (4D-22)]

$$X = 0 \text{ m}$$

$$H = 2.5 \text{ m (8.2 ft)}$$

$$C_D = 1.05$$

$$A = 25 \text{ m}^2 (269 \text{ ft}^2)$$

$$M = 2.8 \times 10^5 \text{ kg (6.17} \times 10^5 \text{ lb}_m)$$

Since the appurtenance is on the ground,

$$K = 4$$

Nondimensional pressure \bar{P} is then

$$\frac{P_s}{P_0} = \frac{1.0 \times 10^5 \text{ Pa}}{1.0135 \times 10^5 \text{ Pa}}$$

$$\bar{P}_s = 0.99$$

Nondimensional impulse \bar{I}_s is

$$\bar{I}_s = \frac{C_D I_s a_0}{P_s (KH + X)} = \frac{(1.05)(1.9 \times 10^4)(340)}{(1.0 \times 10^5) [(4)(2.5) + 0]}$$

366

TABLE OF CONTENTS

	<u>Page</u>
INTRODUCTION	1 1/A12
I. ESTIMATES OF EXPLOSIVE YIELD	8 1/B5
1-1 Explosive Yield as a Function of Propellant Type and Accident Conditions	8 1/B5
1-2 Explosive Yield as a Function of Fluid Type and Initial Conditions for Gas Vessel Bursts	26 1/C9
List of References	29 1/C12
II. CHARACTERISTICS OF PRESSURE WAVES	31 1/C14
2-1 General	31 1/C14
2-2 Pressure Waves from Propellant Explosions	40 1/D9
2-3 Pressure Waves from Gas Vessel Bursts	56 1/E11
List of References	68 1/F9
II. A GAS VESSEL BURST	70 1/F11
2A-1 Nondimensional Parameters	70 1/F11
2A-2 Source of Data	70 1/F11
2A-3 Overpressure Calculation	71 1/F12
2A-4 Impulse Calculation	74 1/G1
2A-5 Effect of Cylindrical Geometry	74 1/G1
2A-6 Effect of Reflecting Surface (Burst at Ground Level)	74 1/G1
List of References	78 1/G5
Symbols	79 1/G6

TABLE OF CONTENTS (Cont'd)

		<u>Page</u>
III.	EFFECTS OF PRESSURE WAVES	80 1/G7
3-1	Damage Estimates to Structures	80 1/G7
3-2	Injury Estimates to Humans	99 2/B3
	List of References	125 2/D1
III.A	STRUCTURAL RESPONSE	128 2/D4
3A-1	Overshooting Analysis	128 2/D4
3A-2	Development of Beam Equations	134 2/D10
3A-3	Development of Plate Equations	142 2/E4
3A-4	Development of Membrane Equations	153 2/F1
	List of References	158 2/F6
III.B	PRESSURE/IMPULSE COMBINATIONS PRODUCING LUNG DAMAGE	159 2/F7
	List of References	169 2/G3
III.C	PRESSURE/IMPULSE COMBINATIONS PRODUCING LOSS OF HEARING	171 2/G5
	List of References	175 2/G9
III.D	PRESSURE/IMPULSE COMBINATIONS PRODUCING WHOLE-BODY DISPLACEMENT AND SUBSEQUENT DAMAGE TO THE HEAD AND BODY	176 2/G10
	List of References	190 3/B1
IV.	CHARACTERISTICS OF FRAGMENTS	191 3/B2
4-1	General	191 3/B2
4-2	Methods for Estimating Fragment Initial Velocities for Spheres and Cylinders Bursting into Many Fragments	191 3/B2

TABLE OF CONTENTS (Cont'd)

		<u>Page</u>
4-3	Estimate of Initial Velocities of Fragments from Spheres and Cylinders Bursting into Two Equal Halves	218 3/D1
4-4	Determination of Appurtenance Velocity	228 3/D11
4-5	Methods for Computing Fragment Ranges and Impact Conditions	240 3/E9
4-6	Fragment Mass Distribution	279 4/A11
4-7	Probability of Fragment Arrival Versus Range	286 4/B4
	List of References	292 4/B10
IV.A	METHODS FOR ESTIMATING FRAGMENT INITIAL VELOCITIES	293 4/B11
	List of References	315 4/D5
IV.B	COMPARISON OF EXPERIMENTAL RESULTS WITH CODE PREDICTIONS	316 4/D6
	List of References	318 4/D8
IV.C	ESTIMATE OF INITIAL VELOCITIES OF FRAGMENTS FROM SPHERES AND CYLINDERS BURSTING INTO TWO EQUAL HALVES	319 4/D9
	List of References	354 4/G2
IV.D	ESTIMATION OF VELOCITIES ATTAINED BY APPURTENANCES SUBJECTED TO BLAST LOADING	355 4/G3
	List of References	377 5/B2
IV.E	ANALYSES FOR FRAGMENT TRAJECTORIES	378 5/B3
	List of References	401 5/C12

TABLE OF CONTENTS (Cont'd)

	<u>Page</u>
IV.F STATISTICAL FITTING TO FRAGMENT DATA	402 5/C13
4F-1 Derivation of Figures 4-46 Through 4-49	402 5/C13
4F-2 Derivation of Figure 4-50	402 5/C13
4F-3 Rationale for Averaging Fragment Mass Distribution for Events 3, 4, and 5	403 5/C14
4F-4 Fragment Mass Distributions for Gas Vessel Bursts	406 5/D3
4F-5 Rationale for Averaging Fragment Mass Distributions for Tanks A and B and Tanks D and E	412 5/D9
4F-6 Derivation of Figure 4-57, Fragment Distance Versus Percent Yield for Propellant Explosions	413 5/D10
4F-7 Derivation of Simulated Fragment Range Distribution for Gas Vessel Bursts	415 5/D12
4F-8 Rationale for Combining Simulated Range Distribution for Tanks A and B and for Tanks D and E	423 5/E6
List of References	424 5/E7
V. EFFECTS OF FRAGMENTS	425 5/E8
5-1 Damage Estimates to Structures and Facilities	425 5/E8
5-2 Damage Estimates to People from Secondary Fragments	433 5/F2
List of References	442 5/F11
V.A EFFECTS OF FRAGMENTS ON STRUCTURES	444 5/F13
List of References	446 5/G1

TABLE OF CONTENTS (Concl'd)

		<u>Page</u>
V. B	DAMAGE ESTIMATES TO PEOPLE FROM SECONDARY FRAGMENTS	447 5/G2
	5B-1 Penetrating Fragments	447 5/G2
	5B-2 Nonpenetrating Fragments	455 5/G10
	List of References	456 5/G11
VI.	RISK ASSESSMENT AND INTEGRATED EFFECTS	458 5/G13
	6-1 Risk Assessment	458 5/G13
	6-2 Prediction of Relative Blast and Fragment Effects	461 6/A7
	List of References	507 6/D11
VII.	DISCUSSION OF RESULTS	508 6/D12
VIII.	CONCLUSIONS	511 6/E1
IX.	RECOMMENDATIONS	513 6/E3
LIST OF SYMBOLS		516 6/E6
CONVERSION FACTORS		523 6/E13
GLOSSARY OF TERMS		525 6/F1
BIBLIOGRAPHY		528 6/F4

$$\bar{I}_s = 6.8$$

Locating the point (P_s, I_s) on Figure 4D-5, one can find that it lies very near the 5.0 nondimensional velocity \bar{V} curve. Choosing \bar{V} equal to 5.0, appurtenance velocity can be calculated as follows:

$$\frac{M V a_0}{p_0 A (K \bar{H} + X)} = 5.0$$

$$V = \frac{(5.0) p_0 A (K \bar{H} + X)}{M a_0}$$

$$V \approx \frac{(5.0)(1.0135 \times 10^5 \text{ Pa})(25 \text{ m}^2)[(4)(2.5 \text{ m}) + (0)]}{(2.8 \times 10^5 \text{ kg})(340 \text{ m/s})}$$

$$V \approx 1.33 \text{ m/s (4.36 ft/sec)}$$

The listing of variables and list of the computer program follow.

COMPUTER PROGRAM ENTITLED /NDAPVE/ IN FORTRAN IV

Function:

This program computes nondimensional appurtenance velocities for various nondimensional pressures and nondimensional impulses.
Input data are:

(A) Nondimensional values for calculations

(PB, BB) Ordered pairs of nondimensional peak incident overpressure \bar{P} and dimensionless time constant b .

(PBB, UB, QB, PRB) Ordered quadruplets of nondimensional values of incident overpressure \bar{P} , shock front velocity \bar{U} , dynamic pressure \bar{Q} , and reflected pressure \bar{P}_r .

(NDV)	Nondimensional velocity values.
(B) Blast wave characteristics	
[P(I)]	Peak incident overpressure
[PI(I)]	Specific impulse
(C) Ambient conditions	
[PO(I)]	Atmospheric pressure p_0
[AO(I)]	Speed of sound a_0
(D) Appurtenance characteristics	
(X)	Distance X from front of object to location of largest cross- sectional area.
(H)	Minimum transverse distance H of the mean presented area of the appurtenance.
(CD)	Drag coefficient C_D
(A)	Mean presented area A
(TM)	Mass M of appurtenance

Variables:

The definition and units of the variables in this program are given in the following table.

TABLE 4D-1. DEFINITION OF PROGRAM VARIABLES
FOR APPURTEINANCE PROGRAM

<u>Program Variable</u>	<u>Variable</u>	<u>Definition</u>	<u>Units</u>
PB	\bar{P}	nondimensional pressure for calculating b	---
BB	b	dimensionless time constant b	---
PBB	\bar{P}	nondimensional peak incident pressure for calculating \bar{U} , Q, \bar{P}_r	---
UB	\bar{U}	nondimensional shock front velocity	---
QB	\bar{Q}	nondimensional peak dynamic pressure	---
PBR	\bar{P}_r	nondimensional peak reflected pressure	---
NDV	\bar{V}	nondimensional velocity for internal calculations	---
P(I)	P_s	peak incident overpressure values	Pa
PI(I)	I_s	incident specific impulse values	Pa·s
PO(I)	P_o	atmospheric pressure values	Pa
AO(I)	a_o	speed of sound values	m/s
X	X	distance from front of object to location of largest mean presented area	m
H	H	minimum transverse distance of mean presented area of appurtenance	m
CD	C_D	drag coefficient	---
A	A	mean presented area	m^2
TM	M	mass of appurtenance	kg
G	--	number of P_o , a_o input combinations	---
V	--	number of P(I) input values	---
R	--	number of PI(I) input values	---
S	--	number of NDV(I) input values	---
PBAR	\bar{P}	nondimensional peak incident pressure for a particular iteration	---
T	T, T_3	total duration of blast wave	s
PBARR	\bar{P}_r	nondimensional peak reflected pressure for a particular iteration	---

TABLE 4D-1. (CONT'D)

<u>Program Variable</u>	<u>Variable</u>	<u>Definition</u>	<u>Units</u>
QBAR	\bar{Q}	nondimensional dynamic pressure for a particular iteration	---
UBAR	\bar{U}	nondimensional shock front velocity for a particular iteration	---
PR	P_r	peak reflected pressure	Pa
Q	Q	peak dynamic pressure	Pa
U	U	shock front velocity	m/s
T_1	T_1	time corresponding to occurrence of peak reflected pressure	s
T_2	T_2	time corresponding to second interaction of diffracted and drag phase of loading curves	s
QT2	$q(T_2)$	dynamic pressure at time T_2	Pa
CDQ	--	intermediate calculation for T_1	---
TL	T_f	time at which diffracted phase of loading is over	s
APR	--	intermediate calculation for I_D	Pa·s
ACDQ	--	intermediate calculation for I_D	Pa·s
B1	--	intermediate calculation for I_D	---
EXPT3	--	intermediate calculation for I_D	Pa·s
TIMET3	--	intermediate calculation for I_D	---
EXPT2	--	intermediate calculation for I_D	Pa·s
TIMET2	--	intermediate calculation for I_D	---
IGRAL	I_D	calculation for integral I_D	Pa·s
XT3(k)	V	calculated appurtenance velocity	m/s
NNDV(k)	\bar{V}	calculated nondimensional velocity \bar{V}	---
FIND	--	"1" means calculated \bar{V} is far from input \bar{V} "2" means calculated \bar{V} is near input \bar{V}	---

TABLE 4D-1. (CONCL'D)

<u>Program Variable</u>	<u>Variable</u>	<u>Definition</u>	<u>Units</u>
NNNDV(M, J, L)	\bar{V}	final calculated \bar{V}	---
XXT3(M, J, L)	V	final calculated V	m/s
PP(M, J, L)	P	peak incident pressure for a particular final calculated V and input values	Pa
PPI(M, J, L)	I	specific impulse for particular final calculated and input values	Pa·s
POO(M, J, L)	p_0	atmospheric pressure	Pa
AOO(M, J, L)	a_0	speed of sound	m/s
Y(M, J, L)	\bar{P}	nondimensional pressure for particular calculated \bar{V} and input parameters	---
XX(M, J, L)	\bar{I}	nondimensional impulse for particular calculated \bar{V} and input parameters	---
PBARXO	--	subroutine variable used to calculate b	---
PBARX	--	subroutine variable used to calculate b	---
PBXO	--	subroutine variable used to calculate \bar{U} , \bar{Q} , \bar{P}_r	---
PBX	--	subroutine variable used to calculate \bar{U} , \bar{Q} , \bar{P}_r	---

Indicators of limits of calculations:

NNNDV = XXT3 = -1.0 indicates $P_s > 67.9$

NNNDV = XXT3 = -2.0 indicates $T_2 > T$ (or T_3)

NNNDV = -3.0 indicates input \bar{V} is greater than maximum calculated \bar{V}

NNNDV = -4.0 indicates input \bar{V} is less than minimum calculated \bar{V}

PROGRAM NDAPVE(INPUT,OUTPUT)

```

C
C
C      THIS PROGRAM DETERMINES THE COMBINATIONS OF NONDIMENSIONAL
C      QUANTITIES WHICH WILL PRODUCE A SPECIFIED NONDIMENSIONAL VALUE O
C      NDV (NONDIMENSIONAL VELOCITY) FOR VARIOUS APPURTEANCES.
C      NDAPVE OR N-D-A-P-V-E IS A CODE NAME DESIGNATING--NONDIMENSIONAL
C      APPURTEANCE VELOCITY.
C
C      DIMENSION PB(30),BB(30),PBB(5),UB(5),QB(5),PBR(5),PO(4),AO(4),
C      1P(50),PI(50),PP(20,4,50),PPI(20,4,50),P00(20,4,50),A00(20,4,50),
C      2XX(20,4,50),Y(20,4,50),XT3(50),XXT3(20,4,50)
C      INTEGER G,R,S,V,FIND
C      REAL IGRAL,NDV(20),NNNDV(50),NNNDV(20,4,50)
C
C      READ IN CURVES FOR PBAR VS. B AND
C      PBAR VS. URAR,QBAR,PBARR
C      PO = ATMOSPHERIC PRESSURE
C      AO = SPEED OF SOUND
C      G, 1 = OBJECT IN AIR
C            2 = OBJECT ON GROUND
C      P = PRESSURE
C      PI = IMPULSE
C      X = DIST. FROM FRONT OF OBJECT TO LOCATION OF LARGEST MEAN
C      SECTIONAL PRESENTED AREA
C      H = MINIMUM TRANSVERSE (TO SHOCK WAVE DIRECTION) DISTANCE AS
C      LOCATION OF LARGEST MEAN PRESENTED AREA
C      CD = DRAG COEFFICIENT
C      A = MEAN PRESENTED AREA
C      TM = OBJECT MASS
C      XT3 = VELOCITY OF APPURTEANCE
C      NDV = CONSTANT VALUE FOR TM*AO*XT3/((PO*A)(G+H+X))
C
C      READ 900,(PB(I),BB(I),I=1,21)
C      READ 901,(PBB(I),UB(I),QB(I),PBR(I),I=1,5)
C      READ 120,G
C      READ 100,(PO(I),AO(I),I=1,4)
C      READ 120,V
C      READ 130,(P(I),I=1,V)
C      READ 120,R
C      READ 130,(PI(I),I=1,R)
C      READ 120,S
C      READ 901,(NDV(I),I=1,S)
C      300 READ 110,X,H,CD,A,7M
C      IF(X,EQ.0.0) GO TO 301
C      DO 11 M=1,S
C      DO 11 J=1,4
C      DO 11 L=1,R
C      DO 10 K=1,V
C      FIND=1
C      12 PBAR=P(K)/PO(J)
C      CALL PARAMB(H,PBAR,PB,BB)
C      IF(B,EQ.0.0) GO TO 30
C      T=PT(L)*B/(P(K)*(1.0-((1.0-EXP(-B))/B)))
C      IF(PBAR.GT.1.5) GO TO 305
C      PBAR=2.0*PBAR+1.0*PBAR**2.0/4.0

```

```

      QBAR=5.0/2.0*PBAR**2.0/(7.0*PBAR)
      UBAR=SGRT(1.0*6.0*PBAR/7.0)
      GO TO 307
 305 CALL PARUQP(PRAR,UBAR,QBAR,PBARR,PBB,UB,QB,PBR)
      IF(UBAR,EQ,0.0) GO TO 30
 307 PR=PBARR*PO(J)
      Q=QBAR*PO(J)
      U=UBAR*AO(J)
      T1=X/U
      IF(G,EQ,1) GO TO 308
      T2=4.0*H/U+T1
      GO TO 309
 308 T2=2.0*H/U+T1
 309 CONTINUE
      IF(T2,GT,T) GO TO 32
      QT2=0*(1.0-T2/T)**2.0*EXP(-B*T2/T)
      CDG=CD*QT2/PR
      TL=(T2-CDG*T1)/(1.0-CDG)
      APR=PR*TL/2.0
      ACDO=CD*QT2*(TL-T2)/2.0
      B1=(2.0/H)-(2.0/H**2.0)*1.0
      EXPT3=CD*Q*T*EXP(-B)/B
      TIMET3=1.0-2.0/H
      EXPT2=CD*Q*T*EXP(-B*T2/T)/B
      TIMET2=(P.0*T2/T)-(2.0*T2/(B*T))-(T2/T)**2.0
      IGRL=(EXPT3*(TIMET3+B1))-(EXPT2*(TIMET2+B1))
      XT3(K)=A/TM*(APR+IGRL-ACDO)
      NNDV(K)=TM*AO(J)*XT3(K)/((PO(J)*A)*(G+H*X))
      IF(ABS((NNDV(M)-NNDV(K))/NDV(M)),LE,0.005) GO TO 16
      IF(NDV(M),LT,NNDV(1)) GO TO 17
      IF(K,EQ,1) GO TO 10
      IF(FIND,EQ,2) GO TO 13
      IF(NDV(M),GT,NNDV(K)) GO TO 10
      FIND=2
 14 P(K+1)=P(K)
      P(K)=P(K-1)+(P(K+1)-P(K-1))/2.0
      GO TO 12
 13 IF(NNDV(K),GT,NDV(M)) GO TO 14
      P(K-1)=P(K)
      P(K)=P(K-1)+(P(K+1)-P(K-1))/2.0
      GO TO 12
 10 CONTINUE
      K=V
      NNDV(K)=3.0
      GO TO 16
 17 NNDV(K)=4.0
      GO TO 16
 30 NNDV(K)=XT3(K)=1.0
      GO TO 16
 32 NNDV(K)=XT3(K)=2.0
 16 NNNDV(M,J,L)=NNDV(K)
      XXT3(M,J,L)=XT3(K)
      PP(M,J,L)=P(K)
      PPI(M,J,L)=PI(L)
      POO(M,J,L)=PO(J)
      AOO(M,J,L)=AO(J)
      Y(M,J,L)=P(K)/PO(J)

```

NDAPVE 74/74 OPT=1

FTN 4,2+7+325

04/02/75

$$XX(M,J,L) = CD * PI(L) * AO(J) / ((P(K)) * (G + X))$$

11 CONTINUE

PRINT OUT RESULTS

PPI=IMPULSE

PP=PRESSURE

XXT3=VELOCITY OF APPURTEANCE

NNNDV=XXT3=-1.0 INDICATES PP ,GT, 67,9

NNNDV=XXT3=-2.0 INDICATES T2 ,GT,T

NNNDV=-3.0 INDICATES NDV(M) ,GT, NNDV(V)

NNNDV=-4.0 INDICATES NDV(M) ,LT, NNDV(I).

Y=NONDIMENSIONAL PRESSURE

XX=NONDIMENSIONAL IMPULSE

IF(G,EQ,2) GO TO 400

PRINT 499,X,M,CD,A,TH

GO TO 401

400 PRINT 500,X,M,CD,A,TH

401 PRINT 501

DO 20 M=1,8

DO 20 J=1,4

DO 20 L=1,R

20 PRINT 502,P00(M,J,L),AO0(M,J,L),PPI(M,J,L),PP(M,J,L),XXT3(M,J,L),
1NDV(M),NNNDV(M,J,L),XX(M,J,L),Y(M,J,L)

GO TO 300

301 CONTINUE

100 FORMAT(2F15.5)

110 FORMAT(5F15.5)

120 FORMAT(I2)

130 FORMAT(BF10.2)

999 FORMAT(1H1,5H X = ,E12.5,/,6H M = ,E12.5,/,6H CD = ,E12.5,/,
16H A = ,E12.5,/,6H TH = ,E12.5,/,20H APPURTEANCE IN AIR)500 FORMAT(1H1,5H X = ,E12.5,/,5H M = ,E12.5,/,6H CD = ,E12.5,/,
16H A = ,E12.5,/,6H TH = ,E12.5,/,23H APPURTEANCE ON GROUND)501 FORMAT(1H1,5X,3H P0,4X,3H AO,4X,4H PPI,4X,3H PP,4X,5H XXT3,7H,
14H NDV,7X,6H NNNDV,7X,3H XX,4X,2H Y)

502 FORMAT(1H ,4E12.5)

900 FORMAT(BF12.4)

901 FORMAT(1HF5.2)

STOP

END

```
SUBROUTINE PARAMB(B,PBAR,PB,BB)
DIMENSION PB(30),BB(30)
REAL B,PBAR
IF(PBAR.LE.PB(21)) GO TO 20
B=0.0
GO TO 11
20 DO 10 I=1,21
IF(PBAR.EQ.PB(I)) GO TO 4.
K=I+1
PBARI0=ABS(PB(K)-PB(I))
PBARI=ABS(PBAR-PB(I))
IF (PBARI.GT.PBARI0) GO TO 10
B=(BB(K)-BB(I))/(PB(K)-PB(I))+(PBAR-PB(I))+BB(I)
GO TO 11
4 B=BB(I)
GO TO 11
10 CONTINUE
11 RETURN
END
```

PARUQP 74/74 OPT=1

FTN 4,2+74325

09/02/75 09,

```
SUBROUTINE PARUQP(PBAR,UBAR,QBAR,PBARR,PBB,UB,QB,PBR)
DIMENSION PBH(5),UB(5),QB(5),PBR(5)
REAL PBAR,UBAR,QBAR,PBARR
IF(PBAR.LE.PBB(5)) GO TO 20
UBAR=QBAR=PBARR=0.0
GO TO 11
20 DO 10 I=1,5
IF (PBAR.EQ.PBB(I)) GO TO 9
K=I+1
PBX0=ARS(PBB(K)-PBB(I))
PBX=ABS(PBAR-PBH(I))
IF (PBX.GT.PBX0) GO TO 10
UBAR=(UB(K)-UB(I))/(PBH(K)-PBB(I))*(PBAR-PBB(I))+UB(I)
QBAR=(QB(K)-QB(I))/(PBH(K)-PBB(I))*(PBAR-PBB(I))+QB(I)
PBARR=(PBR(K)-PBR(I))/(PBH(K)-PBB(I))*(PBAR-PBB(I))+PBR(I)
GO TO 11
9 UBAR=UB(I)
QBAR=QB(I)
PBARR=PBR(I)
GO TO 11
10 CONTINUE
11 RETURN
END
```

LIST OF REFERENCES

1. Baker, W. E., V. B. Parr, R. L. Bessey, and P. A. Cox, "Assembly and Analysis of Fragmentation Data for Liquid Propellant Vessels," NASA CR-134538, NASA Lewis Research Center, January 1974.
2. Baker, Wilfred E., Explosions in Air, University of Texas Press, Austin, Texas, May 1973.
3. Glasstone, Samuel, The Effects of Nuclear Weapons, U. S. Government Printing Office, Revised Edition, April 1962.
4. Norris, C. H., R. J. Hansen, M. J. Holley, J. M. Biggs, S. Namyat, and J. V. Minami, Structural Design for Dynamic Loads, McGraw-Hill Book Co., New York, 1959.

(d)

APPENDIX IV. E
ANALYSES FOR FRAGMENT TRAJECTORIES

Analysis for Obtaining Fragment Range and Terminal
Velocities for Disc-Shaped Fragments

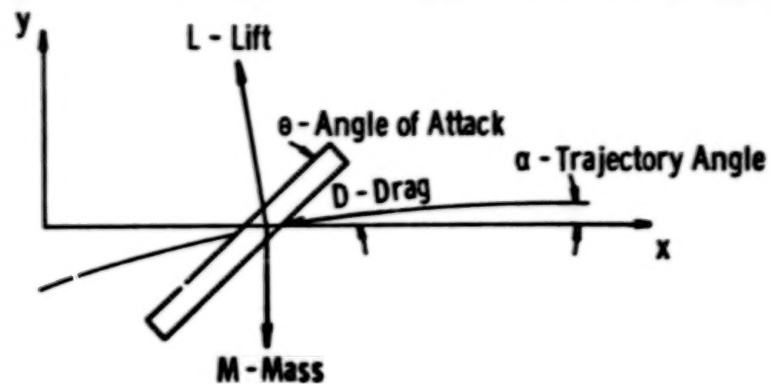
List of Variables

A	-	planform area - m ²
AP	-	projected area - m ²
AR	-	disc aspect ratio (diameter/thickness)
C	-	chord or width of rotor blade - m
C _D	-	drag coefficient
C _L	-	lift coefficient
D _p	-	profile drag - N
I	-	mass moment of inertia of rotor
L	-	lift - N
M	-	mass - kg
Q	-	torque - N-m
R	-	radius of rotor
T	-	thrust - N
V _c	-	rotor blade velocity along rotational axis
V _i	-	initial velocity of fragment
V _t	-	tip velocity of rotor
V _{in}	-	induced velocity from thrust
X	-	range - m

List of Variables (Cont'd)

Y	-	altitude - m
\dot{X}	-	horizontal velocity
\dot{Y}	-	vertical velocity
\ddot{X}	-	horizontal acceleration
\ddot{Y}	-	vertical acceleration
a	-	airfoil curve slope
b	-	number of rotor blades
d	-	disc diameter
g	-	acceleration of gravity
r	-	disc radius
t	-	disc thickness
Δt	-	time increment
α	-	trajectory angle - rad
α_i	-	initial trajectory angle - rad
ρ	-	density of air - kg/m ³
θ	-	angle of attack of disc - rad
ω	-	angular velocity - rad/sec

The range of disc-shaped flying fragments from an explosion was determined from the fragment accelerations due to lift and drag forces. The forces acting on the particle are as follows:



The acceleration in the Y direction is:

$$\therefore \ddot{Y} = -g - \frac{AC_D \rho (\dot{X}^2 + \dot{Y}^2)}{2M} \sin \alpha + \frac{AC_L \rho (\dot{X}^2 + \dot{Y}^2)}{M} \cos \alpha \quad (4E-1)$$

and for the X direction

$$\therefore \ddot{X} = - \frac{AC_D \rho (\dot{X}^2 + \dot{Y}^2)}{2M} \cos \alpha - \frac{AC_L \rho (\dot{X}^2 + \dot{Y}^2)}{M} \sin \alpha \quad (4E-2)$$

where

A = area of fragment

C_D = drag coefficient

C_L = lift coefficient

At $t = 0$

$$\dot{X} = V_i \cos \alpha_i \quad (4E-3)$$

$$\dot{Y} = V_i \sin \alpha_i \quad (4E-4)$$

where

V_i = initial velocity

α_i = initial trajectory angle

It is assumed that the fragment is spinning about its Y axis. This motion gives the required stability for flight and allows the fragment to maintain a constant angle with respect to the relative wind.

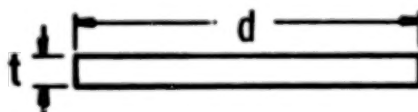
A complete program (FRISB) was written to determine the particle trajectory from these equations. The second order differential equations were solved simultaneously using a fourth order Runge-Kutta method. These solutions gave the velocities, which were then numerically integrated to yield the distances.

The lift coefficient based on the planform area was determined from

$$C_L = 1.82 \tan(\theta) \quad (\text{see Reference 1}) \quad (4E-5)$$

which is valid for a "thin" circular wing. It was assumed that the particle retained a constant angle of attack throughout the flight, which resulted in a constant lift coefficient. The maximum lift coefficient would be for approximately a 10° angle of attack. Larger angles would result in stall or total loss of lift. Using $\theta = 10^\circ$ in Equation (4E-5), $C_L = 0.32$.

The drag coefficient was chosen from Hoerner² for a fragment with a rectangular cross section



For a "thin" disc or $d/t \geq 3$, the drag coefficient based on the projected area is constant at 0.85.

As can be seen by examining Equations (4E-1) through (4E-4), the trajectory of a fragment is governed by a number of dependent and independent variables. The dependent variables are displacements X and Y; the independent variable list includes α_i , V_i , M, A, and AP. To construct a useful system of graphs, a spectrum of values for the independent variables was input to FRISB, which gave the flight trajectories.

The input data were selected by assuming a disc aspect ratio

$$AR = \frac{d}{t} \quad (4E-6)$$

and values of fragment mass and density. The mass is expressed as

$$M = \pi r^2 t \rho = \frac{2 \pi r^3 \rho}{AR} \quad (4E-7)$$

and

$$r = \left(\frac{MAR}{2\pi\rho} \right)^{1/3} \quad (4E-8)$$

Now the planform or lift area is given as

$$A = \pi \left(\frac{MAR}{2\pi\rho} \right)^{2/3} \quad (4E-9)$$

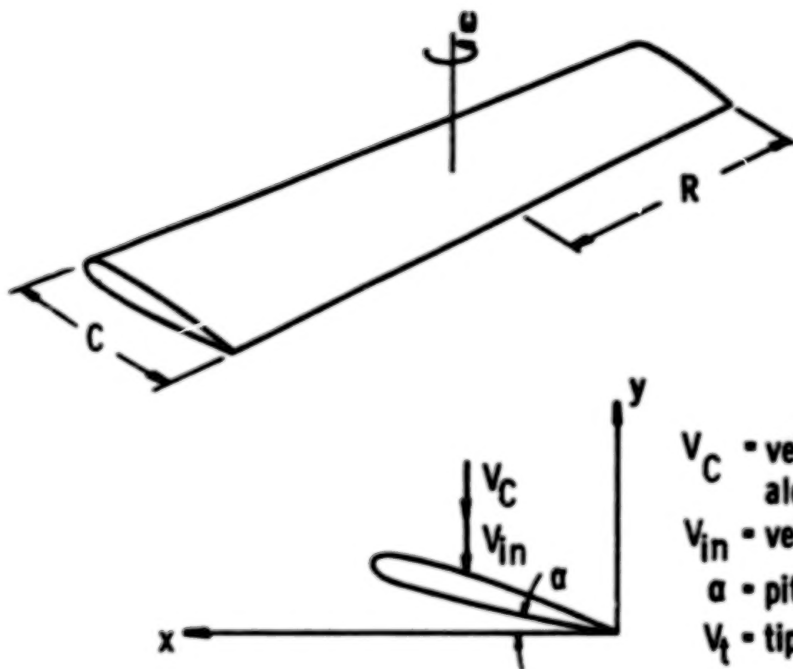
The projected or drag area is

$$AP = dt \quad (4E-10)$$

where d is calculated from Equation (4E-8), and t is determined from Equation (4E-6) for a given value of AR. The independent variables used in various computer runs are shown in Table 4-1 of the text. The results of these runs are plotted in Figures 4-27 through 4-36 of the text. The graph shows the maximum range of the fragment versus the initial trajectory angle. For a given velocity and aspect ratio, a family of curves is shown for various values of M/A. For several cases the lift force would act to pull the fragment up into a completely vertical flight. When this occurred, it was assumed that the fragment became unstable and fell straight to the ground. This phenomenon generally occurred for relatively high initial velocities and/or trajectory angles. A line has been drawn on Figures 4-28 through 4-35 to depict this occurrence. All points to the right of the line represent a "normal" flight, and those to the left are for the fragments that attained a vertical flight.

The value 300 m/s (938 ft/s) was used as a maximum initial velocity for the test cases. This velocity is very close to Mach 1 for STP conditions, and velocities above this would result in the need for a more complex aerodynamic analysis. The FRISB code would most likely predict larger ranges than would actually occur at higher velocities due to the increased drag at supersonic speeds. Therefore, for the purpose of estimation, the results from FRISB could be used for higher velocities.

Some fragments may not be disc or spherical shaped, but long and thin as a helicopter blade. The disc analysis is not valid for such a fragment because of the differing mechanisms of flight. The disc depends upon the forward motion to generate lift, where a whirling blade would generate most of its lift from the thrust due to the whirling motion, much the same as a helicopter rotor blade. Due to the possible need for such an analysis, the FRISB code was adapted with a subprogram to compute the trajectory of a fragment that flies, such as a helicopter rotor blade. The fragment geometry is as follows:



v_C = velocity at which blade moves along vertical axis
 v_{in} = velocity induced by thrust of blade
 α = pitch or trajectory angle
 v_t = tip speed = $R\omega$

The induced velocity is obtained from (see Reference 3):

$$v_{in} = v_t \left[- \left(\frac{abc}{16\pi R} + \frac{v_c}{2v_t} \right) + \sqrt{\left(\frac{abc}{16\pi R} + \frac{v_c}{2v_t} \right)^2 + \frac{abc\alpha}{8\pi R} - \frac{abc v_c}{8\pi R v_t}} \right] \quad (4E-11)$$

The thrust is determined by

$$T = \frac{1}{2} C_L v_t^2 \rho \frac{bcR}{g} \quad (4E-12)$$

The acceleration in the y direction due to the thrust is

$$\ddot{y} = \left[\left\{ \left(\frac{Tg}{M} \right) \cos \alpha - g \right\}^2 + \left\{ \left(\frac{Tg}{M} \right) \sin \alpha \right\}^2 \right]^{1/2} \quad (4E-13)$$

The change in vertical velocity is

$$\Delta V_c = \ddot{Y} \Delta t \quad (4E-14)$$

The torque produced by the rotating blade is

$$Q = \left\{ \frac{T(V_c + V_{in})}{V_t} + D_p \right\} R \quad (4E-15)$$

where D_p is the profile drag, which is given by:

$$D_p = \frac{1}{2} \rho C_D \frac{V_t^2 C R}{g} \quad (4E-16)$$

The change in angular rotation is

$$-\Delta\omega = \frac{Q \Delta t}{I} \quad (4E-17)$$

where I is the mass moment of inertia of the blade.

A fragment flying in this fashion would eventually lose its angular velocity due to drag, and thus lose its lift. This procedure differs from that for a disc in that it assumes that the lift force comes from the rotation of the fragment and not the fragment forward motion. The drag due to the forward motion of the fragment blade is considered when the computation is returned from the subroutine to the main program.

Input Data

1st data card NN - number of test runs included in data check

2nd data card N - number of differential equations to be solved by
Runge-Kutta = 2

X - initial time - 0.0

H - time increment (0.1 sec is usually sufficient)

* AP - projected area and drag area - m^2

OPER - 1 for disc - 2 for rotor blade

* If rotor subprogram is used, this is read in as anything because it will not be used.

3rd data card ρ_0 - density of air - kg/m^3
 A - lift area (planform) - m^2
 CL - lift coefficient
 CD - drag coefficient
 AMASS - fragment mass - kg
 ALPHAO - initial trajectory angle - rad
 VO - initial fragment velocity - m/s
 G - acceleration of gravity - m/s^2

4th data card
(only if using
rotor analysis) EMEGA - angular velocity - rad/s
 R - radius of blade - m
 ASLP - lift curve slope of rotor airfoil $\approx 2\pi$
 C - chord or width of rotor
 B - number of rotor blades - 2
 EMI - mass moment of inertia - $\text{N}\cdot\text{s}^2\cdot\text{m}$

PROGRAM FRISB (INPUT,OUTPUT,TAPES =OUTPUT)

THIS PROGRAM SOLVES THE SECOND ORDER DIFFERENTIAL EQUATIONS THAT GOVERN THE TRAJECTORY OF AN EXPLOSION FRAGMENT. THE SECOND ORDER EQUATIONS ARE WRITTEN AS FIRST ORDER AND SOLVED BY RUNGE KUTTA TECHNIQUES. THE SOLUTIONS ARE THEN INTEGRATED TO OBTAIN THE FRAGMENT TRAJECTORY.

THE INPUT VARIABLES ARE; X=INITIAL TIME, N=NUMBER OF EQUATIONS, R0=AIR DENSITY, A=FRAGMENT PLANFORM AREA, CL=LIFT COEFFICIENT, CD=DRAG COEFFICIENT, AMASS=PARTICLE MASS, ALPHAO=INITIAL TRAJECTORY ANGLE, VO=INITIAL VELOCITY, THETA=ANGLE OF ATTACK, H=TIME INCREMENT, AP=PROJECT AREA, OPER= SIGNALS USE OF ROTOR SUBROUTINE, OPER=1=DISC, OPER=2=ROTOR

DIMENSION Y(2),F(2),AA(2),BB(2),DSUMY(1000),DSUMX(1000),DXDDOT(2)

INTEGER OPER

READ 25,NN

DO 999 K=1,NN

READ 99,N,X,H,AP,OPER

READ 100,R0,A,CL,CD,AMASS,ALPHAO,VO,G

IF(OPER,NE,2)GO TO 319

READ 1000,EMEGA,R,ASLP,C,B,EMI

319 CONTINUE

PRINT 106

PRINT 112,CL,CD

PRINT 116

PRINT 113,AMASS

PRINT 116

PRINT 263,A

PRINT 116

PRINT 114,ALPHAO

PRINT 116

PRINT 115,VO

PRINT 116

PRINT 111,H

PRINT 116

PRINT 110

PRINT 116

1 CONTINUE

LL=0

I=0

VC=0.

ALPHA=ALPHAO

NT=0

SUMY=0.0

SUMX=0.0

ICNT=0

Y(1)=0.0

Y(2)=0.0

29 CONTINUE

*CNY=ICNT+1

Y(1)=Y(1)+VO*SIN(ALPHAO)

(OPER,EQ,2)YDOT=YDOT+VC*COS(ALPHA)

XDOT=Y(2)+VO*COS(ALPHAO)

```

IF(OPER,EQ,2)XDOT=XDOT-VC*SIN(ALPHA)
DXDOT(1)=XDOT
DALPHA=ATAN(YDOT/XDOT)
ALPHA=DALPHA
IF(ALPHA,GT,1.5) GO TO 997
IF(ALPHA,LT,-1.4) GO TO 997
IF(OPER,NE,2) GO TO 320
CALL ROTOR(FMEGA,R,CL,CD,ALPHAO,ASLP,C,B,EMI,RO,YC,DVC,H,G,AMASS,A,
1LPHA)
320 CONTINUE
AA(1)=Y(1)
BB(1)=Y(2)
BETA=.5*RO*AP*CD/AMASS
GAM=.5*RO*A*CL/AMASS
IF(OPER,EQ,2)GAM=.0
22 CONTINUE
YSPXS=Y(1)**2+Y(2)**2+2*Y(1)*V0*SIN(ALPHAO)+2*Y(2)*V0*COS(
SALPHAO)+V0**2
F(1)=-G-BETA*(YSPXS)*SIN(ALPHA)+GAM*(YSPXS)*COS(ALPHA)
F(2)=-BETA*(YSPXS)*COS(ALPHA)-GAM*(YSPXS)*SIN(ALPHA)
S=RKLDEQ(N,Y,F,X,H,NT)
SS=S-1.0
IF(SS,EQ,0.0)GO TO 22
AA(2)=Y(1)
BB(2)=Y(2)
YDOT=Y(1)+V0*SIN(ALPHAO)
IF(OPER,EQ,2)YDOT=YDOT+VC*COS(ALPHA)
XDOT=Y(2)+V0*COS(ALPHAO)
IF(OPER,EQ,2)XDOT=XDOT-VC*SIN(ALPHA)
DYDNT(2)=XDOT
IF(X,GE,0.5) GO TO 13
13 CONTINUE
DISY=(AA(1)+(AA(2)-AA(1))/2.)*H+V0*SIN(ALPHAO)*H
DISX=(BB(1)+(BB(2)-BB(1))/2.)*H+V0*COS(ALPHAO)*H
IF(OPER,EQ,2)DISY=DISY+DVC*H
SUMY=SUMY+DISY
SUMX=SUMX+DISX
LL=LL+1
LL=0
6 CONTINUE
I=I+1
DSUMY(I)=SUMY
DSUMX(I)=SUMX
PRINT 101,X,SUMY,SUMX,YDOT,XDOT,ALPHA
101 FORMAT(SX,F10.5,10X,F10.3,10X,F10.3,10X,F10.3,10X,F10.3)
7 CONTINUE
IF(SUMX,LT,0.) GO TO 997
IF(SUMY,GT,0.0)GO TO 24
997 CONTINUE
IN= ALOG10(SUMX)
MM=(SUMX/(10**IN))+1
XMAX= MM*10**IN
CALL EXTRAL(DSUMY,ICNT,YMAX,DMIN)
PRINT 3001
3001 FORMAT(1H1)
CALL PLOT1(2,2)
CALL PLOT2(XMAX,0.,YMAX,0.)
CALL PLOT3(1HX,DSUMX,DSUMY,I)

```

```
CALL PLOT*(0,0,1H )
994 CONTINUE
25 FORMAT(I10)
100 FORMAT(8F10.6)
104 FORMAT(1M1)
110 FORMAT(7X,*TIME*,12X,*Y DISPLACEMENT*,6X,*X DISPLACEMENT*,4X,*Y VE
 *LOCITY*,11X,*X VELOCITY*,12X,*ALPHA*)
111 FORMAT(10X,*TIME INCREMENT = *,F5.2,*SEC*)
112 FORMAT(10X,*LIFT COEFFICIENT = *,F10.5,10X,*DRAG COEFFICIENT = *,F
 810.5)
113 FORMAT(10X,*INITIAL MASS = *,F10.6,*KG*)
114 FORMAT(10X,*INITIAL TRAJECTORY ANGLE = *,F10.8,*RADIAN8*)
115 FORMAT(10X,*INITIAL VELOCITY = *,F10.3,*M/SEC*)
116 FORMAT(1M0)
263 FORMAT(10X,*FRAGMENT AREA = *,F10.4,*SQ. METERS*)
1000 FORMAT(6F10.5)
99 FORMAT(I10,3F10.6,I10)
STOP
END
```

SUBROUTINE PLOT1(NVS,NHS)
COMMON/GRAPH2/POINT(*1,101),CH

```
C  
C ***** INPUT *****  
C  
C NVS = NO. OF VERTICAL GRID LINES (MUST EQ. 11,6,3, OR 2)  
C NHS = NO. OF HORIZONTAL GRID LINES (MUST EQ. 5,3, OR 2)  
C  
C THIS IS A FORTRAN PROGRAM WHICH BUILDS A PLOT GRID FOR A PRINTER-PLOT  
C THE FOLLOWING PROGRAMS HAVE TO BE USED IN CONJUNCTION WITH THIS PROGRAM  
C  
C A SUBROUTINE PLOT2  
C B SUBROUTINE PLOT3  
C C SUBROUTINE PLOT4  
C  
C *****  
C  
BL = 1H  
VC = 1H  
HC = 1H  
C = 1H  
C. BLANK OUT THE PLOT AREA  
DO 1 I=1,41  
DO 1 J=1,101  
1 POINT(I,J) = BL  
C DETERMINE TYPE OF GRID TO BE USED  
JS = 100/(NVS - 1)  
IS = 40/(NHS - 1)  
C BUILD THE HORIZONTAL GRID LINES.  
DO 2 I=1,41,IS  
DO 2 J=1,101  
2 POINT(I,J)=HC  
C BUILD THE VERTICAL GRID LINES, AND PUT CHARACTER AT INTERSECTING  
C POINTS  
DO 3 J=1,101,JS  
DO 3 I=1,41  
IF(POINT(I,J),EQ.,HC) GO TO 9  
POINT(I,J) = VC  
GO TO 3  
9 POINT(I,J) = C  
3 CONTINUE  
C PUT CHARACTER AT EACH TENTH SPOT OF THE PERIMETER OF THE GRID  
DO 5 J=1,101,10  
DO 5 I=1,41,10  
5 POINT(I,J) = C  
DO 6 I=11,31,10  
DO 6 J=1,101,100  
6 POINT(I,J) = C  
RETURN  
END
```

```
FUNCTION RKLDFQ(N,Y,F,X,H,NT)
C D2 UCSD RKLDEQ RUNGE-KUTTA-GILL LINEAR DIFFERENTIAL EQUATION SOLVER
C D2 UCSD RKLDEQ
C MODIFIED MAY 1963 (Q REMOVED FROM CALLING SEQUENCE)
C TEST OF ALGOL ALGORITHM
C DIMENSION Y(10),F(10),Q(10)
C REAL X,H--INTEGER N,NT--COMMENT--BEGIN INTEGER I,J,L=REAL A
NT=NT+1
GO TO (1,2,3,4),NT
C GO TO S(NT)
1 DO 11 J=1,N
11 Q(J)=0,
A=.5
X=X+H/2,
GO TO 5
2 A=.29284321881
GO TO 5
3 A=1.7071067812
X=X+H/2,
GO TO 5
4 DO 41 I=1,N
41 Y(I)=Y(I)+H*F(I)/6,-Q(I)/3,
NT=0
RKLDEQ=2,
GO TO 6
5 DO 51 L=1,N
51 Y(L)=Y(L)+A*(H*F(L)-Q(L))
51 Q(L)=2.*A*H*F(L)+(1.-3.*A)*Q(L)
RKLDEQ=1,
6 CONTINUE
RETURN
END
```

```

SUBROUTINE ROTOR(EMEGA,R,CL,CD,ALPHAO,ASLP,C,B,EMI,RO,VC,DVC,H,G,A
1MASS,ALPHA)
ZZ = VC
VT = EMEGA*R
VA = VT/2.
DD = ASLP*B/(3.1417*R)
VI = VT*(=DD/16. - VC/(2.*VT) + ((DD/16. + VC/(2*VT))**2.+{DD+ALPH
1AO)/8. - (DD*(C)/(B.*VT))**.5)
T = .5*CL*(VA**2)*RO*B*C/R/G
ACC = (((T*G/A MASS))=COS(ALPHA)=G)**2 + ((T*G/A MASS)*SIN(ALPHA))**2
1)**.5
DP = .5*RO*CD*(VA**2)*.0032/G
Q = (T*((VC + VI)/VA) + DP )*R
DMEGA = Q*H/EMI
EMEGA = EMEGA - DMEGA
VC = ACC*H
DVC = VC - ZZ
PRINT191,EMEGA,VC,T,Q
191 FORMAT(5X,=EMEGA =*,F10.2,5X,=VC=,F10.4,5X,=T=,F10.4,5X,=Q=,F10
.,4)
RETURN
END

```

```
SUBROUTINE PLOT2(XMAX,XMIN,YMAX,YMIN)
COMMON/GRAPH1/X(100),Y(100),XF,XL,YF,YL,NPTS
```

```
C ***** INPUT *****
C
C   XMAX = XL = THE MAX. SCALE VALUE FOR THE X-AXIS
C   XMIN = XF = THE MIN. SCALE VALUE FOR THE X-AXIS
C   YMAX = YL = THE MAX. SCALE VALUE FOR THE Y-AXIS
C   YMIN = YF = THE MIN. SCALE VALUE FOR THE Y-AXIS
C
C   THIS IS A FORTRAN PROGRAM WHICH SETS THE PLOT SCALE
C
C ***** *****
C
XL = XMAX
XF = XMIN
YL = YMAX
YF = YMIN
RETURN
END
```

```
SUBROUTINE PLOT3(CHAR,XARAY,YARAY,N)
DIMENSION XARAY(200),YARAY(200)
COMMON/GRAPH1/X(100),Y(100),XF,XL,YF,YL,NPTS
COMMON/GRAPH2/POINT(41,101),CH
C
C ***** INPUT *****
C
C   CHAR = PLOT CHARACTER TO BE USED
C   XARAY = VALUES OF X TO PLOT
C   YARAY = VALUES OF Y TO PLOT
C   N    = NO. OF POINTS (OR DIMENSION OF XARAY, AND YARAY)TO PLOT
C          IF .GT. 100 THE ARRAY WILL BE SCALED TO .LE. 100
C
C   THIS IS A FORTRAN PROGRAM WHICH SCALES ARRAYS TO BE PLOTTED.
C
C ***** *****
C
J=0
CH=CHAR
ISTEP=N/100+1
DO 1 I=1,N,ISTEP
J=J+1
X(J)=XARAY(I)
Y(J)=YARAY(I)
NPTS=J
CALL PLOT
RETURN
END
```

```

SUBROUTINE PLOT
COMMON/GPGRAPH1/X(100),Y(100),XF,XL,YF,YL,N
COMMON/GPGRAPH2/POINT(41,101),CH
COMMON/GPGRAPH3/S(11),T(5)
C1=1H
C2=1H
C3=1H-
C4=1H+
C5=1H+
KOLD = 102
LOLD = 42
IF(XL .EQ. XF)RETURN
IF(YL .EQ. YF)RETURN
A = 100./(XL - XF)
B = 40.0/(YL - YF)
DX = (XL - XF)/10.0
DY = (YL - YF)/4.0
S(1) = XF
T(1) = YF
DO 6 I=1,10
  6 S(I+1) = S(I) + DX
  DO 61 I=1,4
    61 T(I+1) = T(I) + DY
  DO 10 I=1,N
    K = (X(I) - XF)*A + 1.5
    L = 40.0 - (Y(I) - YF)*B + 1.5
    IF(K .GT. 101)GO TO 10
    IF(L .LT. 0)GO TO 10
    IF(L .GT. 41)GO TO 10
    IF(K .EQ. KOLD)GO TO 11
    GO TO 12
  11 IF(L .EQ. LOLD) GO TO 10
  12 KOLD = K
  LOLD = L
  IF(POINT(L,K).NE.C1.AND.POINT(L,K).NE.C2.AND.POINT(L,K).NE.
  S C3.AND.POINT(L,K).NE.C4)GO TO 9
  POINT(L,K) = CH
  GO TO 10
  9 CONTINUE
  POINT(L,K)=C5
  10 CONTINUE
  RETURN
END

```

```

SUBROUTINE PLOT4(NCY,NCX,LABEL)
COMMON/GRAPH1/X(100),Y(100),XF,XL,YF,YL,N
COMMON/GRAPH2/POINT(41,101),CH
COMMON/GRAPH3/S(11),T(5)
DIMENSION LABEL(26)

C **** INPUT ****
C
C NCY = SWITCH INDICATING Y-AXIS CAPTION
C   = 0, NO CAPTION
C   = 1, UP TO 12 BCD CHARACTERS IN TITLE
C NCX = SWITCH INDICATING X-AXIS CAPTION
C   = 0, NO CAPTION
C   = 1, UP TO 72 BCD CHARACTERS TO BE PRINTED AS A HEADING
C       ABOVE THE PLOT, AND UP TO 72 BCD CHARACTERS TO BE PRINTED
C       ON A LINE BELOW THE PLOT
C
C THIS IS A FORTRAN PROGRAM WHICH PRINTS THE PLOTS, CAPTIONS AND SCALES
C OF THE DESIRED GRAPHS
C ****
C
IF(NCX .EQ. 0) GO TO 1
PRINT 101,(LABEL(IX),IX=3,14)
101 FORMAT(1H1,/,>29X,4H*** ,12A6,1X,3H***,//)
1 DO 40 I=1,15
IF(MOD(I,10) .EQ. 1) GO TO 45
PRINT 110,(POINT(I,J),J=1,101)
110 FORMAT(20X,101A1)
GO TO 40
45 INDX = 6 - (I+11)/10
PRINT 180,T(INDX),(POINT(I,J),J=1,101)
180 FORMAT(3X,E15.3,2X,101A1)
40 CONTINUE
IF(NCY .EQ. 0)GO TO 2
PRINT 120,(LABEL(IY),IY=1,2),(POINT(16,J),J=1,101)
120 FORMAT(8X,2A6,101A1)
GO TO 3
2 PRINT 110,(POINT(16,J),J=1,101)
3 DO 50 I=17,41
IF(MOD(I,10) .EQ. 1) GO TO 55
PRINT 110,(POINT(I,J),J=1,101)
GO TO 50
55 INDX = 6 - (I + 11)/10
PRINT 180,T(INDX),(POINT(I,J),J=1,101)
50 CONTINUE
PRINT 130,(S(I),I=1,11,2)
130 FORMAT(1H0,6X,E15.3,5(6X,E15.3))
IF(NCX .EQ. 0) GO TO 4
* RETURN
END

```

```
SUBROUTINE EXTVAL(X,N,XMAX,XMIN)
DIMENSION X(1)
```

```
C
C FIND MAXIMUM AND MINIMUM VALUES IN THE ARRAY X WHICH HAS N ENTRIES
XMAX=X(1)
XMIN=X(1)
DO 200 I=2,N
IF (XMAX.GT.,X(I)) GO TO 100
XMAX=X(I)
100 IF (XMIN.LT.,X(I)) GO TO 200
XMIN=X(I)
200 CONTINUE
NN= ALOG10(XMAX)
M=(XMAX/(10**NN))-1
XMAX = M*10**NN
RETURN
END
```

**Computer Code TRAJE for Obtaining the Range and
Terminal Velocities of Drag Fragments**

The following computer code, TRAJE, was used to generate figures for fragment range versus initial trajectory angle for fragments which experience no lift forces. It can be used to determine the terminal velocity of fragments at their maximum range. The program is based on a perturbation technique described in Reference 4. The following table lists the program variables used in TRAJE that were not previously defined in FRISB.

<u>Program Variable</u>	<u>Definition</u>	<u>Unit</u>
FM	input fragment mass	kg
AF	input fragment characteristic area	m^2
CD	input fragment drag coefficient	--
NCD	input branch constant (for NCD ≥ 1 the velocity dependent drag coefficient is introduced)	--
DT	input time increment	s
TM	input maximum time limit	s
V \emptyset	initial fragment velocity	m/s
AL \emptyset	initial trajectory angle	rad
BBT	drag constant	N/kg
TT	test time	s
XQ	fragment horizontal displacement	m
Y	fragment vertical displacement	m
VX	fragment instantaneous horizontal velocity	m/s
VY	fragment instantaneous vertical velocity	m/s
ALP	instantaneous trajectory angle	rad
V	total fragment velocity	m/s

```

PROGRAM TRAJE (INPUT,OUTPUT,TAPE1 =OUTPUT,TAPE2 =INPUT)
COMMON /VAR/ BET, AF,FM
1 FORMAT (E12.5)
2 FORMAT (2E12.5)
3 FORMAT (/,7H ALPHA=,E11.9,4H RAD, V0=,E11.9,6H M/SEC)
4 FORMAT (/,6H MASS=,E11.9,11H KG, AREA=,E11.9,5H SQ,M)
5 FORMAT (/,4H CD=,E11.9)
6 FORMAT (/,17H TEST TIME VALUE=,E11.9)
10 FORMAT (2/,62H TIME X-DISP Y-DISP X-VEL Y-VEL
1 ANG )
11 FORMAT (6H (SEC) (METER) (METER) (M/SEC) (M/SEC)
1 (RAD) )
12 FORMAT (/,HE11.9)
13 FORMAT (/,HE11.9)
16 FORMAT (I2)
DO 105 K=1,10
READ (2,2) FM,AF
WRITE (1,5) FM,AF
RFAD (2,1) CD
WRITE (1,7) CD
RFAD (2,16) NCO
READ (2,2) DT,TM
V0=0.0
DO 500 II=1,3
AL0=0.0
V0= V0+100.
DO 501 IJ=1,b
AL0= AL0+ 0.1795
111 WRITE (1,3) AL0,V0
BET= (CD*AF+1.2050)/(2.*FM)
TT=(HET*9.81)**=-0.5
WRITE (1,8) TT
SET INITIAL VALUES
X=0.0
Y=0.0
VX=V0*COS(AL0)
VY=V0*SIN(AL0)
DX=0.0
DY=0.0
DA=0.0
DVX=0.0
DVY=0.0
DO 100 I=1,900
IF (I-1) 120,120,121
120 ALP=AL0
GO TO 122
121 ALP=DA
122 CONTINUE
X=X+DX
Y=Y+DY
IF (Y>10.) 503,502,502
503 CONTINUE
PRINT OUT VALUES
IF (I-1,) 101,101,102
101 T=0.0
WRITE (1,10)
WRITE (1,11)

```

```
      WRITE (1,12) T,X,Y,VX,VY,ALP
      GO TO 103
102 WRITE (1,13) T,X,Y,VX,VY,ALP
502 CONTINUE
      IF (V) 501,106,106
106 CONTINUE
      CALC. NEW INPUT PARAMETERS
103 T= T+DT
      IF (T-TM) 104,104,105
104 VI=((VX**2)+(VY**2))**0.5
      IF (NCD-1) 300,301,301
301 IF (VI-150.) 302,302,303
302 CD=1.28
      GO TO 300
303 IF(VI-275.) 304,304,305
304 CD=(.00375*(VI-150.))+1.28
      GO TO 300
305 IF (VI-335.) 306,306,307
306 CD=(.004917*(VI-275.))+1.75
      GO TO 300
307 IF(VI-475.) 308,308,309
308 CD=(.00393*(VI-335.))+2.30
      GO TO 300
309 IF(VI-675.) 310,310,311
310 CD=(.001*(VI-475.))+2.85
      GO TO 300
311 CD=(.000461*(VI-675.))+3.05
300 CONTINUE
      BET=(CD*AF*1.2050)/(2.*FM)
      CALC. CHGS. FOR NEW T
      CALL DEL (DT,ALP,VI,DX,DY,VX,VY,DA)
100 CONTINUE
501 CONTINUE
500 CONTINUE
105 CONTINUE
      END
```

```

SUBROUTINE DEL (DT,ALP,VI,DY,DVX,VY,DVY)
REAL LNF
COMMON/VAR/BET, AF,FM
150 FORMAT (RE12.5)
G=9.81
EK=BET*VI
U=EK*DT
DEFINITION VALUE OF LOG FUNC,
IF (U=.0001) 201,201,202
201 LNF=1-(0.5*(U**2))+((1.0/3.0)*(U**3))-(0.25*(U**4))
S=(1.+U)
GO TO 203
202 S=(1.+U)
LNF= ALOG(S)
CALC. DX AND DVX IN MOVING COORD,
203 X0=LNF/BET
X0D=VI/S
GS=G*SIN(ALP)
GC=G*COS(ALP)
XP=0.5*GS*(DT)**2+(1.+(U/3))*S
XPD=-GS*DT*(1.+U+((1./3.)*U**2))/(S**2)
DX=X0+XP
DVX=X0D+XPD
CALC. DY AND DVY IN MOVING COORD,
YPD= -(GC*0.5/EK)*(S-(1./S))
TS=(S**2)/2.
SMT2=(TS-LNF-0.5)
YP=(-(0.5*GC/(EK**2))*SMT2)
DY=YP
DVY=YPD
CALC. DX DY DVX DVY IN FIXED COORD,
DX=(DX*COS(ALP))-(DY*SIN(ALP))
DY=(DX*SIN(ALP))+(DY*COS(ALP))
VX=(DVX*COS(ALP))-(DVY*SIN(ALP))
VY=(DVX*SIN(ALP))+(DVY*COS(ALP))
DA=ATAN( VY/ VX)
V=((VX**2)+(VY**2))**0.5
RETURN
END

```

REFERENCES

1. Milne-Thompson, L. M., Theoretical Aerodynamics, MacMillan, London, 1966, 4th Edition, p. 230.
2. Hoerner, S. F., Fluid Dynamic Drag, S. F. Hoerner, 1958, USA, pp. 3-12.
3. Stepniewski, W. Z., "Basic Aerodynamics and Performance of the Helicopter," Helicopter Aerodynamics and Dynamics--AGARD Lecture Series No. 63, AGARD-LS-63, April 1973.
4. Zaker, T. A., "Trajectory Calculations in Fragment Hazard Analysis," Minutes of 13th Annual Explosives Safety Seminar, September 1971, p. 101.

APPENDIX IV. F

STATISTICAL FITTING TO FRAGMENT DATA

4F-1 Derivation of Figures 4-46 through 4-49

From the initial fragment velocity data on grouped tests by propellant and configuration given on page 102 of Reference 1, the following estimated means and standard deviations for the log-normal (to the base e) distributions are shown in Table 4F-1.

TABLE 4F-1. LOG NORMAL DISTRIBUTIONS OF FRAGMENT INITIAL VELOCITY (TO THE BASE e) BY PROPELLANT TYPE AND CONFIGURATION

	<u>CBM</u> <u>LO₂/LH₂</u>	<u>CBM</u> <u>LO₂/RP-1</u>	<u>CBGS</u> <u>LO₂/LH₂</u>	<u>CBGS</u> <u>LO₂/RP-1</u>
Estimated Mean	5.2759*	5.5249	4.9410	4.7739
Estimated Std. Dev.	0.9875	5.5249	0.7715	0.6387

These distributions are plotted on Figures 4-46 through 4-49, respectively. The goodness of fit statistics (W) are given in Reference 1.

4F-2 Derivation of Figure 4-50

The data from page 86 of Reference 1 for fragment initial velocity measurements were used to determine the regression line (least squares fit) shown of initial velocity, U, in Figure 4-50. The 95th percentile (U_{95}) estimate was constructed by taking the estimate for the standard deviation (σ) from the CBM LO₂/LH₂ group in Section 4F-1 above, establishing a point 1.65 σ above the point $U = 73.96$, $Y = 1\%$ by the formula:

$$\begin{aligned} U_{95} &= \exp [\ln 73.96 + (1.65)(0.9875)] \\ &= 377.24 \text{ meters (1237.7 ft)} \end{aligned}$$

* To determine the geometric mean in meters/second, raise e to the power shown.

A line was then extended from the point $U = 377.24$, $Y = 1$, parallel to the regression line for U on Y ($U = 73.96 Y^{0.4296}$).

The values for nine tests from Reference 1 are presented in Table 4F-2.

TABLE 4F-2. MEAN AND MAXIMUM FRAGMENT INITIAL VELOCITY FOR LO₂/LH₂ CBM

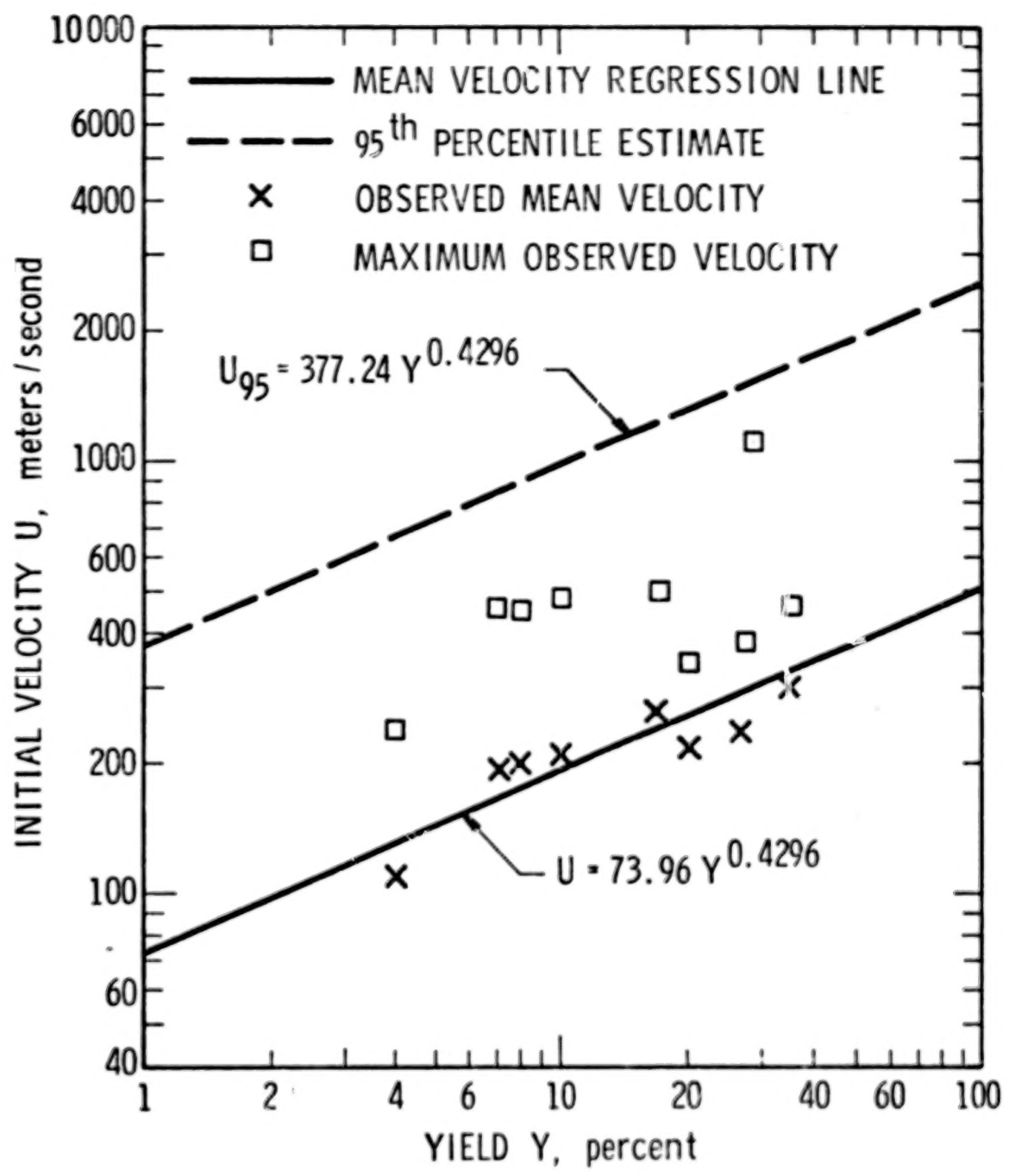
Test No.	Yield (%)	Mean Velocity	Maximum Velocity
		m/s	Measured
053	4	110.3	240
091	29	457.2	1100
118	20	216.4	340
199	8	201.2	455
200	17	268.2	504
210	7	198.1	462
212	27	240.8	383
213	35	301.8	459
265	10	210.3	441

Figure 4F-1 shows the regression line, the estimated 95th percentile line, and the mean and maximum observed velocity points.

4F-3 Rationale for Averaging Fragment Mass Distribution for Events 3, 4, and 5

The estimated means and standard deviations (log-normal to the base e) for the fragment mass for the five events from Reference 1 are shown in Table 4F-3.

The estimated means and standard deviations of events 3, 4, and 5 were fairly close to each other, and the events were of the same type. Therefore, it seemed reasonable to apply a "t" test (see Reference 8) for significant difference in means. This test was applied to events 3 and 4 since the difference in estimated means was the greatest for any pair of estimated means from events 3, 4, and 5.



(ft/sec = m/s X 3.281)

Figure 4F-1. Initial Velocity Vs Yield,
CBM, LO₂/LH₂

TABLE 4F-3. ESTIMATED MEAN AND STANDARD DEVIATION FOR FRAGMENT MASS DISTRIBUTION (LOG NORMAL TO BASE e) FOR FIVE EVENTS

<u>Event No.</u>	<u>Fragment Mass Distribution</u>		<u>Percent Yield</u>
	<u>Mean</u>	<u>Standard Dev.</u>	
1	7.7226*	0.8020	5.0
2	9.3940	1.1442	1.1
3	9.7761	1.1787	23.0
4	10.1488	1.0367	24.4
5	10.0522	0.8838	62.6

The "t" test is applied using the following steps:

- (1) The pooled estimate for the standard deviation (S_p) is calculated by:

$$S_p = \sqrt{(S_1^2 + S_2^2)/2}$$

- (2) The "t" statistic is calculated by

$$t = (\bar{W}_1 - \bar{W}_2)/(S_p (\sqrt{2/n})),$$

where n is the number of points to estimate \bar{W}_1 and \bar{W}_2 in our case n = 9.

- (3) The "t" statistic is then compared to a value in the t distribution table, $t_{\alpha/2}(n - 1)$, where α is the probability of type I error or risk of accepting the hypothesis that there is no significant difference in means where there is, and $2(n - 1)$ is a parameter in the t distribution (degree of freedom) used to find the tabled value.
- (4) If the calculated value of t (from step 2) is between $\pm t_{\alpha/2}(n - 1)$ (the table value), we accept the hypothesis

* To determine geometric mean weight, raise e to power shown in table.

that there is no significant difference in the means. If not, we reject the hypothesis, and conclude there is a significant difference in the means.

Choosing an α of 0.20, the table value of t for 16 degrees of freedom is ± 1.337 .

The formula for calculating "t" can be further simplified to:

$$t = \frac{\sqrt{n} (\bar{W}_1 - \bar{W}_2)}{\sqrt{s_1^2 + s_2^2}} \quad (4F-1)$$

Using the above formula, the calculated value of t is:

$$t = \frac{3 (10.1488 - 9.7761)}{\sqrt{1.0367^2 + 1.1787^2}} = 0.712$$

Since the calculated value of t of 0.712 lies between the table value ± 1.337 , we accept the hypothesis that there is no significant difference in means and can use a single distribution for the fragment mass distribution for events 3, 4, and 5. Averaging the means of events 3, 4, and 5 yielded an average value of 9.9924, and for the standard deviation an average value of 1.0331. These values were used to construct Figure 4-53.

4F-4 Fragment Mass Distributions For Gas Vessel Bursts

The fragment mass data from each of the tanks were sorted in ascending order; the values for the mass for the 10th to the 90th percentiles in 10% steps were identified. Table 4F-4 is a listing of these values.

Figures 4F-2 through 4F-5 are plots of the percentile points on log normal probability paper for tanks A, B, D and E, respectively.

Table 4F-5 is a listing of the estimated means and standard deviations for the log normal (to the base e) distributions.

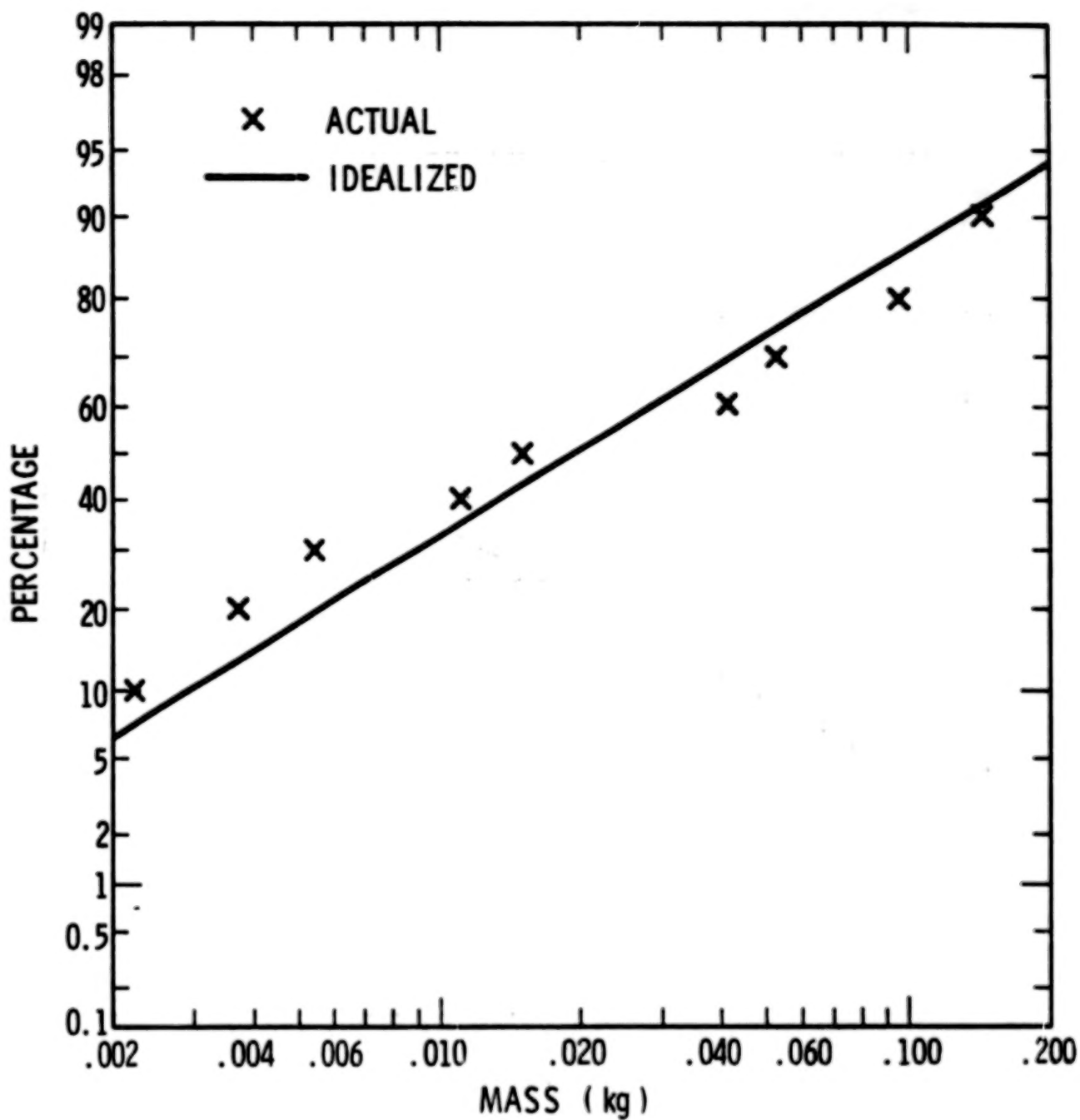
A "W" statistic (see Reference 9) for goodness of fit was calculated for each of the distributions. The approximate probability of obtaining the calculated test statistic, given that the chosen distribution is correct, was then determined. The results are shown in Table 4F-6.

**TABLE 4F-4. PERCENTILES FOR PLOTTING FRAGMENT
MASSES OF TANKS A, B, D, AND E**

<u>Percent</u>	<u>Mass (g)</u>			
	<u>Tank A</u>	<u>Tank B</u>	<u>Tank D</u>	<u>Tank E</u>
10	2.2	1.1	85	61
20	3.7	4.6	199	199
30	5.2	6.6	454	454
40	11.0	24.0	624	738
50	15.0	31.0	1731	1277
60	42.0	38.0	2015	1617
70	53.0	63.0	2156	1873
80	96.0	92.0	2270	2270
90	145.0	125.0	2639	3036

**TABLE 4F-5. LISTING OF ESTIMATED MEANS AND STANDARD
DEVIATIONS FOR LOG-NORMAL DISTRIBUTION
(TO THE BASE e) FOR GAS VESSELS**

<u>Tank No.</u>	<u>Estimated Mean</u>	<u>Estimated Standard Deviation</u>
A	2.9730	1.4821
B	3.0327	1.6829
D	6.5698	1.8080
E	6.6782	1.5815



$$(1 \text{ lb}_m = \text{kg} \times 2.205)$$

Figure 4F-2. Fragment Mass Distribution, Tank A

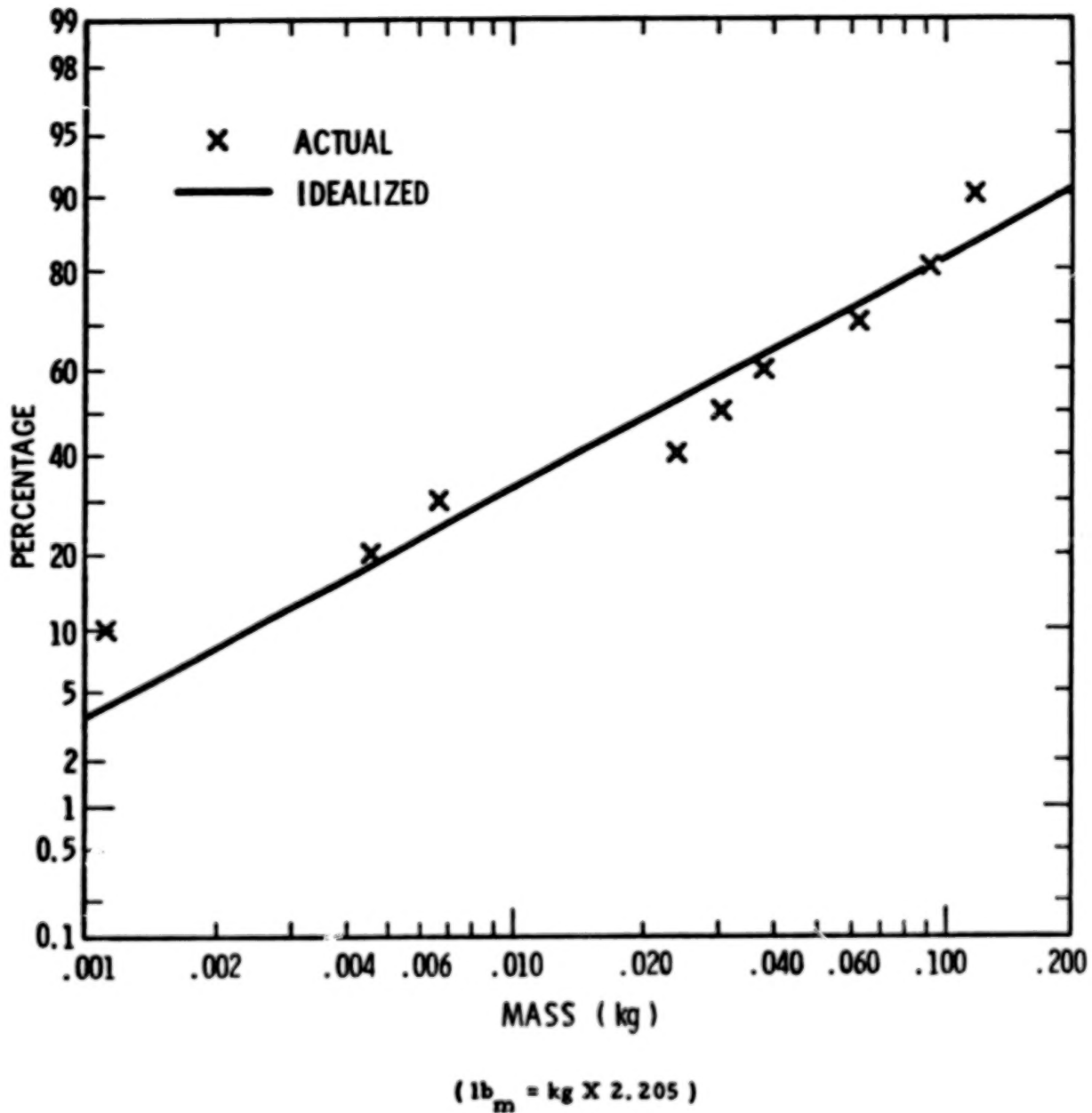
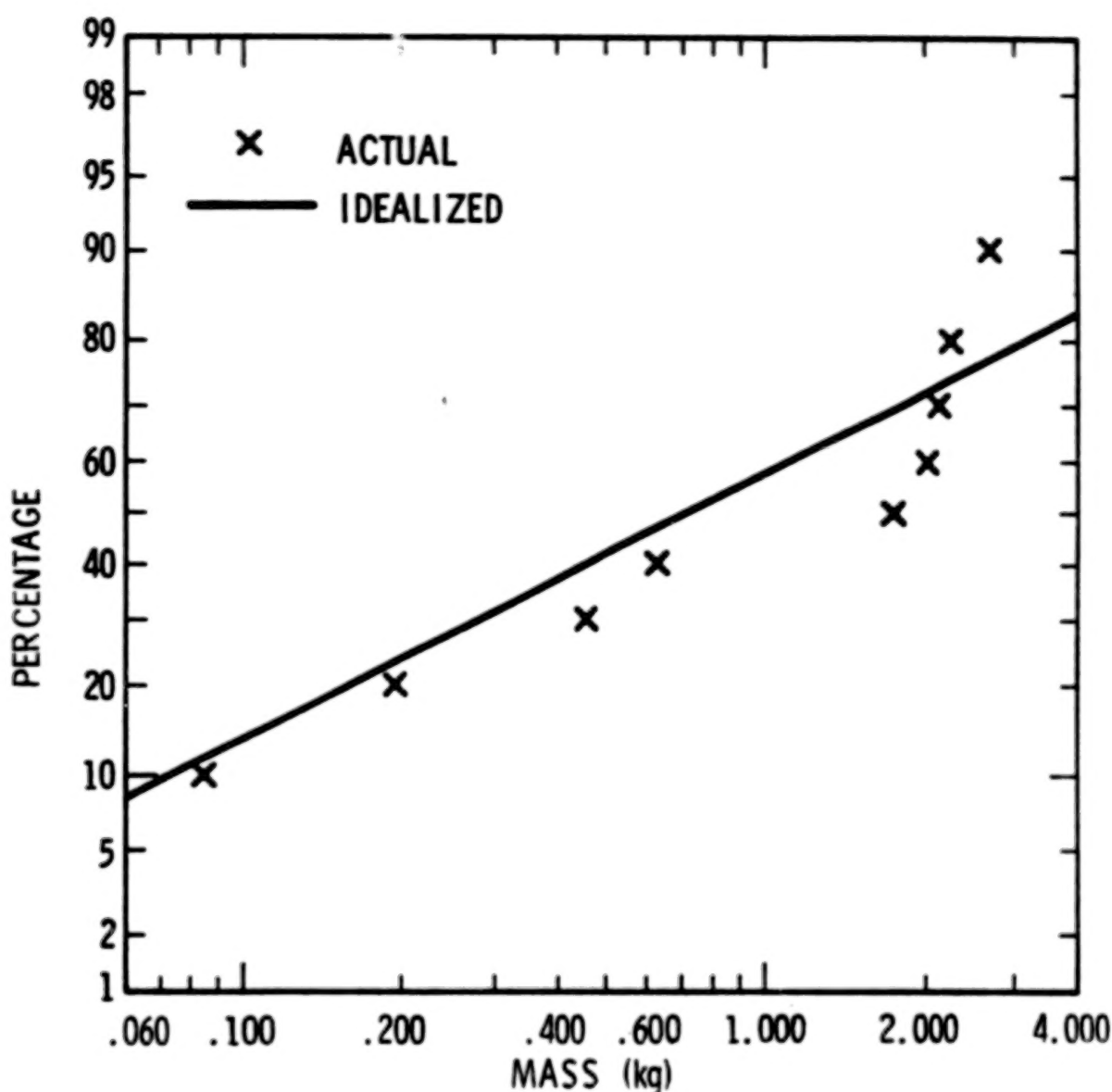


Figure 4F-3. Fragment Mass Distribution, Tank B



$$(1b_m = kg \times 2.205)$$

Figure 4F-4. Fragment Mass Distribution, Tank D

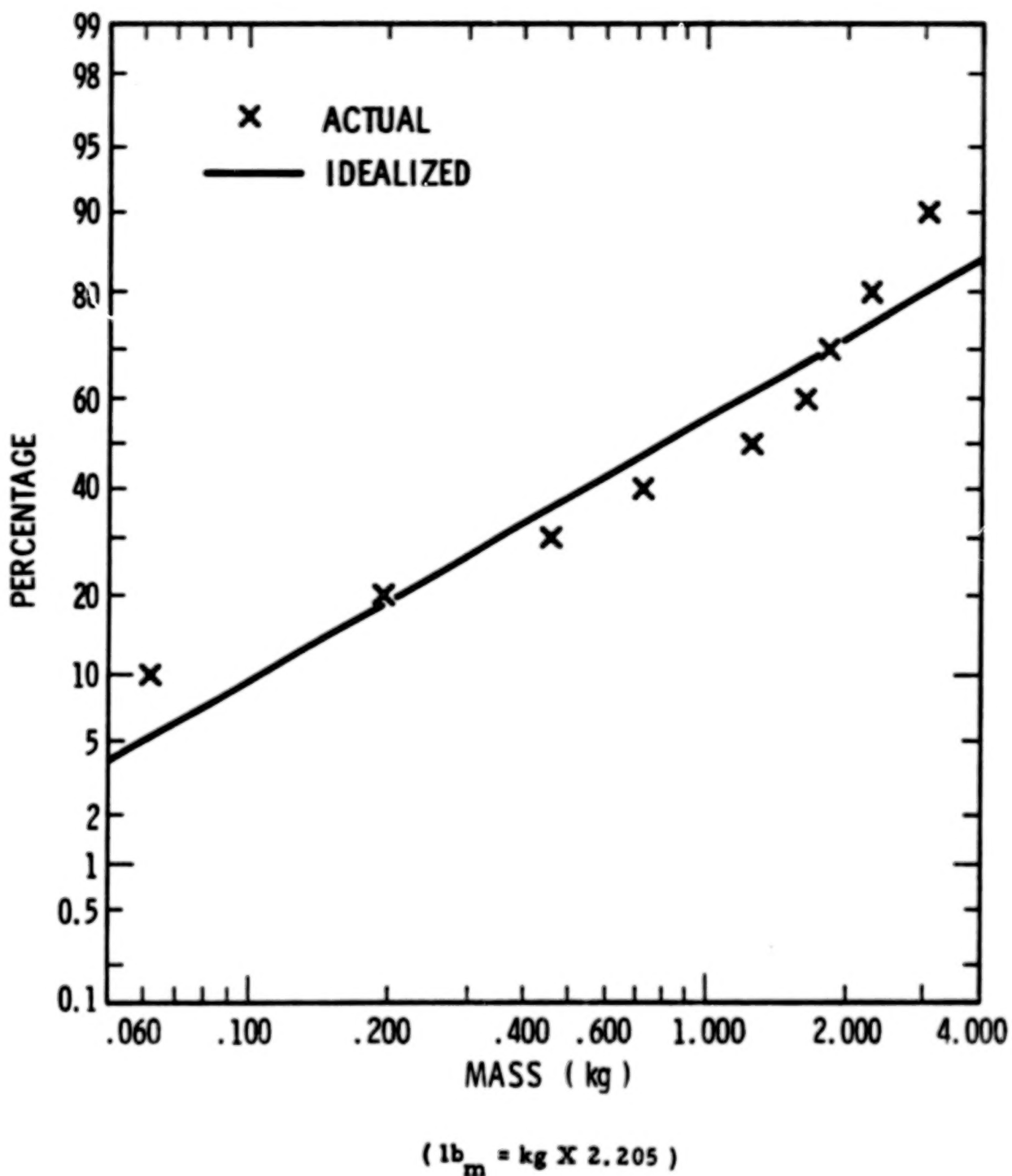


Figure 4F-5. Fragment Mass Distribution, Tank E

TABLE 4F-6. SUMMARY OF "W" TEST ON NORMALITY FOR
FRAGMENT MASS DISTRIBUTION FOR
TANKS A, B, D, AND E

<u>Tank No.</u>	<u>"W"</u>	<u>Probability</u>
A	.948	.65
B	.929	.45
D	.851	.08
E	.956	.74

As it is customary to consider values exceeding 2 to 10% as adequate grounds for not rejecting the hypothesis that the data belong to the chosen distribution, the fits for tanks A, B, and E are more than adequate, and for D somewhat questionable.

Except for Tank D, the other values compare favorably with those obtained for the log-normal fragment distribution for Events 1, 2, 3, 4 and 5 for the propellants (Reference 1).

4F-5 Rationale For Averaging Fragment Mass Distributions For Tanks A and B and Tanks D and E

A "t" test for significant difference in means was made for each of the pairs of tanks, with the following results:

For tanks A and B, the calculated value of "t" was 0.314 versus the table value of ± 1.337 .

For tanks D and E, the calculated value of "t" was .1354 versus the table value of ± 1.337 .

Thus, no significant difference in means for either pair was found, and a single distribution for each pair was derived by averaging the respective pair of means and standard deviations. Table 4F-7 presents the results, and the distributions are charted in Figures 4-54 and 4-55.

TABLE 4F-7. ESTIMATED MEAN, AND STANDARD DEVIATION
(TO THE BASE e) FOR TANKS A AND B, AND D AND E

<u>Tanks</u>	<u>Estimated Mean</u>	<u>Estimated Standard Dev.</u>
A and B	2.9984	1.583
D and E	6.6240	1.695

4F-6 Derivation of Figure 4-57, Fragment Distance Versus Percent Yield For Propellant Explosions

Table 4F-8 is taken from Reference 1, with some minor corrections. For each of the five events, a 95% upper confidence limit was put on the estimated mean (M) and a 90% upper confidence limit was established for the estimated standard deviation (S), using methods outlined in Reference 8.

The confidence limit on the mean was calculated using the following formula:

$$CL = M + \frac{S}{\sqrt{n}} t_{(n; 95)}$$

n is the number of fragments and $t_{(n; 95)}$ is the value of the t distribution with n degrees of freedom at the 95th percentile.

The confidence interval for the standard deviation was calculated using the following formula:

$$CL = \left[\frac{\sum X_i^2 - (\sum X_i)^2/n}{\chi^2_{(n-1); 90}} \right]^{1/2}$$

where X_i is the distance of the ith fragment, n is the number of fragments, and $\chi^2_{(n-1); 90}$ is the value of a chi square distribution with n - 1 degrees of freedom at the 90th percentile.

Then, using the new upper confidence level values of M and S, the R₉₅ in which 95% of the fragments should fall was calculated as follows:

TABLE 4F-8. CONFIDENCE LIMITS ON MEAN, STANDARD DEVIATION, AND DISTANCE CONTAINING 95% OF FRAGMENTS

Event No.	Sample Size	Yield		Distance (R) (m)							Max Dist
		%	TNT	M	S	S.E.	95% CL M	90% CL S	95% CL Dist		
1	341	5	4.55×10^2	136.3	59.13	3.20	141.4	62.33	244	313	
2	38	1.1	1.08×10^3	102.7	61.87	10.05	132.0	73.15	255	335	
3	105	23	4.03×10^2	253.0	169.77	16.56	280.4	186.23	590	671	
4	86	24.4	4.28×10^2	225.6	104.24	11.23	244.1	115.82	437	504	
5	31	62.6	1.097×10^2	300.5	174.96	31.44	353.9	211.23	712	695	

414

$$R_{95} = M + S t_{(n; 95)}$$

The interval from the mean (M) to R_{95} is indicated for each event on Figure 4F-6 by a bar.

A line was then drawn parallel to the regression line, and just touching the longest bar. Thus, the distances read from this line could be expected to encompass at least 95% of the fragments resulting from a given yield.

4F-7 Derivation of Simulated Fragment Range Distribution for Gas Vessel Bursts

For each tank, the fragments were divided into classes by fragment area. The computer program FRISB was then exercised taking into account fragment shape (from drag) for initial angles of 15, 30, 45, 60, and 75° to determine a range for each angle for each class of fragment. Table 4F-9 presents the results of the range simulation.

In the table the fragments have been divided into groups or classes with the average planform area \bar{A}_L and the average mass \bar{M} of each class listed. The area data were obtained by measurement from the photographs of Reference 2. Mass data were given in the reference for each fragment. \bar{A}_D is the average drag area for each class of fragment; this area is calculated on the basis of the thickness of the fragments and a characteristic width dimension equal to the square root of the fragment, planform area. The maximum range of the classes of fragments for various values of initial trajectory angle ($\alpha = 5 n^\circ$, $n = 3, 15$) was calculated using code FRISB assuming the average characteristics for the fragments in each class, and that the initial velocity was the maximum initial velocity for the fragments measured for each tank.

The fragment ranges were ordered, and the percentiles were determined and are shown in Table 4F-10. Then the percentiles were plotted on normal probability paper and are shown in Figures 4F-7 through 4F-10. The estimates for the mean and standard deviation for each distribution were then calculated and are shown in Table 4F-11.

A "W" goodness of fit statistic was calculated for each distribution and the probability of obtaining the calculated test statistic value, given that the chosen distribution is correct was then determined. The results are shown in Table 4F-12.

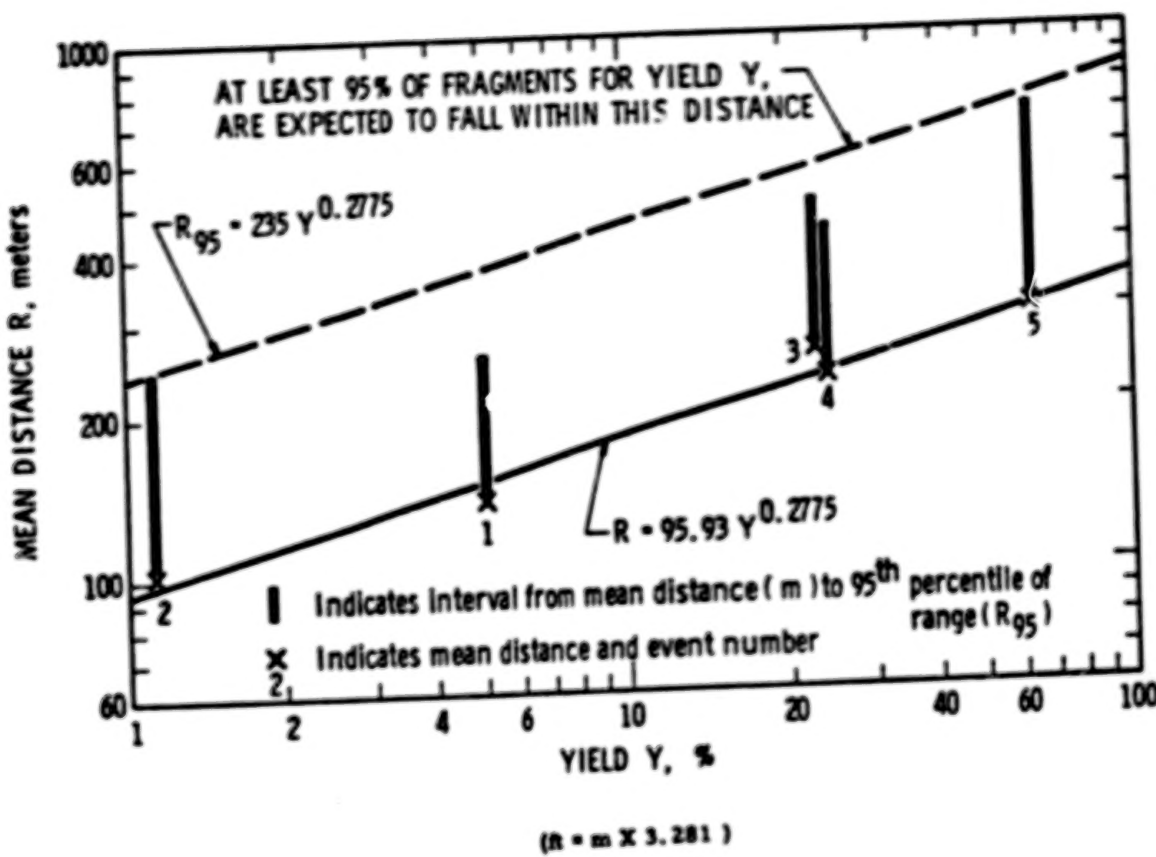


Figure 4F-6. Mean Distance Vs Yield with Estimated Range
Containing 95% of the Fragments (R_{95})

416

TABLE 4F-9. COMPUTER SIMULATED FRAGMENT RANGE FOR GAS VESSEL BURSTS

$$C_L = .32 \quad C_D = .85$$

Frag. Class	No.	$\overline{A}_L (\text{cm}^2)$	$\overline{M}_{\text{frag}}$	$\overline{A}_D + \sqrt{\overline{A}_L} (\text{cm}^2)$	Volume	Range - (m)					
						M^1	M^2	M^3	M^4	M^5	
Task A											
1	1-9	3.22×10^{-2}	1.00×10^{-1}	5.38×10^{-4}	5.51×10^{-3}	317	12.969	8.479	5.187	2.330	.564
2	10-15	1.07×10^{-2}	4.33×10^{-2}		5.48×10^{-3}		15.394	10.526	6.169	2.774	.754
3	16-21, 35	3.11×10^{-3}	1.33×10^{-2}		3.09×10^{-3}		16.502	11.120	6.473	2.967	.836
4	22-33	1.23×10^{-3}	3.81×10^{-3}		1.85×10^{-3}		11.893	8.052	4.717	2.110	.562
5											
Task B											
1	1, 2, 4-9	4.23×10^{-2}	1.20×10^{-1}	5.38×10^{-4}	1.09×10^{-3}	378	11.001	7.418	4.338	1.970	.532
2	3, 10-22	9.70×10^{-3}	4.18×10^{-2}		5.22×10^{-3}		16.298	11.014	6.389	2.945	.767
3	23-38, 35	2.00×10^{-3}	5.55×10^{-3}		2.42×10^{-3}		16.248	6.929	4.061	1.855	.560
4	31-33	1.10×10^{-4}	4.00×10^{-4}		7.68×10^{-4}		16.958	7.369	4.326	1.977	.534
5	34	9.43×10^{-4}	1.81×10^{-1}								
Task D											
1	1-12	5.20×10^{-2}	2.21	5.19×10^{-3}	2.11×10^{-3}	426	161.644	106.395	63.776	28.752	.798
2	13-18	1.29×10^{-2}	4.48×10^{-1}		1.16×10^{-3}		131.644	86.366	51.134	23.486	.637
3	19, 26, 21	4.73×10^{-3}	8.43×10^{-2}		6.32×10^{-4}		66.497	43.814	25.995	11.951	.499
4											
Task E											
1	1-16	5.38×10^{-2}	2.08	5.19×10^{-3}	2.13×10^{-3}	448	166.975	96.547	56.845	25.981	.693
2	17-19	1.47×10^{-2}	5.58×10^{-1}		1.11×10^{-3}		143.262	96.326	55.911	25.389	.661
3	20-22	5.59×10^{-3}	1.78×10^{-1}		6.87×10^{-4}		116.643	77.438	45.372	20.784	.576
4	23, 24	1.20×10^{-3}	4.99×10^{-2}		3.30×10^{-4}		142.168	95.762	56.629	25.291	.611

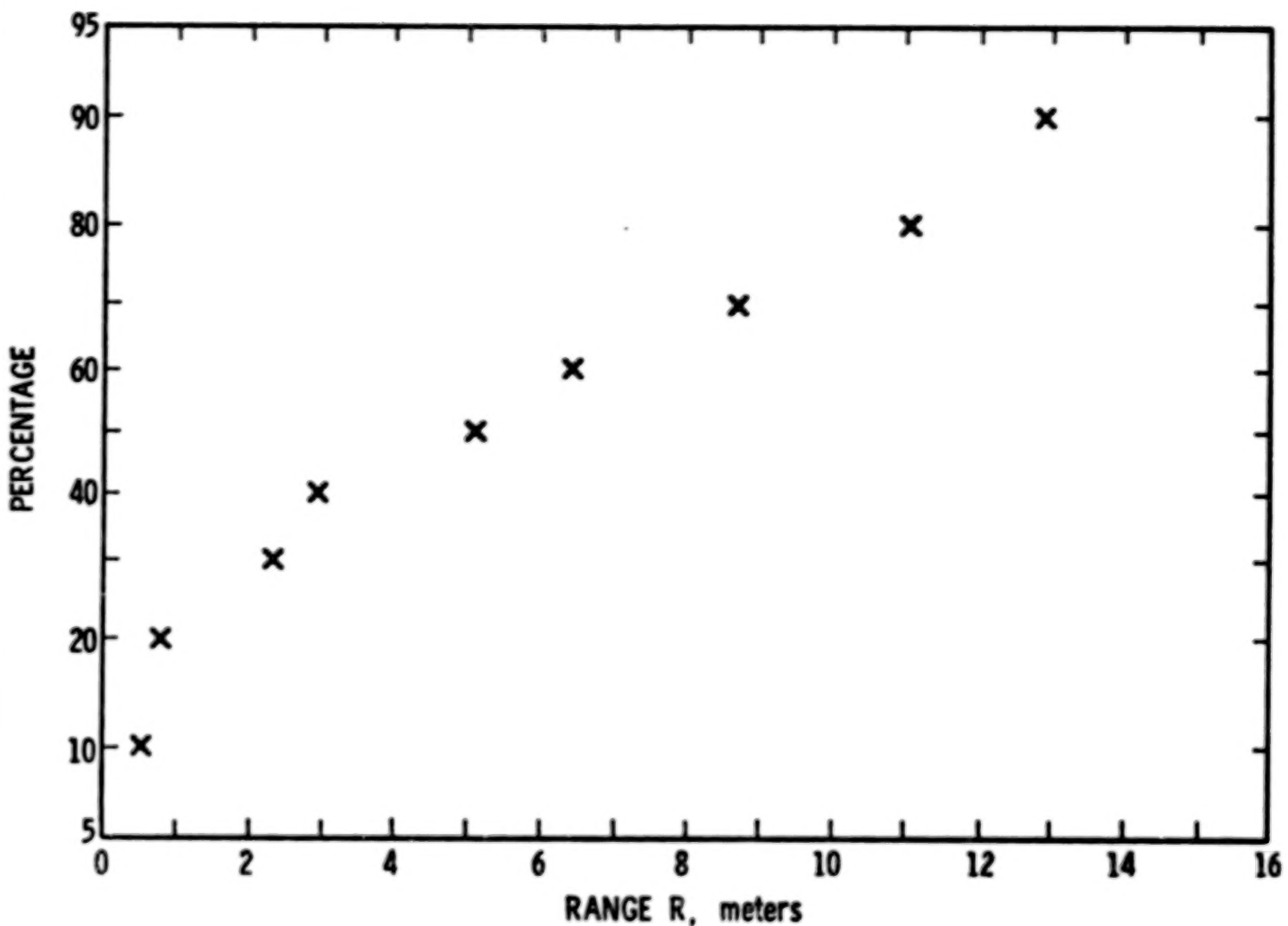
417

TABLE 4F-10. PERCENTILES FOR SIMULATED RANGES
FOR GAS VESSEL BURSTS

<u>Percentile</u>	<u>Tank A</u>	<u>Tank B</u>	<u>Tank D</u>	<u>Tank E</u>
10	0.566	0.532	6.4	6.9
20	0.806	0.747	11.9	20.8
30	2.330	1.98	23.5	25.4
40	2.947	2.95	28.7	45.4
50	5.107	4.33	43.8	56.0
60	6.473	6.38	63.8	77.4
70	8.679	7.39	66.5	96.3
80	11.120	10.25	108.4	114.6
90	12.969	11.00	131.6	143.3

TABLE 4F-11. ESTIMATES FOR MEAN AND STANDARD DEVIATION FOR SIMULATED RANGE DISTRIBUTIONS

<u>Tank No.</u>	<u>Estimate for Mean (M)</u>	<u>Estimate for Standard Deviation (S)</u>
A	5.67	6.72
B	5.06	3.92
D	53.05	44.05
E	65.1	46.20



(ft = m X 3.281)

Figure 4F-7. Simulated Range Distribution for Tank A

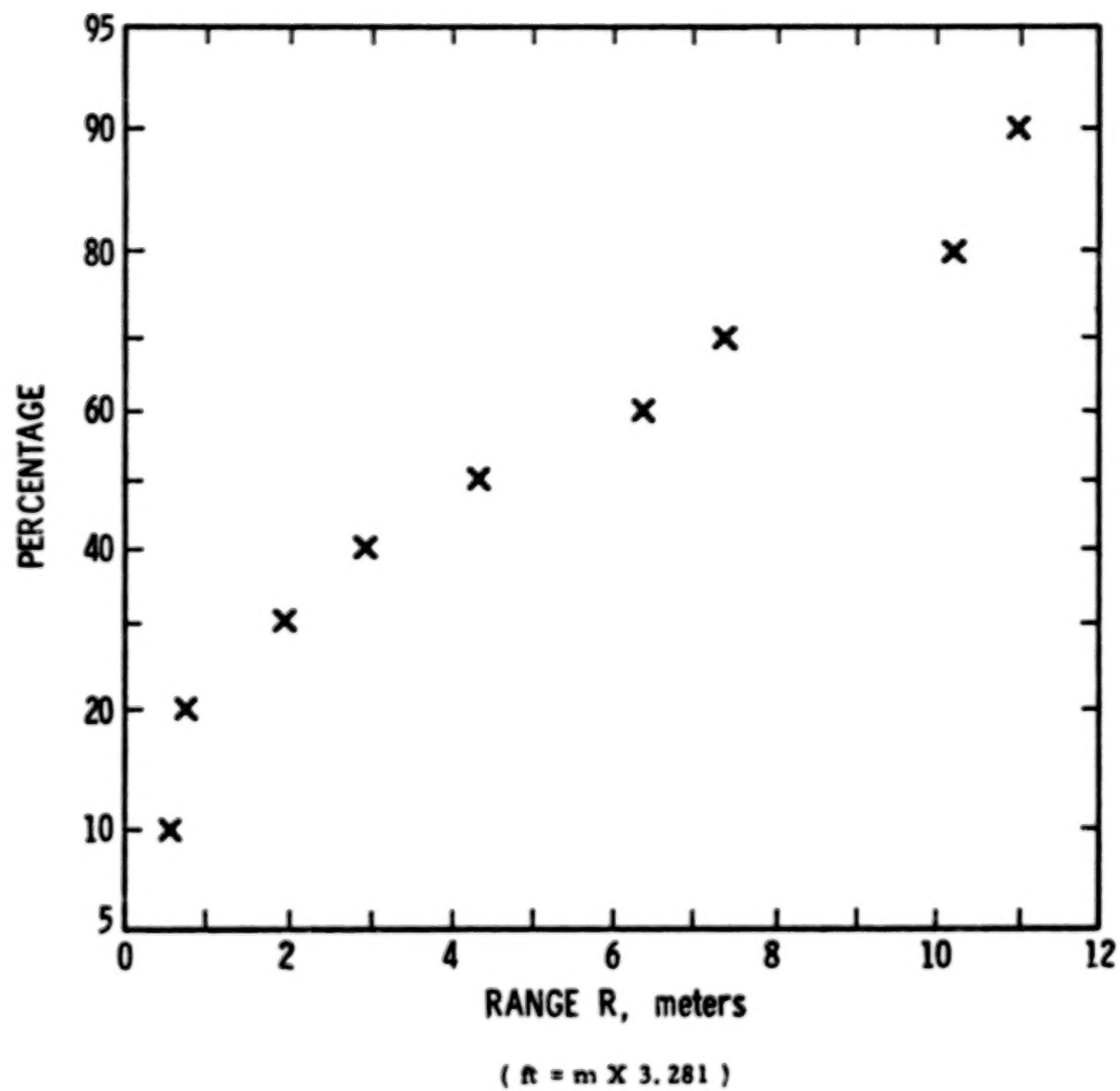


Figure 4F-8. Simulated Range Distribution for Tank B

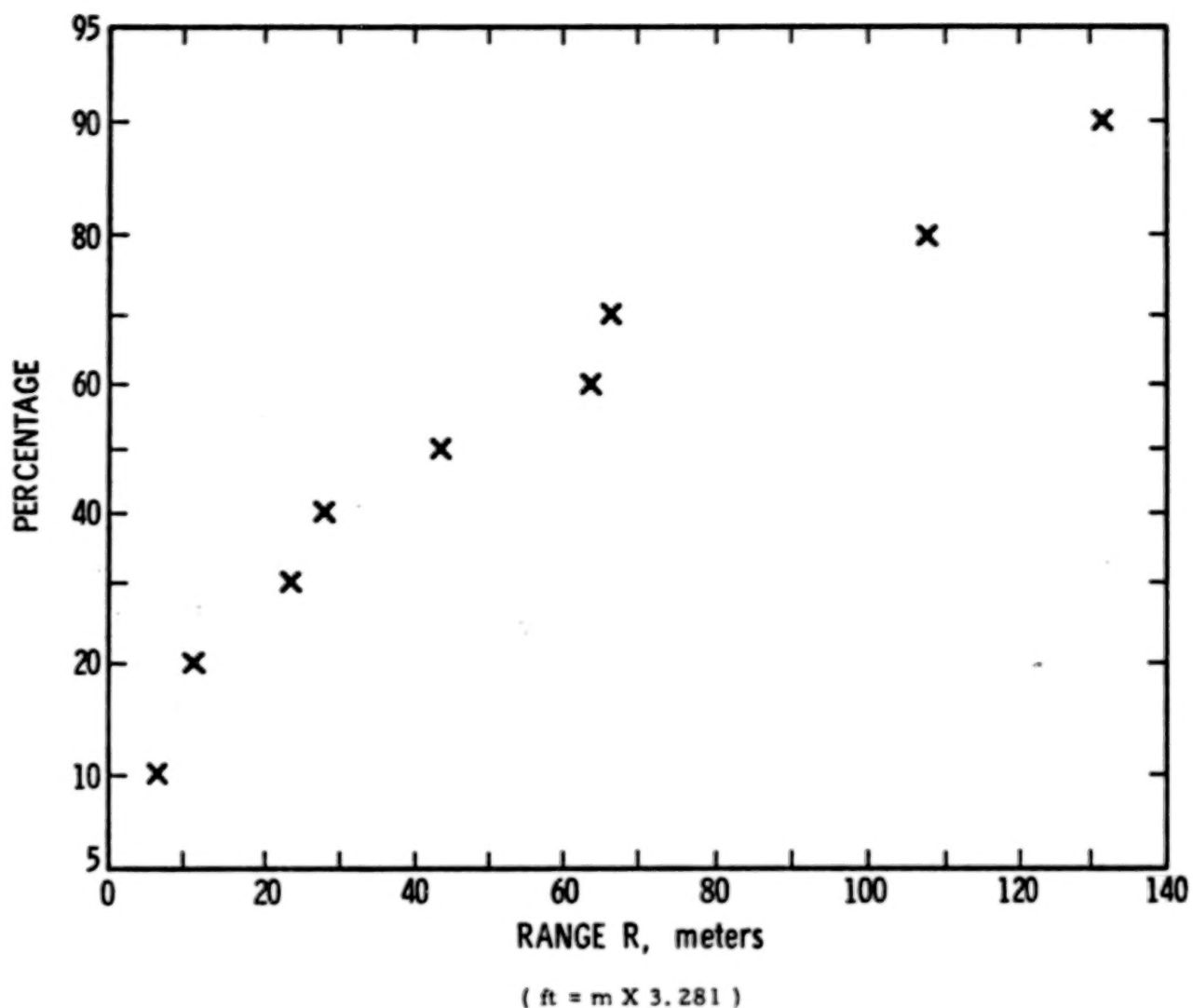
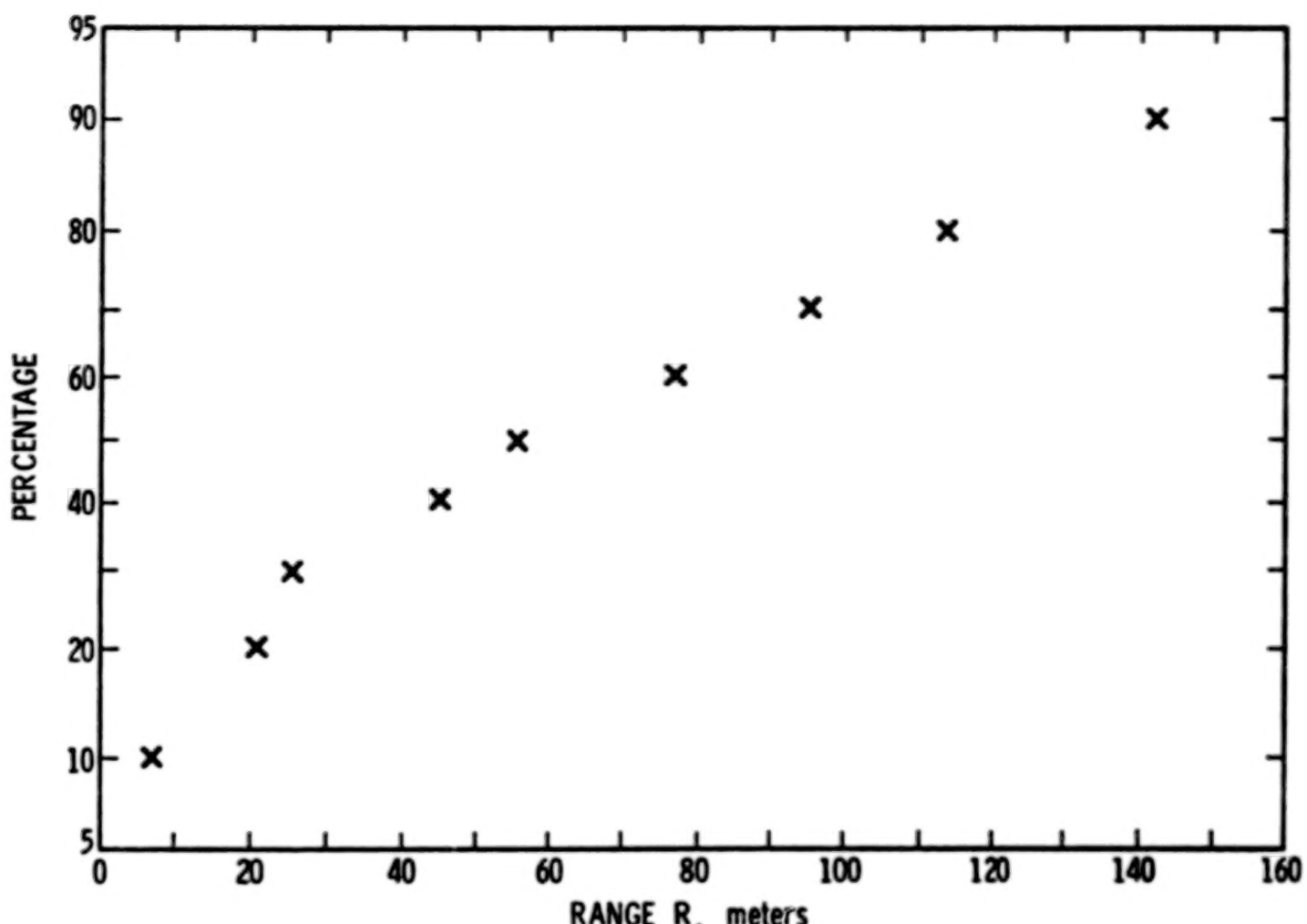


Figure 4F-9. Simulated Range Distribution for Tank D



(ft = m X 3.281)

422

Figure 4F-10. Simulated Range Distribution for Tank E

TABLE 4F-12. SUMMARY OF "W" TEST ON NORMALITY FOR SIMULATED FRAGMENT RANGE DISTRIBUTION FOR GAS VESSEL BURSTS

<u>Tank No.</u>	<u>"W"</u>	<u>Probability</u>
A	.929	.46
B	.921	.37
D	.933	.47
E	.956	.74

As shown from the probability column of Table 4F-12, the normal distributions are fairly good fits to the data.

4F-8 Rationale For Combining Simulated Range Distribution For Tanks A and B and for Tanks D and E

A "t" test for significant differences in means was made for each of the pairs of tanks, with the following results.

For tanks A and B, the calculated value of "t" was 0.235 and for tanks D and E was 0.558 versus the table value of ± 1.337 . Thus, no significant difference in means for either pair was found, and a single distribution for the simulated range for each pair was derived by averaging the respective pair of means and standard deviations. Table 4F-13 presents the results, and the distributions are charted in Figures 4-58 and 4-59.

TABLE 4F-13. ESTIMATED MEAN AND STANDARD DEVIATION FOR SIMULATED RANGE DISTRIBUTION FOR TANKS A AND B, AND TANKS D AND E

<u>Tanks</u>	<u>Estimated Mean</u>	<u>Estimated Standard Deviation</u>
A and B	5.4	5.5
D and E	59.2	45.1

LIST OF REFERENCES

1. Baker, W. E., V. B. Parr, R. L. Bessey, and P. A. Cox, "Assembly and Analysis of Fragmentation Data for Liquid Propellant Vessels," NASA CR-134538, NASA Lewis Research Center, January 1974.
2. Pittman, J. F., "Blast and Fragment Hazards From Bursting High Pressure Tanks," NOLTR 72-102, May 1972.
3. Chelson, Paul O., "Reliability Computation Using Fault Tree Analysis," JPL-TR-32-1542, NASA CR 124740, December 1, 1971.
4. Rasmussen, N. C., "Reactor Safety Study: An Assessment of Accident Risks in U. S. Commercial Nuclear Plants," U. S. Atomic Energy Report WASH-1400, August 1974.
5. Kanda, Kazuo, "Subsystem Safety Analysis Techniques," Annals of Reliability and Maintainability, Vol. 4, pp. 291-297, 1965.
6. Powers, G. J. and F. C. Tompkins, "A Synthesis Strategy For Fault Trees in Chemical Processing Systems," Loss Prevention, CEP Technical Manual, Vol. 8, 1974.
7. Lawley, H. G., "Operability Studies and Hazard Analysis," Loss Prevention, CEP Technical Manual, Vol. 8, 1974.
8. Ostle, B., Statistics in Research, The Iowa State Press, Ames, Iowa, 1960.
9. Hahn, G. J. and S. S. Shapiro, "Statistical Models In Engineering," John Wiley and Sons, Inc., New York, 1967.

CHAPTER V

EFFECTS OF FRAGMENTS

5-1 Damage Estimates to Structures and Facilities

5-1.1 General

One can see from Chapter IV that there are wide variations in characteristics of fragments generated during accidental explosions of the types covered in this handbook. Large sections of pressure vessels, and appurtenances accelerated by the explosions, can be quite massive (over 500 kg or 1000 lb_m), while some fragments thrown to large distances are quite light (less than 1 g or 0.002 lb_m). Impact velocities can range from a few meters per second to several hundred meters per second. Also, in Chapter IV, methods are given for estimating the probability that fragments of given mass and impact velocity will strike a structure located a specified distance from an accident. An important characteristic of fragments from these accidents is that they are of low velocity, and large average mass, compared to fragments from munitions which are intended to cause damage by penetration or perforation.

Conventional structures which can be damaged by fragments include frame or masonry residences, light to heavy industrial buildings, office buildings, public buildings, mobile homes, cars, and others too numerous to name. Damage can be superficial, such as denting of metal panels or breakage of panes of glass. But, massive fragments can cause more extensive damage such as perforation of wooden roofs, severe crushing of mobile homes or cars, etc. Most of the fragments will be nonpenetrating and will cause damage by imparting impulsive loads during impact. Methods similar to those used to establish threshold damage levels under blast loadings can also be used to establish thresholds for impact damage by fragments, i. e., lower limits for superficial damage. The methods will be somewhat simpler because the impacts will almost certainly be of short enough duration to be purely impulsive for almost any "target" structure or structural component. Impact conditions with large fragments which can be certain to cause significant structural damage can probably also be established by equating kinetic energy in the fragment to energy absorption capability for typical roof panels, roof supporting beams, etc.

Launch facilities for liquid-propellant rockets present some special "targets" to fragments from accidental explosions which can be especially susceptible to perforation damage. These are thin-walled tanks for storage or transport of energetic propellant liquids such as

LH₂, RP-1, or LO₂. Fragment impact conditions which would cause perforation of such tanks can be estimated from ballistic perforation formulas for munitions fragments and from hailstone impact data. These formulas will be presented and discussed.

5.1-2 Impact of Fragments on Thin Metal Targets

The following methods can be used for fragment impact on metal sheets or plates. The details of the formulation of these methods are presented in Appendix 5A.

The V₅₀ limit velocity is defined as the velocity at which a projectile will have a 50% chance of penetrating a given target. Knowing the properties of the projectile (fragment) and the target, V₅₀ can be obtained from Figure 5-1.

In this figure, a is the radius of the fragment (assuming a spherical shape), h is the thickness of the target, ρ_p is the density of the fragment (or projectile), ρ_t is the density of the target material, and σ_t is the yield stress of the target material.

The solid line in Figure 5-1 gives the relationship between limit velocity and target thickness. As the graph shows, there is uncertainty in this relation. For hard fragments which are less likely to deform, a lower nondimensional limit velocity (more conservative) should be chosen. For softer fragments, a higher limit velocity can be used. At this time, it is not known whether this relationship holds for values of $\frac{h}{a}$ greater than about 2.2.

This method is good for the impact of a fragment with its velocity normal to the target surface. For oblique impacts, the normal component of the velocity should be used. According to one report, (1) for oblique impacts, the penetration velocity is minimum at an angle of 30° from the normal direction. The difference between the penetration velocities at 0° and at 30° may be as great as 20%. Therefore, if oblique impact is expected, the penetration velocity obtained by use of Figure 5-1 should be multiplied by 0.8.

For fragment velocities less than V₅₀, the permanent deflection at the impact point on the target can be determined. Figure 5-2 is a graph of nondimensional deflection versus nondimensional velocity.

For given fragment properties, a given target, and a given normal component of fragment velocity, δ can be obtained. Of course, for very low fragment velocities, there is no permanent deflection.

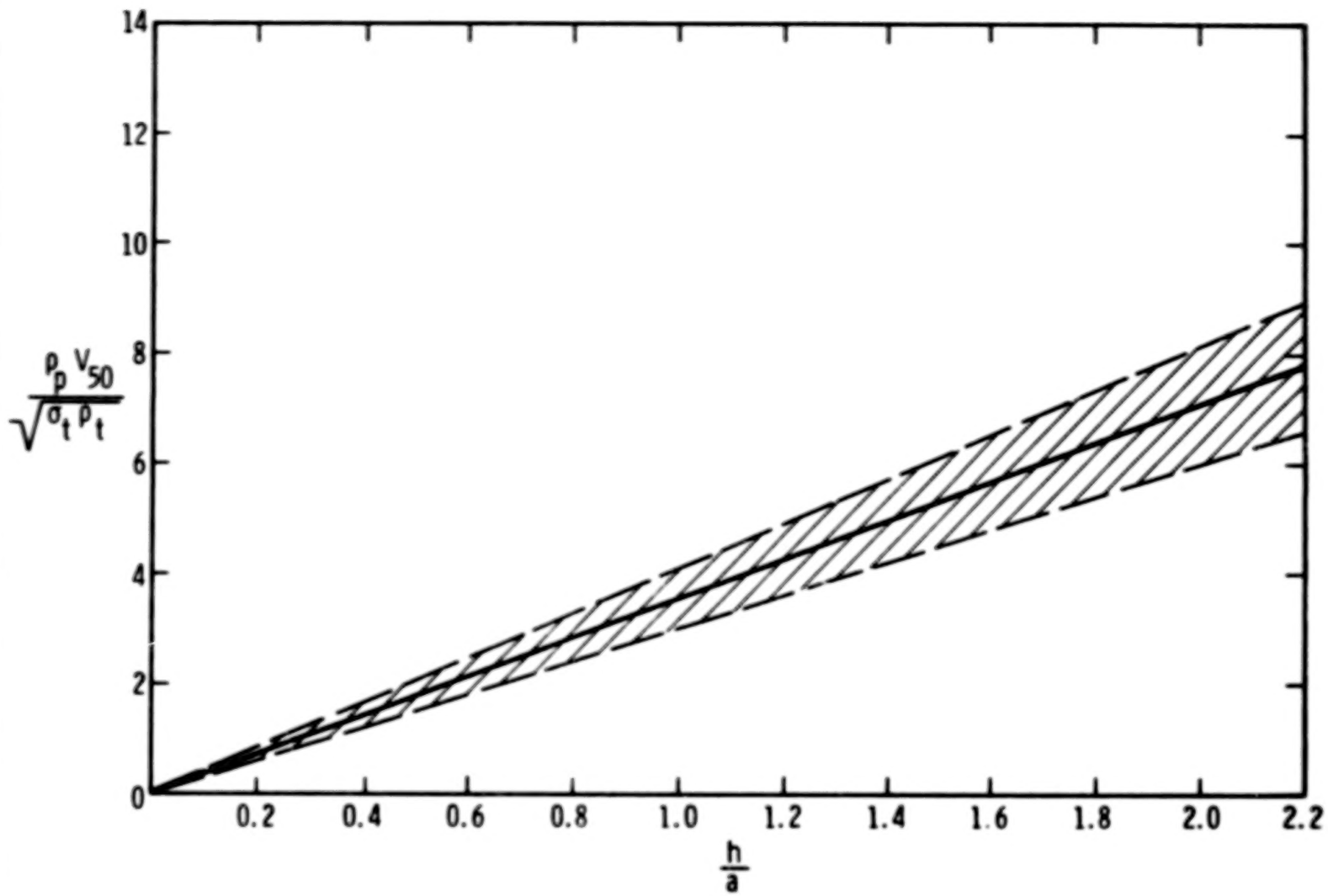


Figure 5-1. Nondimensional Limit Velocity Vs
Nondimensional Thickness

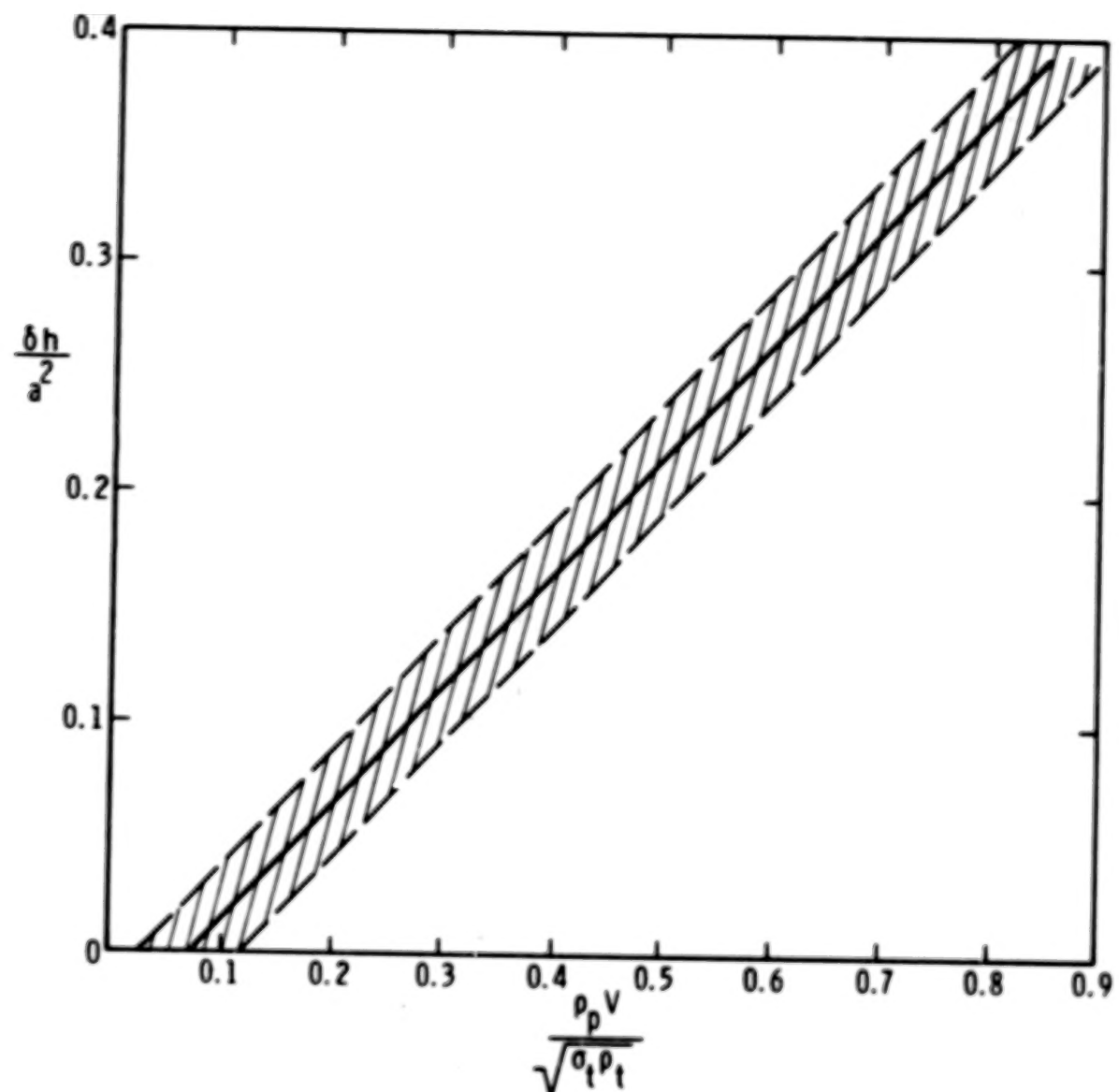


Figure 5-2. Nondimensional Deflection Vs
Nondimensional Velocity

This method was developed for impacts not very close to the edge of a sheet or plate. For fragment impact near the edge of an unsupported or simply-supported sheet or plate, the deflection may be twice the deflection that would be otherwise expected.

This analysis has been formulated for spherical fragments. To apply this to fragments of other shapes, let $a = \left(\frac{m}{\rho_p \frac{4\pi}{3}} \right)^{1/3}$,

where m is the mass of the fragment. More research must be done to determine other effects of fragment shape.

Table 5-1 is a list of the important properties (density and yield stress) of a few selected fragment and target materials.

TABLE 5-1. MATERIAL PROPERTIES
(References 2, 3)

	<u>density ρ</u>		<u>yield stress σ</u>	
	$\frac{\text{kg}}{\text{m}^3}$	$\frac{\text{lb}}{\text{ft}^3}$	Pa	psi
Steel	7850	489		
1015			$3.46 - 4.49 \times 10^8$	50,000 - 65,000
1018			3.66×10^8	53,000
1020 (large grained)			4.42×10^8	64,000
1020 (sheet)			3.11×10^8	45,000
Aluminum Alloys (sheet)	2770	173		
2024-O			8.85×10^7	12,800
2024-T3			3.66×10^8	53,000
2024-T4			3.66×10^8	53,000
Titanium Alloy	4520	282		
6Al4V			1.11×10^9	160,000

Example 1:

Given fragment radius $a = 0.020 \text{ m}$ (0.066 ft) and density $\rho_p = 7000 \text{ kg/m}^3$ ($440 \text{ lb}_m/\text{ft}^3$), target density $\rho_t = 7000 \text{ kg/m}^3$ ($440 \text{ lb}_m/\text{ft}^3$), and yield stress $\sigma_t = 4.40 \times 10^8 \text{ Pa}$ ($6.38 \times 10^4 \text{ psi}$) and fragment velocity $V = 200 \text{ m/s}$ (660 ft/sec), find the minimum target thickness h to prevent penetration. Solution: Nondimensional velocity is computed, and h/a is read from Figure 5-1:

$$\frac{\rho_p V_{50}}{\sqrt{\sigma_t \rho_t}} = \frac{(7000 \text{ kg/m}^3)(200 \text{ m/s})}{[(4.40 \times 10^8 \text{ N/m}^2)(7000 \text{ kg/m}^3)]^{1/2}} = 0.798$$

Then from Figure 5-1, $h/a = 0.202$. For the given a , $h = 0.0040 \text{ m}$ (0.013 ft).

Example 2:

Given fragment radius $a = 0.010 \text{ m}$ (0.033 ft) and density $\rho_p = 7000 \text{ kg/m}^3$ ($440 \text{ lb}_m/\text{ft}^3$), target density $\rho_t = 7000 \text{ kg/m}^3$ ($440 \text{ lb}_m/\text{ft}^3$), yield stress $\sigma_t = 4.40 \times 10^8 \text{ Pa}$ ($6.38 \times 10^4 \text{ psi}$) and thickness $h = 0.0010 \text{ m}$ (0.0033 ft), find V_{50} . Solution: h/a is computed, and the nondimensional velocity is read from Figure 5-1:

$$h/a = \frac{0.0010 \text{ m}}{0.010 \text{ m}} = 0.10$$

Then from Figure 5-1, $\frac{\rho_p V_{50}}{\sqrt{\sigma_t \rho_t}} = 0.43$. For the given properties, $V_{50} = 110 \text{ m/s}$ (360 ft/s).

Example 3:

Given the same fragment and target properties as in Example 2, and a fragment velocity less than the limit velocity $V = 52.0 \text{ m/s}$ (171 ft/s), find the deflection at the impact point on the target.

$$\frac{\rho_p V}{\sqrt{\sigma_t \rho_t}} = \frac{(7000 \text{ kg/m}^3)(52.0 \text{ m/s})}{[(4.40 \times 10^8 \text{ N/m}^2)(7000 \text{ kg/m}^3)]^{1/2}} = 0.207$$

From Figure 5-2, $\frac{\delta h}{2} = 0.068$. Then for this example, $a = 0.0068 \text{ m}$
(0.022 ft).

5-1.3 Impact of Fragments on Roofing Materials

Nearly any impact of a fragment upon the roof of a building will cause at least some superficial damage. Damage which only affects the appearance but which does not interfere with the performance of the roofing will not be discussed here. Serious damage includes cracking and complete penetration.

Because of the many kinds of roofing and the scarcity of data of fragment impact upon roofing materials, the following discussion will be kept as general as possible, presenting only the lower limits of damage for groupings of roofing materials, with the understanding that these are not known very accurately.

The analysis for the impact upon metal targets leads one to believe that the important projectile property is momentum. Until more information is obtained, it must be assumed that momentum is also important in impact upon roofing materials. (The following discussion is based upon data in Reference 4 in which synthetic hailstones were projected at roofing materials targets. The velocities in the tests correspond to the terminal fall velocities of hailstones of the particular sizes used).

The roofing materials can be separated into three classes: asphalt shingles, built-up roofs (alternate layers of bitumen and reinforcing membranes, often topped with pebbles or crushed stone), and miscellaneous materials (asbestos cement shingles, slate, cedar shingles, clay tile, and sheet metal). Lower limits of fragment momentum for serious damage to common roofing materials are given in Table 5-2.

For oblique impact, the component of the velocity normal to the surface of the roof should be used in the calculation of momentum.

Aged shingles may sustain serious damage at a lower fragment momentum than that which is given in the table. Also, the tests were conducted at room temperature. The limiting momentum would be greater for shingles at a higher temperature, and less for shingles at a lower temperature.

**TABLE 5-2. FRAGMENT IMPACT DAMAGE FOR
ROOFING MATERIALS (Reference 4)**

<u>Roofing Material</u>	<u>kg m/s</u>	<u>lb m ft/sec</u>	<u>Comments</u>
Asphalt shingles	0.710	5.13	crack shingle
	6.12	44.1	damage deck
Built-up roof	<0.710	< 5.13	crack tar flood coat
	2.00	14.5	crack surface of conventional built-up roof without top layer of stones
	>4.43	>31.9	with a 14 kg/m ² top layer of slag, there was no damage up to 4.43 kg m/s, which was the maximum momentum of the test
Miscellaneous			
0.003 m (1/8") asbestos cement shingles	0.710	5.13	
0.006 m (1/4") asbestos cement shingles	1.27	9.16	
0.006 m (1/4") green slate	1.27	9.16	
0.006 m (1/4") grey slate	0.710	5.13	
0.013 m (1/2") cedar shingles	0.710	5.13	
0.019 m (3/4") red clay tile	1.27	9.16	
Standing seam terne metal	4.43	31.9	plywood deck cracked

Example 4:

A fragment with a mass of 0.25 kg (0.55 lb_m) and a velocity of 20.0 m/s (65.6 ft/s) strikes a roof of asphalt shingles in a direction normal to the surface of the roof. What kind of damage can be expected? Solution: Calculate the momentum of the fragment, and compare it to the values in Table 5-2. Momentum = $mv = (0.25 \text{ kg})(20.0 \text{ m/s}) = 5.0 \text{ kg m/s}$. According to Table 5-2, this momentum will crack the shingle, but it will not damage the deck.

5-2 Damage Estimates to People from Secondary Fragments

5-2.1 Penetrating Fragments

Fragments can be divided into two categories, penetrating and nonpenetrating. Due to a limited amount of available data, penetrating fragments will refer to fragments weighing up to 0.015 kg (0.033 lb_m) and area-to-mass ratio A/M up to 0.09 m²/kg where A is the cross-sectional area of a fragment along its trajectory and M is the mass of the fragment. Nonpenetrating fragments will refer to fragments weighing 4.54 kg (10 lb_m) or more. Only a summary of the methods for determining fragment damage to people will be presented here. The development of these methods is given in Appendix 5B for the convenience of the interested reader.

To determine whether a fragment can cause severe body penetration damage, it is necessary to determine its striking velocity V in (m/s) and A/M ratio: these parameters can, in general, be determined from other portions of this handbook with the exception of parameters from glass window fragments which follow. The ballistic limit velocity V₅₀ (in m/s), which is the velocity at which half of the missiles incident on the body are expected to perforate the skin with enough residual velocity to cause severe damage is^(5, 6)

$$V_{50} = 1247.1 \left(\frac{A}{M} \right) + 22.03 \text{ m/s} \quad (5-1)$$

for

$$A/M \leq 0.09 \text{ m}^2/\text{kg}, M \leq 0.015 \text{ kg}$$

where

A is the cross-sectional area of the fragment along its trajectory in m²

M is the mass of the fragment in kg

V_{50} is the ballistic limit velocity in m/s

If $V \geq V_{50}$, then one can expect some serious wounds from body penetration.

To determine if a glass fragment from a window pane broken by the blast wave can cause severe body penetration damage, it is necessary to calculate an effective peak overpressure P_e

where

$$P_e = \bar{P}_s p_0 \quad (5-2)$$

for windows oriented side-on or back-on to the approaching blast wave where p_0 is atmospheric pressure in Pa, see Figure 5-3.

or

$$P_e = \bar{P}_r p_0 \quad (5-3)$$

for windows oriented face-on to the approaching blast wave.

for

$$\bar{P}_s \leq 3.5^{(7)}$$

$$\bar{P}_r = 2 \bar{P}_s + \frac{(\gamma + 1) \bar{P}_s^2}{(\gamma - 1) \bar{P}_s + 2\gamma} \quad (5-4)$$

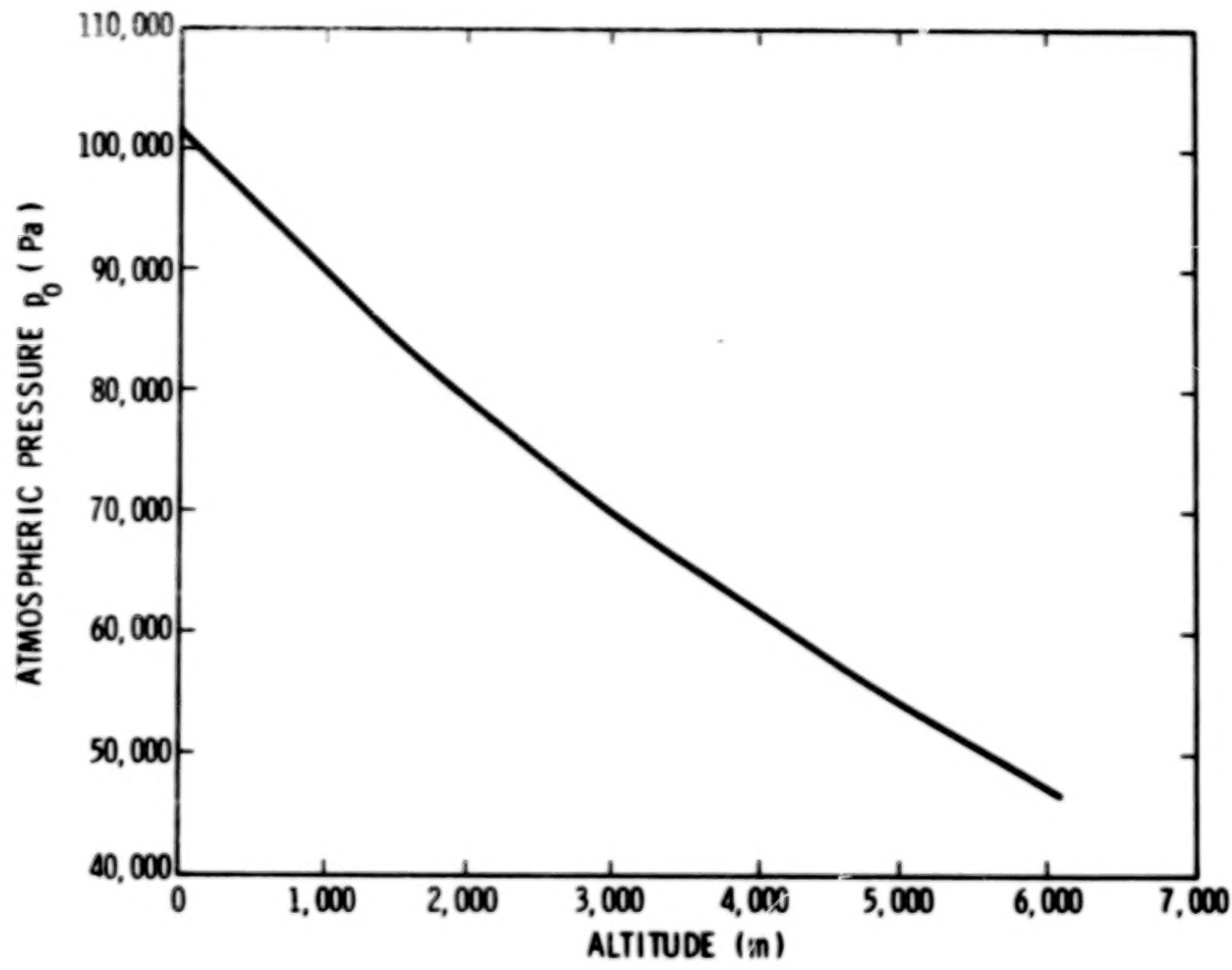
where

$$\gamma \approx 1.4$$

For $\bar{P}_s > 3.5$, \bar{P}_r can be acquired directly from Figure 5-4. The ratio A/M should be chosen as the smaller of

$$\frac{A}{M} = \frac{1}{t_0} \quad (5-5)$$

or



$$(\text{psi} = \text{Pa} \times 1.450 \times 10^{-4})$$

$$(\text{ft} = \text{m} \times 3.281)$$

Figure 5-3. Atmospheric Pressure Vs Altitude Above
Sea Level

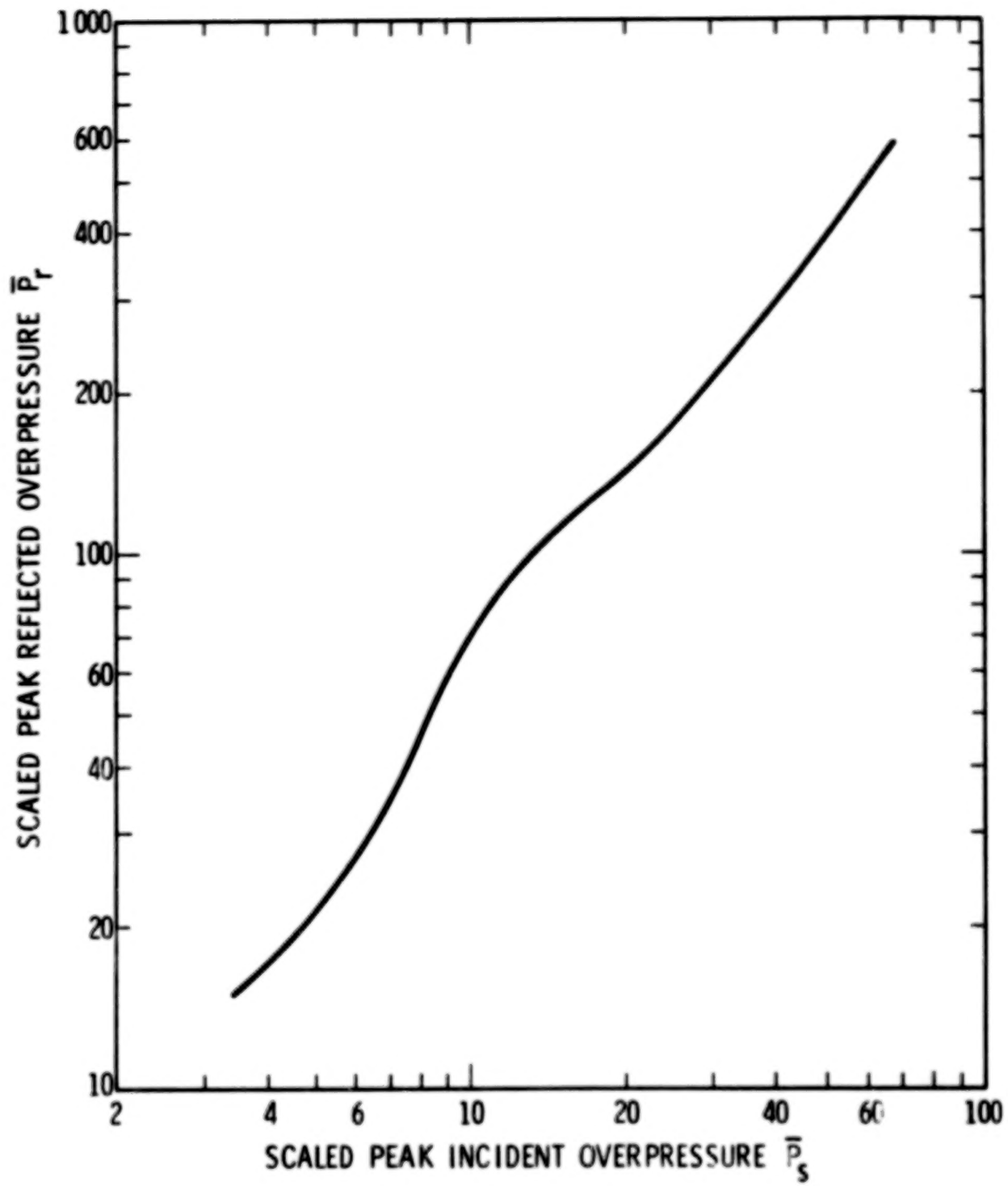


Figure 5-4. Scaled Reflected Overpressure Vs Scaled Side-on Overpressure

$$\frac{A}{M} = \frac{1}{\rho \sqrt{A'}} \quad (5-6)$$

where

t is the thickness of the window pane in meters

ρ is the density of the glass which is approximately 2471 kg/m^3 (from Reference 8)

A' is the geometric mean frontal area of the glass fragment in m^2 expressed by

$$A' = 6.4516 \times 10^{-4} e^{\left[2.4 - \sqrt{12.5 + (5.8566 \times 10^{-5} P_e)^2} \right]} \quad (5-7)$$

for P_e in the range 0 Pa to 96.5 kPa. (From References 8 and 9).

Striking velocity v (in m/s) is

$$v = [(0.2539) + (1.896 \times 10^{-4}) (t - 7.62 \times 10^{-4})^{-0.928}] x \\ [0.3443 P_e^{0.547}] \quad (5-8)$$

for P_e in range 690 Pa to 689 KPa and $t \geq 7.62 \times 10^{-4}$ m.

If $v \geq V_{50}$, then one can expect some serious wounds from body penetration.

5-2.2 Nonpenetrating Fragments

Criteria for body damage from nonpenetrating objects are contained in Table 5-3. It should be noted that damage is dependent on fragment mass and velocity only. The table also only contains one fragment mass value. One can logically assume that larger masses propelled at the same velocities shown in the table will produce more damage than the 4.54 kg (10 lb) mass presented in the table.

TABLE 5-3. TENTATIVE CRITERIA FOR INDIRECT BLAST EFFECTS FROM NONPENETRATING FRAGMENTS
 (References 10, 11, 12)

<u>Mass</u>	<u>Event</u>	<u>Extent of Damage</u>	<u>Impact Velocity</u>
4.54 kg (10 lb _m)	Cerebral Concussion	Mostly "safe"	3.05 m/s (10 ft/sec)
		Threshold	4.57 m/s (15 ft/sec)
	Skull Fracture	Mostly "safe"	3.05 m/s (10 ft/sec)
		Threshold	4.57 m/s (15 ft/sec)
		Near 100%	7.01 m/s (23 ft/sec)

5-2.3 Example Calculations for Determining Damage Estimates to People from Secondary Fragments

Example 1:

Environmental Conditions:

$$P_s = 3.8 \times 10^4 \text{ Pa (4.78 psi)}$$

$$I_s = 1.16 \times 10^3 \text{ Pa} \cdot \text{s (0.168 psi-sec)}$$

$$P_0 = 1.0135 \times 10^5 \text{ Pa (14.7 psi)}$$

Penetrating fragments - Mass M = 0.015 kg (0.033 lb_m)

Velocity V = 40 m/s (131 ft/sec)

Cross sectional area A along trajectory of fragment = 0.00016 m² (0.00172 ft²)

Windows in a nearby building are 0.003175 m (0.125 in.) thick and are face-on to the approaching blast wave.

Nonpenetrating fragment - Mass M = 4.00 kg (8.8 lb_m)

Velocity V = 2.0 m/s (6.6 ft/sec)

(1) Penetrating fragments other than glass from windows:

(a) $\frac{\Delta}{M} = \frac{0.00016 \text{ m}^2}{0.015 \text{ kg}} = 0.0107 \text{ m}^2/\text{kg}$

(b) From Equation (5-1):

$$V_{50} = (1247.1)(0.0107) + 22.03 = 35.4 \text{ m/s}$$

Since $V > V_{50}$, one can expect some severe body penetration damage.

(2) Penetrating fragments from glass windows:

(a) $P_e = \bar{P}_r p_0$ for windows face-on to the approaching blast wave Equation (5-3):

$$\bar{P}_s = \frac{3.8 \times 10^4 \text{ Pa}}{1.0135 \times 10^5 \text{ Pa}} = 0.375 < 3.5$$

Therefore from Equation (5-4),

$$\bar{P}_r = (2)(0.375) + \frac{(2.4)(0.375)^2}{(0.4)(0.375) + 2.8}$$

$$\bar{P}_r = 0.864$$

From Equation (5-3)

$$P_e = \bar{P}_r p_0 = (0.864)(101,350) = 87,567 \text{ Pa}$$

(b) $\left(\frac{\Delta}{M}\right)_1 = \frac{1}{t_p} =$

$$\frac{1}{(3.175 \times 10^{-3} \text{ m})(2.471 \times 10^3 \text{ kg/m}^3)} =$$

$$0.1275 \text{ m}^2/\text{kg}$$

$$\left(\frac{A}{M}\right)_2 = \frac{1}{c \sqrt{A'}}$$

From Equation (5-7):

$$A' = (6.4516 \times 10^{-4}) \times \\ e \left(2.4 - \left\{ 12.5 + [(5.8566 \times 10^{-5})(8.7567 \times 10^4)]^2 \right\}^{1/2} \right) \\ A' = 1.402 \times 10^{-5} \text{ m}^2$$

Therefore,

$$\left(\frac{A}{M}\right)_2 = \frac{1}{(2471) \sqrt{1.402 \times 10^{-5}}} = 0.1081 \text{ m}^2/\text{kg}$$

The smaller value for A/M ($0.1081 \text{ m}^2/\text{kg}$) is the better choice.

- (c) V_{50} for $A/M = 0.1081 \text{ m}^2/\text{kg}$ can be calculated from Equation (5-1):

$$V_{50} = (1247.1)(0.1081) + 22.03$$

$$V_{50} = 157 \text{ m/s (515 ft/sec)}$$

(Note that the limit for A/M in Equation (5-1) has been slightly exceeded, and the V_{50} result is an extrapolation.)

- (d) From Equation (5-8), the striking velocity V is

$$V = \left[(0.2539) + (1.896 \times 10^{-4})(3.175 \times 10^{-3} - 7.62 \times 10^{-4})^{-0.928} \right] \left[(0.3443)(8.7567 \times 10^4)^{0.547} \right]$$

$$V = 53.0 \text{ m/s (174 ft/sec)}$$

(e) Since $V < V_{50}$, one would not expect any severe body penetration damage.

(3) Nonpenetrating fragments:

The mass (4.00 kg) and velocity (2 m/s) of the nonpenetrating fragment are less than the mass and velocity required for the mostly "safe" damage condition shown in Table 5-3. Thus, one would not expect deaths to result from nonpenetrating fragments.

LIST OF REFERENCES

1. McNaughtan, I. L. and S. W. Chisman, "A Study of Hail Impact at High Speed on Light Alloy Plates," Proceedings of the Ninth Annual National Conference on Environmental Effects on Aircraft and Propulsion Systems, Naval Air Propulsion Test Center, October 7-9, 1969, pp. 16-14.
2. Gerberich, W. W., and G. S. Baker, "Toughness of Two-Phase 6 Al-4V Titanium Microstructures," in Applications Related Phenomena in Titanium Alloys, ASTM Special Publication No. 432, 1968.
3. Moore, T. D., ed., Structural Alloys Handbook, Mechanical Properties Data Center, Traverse City, Michigan, 1975.
4. Greenfield, Sidney H., "Hail Resistance of Roofing Products" U. S. Department of Commerce, National Bureau of Standards, Building Science Series 23, August 1969.
5. Sperrazza, J. and W. Kokinakis, "Ballistic Limits of Tissue and Clothing," BRL Technical Note No. 1645, Aberdeen Proving Ground, MD, January 1967.
6. Kokinakis, William, "A New Methodology for Wounding and Safety Criteria," Proceedings of 16th Explosive Safety Seminar, September 1974, pp. 1209-1226.
7. Baker, Wilfred E., Explosions in Air, University of Texas Press, Austin, Texas, May 1973.
8. Fletcher, E. Royce, Donald R. Richmond, and Robert K. Jones, "Velocities, Masses and Spatial Distribution of Glass Fragments from Windows Broken by Airblast," report in preparation for Defense Nuclear Agency, Washington, D. C.
9. E. R. Fletcher, D. R. Richmond, and R. K. Jones, Lovelace Foundation for Medical Education and Research, Albuquerque, New Mexico, 87108.
10. White, Clayton S., "The Scope of Blast and Shock Biology and Problem Areas in Relating Physical and Biological Parameters," Annals of the New York Academy of Sciences, Vol. 152, Art. 1, October 1968, pp. 89+.

11. Clemedson, Carl-Johan, Gustav Hellström, and Sten Lingren, "The Relative Tolerance of the Head, Thorax, and Abdomen to Blunt Trauma," Annals of the New York Academy of Sciences, Vol. 152, Art. 1, October 1968, pp. 1894.
12. White, Clayton S., "The Nature of the Problems Involved in Estimating the Immediate Casualties from Nuclear Explosions," Civil Effects Test Operations, U. S. Atomic Energy Commission, July 1971, DR-1886.

APPENDIX V.A

EFFECTS OF FRAGMENTS ON STRUCTURES

The structures that are considered here are metal plates and sheets. There does not appear to be any effect of the curvature of the target; therefore, it is reasonable to use data for flat targets and apply them to any general shape that may be of interest.

The methods described in Section 5-1 are based upon an examination of data of fragment and hailstone impact upon metal sheets and plates.⁽¹⁻³⁾ In these studies, synthetic hailstones (ice spheres) were fired at target sheets of aluminum alloys, and various shapes of fragments were fired at steel targets. A model analysis was performed, using the methods described in Reference 4. The parameters of interest are listed in Table 5A-1.

TABLE 5A-1. LIST OF PARAMETERS

a	radius of fragment (assuming spherical shape)
h	thickness of target
v	velocity of fragment
b	permanent deflection of target at point of impact
ρ_r	density of fragment (projectile)
ρ_t	density of target
σ_t	yield stress of target material

This analysis is concerned with plastic deformation, which makes the parameter σ_t more important than the modulus of elasticity of the target material. Also, the fragment is assumed to be a rigid body, which makes the strength of the fragment an unnecessary parameter. The model analysis and a study of the data resulted in the nondimensional terms (Table 5A-2).

TABLE 5A-2. NONDIMENSIONAL TERMS

$\left(\frac{\rho_p V}{\sqrt{\sigma_t \rho_t}} \right)$	dimensionless projectile velocity
$\left(\frac{\delta h}{a^2} \right)$	dimensionless target deflection
$\left(\frac{h}{a} \right)$	dimensionless target thickness

When $\left(\frac{\delta h}{a^2} \right)$ is plotted versus $\left(\frac{\rho_p V}{\sqrt{\sigma_t \rho_t}} \right)$, the data follow a straight line with some scatter in the data points (see Figure 5-2 in text). The line intersects the horizontal axis at a positive value of velocity. This is expected because there is a finite fragment velocity below which no permanent target deflection occurs.

Letting the velocity in the dimensionless projectile velocity term be the limit velocity, the locus of $\left(\frac{\rho_p V_{50}}{\sqrt{\sigma_t \rho_t}} \right)$ versus $\left(\frac{h}{a} \right)$ is linear with the data points lying within about 15% of the values on the line (see Figure 5-1 in the text). The hailstone impact data fall in the region above the line (higher limit velocity), and the steel fragment data fall on and below the line (lower limit velocity). This indicates a possible effect of fragment strength. For this reason it may be desirable to be more conservative with steel fragments, choosing a lower limit velocity, and less conservative with aluminum fragments, choosing a higher limit velocity.

LIST OF REFERENCES

1. Kangas, Pell, "Hailstone Impact Tests on Aircraft Structural Components," Civil Aeronautics Administration Technical Development and Evaluation Center, Technical Development Report No. 124, Indianapolis, Indiana, September 1950.
2. McNaughtan, I. I., and S. W. Chisman, "A Study of Hail Impact at High Speed on Light Alloy Plates," Proceedings of the Ninth Annual National Conference on Environmental Effects on Aircraft and Propulsion Systems, Naval Air Propulsion Test Center, October 7-9, 1969, pp. 16-1+.
3. Recht, R. F., "Containing Ballistic Fragments," in Engineering Solids Under Pressure, H. Pugh, ed., Papers presented at the Third International Conference on High Pressure, Aviemore, Scotland, 1970, pp. 51-60.
4. Baker, Wilfred E., Peter S. Westine, and Franklin T. Dodge, Similarity Methods in Engineering Dynamics, Hayden Book Company, Inc., Rochelle Park, New York, 1973.

APPENDIX V.B

DAMAGE ESTIMATES TO PEOPLE FROM SECONDARY FRAGMENTS

5B-1 Penetrating Fragments

Undoubtedly a great deal of research has been conducted to produce classified wound ballistics equations for the military. Although thorough unclassified equations of this type do not exist, some publicly available body penetration data have been accumulated in recent times and some relatively simple analyses have been performed. Methods for predicting body damage from fragments using fragment parameters available in this document are presented in this appendix. More reliable damage criteria will undoubtedly be produced as the state-of-the-art improves.

Sperrazza and Kokinakis^(1,2) concerned themselves with a ballistic limit velocity V_{50} for animal targets. The V_{50} velocity is the striking velocity at which one expects half the impacting missiles to perforate an object. They found that this velocity depended on the area to mass ratio, that is

$$V_{50} \propto \frac{A}{M} \quad (5B-1)$$

where A is cross-sectional area of the projectile along the trajectory, and M is the mass of the projectile. They fired steel cubes, spheres and cylinders of various masses up to 0.015 kg (0.033 lb_m) into 3 mm (0.118 in.) thick isolated skin (human and goat) to establish a ballistic limit. One of their assumptions was that, if the projectile penetrates the skin, its residual velocity would be sufficient enough to cause severe damage. This cautious assumption is appropriate for establishing a certain margin of safety in the calculation. Their conclusions were that, in the range of their data for steel cubes, spheres and cylinders, V_{50} depended linearly on projectile A/M ratio. Specifically,

$$V_{50} = 1247.1 \frac{\text{kg}}{\text{m} \cdot \text{s}} \left(\frac{A}{M} \right) + 22.03 \text{ m/s}^* \quad (5B-2)$$

where A/M is in m^2/kg , and V_{50} is in m/s.

* Equation (5B-2) has been adjusted for SI units.

Kokinakis⁽²⁾ later fired plastic sabots end-on into 20% gelatin that was 1 cm thick. The sabots were fired end-on since this represents the worst case, and 20% gelatin was used because this ballistically simulates isolated human skin. The linear relation of V_{50} versus A/M formulated by Sperrazza and Kokinakis⁽¹⁾ is plotted in Figure 5B-1. The average values for these experiments are located on this graph. Circles on the figure represent the initial experiments using steel cubes, spheres and cylinders weighing up to 0.015 kg (0.033 lb_m), and each average value represents as many as 30 data points. The line drawn on the graph is a least squares fit to these average values. Upward pointed triangles represent the average values for the subsequent experiments with end-on plastic sabots. These average values also lie near the line drawn for the prior study, thus adding a degree of confidence in the analysis.

Unfortunately, other authors have not presented their penetration data in the same form as Sperrazza and Kokinakis. Glasstone⁽³⁾ expressed the probability of glass fragments penetrating the abdominal cavity in terms of the mass of the glass fragments. To compare Glasstone's conclusions with that of Sperrazza and Kokinakis, it is necessary to make a few assumptions. The first assumption is that the glass fragment velocity for 50% probability of penetration of the abdominal cavity is biologically equivalent to the ballistic limit velocity V_{50} for penetrating isolated human skin. This assumption is true provided that, after the glass fragment penetrates the skin, it does not encounter too much resistance before it perforates the abdominal cavity. Glasstone only specifies the mass of the glass required for penetration and does not give its cross-sectional area, thickness or density. For the purpose of comparing the conclusions of Glasstone with those of Sperrazza and Kokinakis, it was assumed that glass fragments are propelled edge-on, which is probably the worst case, and that they are square with thicknesses of 3.175 mm (1/8 in.) to 6.35 mm (1/4 in.). It was also assumed that the glass fragments have an average density of 2471 kg/m³.⁽⁴⁾ With these assumptions, it is not difficult to calculate A/M. If the glass fragment has a thickness t , and edge length y , then for volume

$$V = y^2 t \quad (5B-3)$$

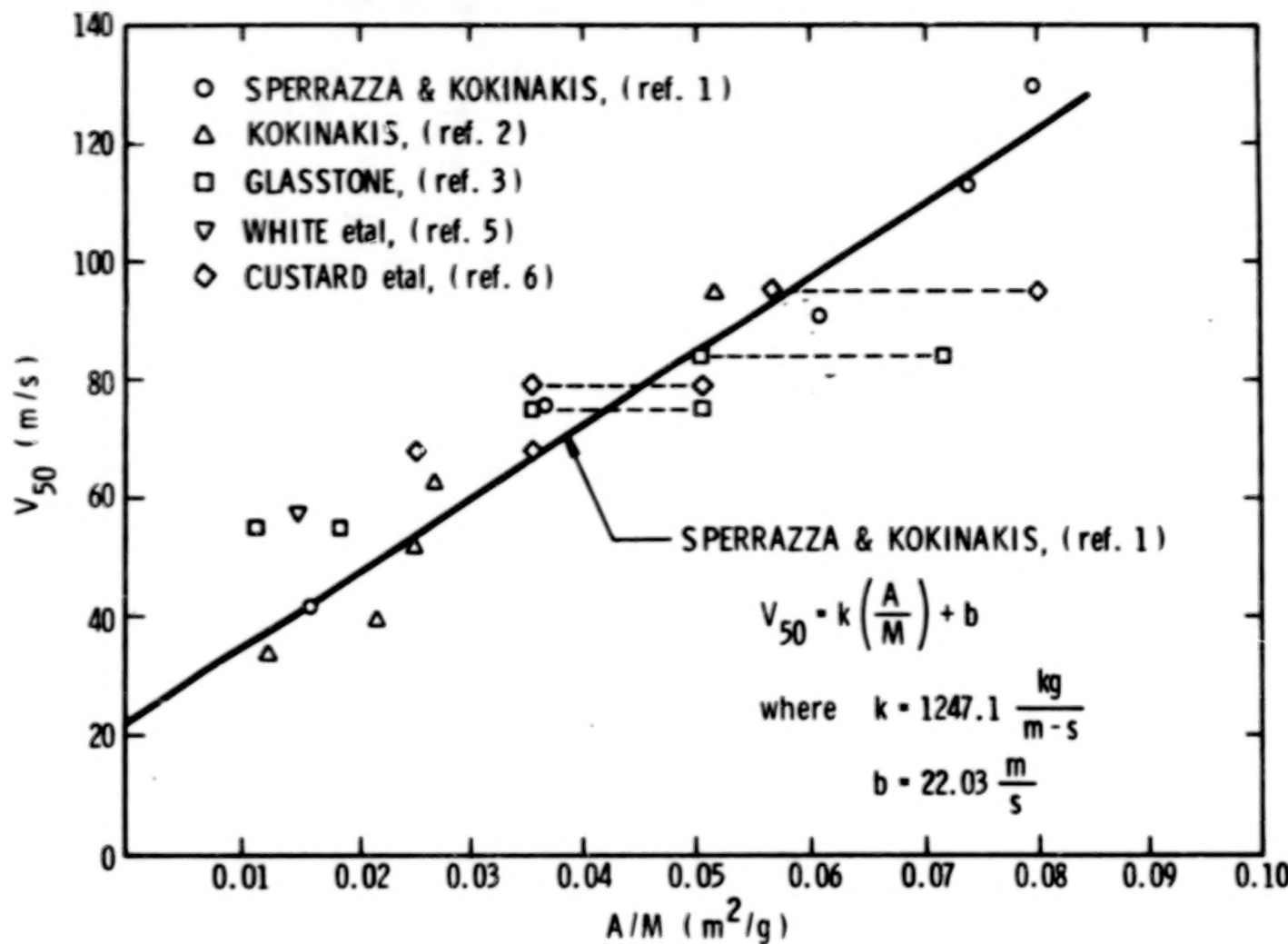
where

V = volume of the fragment

y = edge length

t = thickness

Thus, the mass M of the fragment is



(ft/sec = m/s X 3.281)

($in^2/lb_m = m^2/kg \times 703.1$)

Figure 5B-1. Ballistic Limit (V_{50}) Vs Fragment Area/Mass for Isolated Human and Goat Skin

449

$$M = \rho y^2 t \quad (5B-4)$$

where ρ is the density of the glass. Rearranging Equation (5B-4) gives the edge length,

$$y = \sqrt{\frac{M}{\rho t}} \quad (5B-5)$$

The area-to-mass ratio A/M , assuming edge-on impact, is

$$\frac{A}{M} = \frac{ty}{M} \quad (5B-6)$$

or from Equations (5B-4), (5B-5) and (5B-6),

$$\frac{A}{M} = \sqrt{\frac{t}{\rho M}} \quad (5B-7)$$

Glasstone's criteria for 50% probability of glass fragments penetrating the abdominal cavity are shown in Table 5B-1. This table also contains the estimates for A/M for glass thicknesses of 3.175 mm (1/8 in.) and 6.35 mm (1/4 in.). The velocity values and calculated values for A/M which fall in the range of values used by Sperrazza and Kokinakis are plotted as squares in Figure 5B-1. The dashed lines indicate a range of A/M values for thickness values from 2.175 mm (1/8 in.) to 6.35 mm (1/4 in.). Even with the crude assumptions mentioned above, the calculated points fall very near the line drawn on Figure 5B-1.

White⁽⁵⁾ also related skin penetration velocity to the masses impacting fragments. He concluded that slight skin laceration occurred when spherical bullets with mass 0.0087 kg (0.0191 lb_m) were propelled into the body at 57.9 m/s (190 ft/sec). Assuming that the density ρ of steel is 7925 kg/m³, the A/M ratio can be calculated from

$$\frac{A}{M} = \frac{\pi r^2}{M} \quad (5B-8)$$

where r is the radius of the spherical penetrator or

$$\frac{A}{M} = \frac{\pi}{M} \cdot \left(\frac{3M}{4\pi\rho} \right)^{2/3} \quad (5B-9)$$

TABLE 5B-1. 50 PERCENT PROBABILITY OF GLASS
FRAGMENTS PENETRATING ABDOMINAL
CAVITY^{(3)*}

Mass of Glass Fragment kg	Impact Velocity m/s (ft/sec)	A/M [3.175 mm (1/8 in.) thick] m ² /kg	A/M [6.35 mm (1/4 in.) thick] m ² /kg
0.0001	125 (410)	0.1136	0.1603
0.0005	84 (275)	0.0507	0.0717
0.001	75 (245)	0.0358	0.0507
0.01	55 (180)	0.0113	0.0160

*Table 5B-1 has been adjusted for SI units.

Using Equation (5B-9) and the mass and density mentioned above, A/M becomes 0.0148 m²/kg. The velocity value given above (57.9 m/s) and the calculated value for A/M are plotted on Figure 5B-1 as a downward pointed triangle. This point appears to be a little higher than expected, especially since only slight skin laceration is expected at these velocities instead of 50% penetration.

Custard, et al.,⁽⁶⁾ like Glasstone, specify velocity as a function of mass only for 50% penetration. Making the assumptions that the thickness of the glass can vary from 3.175 mm (1/8 in.) to 6.35 mm (1/4 in.), that the fragments travel edge-on and are square, and that the density of glass is 2471 kg/m³, A/M was calculated from Equation (5B-7). The results are plotted on Figure 5B-1 as diamonds and agree fairly well with the conclusions of Sperrazza and Kokinakis. Thus, for values of A/M up to 0.09 m²/kg and values of M up to 0.015 kg (0.033 lb_m), the functional relationship expressed in Equation (5B-2) and drawn as a solid line in Figure 5B-1 is an adequate representation of 50% probability of skin penetration by a projectile that can result in serious wounds.

Estimates of velocities, presented areas and masses [up to 0.015 kg (0.033 lb_m)] of fragments from a propellant or gas explosion can be acquired from other portions of this document and compared with Figure 5B-1 to determine if penetration is likely. No estimate, however, of the velocity, mass and area of window glass fragments has been made elsewhere in this report. Since wounding from flying glass is a major concern, a method for determining these parameters will be included here. Fletcher, Richmond and Jones^(4,7) conducted blast experiments to obtain information on glass fragments from breaking window panes. From their statistical analysis of the data, they were able to establish functional relationships among several variables. To be able to be used in conjunction with the work of Sperrazza

and Kokinakis,^(1,2) it is necessary to obtain the velocity and area to mass ratio of the glass fragments from the work of Fletcher, et al.^(4,7) After converting their equations to SI units, the geometric mean frontal area A' of fragments become

$$A' = 6.4516 \times 10^{-4} e \left[2.4 - \sqrt{12.5 + (5.8566 \times 10^{-5} P_e)^2} \right] \quad (5B-10)$$

for P_e in range 0 to 96.5 kPa, where P_e is effective peak overpressure in Pascals.

The effective peak overpressure P_e is equivalent to incident peak overpressure P_s for windows oriented side-on or back-on to the approaching blast wave and reflected peak overpressure P_r for windows oriented face-on to the approaching blast wave. This handbook contains methods for determining P_s . For $\bar{P}_s \leq 3.5$ ($\bar{P}_s = P_s/p_0$ where p_0 is atmospheric pressure), $\bar{P}_r = P_r/p_0$ can be determined from

$$\bar{P}_r = 2\bar{P}_s + \frac{(\gamma + 1) \bar{P}_s^2}{(\gamma - 1)\bar{P}_s + 2\gamma} \quad (5B-11)$$

where $\gamma \approx 1.4$.

Atmospheric pressure p_0 can be acquired from Figure 5-3 at sea level and various altitudes above sea level. For $\bar{P}_s > 3.5$, \bar{P}_r can be acquired from Figure 5-4. Effective peak pressure P_e is the

$$P_e = \bar{P}_s p_0 \quad (5B-12)$$

for windows oriented side-on or back-on to the approaching blast wave, or

$$P_e = \bar{P}_r p_0 \quad (5B-13)$$

for windows oriented face-on to the approaching blast wave.

If one assumes that all fragments are square, then mass M can be determined from

$$M = y^2 t \quad (5B-14)$$

where y is the length of a square edge in meters and t is the thickness of the glass in meters.

If all glass fragments travel flat side forward, then

$$A = A' \quad (5B-15)$$

If all glass fragments travel edge forward, then

$$A = t\sqrt{A'} \quad (5B-16)$$

Thus, for these two cases, the ratio A/M is

$$\frac{A}{M} = \frac{1}{t\rho} \quad (5B-17)$$

or

$$\frac{A}{M} = \frac{1}{\rho\sqrt{A'}} \quad (5B-18)$$

Whichever gives the lower value for A/M should be chosen for safety reasons. The geometric mean velocity can be acquired from Fletcher, et al.^(4, 7) After converting their equations to SI units,

$$V = \left[(0.2539) + (1.896 \times 10^{-4}) (t - 7.62 \times 10^{-4})^{-0.928} \right] \\ \times \left[0.3443 P_e^{0.547} \right] \quad (5B-19)$$

for P_e in the range 690 Pa to 689 kPa and $t \geq 7.62 \times 10^{-4}$ m.

A summary of the methods for determining the combinations of parameters which may produce serious penetration damage from fragments less than 0.015 kg (0.033 lb_m) is given here for convenience. To determine whether a fragment can cause severe body penetration damage, it is necessary to determine its striking velocity V (in m/s) and A/M ratio where A is the cross-sectional area of the projectile along its trajectory (in m^2) and M is the mass of the projectile (in kg). These parameters can, in general, be determined from other portions of this handbook. The ballistic limit velocity V_{50} (in m/s) is then

$$V_{50} = 1247.1 \left(\frac{A}{M} \right) + 22.03 \text{ m/s} \quad (5B-20)$$

for $A/M \leq 0.09 \text{ m}^2/\text{kg}$ where A is the cross-sectional area of the fragment along its trajectory in m^2 , M is the mass of the fragment in kg, and

V_{50} is the ballistic limit velocity in m/s. If $V \geq V_{50}$, then one can expect some serious wounds from body penetration.

To determine whether a glass fragment from a window pane broken by the blast wave can cause severe body penetration damage, it is necessary to calculate an effective peak overpressure P_e where

$$P_e = \bar{P}_s P_0 \quad (5B-21)$$

for windows oriented side-on or back-on to the approaching blast wave (P_0 is atmospheric pressure in Pa; see Figure 5-3), or

$$P_e = \bar{P}_r P_0 \quad (5B-22)$$

for windows oriented face-on to the approaching blast wave.

For $\bar{P}_s \leq 3.5$,

$$\bar{P}_r = 2\bar{P}_s + \frac{(\gamma + 1)\bar{P}_s^2}{(\gamma - 1)\bar{P}_s + 2\gamma} \quad (5B-23)$$

where $\gamma \approx 1.4$.

For $\bar{P}_s > 3.5$, \bar{P}_r can be acquired directly from Figure 5-4. The ratio A/M should be chosen as the smaller of

$$\frac{A}{M} = \frac{1}{t\rho} \quad (5B-24)$$

or

$$\frac{A}{M} = \frac{1}{\rho\sqrt{A'}} \quad (5B-25)$$

where t is the thickness of the window pane in meters, ρ is the density of the glass which is approximately 2471 kg/m^3 ,⁽⁴⁾ and A' is the geometric mean frontal area of the glass fragment in m^2 expressed by

$$A' = 6.4516 \times 10^{-4} e \left[2.4 - \sqrt{12.5 + (5.8566 \times 10^{-5} P_e)^2} \right] \quad (5B-26)$$

for P_e in the range 0 Pa to 96.5 kPa.

Striking velocity V (in m/s) is

$$V = \left[(0.2539) + (1.896 \times 10^{-4}) (t - 7.62 \times 10^{-4}) \right]^{-0.928} \\ \times \left[0.3443 P_e^{0.547} \right] \quad (5B-27)$$

for P_e in the range 690 Pa to 689 kPa, and $t > 7.62 \times 10^{-4}$ sec. If $V \geq V_{50}$, then one can expect some serious wounds from body penetration.

5B-2 Nonpenetrating Fragments

Criteria for body damage from nonpenetrating fragments are rather limited. Table 5B-2 contains tentative damage criteria for indirect blast effects involving nonpenetrating objects. It should be noted that the table applies to a fragment of only one mass. One can logically assume that larger masses propelled at the same velocities shown in the table will produce more damage than the 4.54 kg (10 lb) mass presented in the table.

TABLE 5B-2. TENTATIVE CRITERIA FOR INDIRECT BLAST EFFECTS FROM NONPENETRATING FRAGMENTS(9-11)

Mass	Event	Extent of Damage	Impact Velocity
4.54 kg (10 lb)	Cerebral Concussion	Mostly "safe"	3.05 m/s (10 ft/sec)
		Threshold	4.57 m/s (15 ft/sec)
	Skull Fracture	Mostly "safe"	3.05 m/s (10 ft/sec)
		Threshold	4.57 m/s (15 ft/sec)
		Near 100%	7.01 m/s (23 ft/sec)

LIST OF REFERENCES

1. Sperrazza, J., and W. Kokinakis, "Ballistic Limits of Tissue and Clothing," BRL Technical Note No. 1645, Aberdeen Proving Ground, Maryland, January 1967.
2. Kokinakis, William, "A New Methodology for Wounding and Safety Criteria," Proceedings of 16th Explosive Safety Seminar, September 1974, pp. 1209-1226.
3. Glasstone, Samuel, The Effects of Nuclear Weapons, U. S. Government Printing Office, Revised Edition, April 1962.
4. Fletcher, E. R., D. R. Richmond, and R. K. Jones, "Blast Displacement of Prone Dummies," Technical Report to Defense Nuclear Agency. DASA 2710, Lovelace Foundation for Medical Education and Research, June 1971. AD 730-753.
5. White, Clayton S., I. Gerald Bowen, Donald R. Richmond, and Robert L. Corsbie, "Comparative Nuclear Effect of Biomedical Interest," CEX-58.8, Civil Effects Study, U. S. Atomic Energy Commission, January 1961.
6. Custard, G. H., and G. R. Thayer, "Evaluation of Explosive Storage Safety Criteria," Falcon Research and Development Company, Contract DAHC04-69-C-0095, March 1970.
7. Fletcher, E. Royce, Donald R. Richmond, and Robert K. Jones, "Velocities, Masses and Spatial Distribution of Glass Fragments from Windows Broken by Airblast," report in preparation for Defense Nuclear Agency, Washington, D. C.
8. Baker, Wilfred E., Explosions in Air, University of Texas Press, Austin, Texas, May 1973.
9. White, Clayton S., "The Scope of Blast and Shock Biology and Problem Areas in Relating Physical and Biological Parameters," Annals of the New York Academy of Sciences, Vol. 152, Art. 1, October 1968, pp. 89+.
10. Clemedson, Carl-Johan, Gustav Hellström, and Sten Lingren, "The Relative Tolerance of the Head, Thorax, and Abdomen to Blunt Trauma," Annals of the New York Academy of Sciences, Vol. 152, Art. 1, October 1968, pp. 187+.

11. White, Clayton S., "The Nature of Problems Involved in Estimating the Immediate Casualties from Nuclear Explosions," CEX-71.1 Civil Effects Study, U. S. Atomic Energy Commission, July 1971.

CHAPTER VI

RISK ASSESSMENT AND INTEGRATED EFFECTS

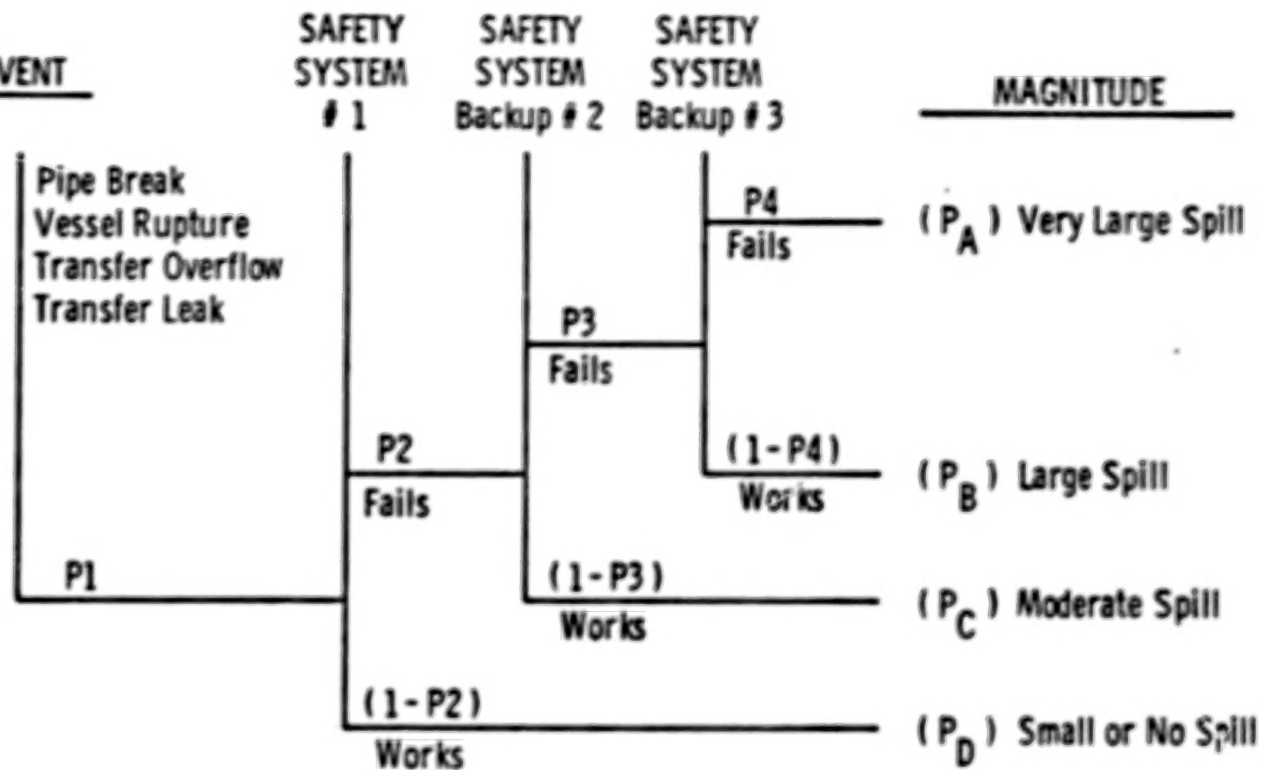
6-1 Risk Assessment

A systematic, effective approach is required to identify the type, magnitude, and probability of occurrence of undesired events in the operation of any given system. Certain well-known related techniques have been used in industry (chemical, aerospace, nuclear and defense) to accomplish this result. These systems analyses are alternately referred to as "Hazard Analysis," "Safety Analysis," "Risk Assessment" and "Reliability Analysis."

Three basic related systematic methods are employed, either singly or in combination, to accomplish these types of analyses. These methods are:

- (1) Event Tree - Starts with an event that initiates a possible accident and develops the possible consequences of the event by considering the response of engineered safety systems that would be called upon as a result of the initial event.
- (2) Fault Tree Provides a method for determining the probabilities needed for the event trees. Fault trees employ a logic almost the reverse of event trees in that they start with an undesired event and identify the ways it may have been caused.
- (3) FMECA The Failure Mode Effects and Criticality Analysis is a systematic procedure for identifying each failure mode of the system and for evaluating the consequences. The FMECA starts with the components of the system, works up through the subsystem to the system level, and identifies the effects of each failure mode on the system operation.

An example of a simple event tree is shown in Figure 6-1 and a simple fault tree in Figure 6-2 for a chemical spill in a storage transfer system. Given an outcome from the event tree, a spill magnitude is defined. For each spill magnitude, a hazard or risk assessment can be made. From the fault tree, the probabilities of failure are determined to assign to each branch of the event tree. Then, the probability (or expected frequency) of occurrence



P = PROBABILITY OF FAILURE

Figure 6-1. Typical Event Tree

459

TABLE OF CONTENTS

	<u>Page</u>
INTRODUCTION	1 1/A12
I. ESTIMATES OF EXPLOSIVE YIELD	8 1/B5
1-1 Explosive Yield as a Function of Propellant Type and Accident Conditions	8 1/B5
1-2 Explosive Yield as a Function of Fluid Type and Initial Conditions for Gas Vessel Bursts	26 1/C9
List of References	29 1/C12
II. CHARACTERISTICS OF PRESSURE WAVES	31 1/C14
2-1 General	31 1/C14
2-2 Pressure Waves from Propellant Explosions	40 1/D9
2-3 Pressure Waves from Gas Vessel Bursts	56 1/E11
List of References	68 1/F9
II. A GAS VESSEL BURST	70 1/F11
2A-1 Nondimensional Parameters	70 1/F11
2A-2 Source of Data	70 1/F11
2A-3 Overpressure Calculation	71 1/F12
2A-4 Impulse Calculation	74 1/G1
2A-5 Effect of Cylindrical Geometry	74 1/G1
2A-6 Effect of Reflecting Surface (Burst at Ground Level)	74 1/G1
List of References	78 1/G5
Symbols	79 1/G6

TABLE OF CONTENTS (Cont'd)

		<u>Page</u>
III.	EFFECTS OF PRESSURE WAVES	80 1/G7
3-1	Damage Estimates to Structures	80 1/G7
3-2	Injury Estimates to Humans	99 2/B3
	List of References	125 2/D1
III.A	STRUCTURAL RESPONSE	128 2/D4
3A-1	Overturning Analysis	128 2/D4
3A-2	Development of Beam Equations	134 2/D10
3A-3	Development of Plate Equations	142 2/E4
3A-4	Development of Membrane Equations	153 2/F1
	List of References	158 2/F6
III.B	PRESSURE/IMPULSE COMBINATIONS PRODUCING LUNG DAMAGE	159 2/F7
	List of References	169 2/G3
III.C	PRESSURE/IMPULSE COMBINATIONS PRODUCING LOSS OF HEARING	171 2/G5
	List of References	175 2/G9
III.D	PRESSURE/IMPULSE COMBINATIONS PRODUCING WHOLE-BODY DISPLACEMENT AND SUBSEQUENT DAMAGE TO THE HEAD AND BODY	176 2/G10
	List of References	190 3/B1
IV.	CHARACTERISTICS OF FRAGMENTS	191 3/B2
4-1	General	191 3/B2
4-2	Methods for Estimating Fragment Initial Velocities for Spheres and Cylinders Bursting into Many Fragments	191 3/B2

TABLE OF CONTENTS (Cont'd)

	<u>Page</u>
4-3 Estimate of Initial Velocities of Fragments from Spheres and Cylinders Bursting into Two Equal Halves	218 3/D1
4-4 Determination of Appurtenance Velocity	228 3/D11
4-5 Methods for Computing Fragment Ranges and Impact Conditions	240 3/E9
4-6 Fragment Mass Distribution	279 4/A11
4-7 Probability of Fragment Arrival Versus Range	286 4/B4
List of References	292 4/B10
IV.A METHODS FOR ESTIMATING FRAGMENT INITIAL VELOCITIES	293 4/B11
List of References	315 4/D5
IV.B COMPARISON OF EXPERIMENTAL RESULTS WITH CODE PREDICTIONS	316 4/D6
List of References	318 4/D8
IV.C ESTIMATE OF INITIAL VELOCITIES OF FRAGMENTS FROM SPHERES AND CYLINDERS BURSTING INTO TWO EQUAL HALVES	319 4/D9
List of References	354 4/G2
IV.D ESTIMATION OF VELOCITIES ATTAINED BY APPURTEANCES SUBJECTED TO BLAST LOADING	355 4/G3
List of References	377 5/B2
IV.E ANALYSES FOR FRAGMENT TRAJECTORIES	378 5/B3
List of References	401 5/C12

TABLE OF CONTENTS (Cont'd)

	<u>Page</u>
IV. F STATISTICAL FITTING TO FRAGMENT DATA	402 5/C13
4F-1 Derivation of Figures 4-46 Through 4-49	402 5/C13
4F-2 Derivation of Figure 4-50	402 5/C13
4F-3 Rationale for Averaging Fragment Mass Distribution for Events 3, 4, and 5	403 5/C14
4F-4 Fragment Mass Distributions for Gas Vessel Bursts	406 5/D3
4F-5 Rationale for Averaging Fragment Mass Distributions for Tanks A and B and Tanks D and E	412 5/D9
4F-6 Derivation of Figure 4-57, Fragment Distance Versus Percent Yield for Propellant Explosions	413 5/D10
4F-7 Derivation of Simulated Fragment Range Distribution for Gas Vessel Bursts	415 5/D12
4F-8 Rationale for Combining Simulated Range Distribution for Tanks A and B and for Tanks D and E	423 5/E6
List of References	424 5/E7
V. EFFECTS OF FRAGMENTS	425 5/E8
5-1 Damage Estimates to Structures and Facilities	425 5/E8
5-2 Damage Estimates to People from Secondary Fragments	433 5/F2
List of References	442 5/F11
V.A EFFECTS OF FRAGMENTS ON STRUCTURES	444 5/F13
List of References	446 5/G1

TABLE OF CONTENTS (Concl'd)

		<u>Page</u>
V. B	DAMAGE ESTIMATES TO PEOPLE FROM SECONDARY FRAGMENTS	447 5/G2
	5B-1 Penetrating Fragments	447 5/G2
	5B-2 Nonpenetrating Fragments	455 5/G10
	List of References	456 5/G11
VI.	RISK ASSESSMENT AND INTEGRATED EFFECTS	458 5/G13
	6-1 Risk Assessment	458 5/G13
	6-2 Prediction of Relative Blast and Fragment Effects	461 6/A7
	List of References	507 6/D11
VII.	DISCUSSION OF RESULTS	508 6/D12
VIII.	CONCLUSIONS	511 6/E1
IX.	RECOMMENDATIONS	513 6/E3
LIST OF SYMBOLS		516 6/E6
CONVERSION FACTORS		523 6/E13
GLOSSARY OF TERMS		525 6/F1
BIBLIOGRAPHY		528 6/F4

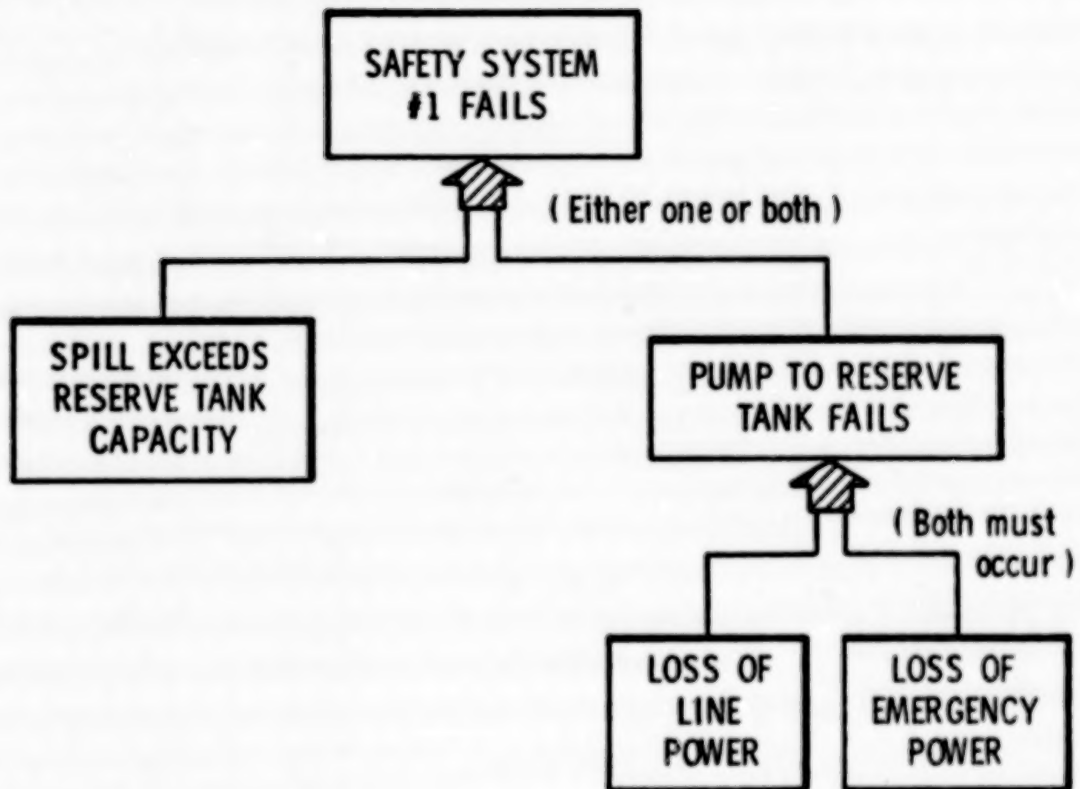


Figure 6-2. Typical Fault-Tree Diagram; Combining of Failure Probabilities

is determined by the proper algebraic combination of the branch probabilities leading to the outcome.

Examples of these types of analyses can be found in references 1, 2, 3, 4, and 5.

For gas vessel or propellant systems, the figures and methods described in Chapters I through V can be used to assess the possible effects of any given undesired event based on the characteristics of fragments (mass initial velocity, and range) or blast phenomena.

The workbook does not give methods for estimating probabilities of catastrophic events occurring, nor does it employ the methods of risk assessment just discussed. It does, however, allow prediction of severity of certain classes of accidental explosion, as well as effects, under the assumption that an explosion does occur.

6-2 Prediction of Relative Blast and Fragment Effects

In Chapters II through IV, we give a number of examples of specific calculations for use of graphs, tables or simple equations each of which provides an estimate of some aspect of explosion hazards or their effects. But here we give a series of more complete examples. Each example represents a possible accident which can occur at aerospace launch or test facilities. Our assessment, as is true for all such estimates which can be made from this workbook, starts with the assumption that an accident has occurred and does not consider the probability of occurrence. Five different accident "scenarios" are presented, and estimates of blast and fragmentation effects are made for each scenario. The quantities of propellant, volumes and types of compressed gases, masses of vehicle structure, etc., are often approximate, but they are realistic values. The problems are intended to illustrate the way in which the data in Chapters II through IV can be used to estimate relative blast and fragment characteristics, for some "typical" accidents.

6-2.1 Scenario #1. Fall-back of Space Shuttle during launch.

The scenario for this accident is a failure of thrust just after lift-off of the space shuttle. This multi-stage vehicle is a large, winged orbiter and landing vehicle similar in configuration to a large aircraft, which is boosted by the solid propellant rocket engines and a liquid-fueled engine. At lift-off, all three engines are firing and delivering thrust. The vehicle is assumed to rise at most a few meters, and then to fall back onto the launch pad with sufficient impact velocity to rupture the liquid rocket tankage. The propellants mix on the ground surface and reach an ignition source after some time delay.

Data for types and amounts of propellant in the Space Shuttle at lift-off, flow rates, and estimates of structural weight are given in Table 6-1. Because this accident occurs immediately after lift-off, all propellant weights are (conservatively) assumed to be the same as at lift-off. Assuming fall-back under gravity from a height of 10 meters (33 ft), the impact velocity is $U_i = 14.0 \text{ m/s}$ (45.9 ft/sec).

The propellants in the solid propellant boosters are assumed not to be explosive. This assumption seems well founded, based on the extensive testing of detonability of solid propellants in Project SOPHY. Furthermore, the quantities of liquid propellants listed for the first four subsystems in Table 6-1 are relatively small, and the type of accident postulated would be unlikely to rupture tanks containing these propellants. So, we assume for this example problem that only the external tank ruptures and spills its propellants in a CBGS type of accident. For estimating fragmentation effects, we also use only the structural mass of the damaged external tankage.

A number of other hazards are obviously associated with this type of accident, but some are not calculable from methods given in this workbook. In particular, the trajectories and impact effects of the propulsive solid propellant boosters, which are burning and thrusting when fall-back occurs, cannot be estimated. Presumably, the orbiter with its human payload can escape by igniting escape rockets in the event of fall-back. If we can estimate its flight location when explosion occurs, some predictions of blast effects can possibly be made. But, we have too little data in hand at present to make this estimate.

6-2.1.1 Yield

The yield is calculated by the methods in Chapter I. According to Table 1-2, Equation 1-2 and Figure 1-7 are used to determine a value for the yield, which is compared with a value obtained from Figure 1-1. The smaller value is used:

$$\begin{aligned} \text{Equation 1-2: } Y_m &= 10\% + \frac{4.43\%}{(\text{m/s})} U_i \quad (0 < U_i < 24.4 \text{ m/s}) \\ &= 10\% + \frac{4.43\% (14.0 \text{ m/s})}{(\text{m/s})} = 72.0\% \end{aligned}$$

In Figure 1-7, choose t_{ignition} for maximum Y : $t_{\text{ignition}} = 0.6 \text{ sec.}$

TABLE 6-1. ON-BOARD PROPELLANT WEIGHTS FOR SPACE SHUTTLE AT LIFT-OFF

Subsystem	Propellant Type	Quantity (kg) (lbm)		Flow Rate (kg/s) (lbm/s)		Structural Mass (kg) (lbm)	
Aux. Power Units (APO)	Hydrozene	281	618	0.04	0.09	--	--
Orbital Maneuvering (OMS)	MMH N_2O_4	4 260 7 010	9370 15,400	3.29 5.42	7.24 11.9	--	--
Reaction Control (RCS)	MMH N_2O_4	1 270 2 030	2790 4470	0.523 0.841	1.15 1.85	--	--
Power Reactant Storage System (fuel cells)	LH_2 Max. mission LO_2 30 day	83.6 502 710 4 260	184 1100 1560 9370	0.000221 -- 0.00176 --	0.000486 -- 0.00387 --	--	--
External Tank	LH_2 LO_2	103 000 608 000	227,000 1,340,000	909 5 450	2000 12,000	--	--
Environmental Control System	NH_3	46.4	102	--	--	--	--
Solid Propellants	--	1 006 000	2,210,000	4 020	8840	251 000	552,000

463

Then

$$\frac{Y + 100}{Y_m} = 62. \quad Y = \frac{62 Y_m}{100} = \frac{(62)(72\%)}{100} = 44.6\%$$

From Figure 1-1 (using a total propellant and oxidizer mass of 711000 kg), $y = 0.06$. The multiplier is 370%. $Y = (0.06)(370\%) = 22.2\%$. Choose the lower value of Y which is 22.2%.

6-2.1.2 Overpressure and Specific Impulse

The overpressure and specific impulse are calculated by the methods in Chapter II. The effective mass is calculated from Equation 2-9: $W = W_T X \frac{Y}{100}$. Table 2-1 gives the procedure for finding the overpressure and specific impulse as functions of distance:

$$W = W_T X \frac{Y}{100} = (711000 \text{ kg}) \frac{22.2\%}{100} = 158000 \text{ kg (348,000 lb}_m)$$

According to Table 2-1, the overpressure is read from Figure 2-16, and the specific impulse is read from Figure 2-17.

The following (Table 6-2) is a list of overpressures (P_o) and specific impulses (I_s) from Figures 2-16 and 2-17. The solid lines in these figures were used. The other terms in Table 6-2 will be explained later.

6-2.1.3 Effect of Blast Waves on Structures.

The methods described in Section 3-1 are used to determine the effects of blast waves on structures.

Glass Breakage

Equation 3-1 relates overpressure for glass breakage to the properties of the glass pane.

$$\left[\frac{P_o X^2}{\sigma_y h^2} \right] = \frac{1.0 + 3.08 \left(\frac{X}{Y} \right)^2 + \left(\frac{X}{Y} \right)^4}{8.68 \left[0.79 + 0.11 \left(\frac{X}{Y} \right)^2 + 0.79 \left(\frac{X}{Y} \right)^4 \right]^{1/2}} \quad (3-1)$$

TABLE 6-2. OVERPRESSURES AND IMPULSES

R (m)	$\frac{R}{W^{1/3}}$	P_s (Pa)	\bar{P}_s	I_s (Pa· s)	$\frac{I_s}{W^{1/3}}$ (Pa· s/kg $^{1/3}$)	$\frac{I_s}{m^{1/3}}$ (Pa· s/kg $^{1/3}$)	$\frac{I_s}{P_0^{1/2} m^{1/3}}$ (Pa $^{1/2}$ · s/kg $^{1/3}$)
32.4	0.6	1.400×10^6	13.8	2.09×10^4	386	1.22×10^4	38.4
54.1	1.0	5.60×10^5	5.53	1.29×10^4	238	7.54×10^3	23.7
108	2.0	1.52×10^5	1.50	7.03×10^3	130	4.11×10^3	12.9
216	4.0	4.71×10^4	0.465	3.82×10^3	70.6	2.23×10^3	7.02
541	10.0	1.31×10^4	0.129	1.71×10^3	31.6	1.00×10^3	3.14
1080	20.0	5.22×10^3	0.0515	9.24×10^2	17.1	5.40×10^2	1.70

(ft = m X 3.281)

(psi = Pa X 1.450×10^{-4})(psi-sec = Pa · s X 1.450×10^{-4})

465

$P_r = 2P_s$ for a blast wave striking a window head-on.

$P_r = P_s$ for a blast wave traveling parallel to the surface of the glass.

It can be shown that P_r increases as $\frac{X}{Y}$ increases. For the lowest P_r to break any kind of glass that is likely to be found, choose $\frac{X}{Y} = 0.20$, and $X = 0.300$ m (0.98 ft). Then, $P_s = 2420$ Pa (0.351 psi) for glass breakage with the glass surface perpendicular to the direction of travel of the blast wave. $P_s = 4840$ Pa (0.702 psi) for glass breakage with the direction of propagation of the blast wave parallel to the surface of the window.

Looking at the data in Table 6-2, it can be seen that, for no glass breakage with windows facing the source of the blast wave, the distance must be much greater than 1080 m (3500 ft). (By extrapolating curve #1, the i_s vs P_s curve in the next Figure, Figure 6-3, it appears that the distance for an overpressure of 2420 Pa is near 2000 m (6000 ft).) With the glass surface parallel to the direction of travel of the blast wave, the distance for no glass breakage must be about 1100 m (3600 ft.).

Building Damage

The degree of building damage as a function of distance from the source of the blast wave can be observed in Figure 6-3. Figure 6-3 is a copy of Figure 3-2, with the (impulse, overpressure, points for selected distances R . The (i_s , P_s) paths for four of the scenarios to be discussed in this chapter are included in this figure. The paths cross the limit of damage lines. By finding the values of R at which they cross one knows the minimum distance at which a given degree of safety exists. One can interpolate between two adjacent values of R by assuming a logarithmic scale for R on Figure 6-3. Alternatively, one can determine the overpressure or impulse at the point of the intersection of the (i_s , P_s) path and the damage limit curve, and then go back to the figure in the text where the overpressure or impulse was obtained and find the corresponding distance. The resulting building damage for this scenario (#1) is presented in Table 6-3.

Overturning of Objects

One can use the methods of Section 3-1.3 to determine the minimum distance from this explosion at which a Saturn V rocket may be placed, for which it will not be overturned by the blast wave. Assume that the fueled Saturn V is standing vertically without restraints. Assume standard atmospheric temperature and pressure. Let $h = 110$ m (360 ft), $h_{cg} = 30$ m (100 ft), $b = 10.1$ m (33 ft), $H = 10.1$ m (33 ft), $h_{bl} = h/2 = 55$ m (180 ft), $m = 2.8 \times 10^6$

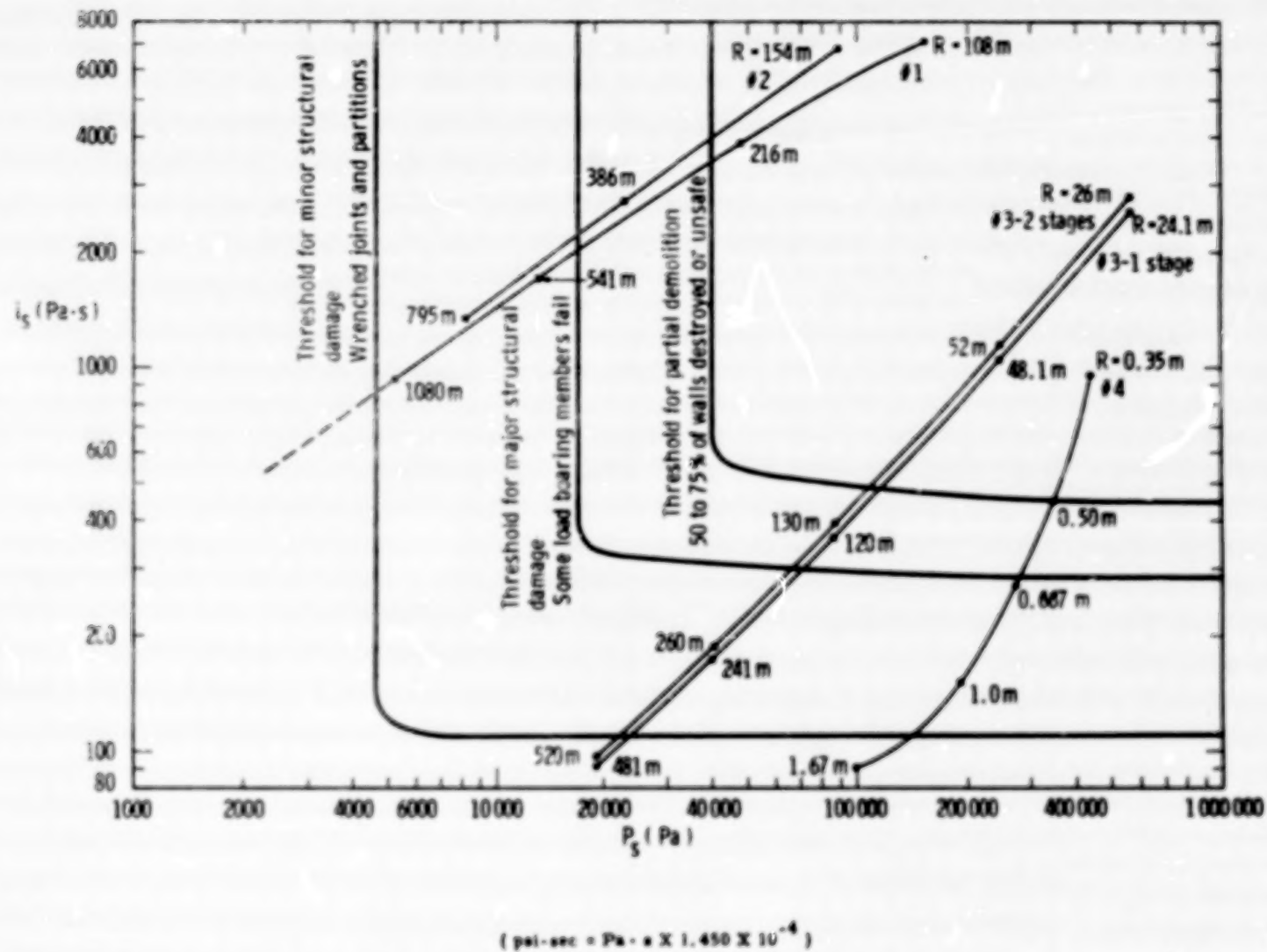


Figure 6-3. Pressure Vs Impulse Diagram for Building Damage with Blast Curves for Scenarios 1 Through 4

4607

TABLE 6-3. BUILDING DAMAGE

Degree of Damage	Distance (m)	Distance (ft)
threshold of minor structural damage	1200	3900
threshold of major structural damage (some load-bearing members fail)	470	1500
threshold of partial demolition	270	890

$kg (6.2 \times 10^6 lb_m)$, and $C_D = 1.2$. Then, $A = 1100 m^2 (12000 ft^2)$, $h/b = 10.9$, and $h_{cg}/h = 0.273$. The procedure is to find the minimum impulse i_0 for overturning. Setting this equal to the applied impulse i_t allows one to find the maximum distance for which the vehicle will overturn. For all larger distances, the vehicle will not overturn.

h/b is too large for Figure 3-4, so use Equation 3-4.

$$\frac{i_0 Ah_{bt}}{mg^{1/2} b^{3/2}} = -\sqrt{\left[\frac{2}{3} + \frac{h^2}{6b^2} + \frac{2h^2}{b^2} \left(\frac{h_{cg}^2}{h^2} \right) \right] \left[-\sqrt{\frac{1}{4} + \left(\frac{h^2}{b^2} \right) \left(\frac{h_{cg}^2}{h^2} \right)} - \left(\frac{h}{b} \right) \left(\frac{h_{cg}}{h} \right) \right]}$$

$$= 1.25. \text{ Then } i_0 = 5810 \text{ Pa} \cdot \text{s. (.843 psi - sec)}$$

Let $i_t = 5810 \text{ Pa} \cdot \text{s.}$ Then $a_0 i_t / p_0 H = 1.77.$ This is the minimum nondimensional applied impulse for overturning which is shown on Figure 6-4, a copy of Figure 3-3. The points $(a_0 C_D i_t / p_0 H, P_g)$ were plotted on Figure 6-4 for several values of $R.$ The place where this curve (curve #1) crosses the line of minimum applied impulse for overturning gives the value of R for the "threshold" of overturning. For Scenario #1, this distance is 160 m (520 ft). At distances greater than 160 m (520 ft), a Saturn V will not be overturned by a blast wave from this explosion.

6-2.1.4 Effect of Blast Waves on Humans

468 The methods described in Section 3-2 are used to determine the effects of blast waves on humans.

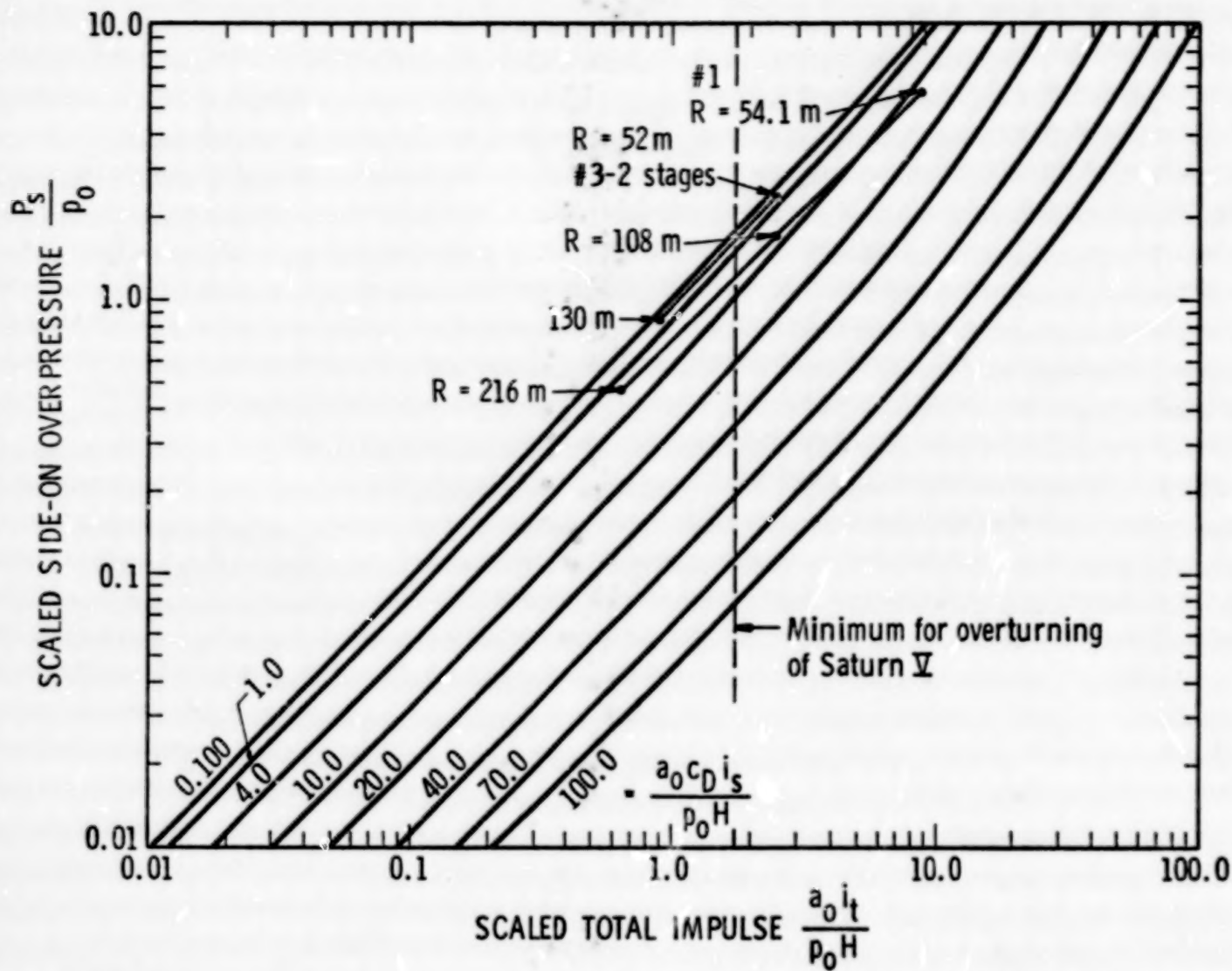


Figure 6-4. Specific Impulse Imparted to a Target Which Might Overturn with Curves for Scenarios 1 and 3

Lung Damage

Figure 3-10 in Section 3-2 is used to determine the extent of damage to the lungs of humans by blast waves. Figure 6-5 is a copy of Figure 3-10 with the $(\bar{P}_s, \frac{I_s}{p_0^{1/2} m^{1/3}})$ points for selected values of R [$p_0 = 1.013 \times 10^5 \text{ Pa}$ (14.7 psi)]. The value of m is chosen as 5.00 kg (11 lb_m). The same procedure as the one that was used for building damage is also used here to determine the values of R for various degrees of lung damage. The results are presented in Table 6-4.

TABLE 6-4. LUNG DAMAGE

Chance of Survival	Distance (m)	Distance (ft)
threshold of lung damage	170	560
99%	100	330
90%	100	330
50%	90	300
10%	70	230
1%	70	230

Ear Damage

Figure 3-11 is used to determine the extent of damage to the ears of humans by blast waves. Figure 6-6 is a copy of Figure 3-11 in Section 3-2 with the (P_s, I_s) points for selected values of R . Table 6-5 shows the results. Note that a value of R cannot be determined for TTS because the curve for Scenario #1 never reaches the TTS damage limit curve, and it is inadvisable to try to extrapolate this curve.

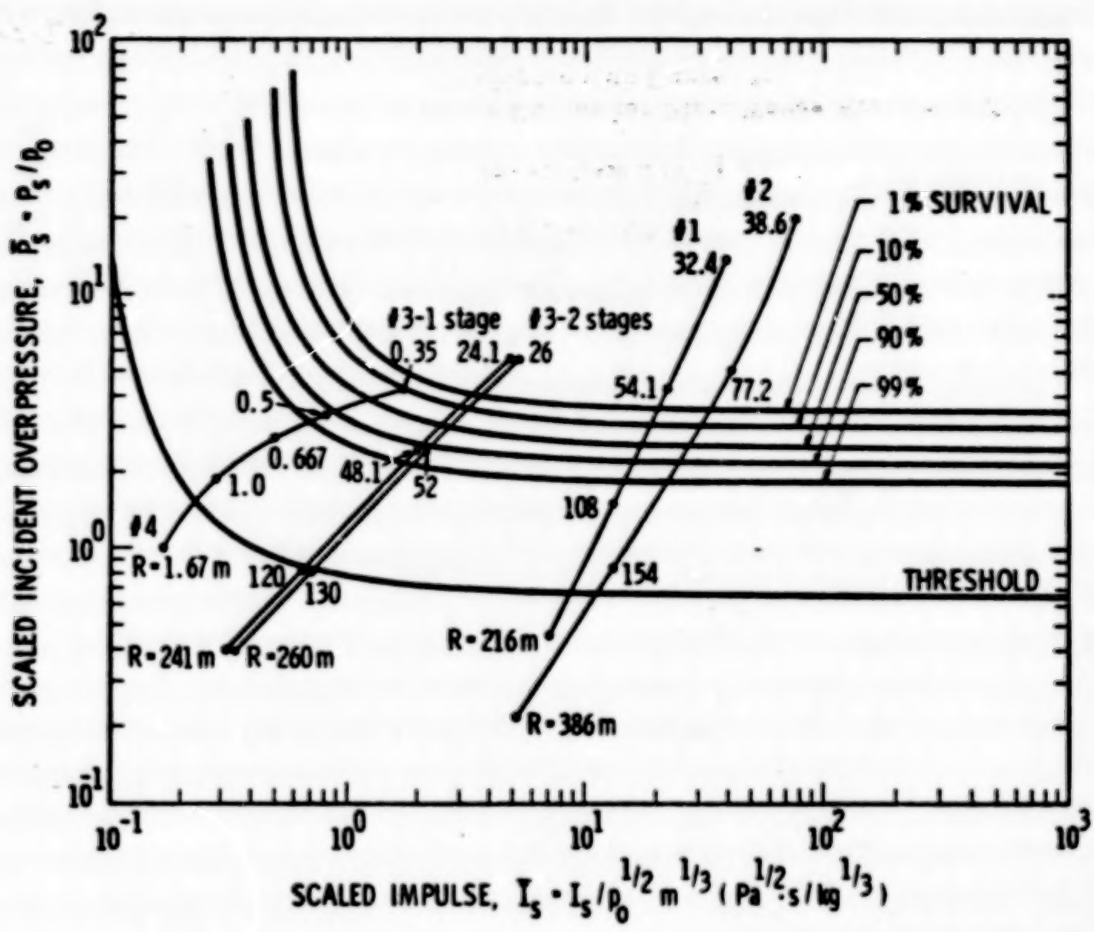
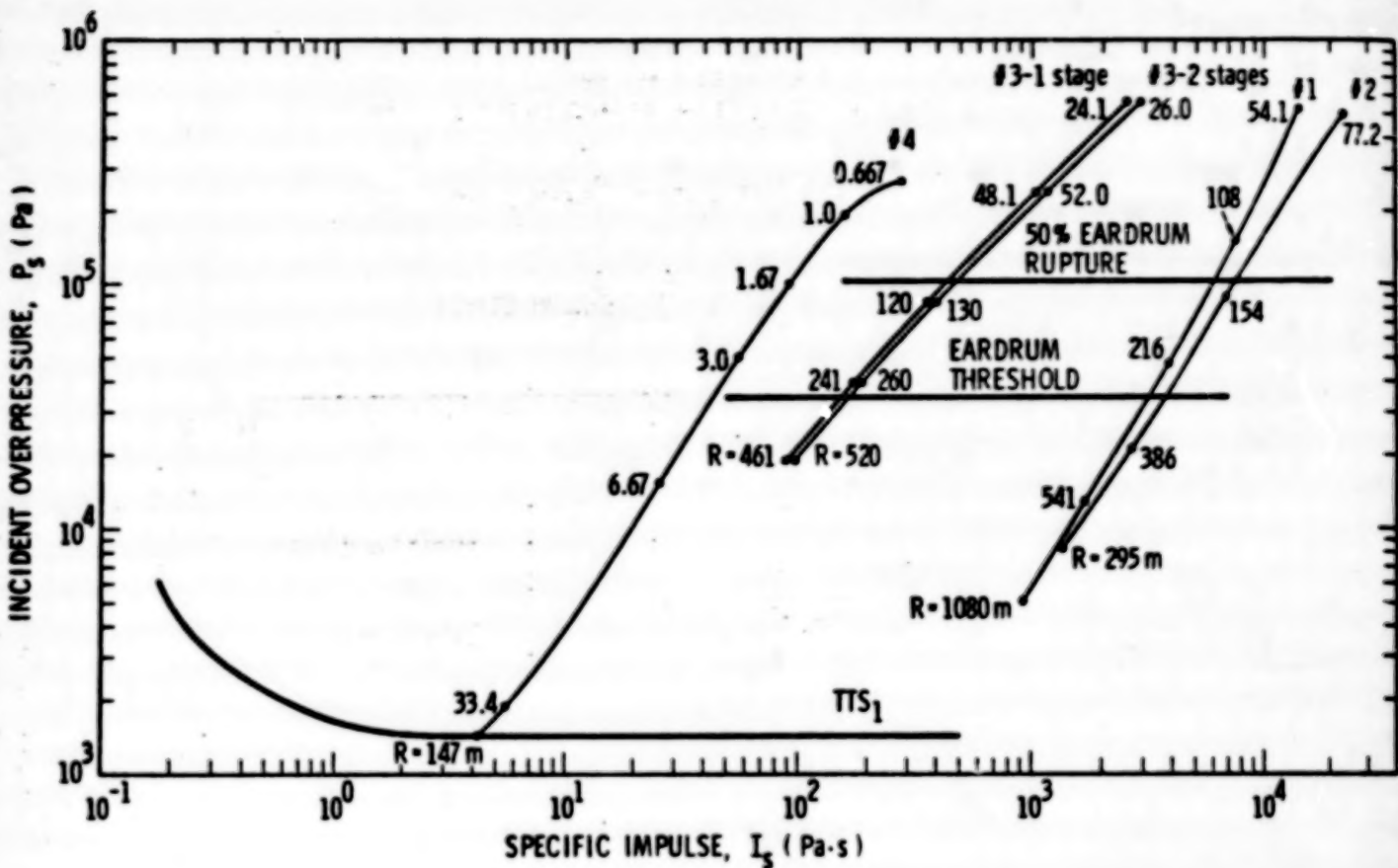


Figure 6-5. Survival Curves for Lung Damage with Curves for Scenarios 1 Through 4



$$(\text{psi} = \text{Pa} \times 1.450 \times 10^{-4})$$

$$(\text{psi-sec} = \text{Pa} \cdot \text{s} \times 1.450 \times 10^{-4})$$

Figure 6-6. Human Ear Damage Curves for Blast Waves Arriving at Normal Angle of Incidence with Curves for Scenarios 1 Through 4

472

TABLE 6-5. EAR DAMAGE

Degree of Damage		Distance (m)	Distance (ft)
temporary threshold shift (TTS) (90%-no loss)		over 2000	over 6000
threshold of eardrum rupture		270	890
50% eardrum rupture		130	430

Skull Fracture

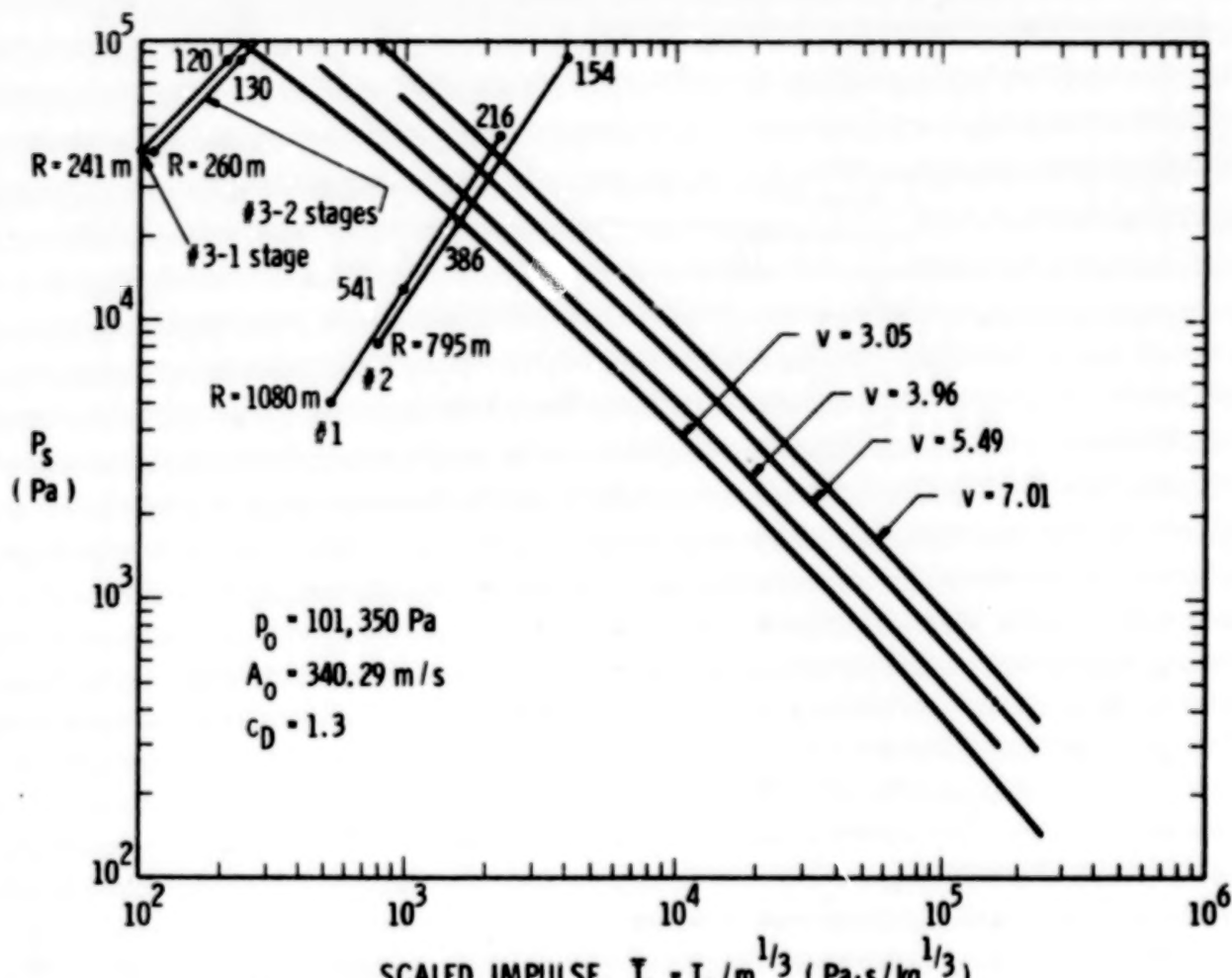
Figure 3-12 is used to determine the chance of Skull Fracture due to bodily translation and impact caused by blast waves. Figure 6-7 is a copy of Figure 3-12 with the $(P_s, \frac{I_s}{m^{1/3}})$ points for selected values of R. The body mass, m, is chosen as 5.00 kg (11 lb_m). The results are presented in Table 6-6.

TABLE 6-6. SKULL FRACTURE

Chance of Skull Fracture		Distance (m)	Distance (ft)
mostly safe		350	1100
threshold		310	1000
50%		270	890
near 100%		240	790

Body Translation and Impact

Figure 3-16 is used to determine the probability of mortality from whole body translation and impact upon a hard surface caused by blast waves. Figure 6-8 is a copy of that figure with the $(P_s, \frac{I_s}{m^{1/3}})$ points for selected values of R. The body mass m is chosen as 5.00 kg. Table 6-7 shows the results. Note that no value of distance is given for "near 100% mortality" because it is inadvisable to extrapolate the curves in Figure 6-8.



$$(\text{psi} = \text{Pa} \times 1.450 \times 10^{-4})$$

$$(\text{psi-sec/lb}_m^{1/3} = \text{Pa} \cdot \text{s}/\text{kg}^{1/3} \times 1.114 \times 10^{-4})$$

Figure 6-7. Skull Fracture, 0 m Altitude, with Curves for Scenarios 1, 2, and 3

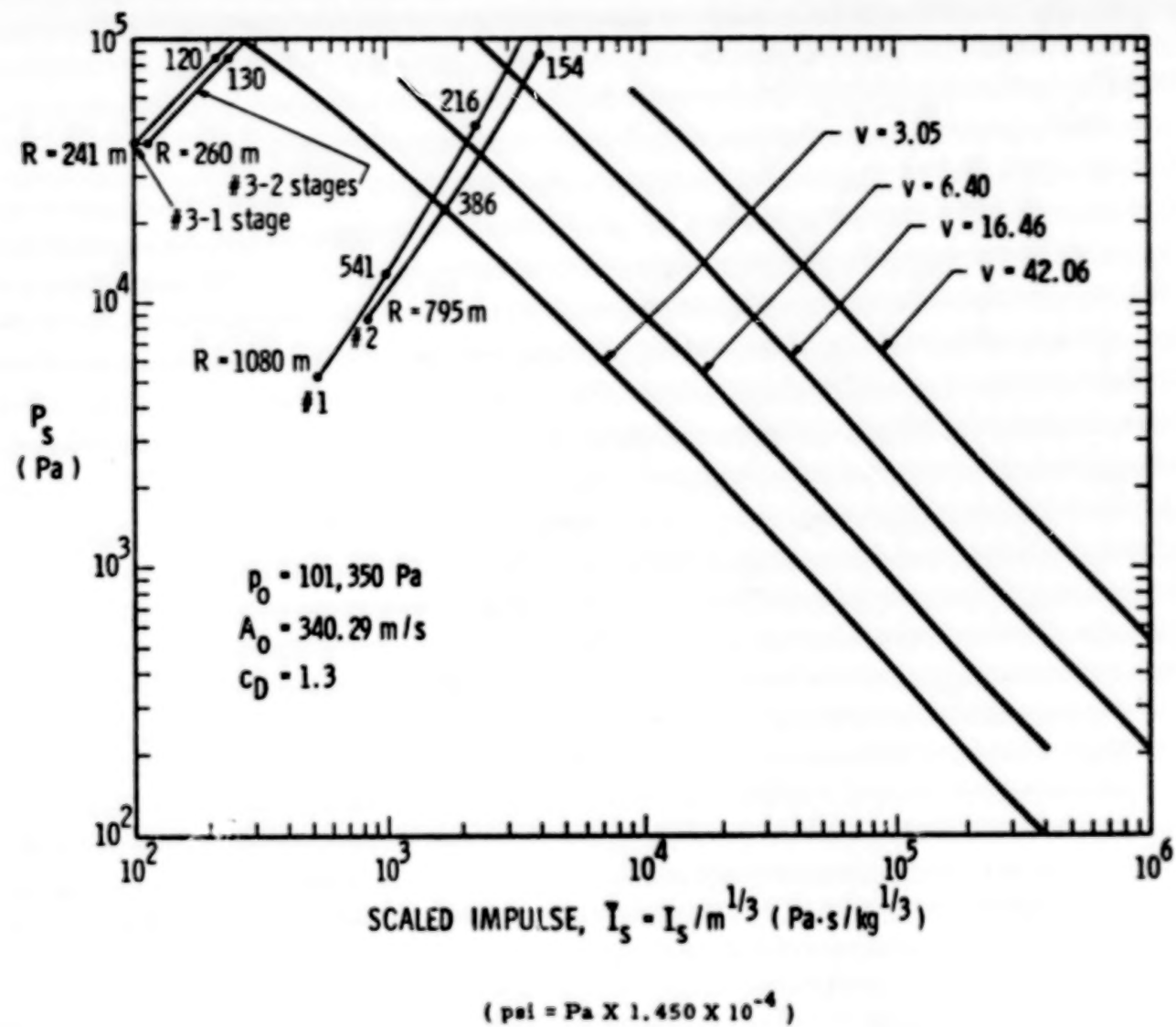


Figure 6-8. Lethality from Whole Body Translation, 0 m Altitude, with Curves for Scenarios 1, 2, and 3

TABLE 6-7. MORTALITY FROM BODY IMPACT

Degree of Mortality	Distance (m)	Distance (ft)
mostly safe	340	1100
threshold of lethality	240	790
50% mortality	160	520

6-2.1.5 Fragment Characteristics

The initial fragment velocity distribution is obtained from Figure 4-48. 95% of the fragments have an initial velocity less than or equal to 500 m/s (1600 ft/sec).

The fragment mass distribution is obtained from Figure 4-53. 95% of the fragments have a mass less than or equal to 120 kg (264 lb_m).

The fragment range is obtained from Figure 4-57. 95% of the fragments will strike the ground at a distance less than or equal to 580 m (1900 ft).

6-2.1.6 Appurtenances

As an example of an appurtenance, a cement block identical to that described in Example 1 of Section 4-4 will be used. Suppose that it is located at a distance of 108 m (350 ft) from the source of the blast wave, and one must know its velocity after being picked up by the blast wave.

At $R = 108 \text{ m}$, $P_o = 1.52 \times 10^5 \text{ Pa}$, $\bar{P}_s = 1.50$, and $I_s = 7.03 \times 10^3 \text{ Pa} \cdot \text{s}$. The nondimensional impulse is

$$\bar{I}_s = \frac{C_D I_s a_0}{P_s (K \dot{H} + X)} = \frac{1.05(7.03 \times 10^3)(340)}{1.52 \times 10^5 [4(2.5) + 0]} = 1.65 .$$

Locating the (\bar{P}_s, \bar{I}_s) point on Figure 4-26, one finds that $\bar{V} \approx 3.5$. Then,

$$V = \frac{\bar{V} P_o A (K \dot{H} + X)}{M a_0} = \frac{(3.5)(1.013 \times 10^5)(6.25)[4(2.5) + 0]}{(2.8 \times 10^4)(340)}$$

This cement block would be thrown at a very low velocity.

6-2.1.7 Effect of Fragments on Humans

The effect on humans of flying glass from windows broken by blast waves will be considered. In Example 1 of Section 5-2, the 50% penetration limit velocity V_{50} for typical glass was found to be 157 m/s (515 ft/sec). Equation 5-8 relates striking velocity V to overpressure P_e , which may be P_s or P_r , depending upon the orientation of the glass with the blast wave.

$$V = \left[0.2539 + (1.896 \times 10^{-4}) (t - 7.62 \times 10^{-4})^{-0.928} \right] \left[0.3443 P_e^{0.547} \right] \quad (5-8)$$

Setting $V = V_{50}$, one can solve for the minimum P_e for human injury from flying glass. Letting $t = 3.175 \times 10^{-3}$ m, $P_e = 6.37 \times 10^5$ Pa (92.4 psi).

For windows where the direction of propagation of the blast wave is parallel to the glass surface, $P_e = P_s$. Then $P_s = 6.37 \times 10^5$ Pa. From Figure 2-16, $R = 50$ m (164 ft). At any distance s less than 50 m, there is likelihood of human injury by flying glass from windows with surfaces parallel to the direction of propagation of the blast wave.

For windows where the direction of propagation of the blast wave is normal to the glass surface, $P_e = P_r$. Solving 5-4 for P_s and manipulating gives $P_s = 1.94 \times 10^5$ Pa (28.1 psi). From Figure 2-16, $R = 97.3$ m (319 ft). Tables 6-8 and 6-9 summarize the damage and injury that can be expected.

6-2.2 Scenario #2. Explosion of Space Shuttle Propellant Tanks in Early Stages of Flight

In this "scenario", the Space Shuttle has lifted off from the pad and started its ascent. A failure occurs in the tankage for the main liquid propellant rocket engine, causing the LH_2 and LO_2 to mix and ignite within the tanks (CBM). The explosion occurs at about 1000 m (3280 ft) altitude, where ground reflections do not affect the blast wave properties. This altitude is not great enough, however, to affect blast wave characteristics other than by lack of ground reflection. The initial quantities of propellants at lift-off are given in Table 6-1. Assuming 30 seconds of propellant consumption, remaining weights are:

External Tank - LH_2 , 75 700 kg (167,000 lb_m)

LO_2 , 444 000 kg (977,000 lb_m)

Solid Propellants - 885 000 kg (1,950,000 lb_m)

TABLE 6-8 SCENARIO 1: DAMAGE TO STRUCTURES

Damage to Structures	Distance (m)	Distance (ft)
threshold of overturning Saturn V	160	520
threshold of partial demolition	270	890
threshold of major structural damage	470	1500
95% of fragments will strike the ground within this distance	580	1900
threshold of side-on glass breakage	1100	3600
threshold of minor structural damage	1200	3900
threshold of face-on glass breakage	2000	6000

TABLE 6-9 SCENARIO 1: HUMAN INJURY

Human Injury	Distance (m)	Distance (ft)
1%-10% survival (lung damage)	70	230
50% survival (lung damage)	90	300
90-99% survival (lung damage)	100	330
50% eardrum rupture	130	430
50% mortality from body impact	160	520
threshold of lung damage	170	560
near 100% chance of skull fracture		
threshold of lethality from body impact	240	790

TABLE 6-9 SCENARIO 1: HUMAN INJURY (CONCLUDED)

Human Injury		Distance (m)	Distance (ft)
threshold of eardrum rupture 50% chance of skull fracture		270	890
threshold of skull fracture		310	1000
mostly safe from body impact injury, mostly safe from skull fracture		350	1100
threshold of injury from flying glass (side-on)		50	164
threshold of injury from flying glass (face-on)		97	319
temporary threshold shift (hearing)	over 2000	over 6000	

In this type of accident, we can estimate explosive yield and blast effects, as well as initial velocities of fragments, making the same restrictive assumptions as for Scenario #1. But, fragment trajectories and impact conditions cannot be estimated, because all of the graphs in Chapter IV relating to these properties of fragments are based on explosions which occur on the ground surface. The methods for computing fragment trajectories are applicable, but the appropriate computer programs have not been exercised for initial conditions of significant altitudes above the ground. Because we cannot estimate impact conditions, we, of course, cannot use the methods of Chapter V for predicting damaging effects of fragments.

6-2.2.1 Yield

The yield is calculated by the methods in Chapter I. According to Table 1-2, values for the yield are obtained from Figures 1-1 and 1-6, and the lower value is used:

From Figure 1-1, for a fuel and oxidizer mass of 5.20×10^5 kg, $y = 0.06$. The multiplier is 370%. $Y = (0.06)(370\%) = 22.2\%$

In Figure 1-6, choose t_{ignition} for maximum Y. Then $Y = 58\%$. Using the lower value, $Y = 22.2\%$.

The overpressure and impulse curves for propellant explosions were obtained from data of explosions occurring on the ground. An argument similar to that used on page 75 can be used here. The ground explosion can be approximated by the vessel in Figure 2A-4b, where half of the energy is released above the ground. To apply the analysis to an explosion in free air, the energy (or yield) must be halved. Then $Y = 11.1\%$.

6-2.2.2 . Overpressure and specific impulse

The overpressure and specific impulse are calculated by the methods in Chapter II. The effective mass is calculated from Equation 2-9:

$W = W_T \times \frac{Y}{100}$. Table 2-1 gives the procedure for finding the overpressure and specific impulse as functions of distance:

$$W = W_T \times \frac{Y}{100} = (5.20 \times 10^5 \text{ kg}) \frac{11.1\%}{100\%} = 57500 \text{ kg (126,000 lb}_m)$$

According to Table 2-1, the overpressure is read from Figure 2-14, and the specific impulse is read from Figure 2-15.

The following (Table 6-10) is a list of overpressures (P_s) and specific impulses (I_s) from Figure 2-14 and 2-15. The solid lines in these figures were used.

TABLE 6-10. OVERPRESSURES AND IMPULSES

R (m)	$\frac{W}{W^{1/3}}$ ($m/kg^{1/3}$)	P_s (Pa)	\bar{P}_s	P_r (Pa)	$\frac{I_r}{W^{1/3}}$ ($Pa \cdot s/kg^{1/3}$)	I_s ($Pa \cdot s$)	I_r ($Pa \cdot s$)	$\frac{I_r}{m^{1/3}}$ ($Pa \cdot s/kg^{1/3}$)	$\frac{I}{P_o^{1/2} m^{1/3}}$ ($Pa^{1/2} \cdot s/kg^{1/3}$)	\bar{P}_r
15.4	0.400	2.48×10^6	24.5	1.77×10^7	451	1.74×10^4	1.24×10^5	7.25×10^4	2.28×10^2	175
23.2	0.600	1.13×10^6	11.2	7.70×10^6	344	1.33×10^4	9.02×10^4	5.28×10^4	1.66×10^2	76
38.6	1.00	4.39×10^5	4.33	2.30×10^6	237	9.15×10^3	4.23×10^5	2.47×10^4	7.77×10^1	20
77.2	2.00	1.23×10^5	1.21	5.27×10^5	137	5.29×10^3	2.27×10^4	1.33×10^4	4.17×10^1	5.2
154	4.00	3.83×10^4	0.378	8.84×10^4	76.9	2.97×10^3	6.85×10^3	4.00×10^3	1.26×10^1	0.872
306	10.0	1.08×10^4	0.107	2.27×10^4	33.8	1.30×10^3	2.72×10^3	1.39×10^3	5.00	0.224
795	20.6	4.02×10^3	0.0396	8.16×10^3	17.2	6.64×10^2	1.35×10^3	7.89×10^2	2.48	0.0895

(ft = m X 3.281)

(psi-sec = Pa · s X 1.450×10^{-4})(psi = Pa X 1.450×10^{-4})

6-2.2.3 Effect of Blast Waves on Structures

The methods described in Section 3-1 are used to determine the effects of blast waves on structures.

Glass Breakage

In Scenario #1, it was found that the minimum overpressure to break a typical pane of glass facing the explosion is 2420 Pa. For a pane of glass parallel to the path of the blast wave the minimum overpressure required to break it is 4840 Pa. We are concerned with damage on the ground. The blast wave will be reflected by the ground. Therefore, the reflected overpressure is important here. Replace P_0 by P_r and calculate the new P_r . From Equation 2-3, $P_r = 2420 \text{ Pa} (0.351 \text{ psi})$, $P_r = 1280 \text{ Pa} (0.186 \text{ psi})$. For $P_r = 4840 \text{ Pa} (0.702 \text{ psi})$, $P_r = 2420 \text{ Pa} (0.351 \text{ psi})$. As in this particular calculation, P_r and I_r will be used in place of P_0 and I_0 throughout this scenario. From Figure 2-14, one would expect to be able to obtain the distance at which these overpressures would be observed for Scenario #2. For $P_r = 2420 \text{ Pa}$, or $P_r = 1280 \text{ Pa}$ a value of $R/W^{1/3}$ cannot be read from Figure 2-14, but it can be seen that the distance R must be over 1000 m (3000 ft). Therefore, glass breakage will occur on the ground below the explosion.

Building Damage

The (i, P_r) points for selected values of R for Scenario #2 are included in Figure 6-3. Using the same techniques as in Scenario #1, but using the reflected overpressures and impulses, Table 6-11 was assembled. (The reflected impulses are calculated by Equation 2-4). For this explosion at an altitude of 1000 m, there might be building damage on the ground (possibly minor structural damage).

TABLE 6-11. BUILDING DAMAGE

Degree of Damage	Distance (m)	Distance (ft)
threshold of minor structural damage	over 800	over 2600
threshold of major structural damage	450	1500
threshold of partial demolition	300	980

6-2.2.4 Effect of Blast Waves on Humans

The methods described in Section 3-2 are used to determine the effects of blast waves on humans.

Lung Damage

The $(\bar{P}_s, \frac{I_s}{p_0^{1/2} m^{1/3}})$ points for selected values of R for Scenario #2 are included in Figure 6-5. Table 6-12 was obtained from this figure. There will be no lung damage to humans from this explosion.

TABLE 6-12. LUNG DAMAGE

Chance of Survival	Distance	
	(m)	(ft)
threshold of lung damage	170	560
99%	100	330
90%	100	330
50%	90	300
10%	90	300
1%	90	300

Ear Damage

The (P_s, I_s) points for selected values of R for Scenario #2 are included in Figure 6-6. Table 6-13 was assembled using this figure. The data could not be extrapolated to find the distance for "Temporary Threshold Shift."

TABLE 6-13. EAR DAMAGE

Degree of Damage	Distance	
	(m)	(ft)
threshold of eardrum rupture	340	1100
50% eardrum rupture	150	490

Skull Fracture

$$\frac{I_s}{P_s, m^{1/3}}$$

The $(P_s, \frac{I_s}{m^{1/3}})$ points for selected values of R for Scenario #2 are included in Figure 6-7. Table 6-14 is the result.

TABLE 6-14. SKULL FRACTURE

Chance of Skull Fracture	Distance	
	(m)	(ft)
mostly safe	390	1300
threshold	360	1200
50%	340	1100
near 100%	320	1000

Body Translation and Impact

$$\frac{I_s}{P_s, m^{1/3}}$$

The $(P_s, \frac{I_s}{m^{1/3}})$ points for selected values of R for Scenario #2 are included in Figure 6-8. In the result, Table 6-15, note that no value of R is given for "near 100% mortality" because extrapolation is not recommended.

TABLE 6-15. MORTALITY FROM BODY IMPACT

Degree of Mortality	(m)	Distance (ft)
mostly safe	390	1300
threshold of lethality	330	1100
50% mortality	170	560

There would be injury to people on the ground due to the blast wave.

6-2.2.5 Fragment Characteristics

The initial fragment velocity distribution is obtained from Figure 4-50; 95% of the fragments have an initial velocity less than or equal to 1000 m/s (3300 ft/s).

The fragment mass distribution cannot be determined with the methods that are presently available. Figures 4-51 and 4-52 show the mass distribution for CBM explosions with yields of 5% and 1.1%. There is obviously a strong dependence of mass distribution upon yield, and it is not valid to attempt to extrapolate the information in these figures to a yield of 11.1%.

6-2.2.6 Effect of Fragments on Humans

The effect on humans of flying glass from windows broken by blast waves will be considered. In Scenario #1, it was shown that for injury from flying glass, $P_s = 1.94 \times 10^5 \text{ Pa}$ (28.1 psi) with the blast wave striking the pane of glass head-on, and $P_s = 6.37 \times 10^5 \text{ Pa}$ (92.4 psi) with the blast wave propagating in a direction parallel to the surface of the glass.

As for other types of damage in this Scenario, the reflected over-pressure must be used in place of P_s . Then, $P_s = 1.94 \times 10^5 \text{ Pa}$ for normal blast impact and $P_s = 6.37 \times 10^5 \text{ Pa}$ for blast impact parallel to the glass surface. The corresponding values of P_s are then $7.52 \times 10^4 \text{ Pa}$ (10.9 psi) and $1.94 \times 10^5 \text{ Pa}$ (28.1 psi). From Figure 2-14 of Chapter II, at a distance R less than 124 m (405 ft), there is likelihood of human injury by flying glass from windows normal to the direction of travel of the blast wave. The corresponding distance for windows parallel to the direction of travel is 70 m (230 ft).

There will be no injury by flying glass to humans on the ground.

6-2.3 Scenario #3. Fall Back of the Titan Centaur Vehicle During Launch

The scenario for this accident is nearly identical to the first, except that the launch vehicle is different. The Titan Centaur is a three-stage, liquid-fueled rocket vehicle with a mass fraction of 0.85. The first two stages are fueled with the hypergolic propellant combination N_2O_4 and Aerozine 50, and the third stage with LO_2 and LH_2 . The missile is assumed to rise a short distance when loss of thrust in the first stage allows it to fall back on the launch pad. The impact is assumed to be sufficiently violent that at least the first stage ruptures and spills its propellant on the launch pad. Impact velocity is 14.0 m/s (45.9 ft/s). Table 6-16 gives propellant masses and estimates of structural masses for each stage, based on the mass fraction of 0.85.

Several possible assumptions regarding severity of the fall-back accident can be made. We will make two such assumptions, and predict effects for both. These assumptions are:

- (1) Only the first stage ruptures and explodes, and
- (2) Both first and second stages rupture and explode

For the first assumption, the structure of the first stage is assumed to be the only source of fragments, while for the second assumption, the structures of both first and second stages are fragment sources.

TABLE 6-16. PROPELLANTS AND STRUCTURES
AT LIFT-OFF OF TITAN CENTAUR ROCKET

Stage	Propellants	Propellant Masses (kg)	Structure Masses (kg)	Propellant Masses (lb _m)	Structure Masses (lb _m)
Titan First	N_2O_4	75 900	20 600	167,000	45,300
	Aerozine 50	40 400	--	88,900	--
Titan Second	N_2O_4	19 500	5 360	42,900	11,800
	Aerozine 50	10 900	--	24,000	--
Centaur (Third)	LO_2	11 400	2 410	25,100	5300
	LH_2	2 270	--	4990	--

6-2.3.1 Yield

The yield is calculated by the methods in Chapter I. According to Table 1-2 values for the yield are obtained from Figure 1-1 and Table 1-1, and the lower value is used:

From Figure 1-1, for a fuel and oxidizer mass of 116 000 kg (255,000 lb_m) (only the first stage), or 146 000 kg (321,000 lb_m) (first and second stages), $y = 0.06$. The multiplier is 240%. $Y = (0.06)(240\%) = 14.4\%$. From Table 1-1, $Y = 1.5\%$. Using the lower value, $Y = 1.5\%$.

6-2.3.2 Overpressure and Specific Impulse

The overpressure and specific impulse are calculated by the methods in Chapter II. The effective mass is calculated from Equation 2-9.

$W = W_T \times \frac{Y}{100}$. Table 2-1 gives the procedure for finding the overpressure and specific impulse as functions of distance:

$$W_1 = W_{T_1} \times \frac{Y}{100} = (1.16 \times 10^5 \text{ kg}) \frac{1.5\%}{100\%} = 1740 \text{ kg (3820 lb}_m)$$

(only the first stage)

$$W_{1+2} = (1.46 \times 10^5 \text{ kg}) \frac{1.5\%}{100\%} = 2190 \text{ kg (4820 lb}_m)$$

(first and second stages)

According to Table 2-1, the overpressure is read from Figure 2-7, and specific impulse is read from Figure 2-8.

The following (Table 6-17) is a list of overpressures (P_s) and specific impulses (I_s) from Figures 2-7 and 2-8. The solid lines in the figures were used.

6-2.3.3 Effect of Blast Waves on Structures

The methods described in Section 3-1 are used to determine the effects of blast waves on structures.

Glass Breakage

In Scenario #1, it was found that the minimum overpressure to break a typical pane of glass facing the explosion is 2420 Pa (.351 psi). For a pane of glass parallel to the path of the blast wave, the minimum overpressure required to break it is 4840 Pa (.702 psi). From Figure 2-7 one would expect to be able to obtain the distance at which these overpressures would be observed for Scenario #3. For $P_s = 2420 \text{ Pa or } 4840 \text{ Pa}$, a value of

TABLE 6-17. OVERPRESSURES AND IMPULSES

$\frac{R}{W}^{1/3}$ (m/kg ^{1/3})	\bar{P}_a (Pa)	P_o (Pa)	$\frac{1}{W}^{1/3}$ (Pa · s/kg ^{1/3})	1st Stage				2nd Stage			
				T_a (Pa · s)	R (m)	$\frac{T_a}{m^{1/3}}$ (Pa · s/kg ^{1/3})	$\frac{P_o}{T_a^{1/2}}^{1/3}$ (Pa ^{1/2} · s/kg ^{1/3})	R (m)	T_a (Pa · s)	$\frac{T_a}{m^{1/3}}$ (Pa · s/kg ^{1/3})	$\frac{P_o}{T_a^{1/2}}^{1/3}$ (Pa ^{1/2} · s/kg ^{1/3})
2.00	5.64	5.71×10^5	216	2600	24.1	1520	4.78	26.0	2800	1640	5.14
4.00	2.42	2.45×10^5	87.7	1060	48.1	620	1.95	52.0	1140	667	2.09
10.00	0.850	8.61×10^4	30.3	365	120	213	0.671	130	394	230	0.724
20.00	0.397	4.02×10^4	14.5	174	241	102	0.320	260	188	110	0.345
40.00	0.190	1.92×10^4	7.47	89.9	481	52.6	0.165	520	97.0	56.7	0.178

(R = m X 3.281)

(pa = Pa X 1.450×10^{-4})(pa-sec = Pa · s X 1.450×10^{-4})

$R/W^{1/3}$ cannot be read from Figure 2-7, but it can be seen that $R/W^{1/3}$ must be over 60, corresponding to R greater than 720 m (2400 ft) for only one stage exploding and R greater than 780 m (2600 ft) for both the first and second stages exploding.

Building Damage

The (i, P_s) , points for selected values of R for Scenario #3 are included in Figure 6-3. Using the same technique as in Scenario #1, Table 6-18 was assembled.

TABLE 6-18. BUILDING DAMAGE

Degree of Damage	Distance			
	1st Stage (m)	1st Stage (ft)	1st and 2nd Stages	
threshold of minor structural damage	380	1200	416	1400
threshold of major structural damage	140	460	160	520
threshold of partial demolition	95	310	100	330

OVERTURNING OF OBJECTS - TWO STAGES EXPLODING

The $(\frac{a_o C_d i}{p_o H}, \bar{P}_s)$ points for selected values of R are included in Figure 6-4. For R less than or equal to 70 m (230 ft), a Saturn V rocket can be expected to overturn as a result of this explosion.

6-2.3.4 Effect of Blast Waves on Humans

The methods described in Section 3-2 are used to determine the effects of blast waves on humans.

Lung Damage

The $(\bar{P}_s, \frac{I_s}{p_o^{1/2} m^{1/3}})$ points for selected values of R for Scenario #3 are included in Figure 6-5. Table 6-19 was obtained from this figure.

TABLE 6-19. LUNG DAMAGE

Chance of Survival	Distance			
	1st Stage (m)	1st Stage (ft)	1st and 2nd Stages (m)	1st and 2nd Stages (ft)
threshold of lung damage	120	390	130	430
99%	53	170	55	180
90%	46	150	52	170
50%	39	130	45	150
10%	35	110	40	130
1%	32	100	36	120

Ear Damage

The (P_s, I_s) points for selected values of R for Scenario #3 are included in Figure 6-6. Table 6-20 was assembled using this figure. The data could not be extrapolated to find the distance for "Temporary Threshold Shift".

TABLE 6-20. EAR DAMAGE

Degree of Damage	Distance			
	1st Stage (m)	1st Stage (ft)	1st and 2nd Stages (m)	1st and 2nd Stages (ft)
threshold of eardrum rupture	260	850	280	920
50% eardrum rupture	110	360	120	390

Skull Fracture

The $(P_s, \frac{I_s}{m^{1/3}})$ points for selected values of R for Scenario #3 are included in Figure 6-7. Table 6-21 is the result. The curves in Figure 6-6 should not be extrapolated to find the damage limits beyond "mostly safe".

TABLE 6-21. SKULL FRACTURE

Chance of Skull Fracture	Distances			
	1st Stage (m)	1st and 2nd Stages (m)	(ft)	(ft)
mostly safe	110	360	120	390

Body Translation and Impact

The $(P_s, \frac{I}{m^{1/3}})$ points for selected values of R for Scenario #3 are included in Figure 6-8. In the result, Table 6-22, note that a value of R is given only for "mostly safe" because extrapolation is not recommended.

TABLE 6-22. MORTALITY FROM BODY IMPACT

Degree of Mortality	Distances			
	1st Stage (m)	1st and 2nd Stages (m)	(ft)	(ft)
mostly safe	110	360	120	390

6-2.3.5 Fragment Characteristics

The fragment mass and initial velocity distributions cannot be determined by the methods in Chapter IV because the figures there are not to be used for hypergolic propellants.

The fragment range is obtained from Figure 4-57. 95% of the fragments will strike the ground at a distance less than or equal to 270 m (890 ft).

6-2.3.6 Appurtenances

As an example of an appurtenance a cement block will be used as in Scenario #1. The stand-off distance is 52 m (170 ft), where $P = 2.45 \times 10^5$ Pa, $P_c = 2.42$, and $I = 1140$ Pa · s. Then $I = 0.268$. Locating the (P_s, I) point on Figure 4-26, one finds that $\bar{V} = 5.0$. Then $V = 3.3$ m/s (11 ft/s). Thus, this cement block would be thrown at a low velocity.

6-2.3.7 Effect of Fragment on Humans

The effect on humans of flying glass from windows broken by blast waves will be considered. In Scenario #1, it was shown that for injury from flying glass, $P_s = 1.94 \times 10^5$ Pa with the blast wave striking the pane of glass head-on, and $P_s = 6.37 \times 10^5$ Pa with the blast wave propagating in a direction parallel to the surface of the glass. From Figure 2-7, at a distance $R/W^{1/3}$ less than 1.8, there is likelihood of human injury by flying glass from windows parallel to the direction of travel of the blast wave. The corresponding distance $R/W^{1/3}$ for windows normal to the direction of travel is 5.0. The maximum distances from the explosion for human injury from flying glass are shown in Table 6-23.

The damage and injury to be expected in Scenario #3 are summarized in Tables 6-24 and 6-25.

TABLE 6-23. MINIMUM SAFE DISTANCE FOR INJURY BY FLYING GLASS

Orientation of Glass to Direction of Travel of Blast Wave	Distance			
	1st Stage (m)	1st Stage (ft)	1st and 2nd Stages (m)	1st and 2nd Stages (ft)
parallel	22	72	23	75
normal	60	197	65	213

TABLE 6-24. SCENARIO 3: DAMAGE TO STRUCTURES

Damage to Structures	Distance			
	1st Stage (m)	1st Stage (ft)	1st and 2nd Stages (m)	1st and 2nd Stages (ft)
Saturn V overturning threshold of partial demolition	--	---	70	230
	95	310	100	330
threshold major structural damage	140	460	160	520
95% of fragments will strike the ground within this distance	270	890	270	890
threshold minor structural damage	380	1200	416	1400
threshold of side on glass breakage	> 720	> 2400	> 780	> 2600

TABLE 6-25. SCENARIO 3: HUMAN INJURY

Human Injury	Distance			
	1st Stage (m)	1st and 2nd Stages (ft)	1st and 2nd Stages (m)	1st and 2nd Stages (ft)
1% survival (lung damage)	32	100	36	120
10% survival (lung damage)	35	110	40	130
50% survival (lung damage)	39	130	45	150
90% survival (lung damage)	46	150	52	170
99% survival (lung damage)	53	170	55	180
50% eardrum rupture, mostly safe from skull fracture and body impact	110	360	120	390
threshold of lung damage	120	390	130	430
threshold of eardrum rupture	260	850	280	920
threshold injury from flying glass (side-on)	460	1500	490	1600

6-2.4 Scenario #4. Pressure Burst of a Centaur Pressurant Tank During Pneumatic Strength Testing in a Shop Area

One of the spherical pressurant tanks for the Centaur launch vehicle is assumed to fail catastrophically while it is being proof tested in a shop area. The vessel is spherical, made of Ti-6 Al4V alloy, has a volume of 0.1206 m^3 (4.26 ft^3), and fails at the design pressure of 20.7 MPa (3000 psi), and at room temperature of 25°C (77°F). The vessel is being pressurized with helium, with a γ of 1.67. The radius of the vessel is 0.307 m (1.00 ft), and the wall thickness is 4.60 mm (0.0151 ft). The density of the titanium alloy is 4.48 Mg/m^3 ($279 \text{ lb}_\text{m}/\text{ft}^3$), making the mass of the vessel 24.3 kg (53.5 lb_m).

6-2.4.1 Overpressure and Specific Impulse

Determine the starting point and locate it on Figure 2-18. Use the nearest curves to find the overpressure versus distance behavior. Use Figure 2-23 to determine the specific impulse versus distance behavior:

$$p_1 = 2.07 \times 10^7 \text{ Pa (g)} = 2.08 \times 10^7 \text{ Pa (absolute)}$$

$$p_a = 1.013 \times 10^5 \text{ Pa. Then } p_1/p_a = 205.3$$

$$T_1 = T_a = 298^\circ\text{K.} \text{ Then } T_1/T_a = 1.00.$$

For $\gamma_1 = 1.667$, from Figure 2-21, $\bar{P}_{so} = 4.8$.

$$\bar{R}_o = \left[\frac{1}{\frac{4\pi}{3} \left(\frac{p_1}{p_a} - 1 \right)} \right]^{1/3} = \left[\frac{1}{\frac{4\pi}{3} \left(\frac{2.08 \times 10^7 \text{ Pa}}{1.013 \times 10^5 \text{ Pa}} - 1 \right)} \right]^{1/3} = 0.092 \text{ m}$$

In Figure 2-18 the point $(\bar{R}_o, \bar{P}_{so})$ lies nearest the 4th curve from the bottom. This gives \bar{P}_s versus \bar{R} .

$$\bar{R} = \left[\frac{\bar{r}}{\bar{r}_o} \right]^{1/3} . \text{ Then } \bar{r} = \bar{R} \bar{r}_o \left[\frac{\frac{4\pi}{3} \left(\frac{p_1}{p_a} - 1 \right)}{\gamma_1 - 1} \right]^{1/3}$$

$$= \bar{R}(0.307 \text{ m}) \left[\frac{\frac{4\pi}{3} \left(\frac{2.08 \times 10^7 \text{ Pa}}{1.013 \times 10^5 \text{ Pa}} - 1 \right)}{1.667 - 1} \right]^{1/3} = \bar{R}(3.336) \text{ (r in m)}$$

$$\bar{P}_s = \frac{p_s - p_a}{p_a} . \text{ Then } p_s - p_a = p_a \bar{P}_s = (1.013 \times 10^5 \text{ Pa}) \bar{P}_s \text{ (p}_s \text{ in Pa)}$$

$$E = \frac{P_1 - P_a}{Y_1 - 1} V_i = \frac{(2.08 \times 10^7 \text{ Pa} - 1.013 \times 10^5 \text{ Pa})(0.1206 \text{ m}^3)}{1.667 - 1}$$

$$= 3.74 \times 10^6 \text{ J}$$

$$\bar{I} = \frac{I a_a}{P_a^{2/3} E^{1/3}} . \text{ Then } I = \frac{\bar{I} P_a^{2/3} E^{1/3}}{a_a}$$

$$= \frac{\bar{I} (1.013 \times 10^5 \text{ Pa})^{2/3} (3.743 \times 10^6 \text{ J})^{1/3}}{331 \frac{\text{m}}{\text{s}}} = 1019 \bar{I} . \text{ (I in Pa} \cdot \text{s)}$$

Overpressures and specific impulses versus distance are listed in Table 6-26 and graphed in Figures 6-9 and 6-10.

6-2.4.2 Effect of Blast Waves on Structures

The methods described in Section 3-1 are used to determine the effects of blast waves on structures.

Glass Breakage

In Scenario #1, it was found that the minimum overpressure to break a typical pane of glass facing the explosion is 2420 Pa. For a pane of glass parallel to the path of the blast wave, the minimum overpressure required to break it is 4840 Pa. From Figure 6-9 one can obtain the distance at which these overpressures would be observed for Scenario #4. For $P_o = 2420 \text{ Pa}$, it can be seen that the distance R must be 28 m (92 ft). For $P_o = 4840 \text{ Pa}$, the distance R is 16 m (52 ft).

Building Damage

The (i, P_o) points for selected values of R for Scenario #4 are included in Figure 6-3. Using the same techniques as in Scenario #1, Table 6-27 was assembled. It is unlikely that any building damage will result.

TABLE 6-26. OVERPRESSURES AND SPECIFIC IMPULSES FOR A BURSTING PRESSURANT TANK

\bar{R}	r (m)	\bar{P}_s	P_s (Pa)	T	$\frac{I}{\bar{r}}$ (Pa · s)	$\frac{I}{(P_s \cdot r)^{1/3}}$ (Pa · s/kg ^{1/3})	$\frac{1}{\bar{P}_s^{1/2} \bar{r}^{1/3}}$ (Pa ^{-1/2} · s/kg ^{1/3})
0.092	0.307	4.8	4.9×10^5	--	--	--	--
0.10	0.33	4.6	4.6×10^5	1.1	1100	660	2.1
0.20	0.67	2.7	2.7×10^5	2.7×10^{-1}	280	160	5.1×10^{-1}
0.30	1.0	1.9	1.9×10^5	1.5×10^{-1}	150	90	2.8×10^{-1}
0.50	1.7	1.0	1.0×10^5	9.2×10^{-2}	94	55	1.7×10^{-1}
0.90	3.0	0.49	5.0×10^4	5.4×10^{-2}	55	32	1.0×10^{-1}
2.0	6.7	0.16	1.62×10^4	2.6×10^{-2}	26	16	4.9×10^{-2}
10	33	0.019	1.9×10^3	3.4×10^{-3}	5.5	3.2	1.0×10^{-2}
44	150	0.014	1.4×10^3	4.1×10^{-3}	4.2	--	--
100	330	1.4×10^3	1.4×10^2	4.7×10^{-4}	0.48	0.28	8.8×10^{-4}
1000	2900	1.1×10^4	1.1×10^1	4.6×10^{-5}	0.047	0.027	8.6×10^{-5}

(R = m X 3.281)

(psi = Pa X 1.450 X 10⁻⁴)(psi-sec = Pa · s X 1.450 X 10⁻⁴)

496

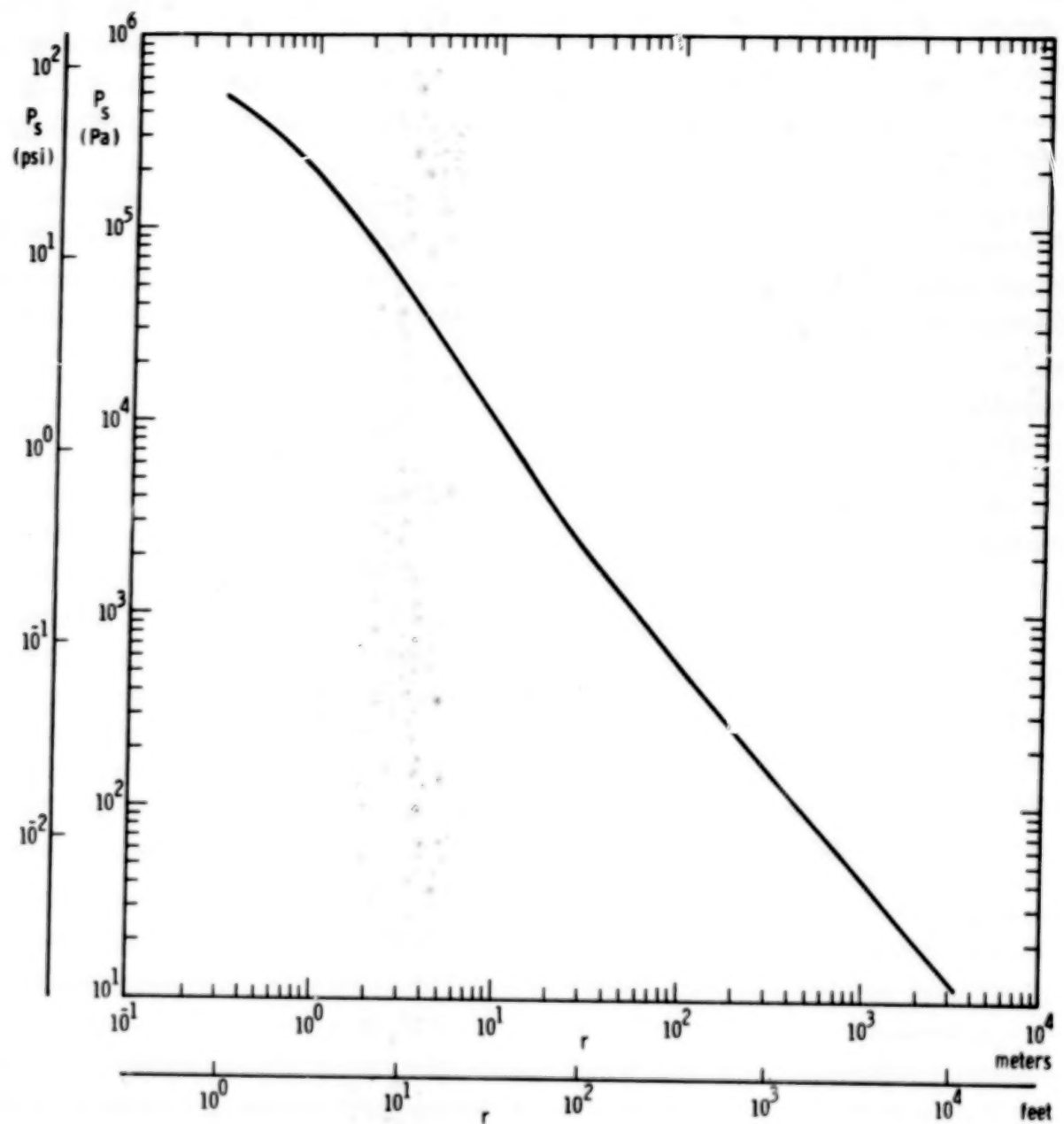


Figure 6-9. Overpressure Vs Distance for Pressurant Tank Burst

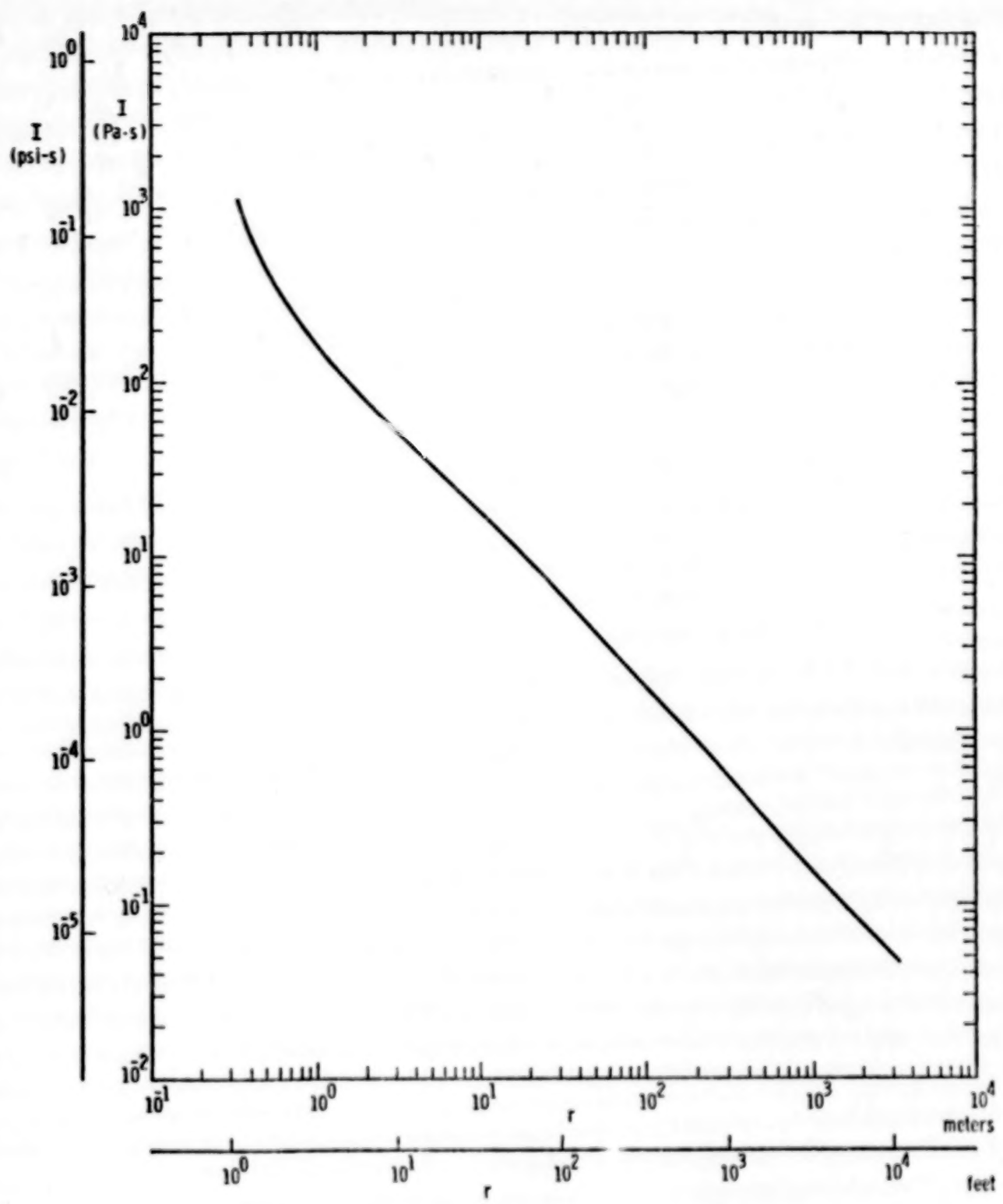


Figure 6-10. Specific Impulse Vs Distance for Pressurant Tank Burst

TABLE 6-27. BUILDING DAMAGE

Degree of Damage	Distance (m)	Distance (ft)
threshold of minor structural damage	1.3	4.3
threshold of major structural damage	0.6	2
threshold of partial demolition	0.5	1.6

6-2.4.3 Effect of Blast Waves on Humans

The methods described in Section 3-2 are used to determine the effects of blast waves on humans.

Lung Damage

The $(P_s, \frac{I_s}{p_0^{1/2} m^{1/3}})$ points for selected values of R for Scenario #4

are included in Figure 6-5. Table 6-28 was obtained from this figure. The "1% survivability" limit cannot be determined, but it certainly lies within the gas vessel, and therefore is of no interest.

TABLE 6-28. LUNG DAMAGE

Chance of Survival	Distance (m)	Distance (ft)
threshold of lung damage	1.2	3.9
99%	0.54	1.7
90%	0.48	1.6
50%	0.41	1.4
10%	0.35	1.1

Ear Damage

The (P_s, I_s) points for selected values of R for Scenario #4 are

included in Figure 6-6. Table 6-29 was assembled using this figure. Although it is inadvisable to extrapolate the curves in Figure 6-6, one can estimate values of R for "threshold of eardrum rupture" and "50% eardrum rupture".

TABLE 6-29. EAR DAMAGE

Degree of Damage	Distance (m)	Distance (ft)
threshold of eardrum rupture	4(approx.)	13(approx.)
50% eardrum rupture	1.6(approx.)	5(approx.)
TTS	147	480

Skull Fracture

The $(P_s, \frac{I}{m^{1/3}})$ points for selected values of R for Scenario #4

could not be included in Figure 6-7. Because extrapolation is not recommended, little information on safe stand-off distances (with respect to skull fracture) can be obtained. It appears that distances greater than about 1 m (3ft) will be safe for humans for this type of injury.

Body Translation and Impact

The $(P_s, \frac{I}{m^{1/3}})$ points for selected values of R for Scenario #4

could not be included in Figure 6-8. As above, it seems that a safe distance for humans, considering whole body translation and impact, is about 1 m (3 ft).

6-2.4.4 Appurtenances

This vessel burst occurs in a laboratory. A reasonable object for an appurtenance might be a hammer. This is grossly idealized as two vertical cylinders, one on top of the other. The top cylinder, the head, has a radius of 0.01905 m (0.75 in), a length of 0.1016 m (4.0 in), and a mass of 0.918 kg (2.0 lb m^3). The lower cylinder (the handle) has a radius of 0.01905 m (0.75 in), a length of 0.254 m (10 in), and a mass of 0.679 kg (1.5 lb m^3). The total mass is 1.60 kg (3.537 lb m^3), and the cross-sectional area facing the blast wave A is 0.0135 m^2 (0.145 ft^2). $C_D = 1.20$. $K = 4$.

Then, $X = 0$, and $H = 0.01905 \text{ m}$ (0.06250 ft). Assume that the hammer is located 0.667 m (2.19 ft) from the center of the vessel. At this distance, $P_s = 2.74 \times 10^5 \text{ Pa}$ (39.7 psi), $\bar{P}_s = 2.7$, and $I_s = 275 \text{ Pa} \cdot \text{s}$ (0.0399 psi-sec).

$$\text{For Figure 4-26, } \bar{I}_s = \frac{C_D I_a}{P_s (KH + X)}$$

$$= \frac{(1.20)(275)(331)}{(2.74 \times 10^5)[4(0.01905) + 0]} = 5.23. \text{ From that graph, } \bar{V} \approx 20.$$

$$\text{Then } V = \frac{\bar{V} p_o A (KH + X)}{M a_o} = \frac{(20)(1.013 \times 10^5)(0.0135)[4(0.01905) + 0]}{(1.60)(331)} = 4 \text{ m/s}$$

(13 ft/s). A hammer can be thrown at a high enough velocity to be dangerous.

6-2.4.5 Effect of Fragments on Humans

The effect on humans of flying glass from windows broken by blast waves will be considered. In Scenario #1, it was shown that for injury from flying glass, $P_s = 1.94 \times 10^5 \text{ Pa}$ with the blast wave striking the pane of glass head-on, and $P_s = 6.37 \times 10^5 \text{ Pa}$ with the blast wave propagating in a direction parallel to the surface of the glass. From Figure 6-9, at a distance R less than 1.0 m (3.3 ft), there is likelihood of human injury by flying glass from windows normal to the direction of travel of the blast wave. The corresponding distance for windows parallel to the direction of travel is less than 0.3 m (1.0 ft).

A summary of damage and injury for Scenario #4 is given in Table 6-30.

6-2.4.6 Fragment Barrier

A metal sheet or plate can be used as a barrier to stop fragments from a bursting pressurant tank. It was found that the initial fragment velocity is 311 m/s. Assume that the barrier is close enough to the vessel that the fragment velocity does not decrease significantly before the fragment strikes the barrier.

For a barrier, assume a steel sheet or plate ($\rho_t = 7850 \text{ kg/m}^3$, $\sigma_t = 3.11 \times 10^9 \text{ N/m}^2$). The barrier may surround the vessel, but effects of curvature and oblique impact will be ignored.

TABLE 6-30. SCENARIO 4: DAMAGE TO STRUCTURES
AND INJURY

<u>Damage and Injury</u>	<u>Distance</u>	
	<u>(m)</u>	<u>(ft)</u>
10% survival (lung damage)	0.35	1.1
50% survival (lung damage)	0.41	1.4
90% survival (lung damage)	0.48	1.6
99% survival (lung damage)	0.54	1.7
mostly safe from skull fracture and mortality due to body impact	-1	-3
threshold of lung damage	1.2	3.9
50% eardrum rupture	-1.6	-5
threshold of eardrum rupture	-4	-13
threshold of injury from flying glass (face-on)	1.0	3.3
threshold of injury from flying glass (side-on)	0.3	1.0
threshold of side-on glass breakage	16	52
threshold face-on glass breakage	28	92
temporary threshold shift	147	480

The fragment mass is determined by choosing the 90th percentile of distribution of fragment mass (the mass which would equal or exceed the mass of 90% of the fragments). From Figure 4-55, the fragment mass is then 6.6 kg (15 lb_m). Assume that the fragment is a sphere of radius a .

$$a = \left(\frac{m}{\sigma_p \frac{4\pi}{3}} \right)^{1/3} = \left(\frac{6.6 \text{ kg}}{4520 \frac{\text{kg}}{\text{m}^3} \frac{4\pi}{3}} \right)^{1/3} = 0.0704 \text{ m (0.231 ft)}$$

The nondimensional limit velocity is

$$\frac{\sigma_p V_{50}}{\sqrt{\sigma_t \sigma_t}} = \frac{(4520 \frac{\text{kg}}{\text{m}^3})(311 \frac{\text{m}}{\text{s}})}{\sqrt{(3.11 \times 10^8 \frac{\text{N}}{\text{m}^2})(7850 \frac{\text{kg}}{\text{m}^3})}} = 0.900$$

From Figure 5-1, h/a to stop the fragment is 0.23. Then $h = 0.23 a = (0.23)(0.0704) = 0.016 \text{ m} = 0.052 \text{ ft} = 0.63 \text{ in}$.

A steel plate of 0.016 m (0.63 in) thickness would stop 50% of the fragments with the given initial velocity. Before such a barrier is used, the blast loading should also be determined.

6-2.5 Scenario #5. Rotor Burst of an Aircraft Gas Turbine Running on a Test Stand

This problem is quite different from the previous four. It does not involve accidental explosions at all and is included to demonstrate the utility of some of the methods given in the workbook to safety problems other than the primary intended ones.

The problem is as follows: Predict the maximum range and terminal velocity for a fan blade fragment of a gas turbine engine assuming that the blade failure occurs at its connection to the rotor disk.

For Case I, assume the spinning blade leaves through the engine inlet with a deflection that tips it into the horizontal plane within an initial trajectory greater than 33°, with no loss of kinetic energy. Although the twist in blade may not contribute to the assumption of lift forces, assume that the blade is a spinning body or deformed into a boomerang-like shape. Identify the angle-of-attack and trajectory angle for maximum fragment range.

For Case II - The fan blade is deflected and deforms by curling into a cylinder or sphere-like shape upon leaving the inlet to the gas turbine with

a loss of 10% of the translational kinetic energy. In this case, predict the maximum possible range and terminal velocity using drag coefficients for a cylinder or sphere.

Fragment characteristics are as follows:

Geometrical shape (see figure on p. 4E-6)

Rotational kinetic energy	= 17,400 J
Translational kinetic energy	= 260 J
Mass	= 0.5 kg
Fan blade tip speed	= 393 m/s
Fan speed	= 123.1 RPS
Fan jet velocity	= 255 m/s
Location of fan blade center of gravity (CG) from C_L of engine	= 0.342 m
Location of fan blade CG from failure	= 0.116 m

These types of jet engine rotor failures have occasionally occurred during takeoff and climb-out. Some have also occurred on static jet engine test stands. Documented evidence shows that trajectories have been as much as 57° forward, relative to the plane of failure for fan rotors. Containment barriers cannot be provided at the inlet of engines on static test stands without upsetting inlet performance data. Thus, it becomes important to identify hazards to people and risk of damage to facilities for such failures.

Case I was run under two sets of assumptions. Since FRISB was written for "disc" fragments, it was necessary to assume that the blade curled into a disc shape. The planform area of the blade fragment was set equal to the surface area of a representational disc. The planform thickness of the blade as viewed from the front was set equal to the thickness of a representational disc. The optimal lift coefficient for a circular wing ($C_L = 0.32$) was taken, assuming gyro stability for the circular disc and assuming a constant angle of attack. A drag coefficient of 0.85 was obtained from tables relating drag coefficient to the thickness-to-diameter ratio of a plate-shaped fragment.⁶ The area over which pressure drag acted was taken as the thickness times the diameter of the representational disc. The initial velocity of the disc was assumed to be the initial translational velocity of the fragment. The rotational velocity of the fragment only contributes to the gyro stability of the disc. Results were obtained from the spectrum of initial trajectory angles from 30 to 70° in five-degree intervals. The results given in Table 6-31 are for the maximum range obtained.

As a check on the results obtained for Case I under the assumptions of the disc geometry, the trajectory characteristics of the fragment were determined under a different set of assumptions relating to lift. For these

"thrust" assumptions, the blade was assumed to spin about an axis normal to its planform area, producing a thrust like a helicopter rotor blade, and thus lift. All other sources of lift were ignored. The fragment was approximated from drawings to have the shape of a NACA 4412 air foil. The rotational kinetic energy contributing to the thrust is assumed to dissipate as a result of pressure drag forces as a function of the average linear velocity of the blade in rotation. The rotation of the blade contributes only to lift. The initial velocity of the blade is the initial translational velocity as in the disc case. The drag resulting from the translational velocity of the blade acts to dissipate the translational kinetic energy.

For Case II in which no lift is considered, the fragment was assumed to deform into a cylindrical shape, and a pressure drag coefficient of 0.85 was used (which is approximately correct for cylindrical fragments traveling at Mach numbers less than 1/2). Trajectory differential equations were solved both by the use of Runge-Kutta techniques and the time interval perturbation technique as of Zaker.⁷ Results were the same. Predictably, for the no lift case the maximum range is less than for the case where lift is assumed. The terminal velocity is also slightly less. See Table 6-31.

TABLE 6-31

α_i deg	R m	V _t m/s	θ deg
-------------------	--------	-----------------------	-----------------

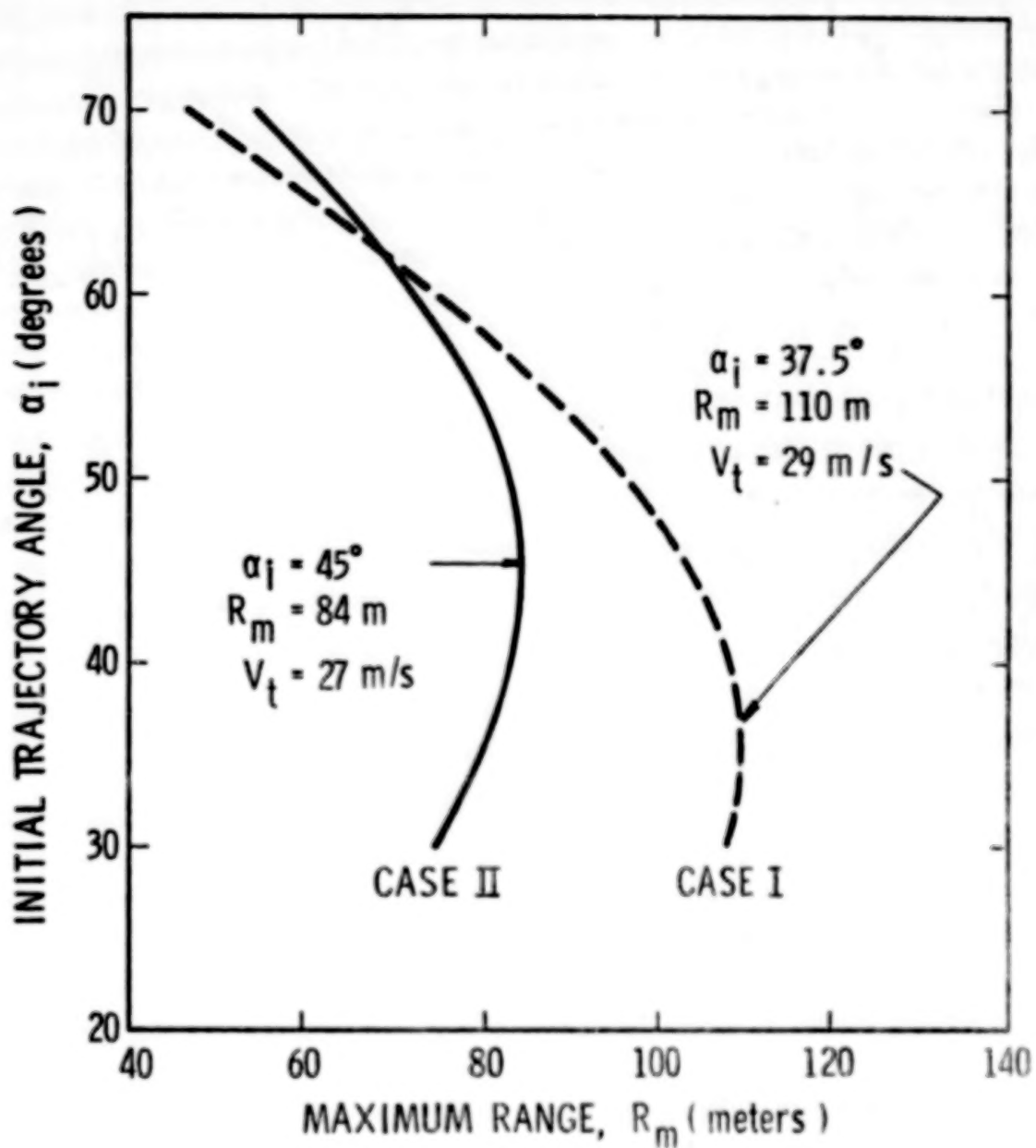
Case I

Disc	37.5	110	29.0	38
Thrust	40	97	27.9	24

Case II

No lift	45	84	27.0	47
---------	----	----	------	----

Table 6-31 and Figure 6-11 show the results of predictions obtained for both cases for the optimum initial trajectory angle α_i and under various assumptions to be described. The maximum range in meters R_m is given, as well as the terminal velocity V_t in meters per second, and the terminal ballistic angle of attack in degrees θ . From the table it may be seen that the maximum range expected under any of these sets of assumptions is 112 meters (367 ft) and the terminal velocity is only slightly less than the initial translational velocity of 30 meters per second (98 ft/sec). To put the damage potential of this fragment in perspective, a spherical fragment having the same mass with this terminal velocity could penetrate a 0.6-mm-thick (.0236 in) steel plate or a 1.6-mm-thick (.06299 in) aluminum plate.



(ft = m X 3.281)

Figure 6-11. Maximum Range as a Function of Initial Trajectory Angle, Cases I and II, Turbine Rotorblade Example

LIST OF REFERENCES

1. Chelson, Paul O., "Reliability Computation Using Fault Tree Analysis," NASA Technical Report 32-1542, December 1, 1971.
2. Rasmussen, Norman C., "Reactor Safety Study, an Assessment of Accident Risks in U.S. Commercial Nuclear Plants," U.S. Atomic Energy Commission Report WASH-1400, August 1974.
3. Kanda, Kazuo, "Subsystem Safety Analysis Techniques," Annals of Reliability and Maintainability, 1965.
4. Powers, G. J., and F. C. Tompkins, "A Synthesis Strategy for Fault Trees in Chemical Processing Systems," Loss Prevention, CEP Technical Manual, Volume 8, 1974.
5. Lawley, H. G., "Operability Studies and Hazard Analysis," Loss Prevention, CEP Technical Manual, Volume 8, 1974.
6. Hoerner, S. F., Fluid Dynamic Drag, published by author, 1958.
7. Zaker, T. A., "Trajectory Calculations in Fragment Hazard Analysis," Minutes 13th ASESB Seminar, September 1971.

CHAPTER VII

DISCUSSION OF RESULTS

Chapters I through VI in this workbook give a number of simplified prediction methods which hopefully can be used by a typical safety engineer to estimate damaging effects for certain classes of accidental explosions in aerospace launch facilities and flight vehicles. All prediction methods employ relatively simple graphs or equations, and require at most the use of a desk calculator or slide rule to make estimates. Example calculations are given in each chapter to illustrate use of the graphs.

Generally, the first step in predicting the effects of an accident is to estimate the total explosive yield or energy. For accidents involving the liquid propellants commonly used in rocket vehicles, a number of curves are presented in Chapter I for prediction of explosive yields given the propellant mixture and type of postulated accident. These graphs are based primarily on scaled results from Project PYRO tests, with upper limits established by other related work. This chapter also contains scaled graphs for estimating explosive energy release for gas vessel bursts, given the vessel characteristics and size, type of gas, and initial conditions. These graphs are based primarily on computer code solutions rather than experimental data.

Once explosive yields or energies are estimated from Chapter I, they can be used as inputs to graphs in Chapter II to obtain predictions of blast wave characteristics over a range of distances from the explosive sources. The primary blast wave properties included in Chapter II are side-on peak overpressure P_s and side-on impulse I_s , although we include discussions of other properties such as reflected peak overpressure P_r and time histories of drag pressure q . Again, blast data for liquid propellants are based primarily on experiment, while data for bursting gas vessels are estimated from computer code solutions for such waves.

Chapter III is devoted to prediction of damaging effects of blast waves, and is designed to give such predictions once blast pressures and impulses are known. The chapter therefore contains a number of scaled P-I (pressure-impulse) curves which are associated with various levels of damage or injury to a variety of structures, structural elements, and people. From different graphs, one can estimate minor damage through complete collapse of residences, threshold for glass breakage, incipient damage to beams or plates, and incipient toppling or overturning of a vehicle. Probability of injury or mortality of people can be predicted

from other scaled graphs. These give estimates of threshold of ear damage, various probabilities of mortality as functions of size of an individual as well as blast wave properties, tertiary blast damage from individuals being tumbled by a blast wave, and probability of injury from flying glass from windows destroyed by blast waves. The prediction methods for blast damage to structures are based on bomb damage studies from World War II, and a variety of other analytic and experimental sources. Extensive work by Lovelace Foundation over a number of years is the primary basis for the estimates of injury and mortality to people.

Knowledge or estimates of some of the general characteristics of vessels involved in accidental explosions, and explosive yield estimates from Chapter I, will allow one to estimate characteristics of fragments generated by these explosions. The first set of graphs allows estimation of fragment initial velocities. These, and fragment mass and shape distributions, allow use of other graphs to predict fragment terminal velocities and impact conditions. Finally, several curves give probability of fragment arrival versus range. Most of the predictions from this chapter are statistical functions because of the inherent statistical nature of fragmentation. The graphs for fragment initial velocities are based on exercise of computer program developed under this contract and a previous one, supported by limited experimental data. Graphs for mass and shape distributions of fragments are, on the other hand, based entirely on fits of statistical functions to experimental "missile maps".

Once fragment impact conditions are known, one should then be able to estimate effects of such impacts on structures, facilities and people. Chapter V provides data for making some such predictions. These include incipient damage to light structures or panels, and blunt object impact injury to people. Some data on thresholds of penetration of light panels are also given. This part of the workbook is, because of lack of sufficient experimental data or analyses, and in some instances the classified nature of fragment impact effects on humans, less complete than other chapters. Some of the graphs for impact damage are based on tests and analysis of what one might think to be an unrelated field, i.e., i.e., damage to aircraft and ground structures.

The sixth chapter includes a brief discussion of the more complete field of risk assessment, of which damage estimation is a part. We point out that a more complete analysis is needed if one is to estimate the probability of an accident occurring, which type of accident is more probable than another, etc. Most of Chapter VI is devoted to a series of illustrations of use of the methods of Chapters I through V in predicting both blast and fragmentation effects for five accident "scenarios". The five postulated accidents include several which could occur during launch or flight of multi-stage rocket vehicles, or during tests of components in

a test bay or laboratory. Hopefully, study of these examples should lead the reader through the workbook methods for reasonably complete estimates of effects of certain accidents, as opposed to calculation of separate parts of the effects given in previous chapters.

Throughout the workbook, the "tolerances", or possible errors, involved in various calculations are indicated. These are included in various ways, such as error bands about groups of measured data, a range of probabilities of mortality or fragment impact, etc. A wide error band indicates either large inherent spread of data or considerable uncertainty in the method of estimation because it has not been validated by experiment. Factors of safety are not included as such, although use of upper bounds to loading parameters such as blast pressure and impulse or impact velocities of fragments will assure conservation.

CHAPTER VIII

CONCLUSIONS

Some conclusions can be drawn regarding the applications of this workbook, and limitations to its use. These are discussed in this brief chapter.

It is possible using methods given in the workbook to make reasonable estimates of blast wave characteristics over a wide range of distances from the source of the accident. These characteristics can then be used to predict damage to structures, for a number of types of structures and damage modes, and can also be used to predict various levels of injury to and probability of mortality of humans. Confidence in blast damage and injury prediction is good, given knowledge of the blast wave properties, because of extensive past testing and analysis. The blast damage prediction methods are cast in a format which allow their use for other types of explosions.

Prediction methods are given for estimating initial velocities, ranges, masses, and impact conditions for fragments generated by propellant explosions and gas vessel bursts. The methods for predicting initial velocities are reasonably well founded on theoretical analyses and experimental data, and apply over a wide range of simulated burst conditions. Methods for predicting fragment ranges and impact conditions have a good theoretical basis, and can be used for other predictions involving flight through the air of high-velocity objects. Such predictions can be made for objects launched over a very wide range of initial Mach numbers. Methods for predicting fragment mass and shape distributions are entirely based on statistical fits to quite limited data, and therefore involve considerable uncertainty, as well as being impossible to accurately extrapolate.

Some predictions can be made of fragment impact effects on structures and structural elements from graphs and equations given in the workbook. These effects are much less well-known than are blast effects, so only limited predictions are possible. Some effects of fragment impact on humans can also be predicted, but these predictions are limited by security restrictions on wounding potential of fragments. Throughout the workbook, limitations such as this are noted when they are known.

This workbook is hopefully presented in a manner which allows easy use by typical safety engineers. For readers who are interested in the detail behind the relatively simple equations or graphs used to make predictions, a number of detailed appendices are included in appropriate

chapters. We believe that the workbook is the first to provide safety engineers with relatively simple estimates of blast and fragment hazards for accidental explosions in liquid-propellant fueled flight vehicles.

As noted before, some parts of the workbook have wider potential application than explosive hazard prediction for liquid-fueled rockets. The sections on fragment trajectory prediction, or the associated computer programs, can be used to predict ranges and impact conditions for many types of fragments or objects thrown into the air. The sections on blast effects apply for blast loads from any source. The methods for estimating fragment impact damage, though limited, are independent of the sources of these fragments or impacting objects.

CHAPTER IX

RECOMMENDATIONS

This workbook will allow prediction of blast and fragmentation effects for a wide variety of explosive accidents which could occur at aerospace launch and test facilities. It is based on a rather exhaustive review of existing test and accident data; analyses of blast and shock wave physics and effects of such waves on objects and humans; and analyses of fragment velocities, trajectories, impact conditions, and effects of impacts. A number of supporting studies have been made in generating relatively simple application formulas or graphs - these are reported in appropriate appendices.

The bases for the prediction methods given in this workbook range from a firm foundation of extensive testing and analysis, through analyses supported by limited testing or accident reporting, to some predictions which are quite speculative because of little or no corroborating evidence. Predictions in the latter case could often be improved by additional research. Also, some of the methods which have been developed here have potentially wide application to problems in hazards prediction other than explosive effects for flight-weight aerospace vehicles. We therefore give in this short chapter a list of recommendations for areas in which we feel there is a need for additional testing, analysis, or correlation of prediction methods.

Some of these areas are:

- (1) Definition of fragmentation characteristics for bursting gas storage bottles. Existing data consist of only five tests for two bottle geometries, one material, and one gas. There are no reliable "missile maps" for such bursts. Curves for fragment range presented in the workbook are based on computer-generated predictions, which should be validated by test.
- (2) Definition of blast wave characteristics for burst of cylindrical gas storage vessels, either analytically or experimentally. Present methods are limited to essentially spherically symmetric cases.

The analysis in this workbook is based upon data generated by a computer program. It has been confirmed to some extent by experimental data, but more experiments are needed. More work must be done to determine specific

impulse versus distance for gas vessel bursts. Then, a good nomograph should be developed.

The effects of changing the vessel shape from spherical to cylindrical should be investigated, both theoretically and experimentally.

In this analysis of the blast wave, the energy required to burst a pressure vessel and accelerate the fragments was neglected. Analytical and experimental studies would allow this effect to be included in the calculation of the blast wave parameters.

- (3) This workbook deals with very particular types of fragments and targets. The analysis should be extended to include shapes of fragments other than spherical and targets other than metal sheets and plates.

Targets that might be studied include wood, concrete, brick and glass. Also, it may not be desirable to treat the side of a fuel tank as an unsupported metal sheet or plate. There is probably some effect of the liquid, and one is concerned with the possibility of a fragment igniting a fuel tank, in addition to only puncturing it.

Oblique impacts by fragments deserve more study, and the effects of the strength of fragments is presently unknown. A model-scale experimental program is recommended to fill this void.

- (4) We recommend extension of the present work to accidental explosions in thick-walled storage vessels typical of ground transport and storage vessels. The current work is directed toward explosions of flight-weight hardware. Blast and fragmentation characteristics can be drastically different for heavier vessels, and consequently, so can the effects on structures, facilities, vehicles and humans. Included in this work should be exercise of the SPHER and CYLIN codes for typical initial conditions for massive vessels.
- (5) The analyses used to develop scaled curves for fragment range and impact conditions, for both lifting and drag-type fragments, have potentially wider application than generation of some of the scaled curves of Chapter IV. We

recommend that those programs be used to develop more nomographs which include other parameters such as initial altitude of an explosion, flight velocity as a function of this altitude, and additional mass to area ratios typical of ground storage vessels. We also recommend that the programs be used for other types of accidents involving high-velocity missiles or fragments such as the pieces from a turbine rotor burst postulated in the fifth application problem in Chapter VI.

- (6) The existing codes for predicting initial fragment velocities are limited to one space dimension and time (1-D codes). We recommend the development of a limited 2-D code for cylinder fragmentation, based on a combination of the assumptions inherent in the FRAG-2 and CYLIN codes used in this workbook. Such a code should more accurately predict initial fragment velocities for real vessels, but would certainly be more complex and more expensive to run than either of the existing codes.
- (7) As a part of studies of accidental explosions of thick-walled vessels, we recommend a literature search for tests or accident cases, where data on projection of large parts of tanks could be compared with predictions from FRAG-2, which assumes that a tank separates into two pieces which are propelled by the exhausting fluids. Rail tank car accident reports, and burst tests of tank cars conducted at White Sands Missile Range, would perhaps be appropriate sources of such data.
- (8) We recommend using the programs for prediction of fragment ballistics to generate tables for range and terminal impact conditions, such as was done in a limited sense for fragments from bursting gas spheres in Chapter IV. These predictions would supplement, or could conceivably supplant, missile map data for this class of explosion.

The specific recommendations listed before can be supplemented by a last general recommendation. This workbook contains, we believe, the most accurate assessments which can be made based on the current state of the art. In almost all areas covered, either ongoing or future studies may well alter the prediction methods, or the results of applying the prediction methods. The workbook is so organized that alterations or modifications can be made to individual chapters, without a complete revision of the entire book. It is strongly recommended that revisions be considered on some regular schedule, say at two-year intervals.

LIST OF SYMBOLS

A, B, C, D	- terms in equations for bursting vessel motion
A	- presented target area - area of an object presented to the blast front - planform or top surface area of fragment - cross-sectional area of a fragment along its trajectory - mean presented area of object
<u>AD</u>	- average drag area
<u>AL</u>	- average planform area
A_f	- fragment area
A^l	- geometric mean frontal area of glass fragment
a	- radius of a fragment - airfoil curve slope
a_s	- critical sound speed in mass flow equation
a_o	- ambient sound velocity
a_{oo}	- sound speed in confined gas, $\tau = 0$
b	- vehicle track width or depth of target base - number of rotor blades
C_D, C_d	- drag coefficient
C_L	- lift coefficient
C_l	- cylinder length
C_t	- cylinder thickness
$C(\tau)$	- mass of gas confined at high pressure as a function of time

LIST OF SYMBOLS (Cont'd)

D_p	- profile drag
d	- diameter of fragment
	- width of fragment segment
E	- modulus of elasticity
	- effective blast energy
	- bulk modulus
E_l	- end cap length
E_t	- end cap thickness
e	- stored energy ratio
F	- fragment projected area
g	- nondimensionalized displacement of a fragment
	- acceleration of gravity
H	- minimum transverse dimension at location of largest presented area of object
h	- thickness of a target, glass, or plate
	- sphere wall thickness
	- segment height
I	- mass moment of inertia of rotor
\bar{I}	- nondimensional specific impulse
I_d	- total drag and diffraction impulse
I_s	- incident specific impulse
\bar{I}_s	- nondimensional incident specific impulse
i	- initial trajectory angle of the fragment
i_s	- side-on impulse

LIST OF SYMBOLS (Cont'd)

i_0	- threshold impulse
K	- adiabatic exponent (ratio of specific heats)
	- constant (+ if appurtenance is on the ground and 2 if appurtenance is in air)
	- value from the normal distribution table
k	- mass flow rate coefficient
L	- cylinder length
L/D	- length-to-diameter ratio
M	- mass of fragment; of contained gas
\bar{M}	- average mass
M_f	- fragment mass
M_t	- cylindrical shell mass
m	- total mass of target; of fragment
n	- number of fragments
P	- pressure of confined gas
	- crack perimeter about a fragment
\bar{P}	- nondimensional pressure
P_e	- peak overpressure
P_o	- pressure of confined gas at any instant
P_{oo}	- initial pressure of confined gas
P_r	- threshold applied maximum reflected pressure
	- reflected peak overpressure

LIST OF SYMBOLS (Cont'd)

P_r	- peak reflected pressure
P_s	- peak side-on overpressure
P_*	- nondimensional pressure
P_o	- ambient air pressure
$p(t)$	- net transverse pressure
Q	- peak dynamic pressure
	- peak dynamic overpressure
R	- gas constant
	- sphere radius before burst
	- radius of rotor
	- initial cylinder radius
r	- distance from center of a vessel
	- cylinder radius
	- disc radius
	- fragment displacement at any instant
SE	- strain energy stored in vessel
s	- estimate for the standard deviation
s	- segment length
T	- duration of the positive phase of the blast wave
	- temperature
T_o	- temperature of confined gas at any instant

LIST OF SYMBOLS (Cont'd)

T_{∞}	- temperature
t	- thickness of fragment; disc; window pane
t_a	- time of arrival
t_h	- shell thickness
U	- shock velocity
U_s	- peak particle velocity
V	- velocity of fragment
	- volume
\bar{V}	- nondimensional velocity
	- initial velocity ratio
V_c	- rotor blade velocity along rotational axis
V_i	- volume of the vessel before it bursts
	- initial fragment velocity
V_{in}	- induced velocity from thrust
V_o	- volume of confined gas at any instant
V_s	- volume of shell material
V_t	- tip velocity of rotor
V_{50}	- ballistic limit velocity
W	- effective mass of propellant
\bar{W}	mean mass
W_T	- total mass of propellant and oxidizer
w	- crack width

LIST OF SYMBOLS (Cont'd)

X	- displacement of an object
	- distance from the front of object to location of largest cross-sectional area
	- the distance from the front of the object to the plane facing the approaching blast wave
\dot{X}	- horizontal velocity
\ddot{X}	- horizontal acceleration
x	- short halfspan
	- nondimensionalizing constant for displacement
Y	- terminal blast yield
\dot{Y}	- vertical velocity
\ddot{Y}	- vertical acceleration
y	- edge length
	- long half span
α	- nondimensional constant
α_i	- initial trajectory angle
β	- nondimensional constant
δ	- permanent deflection of target at point of impact
Δt	- time increment
ϵ	- nondimensionalizing constant for time
θ	- angle of attack of disc
	- angle subtended at the center of the cylinder by a fragment $\tau = 0$

LIST OF SYMBOLS (Cont'd)

κ	- ratio of specific heats for confined gas
γ	- ratio of specific heats for confined gas
ν	- Poisson's ratio for the material
ξ	- nondimensionalized time
ρ	- density of glass, air
ρ_0	- confined gas density at any instant
ρ_p	- density of a fragment (or projectile)
ρ_r	- density of fragment
ρ_s	- density of shell material
	- peak density in shock wave
ρ_t	- density of target
ρ_c	- critical density of gas in mass flow equation
σ_t	- yield stress of target material
σ_y	- yield stress of glass; plate
	- stress in container wall
τ	- time
Φ_i	- impulse shape factors
Φ_p	- pressure shape factors
ω	- angular velocity

CONVERSION FACTORS

The following table provides multiplying factors for converting numbers and miscellaneous units to corresponding new numbers and SI units.

The first two digits of each numerical entry represent a power of 10. An asterisk follows each number which expresses an exact definition. For example, the entry "-02 2.54*" expresses the fact that 1 inch = 2.54×10^{-2} meter, exactly, by definition. Most of the definitions are extracted from National Bureau of Standards documents. Numbers not followed by an asterisk are only approximate representations of definitions, or are the results of physical measurements.

<u>To convert from</u>	<u>to</u>	<u>multiply by</u>
atmosphere	newton/meter ²	+05 1.013 25*
bar	newton/meter ²	+05 1.00*
British thermal unit (mean)	joule	+03 1.055 87
calorie (mean)	joule	+00 4.190 02
dyne	newton	-05 1.00*
erg	joule	-07 1.00*
Fahrenheit (temperature)	Celsius	$t_C = (5/9)(t_F - 32)$
foot	meter	-01 3.048*
inch	meter	-02 2.54*
lb _f (pound force, avoirdupois)	newton	+00 4.448 221 651 260 5*
lb _m (pound mass, avoirdupois)	kilogram	-01 4.535 923 7*
pascal	newton/meter ²	+00 1.00*
pound force (lb _f avoirdupois)	newton	+00 4.448 221 615 260 5*
pound mass (lb _m avoirdupois)	kilogram	-01 4.535 923 7*
poundal	newton	-01 1.382 549 543 76*
slug	kilogram	+01 1.459 390 29

<u>To convert from</u>	<u>to</u>	<u>multiply by</u>
foot/second ²	meter/second ²	-01 3.048 ⁰
inch/second ²	meter/second ²	-02 2.54 ⁰
gram/centimeter ³	kilogram/meter ³	+03 1.00 ⁰
lb _m /inch ³	kilogram/meter ³	+04 2.767 990 5
lb _m /foot ³	kilogram/meter ³	+01 1.601 846 3
slug/foot ³	kilogram/meter ³	+02 5.153 79
lb _f /foot ²	newton/meter ²	+01 4.788 025 8
lb _f /inch ² (psi)	newton/meter ²	+03 6.894 757 2
foot/second	meter/second	-01 3.048 ⁰
inch/second	meter/second	-02 2.54
foot ³	meter ³	-02 2.831 684 659 2 ⁰
inch ³	meter ³	-05 1.638 706 4 ⁰

GLOSSARY OF TERMS

Air-embolic insult - air bubbles circulating in the blood which can contribute to the collapse of the heart.

Angle of attack - angle between fragment horizontal axis and the relative wind vector.

Applied impulse - actual impulsive loading applied to a "target".

Appurtenance - a piece of equipment or an object located near a source of an explosion, which can be accelerated by the blast wave from the explosion.

Blast yield - energy release in an explosion inferred from measurements of the characteristics of blast waves generated by the explosion.

Blunt trauma - injury caused by a nonpenetrating object.

Burst pressure - the pressure at which a gas storage vessel bursts or fails.

CBGS - Confined by Ground Surface. This abbreviation designates a liquid propellant explosion occurring on the ground after spill and mixing.

CBM - Confined by Missile. This abbreviation designates an explosion within the tankage of a liquid propellant vessel or rocket.

Critical threshold impulse - blast wave impulse which determines the impulse asymptote for an isodamage contour.

Drag coefficient - ratio of drag force to dynamic force exerted by wind pressure on a reference area.

Edema - abnormal accumulation of fluid in connective tissues causing local swelling.

Energy of detonation - the energy in an explosion which drives a blast wave.

Event tree - a method employed in risk assessment for systematic estimation of consequences of an accident.

Explosive yield - energy released in an explosion, often expressed as a percent or fraction of energy which would be released by the same mass of a standard high explosive such as TNT.

FMECA - abbreviation for Failure Mode Effects and Criticality Analysis. A systematic procedure for identifying failure modes of a system and for evaluating consequences of failures.

Fall-back - an accident in which a launch vehicle settles or falls back to earth in initial stages of launch.

Fault tree - a method employed in risk assessment for determining probabilities for event trees (see event tree).

Fibrotic foci - fine scars of the lungs.

Free-field impulse - see side-on impulse.

Free-field pressure - see side-on overpressure.

HVI - High Velocity Impact. This abbreviation designates a liquid propellant explosion occurring after a vehicle with unburned propellant impacts the earth at relatively high velocity.

Ignition time - time after beginning of an accident involving liquid propellants at which initiation of an explosion occurs.

Induced velocity - velocity along rotor axis, induced by thrust generated by the whirling blade.

Initial trajectory angle - angle of fragment's horizontal axis relative to the ground surface at the beginning of the flight.

Isodamage line - Loci of combinations of overpressure and impulse which produce the same level of blast damage to a given "target".

Lift coefficient - ratio of lift force to dynamic force exerted by wind pressure on a reference area.

Limit velocity (V_{50}) - impact velocity, for a fragment or missile striking a target, at which 50% perforations occur.

Major structural damage - damage to a residence involving partial or total collapse of roof, partial demolition of one or two external walls, or severe damage to load-bearing partitions requiring replacement.

Minor structural damage - damage to a residence involving window breakage and wall and support cracking.

Overpressure - pressure in a blast wave above atmospheric pressure.

Partial demolition - damage to a residence in which 50% to 75% of the external brick work is destroyed, or the building is rendered so unsafe that it must be demolished.

Planform area - the area viewed by looking down on the fragment - top surface area.

Plate aspect ratio - ratio of length to width for a rectangular plate.

Projected area - area of fragment viewed perpendicular to the top surface area.

Pulmonary hemorrhage - internal bleeding occurring in the lungs.

Reflected impulse - integral of reflected pressure-time history.

Relative wind vector - vector along which the fragment flies.

Side-on impulse - integral of time history of side-on overpressure.

Side-on overpressure - blast wave overpressure in an undisturbed blast wave.

Standoff distance - distance from center of an explosion.

Temporary threshold shift - the case where 90 percent of those exposed to a blast wave advancing at normal angle of incidence to the earth are not likely to suffer an excessive degree of hearing loss.

Terminal yield - blast yield from measurements made far enough from an explosion that the waves are similar to those generated by a specified mass of TNT.

Threshold bending impulse - blast wave impulse which produces an incipient bending failure.

Threshold membrane impulse - blast wave impulse which produces an incipient stretching failure.

BIBLIOGRAPHY

Ablow, C. M and R. W. Woolfolk, "Blast Effects from Non-Ideal Explosions," SRI Final Report, Contract No. 0017-71-C-4421, Stanford Research Institute, Menlo Park, California, December 1972.

Adderton, D. V., "Gas Inferno Rages," The News Gazette, Champaign, Illinois, September 15, 1974.

Ahlers, E. B., "Fragment Hazard Study," Minutes of the Eleventh Explosives Safety Seminar, pp. 81-107, September 1969.

Alstor, J., Editor, Proceedings of the Conference on Mechanisms of Explosion and Blast Waves, Sponsored by The Joint Technical Coordinating Group for Air Launched Non-Nuclear Ordnance Working Party for Explosives, November 1973.

Anderson, W. H. and N. A. Louie, "Effect of Energy Release Rate on the Blast Produced by Fuel-Air Explosions," SH-TR-75-01, Shock Hydrodynamics Division, Whittaker Corporation, North Hollywood, California, January 1975.

Angiullo, F. J., "Explosion of a Chloronitrotoluene Distillation Column," Paper No. 90a, Presented at the AIChE Symposium on Loss Prevention in the Chemical Industry, Houston, Texas, March 18-20, 1975; to be published in the Loss Prevention Journal, Vol. 8, 1975.

Anonymous, "Essais D'Ependage de Gas Naturel Liquefie Sur de Sol," Report on the experiments conducted by Gas De France, September 1972.

Anonymous, SIV All Systems Vehicle Malfunction, Douglas Missile & Space Division, Santa Monica, California, January 24, 1964.

Anonymous, "Spacecraft Incident Investigation, Panel I," Vols. I, II and III, NASA TMX-66922, 66921 and 66934, June, July and September 1970.

Anonymous, "Summary Report on a Study of the Blast Effect of a Saturn Vehicle," Report No. C63850, Arthur D. Little, Inc., Cambridge, Massachusetts, February 1962.

Bach, G. G., and J. H. S. Lee, "An Analytic Solution for Blast Waves," AIAA Journal, Vol. 8, pp. 271-275, 1970.

Baker, W. E., "An Accidental Acetylene-Air Explosion," letter report, September 1974.

Baker, W. E., Explosions in Air, University of Texas Press, Austin, Texas, May 1973.

Baker, W. E., "Scale Model Tests for Evaluating Outer Containment Structures for Nuclear Reactors," Proceedings of the Second International Conference on the Peaceful Uses of Atomic Energy, United Nations, Geneva, Vol. 11, pp. 79-84, 1958.

Baker, W. E., W. D. Ewing, Jr., and J. W. Hanna, Laws For Large Elastic Response And Permanent Deformation of Model Structures Subjected to Blast Loading, BRL Report No. 1060, December 1958.

Baker, W. E., V. B. Parr, R. L. Bessey, and P. A. Cox, "Assembly and Analysis of Fragmentation Data for Liquid Propellant Vessels," NASA CR-134538, NASA Lewis Research Center, January 1974.

Baker, W. E., S. Silverman, P. A. Cox, and D. Young, "Methods of Computing Structural Response of Helicopters to Weapons Muzzle and Breech Blast," The Shock and Vibration Bulletin, 40, Part 2, pp. 227-241, December 1969.

Baker, W. E., S. Silverman and T. D. Dunham, "Studies of Explosions in the NASA-MSC Vibration and Acoustic Test Facility (VATF)", Final Report on Contract NAS9-7749, Southwest Research Institute, March 1968.

Baker, W. E. and P. S. Westine, "Methods of Predicting Loading and Blast Field Outside Suppressive Structures," Minutes of 16th Annual Explosive Safety Seminar, Department of Defense Safety Board, 1974.

Baker, W. E., P. S. Westine, and R. L. Bessey, "Blast Fields About Rockets and Recoilless Rifles," Final Technical Report Contract No. DAAD05-70-C-0170, Southwest Research Institute, San Antonio, Texas, May 1971.

Baker, W. E., P. S. Westine, and F. T. Dodge, Similarity Methods in Engineering Dynamics: Theory and Practice of Scale Modeling, Spartan Books, Rochell Park, New Jersey, 1973.

Bendler, A. J., J. K. Roros, and N. H. Wagner, "Fast Transient Heating and Explosion of Metals Under Stagnant Liquids," AECU-3623, Contract AT (30-3)-187, Task II, Columbia University, Department of Chemical Engineering, February 1958.

Bethe, H. A., K. Fuchs, H. O. Hirschfelder, J. L. Magee, R. E. Peierls, and J. von Neumann, "Blast Wave," LASL 2000, Los Alamos Scientific Laboratory, August 1947, distributed March 27, 1958.

Bethe, H. A., K. Fuchs, J. von Neumann, R. Peierls, and W. G. Penney, "Shock Hydrodynamics and Blast Waves," AECE 2860, October 1944.

Boger, R. C. and G. D. Waldman, "Blast Wave Interactions from Multiple Explosions," Paper No. XII, Proceedings of the Conference on Mechanisms of Explosion and Blast Waves, J. Alstor, Editor, Sponsored by The Joint Technical Coordinating Group for Air Launched Non-Nuclear Ordnance Working Party for Explosives, November 1973.

Bogo, V., R. A. Hutton, and A. Bruner, "The Effects of Airblast on Discriminated Avoidance Behavior in Rhesus Monkey," Technical Report to Defense Atomic Support Agency, DASA 2659, Lovelace Foundation for Medical Education and Research, AD 742819, March 1971.

Bowen, I. G., E. R. Fletcher, D. R. Richmond, "Estimate of Man's Tolerance to the Direct Effects of Air Blast," Technical Report to Defense Atomic Support Agency, DASA 2113, Lovelace Foundation for Medical Education and Research, AD 693105, October 1968.

Boyer, D. W., H. L. Brode, I. I. Glass, and J. G. Hall, Blast From a Pressurized Sphere, UTIA Report No. 48, Institute of Aerophysics, University of Toronto, 1958.

Bracco, F. V., "Air Blast Parameters Close to a Liquid Propellant Explosion," ICRPG Hazards Working Group Publication 113, June 1966; 2nd Meeting Bulletin CPIA, Silver Spring, Maryland (Includes response by A. B. Willoughby).

Brasie, W. C. and D. W. Simpson, "Guidelines for Estimating Damage from Chemical Explosions," Preprint 21A, Paper presented at the Symposium on Loss Prevention in the Process Industries, 63rd National Meeting AIChE, St. Louis, Missouri, February 1968.

Brinkley, S. R., "Determination of Explosion Yields," AICHE Loss Prevention, Vol. 3, pp. 79-82, 1969.

Brinkley, S. R., "Shock Waves in Air Generated by Deflagration Explosions," Paper presented at Disaster Hazards Meeting of CSSCI, Houston, Texas, April 1970.

Brinkley, S. R., and J. G. Kirkwood, "Theory of the Propagation of Shock Waves," Phys. Rev., Vol. 71, p. 606, 1947.

Brode, H. L., "Blast Wave From a Spherical Charge," Physics of Fluids, Vol. 2, No. 217, 1959.

Brode, H. L., "Numerical Solutions of Spherical Blast Waves," J. App. Phys., Vol. 26, pp. 766-775, 1955.

Brown, J. A., A Study of the Growing Danger of Detonation in Unconfined Gas Cloud Explosions, John Brown Associates, Inc., Berkeley Heights, New Jersey, December 1973.

Burenin, P. I., "Effect of Shock Waves," Final Report on Contract NASA-2485, Techtran Corporation, March 1974.

Burgess, D. S., J. N. Murphy, N. E. Hanna, and R. W. Van Dolah, "Large Scale Studies of Gas Detonations," Report of Investigations 7196, U. S. Department of the Interior, Bureau of Mines, Washington, D. C., November 1968.

Burgess, D. S., J. N. Murphy, and M. G. Zabetakis, "Hazards Associated with Spillage of Liquefied Natural Gas on Water," U. S. Bureau of Mines, RI 7448, November 1970.

Burgess, D. S., J. N. Murphy, and M. G. Zabetakis, "Hazards of LNG Spillage in Marine Transportation," SRC Report #S-4105, Final Report, MIPR No. Z-70099-9-92317. Project 714152, U. S. Coast Guard, Washington, D.C., February 1970.

Burgess, D. S., J. N. Murphy, M. G. Zabetakis, and H. E. Perlee, Volume of Flammable Mixtures Resulting from the Atmospheric Dispersion of a Leak or Spill, Fifteenth International Symposium on Combustion, The Combustion Institute, Pittsburgh, Pennsylvania, Paper #29 (in press).

Burgess, D. S. and M. G. Zabetakis, Detonation of a Flammable Cloud Following a Propane Pipeline Break, The December 9, 1970, Explosion in Port Hudson, Missouri, Report of Investigations 7752, U. S. Department of the Interior, Bureau of Mines, Washington, D. C., 1973.

Burgess, D. S. and M. G. Zabetakis, "Fire and Explosion Hazards Associated with Liquefied Natural Gas," U. S. Department of the Interior, RI 6099, 1962.

Carmichael, J. B., Jr. and H. E. von Gierke, "Biodynamic Applications Regarding Isolation of Humans from Shock and Vibration," Aerospace Medical Research Laboratory, Wright-Patterson Air Force Base, Ohio, AD 770316, September 1973.

Carter, P. B., Jr., "A Method of Evaluating Blast Parameters Resulting from Detonation of Rocket Propellants," AEDC-TDR-64-200, Arnold Engineering Dev. Center, Air Force Systems Command, Ad 450140, October 1964.

Champion, K. S. W., W. J. O'Sullivan, Jr., and Sidney Jeweles, U. S. Standard Atmosphere, 1962, U. S. Government Printing Office, Washington, D. C., December 1962.

Charney, M., "Explosive Venting Versus Explosion Venting," Presented at AIChE Petrochemical Refining Exposition, Houston, Texas, February 2, 1967.

Charney, M., "Flame Inhibition of Vapor Air Mixture," Presented to AIChE Petrochemical and Refining Exposition, New Orleans, Louisiana, March 18, 1969.

Chelson, Paul O., "Reliability Computation Using Fault Tree Analysis," JPL-TR-32-1542, NASA CR 124740, December 1, 1971.

Clayden, W. A., Editor, "Symposium: The Problems Arising from Gunfire and Detonation Noise," Tech. Report 1/71, Ministry of Defence, CSR (A), England, 1971.

Clemedson, Carl-Johan, Gustav Hellström, and Sten Lingren, "The Relative Tolerance of the Head, Thorax, and Abdomen to Blunt Trauma," Annals of the New York Academy of Sciences, Vol. 152, Art. 1, October 1968.

Coevert, K., Th. M. Groothuizen, H. J. Pasman, and R. W. Trese, "Explosions of Unconfined Vapour Clouds," Presented at the Loss Prevention Symposium, The Hague, Netherlands, May 1974.

Cohen, Edward, Consulting Editor, "Prevention of and Protection Against Accidental Explosion of Munitions, Fuels and Other Hazardous Mixtures," Annals of the New York Academy of Sciences, Vol. 152, Art. 1, PP. 1-913, October 28, 1968.

Cole, R. H., Underwater Explosions, Dover Publications, Inc., 1965.

Corben, H. C., "Power Bursts In Nuclear Reactors," RWC 22-127, Contract AT (04-3)-165 with U. S. AEC, The Ramo-Wooldridge Corporation, Los Angeles, California, September 1958.

Cox, P. A. and E. D. Esparza, "Design of a Suppressive Structure for a Melt Loading Operation," Minutes of 16th Annual Explosion Safety Seminar, Department of Defense Safety Board, 1974.

Cranz, C., Lehrbuch der Ballistik, Springer-Verlag, Berlin, 1926.

Craven, A. D. and T. R. Grieg, "The Development of Detonation Over-Pressures in Pipelines," I. Chem. E. Series No. 25, Institution of Chemical Engineers, London, 1968.

Crocker, M. J. and R. R. Hudson, "Structural Response to Sonic Booms," J. Sound & Vibration, Vol. 9, pp. 454-468, 1969.

Custard, G. H. and J. R. Thayer, "Evaluation of Explosive Storage Safety Criteria," Falcon Research and Development Co., Contract DAHC04-69-C-0095, March 1970.

Custard, G. H. and J. R. Thayer, "Evaluation of Explosive Blast," Falcon Research and Development Co., September 1970.

Dabora, E. K., "Variable Energy Blast Waves," AIAA Journal, Vol. 10, p. 1385, 1972.

Dabora, E. K., M. N. Director and R. L. Stoy, "Analytical and Experimental Studies of Variable Energy Blast Waves," Paper #III, Proceedings of the Conference on Mechanisms of Explosion and Blast Waves, J. Alstor, Editor, Sponsored by The Joint Technical Coordinating Group for Air Launched Non-Nuclear Ordnance Working Party for Explosives, November 1973.

Damon, Edward G., Ernest A. Henderson, and Robert K. Jones, "The Effects of Intermittent Positive Pressure Respiration on Occurrence of Air Embolism and Mortality Following Primary Blast Injury," Technical Report to Defense Nuclear Agency, DNA 2989F, Lovelace Foundation for Medical Education and Research, AD 754448, January 1973.

Damon, Edward G., Donald R. Richmond, E. Royce Fletcher, and Robert K. Jones, "The Tolerance of Birds to Airblast," Final Report to Defense Nuclear Agency, DNA 3314F, Lovelace Foundation for Medical Education and Research, AD 785259, July 1974.

Damon, Edward G., John T. Yelverton, Ulrich C. Luft, Kabby Mitchell, Jr., and Robert K. Jones, "The Acute Effects of Air Blast on Pulmonary Function in Dogs and Sheep," Technical Progress Report to Defense Atomic Support Agency, DASA 2461, Lovelace Foundation for Medical Education and Research, AD 709972, March 1970.

Damon, Edward G., John T. Yelverton, Ulrich C. Luft, and Robert K. Jones, "Recovery of the Respiratory System Following Blast Injury," Technical Progress Report to Defense Atomic Support Agency, DASA 2580, Lovelace Foundation for Medical Education and Research, AD 718369, October 1970.

Dartnell, R. C. and T. A Ventrone, "Explosion of a Para-Nitro-Meta-Cresol Unit," Loss Prevention, Vol. 5, pp. 53-56, 1971.

Deese, J. H., "Test Conductors Damage Assessment Report on Auto-Ignition LO₂/LH₂ Mixing Test Experimental Expansion of March 2, 1972," Systems Engineering Division, Kennedy Space Center, NASA.

Dewey, J. M. and J. Sperrazza, "The Effect of Atmospheric Pressure and Temperature on Air Shock," BRL Report 721, Aberdeen Proving Ground, Maryland, 1950.

Dietrich, J. R., "Experimental Investigation of the Self-Limitation of Power During Reactivity Transients in a Subcooled, Water-Moderated Reactor (Borax-I Experiments)," AECD-3668, Argonne National Laboratories, Lemont, Illinois, 1954.

Dow Chemical Company, "Fire and Explosion, Dow's Safety and Loss Prevention Guide. Hazard Classification and Protection," Editor, Chem. Eng. Progress, American Institute of Chemical Engineering, New York, 1973.

Doyle, W. H., "Estimating Losses," Paper presented at CSSCI Meeting in Houston, Texas, April 1970.

Doyle, W. H., "Industrial Explosions and Insurance," Loss Prevention Vol. 3, pp. 11-17, 1969.

Farber, E. A., "Characteristics of Liquid Rocket Propellant Explosion Phenomena, No. 448, Part VIII, Prediction of Explosive Yield and Other Characteristics of Liquid Propellant Rocket Explosions," Vol. XXIII, No. 11, Engineering Progress at the University of Florida, November 1969.

Farber, E. A., "Characteristics of Liquid Rocket Propellant Explosion Phenomena Series, Report No. IX, Critical Mass (Hypothesis and Verification) of Liquid Rocket Propellants," University of Florida, Gainesville, Florida, September 1971.

Farber, E. A., "Explosive Yield Limiting Self-Ignition Phenomena in LO₂/LH₂ and LO₂/RP-1 Mixtures," Minutes of the 15th Explosives Safety Seminar, San Francisco, California, September 18-20, 1973, Department of Defense Explosives Safety Board, 1287-1304.

Farber, E. A. and J. H. Deese, "A Systematic Approach for the Analytical Analysis and Prediction of the Yield from Liquid Propellant Explosions," Tech. Paper No. 347, Eng. Progress at the University of Florida, Vol. XX, No. 3, March 1966.

Farber, E. A., F. W. Klement, and C. F. Bonzon, "Prediction of Explosive Yield and Other Characteristics of Liquid Propellant Rocket Explosions," Final Report Contract NAS 10-1255, University of Florida Engineering Experiment Station, October 31, 1968.

Farber, E. A., J. H. Smith, and E. H. Watts, "Electrostatic Charge Generation and Auto-Ignition Results of Liquid Rocket Propellant Experiments," Report No. X, University of Florida, Gainesville, Florida, October 1972.

Feinstein, D. I., "Fragmentation Hazard Evaluations and Experimental Verification," Minutes of 14th Explosives Safety Seminar, Defense Explosives Safety Board, pp. 1099-1116, New Orleans, Louisiana, November 8-10, 1972.

Feinstein, D. I., "Fragmentation Hazards to Unprotected Personnel," TR IITRI-J6176, January 1972.

Feinstein, D. I. and H. H. Nazooka, "Fragment Hazards From Detonation of Multiple Munitions in Open Stores," TR IITRI-J6176, August 1971.

Fletcher, E. R., D. R. Richmond, and R. K. Jones, "Airblast Effects on Windows in Buildings and Automobiles on the Eskimo II Event," Minutes of the Fifteenth Explosive Safety Seminar, Vol. I, September 18-20, 1973, San Francisco, California, Sponsored by Department of Defense Explosives Safety Board, Washington, D. C., pp. 251-275.

Fletcher, E. R., D. R. Richmond and R. K. Jones, "Blast Displacement of Prone Dummies," Technical Report for Defense Nuclear Agency, DASA 2710, Lovelace Foundation for Medical Education and Research, AD 730753, June 1971.

Fletcher, E. R., D. R. Richmond, and R. K. Jones, "Velocities, Masses and Spatial Distribution of Glass Fragments from Windows Broken by Airblast," Report in preparation for Defense Nuclear Agency, Washington, D. C.

Fletcher, E. R., "A Model to Simulate Thoracic Responses to Air Blast and to Impact," Aerospace Medical Research Laboratory, Paper No. 1, Wright-Patterson Air Force Base, Ohio, AD 740438, December 1971.

Fletcher, R. F., "Characteristics of Liquid Propellant Explosions," Annals of New York Academy of Science, Vol. 152, No. I, pp. 432-440, October 1968.

Fletcher, R. F., "Liquid-Propellant Explosions," Jour. of Spacecraft and Rockets, Vol. 5, No. 10, pp. 1227-1229, October 1968.

Forrest, M. R., "Evaluation of Hazard to Hearing from Impulsive Noise," Report APRE 23/73 (R), Ministry of Defence, Army Personnel Res. Estab., England, 1973.

Freeman, R. H., and M. P. McCready, "Butadiene Explosion at Texas City - 2," Chemical Engineering Progress, Vol. 67, No. 6, pp. 45-50, June 1971.

Freeman, R. H. and M. P. McCready, "Butadiene Explosion at Texas City - 2," Loss Prevention, Vol. 5, pp. 61-66, 1971.

Freese, R. E., "Solvent Recovery from Waste Chemical Sludge -- An Explosion Case History," Loss Prevention, Vol. 7, pp. 108-112, 1973.

Freytag, H. H., Editor, Handbuch der Raumexplosionen, Verlag Chemie, GMBH, Weinheim/Bergstr., 1965.

Fugelso, L. E., L. M. Weiner, T. H. Schiffman, "A Computation Aid for Estimating Blast Damage from Accidental Detonation of Stores Munitions," Minutes of 14th Explosive Safety Seminar, New Orleans, Louisiana, November 8-10, 1973, Department of Defense Explosives Safety Board, pp. 1139-1166.

Gates, R. W., "Containment of Fragments from a Runaway Reactor," Stanford Research Institute, Menlo Park, California, SRIA-117, AEC Research and Development Report UC-80, Reactor Technology TID-4500 (27th Edition), February 15, 1964. Final Report prepared for U. S. Atomic Energy Commission, Contract No. AT (04-3)-115, Project Agreement No. 2.

Gayle, J. B., C. H. Blakewood, J. W. Bransford, W. H. Swindell, and R. W. High, "Preliminary Investigation of Blast Hazards of RP-1/LOX and LH₂/LOX Propellant Combinations," NASA TM X-53240, George C. Marshall Space Flight Center, Huntsville, Alabama, April 1965.

Gerberich, W. W. and G. S. Baker, "Toughness of Two-Phase 6Al-4V Titanium Microstructures," in Applications Related Phenomena in Titanium Alloys, ASTM Special Publication No. 432, 1968.

Glasstone, S., "The Effects of Nuclear Weapons, U. S. Government Printing Office, Revised Edition, April 1962.

Goodman, H. S., "Compiled Free Air Blast Data on Bare Spherical Lentolite," BRL Report 1092, Aberdeen Proving Ground, Maryland, 1960.

Greenfield, Sidney H., "Hail Resistance of Roofing Products," U. S. Department of Commerce, National Bureau of Standards, Building Science Series 23, August 1969.

Grodzovski, G. L., and F. A. Kukanov, "Motion of Fragments of a Vessel Bursting in a Vacuum," Soviet Engineering Journal, March/April 1965.

Guirao, C. M., J. H. Lee, and G. G. Bach, The Propagation of Non-Ideal Blast Waves, AFOSR Interim Scientific Report, AFOSR-TR-74-0187, Department of Mechanical Engineering, McGill University, Montreal, January 1974.

Gurney, R. W., "Fragmentation of Bombs, Shells, and Grenades," BRL Report 635, March 1947.

Gurney, R. W., "The Initial Velocities of Fragments from Bombs, Shells, and Grenades," BRL Report 405, 1943.

Gwaltney, R. C., "Missile Generation and Protection in Light-Water-Cooled Power Reactor Plant," ORNL-NSIC-22, Oak Ridge National Laboratory, September 1968.

Hahn, Gerald J., and Shapiro, Samuel S., Statistical Models in Engineering, John Wiley and Sons Inc., New York, 1967.

Halverson, LCDR F. H., "A Review of Some Recent Accidents in the Marine Transportation Mode," Paper No. 52e, Presented at the AIChE Symposium on Loss Prevention in the Chemical Industry, Houston, Texas, March 18-20, 1975; to be published in the Loss Prevention Journal, Vol. 8.

Hansen, J. V. E., "Body Armor Evaluation," National Defense, pp. 312-313, January-February 1975.

Henry, L. G., "The Gurney Formula and Related Approximations for the High-Explosive Deployment of Fragments," Hughes Aircraft Company, Report No. PUB-189, Culver City, California, April 1967.

Heppner, L. D. and J. E. Steedman, "Drag Coefficient for Fragment Simulating Projectiles, 20 MM, Caliber. 50, and Caliber .30," APG DPS-286, AD 822-489, August 1961.

High, R. W., "The Saturn Fireball," Annals of New York Academy of Science, Vol. 152, Art. 1, pp. 441-451, October 1968.

Hirsch, A. E., "The Tolerance of Man to Impact," Annals of the New York Academy of Sciences, Vol. 152, Art. 1, pp. 168+, October 1968.

Hoerner, S. F., Fluid-Dynamics Drag, Published by the Author, Midland Park, New Jersey, 1958.

Hopkinson, B., British Ordnance Board Minutes 13565, 1915.

Howard, W. B., "Interpretation of a Building Explosion Accident," Loss Prevention, Vol. 6, pp. 68-73, 1972.

Huang, S. L. and P. C. Chou, "Calculations of Expanding Shock Waves and Late-State Equivalence," Final Report, Contract No. DA-18-001-AMC-876 (X), Report 125-12, Drexel Institute of Technology, Philadelphia, Pennsylvania, April 1968.

Hunt, D. L., F. J. Walford and F. C. Wood, "An Experimental Investigation into the Failure of a Pressure Vessel Containing High Temperature Pressurized Water," AEEW-R 97, United Kingdom Atomic Energy Authority, Reactor Group, September 1961.

Iotti, R. C., W. J. Krotiuk, and D. R. DeBoisblanc, "Hazards to Nuclear Plants from On (or Near) Site Gaseous Explosions," Ebasco Services, Inc., 2 Reactor Street, New York, New York, 1974.

Iverson, J. H., Summary of Existing Structures Evaluation, Part II: Window, Glass and Applications, Stanford Research Institute Contract No. OCD-DAHC20-67-C-0136 with Office of Civil Defense, December 1968.

Jarrett, D. E., "Derivation of the British Explosive Safety Distances," Annals of the New York Academy of Sciences, Vol. 152, Art. 1, pp. 32-33, October 1968.

Jarvis, H. C., "Butadiene Explosions at Texas City - 1," Loss Prevention, Vol. 5, pp. 57-60.

Jeffers, S. L., "Fragment Velocity Measurements from Three Project Pyro Experiments," Report SC-DR-69-329, Aerospace Nuclear Safety Department 9510, Sandia Laboratories, Albuquerque, New Mexico, June 1969.

Jensen, Andreas V., Editor, "Chemical Rocket/Propellant Hazards, Vol. I. General Safety Engineering Design Criteria," Chemical Propulsion Information Agency, CPIA Publication No. 194, Vol. I, October 1971.

Johnson, O. T., R. D. Mayerhofer, and W. J. Schuman, Jr., Effect of Blast Upon Simulated and Actual Missiles (Project 14 Operation Snow Ball) (U), BRL Memorandum Report #1655, May 1965.

Kaleps, Ints, and Henning E. von Gierke, "A Five-Degree-Of-Freedom Mathematical Model of the Body," Aerospace Medical Research Laboratory, Paper No. 8, Wright-Patterson Air Force Base, Ohio, AD 740445.

Kanda, Kazuo, "Subsystem Safety Analysis Techniques," Annals of Reliability and Maintainability, pp. 291-297, 1965.

Kangas, Pell, "Hailstone Impact Tests on Aircraft Structural Components," Civil Aeronautics Administration Technical Development and Evaluation Center, Technical Development Report No. 124, Indianapolis, Indiana, September 1950.

Kazarian, L. E. and H. E. von Gierke, "The Effects of Hypogravic and Hypodynamic Environments on the Skeletal System and Acceleration Tolerance," Aerospace Medical Research Laboratory, Paper No. 16, Wright-Patterson Air Force Base, Ohi, AD 740453, December 1971.

Kennedy, W. D., "Explosions and Explosives in Air," Effects of Impact and Explosion, M. T. White, Editor, Summary Technical Report of Div. 2, NDRC, Vol. 1, Washington, D. C., AD 221586, 1946.

Kingery, C. N. and B. F. Pannill, "Peak Overpressure Versus Scaled Distance for TNT Surface Burst (Hemispherical Charges)," BRL Memo Report No. 1518, Aberdeen Proving Ground, Maryland,

Kinnersly, P. "What Really Hapened at Flixborough?" New Scientist, Vol 65, (938), pp. 520-522, February 27, 1972

Kinney, G. F., "Engineering Elements of Explosions," NWC TP4654, Naval Weapons Center, China Lake, California, AD 844917, November 1968.

Kinney, G. F., Explosive Shocks in Air, MacMillan, New York, New Yor, 1962.

Kiwan, A. R., "TAE Flow Calculations Using AFAMF Code (U)," BRL Report 1547, Ballistics Research Laboratories, Aberdeen Proving Ground, Maryland, September 1971.

Kiwan, A. R., "Gas Flow During and After the Deflagration of a Spherical Cloud of Fuel-Air Mixture," BRL R-1511, Ballistic Research Laboratories, Aberdeen Proving Ground, Maryland, November 1970.

Kiwan, A. R., "Self-Similar Flow Outside an Expanding Sphere," BRL Report 1495, Ballistic Research Laboratories, Aberdeen Proving Ground, Maryland, September 1970.

Kletz, T. A., "Lessons to be Learned from Flixborough," Paper No. 67F, Presented at the AIChE Symposium on Loss Prevention in the Chemical Industry, Houston, Texas, March 18-20, 1975; to be published in the Loss Prevention Journal, Vol. 8, 1975.

Kokinakis, William, "A New Methodology for Wounding and Safety Criteria," Proceedings of the 16th Explosive Safety Seminar, pp. 1209-1226, September 1974.

Korobeinikov, V. P., N. S. Mil'nikova, and Ye. V. Ryazanov, The Theory of Point Explosion, Fizmatgiz, Moscow, 1961; English translation, U. S. Department of Commerce, JPRS: 14, 334, CSO: 69-61-N, Washington, D. C.

Kuhl, A. L., N. M. Kamel, and A. K. Oppenheim, "On Flame Generated Self-Similar Blast Waves," 14th Symposium (International) on Combustion, The Combustion Institute, pp. 1201-1214, 1973.

Larson, R. J., and W. C. Olson, "Measurements of Air Blast Effects from Simulated Nuclear Reactor Core Excursions," BRL Memorandum Report No. 1102, Aberdeen Proving Ground, Maryland, September 1957.

Lawley, H. G., "Operability Studies and Hazard Analysis," Loss Prevention, CEP Technical Manual, Volume 8, 1974.

Lee, J. H., R. Knystautas, and G. G. Bach, "Theory of Explosions," Department of Mechanical Engineering, McGill University, AFOSR Scientific Report 69-3090TR, 1969.

Lehto, D. L. and R. A. Larson, "Long Range Propagation of Spherical Shock Waves from Explosions in Air," NOLTR 69-88, Naval Ordnance Laboratory, White Oak, Maryland, 1969.

Leigh, B. R., "Lifetime Concept of Plaster Panels Subjected to Sonic Boom," UTIAS Technical Note 91, Institute for Space Studies, University of Toronto, July 1974.

Lewz, H., "Asymptotic Integration of Fragment Trajectories," APG-BRL Report No. 559 and Technical Note No. 496, September 1951.

Liepmann, H. W., and A. Roshko, "Elements of Gasdynamics," John Wiley and Sons, Inc., New York, 1967.

Lind, D., "Unconfirmed Vapor Cloud Explosion Studies," Paper No. 67e, Presented at the AIChE Symposium on Loss Prevention in the Chemical Industry, Houston, Texas, March 18-20, 1975; to be published in the Loss Prevention Journal, Vol. 8.

Lutzsky, M. and D. Lehto, "Shock Propagation in Spherically Symmetric Exponential Atmospheres," Physical Fluids, Vol. 11, p. 1466, 1968.

McNaughtan, L. I., and S. W. Chisman, "A Study of Hail Impact at High Speed on Light Alloy Plates," Proceedings of the Ninth Annual National Conference on Environmental Effects on Aircraft and Propulsion Systems, Naval Air Propulsion Test Center, pp. 16-14, October 7-9, 1969.

Makino, R., "The Kirkwood-Brinkley Theory of Propagation of Spherical Shock Waves and Its Comparison with Experiment," BRL Report #750, April 1951.

Mastromonico, C. R., "Blast Hazards of CO/N₂O Mixtures," Minutes of the 15th Explosives Safety Seminar, San Francisco, California, Department of Defense Explosives Safety Board, pp. 1305-1357, September 18-20, 1973.

Milne-Thompson, L. M., Theoretical Aerodynamics, MacMillan, London, 4th Edition, p. 230, 1966.

Moore, T. D., Editor, "Structural Alloys Handbook," Mechanical Properties Data Center, Traverse City, Michigan, 1975.

Muzzall, C. E., Editor, "Compendium of Gas Autoclave Engineering Studies," Report Y-1478, Y-12 Engineering Division, Union Carbide Corporation, Nuclear Division, Oak Ridge, Tennessee, November 1964.

Napadensky, H. S., J. J. Swatosh, Jr., D. R. Morita, "TNT Equivalence Studies," Minutes of 14th Explosive Safety Seminar, New Orleans, Louisiana, Department of Defense Explosives Safety Board, pp. 289-312, November 8-10, 1972.

Nelson, W., "A New Theory to Explain Physical Explosions," Combustion, pp. 31-36, May 1973.

Nicholls, R. W., C. F. Johnson, and W. I. Duvall, "Blast Vibrations and Their Effects on Structures," Bureau of Mines Bulletin 656, p. 105, 1971.

Norris, C. H., R. J. Hansen, M. J. Holley, J. M. Biggs, S. Namyot and J. V. Minami, "Structural Design for Dynamic Loads," McGraw-Hill Book Co., New York, 1959.

Oppenheim, A. K., "Elementary Blast Wave Theory and Computations," Paper # I, Proceedings of the Conference on Mechanisms of Explosion and Blast Waves, J. Alstor, Editor, Sponsored by the Joint Technical Coordinating Group for Air Launched Non-Nuclear Ordnance Working Party for Explosives, November 1973.

Oppenheim, A. K., A. L. Kuhl and M. M. Kamel, "On Self-Similar Blast Waves Headed by the Chapman Jouguet Detonation," J. Fluid Mech., Vol. 55, Part 2, pp. 257-270, 1972.

Oppenheim, A. L., A. L. Kuhl, E. A. Lundstrom, and M. M. Kamel, "A Parametric Study of Self-Similar Blast Waves," J. Fluid Mech., Vol. 52, Part 4, pp. 657-682, 1972.

Oppenheim, A. K., E. A. Lundstrom, A. L. Kuhl, and M. M. Kamel, "A Systematic Exposition of the Conservation Equations for Blast Waves," Journal of Applied Mechanics, pp. 783-794, December 1971.

Ordin, P. M., "Review of Hydrogen Accidents and Incidents in NASA Operations," NASA Technical Memorandum X-71565, 1974.

Oslake, J. J., R. J. Getz, R. A. Romine, and K. Sooftov, "Explosive Hazards of Rocket Launchings," Ford Motor Co., Technical Report 4-108:98, AD 25322, November 1960.

Ostle, Bernard, "Statistics in Research," The Iowa State Press, Ames, Iowa, 1960.

Penny, W. G., D. E. J. Samuels, and G. C. Scorgie, "The Nuclear Explosive Yields at Hiroshima and Nagasaki," Phil. Trans. Roy. Soc., Vo. 266, p. 357, 1970.

Perkins, B. J. and W. F. Jackson, "Handbook for Prediction of Air Blast Focusing," BRL Report 1240, Ballistics Research Laboratories, Aberdeen Proving Ground, Maryland, 1964.

Perkins, B. J., P. H. Lorrain, and W. H. Townsend, "Forecasting the Focus of Air Blasts Due to Meteorological Conditions in the Lower Atmosphere," BRL Report 1118, Aberdeen Proving Ground, Maryland, 1960.

Pesante, R. E. and M. Nishibazashi, "Evaluation of the Blast Parameters and Fireball Characteristics of Liquid Oxygen/Liquid Hydrogen Propellant," Report No. 0954001(61) FP, Aerojet-General Corp., Downey, California, April 1967.

Peterson, P. and H. R. Cutler, "Explosion Protection for Centrifuges," Chemical Engineering Progress, Vol. 69, (4), pp. 42-44, April 1973.

Pittman, J. F., "Blast and Fragment Hazards From Bursting High Pressure Tanks," NOLTR 72-102, May 1972.

Pittman, J. F., "Pressures, Fragments, and Damage from Bursting Pressure Tanks," Minutes of 14th Explosives Safety Seminar, New Orleans, Louisiana, Department of Defense Explosives Safety Board, pp. 1117-1138, November 8-10, 1972.

Porzel, F. B., "Introduction to a Unified Theory of Explosions" (UTE), NOLTR 72-209, Naval Ordnance Laboratory, White Oak, Silver Spring, Maryland, AD 758000, September 1972.

Powers, G. J. and F. C. Tompkins, "A Synthesis Strategy for Fault Trees in Chemical Processing Systems," Loss Prevention, CEP Technical Manual, Vol. 8, 1974.

Proceedings of the Second United Nations International Conference on Peaceful Uses of Atomic Energy, Vol. 11, Reactor Safety and Control, United Nations, Geneva, 1958.

Proctor, J. R. and W. S. Filler, "A Computerized Technique for Blast Loads from Confined Explosions," Minutes of 14th Explosives Safety Seminar, New Orleans, Louisiana, Department of Defense Explosives Safety Board, pp. 99-124, November 8-10, 1972.

Rasmussen, N. C., "Reactor Safety Study: An Assessment of Accident Risks in U. S. Commercial Nuclear Plants," U. S. Atomic Energy Commission Report WASH-1400, August 1974.

Recht, R. F., "Containing Ballistic Fragments," Engineering Solids Under Pressure, H. Pugh, Editor, Papers presented at the Third International Conference on High Pressure, Aviemore, Scotland, pp. 51-60, 1970.

Reed, J. W., "Distant Blast Predictions for Explosions," Minutes of the 15th Explosives Safety Seminar, Department of Defense Explosives Safety Board, Washington, D. C., Vol. II, pp. 1403-1424, 1973.

Reed, J. W., "Evaluation of Window Pane Damage Intensity in San Antonio Resulting from Medina Facility Explosion on November 13, 1963," Annals of New York Academy of Science, Vol. 152, Art. 1, pp. 565-584, October 1968.

Reisler, R. C., "Explosive Yield Criteria," Minutes of 14th Explosives Safety Seminar, New Orleans, Louisiana, Department of Defense Explosives Safety Board, pp. 271-288, November 8-10, 1972.

Richards, E., "Comparative Dispersion and Drag of Spheres and Light Cylinders," APG BRL TR-717, March 1950.

Richmond, D. R., E. G. Damon, E. R. Fletcher, I. G. Bowen, and C. S. White, "The Relationship Between Selected Blast-Wave Parameters and the Response of Mammals Exposed to Air Blast," Annals of the New York Academy of Sciences, Vol. 152, Art. 1, pp. 103+, October 1968.

Ricker, R. E., "Blast Waves from Bursting Pressurized Spheres," Department of Aeronautical and Astronautical Engineering, Master of Science Thesis, University of Illinois at Urbana-Champaign, May 1975.

Robinson, C. S., "Explosions, Their Anatomy and Destructiveness," McGraw-Hill Book Co., New York, New York, 1944.

Ross, R., et al, "Criteria for Assessing Hearing Damage Risk from Impulse-Noise Exposure," Human Engineering Laboratory, Aberdeen Proving Ground, Maryland, AD 666206, August 1967.

Ross, R., A. Coles, G. R. Garinther, D. C. Hodge and C. G. Rice, "Criteria for Assessing Hearing Damage Risk from Impulse-Noise Exposure," Tech. Memo. 13-67, U. S. Army Human Eng. Labs., Aberdeen Proving Ground, Maryland, AD 666206, August 1967.

Runes, E., "Explosion Venting," Loss Prevention, Vol. 6, pp. 63-67, 1972.

Sachs, R. G., "The Dependence of Blast on Ambient Pressure and Temperature," BRL Report 466, Aberdeen Proving Ground, Maryland, 1944.

Sakurai, A., "Blast Wave Theory," Basic Developments in Fluid Mechanics, Vol. I, Morris Holt, Editor, Academic Press, New York, New York, pp. 309-375, 1965.

Sewell, R. G. S. and G. F. Kinney, "Response of Structures to Blast: A New Criterion," Annals of New York Academy of Science, Vol. 152 Art. 1, pp. 532-547, October 1968.

Sewell, R. G. S. and G. F. Kinney, "Internal Explosions in Vented and Unvented Chambers," Minutes of 14th Explosives Safety Seminar, New Orleans, Department of Defense Explosives Safety Board, pp. 87-98, November 8-10, 1973.

Sichel, M. and C. Hu, "The Impulse Generated by Blast Waves Propagating Through Combustible Mixtures," Paper VIII, Proceedings of the Conference on Mechanisms of Explosions and Blast Waves, J. Alstor, Editor, Sponsored by the Joint Technical Coordinating Group for Air-Launched Non-Nuclear Ordnance Working Party for Explosives, November 1973.

Siewert, R. D., "Evacuation Areas for Transportation Accidents Involving Propellant Tank Pressure Bursts," NASA Technical Memorandum X-68277, 1972.

Siskind, D. E., "Ground and Air Vibrations From Blasting, Subsection 11.8," SME and Mining Engineering Handbook, A. B. Cummings and I. A. Given, Editors, Soc. of Min. Eng. of the Am. Inst. of Min. Metallur. and Pet. Eng. Inc., New York, Vol. VI, pp. 11-99 to 11-112, 1973.

Siskind, D. E. and Summers, C. R., "Blast Noise Standards Instrumentation," Bureau of Mines, Environmental Research Program, Technical Progress Report 78, U. S. Department of the Interior, May 1974.

Smith, T. L., "Explosion in Wind Tunnel Air Line," BRL Memorandum Report 1235, Ballistic Research Laboratories, Aberdeen Proving Ground, Maryland, September 1959.

Soper, W. G., "Modeling Laws Related to Target Vulnerability," U. S. Naval Weapons Lab Memorandum No. T-9/67, Dahlgren, Virginia, August 1967 (Confidential).

Sperrazza, J., "Modeling of Air Blast," Use of Modeling and Scaling in Shock and Vibration, W. E. Baker, Editor, ASME, New York, pp. 65-78, November 1963.

Sperrazza, J. and W. Kokinakis, "Ballistic Limits of Tissue and Clothing," BRL Technical Note No. 1645, Aberdeen Proving Ground, Maryland, January 1967.

Stepniewski, W. Z., "Basic Aerodynamics and Performance of the Helicopter," Helicopter Aerodynamics and Dynamics - AGARD Lecture Series No. 63, AGARD-LS-63, April 1973.

Sterne, T. E., "A Note on the Initial Velocities of Fragments from Warheads," BRL Report 648, September 1947.

Sterne, T. E., "The Fragment Velocity of a Spherical Shell Containing an Inert Core," BRL Report 753, March 1951.

Strehlow, R. A., "Accidental Non-Ideal Explosions," Progress Report NASA NSG 3008, December 6, 1974.

Strehlow, R. A., "Blast Waves Generated by Constant Velocity Flames--A Simplified Approach," Combustion and Flame, Vol. 24, 1975.

Strehlow, R. A., "Equivalent Explosive Yield of the Explosion in the Alton and Southern Gateway, East St. Louis, Illinois, January 22, 1972," AAE TR 73-3, Department of Aeronautical and Astronautical Engineering, University of Illinois, Urbana, Illinois, June 1973.

Strehlow, R. A., "Unconfined Vapor-Cloud Explosions--An Overview," 14th International Symposium on Combustion, The Combustion Institute, pp. 1189-1200, 1973.

Strehlow, R. A. and A. A. Adamczyk, "On the Nature of Non-Ideal Blast Waves," Technical Report AAE 74-2, UILU-ENG-740502, University of Illinois, Urbana, Illinois, 1974.

Strehlow, R. A. and W. E. Baker, "The Characterization and Evaluation of Accidental Explosions," NASA CR 134779, NASA Grant NSG 3008, June 1975.

Strehlow, R. A., L. D. Savage, and G. M. Vance, "On the Measurement of Energy Release Rates in Vapor Cloud Explosions," Combustion Sciences and Technology, Vol. 6, pp. 307-312, 1973.

Sutherland, L. C., "A Simplified Method of Estimating the Approximate TNT Equivalent From Liquid Propellant Explosions," Minutes of the 15th Explosives Safety Seminar, Department of Defense Explosives Safety Board, Washington, D. C., Vol. II, pp. 1273-1277, 1973.

Taylor, D. B. and C. F. Price, "Velocities of Fragments From Bursting Gas Reservoirs," ASME Transactions, Journal of Engineering for Industry, November 1971.

Taylor, G. I., "The Air Wave Surrounding an Expanding Sphere," Proc. Royal Soc., A, Vol. 186, pp. 273-292, 1946.

Thomas, J. H., "Computing Effect of Distance on Damage by Fragments," APG BRL Report No. 468, May 1944.

Thornhill, C. K., "Explosions in Air," ARDE Memo (B) 57/60, Armament Research and Development Establishment, England, 1960.

Transue, W. R. and K. M. Saramel, "Terminal Ballistics - Fragmentation Effects," TR Institute of Research Lehigh University, December 1947.

U. S. Army Material Command, Engineering Design Handbook, Principles of Explosive Behavior, AMCP 706-180, Washington, D. C., April 1972.

von Gierke, H. E., "Biodynamic Models and Their Applications," Aerospace Medical Research Laboratory, Wright-Patterson Air Force Base, Ohio, AD 736985, 1971.

von Gierke, H. E., "Dynamic Characteristics of the Human Body," Aerospace Medical Research Laboratory, Wright-Patterson Air Force Base, Ohio, AD 769022, 1973.

von Gierke, H. E., "On the Dynamics of Some Head Injury Mechanisms," Aerospace Medical Research Laboratory, Wright-Patterson Air Force Base, Ohio, AD 728885, 1971.

von Gierke, H. E., "Man to Model, or Model to Man," Aerospace Medical Research Laboratory, Wright-Patterson Air Force Base, Ohio, AD 771670, September 1973.

von Gierke, H. E., "Mechanical Behavior of Biological Systems," Aerospace Medical Research Laboratory, Wright-Patterson Air Force Base, Ohio, AD 758963, September 1967.

von Neumann, J. and H. Goldstine, "Blast Wave Calculation," Communication on Pure and Applied Mathematics, Vol. 8, pp. 327-353; reprinted in John von Neumann Collected Works, A. H. Taub, Editor, Vol. VI, Pergamon Press, New York, New York, pp. 386-412, 1955.

Warren, A., "Blast Pressures from Distant Explosions," ARDE Memo 18/58, AD 305732, 1958.

Wenzel, A. B., and R. L. Bessey, "Barricaded and Unbarricaded Blast Measurements," Contract No. DAHC04-69-C-0028, Subcontract I-OU-431, Southwest Research Institute, October 1969.

Westine, P. S., "R-W Plane Analysis for Vulnerability of Targets to Air Blast," The Shock and Vibration Bulletin 42, Part 5, pp. 173-183, January 1972.

Westine, P. S. and W. E. Baker, "Energy Solutions for Predicting Deformations in Blast Loaded Structures," Minutes of 16th Annual Explosion Safety Seminar, Department of Defense Safety Board, 1974.

White, C. S., "The Nature of the Problems Involved in Estimating the Immediate Casualties from Nuclear Explosions," CEX-71.1, Civil Effects Study, U. S. Atomic Energy Commission, DR-1886, July 1971.

White, C. S., "The Scope of Blast and Shock Biology and Problem Areas in Relating Physical and Biological Parameters," Annals of the New York Academy of Sciences, Vol. 152, Art. 1, p. 89+, October 1968.

White, C. S., I. G. Bowen, D. R. Richmond and R. L. Corsbie, "Comparative Nuclear Effect of Biomedical Interest," CEX-58.8, Civil Effects Study, U. S. Atomics Energy Commission, January 1961.

White, C. S., R. K. Jones, E. G. Damon, E. R. Fletcher, and D. R. Richmond, "The Biodynamics of Airblast," Technical Report to Defense Nuclear Agency, DNA 2738T, Lovelace Foundation for Medical Education and Research, AD 734208, July 1971.

Whisham, G. B., "The Propagation of Spherical Blast," Proc. Roy. Soc., Vol. A203, pp. 571-581, 1950.

Williams, F. A., "Qualitative Theory of Non-Ideal Explosions," Phase I, Final Report entitled, "Explosion Hazards Associated with Spills of Large Quantities of Hazardous Materials," by D. C. Lind, Naval Weapons Center, China Lake, California, August 5, 1974, U. S. Coast Guard, Washington, D. C.

Willoughby, A. B., C. Wilton, B. L. Gabrielson, and J. V. Zaccor, "Loading, Structural Response, and Debris Characteristics of Wall Panels, U. R. S. Contract No. 11618 (6300A-250) with Office of Civil Defense, Final Report, AD 693792, July 1969.

Willoughby, A. B., C. Wilton and J. Mansfield, "Liquid Propellant Explosive Hazards, Final Report - December 1968, Vol. I - Technical Documentary Report," AFRPL-TR-68-92, URS-652-35, URS Research Co., Burlingame, California.

Willoughby, A. B., C. Wilton and J. Mansfield, "Liquid Propellant Explosion Hazards, Final Report - December 1968, Vol. II - Test Data," AFRPL-TR-68-92, URS 652-35, URS Research Co., Burlingame, California.

Willoughby, A. B., C. Wilton and J. Mansfield, "Liquid Propellant Explosion Hazards, Final Report - December 1968, Vol. III - Prediction Methods," AFRPL-TR-68-92, URS 652-35, URS Research Co., Burlingame, California.

Wilse, T., "Fire and Explosions Onboard Ships," Veritas, No. 80, pp. 12-16, September 1974.

Wisotski, J. and W. H. Snyer, "Characteristics of Blast Waves Obtained from Cylindrical High Explosive Charges," University of Denver, Denver Research Institute, November 1965.

Woolfolk, R. W. "Correlation of Rate of Explosion with Blast Effects for Non-Ideal Explosions," SRI Final Report for Contract No. 0017-69-C-4432, Stanford Research Institute, Menlo Park, California, January 25, 1971.

Woolfolk, R. W. and C. M. Ablow, "Blast Waves from Non-Ideal Explosions," Paper # IV, Proceedings of the Conference on Mechanisms of Explosion and Blast Waves, J. Alstor, Editor, Sponsored by the Joint Technical Coordinating Group for Air Launched Non-Nuclear Ordnance Working Party for Explosives, November 1973.

Yelverton, J. T., E. G. Damon, R. K. Jones, T. L. Chiffelle, and U. C. Luft, "Effects of Irradiation and Blast on Pulmonary Function in Sheep," Technical Report to Defense Atomic Support Agency, DASA 2630, Lovelace Foundation for Medical Education and Research, AD 721094, January 1971.

Zaker, T. A., "Trajectory Calculations in Fragment Hazard Analysis," Minutes of 13th Annual Explosives Safety Seminar, p. 101, September 1 1.

90

END

1.4.78